PACIFIC EARTHQUAKE ENGINEERING RESEARCH CENTER

Seismic Risk Management in Urban Areas

Proceedings of a U.S.-Iran-Turkey Seismic Workshop
December 14-16, 2010

Istanbul, Turkey

PEER 2011/07
SEPTEMBER 2011

Seismic Risk Management in Urban Areas

Proceedings of a U.S.-Iran-Turkey Seismic Workshop
December 14-16, 2010

Istanbul, Turkey

PEER Report 2011/07
Pacific Earthquake Engineering Research Center
College of Engineering
University of California

September 2011

ABSTRACT

The U.S.-Iran-Turkey seismic workshop was held on December 14-16, 2010 in Istanbul, Turkey. The workshop was supported by the U.S. National Academy of Sciences in collaboration with the Bogazici University–Kandilli Observatory and Earthquake Research Institute, Turkey; Sharif University of Technology, Iran; and the Pacific Earthquake Engineering Research Center, University of California Berkeley, USA. The theme of this workshop was ***Seismic Risk Management in Urban Areas***. This report contains the collection of papers presented at the 2010 seismic workshop.

.

INTRODUCTION

2008 and 2009 U.S. –Iran Seismic Workshops

Following an extended period of planning, on June 8-9, 2008, a U.S. –Iran invitational workshop on *Seismic Performance of Adobe and Masonry Structures* was held at Sharif University of Technology in Tehran. The workshop was organized by Sharif University of Technology, in collaboration with the U.S. National Academy of Sciences and the Pacific Earthquake Engineering Research Center (PEER), University of California, Berkeley. It involved specialists from fourteen Iranian institutions, and seven earthquake experts from the United States.

The topic of adobe and masonry vulnerability was selected because of the extensive damage to this form of construction from earthquakes in Iran, including the Bam earthquake of December 26, 2003. Twenty-three technical papers were presented. The workshop concluded with a panel session that identified topics for future research collaboration. The workshop was followed with a one-day public seminar on June 10, 2008, on *Seismic Hazard Reduction*, also held at Sharif University.

The second U.S.-Iran seismic workshop was held on June 29-July 1, 2009, at the Arnold and Mabel Beckman Center of the National Academies of Sciences and Engineering, Irvine, California. The workshop was supported by the U.S. National Academy of Sciences, in collaboration with the PEER, and Sharif University of Technology. The theme of this workshop was *Improving Earthquake Mitigation through Innovations and Applications in Seismic Science, Engineering, Communication, and Response*. Numerous U.S. and Iranian earthquake engineers and scientists participated in the workshop and gave presentations. The proceedings of the 2009 seismic workshop were published by PEER as *PEER Report 2009/02*.

2010 US-Iran-Turkey Seismic Workshop

The third seismic workshop, the subject of this report, was held with US, Iranian and Turkish earthquake experts on December 14-16, 2010, in Istanbul, Turkey. The theme of the workshop was *Seismic Risk Management in Urban Areas.*

The 2010 seismic workshop was hosted by the Bogazici University–Kandilli Observatory and Earthquake Research Institute in Istanbul, Turkey, in collaboration with the U.S. National Academy of Sciences, Sharif University of Technology, and the PEER. The participants of the workshop included nine experts from the United States, twelve from Iran, and fifteen from Turkey. The agenda of the workshop is presented next. The papers presented at the workshop were edited by Yousef Bozorgnia (PEER, University of California, Berkeley), Sanaz Rezaeian (PEER, University of California, Berkeley), and William Anderson (U.S. National Academy of Sciences).

On December 16, 2010, the final day of the workshop, the participants had an open discussion about possibilities for future cooperation between seismic experts from the U.S., Iran, and Turkey. Several technical topics were suggested by participants for future collaboration; the top three topics were:

(a) Seismic retrofit of buildings, especially schools,

(b) Seismic performance of tall buildings, and

(c) Seismic performance of lifelines.

We thank all participants of the 2010 workshop from the three countries for their time and efforts. The seismic workshops in 2008, 2009, and 2010 would not have been possible without the continuous support and encouragement of **Glenn Schweitzer** of the US National Academy of Sciences. Professor **Mustafa Erdik** of Kandilli Observatory and Earthquake Research Institute was the key coordinator of the seismic workshop in Istanbul; his efforts and cooperation are greatly appreciated. Dr. **Fayaz Rahimzadeh Rofooei** (Sharif University of Technology) was the coordinator of the Iranian team of participants, and we appreciate his continuous cooperation.

Yousef Bozorgnia, Sanaz Rezaeian, and William Anderson

Istanbul, Turkey, December 16, 2010

AGENDA

Seismic Risk Management in Urban Areas

TUESDAY DECEMBER 14, 2010

7:00–8:00 AM	**Breakfast and Registration**
8:00–8:30 AM	**Opening:** Rector of Bogazici University Mustafa Erdik, Fayaz R. Rofooei, and Yousef Bozorgnia
8:30–10:30 AM	**Seismic Hazard: Nuray Aydınoglu,** Session Chair

- **Mustafa Aktar,** Bogazici University
  Observations in Marmara: Basic Science Contribution to Risk Management
- **Mohsen Ghafory-Ashtiany,** International Institute of Earthquake Engineering and Seismology (IIEES)
  Strong Ground Motion Selection for Reliable Nonlinear Dynamic Analysis of Structures
- **Sinan Akkar,** Middle East Technical University
  Recent Developments in Ground-Motion Prediction Equations
- **Sanaz Rezaeian,** PEER, University of California, Berkeley
  Stochastic Simulation of Earthquake Ground Motion Components for Performance-Based Structural Analysis
- **Sedat Inan,** TÜB_TAK Marmara Research Institute
  Earthquake Research Activities of MAM in the Marmara Region

10:30–10:50 AM	**Break**
10:50 AM–12:00	**Seismic Performance of Tall Buildings: Fayaz Rofooei** Session Chair

- **Yousef Bozorgnia,** PEER, University of California, Berkeley
  Tall Buildings Initiative: A Comprehensive Research on Seismic Analysis and Design of New Tall Buildings
- **Nuray Aydinoglu,** Bogazici University
  Draft Seismic Design Code for Tall Buildings in Istanbul Metropolitan Area
- **Hamzeh Shakib,** Tarbiat Modares University
  Architectural Effects on the Seismic Behavior of Tehran Tall Buildings

12:00–13:00 PM	**Lunch**

13:00–14:30 PM **Earthquake Risk Management & Education (I): William Anderson,** Session Chair

- **Mine Betul Demircioglu**, Bogazici University
  Assessment of Earthquake Risk in Istanbul
- **Mustafa Erdik,** Bogazici University
  Mitigation of Earthquake Risk in Istanbul
- **Ifa Kashefi,** City of Los Angeles
  Seismic Issues from a Large City's Perspective
- **Mehmet Emin Akdogan,** UN-HABITAT, Tehran
  Implementation of Sustainable Plan for Disaster Risk Mitigation in Iran: Recommendations on Damage Prevention, Risk Reduction, Emergency Response, and the Role of UN-HABITAT

14:30–14:50 PM **Break**

14:50–16:20 PM **Earthquake Risk Management & Education (II): Sinan Akkar,** Session Chair

- **Atilla Ansal,** Bogazici University
  Seismic Microzonation Case Studies
- **William Anderson,** U.S. National Research Council / National Academies
  Challenges to Public Seismic Education
- **Haluk Sucuoglu,** Middle East Technical University
  Seismic Risk Assessment in Building Stocks through Street Surveys-Implementation to Istanbul
- **Karin Sesetyan,** Bogazici University
  The Earthquake Model of Middle East: EMME Project

17:00–19:00 PM **Reception at Bogazici University**

WEDNESDAY DECEMBER 15, 2010

7:30–8:30 AM **Breakfast**

8:30–10:30 AM **Seismic Performance of Lifelines: Ali Pak,** Session Chair

- **Mohsen Ghaemian,** Sharif University of Technology
  Seismic Response of Arch Dams Subjected to Multiple Support Excitations
- **Stuart Werner,** Principal, Seismic Systems & Engineering Consultants
  Recent Advances in Seismic Risk Analysis of Highway Systems
- **Fardin Jafarzadeh,** Sharif University of Technology
  Vulnerability and Retrofitting of Buried Pipelines and Networks during Earthquakes with Emphasizing in Urban Areas
- **Seyedmagdedin Mir Mohammad Hosseini,** Amirkabir University of Technology
  The Seismic Response of Shallow Tunnels within the Liquefiable Zones
- **Aslı Kurtulus,** Bogazici University
  Pipeline Vulnerability in Adapazarı during 1999 Kocaeli, Turkey, Earthquake

10:30–10:50 AM **Break**

10:50 AM–12:10 PM **Geotechnical Earthquake Engineering: Stuart Werner,** Session Chair

- **Ali Pak,** Sharif University of Technology
  Numerical Modeling of the Liquefaction-induced Settlements of Buildings in Urban Areas
- **Ahmed Elgamal,** University of California at San Diego
  Numerical Modeling and Performance-Based Earthquake Engineering for Soil-Structure Systems
- **Mohammad Hassan Baziar,** Iran University of Science and Technology
  Liquefaction Assessment Using Hollow Torsional Test Results

12:10–13:15 PM **Lunch**

13:15–15:00 PM **Seismic Performance of Structural Systems (I): Atilla Ansal,** Session Chair

- **James Kelly,** University of California, Berkeley
  Seismic Isolation for Housing, Schools, and Hospitals in Urban Environment

- **Fayaz Rahimzadeh Rofooei,** Sharif University of Technology
  On the Dynamic Response of a Base Isolated Structure Equipped With Cylindrical Liquid Tanks through Fluid/Structure Interaction
- **Mansour Ziyaeifar,** International Institute of Earthquake Engineering and Seismology (IIEES)
  A Dual Mass Model for Studying High Damped Structural Systems
- **Mehdi Ahmadizadeh,** Sharif University of Technology
  Improved Integration Methods for Accurate Identification of Dynamic Properties of Structural Components Using Seismic Hybrid Simulation

15:00–15:20 PM **Break**

15:20–17:20 PM **Seismic Performance of Structural Systems (II): Mohsen Ghafory-Ashtiany,** Session Chair

- **Homayoon Esmailpur Estekanchi,** Sharif University of Technology
  Recent Advances in Seismic Assessment of Structures by Endurance Time Method
- **Hasan Boduroglu,** Istanbul Technical University
  Earthquake Performance Assessment of Buildings
- **Ali Bakhshi,** Sharif University of Technology:
  Damage Identification during Earthquake Excitation in Steel Frame Structures utilizing Time-Frequency Method
- **Mahmoud-Reza Banan**, Shiraz University:
  Beyond R-Factor: Design Theory for Damage-Based Seismic Design of RC Buildings
- **Shahrokh Maalek,** University of Tehran:
  An Experimental Investigation of the Behavior of Double I-Shaped Beams as the Link Members of Eccentrically Braced Frames

THURSDAY DECEMBER 16, 2010

7:30–8:30 AM **Breakfast**

8:30–10:00 AM **Insurance, Field Measurement, Retrofit, Urban Renewal, and Tsunami Issues: Ifa Kashefi,** Session Chair

- **DASK:** Ismet Güngör
  Turkish Compulsory Earthquake Insurance
- **Robert Kayen,** U.S. Geological Survey and University of California, Los Angeles
  Active-Source Surface Wave Analysis for Earthquake Site Response and Liquefaction Assessment
- **ISMEP**
  Istanbul Seismic Risk Mitigation and Emergency Preparedness Project
- **Istanbul Metropolitan Municipality**
  Earthquake Focused Urban Renewal Activities
- **Nurcan Ozel,** Bogazici University
  Establishing a Tsunami Warning System in Turkey

10:00–10:30 AM **Break**

10:30 AM–12:00 PM **Future of Seismic Cooperation Discussion: Glenn Schweitzer,** Session Chair

12:00–12:30 PM **Closing Remarks: Mustafa Erdik, Fayaz Rahimzadeh, and Yousef Bozorgnia**

12:30–2:00 PM **Farewell Lunch**

CONTENTS

SESSION 9: INSURANCE, FIELD MEASUREMENT, RETROFIT, URBAN RENEWAL, AND TSUNAMI ISSUES

EXPERİMENTS FOR MODELİNG THE UNKNOWN ASPECTS OF GROUND MOTİON FOR ISTANBUL CİTY

Mustafa Aktar

Department of .Geophysics, Kandilli Observatory and Earthquake Research. Institute, Bogazici University, Ankara, Turkey, aktar@boun.edu.tr

ABSTRACT

The expected variations of the ground velocity depending on the direction and the velocity of the rupture were analyzed. Representative rupture models were developed using *a priori* knowledge about the fault zone and forward models were run to investigate the ground motion variability. Synthetic seismogram were generated across a dense grid covering the metropolitain area of Istanbul, and spacial variation of the ground velocity was mapped. The slip was assumed to be a random variable, and calculations were done for many samples of initial model. The final results were obtained by averaging the outcomes of different scenarios. The directivity effect was seen to be most effective in the line of the strike of the fault as predicted by theory. The effect of rupture speed was analyzed in particular for the case of subshear and supershear velocities. Results show that high amplification values emerged at far distances from the fault (> 40 km) and in the direction parallel to the fault line. At those distances the ground shaking is expected to fall at smaller levels that are less critical for hazard considerations. For locations very close to the fault, the near-field term became so overwhelming that contribution from the other parts of the fault becomes less significant, making the rupture speed of secondary importance.

INTRODUCTION

The city of Istanbul is identifed as one of the most vulnerable location for earthquake hazard wordwide due to the unruptured segment of the North Anatolian fault in Marmara Sea, which runs at 15 km from the city. There is a considerable work currently being conducted for studying the properties of both the seismic source as well as the site conditions in order to come up with a realistic description of the hazard [Parson et al. 2000; Le Pichon 2001; Armijo et al. 2002]. Standard procedures are then applied to quantify the size of the ground motion expected to occur in the occurence of a large event which would rupture the mapped faults crossing the Marmara Sea [Oglesby et al. 2008; Picozzi et al. 2009; Ansal et al. 2009]. In particular, empirical attenuation relations are used for that purpose, and they constitute the standard basis for quantifying the expected ground motion. These laws are obtained by combining various observations from large earthquakes worldwide [Somerville et al. 1997]. Traditionally, the maximum value of the expected acceleration is used as the measure to describe the extent of the ground motion. In recent years, the peak value of the ground velocity is also found to be a suitable choice for design criteira. In particular, the spacial instability of acceleration observations in the near field poses serious problems for deriving reliable empirical attenuation laws [Bouchon and Karabulut 2002]. On the other hand, the ground velocity is not only more stable but also much easier to compute theoretically once the source and the structure is known. In the future it is expected that ground velocity will be used more intensely and possibly replace or at least complement the ground acceleration as a design criteria.

Seismic Hazard

A common problem associated with empirical relations is the fact that it practically ignores everything related to rupture kinematics. For exemple, slip heterogeineities, rupture speed variations, and directivity effects are totally ignored in all procedures that use the traditional empirical relations. However, recent data from near fields and geodedic observations (GPS, InSar, etc.) and improvements in kinematic and dynamic modelling clearly shows that the rupture process is far from being a uniform process as was previously assumed [Bouchon et al. 2002; Cakir et al. 2003]. The slip is distributed across the fault plane in a very heterogeneous fashion and reaches two-three times its average value on asperity patches [Clévédé et al. 2004]. The rupture velocity, which is usually assumed to be fixed to a value close to 80-90% of the shear wave velocity, not only shows strong fluctuations but may also reach very high values close to the speed of the compressional wave [Bouchon et al. 2001]. Finally, rupture directivity, theoretically known for a long time, is also seen to be more effective than previously assumed. In this study, the last two effects are studied for the case of Istanbul. Ground velocity was analyzed for assessing the characteristics of the ground motion variations. In particular, representative rupture models were assumed based on *a priori* information and forward models were generated to investigate the ground motion for a given source complexity. The motivation of choosing representative rupture models is discussed in detail in view of recent observations in other large earthquakes, in particular Izmit (1999, M=7.4) and Düzce (1999, M=7.2) earthquakes [Bouchon et al. 2002; Bouin et al. 2004].

Rupture Modellıng For Future Marmara Earthquake

The active fault structure in Marmara Sea has been studied in much detail during the last decade using wide range of methods including microseismicity, seismic profiling, coring, etc. [Laigle et al. 2008; Becel et al. 2008]. The main issue in the fault identification is the question related to the complex relation between the existing basin morphology and the actual segmentation of faults. This debate somehow culminated in a basic question of determining whether the whole of the unruptured segment of North Anatolian fault traversing the Marmara Sea could rupture in a single event or not [Le Pichon 2001; Armijo et al. 2002]. In the present day, the general consensus is to accept that in a worst case scenario the rupture is likely to accumulate sufficient energy to cut through various morphological barriers (bends, jogs, pull-aparts), creating a single event to release most of the accumulated strain. Accordingly, most of the scenarios that constitute the basis of vulnarability estimations are based on a single rupture model. However, since this work concentrates on the effect of some particular source complexities, we only considered the rectilinear segment that crosses Takirdag and Central basins and implemented the source complexities on this segment. The Cinarcik basin is excluded since directionwise it is not in the line of the major rectilinear fault.

In order to get insight for the range of source complexities that are likely to be observed on this part of North Anatolian fault, it is best to look at the closest event that has occured in relatively recent time: the Izmit earthquake of 17 August 1999, Ml=7.4. Several studies have produced rupture models for the Izmit earthquake using a variety of data covering various parts of the observation spectrum: geodetic data based on offset measurements from surface breaks, GPS, InSAR, and SPOT images, as well as seismological data from near-field and teleseismic records (see Clévédé [2004] for a general review). The models show considerable differences between them both in terms of the distribution of the slip and the kinematics of the rupture. All models predict a high slip patch below Golcuk (20 km west of hypocenter). Similarly, many of them predict a second high slip below Sapanca Lake (30 km west of hypocenter). Bouchon et al. [2002] and Cakir et al. [2003] predict a high slip at Karadere segment (50 km west of hypocenter, east of sharp bending) in deep layers, while others predict very small or even no co-seismic slip on this segment. The model by DeLouis et al. [2002] differs from the others by extending the rupture into the Duzce segment, which eventually broke 87 days following the Izmit event (Duzce earthquake of 12 November 1999, Ml=7.2).

Two slip models were used in this study: uniform slip and varying slip. Considering the large variations of slip in the Izmit earthquakes, it is clearly unrealistic to assume the uniform slip model. However, it helps to identify better certain extreme behavior of the ground motion; therefore, it was used occasionally in this work, assuming a constant slip of 2.5 m. The variable slip model was produced by dividing the rupture area into an array of 4×4 km cells and assuming a random slip for each cell having a normal distribution with a given mean and variance. Dividing the rupture area into a grid is a common approach for slip inversion procedures. However, the random distribution (Gaussian) for the slip values leads to a very rapid variation of the slip that is not a realistic representation of what actually is happening in real life. Nevertheless, it helps to remove all the artificial effects due to uniform distribution of slip and tends to smear out the final ground displacement estimation.

The assumption of a location for nucleation point is another issue that is very difficult to estimate, and, therefore, is totally ignored in engineering-oriented hazard analysis. In the Izmit earthquake, the rupture nucleated at a location where a continuous swarm activity had been observed since the beginning of the instrumentation of the area, namely for about 40 years. The area was studied in detail in early 1980s for dilatancy testing. It was found that nearly all the swarm events have normal FPS, pointing to a local extension zone that reduces the normal stress. Durand et al. [2010] noted that similar swarm activities associated with the majority of normal events also exist in other parts of the North Anatolian fault. They also noted that similar to the Izmit case, the local extension at Cerkes (32.88E, 40.82N) coincided with the nucleation point of two major earthquakes of 1943 (M=7.6) and 1944 (M=7.3). This observations leads to the possibility that local extensions zones, marked by swarms of normal events, can be considered as candidates for the nucleation of future ruptures, in particular, the prominent one that is expected to occur in the Marmara Sea. Two locations are observed to show swarm activity with majority of events having normal fault plane solutions: (a) west of Tekirdag Basin on the west, and (b) east of Cinarcik basin on the east. In the models presented herein, these are the two locations were chosen to be the possible nucleation points for the future Marmara earthquake.

The final unknown parameter for the source model is the rupture velocity. This issue is not usually considered in standard hazard analysis mainly because the rupture velocity was assumed to be theoretically limited to about 90% of the shear velocity. An interesting property of both the Izmit and Duzce ruptures is the observation of the supershear rupture speed as part of the co-seismic process. The next question is then: can we identify candidates for supershear segments for faults that have not ruptured yet? Bouchon and Karabulut [2002] pointed out to the geometric simplicity of the rupture plane on supershear zones. They also noted a distinguishing characteristic of the aftershock distribution along the supershear segments. The first thing that was observed is that the supershear segment of Izmit rupture was remarkably rectilinear with no sign of jogs or bends. Furthermore the aftershocks along the supershear part were not located exactly on the fault plane and were also much reduced in number. In Izmit earthquake, along the subshear part to the west of the epicenter, the aftershocks followed the rupture line at a close distance and in a regular fashion without leaving too much of a quiet zone. The off-the-fault aftershocks only appeared at the very end of the rupture where the fault splays. The supershear section had a totally different character. The activity this time was not located on the rupture itself but on adjacent faults. These are probably aftershock activities that were triggered on the secondary and probably ancient weakness zones. Bouchon and Karabulut [2002] concluded that supershear should be expected on sections where the fault has a simple rectilinear geometry and characterized by a general lack of micro-seismicity. By comparison, the linear and quiet section of the Marmara Sea fault east of the Central Basin is considered to be a candidate for supershear and is modeled as such (see Figure 1).

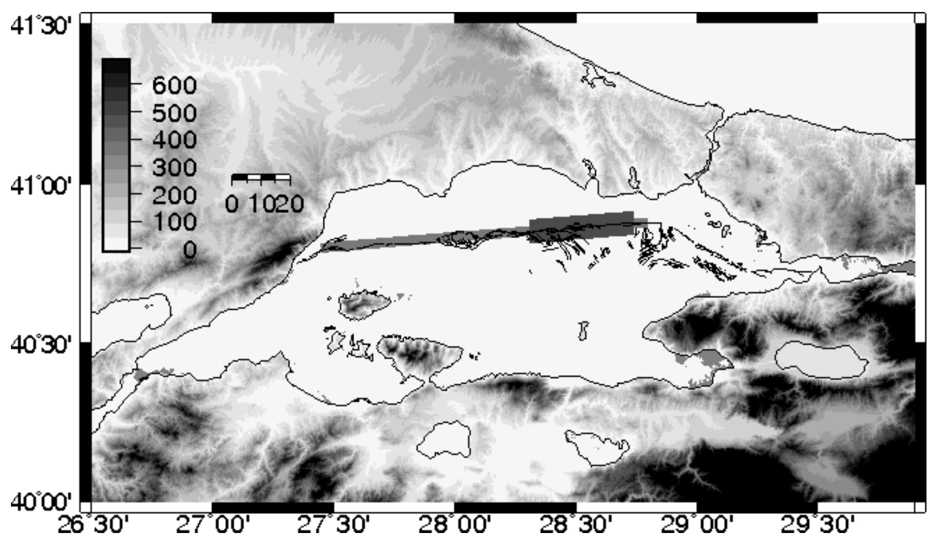

Figure 1 Topographic map of Marmara Sea surrounding. The submarine faults are taken from Le Pichon et al. [2001]. The thin grey line shows the rupture line, and the thick darker grey line shows the segment where the supershear is assumed to have occurred.

Results

The first experiment for ground motion analysis concentrated on the expected variation of the ground velocity depending upon the direction of rupture. The ground velocity was calculated for a grid of 40 points covering the metropolitan area of Istanbul (Figure 2). The rupture velocity was assumed to have a subshear with a value of 2.6 km/sec (85% of the shear velocity). The frequency-wave number method [Bouchon 1981] was used for generating the seismograms. The slip distribution was assumed to be random as described above, with mean of 2.5 and variance of 0.8. Ten different experiments were made, each time with a different random choice of slip distribution. The final results were the average value of these ten experiments. The rupture was assumed to be unilateral and initiated at the east (an east-to-west rupture) for the least effective directivity and at the west (a west-to-east rupture) for the highest directivity. The ground velocity was estimated for both models where the rupture propagates in two opposite directions. Figure 2 shows the ratio of the maximum velocity in horizontal components (NS and EW) for each direction of propagation.

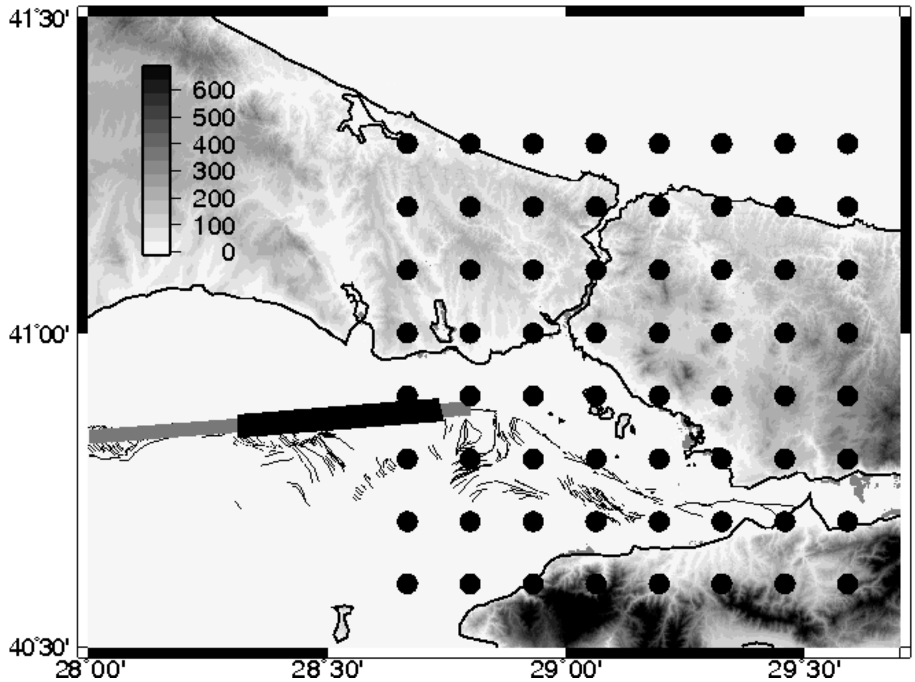

Figure 2 **Topographic map of Istanbul city and surrounding. The submarine faults are taken from Le Pichon et al. [2001]. The thin grey line shows the rupture line, and the thick darker grey line shows the segment where the supershear is assumed to occur. The dots represent the grid points where synthetic ground velocities are computed.**

The second experiment evaluated the expected effect of the supershear rupture if ever it occurs during the Marmara earthquake. Similar conditions were assumed as the previous experiment. The supershear segment is indicated on the Figure 3 by the thick line, covering 36 km of the eastern end of the fault, which is the closest part to Istanbul. The direction of rupture propogation was assumed to be from west to east, both for the subshear and supershear rupture cases. Figure 4 shows the change in the horizontal components (NS and EW) at a given location due to the variation of the rupture velocity. This location is on the north of the rupture, close to the eastern end, 5-km distance from the fault. Rupture velocities between 0.85 V_s to 1.73 V_s were tested, where V_s indicates the shear velocity of the rupturing medium. The slip distribution was assumed to be constant at 2.5 m. Note that as the rupture velocity increases, all swings of the shear pulse are squeezed into single main lobe whose amplitude increases slightly. This corresponds to the sharp arrival of the shear wave associated with Mach cone. This also means that the radiated energy gets larger as the rupture velocity increases. As the rupture velocity increases above the critical value of 1.41 V_s, the main pulse seems to broaden again but not significantly. This property holds for both the NS and EW components.

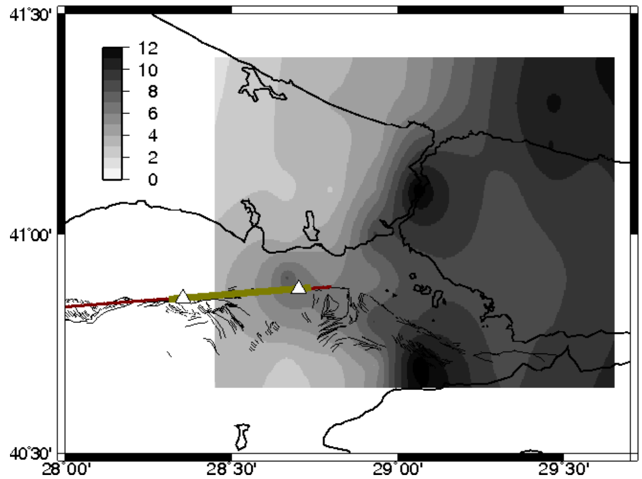

(a) North-south component of ground velocity

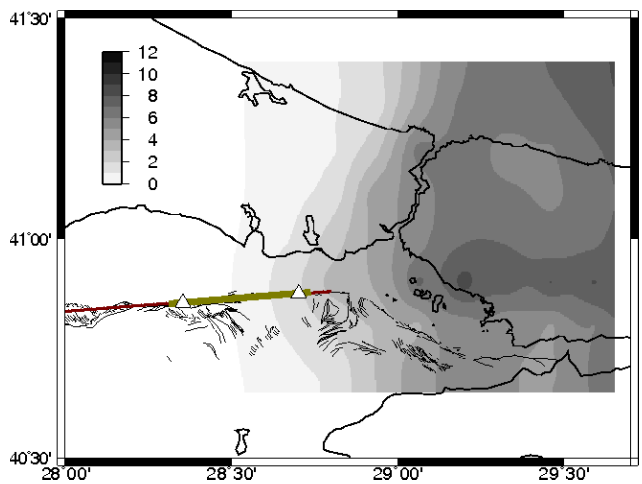

(b) East-west component of ground velocity

Figure 3 **The amplification factor due to directivity on horizontal components where the amplification factor is the ratio of the maximum peak value of synthetic seismogram generated for unilateral East-to-west and unilateral west-to-east ruptures. High amplification values are seen in the direction of eastern propogation of the fault line. The deviations from symmetry about fault line are due to the non-symmetrical positions of the grid points with respect to the fault line. The submarine faults are taken from Le Pichon et al. [2001]. The thin grey line shows the rupture line, the thick darker grey line shows the segment where the supershear is modelled to occur.**

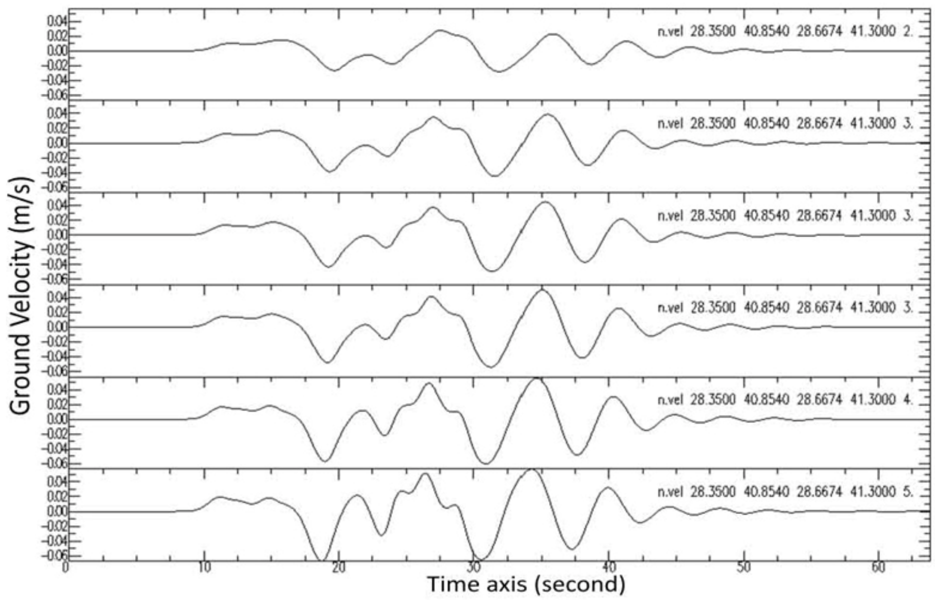

(a) North-south component of ground velocity

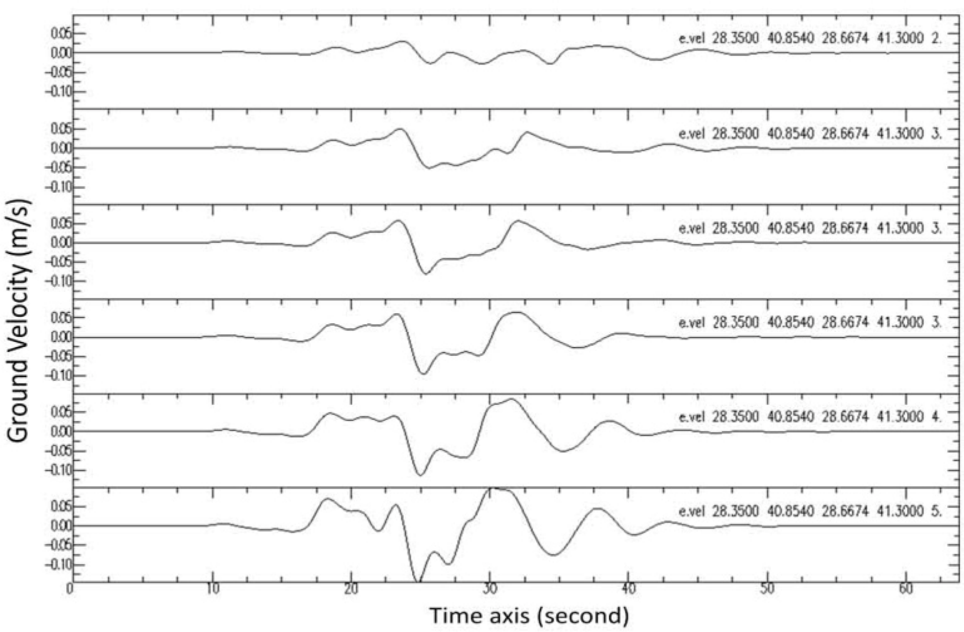

(b) East-west component of ground velocity

Figure 4 The variation of the horizontal velocity components due to the rupture velocity increase at 5-km distance north of the fault. Rupture velocities used were 0.85, 1.00, 1.10, 1.20, 1.41, and 1.73 times the shear velocity (from top to bottom). The slip distribution was assumed to be constant at 2.5 m. Note that as the rupture velocity increases, all swings of the shear pulse are squeezed into single main lobe whose amplitude increases slightly. This corresponds to the sharp arrival of the shear wave associated with Mach cone. [The ground velocity (vertical axis) is given in m/sec, and the time (horizontal axis) in seconds].

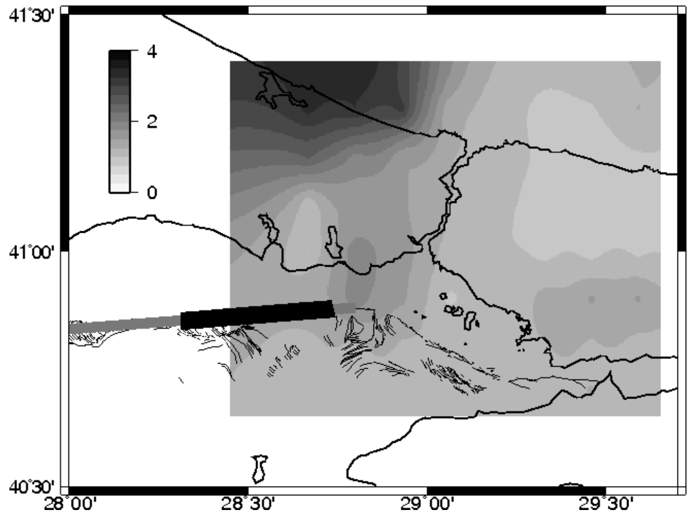

(a) North-south component

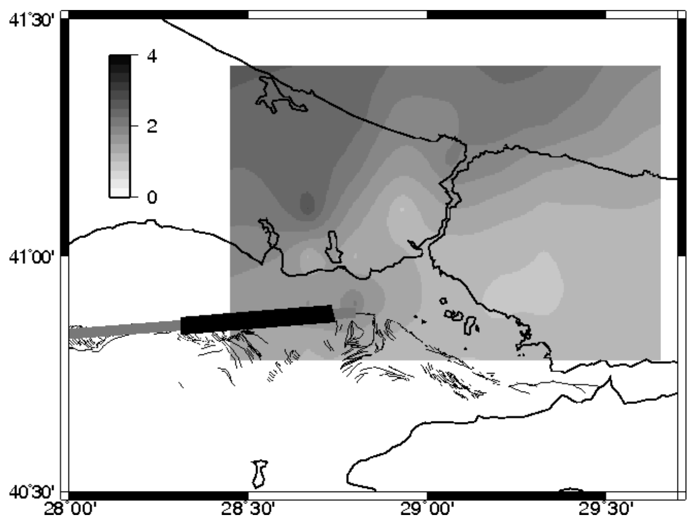

(b) East-west component

Figure 5 The amplification factor on horizontal components due to supershear rupture, where the amplification factor is the ratio of the maximum peak value of synthetic seismogram generated for two rupture velocities: $V_r = 0.85V_s$ (subshear) and $V_r = 1.41V_s$ (supershear). West to east unilateral rupture is assumed in both cases. High amplification values are seen at far distances from the fault (> 40 km) and in the direction parallel to the fault line. At those distances the ground shaking is expected to fall to smaller levels which are less critical for hazard considerations. The deviations from symmetry about fault line are due to the non-symetrical positions of the grid points with respect to the fault line. The submarine faults are taken from Le Pichon et al. [2001]. The thin grey line shows the rupture line, and the thick darker grey line shows the segment where the supershear is assumed to occur.

Figure 5 compares two extreme situations (subshear $V_r = 0.85V_S$ and supershear $V_r = 1.41V_S$) on a grid of 40 points similar to the previous experiment. The slip distribution has mean and variance of 2.5 and 0.8, respectively. The maximum value of the horizontal components are compared at each grid point by taking the ratio of maximum velocity in supershear and subshear cases. For all grid points the ratio has a value slighty larger than one showing that the supershear always leads to an increase of the ground velocity. The value is mapped for the total metropolitain area of Istanbul. For both components (NS and EW) the increase in ground velocity becomes significant (peak amplitude ratio around 2-3) at distances far from the fault (>40-50 km) and in the direction normal to the fault line. These is again sign of the efficient propogation of mach cone. For these distances, however, the ground velocity start to decrease to values which are often too small to take into for hazard estimation. For locations very close to the fault, the near-field term becomes so overwhelming that contribution from the other parts of the fault becomes less significant, making the rupture speed of secondary importance. So at these very close locations (<5 km) whether or not the rupture is supershear does not modify the peak ground velocity significantly. Overall, as the rupture increases into supershear mode, the ground velocity is amplified but not significantly as compared to the directivity effect.

CONCLUSIONS

In ground motion modelling directions and velocities of the rupture are generally ignored because they are difficult to estimate. In this work, a forward modelling approach was used to analyze the variation of the ground velocity for various directions and velocities of the rupture. Simple models were developed in order to expose typical characteristics. The directivity effect was seen to be most effective in the line of the strike of the fault as predicted by theory. The effect of rupture speed was analysed particularly for the case of subshear and supershear velocities. Results show that high amplification values emerged seen only at far distances from the fault (> 40 km), which are less critical for hazard considerations. This work is a partial outline of a more comprehensive study that is currently being carried for the investigation of ground motion in the city of Istanbul based on synthetic seismograms. In the future, waveform based information are expected to play a more critical role in studying hazard problems as compared to empirical attenuation laws currently being used.

REFERENCES

Ansal A, Akinci A, Cultrera G, Erdik M, Pessina V, Tönük G, Ameri G (2009). Loss estimation in Istanbul based on deterministic earthquake scenarios of the Marmara Sea region (Turkey), *Soil Dyn. Earthq. Engng.,* 29(4):699–709.

Armijo R, Meyer B. Navarro S, King G, Barka A (2002). Asymmetric slip partitioning in the Sea of Marmara pull-apart: a clue to propagation processes of the North Anatolian fault?, *Terranova* 14:80–86.

Bécel A, Laigle M, de Voogd B, Hirn A, Taymaz T, Galvé A. Shimamura H, Murai Y, Lépine J-C. Sapin M. Ozalaybey S (2008). Moho, crustal architecture and deep deformation under the North Marmara Trough, from the SEISMARMARA Leg 1 offshore–onshore reflection–refraction survey, *Tectonophysics*, 467(1–4):1–21.

Bouchon M, Karabulut, H (2002). A note on seismic activity near the eastern termination of the Izmit rupture in the hours preceding the Duzce earthquake, *Bull. Seism. Soc. Am.,* 92**:**406–410.

Bouchon M (1981). A simple method to calculate Green's functions in elastic layered media, *Bull. Seism. Soc. Am.*, 71**:**959–971.

Seismic Hazard

Bouchon M, Toksoz N, Karabulut H, Bouin M-P, Dieterich M, Aktar M, Edie M (2002). Space and time evolution of rupture and faulting during the 1999 Izmit (Turkey) earthquake, *Bull. Seism. Soc. Am.*, 92**:**256–266.

Bouin M-P, Bouchon M, Karabulut H, Aktar M (2004). Rupture process of the 1999 November 12 Duzce (Turkey) earthquake deduced from strong motion and GPS measurements, *Geophys. J. Int.,* 159**:**207–211

Cakir Z, de Chabalier J-B, Armijo R, Meyer B, Barka A, Peltzer G (2003). Coseismic and early post-seismic slip associated with the 1999 Izmit earthquake (Turkey), from SAR interferometry and tectonic field observations, *Geophys. J. Int*., 155:93–110.

Clévédé E, Bouin M-P, Bukchin B, Mostinskiy A, Patau G (2004). New constraints on the rupture process of 1999 August 17 Izmit earthquake deduced from estimates of stress glut rate moments, *Geophys. J. Int.*, 159:931–942

Delouis, B, Giardini D, Lundgren P, Salichon J (2002). Joint inversion of InSAR, GPS, teleseismic, and strong-motion data for spatial and temporal distribution of earthquake slip: application to the 1999 Izmit mainshock, *Bull. Seism. Soc. Am.*, 92**:**278–299.

Durand V, Bouchon M, Karabulut H, Marsan D, Schmittbuhl J, Bouin M-P, Aktar M, Daniel G (2010). Seismic interaction and delayed triggering along the North Anatolian fault, *Geophys. Res. Lett*., 37, L18310

Laigle, M., Becel A, de Voogd B, Hirn A, Taymaz T, Ozalaybey S (2008). Members of SEISMARMARA Leg1 Team A first deep seismic survey in the Sea of Marmara: Deep basins and whole crust architecture and evolution , 2008, *Earth Planet. Sci. Lett.,* 270:168–179

Le Pichon X, Sengör AMC, Demirbag E, Rangin C, Imren C, Armijo R, Görür N, Cagatay N, Mercier de Lepinay B, Meyer B, Saatcilar R, Tok B (2001). The active main Marmara fault. *Earth Planet. Sci. Lett*., 192:595–616.

Oglesby DD, Mai PM, Atakan K, Pucci S (2008). Dynamic models of earthquakes on the North Anatolian fault zone under the Sea of Marmara: Effect of hypocenter location, *Geophys. Res. Lett*., 35, L18302

Parsons T, Toda S, Stein RS, Barka A, Dieterich JH (2000). Heightened odds of large earthquakes near Istanbul: An interaction-based probability calculation, *Science*, 288:661 –664.

Picozzi M, Strollo A, Parolai S, Durukal E, Özel O, Karabulut S, Zschau J, Erdik M. (2009). Site characterization by seismic noise in Istanbul, Turkey, *Soil Dyn. Earthq. Engng*., 29(3):469–482.

Somerville PG, Smith NF, Graves RW, Abrahamson NA (1997). Modification of empirical strong ground motion attenuation relation to include the amplitude and duration effects of rupture directivity, *Seism. Res. Lett.*, 68:199-222.

ETA-BASED STRONG GROUND MOTION SELECTION FOR RELIABLE NONLINEAR DYNAMIC ANALYSIS OF STRUCTURES

Mohsen Ghafory-Ashtiany[1], Mehdi Mousavi[2], and Alireza Azarbakht[2]

[1] *International Institute of Earthquake Engineering and Seismology, Tehran, Iran,* [2]*Department of Civil Engineering, Faculty of Engineering, Arak University, Iran*

ABSTRACT

The reliability of record selection based on ε-filtration is limited by the strength of the correlation between the structural non-linear response and the ε values. In this paper, an alternative indicator of spectral shape is proposed, which results in a more reliable prediction of the nonlinear response. This new parameter, named eta (η), is a linear combination of ε and the peak ground velocity epsilon (ε_{PGV}). It is shown that η, as a nonlinear response predictor, is remarkably more efficient than the well-known and convenient parameter ε. The influence of η-filtration in the collapse analysis of an eight-story reinforced concrete structure with special moment-resisting frames was studied. Statistical analysis of the results confirmed that the difference between ε-filtration and η-filtration can be very significant at some hazard levels.

INTRODUCTION

It has been shown that the shape of the uniform hazard spectrum (UHS) can be quite different from the shape of the expected response spectrum of a real ground motion record having an equally high spectral amplitude at a particular period [Baker and Cornell 2006b]. For this reason, the current code-based practice is usually conservatively biased for structural analysis, especially in collapse capacity assessment [Baker and Cornell 2006b].

It is quite well-known that the response spectra epsilon (ε) is an indicator of the elastic spectral shape of ground motion records [Baker and Cornell 2006b]. The parameter ε is a measure of the difference between the spectral acceleration of a record and the mean value of the spectral acceleration, obtained from a ground motion prediction equation at a given period. It is noteworthy that the parameter ε has a seismological origin. The three parameters that can vary for a given site and a given fault are magnitude (M_w), distance (R), and ε [Kramer 1996]. Therefore, the most direct approach that can be used to account for the spectral shape in structural analysis is to select ground motion records that have M_w, R, and ε values that match the target values obtained from the corresponding disaggregation analysis.

The parameter ε is not a perfect indicator of spectral shape due to the random nature of ground motion records. The ε values of ground motion records and the associated nonlinear response of a given structure are in partial correlation. The ability of ε to predict the nonlinear response of a given structure depends on the strength of this correlation. The objective of this study is to establish a more reliable indicator of the elastic spectral shape—leading to a better prediction of nonlinear response—by incorporating time-domain intensity measures (i.e., PGA, PGV, and PGD) into frequency-domain intensity measures (i.e., the spectral values).

EPSILON; A PREDICTOR OF NONLINEAR RESPONSE

In order to investigate the effect of ε on the nonlinear response of a structure, a set of nonlinear single-degree-of-freedom (SDOF) systems, as well as an appropriate bin of ground motion records, was considered. A period range of 0.1 to 2.0 sec, as well as a ductility range of 2 to 12, was used for the SDOF systems. The collapse capacity values were calculated using incremental dynamic analysis (IDA), and a precise trace of the collapse capacity point was performed using the Hunt and Fill algorithm [Vamvatsikos and Cornell 2002]. The bin of applied ground motion records includes 78 records, with a magnitude range of 6.5 to 7.8. The selection criteria and the other information can be found in [Haselton and Deierlein 2007].

Figure 1 shows the correlation between the parameter ε and the collapse capacity values for two SDOF systems with periods of 1.0 and 2.0 sec, and ductility values equal to 6 and 12. The epsilon values were determined based on the Campbell and Bozorgnia attenuation relationship [2008]. The correlation shown in the Figure 1 confirms the influence of the parameter ε on the nonlinear response. Due to this correlation, it is anticipated that the selection of ground motion records based on ε-filtration results in a reduction in the potential bias in the prediction of the structural nonlinear response. It is clear that the amount by which the potential bias can be reduced strongly depends on the size of the correlation between the non-linear response and the parameter ε_{Sa}.

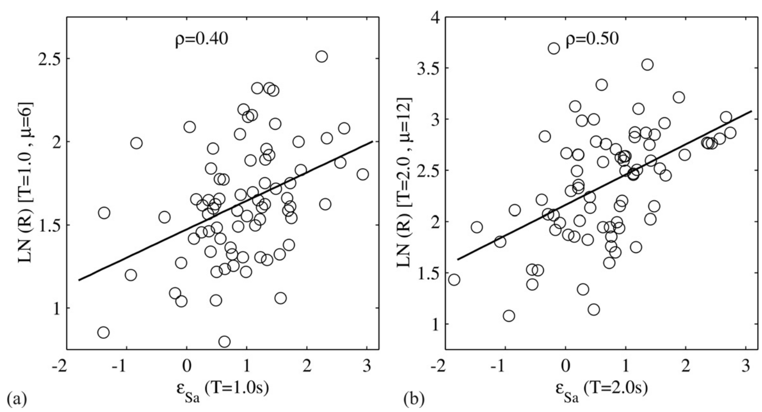

Figure 1 The correlation between the parameter ε and the collapse capacity values

The above analysis for all of the considered SDOF systems showed that the average correlation coefficient is just 0.43. It is reasonable to take this correlation coefficient as an index of efficiency of the parameter ε for reducing bias in the nonlinear response. The main contribution of this study is that a more robust predictor of nonlinear response has been obtained by considering the parameter η as a linear combination of different epsilons, i.e., ε_{PGA} and ε_{PGV}. This hypothesis is studied in the following sections.

ETA (η), A MORE ROBUST PREDICTOR OF NONLINEAR RESPONSE

Each of the IM epsilons can reflect a part of information hidden in a given ground motion record. Here it is shown that a combination of IM epsilons can result in a more robust prediction of the structural response as a result of the inherent distinction between the time domain and frequency response domain parameters, which have a high potential to enhance each other as response predictors. Again, let us assume a SDOF system with a period of 2.0 sec and ductility equal to 12. As expected, a linear trend exists between ε_{Sa} and the nonlinear response, as shown in Figure 1b. The coefficient of correlation between these variables was determined to be equal to 0.50. Now consider the parameter η as a linear combination of ε_{Sa}, ε_{PGA}, ε_{PGV}, and ε_{PGD} as written in Equation (1):

$$\eta = \varepsilon_{Sa} + c_1\varepsilon_{PGA} + c_2\varepsilon_{PGV} + c_3\varepsilon_{PGD} \tag{1}$$

The objective is to find the best values for the constant coefficients (c1, c2, and c3) that result in the maximum correlation between η and the nonlinear response. By application of the Genetic Algorithm (GA) [Goldberg 1989] as a powerful tool for optimization, the optimum constant coefficients were determined to be equal to:

$$c_1 = 0.50 \quad c_2 = -0.74 \quad c_3 = -0.42$$

The achieved coefficient of correlation is 0.75, which is significantly greater than the previously obtained value, as shown in Figure 2b. It is thus reasonable to claim that the potential of η is greater than ε_{Sa} to predict the nonlinear response.

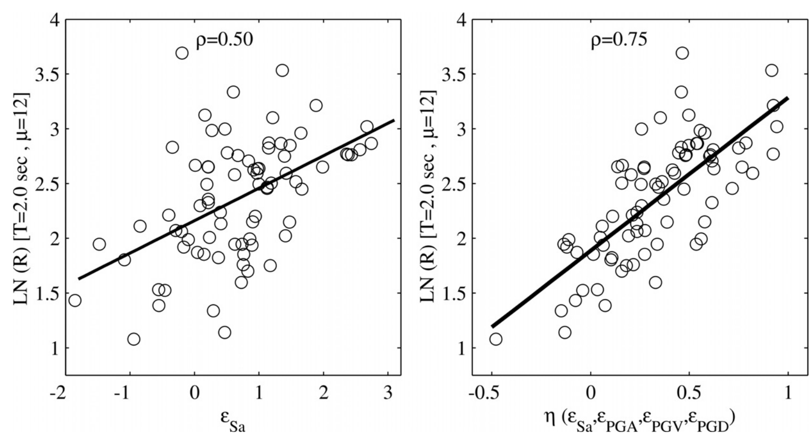

(a) **(b)**

Figure 2 The correlation between the response predictors and the collapse capacity: (a) ε_{Sa} as a response predictor, and (b) η as a response predictor.

Equation 1 was based on just one particular case; therefore, it does not represent all of the investigated SDOF systems. A regression analysis for the response of all of the SDOF systems is needed in order to develop a general response predictor. After normalization of all of the SDOF response values, a vector of size 6552 (84×78) was obtained. Corresponding to this vector, a 6552×4 matrix, including four epsilon values for each record and each SDOF system, was considered. Similarly to the above approach, the response predictor (η) can be defined. For sensitivity analysis, too, different combinations of epsilons are involved in the regression analysis; the results are summarized in Table 1.

Table 1 Determination of the coefficients for η for different linear combinations of ε.

No.	ε_{Sa}	ε_{PGA}	ε_{PGV}	ε_{PGD}	ρ
1	1	-	-	-	0.43
2	-	1	-	-	0.18
3	-	-	1	-	0.08
4	-	-	-	1	0.13
5	1	-0.373	-	-	0.47
6	1	-	-0.823	-	0.64
7	1	-	-	-0.676	0.54
8	1	0.123	-0.958	-	0.65
9	1	-0.289	-	-0.540	0.56
10	1	0.186	-1.016	0.057	0.65

The last case, which involves all of the epsilons, provides the most efficient response predictor, with $\rho = 0.65$ (see Table 1). However, it can be seen that the efficiency of the dual combination of ε_{Sa} and ε_{PGV} (the sixth item in Table 1) is approximately equal to that of the last combination. Thus, a simple definition of the parameter η can be introduced as:

$$\eta = \varepsilon_{Sa} - b\varepsilon_{PGV}, \qquad b = 0.823 \tag{2}$$

Figures 3a and 3b show, respectively, the coefficient of correlation between the parameters η and ε_{Sa} and the nonlinear response for all of the investigated SDOF systems. The parameter η is a more robust predictor of response as shown in Figure 4, with an average of a 50% improvement in the coefficient of correlation.

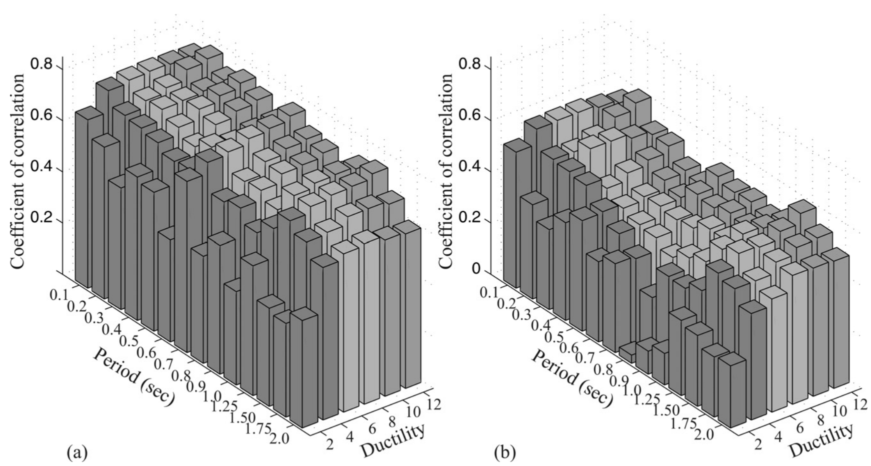

Figure 3 Comparison of the efficiency of η and ε as response predictors: (a) correlation of the response and η; and (b) correlation of the response and εPGV.

The improved efficiency of η as a response predictor may be due to the fact that η is a better indicator of the spectral shape than ε_{Sa}. This hypothesis is demonstrated in Figure 4. The ground motion records were sorted based on the ε_{Sa} value and also based on η, and then two higher and lower subsets with *N* elements were selected from each sorted list. The mean of the response spectra of both subsets were then plotted, so that the left-hand figures are based on ε_{Sa} sorting, and the right-hand figures are based on η-based sorting. Two subsets with size 8, as shown in Figure 4a, result in different spectral shapes. This finding is similar to the results obtained in other studies (i.e., Baker and Cornell [2006b]). The procedure is repeated for η filtration in Figure 4b. The difference between two resulting spectra is more significant for the η filtration case in comparison with the ε_{Sa}-filtration approach. This analysis was repeated for a selection of 16 records, and the corresponding results are shown in Figure 4c and 4d, for each of the filtration approaches. This case fully confirms the better ability of η to make a distinction between records with different spectral shapes.

DETERMINATION OF THE TARGET ETA FOR DIFFERENT HAZARD LEVELS

A practical challenge faced when using η for record selection is the choice of target epsilons. The standard hazard disaggregation analysis only provides the target ε_{Sa}, but the target ε_{PGV} is still undetermined. Assuming equal values for epsilons may be challengeable since equal epsilons may not necessarily correspond to a particular hazard level.

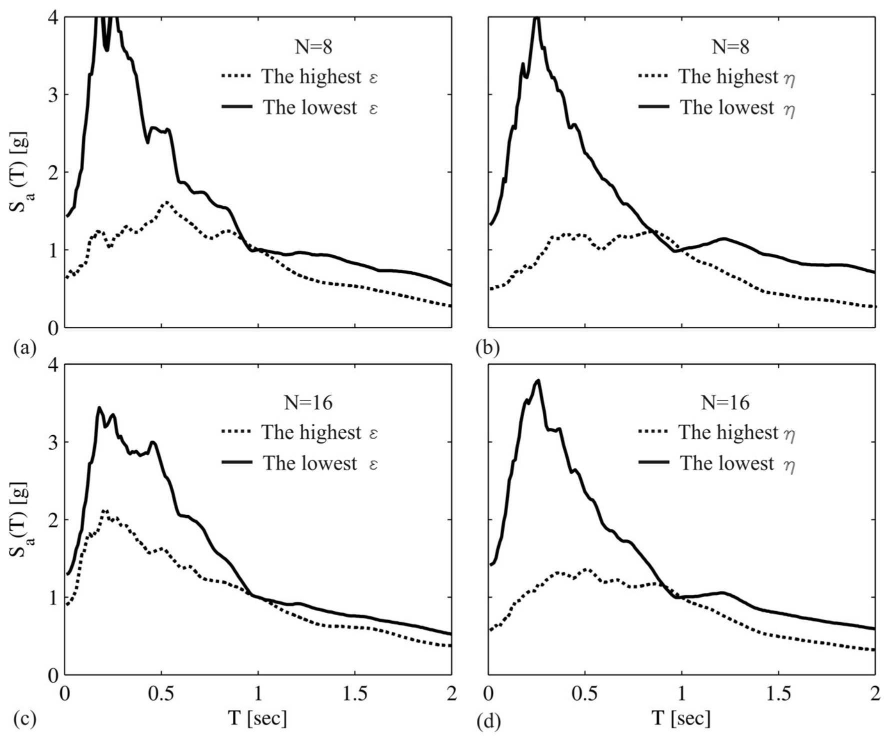

Figure 4 **(a) Comparison of η and εSa indicators of spectral shape; (a) and (b) selection of 8 ground motions with highest/lowest values of η and εS_a ; and (c) and (d) selection of 16 ground motions with highest/lowest values of η and ε S_a.**

Seismic Hazard

The correlation between ε_{PGV} and ε_{Sa} in different period ranges is studied next, and linear regression is implemented in order to develop an analytical equation for the evaluation of ε_{PGV} for a given ε_{Sa}.

The results presented in this section were derived empirically from a strong ground motion records (SGMR's) data set based on worldwide recordings of shallow crustal earthquakes. This set, which was used by Baker and Cornell [2006a] to analyze the correlation of response spectral values, includes 267 pairs of horizontal ground motion records with magnitudes greater than 5.5 and source-to-site distances of less than 100 km.

The correlation between ε_{PGV} and ε_{Sa} can be represented by the following model:

$$\varepsilon_{PGV} = 0.24 + 0.72\varepsilon_{Sa} \tag{3}$$

In this simple model, different values of ε_{Sa} associated with a range of periods were employed in order to develop a unique equation. The range of applied periods was 0.1 to 3.0 sec, including 58 data points. Figure 5 shows ε_{PGV} versus ε_{Sa} for the stated data points.

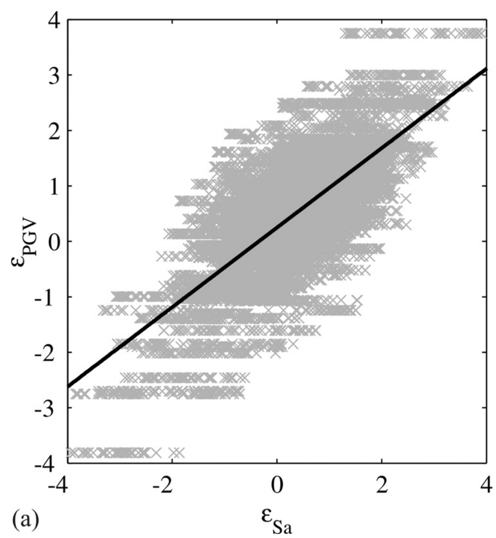

Figure 5 The relationship between ε_{PGV} and ε_{Sa}

A direct method to account for the target η in structural collapse assessment is to determine the expected ε_{PGV} value from Equation (3) for any considered hazard level, then to calculate the target η from Equation (2), and finally, to select the ground motions that are consistent with the target η. For the purposes of simplicity, Equation (2) can be revised to normalize the target η values to the target ε_{Sa} values, as described below.

$$\eta = 0.485 + 2.454\varepsilon_{Sa} - 2.020\varepsilon_{PGV} \tag{4}$$

The target η value can now be considered to be equal to the target ε_{Sa}, which is achievable from the disaggregation analysis. The details of this procedure are outlined by Mousavi et al. [in press]. In the following section, a η-based selection of ground motion records is presented for the collapse simulation of a MDOF structure.

EXAMPLE: COLLAPSE CAPACITY ASSESSMENT OF A MDOF STRUCTURE

In this section the seismic collapse capacity of a MDOF test structure based on an η-based record selection is discussed. The considered structure is an eight-story reinforced concrete building with special moment resisting frames. The building is 36.5×36.5 m in plan, uses a three-bay perimeter frame system with a spacing of 6.1 m, and has a fundamental period (T_1) of 1.71 sec. This building is ID 1011 from Haselton et al. [in press]. It was assumed that this structure is located at an idealized site where the ground motion hazard is dominated by a single characteristic event with a return period of 200 years: M_w = 7.2, R = 11.0 km and Vs_30 = 360m/sec. From basic probability, the target epsilons for different hazard levels are given in Table 2.

Table 2 The target parameters for different hazard levels.

Return Period (Year)	Probability in 50 years	Target epsilon
125	33%	-0.80
200	22%	0.00
475	10%	+0.80
2475	2%	+1.75

For each hazard level, 20 ground motion records were selected using both η-filtration and ε-filtration procedures. The resulting fragility curves for different hazard levels are shown in Figure 6, where the differences between the ε and η filtrations are, in the case of some of the epsilons, significant, whereas in the case of the remaining epsilons they are not significant.

In order to study further the influence of η filtration, the ground motion selection was performed for a relatively wide range of hazard levels. The results are shown in Figure 7a, compared with the results obtained by ε_{Sa} filtration. A standard hypothesis test [Hogg and Ledolter 1987] was implemented for each discrete ε_{Sa} in order to determine whether or not this difference is meaningful. The null hypothesis is the equality of the two means. Figure 7b shows the resulting p-value for each ε_{Sa} value. The p-value indicates the lowest level of significance that would lead to rejection of the null hypothesis with the given data. By assuming a common significant level (i.e., 0.05), as shown in Figure 7b, the null hypothesis can be rejected for $\varepsilon_{Sa} = 0.25, 0.5$. It can therefore be concluded that a record selection based on η filtration may, at some hazard levels, lead to quite different results to those obtained by convenient ε_{Sa} filtration.

Seismic Hazard

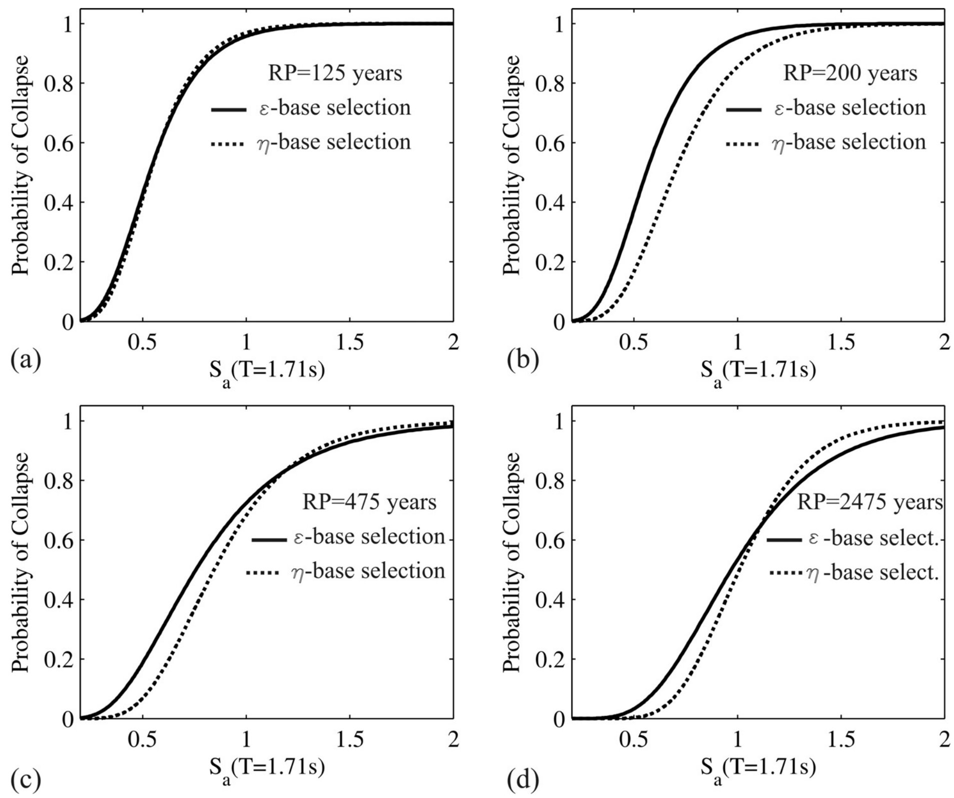

Figure 6 The fragility curves for different hazard levels.

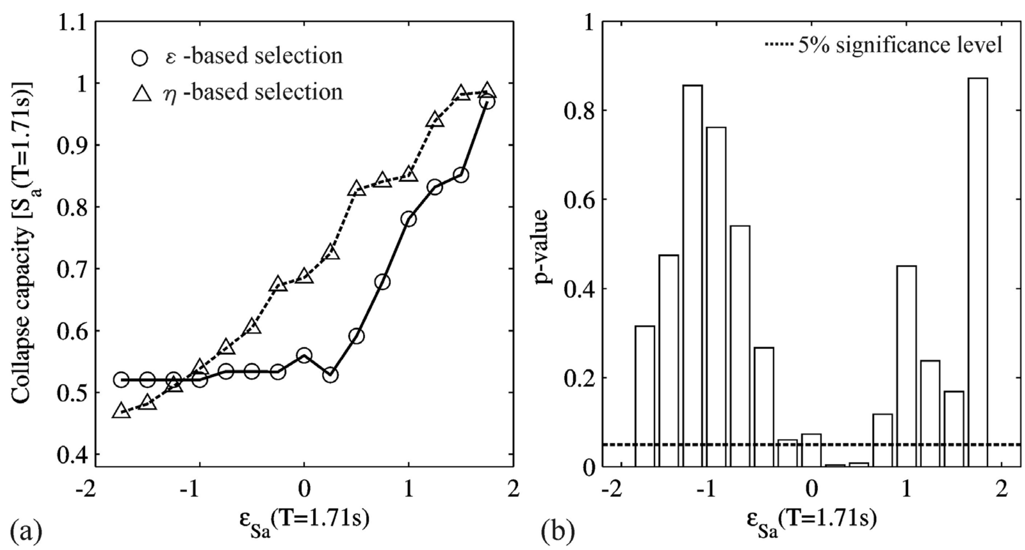

Figure 7 Mean collapse capacity of the MDOF structure based on ε_{Sa} and η filtration: (a) the difference between the two filtration approaches at difference levels of epsilon; and (b) the results of the statistical hypothesis test for the equality of collapse capacity based on the two filtration approaches.

For further investigation, the mean annual frequency (MAF) of collapse was computed based on each of the filtration approaches. Figure 8a shows the hazard curve for the assumed site. The MAF of collapse due to $S_a(T = 1.71\sec) = x$ is shown in Figure 8b, for both record selection methods. The MAF of collapse is also shown in Figure 8b for the case when all the records were used (without any filtration). The MAF of collapse is less for ε-filtration in comparison with the no-filtration approach, which has also been addressed by other studies (e.g., Baker and Cornell [2006b]). This figure also shows that the MAF of collapse for η-filtration is remarkably lower than that for the ε-filtration. The absolute value of MAF, calculated by integrating MAF over S_a, was 6.4×10^{-5}, 3.6×10^{-5} and 1.6×10^{-5} for the no-filtration, ε-filtration and η-filtration approaches, respectively.

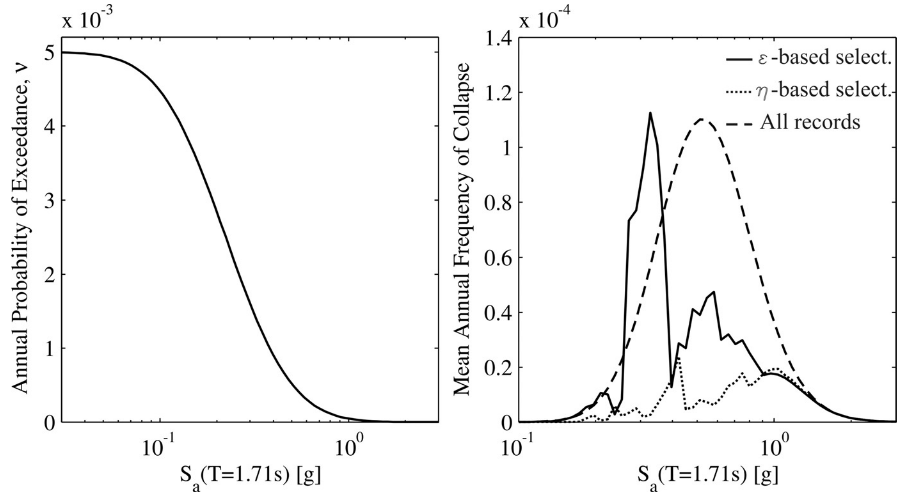

Figure 8 The effect of different filtration approaches in MAF analysis (a) the hazard curve; (b) the MAF of collapse due to $S_a(T = 1.71\sec) = x$.

CONCLUSION

In order to improve the reliability of the record selection procedure, a new parameter named eta (η) has been proposed as a linear combination of ε and ε_{PGV}. It was shown that the correlation between η and the nonlinear response is about 50% better than the correlation between ε and the response. It has also been shown that the parameter-η is a better indicator of spectral shape compared with the parameter ε. Finally, the absolute MAF of collapse for the η-filtration approach is remarkably lower than that corresponding to ε-filtration.

ACKNOWLEDGMENT

The research conducted by the authors has been funded by the International Institute of Earthquake Engineering and Seismology (IIEES) under Award Number 7134. This support is gratefully acknowledged.

REFERENCES

Baker JW, Cornell CA (2006a). Correlation of response spectral values for multi-component ground motions, *Bull. Seismo. Soc. Am.*, 96(1):215–227.

Baker JW, Cornell CA (2006b). Spectral shape, epsilon and record selection, *Earthq. Engng Struct. Dyn.,*35(9):1077–1095.

Campbell KW, Bozorgnia Y (2007). Campbell-Bozorgnia NGA ground motion relations for the geometric mean horizontal component of peak and spectral ground motion parameters. *PEER Report 2007/02*, Pacific Earthquake Engineering Research Center, University of California, Berkeley, CA.

Goldberg DE (1989). *Genetic Algorithms in search, Optimization, and Machine Learning*. Addison-Wesley: Reading, MA.

Haselton CB, Deierlein GG (2007). Assessing seismic collapse safety of modern reinforced concrete moment-frame buildings, *PEER Report 2007/08*, Pacific Earthquake Engineering Research Center, University of California, Berkeley, CA.

Haselton CB, Baker JW, Liel AB, Deierlein GG (in press). Accounting for ground motion spectral shape characteristics in structural collapse assessment through an adjustment for epsilon., *ASCE J. Struct. Engng*.

Hogg RV, Ledolter J (1987). *Engineering Statistics*, MacMillan Publishing Company: New York.

Kramer SL (1996). *Geotechnical Earthquake Engineering*, Prentice Hall, Upper Saddle River, NJ, 653 pgs.

Mousavi M, Ghafory-Ashtiany M, Azarbakht A (in press). A new indicator of elastic spectral shape for the reliable selection of ground motion records. *Earthq. Engng. Struct. Dyn*.

Vamvatsikos D, Cornell CA (2002). Incremental dynamic analysis. *Earthq. Engng Struct. Dyn.,* 31(3):491–514.

A REVIEW OF GROUND-MOTION PREDICTION EQUATIONS IN EUROPE AND SURROUNDING REGIONS

Sinan Akkar

Earthquake Engineering Research Center, Middle East Technical University, Ankara, Turkey

ABSTRACT

This paper summarizes the ground-motion prediction equations (GMPEs) developed in Europe and surrounding regions. Several statistics are presented to describe the general features of more than 100 published models for the subject geographical region. The paper also discusses the aleatory variability and epistemic uncertainty associated with these models, and compares some of the selected GMPEs with ground-motion models from other parts of the world.

INTRODUCTION

Ground-motion prediction equations (GMPEs) describe the probability of a ground-motion parameter conditioned on the earthquake source properties and location of the site. The empirical equations have been developed approximately after mid-1960s [Esteva and Rosenblueth 1964], and since then more than 200 models have been published for estimating peak ground acceleration (PGA) and elastic spectral ordinates [Douglas 2011]. Owing to the increased number and quality of strong-motion recordings, in particular during the last decade, the model developers had the opportunity of investigating the major physical mechanisms influencing the nature of ground motions. In parallel, the empirical functional forms have become more complex by including additional estimator parameters to better address the peculiar behavior of ground motion under different scenarios. The sophisticated functional forms are expected to define aleatory variability in a more rational way and reduce epistemic uncertainty in ground-motion prediction. The aleatory variability and epistemic uncertainty are the widely acknowledged challenges in probabilistic seismic hazard assessment (PSHA) that should be handled carefully for a proper estimation of hazard due to future earthquakes.

This article describes the development of GMPEs in Europe and surrounding regions that estimate PGA and spectral acceleration (SA). The paper shows the current state of aleatory variability and epistemic uncertainty in these predictive models by making comparisons between country-based (local) and pan-European GMPEs. The paper also compares some of the selected models form this study with GMPEs derived using data from other parts of the world. The comparative case studies indicate that aleatory variability and epistemic uncertainty are more pronounced in the local models. The limited comparisons also indicate that the ground motions in Europe and neighboring countries are arguably low with respect to the ground motions in the other parts of the world with similar seismotectonic features.

SOME STATISTICAL INFORMATION ON THE CONSIDERED GROUND-MOTION MODELS

The first ground-motion predictive model for Europe was published in 1975 by Ambraseys (see details in Douglas [2011]). Since then, more than 100 GMPEs have been developed in Europe and surrounding countries. Figure 1a shows the number of published GMPEs in the region of interest on yearly basis. The number of published GMPEs shows a considerable increase after 1990, mostly due to the accumulation of strong-motion recordings in the region. The other motivating factor for the development of larger number of GMPEs after 1990 can be increased public awareness on the importance of seismic hazard in the region. The country-based distribution of published GMPEs in Figure 1b supports the above remarks; countries suffering from high seismic activity in the region with large strong-motion data tend to develop higher number of GMPEs (e.g., former Yugoslavia, Greece, Iceland, Iran, Italy, Romania, and Turkey). Figure 1b also shows the number of pan-European GMPEs that are derived from the compilation of larger strong-motion datasets consisting of recordings from different countries in the region.

Most of the pan-European GMPEs are derived from the strong-motion recordings that have been routinely collected, compiled, and processed since 1971 by the researchers at Imperial College, London [Ambraseys et al. 2004]. Figure 1c shows the number of recordings used in the compiled GMPEs that estimate horizontal ground-motion parameters. The inherent increase in the accumulated strong-motion data is reflected to the number of recordings used in the derivation of GMPEs. On average, the number of data is less than 100 in GMPEs derived before 1990, whereas many model developers between 1990 and 2000 use more than 100 recordings in the derivation of their models. This number is further increased in GMPEs derived after 2000. As it is depicted in Figure 1d, GMPEs from the region of interest mainly focus on the estimation of PGA because this parameter is easy to obtain from accelerograms without running detailed data processing. Moreover PGA has been used intensively by engineers in this region for seismic design and scaling of design spectrum {e.g., Eurocode 8 (CEN [2004])}. These PGA models are followed with GMPEs predicting both PGA and SA (either absolute spectral acceleration or pseudo spectral (the latter being the more viable intensity parameter for engineers); there are fewer models that only estimate SA. Note that ground-motion models that estimate peak ground velocity (PGV) do exist for this region but are not included in the current study. The interested reader is referred to Akkar and Bommer [2007] for GMPEs derived from Europe and surrounding countries.

Figure 2 provides statistical information about main estimator parameters used in the ground-motion models compiled in this paper. Most of the predictive models use either epicentral distance (R_{epi}) or hypocentral distance (R_{hyp}) as the distance measures (Figure 2a). Although finite-source distance metrics (R_{jb} or R_{rup}) are more appropriate for describing distance-dependent variation of ground-motion amplitude, they are used in fewer models. Some models use a combination of above distance measures. The major reason behind the extensive use of point-source distance metrics is the robustness in their calculation. Calculation of finite-source distances requires reliable metadata information about source that is not the case for R_{epi} and R_{hyp}. Figure 2b indicates that the majority of predictive models use M_L, M_s and M_w to describe the magnitude-dependent variation of ground motions. Among these magnitude types, M_w should be the preferred magnitude scale since it does not suffer from saturation. M_L is mainly used in the pre-1990 models. It is also used in the local GMPEs that are derived from datasets that lack a proper M_w conversion. Some ground-motion models combine two or more magnitude types as their datasets do not show a homogenous magnitude scaling. Most of the GMPEs inadequately consider the site effects on the ground-motion amplitude. As presented in Figure 2c, almost all GMPEs exclusively use generic site class definitions. The generic site classes are defined either from average shear-wave velocity in the upper 30 m of the soil profile (V_{S30}) or geotechnical and geological features of the site. Consistency in these classifications is sometimes questionable as many strong-motion sites in the considered region lack reliable geotechnical and geophysical *in-situ* measurements. Recent efforts in the Turkish and Italian strong-motion databases [Sandıkkaya et al. 2010; Akkar et al. 2010; Luzi et al. 2008] have resulted in improvements in strong-motion site characterization in these countries. Beneficial effects of these efforts have yet to be observed on ground-motion models in the region.

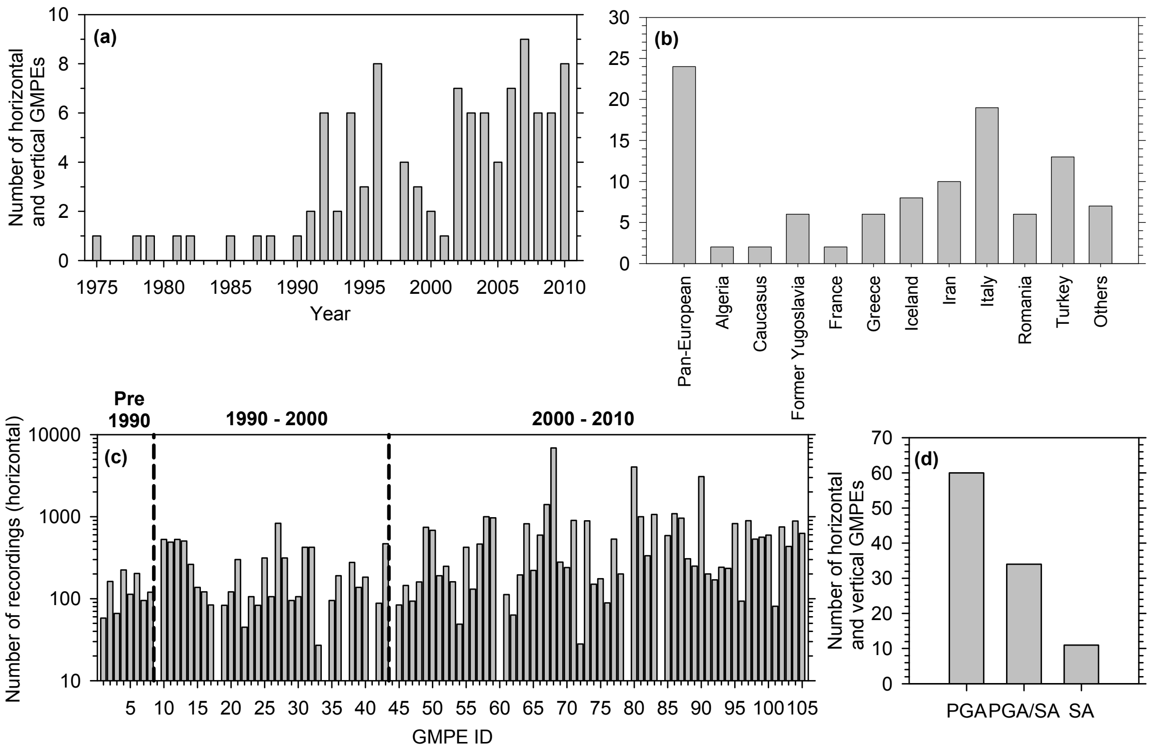

Figure 1 **Distribution of predictive models in Europe and surrounding regions by (a) year; (b) country; (c) number of horizontal recordings used in the derivation of horizontal GMPEs; and (d) estimated ground-motion parameter (i.e., PGA and SA).**

The majority of GMPEs lump their entire dataset in one broad site class or distinguish strong motions as recordings from soil and rock sites. The third largest group in Figure 2c mainly classifies the data as soft, stiff, and rock site recordings. The models falling into this group are mainly from pan-European GMPEs. Marginal number of predictive equations considers site response as a continuous function of V_{S30} and only one predictive model includes soil nonlinearity (e.g., Akkar and Çağnan [2010]) in the ground-motion estimations. The histogram plot in Figure 2d suggests that many models in Europe and surrounding countries disregard the influence of style of faulting on the ground-motion estimations. The major reason behind this observation can be once again the lack of reliable source information in the metadata of strong-motion recordings. The local and pan-European models that associate style-of-faulting information are almost exclusively derived after 2000, owing to the efforts on the improvement of metadata information of strong-motion data recorded in the region.

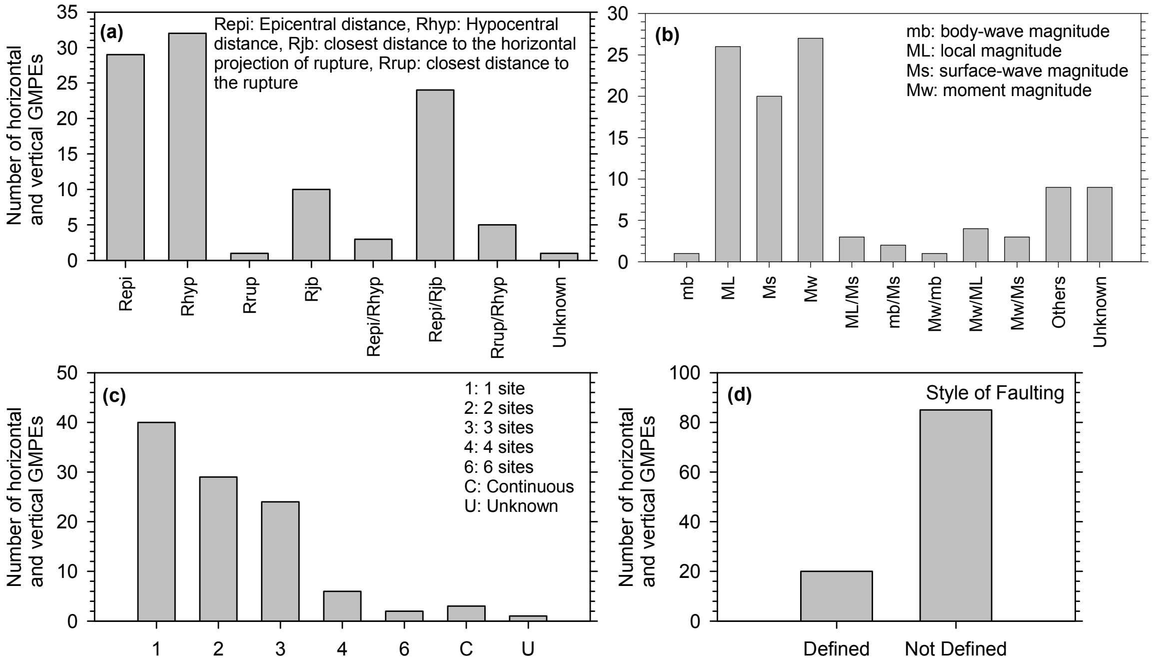

Figure 2 Statistics of horizontal and vertical predictive models in Europe and surrounding regions in terms of (a) distance metrics; (b) magnitude scale; (c) site class; and (d) style-of-faulting.

ALEATORY VARIABILITY AND EPISTEMIC UNCERTAINTY IN THE CONSIDERED GROUND-MOTION MODELS

Trends in the standard deviation (sigma) for GMPEs that estimate horizontal PGA are presented in Figure 3 to assess the level of aleatory variability in the ground-motion models of interest. The standard deviations of local and pan-European GMPEs are plotted in separate colors to observe the existence of possible differences between these 2 groups. The overall variation of sigma, except for some of the outliers, ranges between 0.45 and 0.9. Although some of the sigma values in pan-European models are appreciably high, their standard deviations tend to attain values below 0.65; closer to the lower bound in the overall sigma variation. Speculatively, poorly constrained local databases in terms of main estimator parameters (i.e*.,* magnitude, distance and site-class) as well as their deficient metadata information (i.e., uncertainties associated with the above estimator parameters) play a major role for relatively high sigma in local GMPEs. Higher sigma in local GMPEs can also be attributed to their oversimplified functional forms due to the poorly constrained local databases that trigger the scatter between observed and estimated ground-motion parameters. It is, however, noted that sigma trends for PGA GMPEs published all around the world reveal a similar behavior to those presented in Figure 3 [Strasser et al. 2009]. Thus, the above remarks regarding functional forms and database problems are not specific to the GMPEs derived in Europe and surrounding regions.

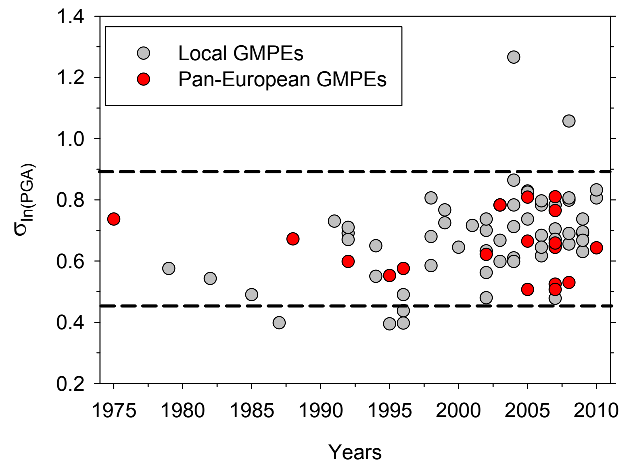

Figure 3 **Comparison of aleatory variability (in terms of logarithmic standard deviation) between country-based (local) and pan-European models. The horizontal dashed lines draw a band where most of the sigma values are accumulated for the entire time span considered in the study.**

Figure 4 compares PGA estimations between pan-European and local predictive models that are mainly tailored for shallow-crustal active seismic regions. The first panel in Figure 4 shows median PGA estimations of pan-European GMPEs. The rest of the panels show median PGA estimations of local GMPEs for countries providing the major fraction of strong-motion data to the databases used in pan-European GMPEs. The comparisons focus on the epistemic uncertainty in the GMPEs derived from the region of interest. The comparisons are done for a scenario event of magnitude (M_w) 6. The fault mechanism is strike-slip with a dip angle of 90º. The depth of the scenario event is considered as 10 km, and a generic rock site was chosen since most of the considered GMPEs lack a detailed site classification. Majority of selected predictive models used M_w and M_s, except for the Italian GMPEs that were mainly derived for M_L. For the given scenario magnitude (M_w 6), both M_s and M_L are not expected to differ significantly from M_w (i.e., no magnitude saturation in M_L and M_s). Therefore, no magnitude conversion was applied between the selected GMPEs. The magnitude range of few Italian GMPEs barely covers the scenario magnitude that may result in biased PGA estimations [Bommer et al. 2007]. They were kept in the list of selected GMPEs to bring forward the modeling (epistemic) uncertainty. R_{jb}, R_{epi} and R_{hyp} are the source-to-site distance measures used in the selected GMPEs. Fault geometry of the scenario event (strike-slip with a dip angle of 90º) provides the use of $R_{\text{jb}} = R_{\text{epi}}$ and $R_{\text{hyp}} = \sqrt{\text{depth}^2 + R_{\text{jb}}}$ relationships to warrant the uniformity between compared models in terms of distance metric metrics. Empirical relationships provided by Beyer and Bommer [2006] were used to convert estimations of different horizontal component definitions to geometric mean (i.e., PGA_{GM}). The plots in Figure 4 show considerable differences in the estimated PGA values regardless of the origin of GMPEs. Except for a few models, the closer agreement in pan-European GMPEs can be explained by the fact that they are almost exclusively derived from the strong-motion databases collected in Imperial College, London. The differences are more significant for local GMPEs; in particular for those derived from Italian, Greek, and Iranian databases. Significant number of micro-regional ground-motion models in Italy can be one of the deriving factors in the observed dispersion of Italian GMPEs. The outlier median PGA curves in Turkey were also derived from the micro regional strong-motion data with questionable metadata information. Some of the models presented for Iran and Greece are rather old with oversimplified functional forms that may fail to represent the actual variation of ground motion. The large discrepancy in the Greek median curves can also stem from the poor strong-motion database features.

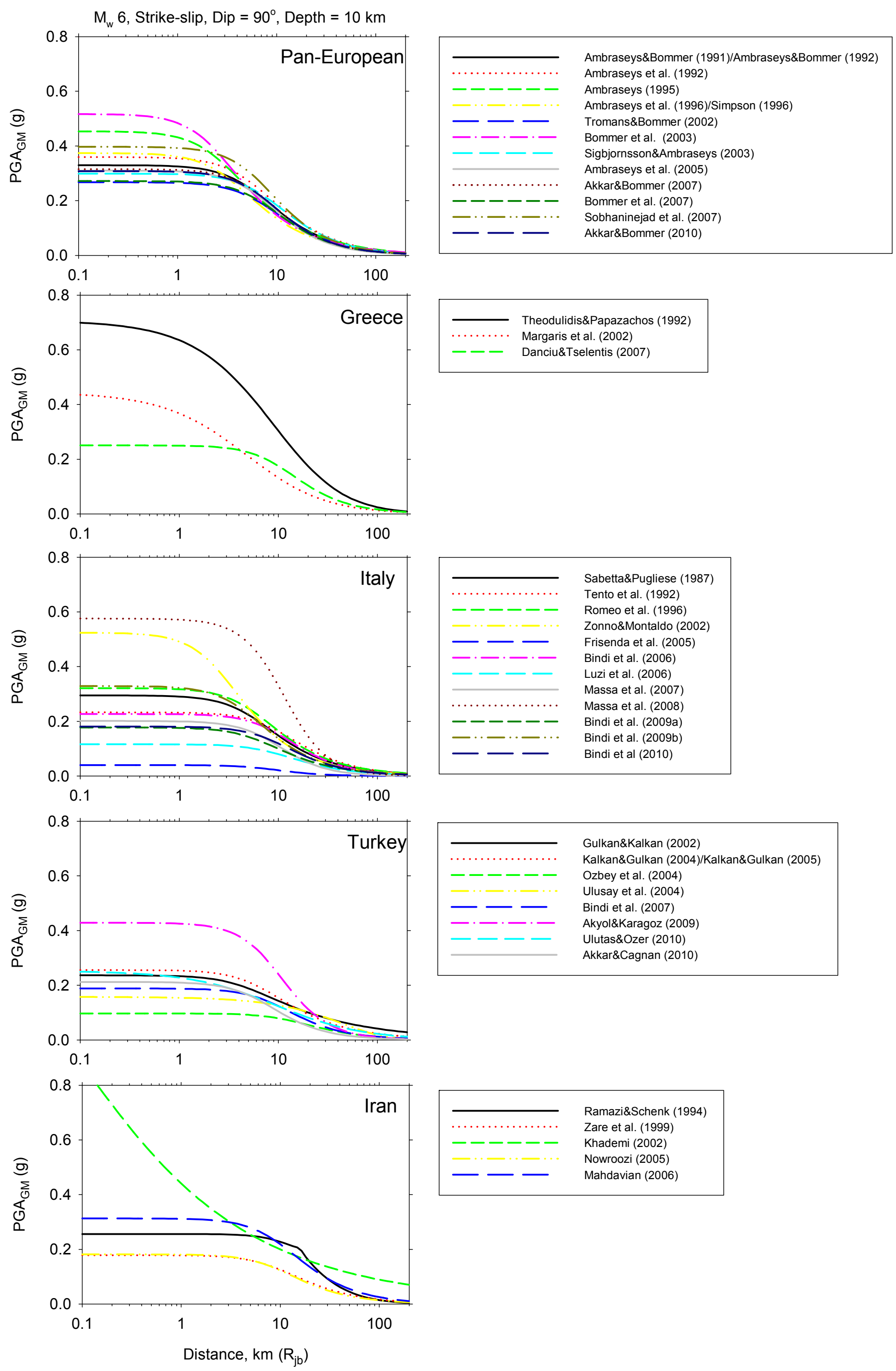

Figure 4 Comparison of pan-European predictive models with local GMPEs derived from Greece, Italy, Turkey and Iran. (The reader is referred to Douglas [2011] for the references of presented GMPEs).

As discussed previously, the local models compiled in this study seem to suffer from poorly constrained databases, as well as the uncertainties associated with metadata information that result in inadequate functional forms, which, in turn, provoke higher sigma (aleatory variability) and modeling (epistemic) uncertainty. The adverse affects of such deficiencies are limited on the pan-European models as they are mainly based on strong-motion databases that have been improved continuously by a specific group of researchers. Recent efforts to improve country-based strong-motion databases as well as the associated metadata (e.g., Akkar et al. [2010]; Luzi et al. [2008]) have provided opportunities to derive local GMPEs using higher quality strong-motion databases with reliable metadata information.

Figure 5 compares two GMPEs derived from such efforts with the recent pan-European ground-motion models. The local predictive models presented in Figure 5 are by Akkar and Çağnan [2010] and Bindi et al. [2010] that use recently compiled Turkish and Italian strong-motion databases, respectively. The latter model estimates for larger horizontal component whereas the former model estimations are on geometric mean. The pan-European GMPEs are from the studies of Ambraseys et al. [2005] and Akkar and Bommer [2010] that use almost the same strong-motion database. The major differences between these two models are as follows: (a) additional quadratic-magnitude term in the functional form of Akkar and Bommer [2010]; and (b) horizontal component definitions in the estimated ground-motion parameters. Ambraseys et al. [2005] predicts for larger horizontal component whereas Akkar and Bommer [2010] uses geometric mean.

The spectral plots in Figure 5 is for a strike-slip event of M_w 6 and for a site located at a distance of R_{jb} = 10 km from the source. Similar to the plots in Figure 4, a generic rock site was chosen in this case study. The component definition adjustments between the compared GMPEs were done using the empirical relationships proposed in Beyer and Bommer [2006]. No other adjustments were required for these models as the rest of the estimator parameters used the same measurements. The functional forms of the models have approximately the same level of complexity. The pan-European GMPEs showed closer agreement with each other, which is not surprising as they are derived from very similar databases. Interestingly, the local predictive models, although they are derived from different databases, show a good resemblance with spectral ordinate estimations lower than those of pan-European GMPEs. Note that the considered pan-European GMPEs mainly contain strong-motion recordings of large magnitude events from the recently updated Turkish strong-motion database. The Italian strong-motion database has gone through major revisions in terms of site classification. Although the comparisons presented in this figure are limited, the highlighted observations and remarks may suggest an update of ground-motion datasets considered in the pan-European GMPEs provided that both Italian and Turkish strong-motion recordings constitute a significant importance for hazard estimation in Europe and surrounding regions.

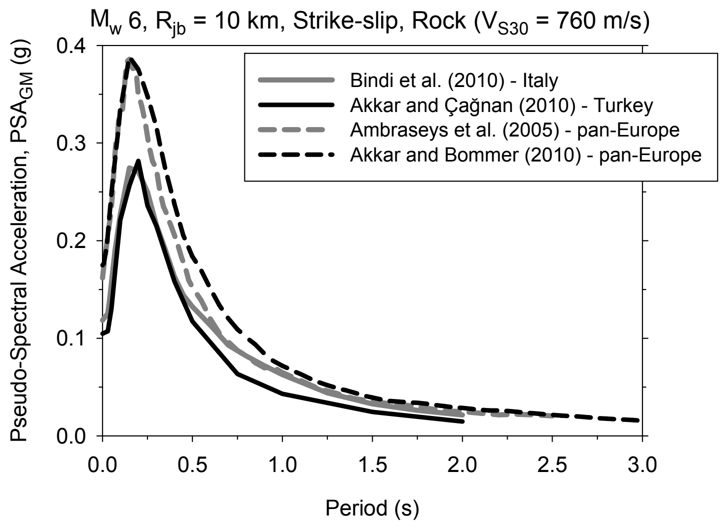

Figure 5 Comparisons between the most recent local and pan-European models derived by using the data from the region of interest.

COMPARISONS BETWEEN EUROPEAN AND NON-EUROPEAN GMPES

This section presents the level of agreement between the selected local and pan-European GMPEs with the Next Generation Attenuation (NGA) predictive models that are derived for shallow crustal earthquakes in the western United States and similar active tectonic regions. The NGA models were developed by five individual teams using ground motions mainly from the western United States and Taiwan. The reader is referred to Douglas [2011] for the general features of NGA GMPEs. Akkar and Bommer [2010] and Akkar and Çağnan [2010] GMPEs were chosen as representative pan-European and local ground-motion models, respectively, that encompass similar tectonic regimes as NGA models. The comparisons (Figure 6) are done for median and median + sigma spectral ordinates for periods up to 2 sec. The fault mechanism was selected as strike-slip with 90° dip angle. 2 magnitude levels (i.e., M_w 5 and M_w 7) are used in the comparisons for a rock site located at a distance of R_{jb} = 10 km. The NGA spectral ordinates were normalized by those computed from Akkar and Bommer [2010] and Akkar and Çağnan [2010] to have a better judgment on the similarity of estimations between these models.

The comparisons show that both Akkar and Bommer [2010] and Akkar and Çağnan [2010] agree fairly well with NGA models for large magnitude ($\mathrm{M_w}$ 7) events. The discrepancy between NGA models and those chosen from this study becomes significant for lower level of seismicity represented by M_w 5. The disagreements towards smaller magnitude events are more prominent in the Akkar and Çağnan [2010] model. The limited observations from this case-specific study may indicate that on average, ground motions in Europe and neighboring regions are lower with respect to those in the other parts of the world, which is in accordance with Douglas [2004]. This should be studied more cautiously because it contradicts to the conclusions drawn by Stafford et al. [2008].

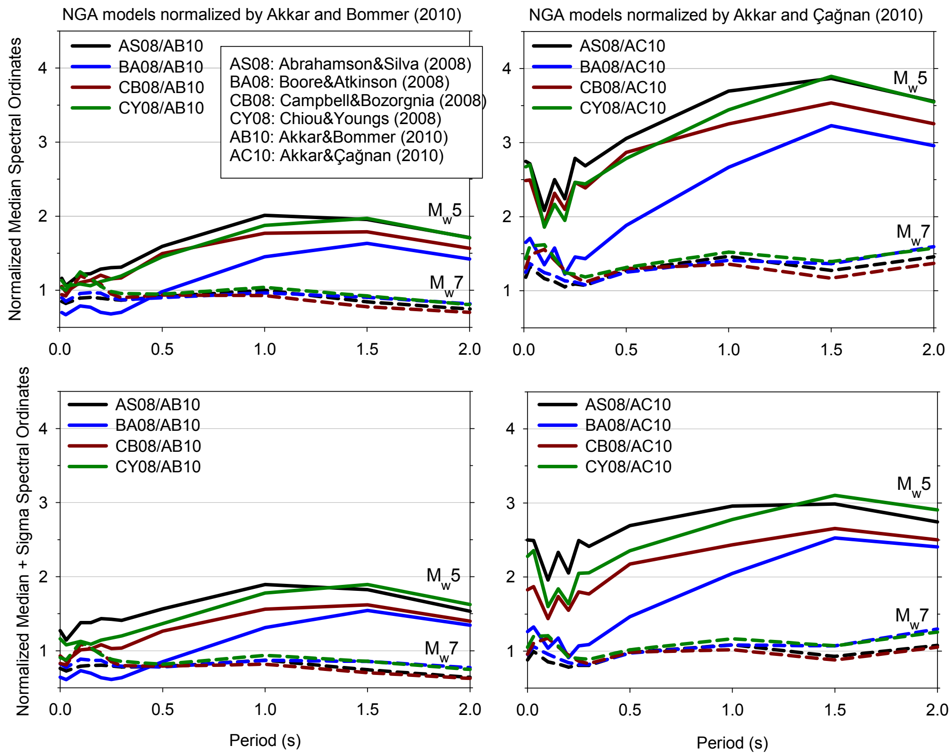

Figure 6 Comparisons of NGA models with Akkar and Bommer (2010) and Akkar and Çağnan (2010) for low (M_w 5) and large (M_w 7) magnitude events (solid and dashed lines, respectively).

SUMMARY AND CONCLUSIONS

This study summarizes the development of ground-motion predictive models in Europe and surrounding regions. The paper presents some simple statistics in order to show the basic features of local and pan-European GMPEs derived from strong-motion data recorded in Europe and neighboring countries. Limited comparisons are given to delineate the aleatory variability and epistemic uncertainty between local and pan-European GMPEs. These comparisons indicate that local GMPEs are more susceptible to higher sigma because their functional forms are generally oversimplified due to poorly constrained local databases, as well as uncertainties in estimator parameter measurements that lead to unreliable metadata information. These factors invoke larger epistemic uncertainty in local predictive models. The recent country-based efforts that aim at improving national strong-motion databases seem to overcome these drawbacks. Such efforts will help the seismological community to understand the regional differences in ground-motion estimations and will improve the use of pan-European GMPEs in the hazard estimations of Europe and neighboring regions. The final part of this article shows a coarse comparison between NGA models and the chosen local and pan-European GMPEs from this study. The comparisons suggest lower ground motions in Europe. This early finding must be investigated further before stating a firm conclusion.

ACKNOWLEDGEMENTS

Figures 1 and 2 were prepared with the help of Özkan Kale. Abdullah Sandıkkaya computed the GMPEs presented in Figure 3 together with the author. The NGA models discussed in Figure 6 were computed by using the software developed by Dr. David M. Boore (USGS, Menlo Park CA).

REFERENCES

Akkar S, Bommer JJ (2010). Empirical equations for the prediction of PGA, PGV and spectral accelerations in Europe, the Mediterranean region and the Middle East, *Seismo. Res. Lett*., 81:195–206.

Akkar S, Çağnan Z (2010). A local ground-motion predictive model for Turkey, and its comparison with other regional and global ground-motion models, *Bull. Seismo. Soc. Am*., 100:2978–2995.

Akkar S, Çağnan Z, Yenier E, Erdoğan Ö, Sandıkkaya MA, Gülkan P (2010). The recently compiled Turkish strong motion database: preliminary investigation for seismological parameters, *J. Seismology*, 14:457–479.

Akkar S, Bommer JJ (2007). Empirical prediction equations for peak ground velocity derived from strong motion records from Europe and the Middle East, *Bull. Seismo. Soc. Am*., 97:511–530.

Ambraseys NN, Douglas J, Sarma SK, Smit PM (2005). Equations for the estimation of strong ground motions from shallow crustal earthquakes using data from Europe and the Middle East: horizontal peak ground acceleration and spectral acceleration, *Bull. Earthq. Engng.,* 3:1–53.

Ambraseys NN, Smit P, Douglas J, Margaris B, Sigbjörnsson R, Ólafsson S, Suhadolc P, Costa G (2004). Internet site for European strong-motion data, *Bollettino di Geofisica Teorica ed Applicata*, 45:113–129

Beyer K, Bommer JJ (2006). Relationships between median values and between aleatory variabilities for different definitions of the horizontal component of motion, *Bull. Seismo. Soc. Am*., 96:1512–1522.

Bindi D, Luzi L, Massa M, Pacor F (2010). Horizontal and vertical ground motion prediction equations derived from the Italian Accelerometric Archive (ITACA), *Bull. Earthq. Engng.,* 8:1209–1230.

Bommer, JJ, Stafford P, Alarcon J, Akkar S (2007). The influence of magnitude range on empirical ground-motion prediction, *Bull. Seismo. Soc. Am*., 97:2152–2170.

Campbell KW, Bozorgnia Y (2008). NGA ground motion model for the geometric mean horizontal component of PGA, PGV, PGD and 5% damped linear elastic response spectra for periods ranging from 0.01 to 10 s, *Earthq. Spectra,* 24:139–171.

CEN (2004). Eurocode 8, Design of structures for earthquake Resistance—Part 1: general rules, seismic actions, and rules for buildings. EN 1998-1:2004. Comité Européen de Normalisation, Brussels.

Douglas J (2011). Ground-motion prediction equations:1964-2010. *Final Report BRGM-RP-59356-FR BRGM*, Orleans, France.

Douglas J (2004). Use of analysis of variance for the investigation of regional dependence of strong ground motions. *Proceedings*, Thirteenth World Conference on Earthquake Engineering, Paper No. 29, Vancouver, Canada.

Esteva L, Rosenblueth E (1964). Espectros de temblores a distancias moderadas y grandes. *Boletin Sociedad Mexicana de Ingenieria Seismica*, 2:1–18 (in Spanish).

Luzi L, Hailemikael S, Bindi D, Pacor F, Mele F, Sabetta F (2008). ITACA (ITalian ACcelerometric Archive): a web portal for the dissemination of the Italian strong motion data, *Seismo. Res. Lett*., 79:716–722.

Sandıkkaya MA, Yılmaz MT, Bakır SB, Yılmaz Ö (2010). Site classification of Turkish national strong-motion stations, *J. Seismology*, 14:543–563.

Stafford PJ, Strasser FO, Bommer JJ (2008). An evaluation of the applicability of the NGA models to ground motion prediction in the Euro-Mediterranean region, *Bull. Earthq. Engng.,* 6:149–177.

Strasser FO, Abrahamson NA, Bommer JJ (2009). Sigma: issues, insights, and challenges, *Seismo. Res. Lett*., 80:40–56.

STOCHASTIC SIMULATION OF EARTHQUAKE GROUND MOTION COMPONENTS FOR PERFORMANCE-BASED STRUCTURAL ANALYSIS

Sanaz Rezaeian[1] and Armen Der Kiureghian[2]

[1]*Postdoctoral Fellow, Pacific Earthquake Engineering Research Center, sanazr128@yahoo.com,*
[2]*Taisei Professor of Civil Engineering, University of California, Berkeley, CA, adk@ce.berkeley.edu*

ABSTRACT

A method for generating an ensemble of orthogonal ground motion components with correlated parameters for specified earthquake and site characteristics is developed. The method employs a parameterized stochastic model that is based on a time-modulated filtered white-noise process with the filter having time-varying characteristics. The stochastic model is fitted to a database of recorded horizontal ground motion component pairs that are rotated into their principal axes, where the components are statistically uncorrelated. Predictive equations are developed for the model parameters in terms of earthquake and site characteristics, and correlation coefficients between parameters of the two components are determined empirically. Given a design scenario, correlated model parameters are randomly simulated and used with two statistically independent white-noise processes to generate a pair of horizontal ground motion components along the principal axes. The simulated components may then be rotated into any desired pair of orthogonal horizontal directions, i.e., the principal axes of a structure.

INTRODUCTION

In seismic design and analysis of structures, development of ground motion time-series is a crucial step because the validity of predicted structural responses depends on the validity of the input ground motion. It is common practice to use acceleration time-series that were recorded during previous earthquakes, either in original or scaled/modified form, as the input excitations to non-linear dynamic analyses. But recorded motions are scarce and are not available for all possible earthquake scenarios and site conditions. Considering that different earthquake and site characteristics can greatly influence the nature of the ground motion, one should refrain from using recorded motions for earthquake scenarios other than the causal scenario. The limited number of recordings has become problematic in the emerging field of performance-based earthquake engineering (PBEE), which considers the entire spectrum of structural response, from linear to grossly nonlinear and even collapse, and thereby requires ground motions with various levels of intensity for different earthquake scenarios. Generating an ensemble of synthetic motions for specified earthquake and site characteristics can therefore benefit PBEE, provided the synthetic motions accurately capture the characteristics of real ground motions and their natural variability. These synthetics can be used to supplant or supplement recorded motions. Furthermore, for earthquake response analysis of three-dimensional structural systems, such as bridges, dams, nuclear power plants, and piping systems, or simply for two-dimensional analysis of asymmetric structures, it is important to simulate components of the ground motion in a consistent manner. This paper presents a method for generating an ensemble of synthetic ground motion components for specified earthquake and site characteristics.

Seismic Hazard

Many ground motion simulation models have been developed in the past. Brief reviews are presented in Rezaeian and Der Kiureghian [2008; 2010]. This study adopts the stochastic model developed in Rezaeian and Der Kiureghian [2008], which is based on a time-modulated filtered white-noise process with the filter having time-varying parameters. The model parameters are identified by fitting statistical characteristics of the stochastic model to those of a recorded acceleration time-series. In a more recent study [Rezaeian and Der Kiureghian 2010], this stochastic model was fitted to a large number of recorded ground motions and predictive equations were developed in terms of earthquake and site characteristics that allow generation of synthetic records without any need for recorded accelerograms. The present paper utilizes these two studies to formulate a new approach for simulation of the horizontal orthogonal components of ground motion for specified earthquake and site characteristics. Though not addressed in this paper, the proposed method can be easily extended to simulate the vertical component as well.

As in previous works related to this subject (e.g., Kubo and Penzien [1979]; Yeh and Wen, [1989]), we employ the model by Penzien and Watabe (1975), which assumes the existence of an orthogonal set of principal axes, along which the ground motion components are statistically independent. However, unlike previous studies, we empirically estimate the correlation coefficients between the model parameters of the components and properly account for them in the simulation. Considering that ground motion components emanate from the same earthquake source and seismic waves travel through the same medium, one expects these correlations to be high. Therefore, they must be carefully modeled in order to obtain realistic synthetics.

The paper starts with a brief review of the concept of principal axes of ground motion. The stochastic ground motion model is then described and a database of ground motion components in principal directions is developed. Based on this database, empirical predictive equations for the model parameters are constructed and correlation coefficients between parameters of the two components are empirically determined. The simulation approach is demonstrated through an example and comparisons are made between simulated and real ground motion components.

PRINCIPAL AXES OF GROUND MOTION

Let $a_1(t)$ and $a_2(t)$ denote two orthogonal horizontal components of ground acceleration at a site. Noting that the ground motion process has zero mean, the temporal correlation coefficient between the two components over the time interval $\tau_1 \le t \le \tau_2$ is defined as

$$\boldsymbol{\rho_{a_1 a_2}} = \frac{\int_{\tau_1}^{\tau_2} \boldsymbol{a_1(t) a_2(t)} \mathbf{d}\boldsymbol{t}}{\sqrt{\int_{\tau_1}^{\tau_2} \boldsymbol{a_1(t)^2} \mathbf{d}\boldsymbol{t} \int_{\tau_1}^{\tau_2} \boldsymbol{a_2(t)^2} \mathbf{d}\boldsymbol{t}}} \tag{1}$$

Penzien and Watabe (1975) examined this correlation coefficient for a number of recorded ground motions and observed that it did not significantly change for different time segments so that $\rho_{a_1 a_2}$ could be computed for the entire length of the record. The correlation coefficient naturally depends on the directions along which the two components are recorded. Let $a_{1,\theta}(t)$ and $a_{2,\theta}(t)$ represent the components of ground motion obtained by a counter-clockwise rotation of angle θ in the horizontal plane:

$$\begin{bmatrix} \boldsymbol{a_{1,\theta}(t)} \\ \boldsymbol{a_{2,\theta}(t)} \end{bmatrix} = \begin{bmatrix} \mathbf{cos}(\boldsymbol{\theta}) & -\mathbf{sin}(\boldsymbol{\theta}) \\ \mathbf{sin}(\boldsymbol{\theta}) & \mathbf{cos}(\boldsymbol{\theta}) \end{bmatrix} \begin{bmatrix} \boldsymbol{a_1(t)} \\ \boldsymbol{a_2(t)} \end{bmatrix} \tag{2}$$

Penzien and Watabe (1975) defined the principal axes of ground motion as the rotated axes along which the three components are statistically uncorrelated, i.e., $\rho_{a_{1,\hat{\theta}}a_{2,\hat{\theta}}} = 0$. The corresponding rotated components, $a_{1,\hat{\theta}}(t)$ and $a_{2,\hat{\theta}}(t)$, are referred to as the major and the intermediate principal components, a_{maj} and a_{int}, in decreasing order of intensities. In this study, we use Arias intensity (for $a(t)$, Arias intensity is $I_a = \frac{\pi}{2g}\int_0^{t_n} a^2(t)\mathrm{d}t$, with t_n denoting the duration of the motion and g denoting the gravitational acceleration) to distinguish between the two components. Based on examination of real accelerograms, Penzien and Watabe (1975) found that a_{maj} usually is horizontal and points in the general direction of the epicenter and a_{int} is horizontal and perpendicular to $a_{maj}(t)$.

STOCHASTIC GROUND MOTION MODEL

The stochastic ground motion model proposed in Rezaeian and Der Kiureghian (2008) represents the ground acceleration process as the response of a linear filter with time-varying parameters to white-noise excitation. The filter response is normalized by its standard deviation and is multiplied by a deterministic time-modulating function. While modulation of the process in time introduces temporal nonstationarity, time-variation of the filter parameters provides spectral nonstationarity. Normalization by the standard deviation of the process prior to time-modulation separates the spectral and temporal nonstationary characteristics of the process, thus greatly facilitating modeling and parameter identification. This model is extended to simulate orthogonal horizontal components of ground motion. In the continuous form, it is formulated as

$$\boldsymbol{x_r(t)} = \boldsymbol{q(t,}\alpha_r\boldsymbol{)}\left\{\frac{\mathbf{1}}{\boldsymbol{\sigma_h(t)}}\int_{-\infty}^{\boldsymbol{t}} \boldsymbol{h[t-\tau,}\lambda_r\boldsymbol{(\tau)]w_r(\tau)\mathrm{d}\tau}\right\}\ ;\ \boldsymbol{r = 1,2} \tag{3}$$

where $x_r(t)$ is acceleration time-series of the r^{th} component; $q(t,\boldsymbol{\alpha}_r)$ is a deterministic, nonnegative, time-modulating function with parameters $\boldsymbol{\alpha}_r$ controlling its shape and intensity; $w_r(\tau)$ is a white-noise process; the integral inside the curved brackets is a filtered white-noise process, where $h[t-\tau,\boldsymbol{\lambda}_r(\tau)]$ denotes the impulse-response function (IRF) of the filter with time-varying parameters $\boldsymbol{\lambda}_r(\tau)$; and $\sigma_h^2(t) = \int_{-\infty}^{t} h^2[t-\tau,\boldsymbol{\lambda}_r(\tau)]\mathrm{d}\tau$ is the variance of the integral process. Due to the normalization by $\sigma_h(t)$, $q(t,\boldsymbol{\alpha}_r)$ equals the standard deviation of $x_r(t)$ and completely controls the temporal characteristics of the process. On the other hand, the form of the IRF and its time-varying parameters control the spectral characteristics of the process.

The time-modulating function and the linear filter employed in this study are similar to those used in Rezaeian and Der Kiureghian (2010). The modulating function has three parameters, $\boldsymbol{\alpha}_r = (\bar{I}_{a,r}, D_{5-95,r}, t_{mid,r})$. These parameters respectively represent: the expected Arias intensity of the acceleration process; the effective duration of the motion, defined as the time interval between the instants at which the 5% and 95% of the expected Arias intensity are reached; and the time at the middle of the strong-shaking phase of the motion, defined as the time at which the 45% level of the expected Arias intensity is reached. The selected filter also has three parameters, $\boldsymbol{\lambda}_r = (\omega_{mid,r}, \omega'_r, \zeta_r)$. Parameters $\omega_{mid,r}$ and ω'_r represent the frequency of the filter, assumed to change linearly with time. $\omega_{mid,r}$ is the filter frequency at time t_{mid} and ω'_r is the rate of change of the frequency with time. ζ_r represents the damping ratio of the filter, assumed to be constant with time. These parameters respectively control the evolutionary predominant frequency and bandwidth of the ground motion process.

As previously mentioned, one would expect high correlations between the sets of parameters for the two components. These correlations are obtained empirically as described later in this paper. While the overall temporal and spectral characteristics of the horizontal ground motion components in Equation (3) are completely defined by the set of 12 parameters, the white noise processes $w_r(t)$, $r = 1,2$, bring in the stochasticity of the motions. For horizontal components along the principal axes, the white-noise processes $w_1(t)$ and $w_2(t)$ are statistically independent.

Given a set of model parameters and two statistically independent white-noise processes, realizations of Equation (3) are easily obtained by a discretization approach proposed in Rezaeian and Der Kiureghian (2008). However, before this process can be regarded as a ground motion time-series, it must undergo high-pass filtering to assure zero residual velocity and displacement, as well as to produce reliable response spectral ordinates at long periods. Details are presented in Rezaeian and Der Kiureghian (2008).

DATABASE OF PRINCIPAL GROUND MOTION COMPONENTS

The strong motion database introduced in Rezaeian and Der Kiureghian (2010) is used, which contains 103 pairs of horizontal recordings, directions of which depend on the orientation of the recording instrument. Each pair is rotated according to Equation (2) for various rotation angels. The pair of rotated components that are statistically uncorrelated, i.e., $a_{1,\hat{\theta}}(t)$ and $a_{2,\hat{\theta}}(t)$, are selected to form the *database of principal ground motion components*. An example is presented in Figure 1.

In Figure 1, the components of as-recorded acceleration time-histories for the 1994 Northridge, California, earthquake at Mt Wilson–CIT Station are plotted on the left side. The pair is rotated according to Equation (2) and correlations between their two components are plotted against the rotation angle on the top. Shown on the right are the corresponding principal components.

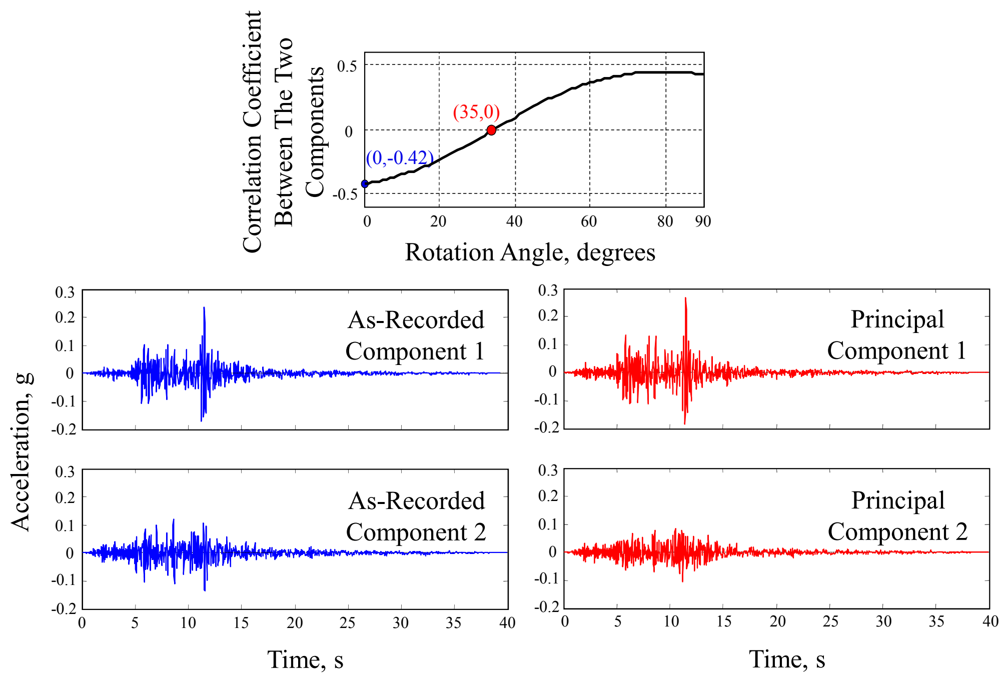

Figure 1 Rotation of a pair of horizontal as-recorded components into principal axes.

EMPIRICAL PREDICTIVE EQUATIONS FOR MODEL PARAMETERS

Sample observations of the model parameters are obtained by fitting the stochastic ground motion model to each pair of records in the database of principal ground motion components. Using this "observational" data, probability distribution models are assigned to each of the six parameters for each component. The data for Arias intensity is divided into two groups: Arias intensity for the major principal component, $I_{a,maj}$, and Arias intensity for the intermediate principal component, $I_{a,int}$. This division reduces the number of data points for statistical analysis from 206 to 103 for each parameter, but it is necessary for simulation of pairs of ground motion components. Lognormal distributions are assigned to $I_{a,maj}$ and $I_{a,int}$ with means of 0.0646 s.g and 0.0290 s.g, and with coefficients of variation equal to 3.45 and 2.24. The statistical analysis for the remainder of model parameters is performed for the entire data set, i.e., data corresponding to both components are combined resulting in 206 data points for each parameter. The identified parameters and the assigned distribution models are reported in Rezaeian (2010).

Predictive equations are developed for each model parameter in terms of earthquake and site characteristics. Four variables that are commonly used to describe a design scenario are selected to describe the earthquake and site characteristics. These variables are F, M, R_{rup}, and V_{S30}, respectively, representing the faulting mechanism, the moment magnitude, the closest distance from the site to the ruptured area, and the shear wave velocity at the top 30 m of the site. Following the constraints of the selected ground motion database, F assumes values of 0 and 1 for strike-slip and reverse types of faulting, $6.0 \leq M$, $10\text{ km} \leq R_{rup} \leq 100\text{ km}$, and $600\text{ m/sec} \leq V_{S30}$. Random-effects regression modeling is performed on the database of identified stochastic model parameters to develop predictive equations of the form

$$\boldsymbol{\Phi^{-1}[F_p(p)] = \beta_{p,0} + \beta_{p,1}(F) + \beta_{p,2}\left(\frac{M}{7.0}\right) + \beta_{p,3}\left(\ln\frac{R_{rup}}{25\ \mathrm{km}}\right) + \beta_{p,4}\left(\ln\frac{V_{S30}}{750\mathrm{m/s}}\right)}$$
$$\boldsymbol{+\eta_p + \epsilon_p \qquad \text{if} \qquad p = \bar{I}_{a,maj}, \bar{I}_{a,int}} \tag{4}$$

$$\boldsymbol{\Phi^{-1}[F_p(p)] = \beta_{p,0} + \beta_{p,1}(F) + \beta_{p,2}\left(\frac{M}{7.0}\right) + \beta_{p,3}\left(\frac{R_{rup}}{25\ \mathrm{km}}\right) + \beta_{p,4}\left(\frac{V_{S30}}{750\mathrm{m/s}}\right)}$$
$$\boldsymbol{+\eta_p + \epsilon_p \qquad \text{if} \qquad p = D_{5-95}, t_{mid}, \omega_{mid}/2\pi\,, \omega'/2\pi\,, \zeta} \tag{5}$$

On the left-hand side, $\Phi^{-1}[.]$ is the inverse of the standard normal cumulative distribution function and $F_p(.)$ is the fitted cumulative distribution function of parameter p. $\Phi^{-1}[F_p(p)]$, which represents transformation of a model parameter to the standard normal space, satisfies the normality criterion required for the response variable in regression analysis. The right-hand side of Equations. (6) and (7) represents the predicted mean of the model parameter in terms of the selected earthquake and site characteristics plus the regression error. The regression error is divided into two components η_p and ϵ_p, representing the inter- and intra-earthquake model error terms, both of which are independent zero-mean normally distributed random variables with variances τ_p^2 and σ_p^2. This formulation accounts for the varying number of records from different earthquakes. The maximum likelihood estimates of the regression coefficients and variance components are presented in Table 1.

Table 1 Maximum likelihood estimates of regression coefficients and error components.

p	$\beta_{p,0}$	$\beta_{p,1}$	$\beta_{p,2}$	$\beta_{p,3}$	$\beta_{p,4}$	τ_p	σ_p
$\bar{I}_{a,maj}$	− 1.841	0.008	3.065	− 1.351	− 0.168	0.176	0.614
$\bar{I}_{a,int}$	− 2.408	− 0.073	3.307	− 1.295	− 0.246	0.474	0.583
D_{5-95}	− 5.859	− 0.707	6.472	0.231	− 0.565	0.475	0.577
t_{mid}	− 5.038	− 0.296	4.614	0.350	− 0.175	0.495	0.431
$\omega_{mid}/2\pi$	2.086	− 0.041	− 1.660	− 0.217	0.037	0.696	0.714
$\omega'/2\pi$	− 3.224	0.067	3.262	0.029	− 0.144	0.168	0.921
ζ	0.692	− 0.676	0.296	− 0.341	0.181	0.704	0.709

In the standard normal space, correlation coefficients between two model parameters are estimated as the sample correlation coefficients between their corresponding total residuals. The correlation coefficients between model parameters of one single component are similar to those reported in Rezaeian and Der Kiureghian (2010). The correlation coefficients between the model parameters of the major and intermediate principal components in the standard normal space are presented in Table 2. In this table, $\nu_1, \ldots, \nu_6$ represent $\Phi^{-1}[F_p(p)]$, respectively for parameters $\bar{I}_a, D_{5-95}, t_{mid}, \omega_{mid}, \omega'$, and ζ. Observe that, as expected, some correlations are high, especially between pairs of similar model parameters of the two components.

Table 2 Sample correlation coefficients between the transformed model parameters.

		Major Component					
		v_1	v_2	v_3	v_4	v_5	v_6
Intermediate Component	v_1	$+0.92$	-0.31	$+0.04$	-0.13	$+0.19$	-0.01
	v_2	-0.30	$+0.89$	$+0.65$	-0.15	-0.21	-0.23
	v_3	-0.03	$+0.68$	$+0.96$	-0.29	-0.22	-0.29
	v_4	-0.13	-0.17	-0.30	$+0.94$	-0.10	$+0.32$
	v_5	$+0.09$	-0.11	-0.24	-0.10	$+0.52$	-0.02
	v_6	$+0.02$	-0.17	-0.21	$+0.29$	-0.13	$+0.75$

SIMULATION IN THE DIRECTION OF PRINCIPAL AXES

Given a design scenario defined by the set of earthquake and site characteristics F, M, R_{rup} and V_{S30}, sets of twelve model parameters (six for each component) are randomly simulated in the transformed space as jointly normal random variables by using the predictive equations and correlation coefficients reported in the previous section. The model parameters in each set are then transformed to their physical space and used in Equation (3) along with two statistically independent white-noise processes to generate a pair of synthetic ground motion components in the directions of principal axes. The pair can then be rotated to any desired direction using the transformation in Equation (2). As an example, Figure 2 shows pairs of acceleration time-histories of the major and intermediate components for one recorded and two simulated ground motions. The corresponding model parameters are presented in Table 3. In Figure 3, the elastic response spectra of the recorded pair are presented along with those of 50 synthetics.

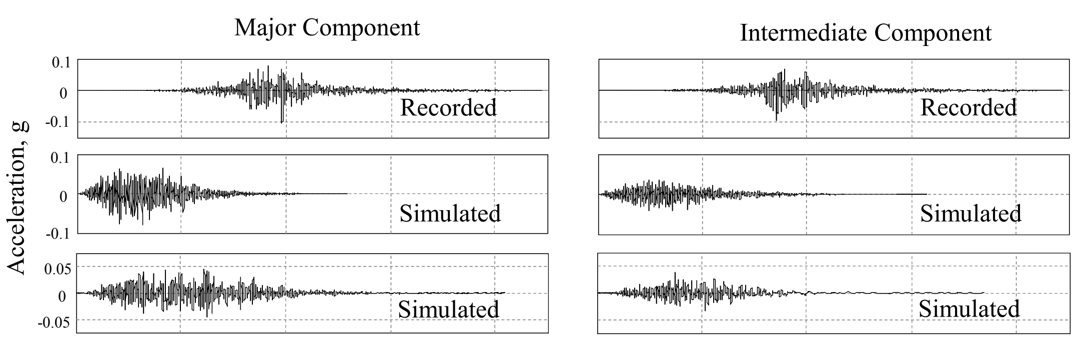

Figure 2 Pairs of horizontal acceleration time-histories corresponding to $F = 1$, $M = 7.62$, $R_{rup} = 51.8$ km and $V_{S30} = 618$ m/sec.

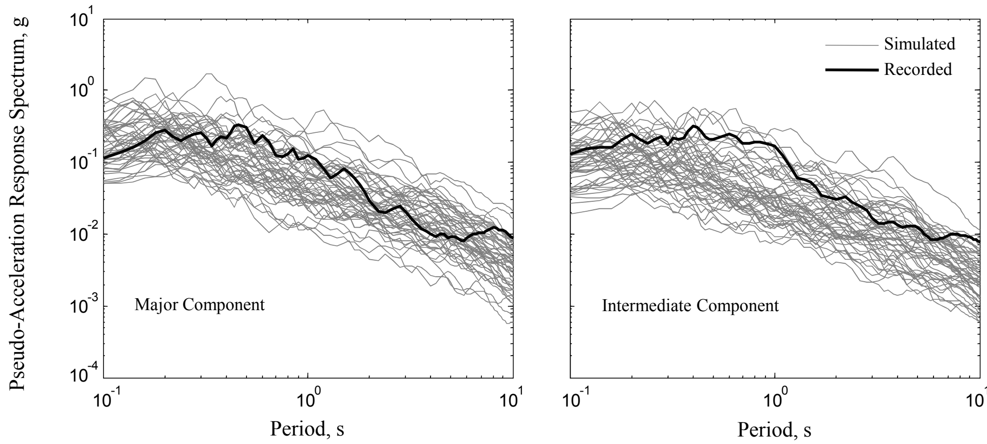

Figure 3 Elastic response spectra (5% damped).

Table 3 Realizations of the model parameters for ground motion components in Figure 2.

Major component						Intermediate component					
I_a s.g	D_{5-95} s	t_{mid} s	$\omega_{mid}/2\pi$ Hz	$\omega'/2\pi$ Hz/s	ζ_f	I_a s.g	D_{5-95} s	t_{mid} s	$\omega_{mid}/2\pi$ Hz	$\omega'/2\pi$ Hz/s	ζ_f
0.0165	16.7	18.3	3.9	−0.08	0.12	0.0135	17.0	17.8	4.1	−0.02	0.11
0.0147	17.3	10.1	8.1	−0.12	0.42	0.0047	21.0	10.7	8.6	−0.18	0.50
0.0099	27.2	17.1	3.2	−0.03	0.20	0.0034	24.8	16.9	3.7	−0.13	0.35

The synthetics are generated for the earthquake and site characteristics of the recorded ground motion pair. Because not only the stochasticity of ground motion time-histories, but also the variability of model parameters are properly accounted for, our simulation method preserves the natural variability of real ground motions for the given design scenario. Observe that at a given spectral period, the spectral ordinates for the pair of recorded motions fall within the range predicted by the synthetics.

CONCLUSION

A method for simulating an ensemble of orthogonal horizontal ground motion components for specified earthquake and site characteristics is developed. A new ground motion database is constructed by rotating recorded horizontal ground motion component pairs into their principal axes. A previously developed stochastic ground motion model is employed and model parameters are identified for each principal component of recorded motions. Predictive equations that express each model parameter in terms of F, M, R_{rup}, and V_{S30}, are developed and correlation coefficients between model parameters of the two horizontal principal components are estimated empirically. The stochastic model, predictive equations, and correlation coefficients are utilized to simulate horizontal ground motion components along the principal axes. The synthetic components can then be rotated into any desired direction, e.g., the input axes of a structure. The proposed simulation procedure does not require any previously recorded motions and is ideal for use in engineering applications. Furthermore, it preserves the natural variability of real ground motions for the given design scenario.

ACKNOWLEDGMENTS

This work was supported by the State of California through the Transportation Systems Research Program of the Pacific Earthquake Engineering Research Center (PEER). Any opinions, findings, and conclusions or recommendations expressed in this material are those of the authors and do not necessarily reflect those of the funding agency.

REFERENCES

Kubo T, Penzien J (1979). Simulation of three-dimensional strong ground motions along principal axes, San Fernando earthquake, *Earthq. Engng. Struct. Dyn.*, 7:279-294.

Penzien J, Watabe, M (1975). Characteristics of 3-dimensional earthquake ground motions, *Earthq. Engng. Struct. Dyn.*, 3:365-373.

Rezaeian S (2010). Stochastic modeling and simulation of ground motions for performance-based earthquake engineering. Ph.D. Thesis, Dept. of Civil Engineering, University of California, Berkeley, CA.

Rezaeian S, Der Kiureghian A (2008). A stochastic ground motion model with separable temporal and spectral nonstationarities, *Earthq. Engng. Struct. Dyn.,* 37:1565-1584.

Rezaeian S, Der Kiureghian A (2010). Simulation of synthetic ground motions for specified earthquake and site characteristics, *Earthq. Engng. Struct. Dyn.*, (in press).

Yeh CH, Wen YK (1989). Modeling of nonstatinary earthquake ground motion and biaxial and torsional response of inelastic structures, Civil Engineering Studies, *Structural Research Series Report No. 546*, University of Illinois, Urbana, IL.

Seismic Hazard

MULTI-DISCIPLINARY EARTHQUAKE RESEARCHES FOLLOWING 17 AUGUST 1999 İZMIT EARTHQUAKE

Sedat İnan, Semih Ergintav, and Onur Tan

TUBITAK Marmara Research Center, Earth and Marine Sciences Institute, Gebze-Kocaeli, Turkey, sedat.inan@mam.gov.tr

Following the devastating Mw 7.4 İzmit earthquake on 17 August 1999, major state-of-the-art earthquake studies were conducted in the Marmara region of northwestern Turkey. Although other faults with the potential to generate big and potentially devastating earthquakes occur in a variety of different tectonic regimes in Turkey, these faults and regions had not received similar attention [Inan et al. 2007]. Different methods for earthquake forecast and hazard estimation are needed to be applied in the high earthquake-risk regions in Turkey, providing different tectonic regimes.

In 2005, The Scientific and Technical Research Council of the Turkish Republic (TÜBİTAK) supported a consortium for a multidisciplinary and multilateral earthquake research project named "Multi-Disciplinary Earthquake Researches in High Risk Regions of Turkey Representing Different Tectonic Regimes" (TÜRDEP Project). This multi-lateral and multi-disciplinary project was completed in October 2010. The project was coordinated by the Earth and Marine Sciences Institute (EMSI) of the Marmara Research Center (MRC) of TÜBİTAK. The end user of the project was defined as the Ministry of Construction and Settlement's General Directorate of Disaster Affairs (GDDA) (later Disaster and Emergency Management Presidency); fourteen Turkish universities were the other consortium members. The main purpose of the project was to collect multi-disciplinary data in order to reveal crustal deformation processes. For this purpose, quite dense networks of observation stations were established in the Marmara, Aegean and the Eastern Mediterranean/Eastern Anatolian region of Turkey (see Figure 1).

This initiative concentrated on monitoring active faults and earthquake activity in different tectonic regimes in order to provide a physical basis for comparative analyses utilizing the continuously operating monitoring stations shown in Figure 1. The initiative has been among the world's first example of a fully integrated earthquake hazards approach that included a variety of tectonic settings. This ambitious project had several goals: micro-seismology aided active fault mapping; improving the macro-seismology observation capacity of GDDA; soil radon monitoring; spring water monitoring; GPS and microgravity studies; borehole tilt measurements in pilot areas; site classification of major cities with microtremors; and GPS-aided crustal deformation modeling.

Before the TÜRDEP Project, between 2001 and 2005—with financial support it received from the Istanbul Metropolitan Municipality—the EMSI had established eleven spring water and eight soil radon monitoring stations in the Marmara Region. This study provided encouraging results in terms of pre-earthquake anomalies [İnan et al. 2008]. However, preliminary results of these studies also suggested that pre-earthquake anomalies largely depend on the tectonic regime; site selections are also important. Thus, the need for establishing geochemical observation networks in different tectonic regimes was determined to be critical. Moreover, geochemical and/or geodetic monitoring was evaluated to be important and useful only when conducted in light of microseismicity. Taking all these considerations, the TÜRDEP Project was designed accordingly and dense monitoring networks were established for continuous observations of different physical and chemical properties of the crustal deformation with respect to pre-earthquake periods in three regions of Turkey (see Figure 2).

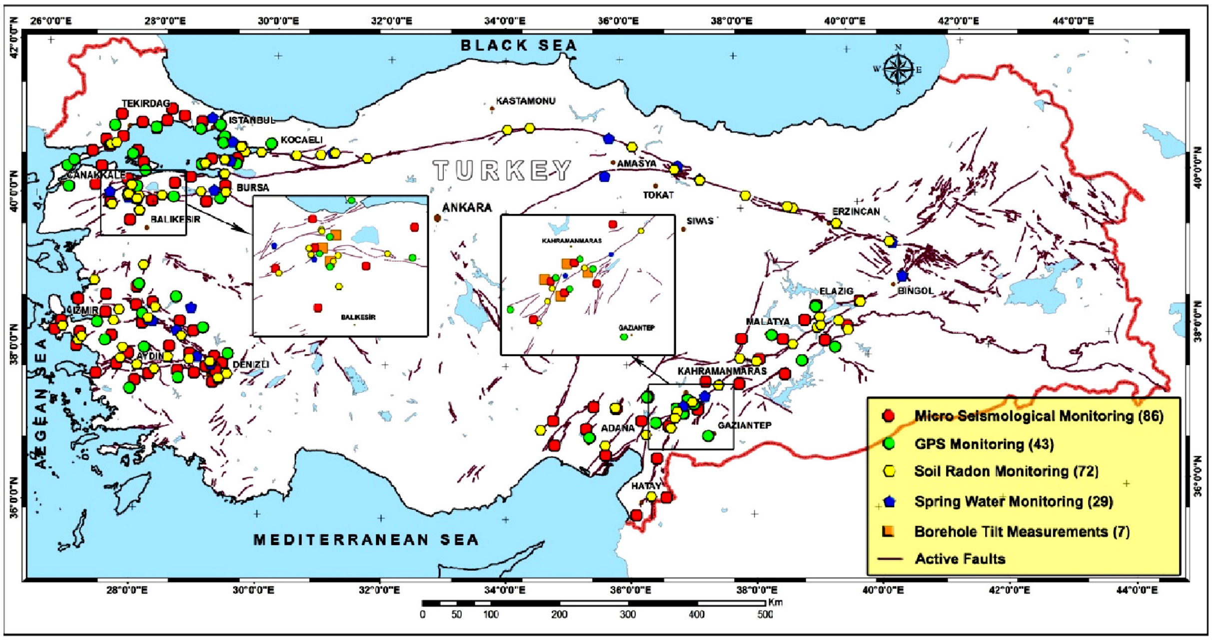

Figure 1 Locations of the established and continuously-run monitoring stations under the scope of the TÜRDEP project. Lines drawn in red are the active faults.

With respect to the Marmara regions, nineteen soil radon, eleven spring water, thirty-two micro-seismology, twenty GPS, three borehole tiltmeter stations, and thirty-one micro-gravity observation sites were established. All observation stations were capable of producing continuous high-resolution data. The important findings based on evalauation of modeling of the continuous data acquired were published by the group. Some examples are: Ergintav et al. [2009]; Baykut et al. [2010]; İnan et al. [2010]; İnan and Seyis [2010]; Seyis et al. [2010]; and Tan et al. [2010].

The benefits of this project can be summurized as follows:

- Online multiparameter (macro and micro seismology, radon gas, and spring water monitoring, as well as GPS, tilt, InSAR, and strain) data have been acquired continuously in the Marmara region and Aegean Extensional Provience (AEP), as well as the area containing the East Anatolian fault system. A database has been compiled, but this effort need to be continued.

- Daily micro-seismological observations were made and the micro-seismicity catalog has been provided to the MTA General Directorate to be used in revising the active fault map of Turkey.

- All the data aquired have been discussed and evaluated in project workshops conducted every six months throughout the project with participation of all parties.

- Scientific awareness for pre-earthquake research in Turkey has been promoted nationally and internationally; cooperating universities initiated this research. Young researchers were hired and trained on the techniques utilized.

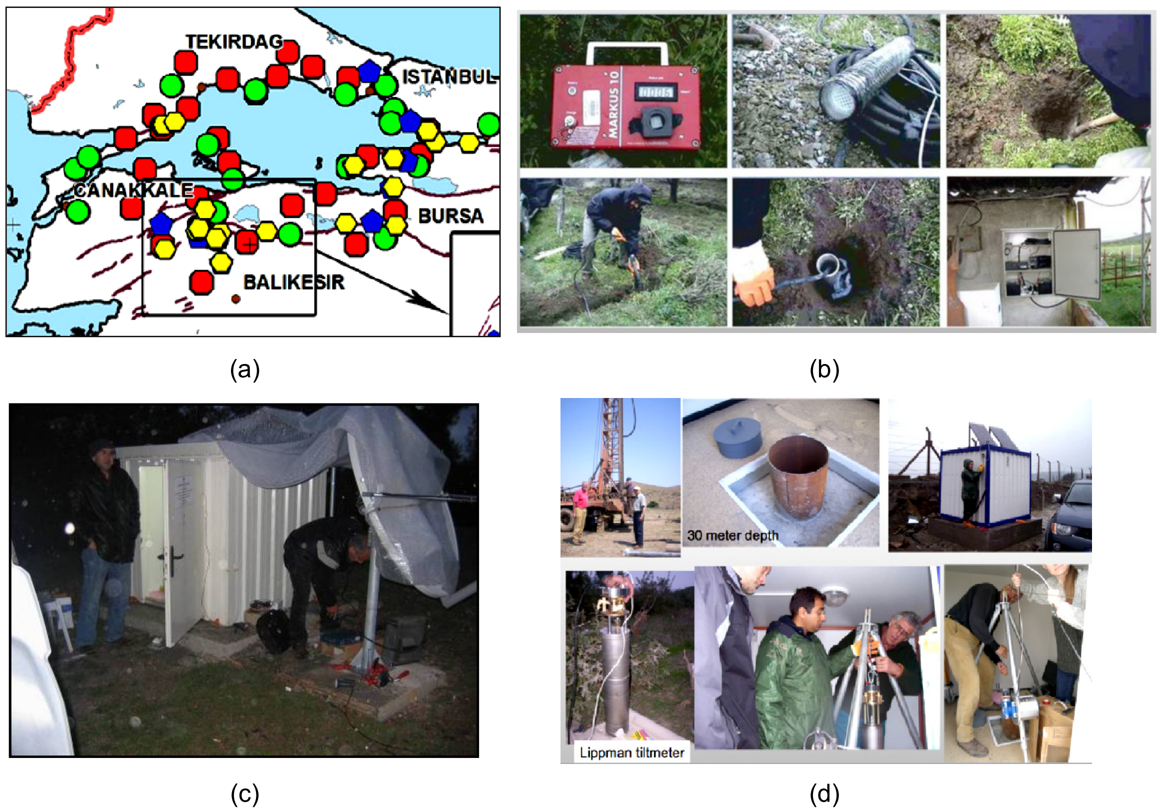

Figure 2. (a) Muti-disiplinary observation stations in the Marmara Region (see Figure 1 for symbols). Examples of establishments of continuous monitoring stations: (b) soil radon gas monitoring; (c) micro-seismology; and (d) borehole tiltmeters.

These efforts require the continuation of ongoing geophysical and geological studies, as well as the application of new methods of observations toward understanding earthquake processes. Multidisciplinary approaches being employed include seismology, borehole tilt/strain measurements, global positioning system (GPS)/interferometric synthetic aperture radar (InSAR), and geochemistry of gas and water emanating from major fracture zones. These observations need to be monitored continuously for several years if not for several decades until sufficient data are acquired to obtain scientifically reliable and accurate explanations for the earthquake phenomena.

We plan to continue with multi-disciplinary monitoring with increasing geodetic measurements (e.g., GPS, microgravity, borehole, tiltmeter, etc.) sites and utilize InSAR data for mapping pre-earthquake deformation in not only the Marmara region but also in the different tectonic regimes in Turkey. Begining in 2010, the EMSI has been involved in EU

Seismic Hazard

FP7 Program-supported projects that will enable continuous comparison between land-derived and satellite derived data for Turkey (e.g., night time thermal images).

REFERENCES

Baykut S, Akgül T, İnan S, Seyis C (2010). Observation and removal of daily quasi-periodic components in soil radon data, *Radiation Measurements*, 45:872-879.

Ergintav S. McClusky S, Hearn EH, Reilinger RE, Çakmak R, Herring T, Ozener H, Lenk O, Tari, E, (2009). Seven years of postseismic deformation following the 1999, M = 7.4 and M = 7.2, Izmit-Düzce, Turkey earthquake sequence, *J. Geophys. Res*., 114:B07403.

İnan S, Ergintav S, Saatçılar R, Tüzel B, İravul Y (2007). Turkey makes major investment in earthquake research, *EOS Trans. AGU*, 88(34):333-334.

İnan S, Akgül T, Seyis C, Saatçılar R, Baykut S, Ergintav S, Baş M (2008). Geochemical monitoring in the Marmara region (NW Turkey): A search for precursors of seismic activity, *J. Geophys. Res*., 113:B0340.

İnan S, Ertekin K, Seyis C, Şimşek Ş, Kulak F, Dikbaş A, Tan O, Ergintav S, Çakmak R, Yörük A, Çergel M, Yakan H, Karakuş H, Saatçilar R, Akçiğ Z, İravul Y, Tüzel B (2010). Multi-disciplinary earthquake researches in Western Turkey: Hints to select sites to study geochemical transients associated to seismicity, *Acta Geophysica*, 58:767-813.

İnan S, Seyis C (2010). Soil radon observations as possible earthquake precursors in Turkey, *Acta Geophysica*, v. 58:828-837.

Seyis C, İnan S, Streil T (2010). Ground and indoor radon measurements in a geothermal area. *Acta Geophysica*, 58:939-946.

Tan O, Tapırdamaz MC, Ergintav S, İnan S, İravul Y, Saatçılar R, Tüzel B, Tarancıoğlu A, Karakısa S, Kartal RF, Zünbül S, Yanık K, Kaplan M, Şaroğlu F, Koçyiğit A, Altunel E, Özel NM (2010). Bala (Ankara) earthquakes: Implications for shallow crustal deformation in Central Anatolian section of the Anatolian Platelet (Turkey), *Turkish J. Earth Sci*.

TALL BUILDINGS INITIATIVE: A COMPREHENSIVE RESEARCH PROGRAM ON SEISMIC ANALYSIS AND DESIGN OF NEW TALL BUILDINGS

Y. Bozorgnia[1] , J. P. Moehle[1] and R.O. Hamburger[2]

[1]Pacific Earthquake Engineering Research Center, University of California, Berkeley, California, USA; [2]Simpson Gumpertz & Heger Inc., San Francisco, California, USA

ABSTRACT

An overview of the Tall Buildings Initiative (TBI), a comprehensive research program on performance-based seismic analysis and design of new tall buildings, is presented in this paper. The TBI was coordinated by the Pacific Earthquake Engineering Research Center (PEER), with close collaboration with practicing structural and geotechnical engineers in the tall building design community. A major outcome of the TBI has been the document *Guidelines for Performance-Based Seismic Design of Tall buildings*. The Guidelines represent the latest practical implementation of performance-based seismic design (PBD), improving upon the PBD procedures developed during the past 10 years. A brief review of the evolution of the PBD in the United States is presented in this paper, followed by an overview of the TBI and development of the *Guidelines*.

INTRODUCTION

In the United States, practical performance-based seismic design (PBD) originated as an effective means to mitigate the seismic risks posed by existing buildings, which was later extended to permit development of new buildings capable of superior seismic performance. The PBD methods were quickly adapted to justify design of new buildings that do not conform to building code requirements, and which are intended only to provide equivalent performance to buildings conforming to code criteria. This practice has become particularly prevalent in the design of very tall buildings in the western United States.

Initial development of PBD procedures in the United States occurred in response to societal reactions to the frequent occurrence of damaging earthquakes in the western United States during the period 1979 through 1994. These earthquakes provided many illustrations of both the strengths and weaknesses of seismic provisions in U.S. building codes, spurring substantial evolution and improvement of these provisions. Most buildings designed to modern code provisions achieved the life-safety intent of the building code, but several experienced extensive damage resulting in large financial loss. These earthquakes also provided frequent reminders that the inventory of existing buildings included many older structures that were susceptible to life-threatening damage and thus posed unacceptable seismic risks.

Some corporations and institutions became interested in voluntary seismic upgrades. Engineers working on their behalf quickly found that decision-makers in these organizations wanted to know how their buildings would perform—in terms meaningful to them—before they would commit to retrofit. Often these decision-makers wanted to tailor retrofit programs to optimize their costs and benefits. These same decision-makers quickly became interested in seismic performance issues in the design of new buildings as well, to assure that their important facilities would adequately protect their business and operational needs, and not encumber them with unacceptable future economic losses.

Many owners of vulnerable buildings were not interested in seismic upgrades, prompting governments to adopt mandatory upgrade programs. To justify adopting such programs, it was necessary to contrast the likely performance of hazardous buildings and the consequences if no action were taken. Performance-based seismic engineering was developed to enable engineers to respond to the need to reliably assess the probable performance of new and existing buildings under a variety of design scenarios.

The Federal Emergency Management Agency (FEMA) provided the primary financial support for development of performance-based seismic engineering procedures by funding the Applied Technology Council's (ATC) development of a series of performance-based engineering criteria and guidelines including *FEMA–273/274* [ATC 1997a, b]; these guidelines formed the basis for present generation performance-based seismic engineering practice. The American Society of Civil Engineers (ASCE) subsequently converted these documents into the ASCE-31 [ASCE 2002] and ASCE–41 [ASCE 2006] standards that could be adopted by building codes.

These first-generation procedures experienced widespread acceptance and application, both in their intended use, evaluation and upgrade of existing buildings; and also for application to the new building design. However, for new building design, the primary application of these procedures is to demonstrate that nonconforming designs have equivalent performance capability as that intended by the building code, allowing development of buildings at lower cost or with other attributes attractive to developers. This practice became particularly popular in design of very tall buildings, contributing to the development of many of these structures in the period 2003 through 2008 in Los Angeles, Seattle, San Francisco, and other western cities with significant seismic hazards.

Many of these structures are tall residential buildings, having post-tensioned concrete flat slabs supported by a ring of perimeter reinforced concrete columns and tubular bearing walls surrounding the central core. Prescriptive U.S. code provisions prohibit such construction in excess of 50 m tall, without provision of a dual special moment-resisting frame capable of resisting at least 25% of specified seismic design forces. By using performance-based procedures, engineers were able to eliminate the moment-resisting frame, saving costs, and, more importantly, permitting exterior designs that accommodated floor to ceiling windows and reduced story heights in buildings extending to 200 m tall.

BUILDING CODE COMPLIANCE

In 2003, western U.S. cities generally adopted and rigorously enforced building regulations based on the *International Building Code* [ICC 2006]. These codes adopt prescriptive seismic design provisions through reference to the *ASCE-7*standard [ASCE 2005], which is based on the *NEHRP Recommended Provisions for Buildings and Other Structures* [BSSC 2003]. The *International Building Code* also includes permissive language that enables the use of alternative procedures demonstrated to provide performance equivalent to the prescriptive requirements. The design professional must demonstrate equivalence to the satisfaction of the building official. Many, but not all, building officials have proven amenable to the use of these procedures.

The code does not limit the procedures that can be used to demonstrate equivalence, nor does the code state, except in generic and qualitative terms, what performance is acceptable. Most engineers and building officials adopt a target performance based on the commentary to the *NEHRP Recommended Provisions*. This commentary states that for ordinary structures the objective is to provide a low conditional probability of collapse, given the occurrence of Maximum Considered Earthquake (MCE) shaking, and to preclude, to the extent practicable, economic losses associated with more frequent and moderate events. The recently published *FEMA –P-695* [ATC 2009a] and *FEMA P-750* [BSSC 2009] reports clarify that the acceptable conditional collapse probability is 10% and specify rigorous analytical and statistical methods for collapse probability quantification. However, these methods are complex and have not yet been adopted into general practice. Instead, engineers have adapted procedures based on *ASCE-41*.

Engineers have typically performed preliminary design in general conformance with the prescriptive code requirements, but taking a limited number of well-defined exceptions. The resulting near conformance to the code requirements provides both building officials and engineers a foundation level of comfort with the designs. Nonlinear response history analysis (RHA) is used to demonstrate adequate collapse resistance. Performance is evaluated on an element by element basis using acceptance criteria contained in the *ASCE-41* standard, sometimes supplemented with project-specific criteria derived from available laboratory testing to demonstrate acceptable behavior. Since analysis tools used in most design offices are incapable of reliably predicting response of structures nearing collapse, acceptance criteria are often conservatively selected to assure response within the range of analysis reliability.

Many building officials lack the technical expertise to review complex analyses or interpret laboratory test reports and have required independent third party review as a condition of acceptance of performance-based designs. Though procedures vary, third party reviews are typically performed by teams including a practicing engineer with expertise in tall building design and seismic technology, a researcher with particular knowledge of the types of structural systems to be employed (e.g., reinforced concrete walls, steel frames, etc.), and a geotechnical engineer. Reviews can be rigorous and include consideration of the design criteria, ground motion selection and scaling, analytical modeling and results, and structural detailing. The review process can be lengthy and can have a significant effect on the design.

FIRST-GENERATION PERFORMANCE-BASED PROCEDURES

Initially engineers adopted ad hoc procedures for performance-based design of tall buildings. Later, documents produced by engineers in Northern California [SEAOC 2007] and Southern California [LATBC 2006] formalized these procedures. Generally, designs conform to the prescriptive code provisions with limited exceptions. These exceptions may include exceedance of code-specified height limits, violation of code requirements with regard to redundancy, and occasional use of materials, e.g., high-strength steel and detailing procedures not specifically recognized by the code. Given the general similarity of these buildings to code-prescriptive designs, the procedures that developed typically include: development and approval of a formal criteria document, preliminary design, code-level analysis, and verification of adequacy for MCE shaking.

Design criteria development and approval is an important first step. The formal criteria document includes: a description of the overall structure and its intended load-resisting mechanisms; identification of any exceptions to the building code requirements and the justification for these exceptions; and identification of analytical procedures, load combinations, design ground motions, material properties, and detailing. The intent is to identify all substantive issues before the designer has expended large effort in actually performing the design. In theory, if all procedures and assumptions are agreed to at project inception, approval of the finished design should be straightforward and attainable without controversy. In practice, however, it is rarely possible to foresee all issues that will arise during the design development, and many substantive criteria issues are resolved through cooperative efforts of the designers and reviewers throughout the project.

The preliminary design provides the basis for succeeding steps. Capacity-based design procedures, wherein a preferred yield mechanism is identified and other elements of the structure are proportioned to remain elastic—essentially—are typically used. Initial sizing of elements is often controlled by considerations of dead, live, and wind loads. In many structures, lateral design for wind forces controls even the final sizing of many elements.

The-code level design is used to confirm the adequacy of preliminary sizing and also to provide building officials with confidence, at a primary level, that the structure is comparable to one designed to conform to the code in all respects. In this step, the engineer typically performs the code-prescribed analyses, and evaluates all relevant code-prescribed strength, deformation, and detailing requirements, except those which were specifically exempted in the formal design criteria. Since the building systems used in these structures are not strictly code-compliant, *R*-coefficients and other factors required in the code procedures are typically selected jointly by the designers and reviewers based on judgment.

Verification of behavior in MCE-level shaking is performed using three-dimensional nonlinear response history analyses. Typically, suites of seven horizontal ground motion pairs are used. Ductile behaviors including wall, slab, and beam flexure are evaluated using the mean of the maxima for relevant demand parameters (flexural strain, plastic rotation, etc.). Brittle behaviors and those with potential to result in catastrophic failure—including wall shear, column axial force, slab punching shear, etc.—are typically evaluated using either maximum demands obtained from the suites of analyses or mean demands that have been amplified by an estimated value of the standard deviation with the intent to provide a low probability of failure. Following procedures contained in *ASCE-41,* models and acceptance criteria for ductile behaviors are typically constructed using expected (mean) values of material properties, considering potential variability and strain hardening effects. Acceptance criteria for brittle and catastrophic behaviors are typically developed using lower bound material properties and sometimes using resistance factors to account for potential dimensional variability and construction quality issues.

THE TALL BUILDINGS INITIATIVE

The PEER Tall Buildings Initiative is a cooperative program of research and development undertaken by PEER researchers and practicing structural and geotechnical engineers experienced in tall building design. Spurred by the rapid growth in the use of performance-based seismic design methodologies for the design of tall buildings, the goal of this initiative is to provide a sound and reliable basis for these procedures and to help assure appropriate seismic performance of the resulting new generation of tall buildings.

Initiated in 2006, the program encompasses a range of tasks intended to investigate the following: the dynamic characteristics of tall buildings; the performance capability of buildings designed using alternative procedures; societal preferences for tall building performance; alternative means of developing ground motions for design; soil-foundation-structure interaction effects, modeling and analysis procedures; and development of design guidelines. An important companion report on modeling, analysis, and acceptance criteria for tall buildings [ATC 2009b] is available from the ATC. Reports on other task activities can be obtained at *http://peer.berkeley.edu/tbi/index.html*.

SEISMIC DESIGN GUIDELINES

The TBI *Guidelines for Performance-Based Seismic Design of Tall Buildings* [PEER 2010] represents an evolutionary step in the practice of performance-based seismic design of tall buildings. The *Guidelines* embrace the same analytical technologies adopted by engineers following the San Francisco AB-083 and Los Angeles Tall Buildings Council criteria but provide more guidance on structural modeling, acceptance criteria, and ground motion selection and scaling. There are two important departures from prior practice. First, the *Guidelines* do not require a code-level analysis in that it is anticipated that the procedures may be applied to structural systems for which the code response modification coefficients will not be defined, leaving the code analysis with questionable value. Second, the *Guidelines* use more advanced procedures for evaluating structural performance, anticipating the availability of software that can reliably assess the response of structures in a near-collapse state.

The *Guidelines* focus evaluation procedures on verification that the design performance objectives can be achieved, rather than verification that the building mostly complies with prescriptive criteria. The design performance objectives are those most commonly adopted by leading earthquake professionals today as the intent of the building code, that is, serviceability with minimal repair for frequent earthquake shaking levels and safety for rare earthquake shaking levels. With the exception of exterior cladding systems, the failure of which could cause numerous casualties in a crowded city, the guidelines address structural performance only. The procedures presume that nonstructural components and systems will be designed to conform to the prescriptive code criteria, but do caution that if a building's response characteristics are substantially different from that of typical code-conforming buildings, additional precautions may be required. The *Guidelines* are written in a "recommendation" and commentary format. Recommendations are written in mandatory language, while commentary explains the basis for the recommendations and warns of significant design issues that may not be adequately covered by the recommendations.

As with the AB-083 and Los Angeles Tall Buildings Council criteria, designers must prepare a formal, project-specific design criteria document. The *Guidelines* recommend independent third party review of the criteria, the analyses, and the design. The *Guidelines* employ two levels of analysis: a Service level and a Maximum Considered level.

Members of the design *Guidelines* development committee are (alphabetically): Yousef Bozorgnia (PEER, UC Berkeley), C. B. Crouse (URS Corp.), Ronald Hamburger (SGH, Inc.), Ron Klemencic (Magnusson-Klemencic Associates), Helmut Krawinkler (Stanford University), James Malley (Degenkolb Engineers), Jack Moehle (PEER, UC Berkeley), Farzad Naeim (John A. Martin & Associates), and Jonathan Stewart (UCLA).

Service-Level Evaluation

The purpose of the Service-level check is to assure that the buildings will not experience significant damage from frequent earthquakes. Much controversy surrounded the selection of a Service-level shaking intensity. The 2008 edition of the Los Angeles Tall Buildings Council guidelines [LATBC 2008] specified service-level shaking with a 50% exceedance probability in 30 years (43–year mean recurrence interval), but permitted Service-level analyses to use 5% viscous damping. Studies conducted by the ATC as part of the TBI effort, and summarized in the ATC-72 [ATC 2009b] report, suggest that 5% viscous damping is excessive for tall buildings, recommending that a 2.5% equivalent viscous damping is more justifiable. In keeping with this rationale, some participants argued for use of a Service-level event with a 25-year mean recurrence, arguing that the response spectrum for such an event, when used with 2.5% damping, would be comparable to the 5%-damped 50%–30-year spectrum. Other participants believed that a 25-year recurrence for onset of damage to these buildings was not an appropriate design objective. Eventually consensus support was achieved for the use of a 2.5% damped, 50% 30-year spectrum as the Service-level loading.

The stated performance goal for the Service-level loading is to avoid onset of damage that would reduce the building's ability to withstand Maximum Considered-level shaking or which would require repair that would necessitate removing the building from service. It is expected that some repair of structural elements may be necessary to restore cosmetic appearance, and fire and weather resistance. Nonstructural damage is anticipated to be minor, but is not specifically evaluated.

The *Guidelines* recommend an elastic, three-dimensional response spectrum analysis for the Service-level because not only is the desired behavior intended to be essentially elastic, but also because it is desired to assure that an elastic analysis is available to benchmark and evaluate nonlinear models used in the Maximum Considered-level evaluation. For Service-Level hazard, carrying out a nonlinear RHA—to distribute the loads on very limited number of overstressed elements—is optional. Analytical models must extend to the structure's true base, which for most tall buildings are located several levels below grade. For Service-level loading, soil-foundation-structure interaction effects need not be explicitly modeled, though it is permitted to do so (Figure 1). Based on analytical studies of typical buildings conducted under the TBI, when soil-foundation-structure interaction effects are not modeled explicitly, neglecting the mass of subgrade levels is permitted.

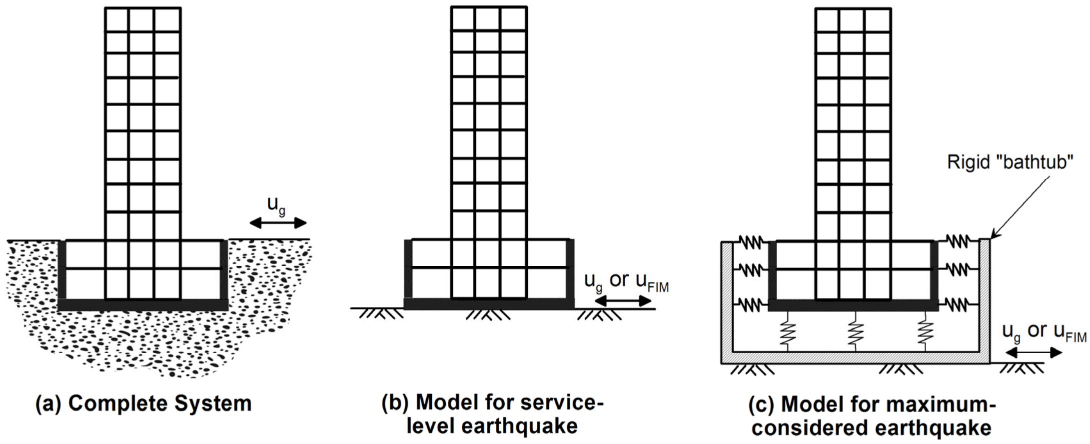

Figure 1: Schematic illustration of tall building with subterranean levels. Figure 1(b) shows the case that soil-foundation interaction effects are neglected. Figure 1(c) presents an approximate representation of soil-foundation-structure interaction. Figure 1(c) only shows springs but parallel dashpots are generally also used.

Acceptance criteria include both strength and deformation. Strength is evaluated by comparing computed strength demands against design strength. Design strength is computed using the strength formula contained in the design specifications referenced by the building code using specified material properties multiplied by strength reduction factors. Recognizing that expected strength will exceed this design strength by a considerable margin, and that some overload is acceptable in a ductile structure, computed demand to capacity ratios may be as large as 1.5. Story drift at any level is not permitted to exceed 0.5% of the story height.

If some computed demand to capacity ratios exceed a value of 1.5, designers are permitted to use three-dimensional nonlinear RHA to demonstrate acceptable Service-level performance. When such analyses are performed, a suite of not less than three horizontal ground motion pairs must be selected and modified to be compatible with the Service-level spectrum previously discussed. Either amplitude scaling or spectral matching may be used to achieve spectrum compatibility following procedures presented in the guidelines. Acceptance criteria must be developed based on suitable laboratory test data. Mean values of response parameters obtained from the suite of analyses cannot exceed demand levels at which the test data suggest the onset of strength degradation or damage, the appearance or repair of which would result in occupancy loss.

The Service-level event in effect serves to define the minimum required base shear strength of the building. In some highly active seismic regions such as Los Angeles and San Francisco, the 2.5% damped 50%–30-year spectrum will result in strength demand comparable to that obtained following the prescriptive code criteria. In regions of lower seismicity—such as Portland, Oregon, and Salt Lake City, Utah—the Service-level spectrum will result in substantially less strength than would be required for a code-conforming building. Commentary warns designers in these regions that additional strength may be required to provide adequate margin against collapse at the Maximum-Considered level.

Maximum Considered-Level Evaluation

Maximum-considered-level evaluations are performed for the same level of shaking specified by the building code for this hazard level. The intent of the MCE evaluation is to demonstrate that the structure is capable of surviving this level of shaking with low probability of collapse. However, since the procedure does not include either explicit collapse or statistical analyses as does the *FEMA P-695* procedure, building adequacy is implied through limiting nonlinear response to levels at which significant margin would seem to remain. Such MCE evaluations are performed using nonlinear RHA and at least seven pairs of motions that are modified, either amplitude scaled or spectrally matched, to be compatible with the MCE spectrum.

The *Guidelines* provide extensive discussion of structural modeling techniques and assumptions. In particular, the subject of strength degradation receives extensive discussion. Where strength degradation is explicitly modeled in a manner that reasonably predicts the hysteretic behavior obtained from testing using varied loading protocols, permissible levels of nonlinear response are relaxed relative to analyses conducted with models that have less explicit incorporation of cyclic strength degradation. Specifically, there are no limitations on the acceptability of nonlinear deformation demand for ductile elements so long as element response remains within levels at which the hysteretic models employed are valid and loss of gravity load carrying capacity does not occur. The *Guidelines* suggest limitations on deformation demand when analytical models are used that do not properly account for element strength and stiffness degradation effects.

As with Service-level evaluations, models must extend to the structure's true base level. Modeling of soil-foundation-structure interaction is not required but can be performed (see Figure 1). Models are based on mean material properties. Acceptance criteria include both strength and deformation considerations.

Actions that are not ductile are evaluated using demand obtained from the equation:

$$Q = D + L_{\text{exp}} + F_E$$

where D is the dead load, and L_{exp} is the expected live load, taken as 25% of the code-specified load. The earthquake effect, F_E , is taken either as 150% of mean earthquake demand $\bar{E}$ computed for the suite of analyses or, for actions with strength demand limited by yielding of other elements, F_E may be taken as $\bar{E} + 1.3\sigma \geq 1.2\bar{E}$, where σ is the standard deviation of the response parameter as obtained from the suite of analyses. It is widely recognized that the true dispersion of responses cannot be adequately gauged using only seven earthquake ground motion pairs. The factor 1.5 applied to the mean response is intended to produce a low probability (around 10%) of exceeding the reliable strength in any one earthquake ground motion at the MCE level. It would be applicable, for example, to wall shear strength. The alternative equation is applicable, for example, to shear in an outrigger beam designed by capacity design methods to be limited by flexural strength. Strength capacities are computed using expected material properties and a resistance factor. The resistance factor may be taken as unity where failure of the element would not result in catastrophic failure and must be taken in accordance with the building code otherwise.

The mean story drift from the suite of response history analyses in any story is not permitted to exceed 3%, and the story drift for any single analysis run is not permitted to exceed 4.5%. These limits were selected somewhat arbitrarily based on the *Guidelines* writers' comfort with the ability of present analytical methods to predict response at very large deformation. In addition to limits on maximum transient story drift, the *Guidelines* also limit maximum residual (permanent) drift. The mean value of residual drift from the suite of analyses cannot exceed 1% of story height in any story, and the maximum residual drift in any story from any analysis cannot exceed 1.5% of story height.

CONCLUSIONS

The PEER TBI has been a successful collaboration of earthquake engineering researchers, practicing structural and geotechnical engineers, and building code officials to address the need for appropriate consensus criteria for performance-based design of tall buildings in the western U.S. Though evolutionary rather than revolutionary in nature, the *TBI Guidelines for Performance-Based Seismic Design of Tall Buildings* introduce significant improvements to practice in the design of these buildings. Of particular note is the provision of modeling guidelines that more realistically account for the nonlinear behavior of buildings than approaches previously used by the profession, together with incorporation of more rational acceptance criteria. The authors believe that the new guidelines will permit the development of tall buildings that are more likely to meet the intended performance objectives embedded in the building code, either than buildings designed to the prescriptive code provisions, or buildings that have been recently designed using performance-based approaches. Future development in this area should include further guidance on selection and scaling of ground motions, direct consideration of nonstructural behaviors, and incorporation of explicit collapse margin investigations.

ACKNOWLEDGEMENTS

The TBI was funded by the California Seismic Safety Commission, California Emergency Management Agency, Charles Pankow Foundation, U.S. National Science Foundation, Federal Emergency Management Agency, California Geologic Survey, and the City of Los Angeles.

REFERENCES

American Society of Civil Engineers (2002). *Seismic Evaluation of Existing Buildings, ASCE-31*, Reston, VA.

American Society of Civil Engineers (2005). *Minimum Design Loads for Buildings and Other Structures, ASCE-7*, Reston, VA.

American Society of Civil Engineers (2006). *Seismic Rehabilitation of Existing Buildings, ASCE-41*, Reston, VA.

Applied Technology Council (1996). *Seismic Evaluation and Retrofit of Buildings, Report No. ATC-40*, Redwood City, CA.

Applied Technology Council (1997a). *NEHRP Guidelines for the Seismic Rehabilitation of Buildings, FEMA-273*, Federal Emergency Management Agency, Washington, D.C.

Applied Technology Council (1997b). *Commentary on the Guidelines for Seismic Rehabilitation of Buildings, FEMA-274*, Federal Emergency Management Agency, Washington, D.C.

Applied Technology Council (2009a). *Qualification of Building Seismic Performance Factors, FEMA P-695*, Federal Emergency Management Agency, Washington, D.C.

Applied Technology Council (2009b). *Interim Guidelines on Modeling and Acceptance Criteria for Seismic Design and analysis of Tall Buildings,* Redwood City, CA.

Building Seismic Safety Council (2003). *NEHRP Recommended Provisions for Seismic Regulation of Buildings and Other Structure, FEMA 450*, Federal Emergency Management Agency, Washington, D.C.

Building Seismic Safety Council (BSSC), 2009, *NEHRP Recommended Provisions for Seismic Regulation of Buildings and Other Structure, FEMA P750*, Federal Emergency Management Agency, Washington, D.C., USA.

International Code Council (2006). *International Building Code*, Whittier, CA.

Los Angeles Tall Buildings Council (2006). *An Alternative Procedure for Seismic Analysis and Design of tall Buildings Located in the Los Angeles Region*, Los Angeles, CA.

Los Angeles Tall Buildings Council (2008). *An Alternative Procedure for Seismic Analysis and Design of tall Buildings Located in the Los Angeles Region*, Los Angeles, CA.

Pacific Earthquake Engineering Research Center (2010). *TBI Guidelines for Performance-Based Seismic Design of Tall Buildings*, *PEER Report 2010/05*, Pacific Earthquake Engineering Research Center, University of California, Berkeley, CA.

Structural Engineers Association of Northern California (2007). *Administrative Bulletin – Requirements and Guidelines for the Seismic Design of New Tall Buildings using Non-Prescriptive Seismic-Design Provisions AB-083*, City of San Francisco, San Francisco, CA.

DRAFT SEISMIC DESIGN CODE FOR TALL BUILDINGS IN ISTANBUL METROPOLITAN AREA

Mehmet Nuray Aydınoğlu

Department of Earthquake Engineering, Kandilli Observatory and Earthquake Research Institute, Boğaziçi University, Istanbul, Turkey

INTRODUCTION

Istanbul is fast becoming a trade, industry, finance, tourism and cultural centre of Eastern Europe and the Middle East. In recent years this development has created a steadily growing demand to construct tall buildings in both European and Asian sectors of the city. In spite of the recent economic slowdown, increasing numbers of tall buildings are under construction or in the design stage. Because of its unique location, however, Istanbul has great potential for experiencing a strong earthquake in the near future. Unfortunately, as is true for other seismic design codes in the world, the current Turkish Seismic Design Code [Ministry of Public Works and Settlement 2007] has not been intended/designed for very tall buildings with continuously increasing story numbers/heights. Indeed, traditional seismic codes are, in many aspects, too restrictive for tall buildings due to their prescriptive nature, while at the same time they lack to cover particular design requirements and special analysis procedures needed for tall buildings.

Because growing numbers of tall buildings are continuing to be constructed in large cities prone to seismic hazard, the development and enforcement of special “tall building seismic design guidelines” has emerged as one of the important agenda items of earthquake engineering. In this respect, special seismic design recommendations / guidelines (consensus documents) for tall buildings have been prepared in recent years by several institutions; these include: Structural Engineers Association of Northern California, Tall Buildings Task Group [SEAONC 2007]; Los Angeles Tall Buildings Structural Design Council [LATBDCD 2005; 2008], and Council on Tall Buildings and Urban Habitat, Seismic Working Group [CTBUH 2008]. At the forefront of this effort, the Pacific Earthquake Engineering Research Center (PEER) has conducted a multi-year collaborative effort, called the *Tall Buildings Initiative* (TBI) to develop a more comprehensive performance-based seismic design guidelines for tall buildings published very recently [PEER 2010a]. In collaboration with the PEER, the Applied Technology Council has providing a supporting document to these guidelines on modeling and acceptance criteria for nonlinear response [ATC 2010].

Encouraged by this development, a draft version of *Istanbul Seismic Design Code for Tall Buildings* [Istanbul Metropolitan Municipality 2008] was prepared upon commission by the Istanbul Metropolitan Municipality composed of working group formed at the Earthquake Engineering Department of Boğaziçi University Kandilli Observatory and Earthquake Research Institute during the period of 2007 through 2008. The draft code has not been officially ratified yet and therefore not officially enforced as of this writing. However, the response from tall building developers and designers has been positive, and has been voluntarily accepted as a performance-based seismic design guideline for tall buildings in Istanbul. The aim of this contribution is to summarize the essential features of the *Draft Istanbul Seismic Design Code for Tall Buildings* [Istanbul Metropolitan Municipality 2008] with emphasis given to performance-based structural design requirements under seismic action.

OBJECTIVE, SCOPE AND GENERAL APPROACH OF CODE

Section 1.2 of the Code sets its objective and scope as follows:

> "This Code shall be applied to earthquake-resistant design of tall buildings to be constructed within the borders of Istanbul Metropolitan Municipality. Tall buildings are minimum 60 meter high buildings measured from the lowest ground level, excluding basement stories that are completely underground and surrounded all around with high-stiffness peripheral walls."

The general approach of the Code is defined as a performance-based design approach, which is described in the same section of the Code as

> "In principle, this Code is based on performance-based design under earthquake action. In this approach, the damage to occur in the elements of structural system under given levels of earthquake ground motion is quantitatively estimated and checked in each element whether it exceeds the acceptable damage limits. The acceptable damage limits are specified under various earthquake levels in conformity with the performance objectives identified for the structure. Since the earthquake damage to be estimated at element level is generally represented by the nonlinear deformations to occur beyond the elastic strain limits, performance-based design approach is directly related to nonlinear analysis methods and the deformation-based design concept. Nevertheless, linear analysis methods are permitted in the Code as well in the framework of strength-based design approach for performance objectives where limited damage is expected."

Finally Section 1.2 of the Code requires a special peer review system for the seismic design of tall buildings as follows:

> "The earthquake-resistant designs of tall buildings to be realized to the requirements of this Code shall be checked and approved by an Independent Review Board."

EARTHQUAKE LEVELS, PERFORMANCE LEVELS / RANGES AND MINIMUM PERFORMANCE OBJECTIVES

Earthquake Levels

In line with the concept of performance-based design, seismic action has been defined for tall buildings in three different levels: E1, E2, and E3 Earthquake Levels with a probability of exceedance of 50%, 10%, and 2% corresponding to return periods of 72, 475, and 2475 years, respectively. The draft code includes contour maps for short-period and 1-sec spectral accelerations estimated for Istanbul metropolitan area.

According to the draft code, a minimum seven sets of earthquake ground motions (acceleration records in two perpendicular horizontal directions) with the following properties shall be selected for the analysis to be performed in the time domain. Real earthquake acceleration records compatible with the scenario earthquake parameters shall be used for each set of ground motion. A strike-slip earthquake source mechanism with a $7.0 < M_w < 7.5$ moment magnitude and a soil class B or C shall be considered in the selection of records for the city of Istanbul. The earthquake distance shall be taken as the shortest distance between the building and the main Marmara Fault line as shown in Figure1.

The resultant spectrum of an earthquake ground motion set shall be obtained through square-root-of-sum-of-squares (SRSS) 5% damped spectra of the two directions. The amplitudes of earthquake ground motions shall be scaled according to a rule such that the average of amplitudes of the resultant spectra of all records between the periods $0.2T$ and $1.2T$ (where T is the predominant natural vibration period of the building) shall not be less than 1.3 times the amplitudes of the design spectrum along the same period range. The scaling of both components shall be made with the same factors.

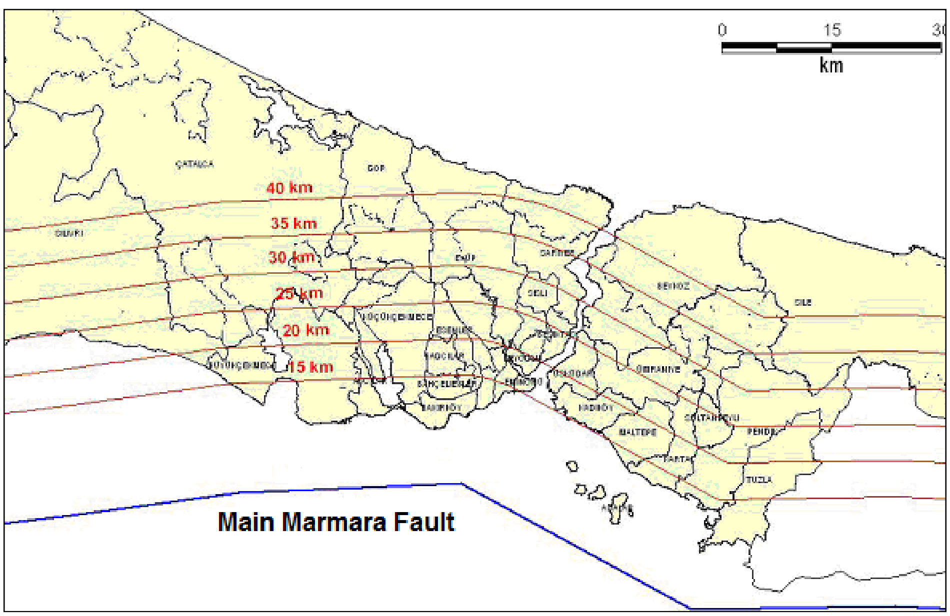

Figure 1 Fault distances to the main Marmara fault.

Performance Levels and Ranges

The draft code defines three discrete performance levels and the corresponding performance ranges in between as Minimum Damage / Uninterrupted Occupancy Performance Level / Range (MD/UO), Controlled Damage / Life Safety Performance Level / Range (CD/LS) and Extensive Damage / No-Collapse Performance Level / Range (ED/NC), respectively. These performance levels/ranges are compatible with those defined in *ASCE 41-06* [ASCE 2007].

Performance Objectives

Performance of tall buildings in *Normal Occupancy Class* (residence, hotel, office building, etc.) is identified to be in *Minimum Damage / Uninterrupted Occupancy Performance Range (MD/UO)* under an (E1) level earthquake, in *Controlled Damage / Life Safety Performance Range (CD/LS)* under an (E2) level earthquake, and in *Extensive Damage / No-Collapse Performance Range (ED/NC)* under an (E3) level earthquake.

Performance of tall buildings in *Special Occupancy Class* (health, education, public administration buildings, etc.) is identified to be in *Minimum Damage/Uninterrupted Occupancy Performance Range (MD/UO)* under an (E2) level earthquake, and in *Controlled Damage/Life Safety Performance Range (CD/LS)* under an (E3) level earthquake.

Upon the preference of the owner, higher performance objectives may be identified for tall buildings in *Normal Occupancy Class* (residence, hotel, office building, etc.) with respect to those defined above.

ANALYSIS AND MODELING REQUIREMENTS

Analysis Requirements

Both linear and nonlinear analysis procedures are specified in the draft code appropriately as indicated in Table 1. In the linear elastic analysis of tall buildings required for design stages described in the section below, the response spectrum analysis (RSA) procedure shall be employed. The complete quadratic combination (CQC) rule shall be used for modal combination to be applied to each response quantity of interest. Sufficient number of modes to be included in RSA shall be determined according to modal story shears.

In nonlinear analysis, a minimum seven earthquake ground motion sets shall be used in accordance with the section above and the acceleration records in the two perpendicular directions shall be applied simultaneously along the principal axes of the structural system. Subsequently, directions of acceleration records shall be rotated by 90^o and the analysis shall be repeated. Design basis seismic demands shall be calculated as the average of results obtained from the minimum 2*7 = 14 analyses.

Modeling Requirements

Modeling of frame elements shall be made with frame finite elements in linear analysis. Modeling in nonlinear analysis can be made with plastic sections (plastic hinges) in the framework of lumped plasticity approach or through fiber elements in the framework of distributed plasticity approach. Regarding the plastic hinge length, an appropriate empirical relationship may be selected from the literature, subject to approval of the *Independent Review Board*. In nonlinear analysis, alternative modeling approaches may be followed upon the approval of *Independent Review Board*. In linear and nonlinear models of steel frames, shear deformation in the beam-column panel zone shall be considered.

Effective bending rigidities shall be used for reinforced concrete frame elements with cracked sections. In linear analysis, modeling of reinforced concrete walls and their parts shall be made with shell finite elements. In order to be consistent with the effective bending rigidities of the frame elements with cracked sections, elastic modulus of shell elements can be reduced accordingly.

Table 1 Performance-based design stages of tall buildings.

Design Stage	Design Stage I–A	Design Stage I–B	Design Stage II	Design Stage III
Design Type	Prelim. Design (dimensioning)	Design	Verification	Verification
Earthquake Level	*Normal class buildings:* (E2) earthquake	*Normal class buildings:* (E2) earthquake	*Normal class buildings:*(E1) earthquake	*Normal class buildings:* (E3) earthquake
	Special class buildings: (E3) earthquake	*Special class buildings:* (E3) earthquake	*Special class buildings:* (E2) earthquake	
Performance Objective	Life Safety	Life Safety	Uninterrupted Occupancy	No-Collapse
Analysis Type	3-D linear response spectrum analysis	3-D nonlinear time-history analysis	3-D linear response spectrum analysis	3-D nonlinear time-history analysis
Structural System Behavior Coefficient	$R \leq 7$	–	$R = 1.5$	–
Story Drift Ratio Limit	% 2	% 2.5	% 1	% 3.5
Section Stiffness in R/C Frame Members	Effective stiffness (from Turkish Seismic Design Code 2007)	Effective stiffness (from moment-curvature analysis)	Effective stiffness (from moment-curvature analysis)	Effective stiffness (from moment-curvature analysis)
Material Strengths	Characteristic strength	Expected strength	Expected strength	Expected strength
Acceptance Criteria	Strength and story drift ratio	Strains & story drift ratio	Strength & story drift ratio	Strains & story drift ratio

In modeling reinforced concrete walls and their parts for nonlinear analysis, fiber elements or alternative modeling options may be used in the framework of distributed plasticity approach, subject to approval of the Independent Review Board. Shear stiffnesses of reinforced concrete walls shall be considered.

In the preliminary design stage described below, design strengths, (f_d), of concrete, reinforcing steel and structural steel are defined as the relevant characteristic strengths, (f_k), divided by material safety factors. In other design and verification stages, expected strengths, (f_e), shall be used as design strengths without any material safety factors. The following relationships may be considered between the expected and characteristic strengths:

Concrete	$f_{ce} = 1.3 f_{ck}$
Reinforcing steel	$f_{ye} = 1.17 f_{yk}$
Structural steel (S 235)	$f_{ye} = 1.5 f_{yk}$
Structural steel (S 275)	$f_{ye} = 1.3 f_{yk}$
Structural steel (S 355)	$f_{ye} = 1.1 f_{yk}$

In floor planes where abrupt changes in the lateral stiffnesses of vertical structural elements occur (as in podium floors), a special care shall be paid for the arrangement of transfer floors with sufficient in-plane stiffness and strength. The stiffness of the foundation and the soil medium shall be considered by appropriate models to be approved by the *Independent Review Board*. When needed, nonlinear behavior of soil-foundation system may be taken into account in design stages as described below.

PERFORMANCE-BASED SEISMIC DESIGN STAGES OF TALL BUILDINGS

A four-stage analysis and design procedure is specified in the draft code as described in the following and outlined in Table 1. The preliminary design (Stage I–A) for the purpose of dimensioning is based on the traditional code design approach for Controlled Damage/Life Safety performance objective under (E2) level earthquake, which the design engineer is already familiar with. This design is then finalized in Stage I–B for the same performance objective with performance-based design procedures based on nonlinear analysis. The other two stages (Stages II and III, respectively) are intended for the verification of design for Minimum Damage/Uninterrupted Occupancy performance objective under (E1) level earthquake and for Extensive Damage/No-Collapse performance objective under (E3) level earthquake.

Design Stage (I–A): Preliminary Design (Dimensioning) with Linear Analysis for Controlled Damage/Life Safety Performance Objective under (E2) Level Earthquake

This design stage aims at preliminary dimensioning for *Controlled Damage/Life Safety* performance objective A linear analysis shall be performed in the framework of *Strength-Based Design* approach with reduced seismic loads similar to Chapter 2 of current Turkish Seismic Design Code (Ministry of Public Works and Settlement 2007) under (E2) level earthquake for *Normal Occupancy Buildings* and under (E3) level earthquake for *Special Occupancy Buildings*. The base shear to be considered in the preliminary design shall not be less than the value given by the following expression:

$$V_{t,\min} = 0.04\, S_{MS(D2)}\, W$$

where $S_{MS(D2)}$ represents the short-period spectral acceleration specified for (E2) level earthquake, and W is a weight representing the total building mass. All internal force quantities obtained from RSA shall be scaled such that the base shear calculated by the same procedure would be equal to the above-given value. The building preliminary design shall generally follow the requirements of the current Turkish Seismic Design Code [Ministry of Public Works and Settlement 2007].

Design Stage (I–B): Design with Nonlinear Analysis for Controlled Damage/Life Safety Performance Objective under (E2) Level Earthquake

The structural system of a tall building, which is preliminarily designed in Design Stage (I–A) using the strength-based design approach under (E2) level earthquake for *Normal Occupancy Buildings* or under (E3) level earthquake for *Special Occupancy Buildings*, shall be designed under the same level of earthquake for *Controlled Damage / Life Safety* performance objective with nonlinear analysis to be performed according to the requirements as stated above (see Table 1). Accidental eccentricity effects need not to be considered in this analysis. The seismic demands obtained as the average of the results of minimum 2*7=14 analysis shall be compared with the following capacities:

(a) Interstory drift ratio of each vertical structural element shall not exceed 0.025 at each story in each direction.
(b) Upper limits of concrete compressive strain at the extreme fiber inside the confinement reinforcement and the reinforcing steel strain are given in the following for reinforced concrete sections satisfying the confinement requirements:

$$\varepsilon_{cg} = 0.0135 \qquad ; \qquad \varepsilon_{s} = 0.04$$

(a) Deformation capacities of structural steel frame elements shall be taken from *ASCE 41-06* [ASCE 2007] for life safety performance objectives.
(b) Shear capacities of reinforced concrete structural elements shall be calculated from the current Turkish Seismic Design Code [Ministry of Public Works and Settlement 2007] using expected strengths given above.
(c) In the event where any of the requirements given in (a) through (d) above is not satisfied, all design stages shall be repeated with a modified structural system.

Design Stage (II): Design Verification with Linear Analysis for Minimum Damage/ Uninterrupted Occupancy Performance Objective under (E1) Level Earthquake

The tall building structural system, which is preliminarily designed in Design Stage (I–A) using the strength-based design approach under (E2) level earthquake for *Normal Occupancy Buildings* or under (E3) level earthquake for *Special Occupancy Buildings*, and subsequently designed in Design Stage (I–B) under the same earthquake level, shall be verified for *Minimum Damage/Uninterrupted Occupancy* performance objective under (E1) level earthquake for *Normal Occupancy Buildings* and under (E2) level earthquake for *Special Occupancy Buildings* with linear analysis to be performed according to requirements given in Table 1. Accidental eccentricity effects need not to be considered in this analysis.

Verification-basis internal forces shall be obtained as those calculated from linear elastic analysis divided by a factor of R_a = 1.5, irrespective of the type of the structural system. Those forces shall be shown not to exceed the strength capacities of cross sections calculated with expected material strengths given above. Interstory drift ratio of each vertical structural element shall not exceed 0.01 at each story in each direction. In the event where above conditions are not verified, all design stages shall be repeated with a modified structural system.

Design Stage (III): Design Verification with Nonlinear Analysis for Extensive Damage/No-Collapse Safety Performance Objective under (E3) Level Earthquake

The tall building structural system preliminarily designed in Design Stage (I – A) using the strength-based design approach under (E2) level earthquake for *Normal Occupancy Buildings* and subsequently designed in Design Stage (I–B) under the same earthquake level, shall be verified for *Extensive Damage / No-Collapse Safety* performance objective under (E3) level earthquake with nonlinear analysis to be performed according to requirements given in Table 1. Accidental eccentricity effects need not to be considered in this analysis.

The seismic demands obtained as definedvabove are the average of the results of minimum 2*7=14 analysis shall be compared with the following capacities:

(a) Interstory drift ratio of each vertical structural element shall not exceed 0.035 at each story in each direction.
(b) Upper limits of concrete compressive strain at the extreme fiber inside the confinement reinforcement and the reinforcing steel strain are given in the following for reinforced concrete sections satisfying the confinement requirements:

$$\varepsilon_{cg} = 0.018 \qquad ; \qquad \varepsilon_s = 0.06$$

(c) Deformation capacities of structural steel frame elements shall be taken from *ASCE 41-06* [ASCE 2007] for the collapse prevention performance objective.
(d) Shear capacities of reinforced concrete structural elements shall be calculated from the current Turkish Seismic Design Code [Ministry of Public Works and Settlement 2007[using expected strengths given above. In the event where any of the requirements given in (a) through (d) above are not satisfied, all design stages shall be repeated with a modified structural system.

CONCLUSIONS

The salient features of the Draft Seismic Design Code for Tall Buildings prepared for the Istanbul Metropolitan Municipality are summarized. The code is intended to be applied to buildings with 60 m height measured from the ground level excluding underground basements. It is based on performance-based design approach with multi-level performance objectives. Earthquake action is defined in terms of three earthquake levels for which contour maps are provided for Istanbul.

A four-stage analysis and design procedure, including a preliminary design stage is adopted as opposed to a two-stage procedure defined in recent documents of the same kind [LATBSDC 2008; PEER 2010]. The more detailed design procedure is intended for the transition period, during which structural designers are in the process of familiarizing with the analysis and design requirements of performance-based design.

The draft code has not been officially ratified yet and therefore not officially enforced as of this writing. However it has been positively responded by the tall building developers and designers, and voluntarily accepted as a performance-based seismic design guideline for tall buildings in Istanbul. It is expected that the Draft Seismic Design Code for Tall Buildings will provide a basis for the relevant design requirements to be included soon in the Turkish Seismic Design Code Code in the form of a dedicated chapter.

REFERENCES

Applied Technology Council (2010). Modeling and acceptance criteria for seismic design and analysis of tall buildings, *ATC-72-1*, Redwood City, CA.

American Society of Civil Engineers (2007). *Seismic Rehabilitation of Existing Buildings, ASCE 41 (*ASCE/SEI 41-06 plus Supplement 1*)*, Reston, VA.

Council on Tall Buildings and Urban Habitat (2008). *Recommendations for the Seismic Design of High-rise Buildings – A Consensus Document*, Seismic Working Group, Chicago, IL.

Istanbul Metropolitan Municipality (2008). *Istanbul Seismic Design Code For Tall Buildings, Draft Version IV*, Istanbul, Turkey.

Los Angeles Tall Buildings Structural Design Council (2005; 2008). *An Alternative Procedure for Seismic Analysis and Design of Tall Buildings Located in the Los Angeles Region – A Consensus Document*, Los Angeles, CA.

Ministry of Public Works and Settlement (2007). *Specification for Buildings to be Built in Seismic Zones*, Ankara, Turkey.

Pacific Earthquake Engineering Research Center (2010). Guidelines for performance-based Seismic design of tall buildings, version 1.0., *PEER Report 2010/05*, University of California, Berkeley, CA.

Structural Engineers Association of Northern California (2007). *Recommended Administrative Bulletin on the Seismic Design and Review of Tall Buildings Using Non-Prescriptive Procedures,* SEAONC Tall Buildings Task Group, San Francisco, CA.

THE EFFECTS OF ARCHITECTURAL REGULATIONS ON THE SEISMIC RESPONSE OF HIGH-RISE BUILDINGS IN TEHRAN

H. Shakib[1], M. Pirizadeh[2], A. Emadi[2], S. Shakib[3]

[1] School of Civil Engineering, Tarbiat Modares University, Tehran, Iran, [2] School of Civil Engineering, Tarbiat Modares University, Tehran, Iran, [3]School of Architecture, University College of Fine Arts, University of Tehran, Tehran, Iran

ABSTRACT

In many mega-cities such as Tehran, the architectural regulations for high-rise buildings construction were approved a few decades ago, limiting the vertical expansion and the total volume of the buildings. These rules bring such factors as zoning, daylight, skyscraper-form requirements, landscaping and built area density into consideration. These factors influence the structural form and configuration of tall buildings and may lead architects and structural engineers to design and construct vertically irregular high-rise buildings. In this paper, the general trends in the seismic behavior of these types of buildings is explored. Building code vertical irregularity requirements and their limitations for seismic design and construction of high-rise buildings are discussed and compared. Also, the variation of the response modification factor and comparison of nonlinear static analysis and rigorous nonlinear dynamic analysis in predicting the seismic demands in 9-story setback buildings are investigated. The results show that the Iranian seismic code regulations for geometric vertical irregularities need to be revised.

INTRODUCTION

The construction of high-rise buildings began in early nineteenth century concurrent with the evolution of the lightweight building frame system and particularly steel structures in industrialized countries. Such buildings demanded the introduction of modern service technologies such as elevators, central ventilation, fire extinguishers, and water pumping systems. At that point in time, high-rise building construction became an important component in the building construction industry. Population growth and the need to build sufficient residential units led countries like Japan, Hong Kong, and Malaysia to follow the same path as industrialized countries. The first high-rise built in Iran was a 10-story building built in 1949 in downtown Tehran. The first residential high-rise complex building was Behjat-Abad, which was built in Tehran in 1970. Upon modification of tax laws, the construction of 20-story Saman residential building complex began in 1970. In this building, prefabricated elements were used for the first time. In the 1970s, residential complex buildings were mostly built in the North and North-West of Tehran. Meanwhile, many buildings for commercial and official use were built in the central and Northern regions of the city. Following the Islamic revolution, there was a hiatus in high-rise building construction for roughly ten years. A new boom of high-rise building construction began in the late 1990s, causing a rise in the price of land in Tehran. Since 1990, architectural regulations led the architects and structural engineers to design and construct irregular high-rise buildings. During this period many irregular buildings have been constructed in Tehran.

The seismic performance of irregular structures has been studied by many researchers. Al-Ali and Krawinkler [1998] investigated the effect of different irregularities on seismic response of structures. They pointed out that the mass irregularity has the lowest influence, whereas strength has more influence than stiffness on the seismic response. They also concluded that the combination of strength and stiffness irregularity has the most influence on the seismic demand. Chintanapakdee and Chopra [2004] studied the accuracy of modal pushover analysis (MPA) in irregular frames, demonstrating that the accuracy of MPA does not deteriorate in the presence of irregularity in the middle or upper stories, but in frames with stiff, strong, stiff and strong first story the MPA is less accurate in predicting the seismic demands. Mazzolani and Piluso [1996] presented an extensive numerical investigation aimed at evaluating the difference in the behavior factor of setback and corresponding regular frames. They concluded that the presence of setbacks does not adversely affect the seismic response, in other words, there was no need for significant decrease of the behavior factor. Romao, et al. [4] showed that structures with setback have appropriate seismic performance and code requirements are suitable for such buildings. In another study performed by Athanassiadou and Bervanakis [2005], two reinforced concrete (RC) frames with setbacks were designed according to Eurocode8 [2003] and that the demand estimated by code was appropriate. Duan and Chandler [1995] stated that neither linear static nor spectral analysis is enough for buildings with setbacks because of the inefficient prediction damage concentrated in the components near the setback level. Khoury, et al. [2005] showed that higher modes have a significant effect on the response of setback buildings, especially in torsion mode, emphasizing that the forgoing investigations on setback buildings must be performed on full-plan asymmetric structures. Fajfar and et al. [2005] showed that the conventional nonlinear static procedure (NSP) is not sufficient for asymmetric buildings and proposed a modification factor to adjust the results of NSP. Athanassiadou [2008] also evaluated the accuracy of NSP in RC frames with setback, showing that NSP does not predict satisfactorily the seismic demands in upper stories. In most of these studies, time history analyses were performed for an ensemble earthquake record set. However, Fragiadakis et al. [2006] showed that the effects of vertical irregularities are highly dependent on the ground motion records.

Pirizadeh and Shakib [2010] evaluated the seismic response of setback buildings subjected to random earthquake excitations by means of the power spectral density analysis (PSD), where the effects of irregularities can be isolated from any record to record variability. In this study, 10-story one-sided setback steel moment frame structures were modeled three dimensionally. Then, the root-mean-squared responses of structures for different setback ratios were compared with a regular structure. Based on the results of this study, the distribution pattern of story drift, velocity, and acceleration over the height of structure varied, depending on the tower of setback structures with respect to regular structure. However, these variations were much more pronounced as the area setback ratios decreased. Moreover, the PSD curves of setback structure's response had a wider frequency content relative to regular structure and a lower peak appeared at the frequency that may correspond to the torsional mode of setback structures.

Based on these studies, it is essential for structural engineers to obtain a better understanding of the seismic response of vertical irregular structures. This paper reviews the architectural rules that influence tall building configurations, which may lead to forming the vertical irregularity in structures. Next, the definition and limitation of vertical irregularities for structural systems in different seismic codes are discussed. Also, in order to check the adequacy of the Iranian seismic code, the variation of response modification factor and comparison of NSP and rigorous nonlinear dynamic analysis (NDP) for predicting the seismic demands for 9-story buildings with setbacks are investigated.

ARCHITECTURAL IRREGULARITY REGULATIONS

In the 1920s because of urban problems resulting from high-rise building construction in many worldwide cities like San Francisco, some architectural rules were set to limit the vertical expansion of the buildings. These rules were based on defining an inclined vertical line in relation to the road axis (Figure 1), expecting to achieve the four primary goals: (i) to provide daylight and ventilation for the buildings and the adjacent streets; (ii) to prevent the buildings from overshadowing one another; (iii) to provide optimal use of solar energy; and (iv) to preserve the visual integrity of the skyline.

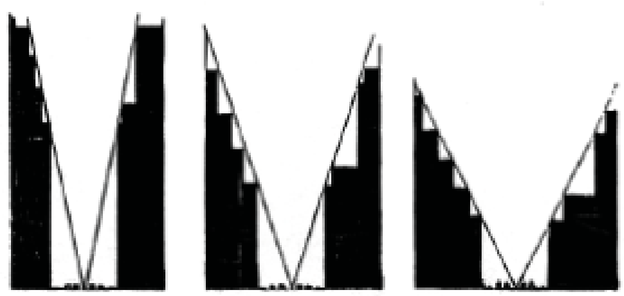

Figure 1 Limitation of the vertical expansion of the buildings.

Since 1990, unplanned high-rise building constructions in Tehran led to architectural, cultural, and environmental problems. In 1998, the Urban Development and Architectural High Council (UDAHC) of Iran passed new rules for the construction of buildings 6-story and higher. Keeping such factors as density and green landscaping in mind, observing these rules results in defining a pyramidal space frame for each piece of land beyond which the building cannot go (Figure 2). The details of these space frames for the detached and attached buildings are as follows [UDACH 1983]:

According to these rules, detached buildings are defined as the buildings that stand on a distance from the neighboring buildings on all four sides with exception of the ground floor. In this type of building the slant of the pyramid frame faces to the street axis and the northern and southern edges in the not adjoining the passage is equal to 200 % (the height 2 to 1 horizon) and the slant of pyramid frame faces from the east and west direction when they are not adjacent to the passage, is equal to 700% (the height 7 to 1 horizon) as shown in Figure 3. According to these principles east and west land pieces are considered as detached buildings, and the slant of the pyramid on the northern and southern edges of land and from axis of road is equal to 200% (the height 2 to 1 horizon).

Attached buildings (row) are adjacent to the neighboring buildings on the east and west directions. The slant of the pyramid sides in these buildings is different in the northern and southern land pieces. In the northern pieces, the pyramid plan from the axis of road is equal to 200 % (the height 2 to 1 horizon) and in the northern of land; the slant is 60% (the height 1 to 1.64 horizon) where this slope is drawn from a line parallel of 10 m from northern edge (Figure 4). In the southern land pieces, the slant of pyramid plan from the opposite side of road is equal to 60% (height 1 to 1.64 horizon) and slope from the southern of land, is equal to 200% (height 2 to 1) . Note that in the row buildings the space frame is perpendicular in two sides on the land surface.

As mentioned above, a pyramid shape was defined for 6-story buildings and higher, and the required landscaping is calculated by Equation (1). Based on this equation, the density of the built area in the enclosed space frames depends on the provision of the area for landscaping. Therefore, in order to obtain the maximum density for the building and to observe the space frame principles, designers in Tehran moved toward designing pyramid-shaped high-rise buildings with setbacks (Figure 5).

In the Tehran Comprehensive Plan (TCP) [UDAHC 2007], the construction of high-rise buildings is limited to specific location provided that seismic site hazard and environmental studies have been conducted. However, in the revised TCP—currently pending final approval—it is stated that the architectural and structural regulations receive the endorsement of the UDAHC. Due to the architectural guidelines that may form the pyramid-shaped buildings with setbacks, it is essential to evaluate the seismic behavior of this type of buildings.

$$A_{Landscaping}= \frac{0.42 \times A \times k \times T}{\sqrt{N}} \tag{1}$$

where $A_{Landscaping}$= the area that needed for landscaping, A= total built area of building, k = coefficient of air pollution , T = coefficient for non-residential buildings, and N= number of stories.

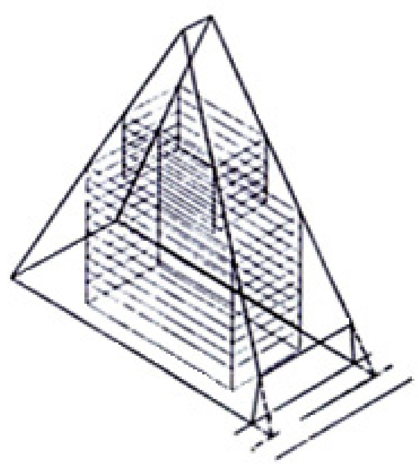

Figure 2 Pyramidal space frame for building.

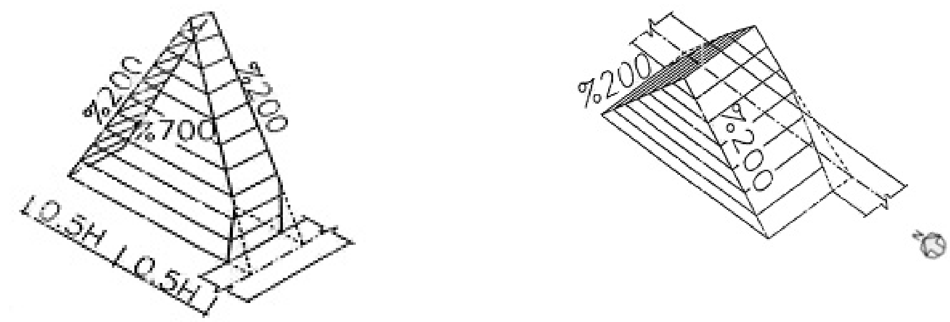

(a) (b)

Figure 3 **Pyramidal space frame for detached buildings: (a) N-S land pieces; and (b) E-W land pieces.**

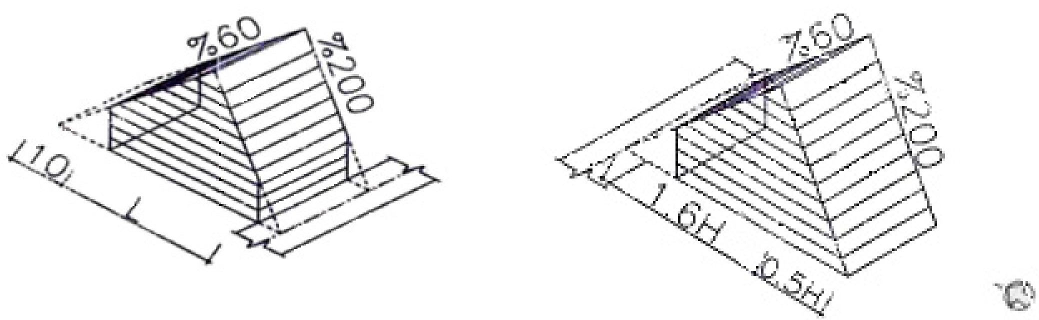

(a) (b)

Figure 4 **Pyramidal space frame for attached buildings: (a) Northern pieces; and (b) Southern pieces.**

Figure 5 **A sample of tall pyramid buildings in Tehran city.**

STRUCTURAL VERTICAL IRREGULARITY REGULATIONS

In general, vertical irregularities can be classified as non-geometric and geometric irregularities (Figure 6). In the geometric irregularity, the plan dimensions suddenly change over the height of building but the non-geometric irregularity, having a non-uniform distribution of seismic lateral resisting properties (such as mass, lateral stiffness, strength) individually or in combination throughout the height of building. Most seismic codes enclose criteria for vertical irregular structures. As shown in Table 1, seismic codes such as UBC 97 [ICBO 1997], ASCE 7-05 [ASCE 2006], the Iranian standard [BHRC 2010], and the Indian standard [NSBI 2002] focus on non-geometric vertical irregularity rather than geometric. However, the Eurocode8 [2003] explicitly defines the setback ratio limits (Figure 7), which is the one main type of geometric vertical irregularity. In general, seismic code regulations attempt to prevent the problem of discontinuity (the abrupt change of lateral load resisting properties over the height of structure).

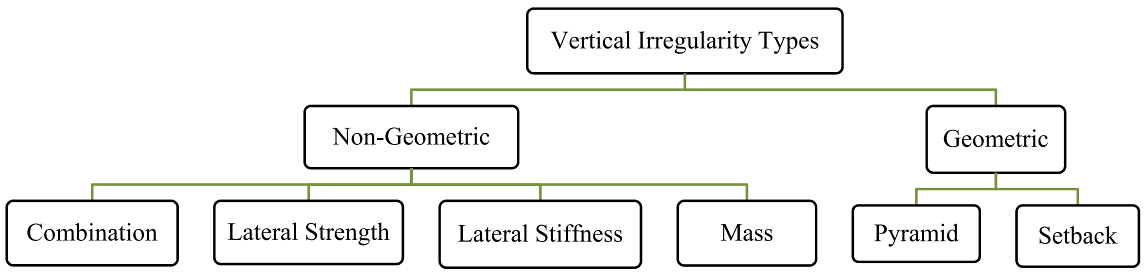

Figure 6 Vertical structural irregularity classification.

The code requirement also focuses on identifying the vertical irregularity conditions for which the equivalent lateral force (ELF) analysis method can be used. When irregularity exceeds certain nominal limit, complete dynamic analysis is a necessity according to most seismic codes. These limitations in the different seismic codes are compared in Table 2. Note, some codes such as Eurocode [2003] do not permit ELF analysis method for vertical irregular buildings, and most of seismic codes limit this method for mid-rise and high-rise vertical irregular structures.

Table 1 Comparison of vertical irregularity definition regulations in the different seismic codes.

Seismic Code	Vertical Structural Irregularity Types			
	Mass (Weight)	Stiffness (Soft Story)	Strength (Weak Story)	Geometric
UBC 97	$\frac{\textit{Effective mass of any story}}{\textit{Effective mass of adjacent story}} > 150\%$	$\frac{\textit{Lateral stiffness of any story}}{\textit{Lateral stiffness of story above}} < 70\%$ $\frac{\textit{Lateral stiffness of any story}}{\textit{Average stiffness of three stories above}} < 80\%$	$\frac{\textit{Lateral strength of any story}}{\textit{Strength of story above}} < 80\%$	$\frac{\text{Horizontal dimensions of lateral force resisting system in any story}}{\text{Adjacent story}} > 130\%$ An in-plane offset of the lateral-load-resisting elements greater than the length of those elements

ASCE7-05; NEHRP (FEMA-450)	$\frac{\text{Effective mass of any story}}{\text{Effective mass of adjacent story}} > 150\%$	Such as UBC97+ Extreme irregularity: $\frac{\text{Lateral stiffness of any story}}{\text{Lateral stiffness of story above}} < 60\%$ $\frac{\text{Lateral stiffness of any story}}{\text{Average stiffness of three stories above}} < 70\%$	Such as UBC97 + Extreme irregularity: $\frac{\text{Strength of any story}}{\text{Strength of story above}} < 65\%$	$\frac{\text{Horizontal dimensions of lateral force resisting system in any story}}{\text{Adjacent story}} > 130\%$ An in-plane offset of the lateral-load-resisting elements greater than the length of those elements or there exists a reduction in stiffness of the resisting element in the story below.
Eurocode	Abrupt changes in the mass of the individual stories from the base to the top (the amount is not declared)	Abrupt changes in the stiffness of the individual stories from the base to the top (the amount is not declared)	Abrupt changes in the strength of the adjacent stories	One sided setback : $\frac{\text{Setback at any floor}}{\text{Previous plan dimension}} > 10\%$ $\frac{\text{Sum of setbacks in all stories}}{\text{Plan dimension at first story}} > 30\%$ Two sided gradual symmetric setback: $\frac{\text{Setback at any floor}}{\text{Previous plan dimension}} > 20\%$ Two sided single setback : $\frac{\text{Setback at floor within the lower 15\% of the total height}}{\text{Previous plan dimension}} > 50\%$ $\frac{\text{Setback at floor above the lower 15 \% of the total height}}{\text{Previous plan dimension}} > 20\%$
Iranian Standard 2800	$\frac{\text{Mass of any story}}{\text{Mass of adjacent story}} > 150\%$	Such as UBC97	Such as UBC97	
Indian Standard	$\frac{\text{Effective mass of any story}}{\text{Effective mass of adjacent story}} > 200\%$	Such as ASCE7-05	Such as ASCE7-05	$\frac{\text{Horizontal dimensions of lateral force resisting system in any story}}{\text{Adjacent story}} > 150\%$ In-plane discontinuity in vertical elements resisting lateral force.

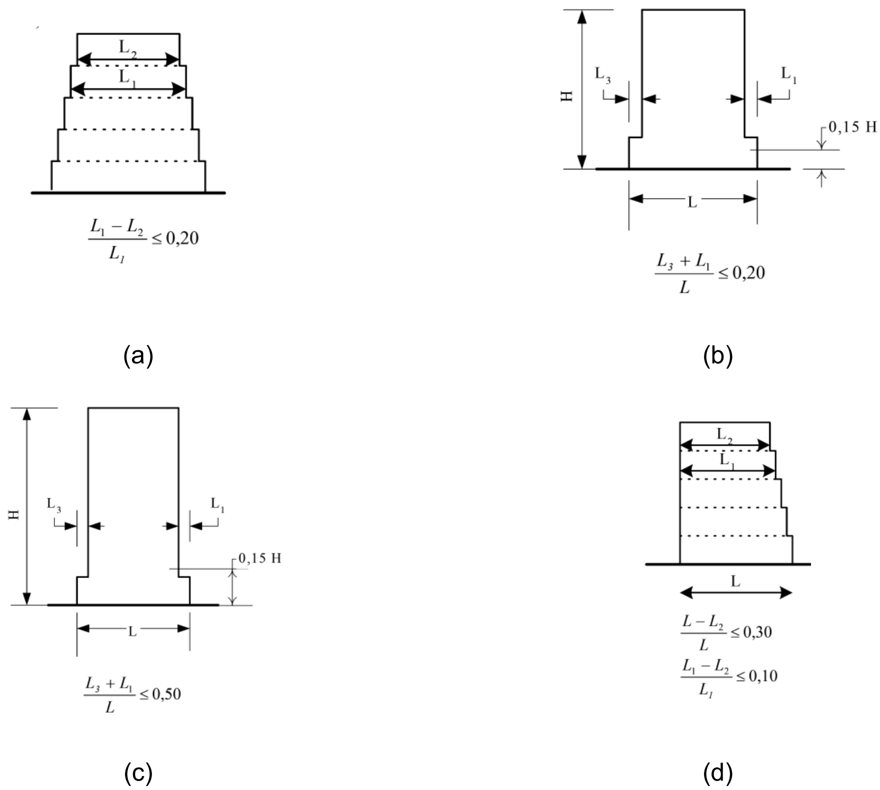

Figure 7 Eurocode [18] criteria for regularity of buildings with setbacks: (a) two-sided gradual symmetric setback: (b) and (c) two sided single setback below and above 15% of building height; and (d) one sided setback.

Table 2 Comparison of the different seismic codes regulations for limiting the simplified static analysis method in the vertical irregular structures.

Seismic Code	Allowable vertical irregular structures for simplified static analysis (equivalent lateral force analysis) method
UBC 97	All structures in Seismic Zone 1 and in Occupancy Categories 4 and 5 in Seismic Zone 2. Irregular structures not more than five stories or 65 feet(19. 8 m) in height. Structures having a flexible upper portion supported on a rigid lower portion where both portions of the structure considered separately can be classified as being regular, the average story stiffness of the lower portion is at least 10 times the average story stiffness of the upper portion and the period of the entire structure is not greater than 1.1 times the period of the upper portion considered as a separate structure fixed at the base.
ASCE7-05 /NEHRP (FEMA-450)	All structures in Seismic Design Category B and C. All structures with $T < 3.5T_s$ with strength irregularity or with in-plane discontinuity in vertical lateral force resisting in Seismic Design Category D, E and F.
Eurocode	None of irregular structures is permitted.
Iranian standard 2800	Irregular structures not more than five stories or 18 meters in height. Structures having a flexible upper portion supported on a rigid lower portion where both portions of the structure considered separately can be classified as being regular, the average story stiffness of the lower portion is at least 10 times the average story stiffness of the upper portion and the period of the entire structure is not greater than 1.1 times the period of the upper portion considered as a separate structure fixed at the base.
Indian standard	Irregular buildings, lesser than 40 m in height in Zones II and III. Irregular buildings, lesser than 12m in height in Zones IV and V.

SEISMIC BEHAVIOR OF IRREGULAR STRUCTURES

As was mentioned in the literature review, some studies indicate that the codes are adequately address buildings with setbacks, while some studies claim they do not. In order to assess the Iranian seismic building criteria code on this issue, a number of three-dimensional buildings with eccentric setbacks in one and two directions were considered. These models were subjected to an ensemble of nine ordinary (i.e., without near-fault effects) earthquake ground motions. All nine-story buildings with strong column and weak beams composed of special steel moment frames satisfy the standard 2800 [BHRC 2010] requirements. Different shapes of eccentric setbacks were created in order to consider a wide range of rational cases. The elevation view of the models with eccentric setbacks in one and two directions is presented in Figure 8. In numbering, the structures suffix (d) means the existence of setback in two directions. The variation of response modification factor and the accuracy of the pushover analysis were checked in these models.

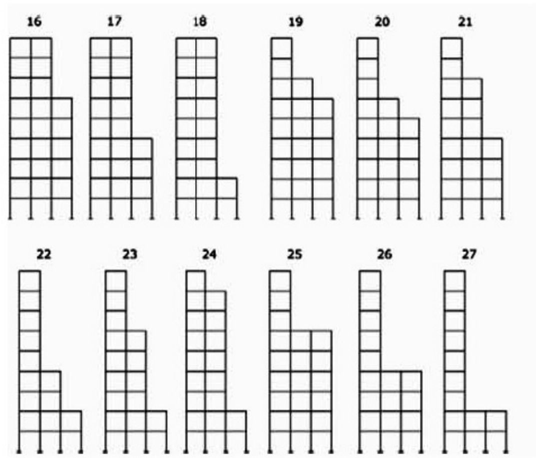

Figure 8 Elevation of models.

Some design codes (as does the Iranian code) consider a constant value for the response modification factor (R) according to the type of structural system without any consideration of configuration and height of structure. In order to determine R, ATC-19 gives the following equation:

$$\mathrm{R} = R_s R_\mu R_r \tag{2}$$

where R_s is the strength factor, R_μ is ductility factor, and R_r is the redundancy factor.

In Figure 9, R values are presented for all models. In both charts, R for regular building (the reference building) is also shown to observe the variation of R by creating setbacks (R_n means the R_μ was calculated from Newmark equation). Note that the existence of setback causes some changes in R values compared to the regular building. Variations in R do not show a consistent pattern, which is mainly due to the complicated behavior of structures.

The accuracy of pushover analysis is also estimated in comparison with rigorous nonlinear dynamic analysis. The majority of structures subjected to conventional NSP [ATC 2005] estimates the target displacement with reasonable accuracy, but underestimate the target displacement in those structures where their responses are complicated, i.e., where load does not match displaced shape according to [ATC 2005] *FEMA-440*. Some examples of such structures are shown in Figure 10 [Ehmadi et al. 2010].

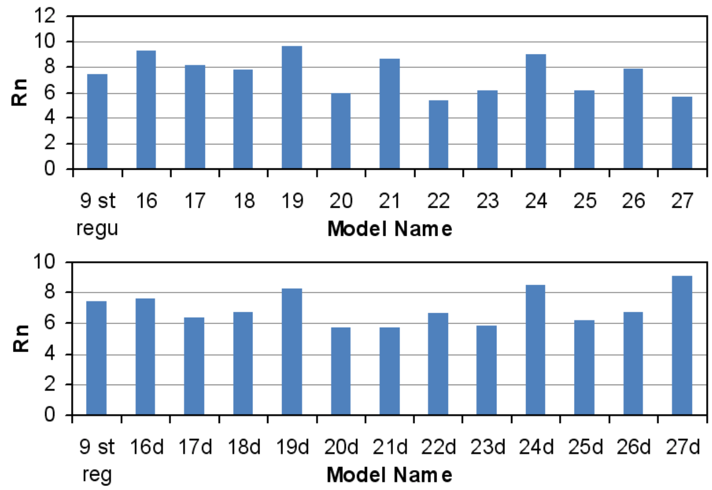

Figure 9 **Response modification factor for all 9-story buildings with eccentric setbacks in one and two directions.**

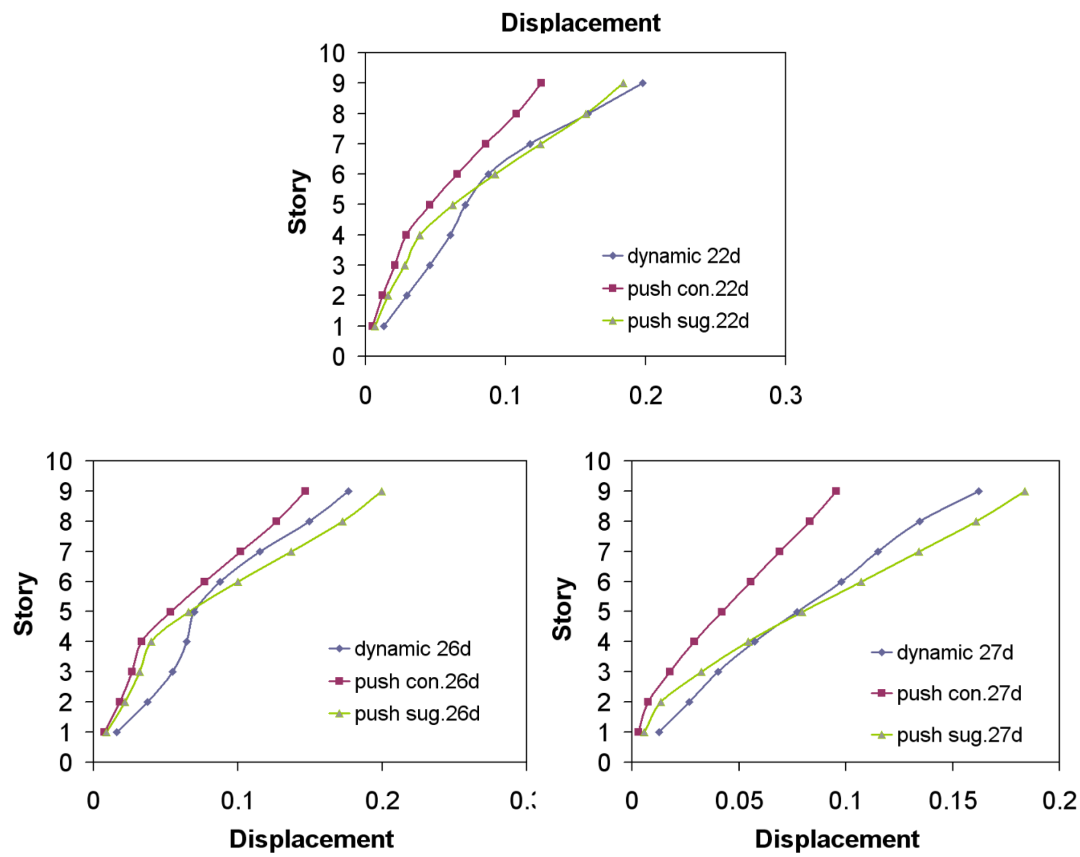

Figure 10 **Comparison between NDP (dynamic), conventional NSP (push con) and the suggestion method (push sug) that modify the relationship of *Sa* and *V*, in determination of displacement in some of the structures.**

According to Figure 10, by modifying the relationship between spectral acceleration and base shear, the displacements in upper stories can be accurately calculated albeit overestimated, while the seismic demands in lower stories are underestimated [Ehmadi et al. 2010].

Generally this underestimation is intensified when an abrupt setback is created because of the damage concentration in one story. In the buildings with setbacks in two directions, the underestimation is greater. Obviously, it is because of the pattern of lateral load, which is conforming to modal distribution obtained from a linear analysis; the codes suggest at least two patterns for lateral load.

In order to investigate the effect of lateral load pattern, the invariant load pattern is also used. In Figure 11, some examples of calculation of seismic demand with two patterns of lateral load (modal and invariant) are illustrated. The target displacements were calculated according to the modified method. Although the results in lower story were more satisfactory—and in some structures like 22 the underestimation was rectified—in some structures (like 27, 22d, 27d) the problem of underestimation was not rectified. It is inherent weak point of NSP for determining all damage modes.

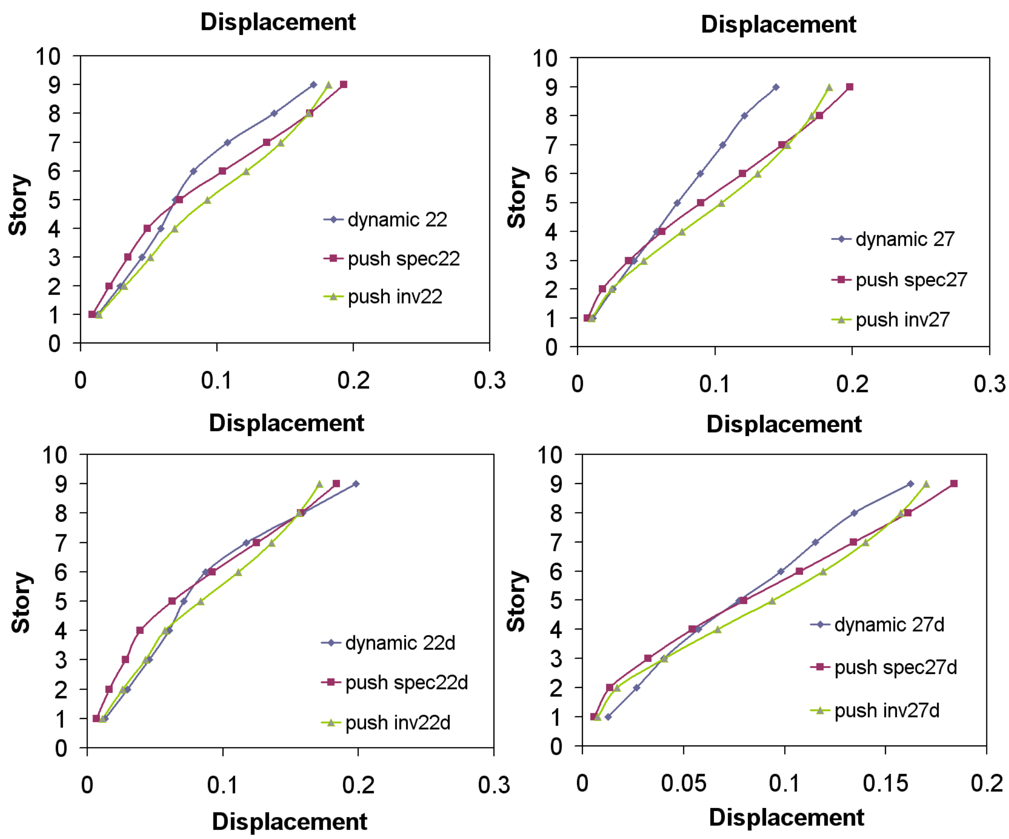

Figure 11 Comparison between NDP (dynamic) and modified NSP by using spectral lateral load pattern (spec) and invariant lateral load pattern (inv) in determination of displacement in some of the structures.

CONCLUSIONS

Since 1990, architectural regulations have been implemented in Tehran for high-rise buildings. These regulations were adopted to provide the necessary daylight and ventilation for buildings and adjacent streets, to prevent the buildings from overshadowing one another, to make optimal use of solar energy, and to preserve the visual integrity of the skyline. The application of these regulations on the design of high-rise buildings was done so without sufficient attention to the seismic structural demands. As a result, many vertical irregular buildings have been constructed during recent decades. Therefore, a comprehensive evaluation of the seismic behavior of such buildings is an important concern. In this study, some of the studies made by different researchers and the seismic code criteria for the vertical irregular structures were reviewed. Also, the adequacy of Iranian seismic code in estimating the seismic demands in 9-story buildings with setbacks was investigated. Some of the conclusions are as the following:

1. The literature review of the studies show that the vertical irregular buildings are much more vulnerable to seismic loading compared to regular buildings. As Tehran is situated in a high seismic risk level region, questions may arise regarding how this type of structure may perform when subjected to a strong ground shaking.
2. A review of seismic codes regulations for geometric irregularities has results in the conclusion that it is essential to revise the vertical irregularity regulations in the Iranian Seismic Building Code. A clear definition of setback ratio limits can prevent the discontinuity problems and minimize the torsional response of these structures.
3. A study of 9-story buildings with setbacks compared to regular buildings demonstrated that variations in response modification factor (R value) is expected; considering one R value without any attention to shape of structures is not justifiable.
4. Displacements in upper stories can be adequately estimated albeit overestimated by modification of the relationship between the spectral acceleration (S_a) and base shear (V). But in all cases (even regular buildings) drift in upper stories is underestimated in nonlinear static analysis (NSP). The deviation becomes more pronounced in the buildings with setback in two directions.

REFERENCES

Al-Ali AAK, Krawinkler H (1998). Effects of vertical irregularities on seismic behavior of building structures, *John A. Blume Earthquake Engineering Center*, Stanford University, Stanford, CA, pp. 130-198.

American Society of Civil Engineers.(2006). Minimum design loads for buildings and other structures, ASCE 7-05, Reston, VA.

Applied Technology Council (2005). Improvement of nonlinear static seismic analysis procedures, *FEMA-440/ATC-55*, Redwood City, CA.

Athanassiadou C (2008). Seismic response of R/C plane frames irregular in elevation, J. Engng. Struct., 30:1250-1261.

Athanassiadou C, Bervanakis S (2005). Seismic behavior of R/C buildings with setbacks designed to EC8, Proceedings, 4th European Workshop on the Seismic Behavior of Irregular and Complex Structures, Thessaloniki, Greece.

Building and Housing Research Center (2010). *Iranian Code of Practice for Seismic Resistant Design of Buildings* (*Standard No. 2800-05*), 3rd ed., Iran.

Chintanapakdee C, Chopra AK (2004). Seismic response of vertically irregular frames: Response history and modal pushover analyses, *J. Struct. Engng.,* 130(8):1177-1185.

Duan XN, Chandler AM (1995). Seismic torsional response and design procedures for a class of setback frame buildings, *Earthq. Engng. Struct. Dyn.,* 24:761–77.

Emadi A, Shakib H, Aghakouchak A (2010). Seismic demand and pushover analysis evaluation in setback buildings, *Earthq.* Spectra (submitted for review).
European Committee for Standardization (2003). *Eurocode 8: Design of Structures for Earthquake Resistance-Part 1: General rules, Seismic Actions and Rules for Buildings*, Draft 6.
Fajfar P, Marusic D, Prus I (2005). Torsional effects in the pushover-based seismic analysis of buildings, *J. Earthq. Engng*., 9(6):831-854.
Fragiadakis M, Vamvatsikos D, Papadrakakis M (2006). Evaluation of the influence of vertical irregularities on the seismic performance of a nine-storey steel frame, *Earthq. Engng. Struct. Dyn.,* 35(12):1489-1509.
International Conference of Building Officials (1997). *Uniform Building Code: Structural Design Requirements*, Vol. 2. Whittier, CA
Khoury W, Rutenberg A, Levy R (2005). On the seismic response of asymmetric setback perimeter-frame structures, *Proceedings*, 4th European Workshop on the Seismic Behavior of Irregular and Complex Structures, Thessaloniki, Greece.
Mazzolani FM, Piluso V (1996). *Theory and Design of Seismic Resistant Steel Frames*, FN & SPON, an Imprint of Chapman & Hall.
National Standard Body of India (2002). Criteria for earthquake resistant design of structures, *IS 1893*, Fifth Revision.
Romeo X, Costa A, Delgado R (2004). Seismic behavior of reinforced concrete frames with setbacks, *Proceedings*, 13th World Conference on Earthquake Engineering, Vancouver, Canada.
Pirizadeh M, Shakib H. (2010). Response of setback frame buildings due to seismic random vibration analysis, *Proceedings*, 14th Symposium on Earthquake Engineering, Indian Institute of Technology, Roorkee.
Urban Development and Architectural High Countril (1983). *Tehran Tall Buildings-Regulations and Zoning Requirements*, Iran.
Urban Development and Architectural High Council (2007). *Tehran Comprehensive Plan* , Iran

ASSESSMENT OF EARTHQUAKE RISK IN ISTANBUL

M. B. Demircioglu, Karin Sesetyan, and M. Erdik

ABSTRACT

Seismic risk can be integrated with components of seismic hazard, physical and social elements exposed to risk, and their respective vulnerabilities and fragilities. Earthquake hazard assessment gives the probability that a certain parameter of ground motion such as MMI, PGA, spectral acceleration, or, more generally, of the seismic process that will be surpassed within a lifetime period. The population, structures, utilities, systems, and socio-economic activities constitute the "Elements at Risk" in urban areas. The physical elements are the built environment such as buildings, lifelines, and the demographic data represent the social elements at risk. There exist numerous studies on the appropriate procedures for the assessment of earthquake risk in Istanbul [IBB-JICA 2002; BÜ- ARC 2002; BU-Munich-Re, IBB-OYO-GRM-BU 2009]. Currently, for the estimation of earthquake losses in the Euro-Mediterranean region, the JRA-3 component of the EU FP6 Project entitled "Network of Research Infrastructures for European Seismology, NERIES" has developed a methodology (which was coded into software called ELER). Recently, ELER methodology and software has been utilized for the assessment of the seismic risk in the Istanbul Province in connection with the "İstanbul'un Olası Deprem Kayıpları Tahminlerinin Güncellenmesi İşi–Updating of the Probabilistic Earthquake Losses in Istanbul Province" of Istanbul Metropolitan Municipality" conducted by OYO International and GRM under the supervision of KOERI [IBB-OYO-GRM-KOERI, 2009].

INTRODUCTION

Generally, seismic risk can be integrated with components of seismic hazard, physical, and social elements exposed to risk and their respective vulnerabilities, and fragilities. Earthquake hazard assessment gives the probability that a certain parameter of ground motion such as MMI, PGA, spectral acceleration, or, more generally, of the seismic process that will be surpassed within a lifetime period. The population, structures, utilities, systems, and socio-economic activities constitute the "Elements at Risk" in urban areas. The physical elements are the built environment such as buildings, lifelines, and the demographic data represent the social elements at risk. Vulnerability is defined as the degree of loss to a given element at risk, or a set of such elements resulting from the occurrence of a hazard. Vulnerability functions (or fragility curves) of an element at risk represent the probability that its response to earthquake excitation exceeds its various performance limit states based on physical and socio-economic considerations. For a population of buildings exposed to earthquake hazard, the vulnerability relationships relate the probability of exceedence of multiple damage limit states (or being in certain damage states) to given measures of the ground motion severity.

There exist numerous studies on the appropriate procedures for the assessment of earthquake risk in Istanbul [IBB-JICA 2002; BÜ-ARC 2002; BU-Munich-Re, IBB-OYO-GRM-BU 2009). Currently, for the estimation of earthquake losses in the Euro-Mediterranean region, the JRA-3 component of the EU FP6 Project entitled "Network of Research Infrastructures for European Seismology, NERIES" has developed a methodology (which was coded into software called ELER). Recently, ELER methodology and software has been utilized for the assessment of the seismic risk in the Istanbul Province in connection with the "İstanbul'un Olası Deprem Kayıpları Tahminlerinin Güncellenmesi İşi – Updating of the Probabilistic Earthquake Losses in Istanbul Province" of Istanbul Metropolitan Municipality" conducted by OYO International and GRM under the supervision of KOERI (IBB-OYO-GRM-KOERI, 2009).

EARTHQUAKE GROUND MOTION

The study of JICA-IBB [2002] included four scenario earthquake models. The earthquake with magnitude M=7.5 on the 120 km fault extending from the west of the rupture segment of Kocaeli earthquake towards Silivri was been assumed in the Model A (Figure 1). Similarly, the study of BU-ARC [2002] was considered, the scenario earthquake with magnitude M=7.5 on un-ruptured main Marmara fault. The peak ground acceleration values observed from BU-ARC [2002] are very close to values of Model A projected by JICA-IBB [2002] as presented in Figure 2.

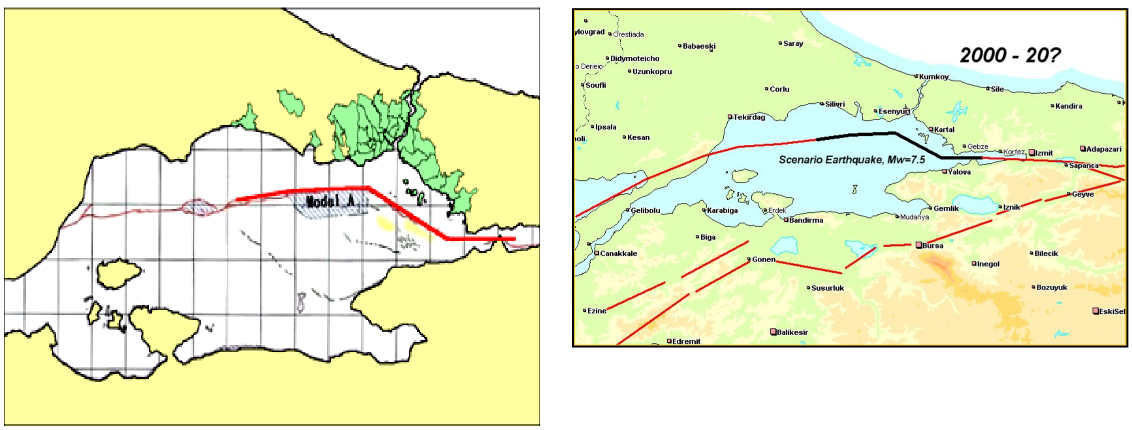

(a) (b)

Figure 1 **Scenario earthquakes: (a) "Model A" in the study of JICA-IBB [2002]; and (b) BÜ- ARC [2002].**

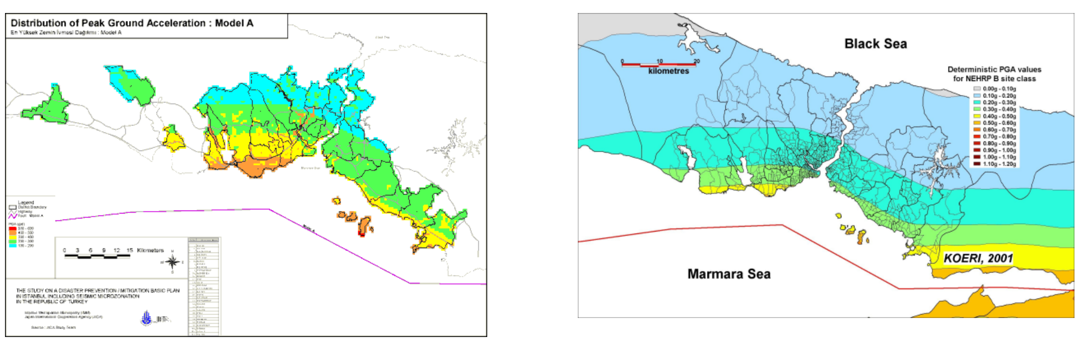

(a) (b)

Figure 2 **Distribution of PGA: (a) JICA-IBB (2002]; and (b) BÜ- ARC [2002].**

The study by IBB–OYO [2002] has been reevaluated with the aim of including recent information and data in the Istanbul earthquake master plan to organize urban disaster management activities and to prioritize regions for urban earthquake structural improvement and urban renewal projects. The purpose of the IBB-OYO-GRM-KOERI [2009] study of Istanbul is to use an updated inventory of buildings and infrastructure, and using earthquake ground motion models to estimate structural damage, casualties, and direct economic losses. Within this project all input information, data and maps received from the official institutions of the Istanbul Metropolitan Municipality and all kinds of existing data and particularly GIS-based data, have been compiled. Similar to the JICA-IBB [2002] and BÜ–ARC [2002] studies, deterministic hazard assessment methodology has been considered to be more appropriate for the assessment of the earthquake risk in Istanbul. The two scenario cases used in the risk assessments are as follows :

- Scenario I: Considering the deaggregation analysis of the probabilistic hazard associated with 50% PE in 50 yrs: Mw=7.5 and ε=0 on the un-erupted segment of the Main Marmara Fault.
- Scenario II: Considering the deaggregation analysis of the probabilistic hazard associated with 10% PE in 50 yrs: Mw=7.25 and ε=1.4 on the un-erupted segment of the Main Marmara Fault.

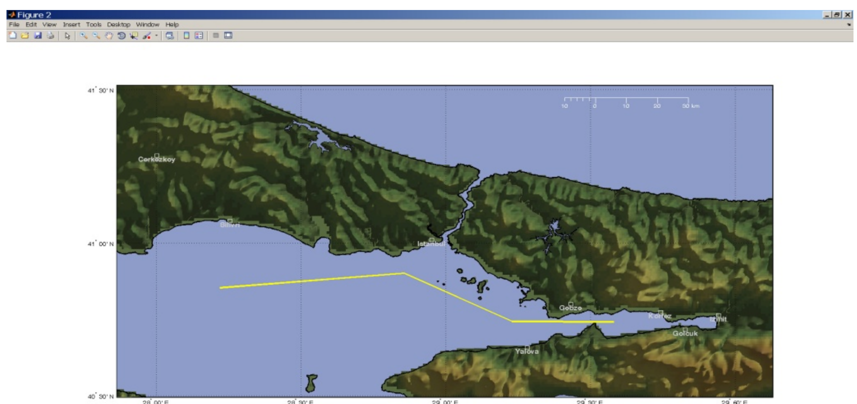

Figure 3 Scenario earthquake used in the study of IBB-OYO-GRM-KOERI [2009].

Considering the deaggregation analysis of the probabilistic hazard associated with 50% PE in 50 years, an earthquake scenario with magnitude *Mw*=7.5 and ε=0 on the unrupted segment of the main Marmara fault was used to estimate building damage. The distribution of ground motion parameters such as PGA, PGV, S_A (T=0.2 sec) and S_A (T=1.0 sec) is presented in Figure 4. Considering the deaggregation analysis of the probabilistic hazard associated with 10% PE in 50 years, an earthquake scenario with magnitude *Mw*=7.25 and ε=1.4 on the unrupted segment of the main Marmara fault was used to estimate building damages. The distribution of ground motion parameters such as PGA, PGV, S_A (T=0.2 sec) and S_A (T=1.0 sec) is presented in Figure 5.

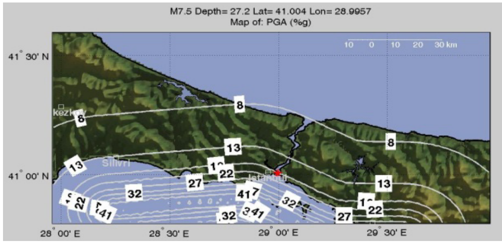

(a)

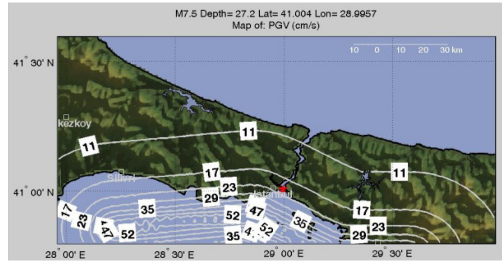

(b)

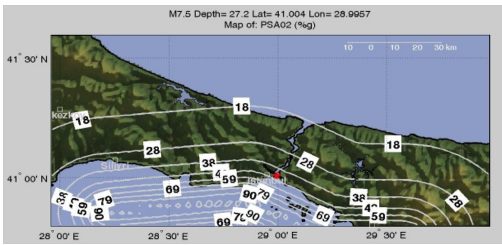

(c)

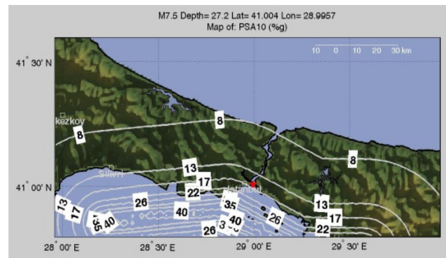

(d)

Figure 4 Distribution of the ground motion parameters for Scenario I: (a) PGA, (b) PGV, (c) *SA* (*T*=0.2 sec), and (d) *SA* (*T*=1.0 sec).

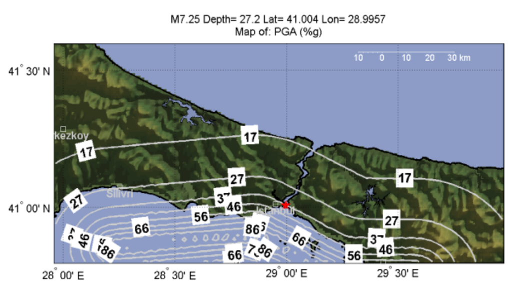

(a)

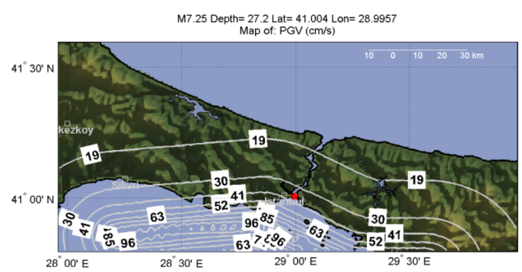

(b)

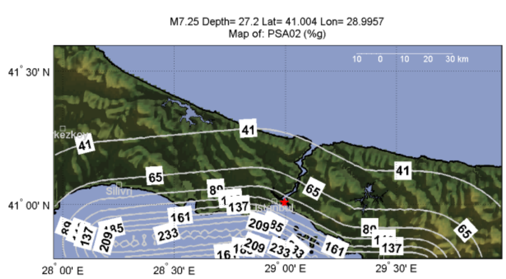

(c)

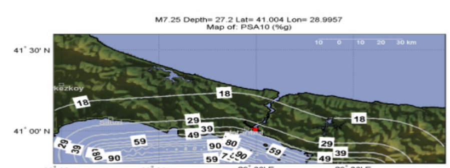

(d)

Figure 5 Distribution of the ground motion parameters for Scenario II: (a) PGA, (b) PGV, (c) S_A (*T*=0.2 sec), and (d) S_A (*T*=1.0 sec).

SITE DEPENDENT GROUND MOTION

The influence of the local geological structure on damage distribution due to ground-motion amplification (also called site effects) is well known [Borcherdt 1994]. The average shear-wave velocity in the upper 30 m (V_{S30}) is mostly used to classify local site conditions. The V_{S30} values together with the site correction methodology of Borcherdt [1978] were used to obtain site corrected ground motion distributions from the assigned V_{S30} values for Istanbul. V_{S30} values for each 0.005 degree grid cells were obtained by averaging ground modeling and site response analysis of each 250-m grid cells, and they were assigned to the 0.005 degree grid cells. Figure 6 shows the distribution of V_{S30} for Istanbul.

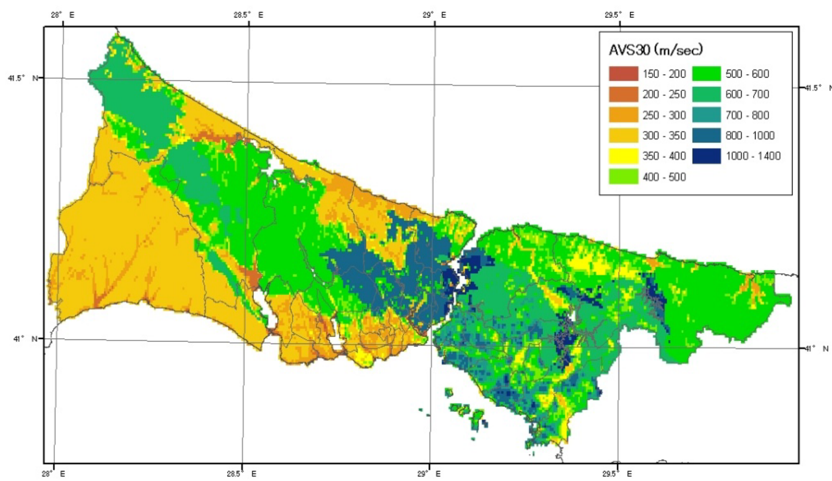

Figure 6 Distribution of the V_s30 for Istanbul.

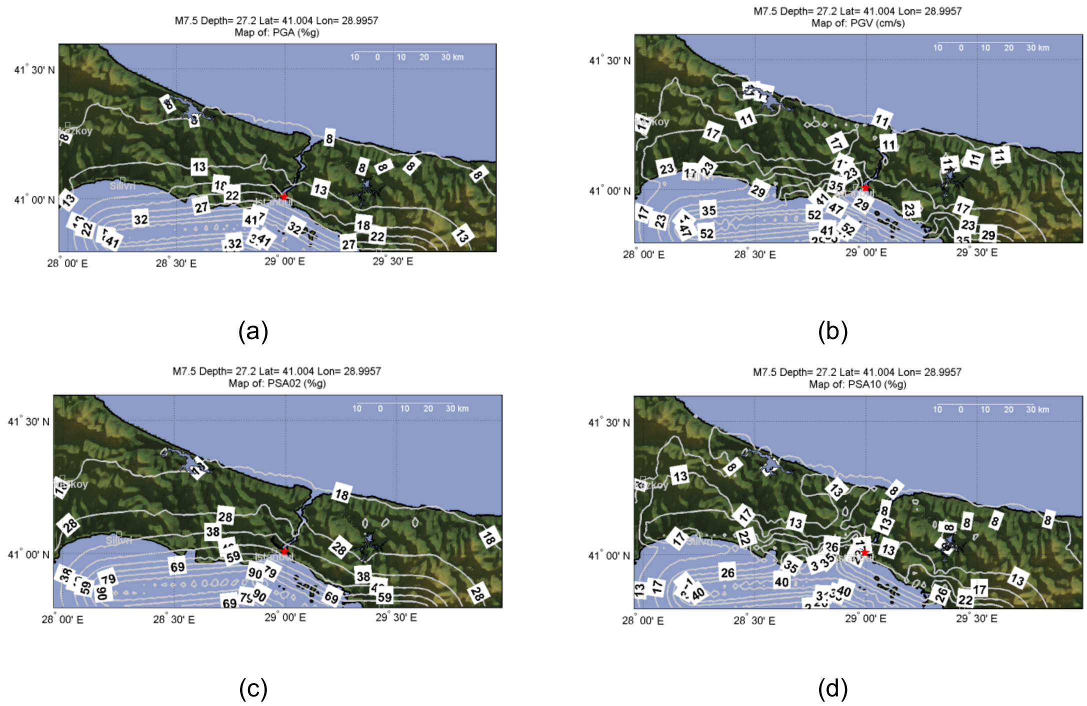

Figure 7 Distribution of the site-dependent ground motion parameters for Scenario I: (a) PGA, (b) PGV, (c) S_A (T=0.2 sec), and (d) S_A (T=1.0 sec).

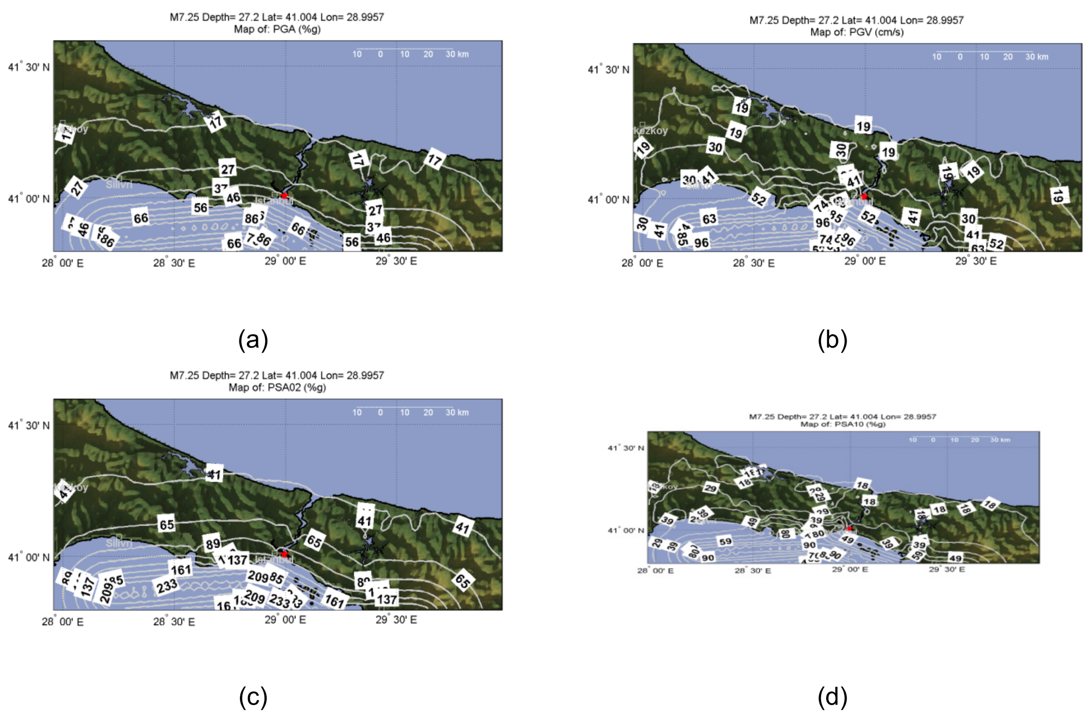

Figure 8 Distribution of the site-dependent ground motion parameters for Scenario II: (a) PGA, (b) PGV, (c) S_A (T=0.2 sec), and (d) S_A (T=1.0 sec).

BUILDING INVENTORY

The structural types considered in the Istanbul Building Classification system are reinforced concrete (R/C) frame, masonry, R/C shear wall, steel, and precast systems. In terms of structural height, the buildings were grouped as low-rise (1-3 floors), mid-rise (4-7 floors), high-rise (9-19 floors), and tall (20 and more floors). The date of construction reflected the state of seismic design applications as pre-1980 buildings having no seismic design considerations, 1980-2000 buildings corresponding to a moderate level of seismic design, and post-2000 buildings corresponding to an acceptable level of seismic design. These three parameters were used to define a building taxonomy, the so-called ‘‘Istanbul Building Classification System’’ composed of 57 classes, and the number of buildings in each building class was determined and assigned to each geo-cell. The results indicate that in Istanbul, low-rise and mid-rise R/C frame buildings constitute about 75% of the building stock. The total number of buildings in Istanbul has been calculated as 1,163,383.

INTENSITY BASED (MACROSEISMIC) BUILDING DAMAGE ESTIMATION

The observed damage based vulnerability method referred to as macroseismic method was originally developed by Giovinazzi and Logomarsino [2004; 2005] Giovinazzi [2005] and Lagomarsino and Giovinazzi [2006] from the definition provided by the European Macroseismic Scale [Grunthal and Levert 1998] making use of classical probability theory and fuzzy-set theory. The aim of a Macroseismic Scale—EMS-98—is to obtain a measure of the earthquake severity from the observation of the damage suffered by the buildings; similarly the scale itself can be used as a vulnerability model for forecast purposes to supply the probable damage distribution for a given intensity.

The EMS-98 scale provides a damage matrix that contains the probability of the buildings belonging to a certain vulnerability class vulnerable to a certain damage level under a given intensity. These damage matrices are limited, providing a vague and incomplete vulnerability model, as the damage probabilities are provided in a fuzzy way through three narrowly overlapping percentage ranges, and the damage matrices are incomplete because they consider only the most common and easily observable situations. In that study the incompleteness matter was solved by introducing a beta distribution to model damage grade variation. This enabled the development of an analytical expression for the relationship between mean damage grade, μ_D (mean of the discrete beta distribution) – intensity, I and vulnerability index, V, allowing estimation of the building damage distribution once vulnerability index V dominant in the area of interest is known.

$$\mu_D = 2.5\left[1+\tanh\left(\frac{I+6.5V-13.1}{2.3}\right)\right] \tag{1}$$

Table 1 Damage estimation results by macroseismic method.

Damage Level	Number of Damaged Buildings
Collapsed to Heavy Damage (D4 + D5)	33,000
Moderate (D3)	91,000
Slight (D2)	188,000
Non-Structural (D1)	270,000

BUILDING DAMAGE ESTIMATION WITH ANALYTICAL METHODS

This study applied the "Spectral Capacity-based Damage Assessment Methodology," which was developed in the United States under the scope of HAZUS project [1999] to estimate building damage using analytical methods. Here, the "capacity spectrum" for every building class and "earthquake demand spectrum" obtained from acceleration spectrum defined for the location of the building are based on the possible nonlinear behavior of structural elements under seismic loads. The spectral displacement value called as "performance point" that corresponds to building bearing capacity is determined by mathematical intersection of "capacity spectrum" and "earthquake demand spectrum" curves. To calculate the performance point, the following four methods are used:

- Capacity Spectrum Method (CMS), ATC-40 [ATC 1996]
- Modified Acceleration-Displacement Response Spectrum (MADRS) Method, *FEMA-440* [FEMA 2005]
- Coefficient Method (CM), *ASCE 41-06* [ASCE 2006]
- KOERI Loss Method (KLM) [ARC-BU 2002; Erdik et al 2003]

Calculating the performance point by using one of above-mentioned four methods, the probabilistic expected damage level of the building is found by entering the "Building Damage Probabilistic Function" that is defined for each building class. Analytic based building damage estimation for each damage level for Scenario I and II are presented in Figure 9 and Figure 10.

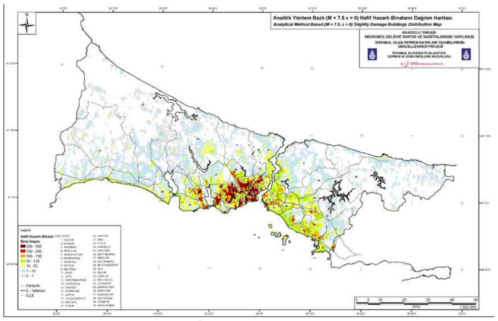

(a) Slight damage

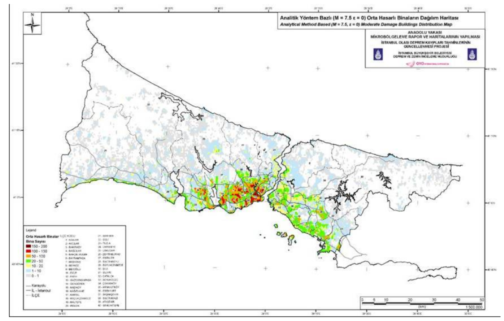

(b) Moderate damage

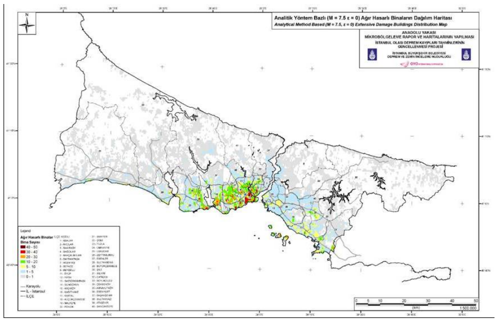

(c) Heavy damage

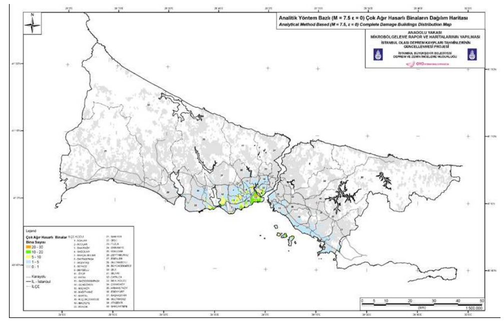

(d) Very heavy damage

Figure 9 Analytic based building damage estimation for Scenario I.

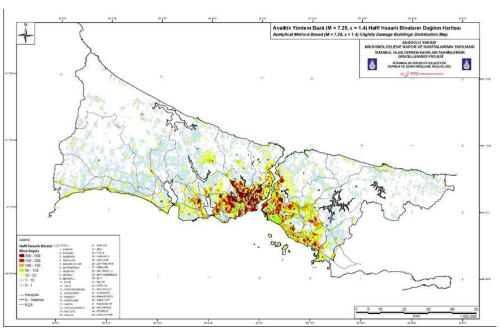

(a) Slight damage

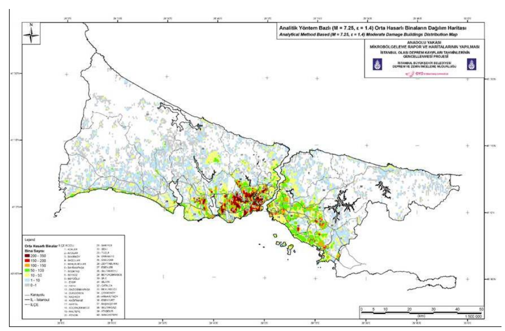

(b) Moderate damage

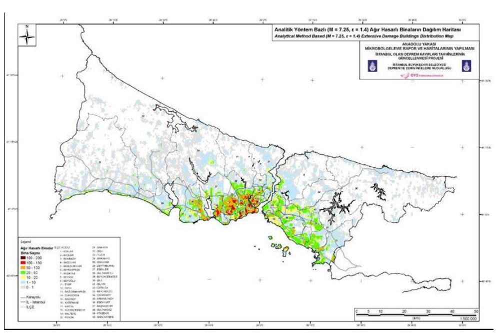

(c) Heavy damage

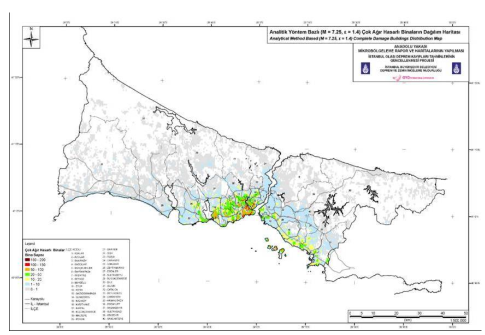

(d) Very heavy damage

Figure 10 Analytic based building damage estimation for Scenario II.

CASUALTY ESTIMATION

Casualty estimation models are generally based on the number of buildings damaged beyond a certain damage state. For instance, Spence and Coburn [2002] provides a casualty estimation model for collapsed (EMS-98 D5) buildings. The KOERI model for Istanbul is based on the number of buildings damaged beyond repair (EMS-98 D4+D5), and hospitalized injury is calculated to multiply by 4 of number of death people. The HAZUS-99 and its more recent versions use four severity levels to categorize injuries, ranging from light injuries (Severity Level 1) to death (Severity Level 4). The model provides casualty rates for different structural types and damage states. Macro-seismic intensity and analytic-based casualty estimation results for Scenario I and II are presented in Tables 2 and 3, respectively.

Table 2 Macro-seismic intensity based casualty estimation.

Severity level	Intensity Based
Death (D4+D5)	33,041
Hospitilized injury	132,164

Table 3 Analytic based casualty estimation.

Severity Level	CSM # of injuries	MADRS_4 # of injuries	CM # of injuries	KOERI_LM # of injuries	Average # injuries
SL3 &4 (Heavy injuries to Death)	24,000	20,000	62,000	26,000	20,000–62,000
SL1 &2 (Meadium to Light injuries)	82,000	75,000	199,000	91,000	82,000–199,000

CONCLUSION

The IBB-OYO-GRM-KOERI study [2009] provided updated building and infrastructure inventories for Istanbul, and used the recent methodology, vulnerability relations, and risk models developed in ELER© (Earthquake Loss Estimation Routine). The selected scenario earthquake corresponds to earthquake ground motion levels expected not to be exceeded with a 50% probability in 50 years. In deterministic hazard analysis, median values of attenuation relations were used. Therefore, statistically the probability that hazard results will be lower or higher than hazard values used in loss calculations is 50%. Building damage estimations based on both empirical and analytical vulnerability relationships indicate that about 2% to 4% of buildings will be either heavily damaged or collapsed after an Istanbul earthquake. About 9% to 15% of the buildings will receive medium damage, and about 20% to 34% of buildings will be damaged lightly. The economic losses based on building damage is estimated at about 12 Billion Euros (as an average figure) and constitutes only a fraction of the total direct and indirect economic losses expected to result from an Istanbul earthquake.

The priorities and optimum approaches in mitigation of earthquake risk in Istanbul can be provided by only exact information on earthquake-induced losses. The results of this work should be used in the development of earthquake risk mitigation strategies and in planning of rapid response studies.

ACKNOWLEDGEMENT

We are thankful to Istanbul Metropolitan Municipality (IBB) and Japan International Cooperation Agency (JICA) for their contribution to the present study. We also express our thanks to the management and engineers of the GRM Risk Management, Inc., that coded and tested the ELER software as well as to our colleagues working at Kandilli Observatory and Earthquake Research Institute, Department of Earthquake Engineering who contributed at all levels of this study.

REFERENCES

American Society of Civil Engineers (2007). Seismic rehabilitation of existing buildings, *ASCE/SEI 41-06*, Reston, VA.

Applied Technology Council (1996). Seismic evaluation and retrofit of concrete buildings, *ATC-40*, Redwood City, CA.

Applied Technology Council (1991) Seismic vulnerability and impact disruption of lifelines in the conterminous United States, *ATC-25*, Redwood City, CA.

Applied Technology Council (1996). Seismic evaluation and retrofit of concrete buildings, *ATC-40*, Redwood City, CA.

BÜ ARC–Kızılhaç Raporu (2003). Earthquake risk assessment for Istanbul metropolitan area, Boğaziçi Üniversitesi, Kandilli Rasathanesi ve Deprem Araştırma Enstitüsü, Deprem Mühendisliği Anabilim Dalı raporu, Bogaziçi Üniversity press. ISBN 975-518-213-6.

BÜ-Munich-Re [2002]. Earthquake risk assessment for industrial facilities in Istanbul, Boğaziçi Üniversitesi, Kandilli Rasathanesi ve Deprem Araştırma Enstitüsü, Deprem Mühendisliği Anabilim Dalı raporu (hazırlayanlar M Erdik, E. Durukal, E. Uckan, K. Sesetyan, M.B. Demircioglu).

Coburn A, Spence R (2002). *Earthquake Protection*, John Wiley & Sons Ltd., Chichester, England.

Erdik M. Demircioğlu MB, Şeşetyan K, Durukal E, Siyahi B (2004). Assessment of probabilistic earthquake hazard in the Marmara region, *Soil Dyn. Earthq. Engrg*., 24:605–631.

Federal Emergency Management Agency (1999). *HAZUS99 User and Technical Manuals*, Washington D.C.

Giovinazzi S, Lagomarsino S (2004). A macroseismic method for the vulnerability assessment of buildings, *Proceedings*, 13th World Conference on Earthquake Engineering, Vancouver, Canada.

Giovinazzi S, Lagomarsino S (2005). Fuzzy-random approach for a seismic vulnerability model. *Proceedings,* ICOSSAR 2005, Rome, Italy.

Giovinazzi S (2005). Vulnerability assessment and the damage scenario in seismic risk analysis, PhD Thesis, Department of Civil Engineering of the Technical University Carolo-Wilhelmina at Braunschweig and Department of Civil Engineering, University of Florence, Italy.

Grünthal G, Levret A (eds.) (2001). European Macroseismic Scale 1998 (EMS-98), Cahiers du Centre Européen de Géodynamique et de Séismologie, Vol. 15, Joseph Beffort, Helfent-Bertrange, Luxembourg.

HAZUS (1999). *Earthquake Loss Estimation Methodology, Technical Manual, RMS, NIBS, and FEMA*, Federal Emergency Manage Agency, Washington, D.C.

IBB-JICA (2002). *The Study on A Disaster Prevention / Mitigation Basic Plan in Istanbul including Seismic Microzonation in the Republic of Turkey*, Report.

IBB-OYO-GRM-BU (2009). *Updating Probable earthquake Losses for Istanbul*, Report.

Lagomarsino S, Giovinazzi S (2006). Macroseismic and mechanical models for the vulnerability and damage assessment of current buildings, *Bull. Earthq. Engng*., 4:415–443.

EARTHQUAKE RISK AND ITS MITIGATION IN ISTANBUL

Mustafa Erdik

Bogazici University, İstanbul, Turkey

ABSTRACT

Physical and societal vulnerability to earthquakes and expected physical, social, economic, and industrial losses in Istanbul are outlined. This risk quantification has served as the basis for the Earthquake Masterplan. Previous risk-mitigation activities and current risk-mitigation activities are discussed.

INTRODUCTION

Istanbul houses approximately one-eighth of the total population and one-half of the industrial potential of Turkey. In addition to the naturally very high earthquake hazard, the earthquake risk in the city has increased because of overcrowding, faulty land-use planning and construction, inadequate infrastructure and services, and environmental degradation. After the losses suffered during the two major earthquakes that struck Turkey in 1999, there has been broad recognition of the need for extensive earthquake preparedness and response planning on the basis of detailed earthquake risk analysis in Istanbul. In this context, the following risk assessment studies have been carried out:

- 1996: Development of Earthquake Loss Scenario for Istanbul–Bogazici University (supported by the World Bank).
- 2002: Earthquake Risk Assessment for Istanbul Metropolitan Area–Bogazici University (supported by American Red Cross).
- 2003: Study on a Disaster Prevention/Mitigation Basic Plan in Istanbul and Seismic Microzonation–OYO and PCI for the Istanbul Metropolitan Municipality (supported by Japan International Cooperation Agency).
- 2004: Earthquake Risk Assessment for Industrial Facilities in Istanbul–Bogazici University (supported by Munich-Re Group).
- 2009: Updating of the Earthquake Risk Assessment–OYO, GRM and Bogazici University (supported by Istanbul Metropolitan Municipality).

These studies provided information on the earthquake risk in Istanbul and also led to the comprehensive report entitled ‘‘Earthquake Masterplan for Istanbul.’’

As it is well known, the basic tenets of earthquake risk management are:

- Understand/quantify the existing hazard and risk.
- Do not increase the existing risk (i.e., build properly).
- Decrease the existing risk (i.e., retrofit).
- Transfer the risk (i.e., insurance).

- Improve emergency management.

Reduction of the structural vulnerability, land-use regulations, design and construction regulations, relocation of communities, and public education/awareness programs are viable measures for the mitigation of earthquake risk. Earthquake performance of cities can be improved by changing the functional characteristics through urban transformation, land-use planning, and increasing the quality and redundancy of the infrastructure. Almost all of these risk management measures are being implemented in Istanbul to prepare the city for a large (Mw=7+) earthquake that has an annual probability of occurrence of about 2%, one of the largest in the world (similar to San Francisco and Tokyo). This earthquake will be termed as the “Istanbul Earthquake.”

EXPECTED EARTHQUAKE LOSSES

On the basis of high conditional probabilities, a deaggregated moment magnitude 7.25 strike-slip earthquake with an epsilon value of 0.0 (i.e., the median value of the associated GMPE) provides a deterministic representation for the ground motion level that would be created by the “Istanbul Earthquake.”Istanbul province houses about 1,200,000 buildings and 13,000,000 people. The losses that would result from this scenario earthquake as reported by 2009 updated risk assessment can be summarized as follows.

Building damage estimations based on both empirical and analytical vulnerability relationships indicate that about 2% to 4% of buildings will be either heavily damaged or collapsed (Figure 1). About 9% to 15% of the buildings will receive medium damage and about 20% to 34% of buildings will be damaged lightly. These assessments would indicate that the number of housing units that would be inhabitable (either due to endangering physical damage or for psychological reasons) would range between 400,000 to 800,000. Out of the province’s total population of 13,000,000 about 0.2% to 0.4% will either lose their lives or will be badly injured. About 0.6% to 2% of the population will receive lesser degrees of injury. About 130,000 people may be in need of hospitalization.

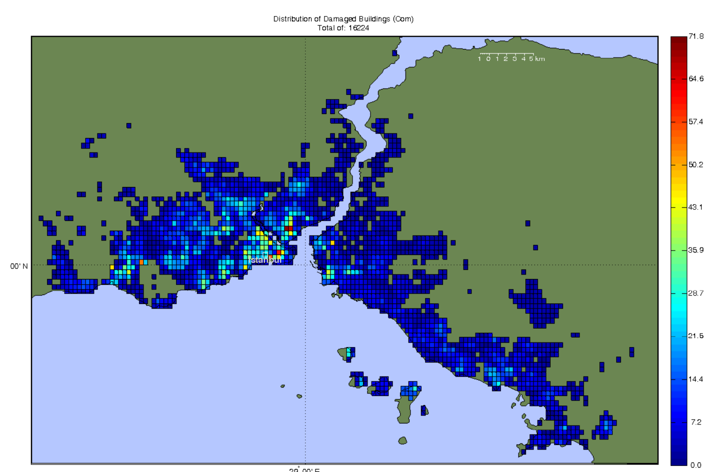

Figure 1 Distribution of heavily damaged buildings.

The building damage based direct economic losses will be about 12 Billion Euros (as an average figure). Note that this figure constitutes only a fraction of the total direct and indirect economic losses, which is expected to be about 50 Billion Euros, as a result of the İstanbul Earthquake.

Two other mega-cities with similar earthquake hazard are San Francisco and Tokyo. In the San Francisco Bay Area, with a population of approximately 10 million and approximately 4.6 million households, a repetition of the 1906 San Francisco earthquake would cause deaths that would vary between 1800 (if the earthquake occurred at night) versus 3400 (if it occurred during the day). Approximately 250,000 residential households and 10,000 commercial buildings will be damaged either extensively or totally [Kircher et al. 2006]. A repeat of the 1923 M7.9 Kanto earthquake in Tokyo (population approximately 30 million, with the number of households approximately 10 million) is estimated to cause 30–60,000 deaths, 80–100,000 hospitalized injuries, and approximately 360,000 totally damaged households [Stein et al. 2006; RMS 2006b]. It is interesting to note that the different building losses in three cities do not justify the striking differences between numbers of casualties.

EARTHQUAKE MASTERPLAN

In 2003, after the portrayal of expected earthquake losses in Istanbul the Metropolitan Municipality commissioned the services of leading Turkish universities (Bogazici Istanbul Technical, Middle East Technical, and Yildiz Technical) to prepare the Earthquake Masterplan for Istanbul. The scope of Earthquake Masterplan for Istanbul comprised:

- Assessment of the current situation.
- Seismic assessment and rehabilitation of existing buildings.
- Urban planning issues.
- Legal issues.
- Financial issues.
- Educational issues.
- Social issues.
- Risk and disaster management issues.

The objective of the Masterplan was the planning of activity in these fields, preparation of implementation programs, and identification of the responsibilities and responsible authorities for earthquake disaster mitigation activity [Earthquake Masterplan for Istanbul 2003]. The Masterplan recognizes that risk mitigation is not only a technical issue but mostly a legal and socio-political issue. All efforts toward risk mitigation will be implemented only as far as they are described in the legal framework, because earthquake risk mitigation activity is closely linked with the legal structure at every stage. The legal recommendations are proposed to indicate that an institutional framework must be developed to ensure successful implementation. The ultimate purpose is to build a disaster-resilient community in Istanbul by creating a culture of prevention to address not only earthquakes but also everyday hazards and managing the risk from natural and human-induced disasters. Four significant outcomes can be achieved by the strategy described in the Masterplan:

- Enhanced institutional capacity development of government and civil society stakeholders in techniques for disaster risk reduction.
- Revised policies, legislation, and plans, informed by knowledge from comprehensive risk analysis, creating a foundation for an all-risk approach to disaster management.
- Application of an effective multidisciplinary, multi-sector, and inter-governmental disaster response and mitigation system for all-risk disaster risk reduction.
- Building up the municipality's capacity to prepare, mitigate, and respond to a multitude of natural and human induced disasters.

Although there is strong institutional and individual commitment to the importance of the implementation of the Masterplan, there is, at the same time, caution over the inadequacy of the bureaucratic system to enact new laws and regulations and to enforce existing ones. The parliamentary process of enacting the needed laws and regulations is active, however, and most of the legal arrangements for urban rehabilitation for earthquake risks are completed.

The essence and the findings of the earthquake Masterplan for Istanbul constituted the objective of the World Bank-financed ISMEP project and the pilot urban transformation projects that the Istanbul Metropolitan Municipality is undertaking. The former project is more geared toward the rehabilitation of public buildings, whereas the latter is involved with residential building stock. Unfortunately, these applications are falling short of the expectations that followed preparation of the Masterplan. The reasons for this inadequate response are that although the Masterplan contains the ingredients for the preparation of roadmaps for earthquake risk mitigation in all sectors of the city, it has not yet evolved into such specific roadmaps, implementation manuals, and public policy support documents.

LEGISLATIVE CHANGES FOR RISK MITIGATION ACTIVITIES

The following important laws related to earthquake risk mitigation have been enacted.

<u>Legislation for Building Design and Construction Supervision (Decree No. 595, 2000):</u> This law enforces mandatory design checking and construction inspection of all buildings (in Istanbul and other 27 large provinces) by government-licensed private ''supervision firms.'' Public buildings are excluded, because the government assumes responsibility for supervision of the design and construction for these. The main objective of this regulation is to verify that the codes and quality standards in private building construction. Supervision firms must be owned by a majority of engineers or architects and are required to hire ''expert'' professionals and have professional-liability insurance. The requirement for mandatory financial-liability insurance, originally intended for offsetting any losses faced by the owner during the first ten years after occupation permit, was later waived, because of problems obtaining liability insurance with uncertain coverage of earthquake damage and other legal complications. Although the system operates with some success, this waiver of the insurance requirement and the other conflict-of-interest issues rather crippled the new supervision system. Fees for design and construction supervision range from 4% to 8% of the estimated building cost and are paid by the owner through an account established by the municipality. In 2001 decree no. 595 was reinstated with modified a law (no. 4708, June 29, 2001) where the insurance cover requirement was removed.

On the basis of cabinet decree dated July 13, 2010, the law on Building Design and Construction Supervision will be implemented throughout the country starting in the beginning of 2011. The law will be applied to all building constructions including those that are self-built. The supervision firms will be responsible for the problems in the structural features for 15 years and for non-structural features for 2 years. It is estimated that the construction prices will increase about 10% due to this supervision.

Compulsory earthquake insurance (Decree No. 587, 1999): Through a World Bank project, a government-sponsored Turkish catastrophic insurance pool (TCIP) was created with the essential objective of transferring the government's financial burden of replacing earthquake-damaged housing to international reinsurance and capital markets. An important feature of this decree is its denial of assistance in accordance with Disasters Law No. 7269 when homeowners have not participated in the pool. All existing and future privately owned property is required to contribute to the Turkish compulsory insurance pool (TCIP). Non-engineered rural housing is excluded. Management of the pool is entrusted to a new entity called the ''Natural Disasters Insurance Council'' (DASK in the Turkish abbreviation). The pool-management model is similar to New Zealand's Earthquake Council (EQC) or the California Earthquake Authority (CEA).

The annual premium, categorized on the basis of earthquake zones and types of structure, varies between 0.220% and 0.044% for reinforced concrete housing units with a 2% deductable. These rates should be compared with 0.5% premium rate and 10–15% deductible in California [California Department of Insurance 2003]. There is a cap of 70,000 EUROs. For the additional value conventional private insurance coverage can be purchased. TCIP has been operational since January 2001 and the penetration rate (as of 2010) throughout the country is approximately 25%; in Istanbul it is approximately 36%. It is the tenth largest insurance program in the world, with a re-insurance cover of 1.4 billion EUROs. The number of policies in Istanbul is about 1,100,000 amounting to a total cover of 35 billion EUROs. If the claims exceed the TCIPs resources, the payment will be pro-rated. Since 2001, approximately 11,000 claims for earthquake damage were processed with a payment of about 9 million EUROs. There are expectations that in the future the TCIP can contribute to the control of construction by differentiation of premiums on the basis of earthquake vulnerability. Several opponents of the plan believe it would be expensive and difficult to find adequate re-insurance capacity in the future.

<u>The law of ''Greater City Municipalities'' (Law No. 5216, 2004):</u> This law enlarged the boundaries of Istanbul Metropolitan Municipality and vested authority for:

- Drawing up city master plans and approving and supervising their implementation by district municipalities.
- Preparation of strategic plans concerning disasters.
- Vacating and demolishing dangerous buildings and all other ''non-conforming'' structures, in partnership with local municipalities and private firms.
- Instituting financial organizations and undertaking many forms of partnership in comprehensive urban regeneration projects.
- Building and operating the major infrastructure installations, for example water and sewerage system, waste water and solid waste treatment plants, gas and central heating system.

- Settling conflicts among the municipalities within their own boundaries.
- Dealing with the other services which are beyond the capacity of district municipalities.

Law on Urban Renewal Processes in the Historic City (Law No. 5366): Law no. 5366 on the 'Preservation by Renovation and Utilization by Revitalizing of Deteriorated Immovable Historical and Cultural Properties', forms the basis of the recent urban transformation projects in historic neighborhoods of Istanbul. Although not necessarily enacted with view of mitigating seismic risk, with its approval by the Council of Ministers in 2005 this law has caused a dramatic change to the dynamics of the urban land transformation processes within the old city and contributed to the improvement of the seismic vulnerabilities. Several historical neighborhoods are declared as renewal areas including Tarlabasi, Sulukule, and Suleymaniye.

Law on the Change of Article 23 of the Law of Municipalities Numbered 5395 (No 5598, Accepted on June 17,2010): With the Law (No.27621, 4.06.2010) on the Change of the 73rd Item of the Law of Municipalities (No. 5393), the municipalities were empowered to protect the historical and cultural texture of the city and to undertake urban renewal projects to mitigate earthquake risks.

DISASTER RISK MANAGEMENT ARRANGEMENTS

The dual organization of local administration in Turkey, with appointed provincial and district governors and elected provincial and district mayors, establishes the basis for their somewhat overlapping role in disaster management. On the basis of law no. 7269 on ''Precautions and Aid Regarding All Types of Disasters that Impacts the Community,'' the governor of Istanbul Province (similar to other provinces in Turkey) assumes every conceivable prerogative to act in disaster (and other extraordinary emergency) conditions. The mayor and other municipal bodies fall under the authority of the governor in these circumstances. The legal regulations do not specify any administrative role for the municipalities and do not allow discretion in planning or mitigation. Trying to improve disaster risk management and preparedness, the Istanbul Governorship and the Istanbul Metropolitan Municipality, respectively, instituted the Disaster Management Center (AYM) and the Disaster Coordination Center (AKOM). The emergency response functions in Istanbul are currently based upon these parallel institutions, derived from the dual administrative systems that govern the metropolis.

An important shift occurred in the disaster management structure of Turkey in 2009. With the law numbered 5902 and dated December, 17 2009, a new governmental entity, called "Disaster and Emergency Management Presidency" (AFAD), under Prime Ministry was established. AFAD combines the activities of General Directorate of Disaster Affairs under Ministry of Public Works and Settlement, General Directorate of Civil Defense under Ministry of Interior and Turkey Emergency Management General Directorate under Prime Ministry. The new law defines the central and provincial level structure of the new unit. There are six departments and three boards under Disaster and Emergency Management Presidency. The departments are: Planning and Mitigation, Earthquake, Recovery, Civil Defense, Response and Administrative Affairs. The three high level boards are: Disaster and Emergency Management Higher Committee, Disaster and Emergency Management Coordination Committee and Earthquake Advisory Committee. Furthermore, the law dictates the formation of Provincial Directorates for Disaster and Emergency Management, under the governor of each province. The assessment of the provincial disaster and emergency risks, preparation and application of response plans and management of the logistic services at the time of disaster and emergency are under the responsibility of these directorates. In Istanbul, the AYM has been effectively absorbed under the Istanbul Directorate for Disaster and Emergency Management. It is believed that with this new re-structuring. local authorities will have more power and responsibility, and there will be more effective and powerful mechanisms for the earthquake disaster management.

RETROFIT OF RESIDENTIAL APARTMENT BUILDINGS

The greatest effect on reduction of human casualties in Istanbul could be achieved by retrofit/rehabilitation of existing building stock. Although several assessment and retrofit applications are in place for public and commercial buildings, serious initiatives have yet to be undertaken to strengthen residential building stock. With the exception of some pilot projects spearheaded by the Istanbul Metropolitan Municipality, none of the current risk-mitigation projects deal with retrofit of residential building stock, although they are the primary reason for loss of human life. New (post-2000) buildings in Istanbul are usually being built much better than the existing building stock. For planned developments, especially, code compliance is very good. For individual housing and/or construction, however, problems still exist. The reasons for the improvement are:

- Application of a new (1998 and 2007) earthquake-resistant design code.
- Increased public awareness and demand for earthquake safety.
- Training and education programs for engineers.
- Better zoning regulations and enforcement by municipalities.
- Control by private construction supervision firms.

A comprehensive retrofit campaign that would involve the earthquake-performance screening of approximately 1,200,000 buildings will be a formidable task. Full retrofit (i.e., in compliance with latest code requirements) of a residential building costs approximately 40% of replacement value, and the building has to be vacated for several months. In addition to this high cost and the inconvenience of moving out, there are strong impediments to retrofitting. In an environment where houses are regarded as commodities and with the evidence that retrofitting will not increase the sales value or rental fee for the property, retrofit is viewed as an investment with no financial return. As such, no conceivable reduction in insurance premium, property tax, or building permit fees would be sufficient to create an incentive for retrofitting. Even neglecting the social and legal constraints of retrofit action in apartment complexes, structural retrofit is, on average, not cost-effective. For a mid-rise reinforced concrete frame building in Istanbul the average loss (mean damage ratio—MDR) in an intensity IX region will be 62% and in an intensity VIII region will be 40%. If these buildings are retrofitted to meet the current earthquake-resistant design code to its full extent, the MDRs will be 16% and 11%, respectively, in intensity IX and VIII regions. Thus retrofit actions will save 46% and 29% of the cost of construction of the building. With an average return period of 50 years, it is impossible to be cost-effective in full-scale retrofit applications. Only for short-term return periods (i.e., 5 years) can it barely reach the break-even point of cost effectiveness in intensity IX regions.

Although building owners will find the future property losses small by comparison with the cost of full retrofit and cannot visualize the benefit, at the macro scale, the society in general will greatly benefit from a retrofit campaign through the reduction of physical, social, and consequential societal losses that will eventually be covered by the public. The current understanding is that such a mitigation effort can only be affected by appropriate urban renewal applications. The most risky areas in Istanbul (in terms of human casualties) are indicated in Figure 2.

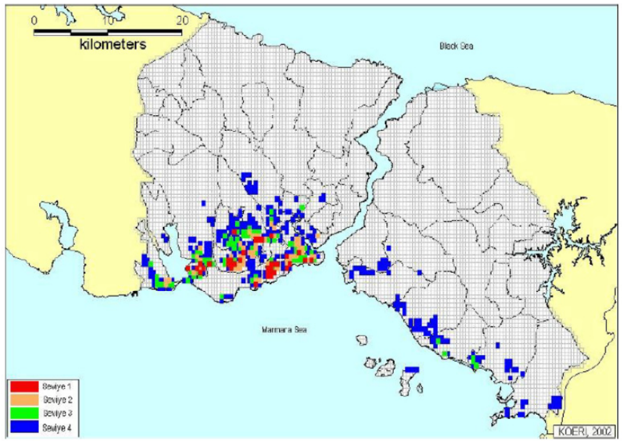

Figure 2 Areas with highest earthquake casualty risk (red is highest) in Istanbul.

EARTHQUAKE FOCUSED URBAN RENEWAL PROJECTS OF THE ISTANBUL METROPOLITAN MUNICIPALITY

The Metropolitan Municipality of Istanbul is implementing a new regulation plan with the objective of instituting a preservation and development balance as a metropolitan settlement that acknowledges its historical, cultural, and natural treasures, and thus regains its status of a world-city in line with its historical and cultural identity. The municipal government is interested in strengthening urban planning processes in the city through the Istanbul Metropolitan Planning and Urban Design Center.

Programs are pursued in urban development, rehabilitation, and transformation, where the focus is strengthening and rehabilitating earthquake risk areas, transformation projects for highly vulnerable building districts, and master projects for rehabilitation and transformation of the historic peninsula. Earthquake performance assessment of buildings and re-development/urban transformation projects are currently in progress in Zeytinburnu, Fatih, and Kucukcekmece districts. A comprehensive seismic microzonation project in the European Asian halves of the city has also been undertaken.

Earthquake loss scenario studies have identified the Zeytinburnu District of Istanbul as one of the most risky areas. To follow-up suggestions contained in the Earthquake Masterplan, Istanbul Metropolitan Municipality has begun the Zeytinburnu Urban Regeneration Pilot Project. The first phase of the project involved the assessment of the earthquake performance of the buildings by teams from leading universities. The results differed and there was no unanimity on prioritization of the vulnerability of the buildings. Approximately 2300 buildings out of a residential stock of 16,000 were eventually selected as the highest-risk group. Although initial plans were for demolition and rebuilding (or extensive retrofit) of these buildings, these plans were not followed because of lack of legal and administrative basis. The current mitigation focus is on urban transformation, and the objective is a joint development platform in which public and private sectors can work together. It is planned to implement the Zeytinburnu urban transformation project in several stages that encompass demolishing the buildings at risk, widening streets, opening evacuation corridors and gathering areas, establishing community centers, strengthening public infrastructure, regenerating housing areas in high priority risk areas, removing industry from the district, and transformation of industry into trade and service. The main problems of such a comprehensive project are inadequate community participation and management of stakeholders and finance.

With the enacting of the Law (No.27621, 4.06.2010) on the Change of the 73rd Item of the Law of Municipalities (No. 5393) the urban renewal activities in Istanbul have gained a new momentum. In this connection, on January 18, 2011, the Istanbul Metropolitan Municipality unanimously decided to approve the new urban plan prepared for the Fikirtepe and three other sub-districts in İstanbul. The new urban plan of these sub-districts gives additional rights and incentives to property owners to combine their small parcels to form large plots to be handed over to real estate developers, a move, that will demolish the existing earthquake vulnerable buildings and rebuilt on an “apartment-for-land” basis.

WORLD BANK FINANCED MITIGATION PROJECTS

The following World Bank financed projects related to earthquake risk mitigation in Istanbul.

Marmara Earthquake Emergency Reconstruction (MEER) Project: The main objectives of the project were to help restore living conditions in the region after the August 17, 1999, Marmara earthquake, support economic recovery and resumption of growth, and develop an institutional framework for disaster risk management and mitigation. The projects undertaken under the MEER project were:

- Feasibility study for the establishment of a disaster-management information system in Istanbul.
- Needs assessment to upgrade the emergency response capacity in Istanbul.
- Feasibility studies for retrofitting residential buildings in Istanbul.
- Feasibility studies for retrofitting selected high-priority public buildings in Istanbul.

Istanbul Seismic Risk Mitigation and Emergency Preparedness (ISMEP) Project: The ISMEP project is a proposed five-year operation with a World Bank loan of 305.35 million EUROS under the jurisdiction of the Governorship of the Province of Istanbul. The overall objectives of the proposed project, in-line with the Istanbul Masterplan, are to save lives and to reduce the social, economic, and financial effects of future earthquakes. With additional funding from the European Investment Bank and EU Development Bank, the current budget has reached 0.86 billion EUROs.

The project consists of three main components: enhancing emergency preparedness; seismic risk mitigation for public facilities; and enforcement of building codes. The bulk of the activities and the budget relate to the retrofitting/reconstruction of priority public facilities (hospitals, clinics, schools, dormitories, and administrative buildings). In Istanbul there are approximately 12,000 buildings serving public functions. The Government has identified approximately 3600 public buildings that are in need of retrofitting. Out of 1783 school complexes and out of 308 hospital complexes about 25% (Figure 3) and 2% were already retrofitted, respectively, under the ISMEP project. Regarding the risk assessment and strengthening of historical and cultural heritage buildings, a project on the earthquake vulnerability assessment of the Istanbul inventory of the Ministry of Culture has been completed. An important pilot project on the assessment of earthquake performance and retrofit design of Hagia Eirene Museum, Mecidiye Kiosk, and the Archeological Museum has been undertaken.

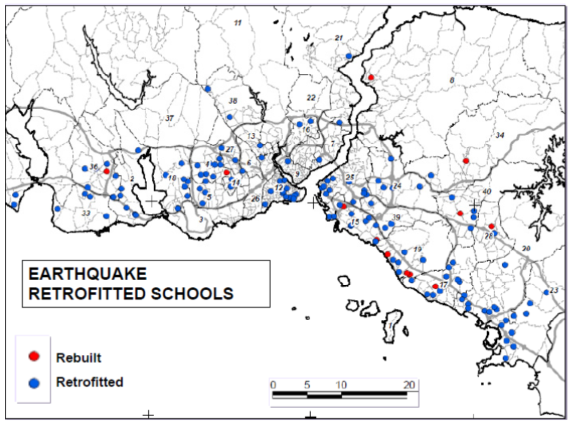

Figure 3 Earthquake retrofitted schools in Istanbul as of 2009.

SEISMIC RETROFIT OF VIADUCTS AND BRIDGES

General Directorate of Highways—17th Division Istanbul has undertaken retrofit of vulnerable viaducts and bridges on the two main freeways (O-1 and O-2) in Istanbul. These freeways run in an E–W direction parallel to the fault and enable, essentially, all local, national, and transnational overland transportation activity. There are 165 main bridges (two of which are major suspension bridges) and 21 main viaducts. Most of these transportation nodes have been retrofitted (Figure 4). Special retrofit applications were conducted on the two suspension bridges and their approach viaducts, the Golden Horn bridges and the Mecidiyekoy Viaduct.

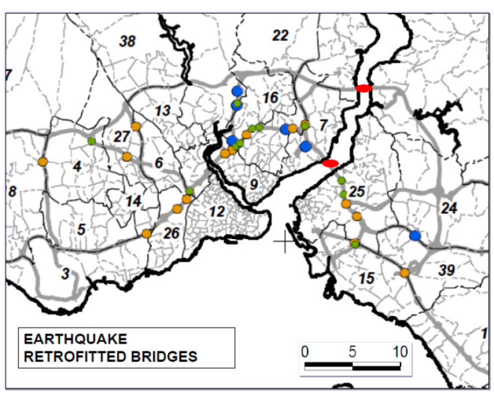

Figure 4 Earthquake retrofitted bridges in Istanbul as of 2009.

CLOSURE

In the almost twelve years since the 1999 Kocaeli and Duzce earthquakes, a multitude of activities have taken place for the assessment and mitigation of the earthquake risk in Istanbul. It is apparent that most of this activity is related to assessment of risk, mitigation planning, institutional strengthening of the legal base, and rehabilitation of public buildings. Although the main cause of casualties will be the residential buildings, very limited coordinated action involves rehabilitation of these buildings through urban renewal and/or transformation projects, which are intrinsically long-term planning projects. Rehabilitation of the existing residential building stock by retrofit is currently left to the discretion and initiative of the tenants and owners of units in apartment blocks.

Inevitably, the earthquake risk faced by one person, one business, or one individual or organization depends on the actions of others. These are external factors, because the actions of others affect you and your actions affect others, and, as such, the involvement of stakeholders in the whole mitigation process is vital for overall success of any mitigation plan. The most important element in this multi-dimensional problem is the self-identification of all stakeholders involved. Because of the perceived risk and urgency of the problem, the media and public criticize the government for the delay in implementation of rehabilitation projects. It is, however, also true that the perception of stakeholders (for example residents of Istanbul, metropolitan and district municipalities, provincial and district governorships, non-governmental organizations and central government) of this urgency becomes a debatable issue. The reasons for the inertia of the stakeholders' involvement in mitigation and ways of overcoming this problem should be assessed properly, because the success of any mitigation plan and/or activity depends on demand by and support from the stakeholders involved.

REFERENCES

Bogazici University-BU (2003). Earthquake risk assessment for industrial facilities in Istanbul–Boğaziçi University (Report prepared for Munich-Re Group), also at http://www.koeri.boun.edu.tr/depremmuh/default.htm under the link 'Research Areas and Applied Projects'.

BU-ARC (2002). Earthquake risk assessment for Istanbul Metropolitan area. Project Report prepared by M. Erdik, M, N. Aydınoglu, A. Barka, O .Yuzugullu, B.Siyahi, E. Durukal, Y. Fahjan, H. Akman, G. Birgoren, Y. Biro, M. Demircioglu, C.Ozbey and K. Sesetyan, Bogazici University Publication.

California Department of Insurance (2003). California earthquake zoning and probable maximum loss evaluation program, Los Angeles, CA.

DASK-Dogal Afet Sigortlari Kurumu (Council for Natural Disaster Insurance) (2007) http://www.dask.-gov.tr/.

Istanbul Metropolitan Municipality (2003). *Earthquake Masterplan for Istanbul*, prepared by Bogazici University, Istanbul Technical University, Middle East Technical University. Yildiz Technical University.

Erdik M, Aydinoglu N, Fahjan Y, Sesetyan K, Demircioglu M, Siyahi B, Durukal E, Ozbey C, Biro Y, Akman H, Yuzugullu O (2003). Earthquake risk assessment for Istanbul metropolitan area. *Earthquake Engng. Engng. Vibration*, 2(1):1–25.

JICA-IMM (2003). The study on a disaster prevention/mitigation basic plan in Istanbul including seismic microzonation in the Republic of Turkey–Japan International Cooperation Agency and Istanbul.

Kircher C, Seligson H, Bouabid J, Morrow G (2006). When the big one strikes again—estimated losses due to a repeat of the 1906 San Francisco earthquake, *Earthq. Spectra*, 22(S2):S297–S339.

RMS (2006a). The 1906 San Francisco earthquake and fire: perspectives on a modern super catastrophe, San Francisco, Ca.

RMS (2006b) Catastrophe mortality in Japan: the impact of catastrophes on life and personal accident insurance, San Francisco, CA.

Stein R, Toda S, Parsons T, Grunewald E (2006). A new probabilistic seismic hazard assessment for greater Tokyo, *Phil. Trans.R. Soc. A.*, 364:1965–1988.

SEISMIC ISSUES FROM A LARGE CITY′S PERSPECTIVE

Ifa Kashefi, Ph.D., S.E.

Department of Building and Safety, City of Los Angele, Los Angeles, California, USA

ABSTRACT

This paper presents an overview describing the functions and responsibilities of the Los Angeles Department of Building and Safety, the largest organization of its kind in the United States. Also, it seeks to share a summary of the Department's code adoption and approval processes for the construction projects along with some of the Department's fundamental seismic related implementations and enforcements, which are expected to result in safe buildings and mitigate loss of life and damage to properties caused by the future earthquakes. All of these essential functions are major contributors in the Department's proactive role in resolving the seismic safety issues in the City of Los Angeles and maintaining a high level of life safety for the residents and visitors of the City.

BACKGROUND

City of Los Angeles

With a population of more than 3.8 million, the City of Los Angeles (LA) is the second largest city in the United States and the largest city in California. It is one of the world's centers for culture, media, academics, business and international trade. It is located in high seismic category zones and has over 500 high-rise buildings. The map of the City of LA and its 15 council districts and some of the active earthquake fault zones in the LA vicinity are shown in Appendix A.

Los Angeles Department of Building and Safety

The Los Angeles Department of Building and Safety (LADBS) is the largest building department in the United States with 200 engineers, 400 inspectors and 180 administrative and support staff. The Department provides services to the residents of the City of LA through 5 construction services centers, 2 testing laboratories and 6 satellite inspection offices covering a metropolitan area of more than 470 square miles.

What Does LADBS DO?

Mission Statement: The Mission of the Department of Building and Safety is to protect the lives and safety of the residents and visitors of the City of Los Angeles and enhance the quality of life, housing, economic prosperity, and job creation. This is accomplished through advising, guiding, and assisting customers to achieve compliance with the Building, Zoning, Plumbing, Mechanical, Electrical, Disabled Access, Energy, and Green codes; and local and State laws through a timely, cooperative, and transparent process for the facilitation of construction and maintenance of commercial, industrial, and residential buildings throughout the City.

Functions and Responsibilities: The responsibilities of the Department of Building and Safety are assigned to the following four bureaus:

The Engineering Bureau is primarily responsible for the plan checking, product approvals, and permit issuance related to building and land use projects within privately owned properties in the City of Los Angeles. In the course of carrying out these responsibilities, the Engineering Bureau enforces the structural, building, disabled access, plumbing, mechanical, electrical, grading, and zoning regulations of the City. In addition, the Engineering Bureau is responsible for reviewing applications for building, plumbing, mechanical and electrical product approvals through its Building Research Section and its Electrical and Mechanical Testing Laboratories.

The Inspection Bureau is responsible for inspection of all construction activities for new and existing buildings, plumbing, mechanical, electrical, elevator and pressure vessel systems, the enforcement of applicable State and Local laws relating to existing buildings and properties, and the administration of various special programs mandated by the City Council. The Inspection Bureau also provides tests and licensing of the deputy inspectors, fabricators and certified testing laboratories.

The Code Enforcement Bureau is responsible for the enforcement of Municipal Code requirements for all violations in existing buildings in the City of Los Angeles except for rental multi-family dwellings. The Bureau handles complaints, citations, processing of vacant and nuisance buildings for repair or demolition, Signs, the Vehicle Establishment Inspection Program, the Proactive Code Enforcement Program, and many more.

The Resource Management Bureau is responsible for the direction and coordination of administrative and financial projects, system development and training. It acts as the emergency disaster coordinator for all Department operations and has developed response and recovery plans for major disaster events.

A Few Facts about LADBS

The following statistics represent the Department's annual construction activities workload:

- Reviews and approves plans for over 34,700 projects
- Issues over 115,200 permits with an estimated valuation of over $3 billion
- Issues over 27,200 e-Permits over the Internet
- Conducts over 667,000 inspections
- Serves over 369,000 walk-in customers
- Serves over 537,300 phone customers
- Brings over 45,500 properties back to compliance
- Issues nearly 14,000 trade licenses for 15 different occupations
- All of these are accomplished by our dedicated, knowledgeable and hard working team of 780 employees.

SEISMIC SAFETY ENHANCEMENTS, IMPLEMENTATIONS AND ENFORCEMENTS

The following code adoptions, implementations and enforcements are essential contributors in the Department's proactive role in resolving building safety and seismic safety issues.

LA City Codes for Design and Construction Projects

The City of LA Building Code was established in 1889 with the appointment of the first superintendent of building. The LA Seismic code design requirements were initiated as a result of a 6.25 magnitude earthquake that struck the City of Long Beach in California on March 10, 1933. Since then, through the intervening years, the LA codes have been amended and revised regularly, mostly every three years, to keep pace with the ever-changing technology of the construction industry and the new proven concepts of structural design.

Three-Year Code Cycle Adoption

The building code is an evolving system. Every three years the International Code Council (ICC) publishes the International Building Code (IBC). Nation-wide, this code is commonly referred to as the model building code. In between the publications of the code, ICC holds code hearings throughout the country to gather input and comments from building officials, engineers, architects, building organizations and other building experts. During this process, the proposals and comments brought up by the various stakeholders are taken to committees within the ICC and to the public for comments. Ultimately, approval by voting is necessary on the proposed changes in order to be included in the next cycle of codes.

Once the IBC is published, each state within the country adopts the code in a certain timeframe. The State of California, like most of the other states, adopts the California Building Code (CBC) after making necessary amendments to the IBC. Local amendments are necessary because the model codes are in a sense too broad and in some cases they can lack specific details for certain regions within the country.

The state of California mandates that all local jurisdictions, such as the City of LA, adopt the California Codes (Building, Mechanical, Plumbing and Electrical) six months after their publications. However, during this period local jurisdictions have the ability to make any necessary amendments to the California Codes. The local amendments to the State codes can only be made due to geologic, topographic or climatic findings and can only be more restrictive.

The City of LA adopts the Los Angeles Building Code (LABC) after making the necessary amendments to the California Building Code (CBC). The LA City has made various local amendments through the years to the California State Codes, which are also carried forward in every three-year code cycle. The new amendments to the Building Code are made by collaborative efforts of committees formed with in-house staff, other local jurisdictions, the Structural Engineers Association of Southern California (SEAOSC), the American Institute of Architects, Los Angeles Tall Buildings Structural Design Council, and other stakeholders. The code enhancements are carefully reviewed based on the past knowledge and experience brought by these highly qualified stakeholders.

Earthquake Risk Management and Education (I)

Current Building Code

The current 2008 LABC is the adopted 2007 CBC, based on the 2006 IBC, with LA's amendments. Earthquake engineering requirements are based on ASCE7-05 published by the American Society of Civil Engineers. The next cycle of City of Los Angeles Building code will be the 2011 LABC.

Approval Process of Construction Projects

The LADBS provides independent review of engineering plans and reports, issues permits and provides inspection at various stages of construction. The LADBS has knowledgeable and experienced plan check engineers and inspectors to perform the work. Most of the engineers are registered Professional Engineers with the State of California. In addition, LADBS has more than 15 supervisors and managers who are registered as Structural Engineers with the State. The Department provides training on a continual basis to its engineers and inspectors to keep them up to date with current engineering practices and code changes and even offers training outside of the Department, for entities such as other agencies and the industry.

Preparation of Plans by Licensed Design Professionals

Construction plans for projects prepared by design professionals are required to be submitted to the LADBS for review and approval. A licensed architect or engineer by the State of California is required for most projects.

Plans/Reports Review and Permit Issuance by LADBS

The process of plan review and construction inspections of permitted projects by LADBS engineers and inspectors is the Department's primary means of ensuring safe buildings. The construction plans, design calculations, and soil and geology reports for building permits are reviewed by the LADBS plan check engineers, soils engineers, and geologists for compliance with the City's codes and regulations. All new buildings, additions, alterations, and tenant improvements require plan check review, permit issuance, and inspection process. This applies to all residential (single family and multi-family dwellings), commercial, industrial, and private school projects. Public schools are handled by a California State Agency. The scope of plan review, permit issuance and inspection of projects are for building, structural, seismic, grading, disabled access, zoning, electrical, mechanical, plumbing, etc.

Required Construction Inspections by LADBS Inspectors

Constructions are inspected by LADBS inspectors in different stages to ensure compliance with the approved plans and to provide quality control and quality assurance necessary for the approved construction. Approval by an LADBS inspector is required before proceeding to each new construction phase. The contractor has to request for inspection after completion of each phase of construction such as grading, foundation, underfloor, framing, shear wall, roof, interior finishes, plumbing, mechanical, electrical, and eventually final inspection. The LADBS inspector identifies work that does not match the approved plans or comply with the city's codes and then prepares written correction notices as needed. Upon completion of the corrections, the contractor requests another inspection.

In addition to the inspections conducted by the LADBS inspection staff, LADBS requires periodic visual structural observations of the engineer or architect of record to assure that major structural elements and connections are properly installed as designed and approved in the construction plans and submittal of structural observation reports to the LADBS Inspector. Also, any phase of work that requires continuous inspection, such as concrete placement or field welding, is required to be witnessed by a third party deputy inspector approved by the City of LA. The deputy inspector provides continuous inspection of the work being performed and provides reports to the LADBS inspectors in order to ensure quality construction. The contractor is held accountable to correct all deficiencies including those identified by the structural observer and deputy inspectors.

Certificate of Occupancy

After completion and approval of all required inspections, a Certificate of Occupancy is issued by an LADBS building inspector. This certificate documents the successful compliance with the requirements of the City's codes and becomes part of the Department's permanent records.

Materials and Products Approval

To assist designers and contractors with selecting code compliant materials and products, LADBS reviews, evaluates, and approves technical reports of materials and products submitted for the Department's approval. These reports are prepared by independent testing agencies approved by the Department using established criteria for fire resistive components, structural connections, materials, etc. The product evaluation criteria are based on American Society for Testing and Materials (ASTM) standards, which are approved by the International Code Council and/or other nationally recognized organizations that develop codes and test standards. The LADBS policy on the approval process is outlined in the LADBS Information Bulletin, "P/BC 2008 -119 Policy on Accepting Alternate Building Materials or Products" can be obtained at: http://ladbs.org/LADBSWeb/information-bulletins.

Lessons Learned from the Past Earthquakes

Every major earthquake provides new knowledge on ground motions and their impact on buildings. It allows engineers to observe and study the performance of the various building constructions during the earthquake and identify necessary modifications to the codes in order to assure safer and more earthquake resistant building designs. The lessons learned from the Northridge Earthquake, a recent major earthquake that hit the LA Basin, have made a significant contribution in enhancing the seismic design requirements of the building code.

In the early morning of January 17, 1994, a 6.7 magnitude earthquake struck Northridge, a populated suburb of Los Angeles (about 30 km. northeast of Los Angeles) in the San Fernando Valley; it caused a lot of damage, particularly in low-rise buildings. This was the worst earthquake to hit the Los Angeles basin since the 1971 San Fernando Earthquake. The Northridge earthquake shaking lasted about 20 sec. Seventy-two deaths were attributed to the earthquake and over 9000 were injured. The earthquake caused an over $30 billion dollars in estimated damage, and it was one of the costliest natural disasters in U.S. history.

Immediately following this earthquake LADBS established a Joint LA City/SEAOSC engineering Task Group to study the earthquake damage to various types of construction. The Task Group looked into the performance and damage of wood frame construction, concrete parking structures, steel frame buildings, non-ductile concrete frame buildings, ground motions, tilt-up wall construction and nonstructural elements, i.e. piping, chimneys, ceilings, etc.

The Northridge earthquake taught us many lessons about the performance of these types of buildings. The results of the studies were used to develop and implement emergency code changes, retrofit standards and code amendments. Some of the reported problems were:

- Narrow wood shear panels, stucco and drywall construction did not perform as expected.
- Numerous hillside residential buildings had severe damage, with some collapsing and causing injuries and a few deaths.
- Masonry and tilt-up concrete wall buildings with wood flexible roof diaphragms needed to be better connected to hold the building components together.
- Numerous steel moment frame welded joints were found to have fractures through the welds and beam-column panels.

The task group later expanded to form an Applied Technology Council (ATC), Structural Engineers Association of California (SEAOC) and California Universities for Research in Earthquake Engineering partnership research program to develop solutions to the problems observed in steel moment-frame buildings. This eventually evolved into the Federal Emergency Management Agency (FEMA) study and the FEMA 350 through 353 documents for steel moment-frame buildings. These documents recommended seismic design criteria for new buildings, seismic evaluation and upgrade criteria for existing buildings, post earthquake evaluation and repair criteria and specifications and quality assurance guidelines, respectively.

LADBS was proactive in proposing code amendments for new construction and mandatory and voluntary seismic retrofit ordinances for existing buildings to mitigate loss of life and damage to property caused by the effects of the next earthquake.

The Northridge Earthquake pointed out the importance of proper detailing and assurance that the load path is maintained. This eventually led the City of Los Angeles to require visual observation of the structural system by the registered design professional in responsible charge for the structural design for general conformance to the approved construction plans at significant construction stages and at completion of the structural system. The structural observation does not include or waive the responsibility for the inspection required by the LADBS inspectors. It also resulted in improved hillside building constructions by requiring new hillside structures to be horizontally anchored to their foundations. In addition, existing wood frame cripple wall buildings are voluntarily being retrofitted with the Los Angeles City’s developed standards, and these are also being used outside the City by other agencies.

Seismic Retrofit Programs in LA

The Seismic Retrofit Programs in the City of Los Angeles (4 mandatory and 5 voluntary programs) are summarized in Tables 1 and 2.

Table 1 Mandatory seismic retrofit program.

Type of Building / Program	Starting Date
Earthquake Hazard Reduction in Existing Unreinforced Masonry Buildings - designed Prior to October 1933 (LABC Chapter 88) 8,080 Buildings Affected	1981
Earthquake Hazard Reduction in Existing Tilt-Up Concrete Wall Buildings - designed Prior to January 1976 (LABC Chapter 91) 2,638 Buildings Affected	1994
Special Provisions for Repair of Welded Steel Moment Frame Buildings in High Earthquake Damaged Areas (Ordinance No. 170406, effective 3/7/95) 520 Buildings Affected	1995
Seismic Gas Shutoff Valves (Ordinance No. 170406, effective 3/7/95)	1995

The above Chapters of the LA City Building Code are found at http://ladbs.org/LADBSWeb/codes.jsf.

Table 2 Voluntary seismic retrofit program.

Type of Building / Program	Starting Date
Earthquake Hazard Reduction in Existing Wood Frame Residential Buildings with Weak Cripple Walls and Unbolted Sill Plates - Anchor LA Program. *Los Angeles City's developed standards, which are being used outside of the City by other agencies* (LABC Chapter 92)	1996
Earthquake Hazard Reduction in Existing Wood Frame Residential Buildings with Soft, Weak or Open Front Walls (LABC Chapter 93)	1998
Earthquake Hazard Reduction in Existing Hillside Buildings (LABC Chapter 94)	1996
Earthquake Hazard Reduction in Existing Reinforced Concrete Buildings and Concrete Frame Buildings with Masonry Infills - *designed Prior to January 1976* (LABC Chapter 95)	1996
Earthquake Hazard Reduction in Existing Reinforced Concrete and Reinforced Masonry Wall Buildings with Flexible Diaphragms - *designed after January 1976* (LABC Chapter 96)	1996

The above Chapters of the LA City Building Code are found at *http://ladbs.org/LADBSWeb/codes.jsf*.

Earthquake Recording Instrumentation

The LABC assists with the future development of earthquake design by requiring strong-motion recording instruments to collect data during seismic events. The LABC requires every new building over ten stories in height or over six stories and more than 60,000 square feet to be equipped with at least three approved recording accelerographs. Installation criteria are described in the LADBS Information Bulletin, "P/BC 2008-048 Specifications for Strong-Motion Accelerographs and Requirements for Installation and Servicing."

In addition, buildings designed using time history analysis methods are required to be equipped with additional instruments. Locations of these instruments are identified during the structural engineering review process. These more complicated building designs are required to use the strong motion system design and criteria described in the LADBS Information Bulletin, "P/BC 2008-117 Structural Monitoring Equipment in Buildings Designed with Nonlinear Response History Procedure." Both of these bulletins may be found at http://ladbs.org/LADBSWeb/information-bulletins.jsf#ib3.

Emergency Response preparedness

The Los Angeles Department of Building and Safety is a key member of the City's Emergency Operations Center (EOC). The Department's EOC will coordinate all resources (i.e., personnel, food, shelter, etc.) within the City family. The LADBS has developed response and recovery plans for major disaster events and continues to update them on a periodic basis. Most of these plans are reviewed annually.

In the event of a catastrophic earthquake, LADBS will:

1. Send mass notification messages to all LADBS employees alerting them of the event and asking them to report their availability.
2. Deploy a team of cadres to respond and assist at EOC.
3. Set up the Building and Safety's Department Operation Center to coordinate all resources within the Department.
4. Set up an Incident Command Post near the epicenter to coordinate all resources within the affected area.
5. Deploy specially trained teams of inspectors and engineers to evaluate whether Essential Government Buildings are safe for continued occupancy or they must be vacated immediately.
6. Direct all other inspection and engineering staff to meet at the Department's Incident Command Post before conducting safety assessment of all other buildings.
7. Damage information is quickly gathered and reported to the Mayor and the City Council. Mutual aid may be requested at this time.
8. Provide rapid evaluation of damaged buildings and post the buildings in accordance with ATC -20 guidelines to inform owners, occupants, and the public about the condition of a damaged building in terms of its suitability for occupancy and general use following an earthquake.

CONCLUSIONS

As described above, the following key functions play critical roles in achieving the Department's mission of enhancing seismic safety in the City of Los Angeles.

- The updated and current City Codes for design and construction with the amendments developed and implemented from lessons learned from past major earthquakes are expected to result in buildings with reliable performance in resisting earthquake forces.
- The LADBS approval process for construction projects has been designed to include independent review of plans and related reports by the Department's experienced and knowledgeable engineers. It also includes inspections by LADBS inspectors in different stages of construction. This process ensures compliance with the City Codes and policies, and construction compliance with the approved plans. It also provides the quality control and quality assurance necessary for the approved constructions.
- The City of Los Angeles earthquake recording instrumentation requirements are result of the Department's remarkable efforts to assist the future development of earthquake designs.
- The Department's emergency response preparedness and recovery plans for major disaster events will assist the City in the recovery phase after catastrophic earthquakes.

Collectively, all of these core functions, along with the LADBS's constant efforts for improving quality control and quality assurance in building constructions, play an integral part to building a safer Los Angeles.

REFERENCES

2008 City of Los Angeles Building Code.

Los Angeles Department of Building and Safety Information Bulletin "P/BC 2008-119 Policy on Accepting Alternate Building Materials or Products."

Los Angeles Department of Building and Safety Information Bulletin, "P/BC 2008-048 Specifications for Strong-Motion Accelerographs and Requirements for Installation and Servicing." *http://ladbs.org/LADBSWeb/information-bulletins.jsf#ib3.*

Los Angeles Department of Building and Safety Information Bulletin, "P/BC 2008-117 Structural Monitoring Equipment in Buildings Designed with Nonlinear Response History Procedure." *http://ladbs.org/LADBSWeb/information-bulletins.jsf#ib3.*

Applied Technology Council (ATC), ATC 20, Procedures for Post Earthquake Safety Evaluation of Buildings (1989) & Addendum (1995).

APPENDIX A

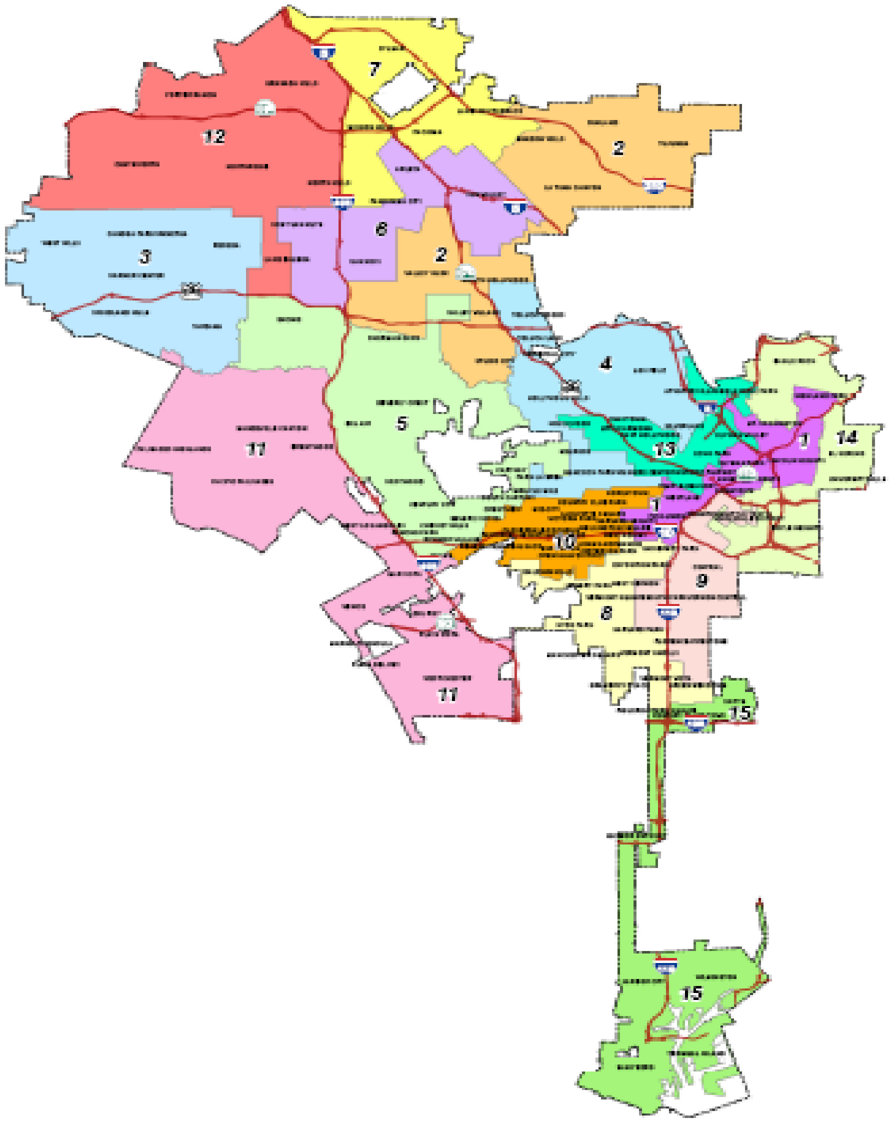

Figure A.1 Map of the City of Los Angeles:15 Council Districts of Los Angeles.

Figure A.2 Seismic fault lines in Los Angeles vicinity.

Source of map:
http://earthquake.usgs.gov/earthquakes/recenteqscanv/FaultMaps/Los_Angeles.html.

Earthquake Risk Management and Education (I)

A STUDY BY UN-HABITAT ON DAMAGE PREVENTION, RISK REDUCTION, AND EMERGENCY RESPONSE OF TEHRAN CITY

Mehmet Emin Akdoğan

UN-HABITAT Tehran Disaster Mitigation Office, I.R.Iran

ABSTRACT

South, West, and Central Asia's vulnerability to disasters, in particular earthquakes, is a historical fact that for centuries has caused the destruction of a huge quantity of habitats and claimed lives of a large number of habitants in this region. Iran is highly vulnerable to natural disasters, particularly earthquakes, and is one of the most arid regions of the world. It suffers from frequent earthquakes, droughts, floods, and landslides. Within the nation's high-risk context, Tehran, the capital and political and economic center of Iran, is one of the most earthquake-prone cities in the world due to its position in the Alpine-Himalayan mountain system, the seismic belt that is one of the most active tectonic regions of the world. In the last few decades, the country has experienced many destructive earthquakes, resulting in the deaths of thousands of people and destruction of many cities and villages, and causing extensive economical damage more than ever in the recent years. The UN-HABITAT Disaster Mitigation Office in Tehran is focused on disaster mitigation and capacity-building in the area of earthquake-resistant housing, with links to disaster mitigation with sustainable relief and reconstruction, including earthquake-resistant technologies. This document addresses some important facts regarding the potential hazard in Iran, the seismicity and vulnerability of Iran, construction and existing types of buildings in Iran and their potential risks, existing building codes in Iran, disaster risk mitigation and disaster risk reduction policies of Iran, and finally the overall role of United Nations and UN-Habitat in Iran. Recommendations and some key challenges within this framework are initiated, and it is hoped that the implementation will provide an assessment of the disaster's impact upon country and local disaster safety policies and programs.

INTRODUCTION

Iran is located between Arabian and Eurasian plates with the occurrence of more than 100 strong earthquakes with magnitude of 7.5 or more in the past centuries, causing extensive human and economic losses. In the last two decades, especially after the Bam and Manjil earthquakes, to ensure the sustainable development and seismic safety of Iran, a multidisciplinary risk reduction strategy with the objective of saving human lives and resources has been initiated. Impacts arising from the potential occurrence of hazards, particularly earthquakes, are to be mitigated through (i) enhancement and following the Iranian and international seismic design requirements; and (ii) developing and implementation of emergency preparedness plans that cover activities to be implemented before, during, and after the occurrence of earthquakes.

A very broad spectrum of Iran's technical and scientific community, and society in general have embraced the overall principles and processes by developing many programs, including the Hyogo Framework for Action and Five Year Development Plans. Achievements during these periods of Actions and Plans have been impressive, but not satisfactory enough.

Seismological research with the objective of more reliable hazard assessment has been the main core of the scientific research needed for risk reduction.

Therefore, as a part of above mentioned implementation plan and to further extend the key objectives resulting in proactive measures, an agreement between the Islamic Republic of Iran and UN-HABITAT signed in April 2007 by Executive Director of UN-HABITAT and the Iranian Minister for Housing and Urban Development to establish the UN-HABITAT Disaster Mitigation Office in Tehran is focused on disaster mitigation and capacity-building in the area of earthquake-resistant housing, with links to disaster mitigation with sustainable relief and reconstruction, including earthquake-resistant technologies. The objectives are to improve Iran's preparedness for potential disasters and earthquakes through promoting the development, dissemination and application of the expertise, experience, applied research, and information on earthquake-resistant construction, strengthening of critical public facilities for earthquake resistance, and supporting measures for better enforcement of building codes and urban development.

This paper focuses on the key observations on the potential seismic hazard in Iran, including the vulnerability of existing buildings, seismic codes, disaster mitigation and disaster risk reduction initiatives, and the overall role of United Nations and UN-Habitat in Iran. In addition, this paper presents the results from a reconnaissance survey conducted by the authors, with particular attention to schools and hospitals that might experience disproportional failures during an earthquake. Finally, efforts underway to develop recommendations to mitigate future seismic damage in the region are summarized.

ABOUT IRAN

Iran, located in Southeast Asia in the Middle East, borders several countries and the Caspian Sea. It is the eighteenth largest country in the world in terms of area at 1,648,195 km, and the country has particular geostrategic significance owing to its location in the Middle East and central Eurasia. The terrain is rugged and very mountainous, and periodic floods, droughts, dust storms, sandstorms, and earthquakes are some of the natural hazards that seriously affect Iran's habitants. Some disasters—for example, floods and droughts—have become more frequent and destructive partly because of global climate change and partly because of local environmental damage. Moreover, Iran is ranked as the fourth most disaster-prone country in the world, and earthquakes in this country pose a great threat owing to the high concentration of population in its major cities, more than three quarters of which are located in potential major earthquakes zones.

Some statistics regarding the potential hazard and disasters in Islamic Republic of Iran can be classified:

- Earthquakes
    - 97% of the country is located on major seismic fault zones
    - 90% of the population lives in seismically active areas
    - 75% of damaged buildings and 64% of total disaster losses in the last century are due to earthquakes

- Recurrent droughts
    - Drought affects more than half of Iran's population of 70 million people
    - About 80% of Iran's total area has arid or semiarid climate
    - A severe drought, such as the one that occurred in the crop year 1999–2000, imposes a direct cost of 1605 million USD, equivalent to 30.3% of the total value
- Flash floods
    - Northeastern and southeastern Iran are well known for deadly flash floods (Oman, Shiraz, Golestan)
    - The Great Iran Flood in 1954, which caused 10,000 fatalities due to flash flooding and landslides, occurred at Isfahan, Bandar Abass.

Tehran, densely populated metropolitan area and home to an estimated 10-12 million people, is covered with seismically hazardous buildings built with no provisions of earthquake-proof seismic codes. Tehran, situated at the foot of the Alborz Mountains, extends to the Alps-Himalaya orogenic zone. The North Tehran and Mosha faults situated towards the northern side of Greater Tehran and the Ray Fault on the southern limits of the city have the potential to generate M_W = 7.2 and 6.7 earthquakes, respectively, which are estimated to cause 150,000 to 500,000 deaths, according to earthquake scenarios developed under the JICA-CEST projects "Study on the Seismic Microzoning of the Greater Tehran Area," [1999-2004].

VULNERABILITY AND SEISMIC HAZARD

Faulting and Tectonics

Earthquakes in Iran are closely connected to their position within the geologically active plateaus, characterized by active faulting, active folding, recent volcanic activities, and considerable elevation contrasts along the Alpine-Himalayan mountain belt, which is the last and the youngest mountainous area in the world and subjected to constant transformation. Geologically, in Iran the plate movement is complicated due to involving three plates on conservative margins: the Arabian plate, the Eurasian plate, and Indo-Australian plate. The spreading of the Red Sea is causing the Arabian plates to move towards Iran (Figure 1).

Much of the mechanical deformation resulting from Arabia-Eurasia collision is accommodated by the Zagros Ranges in the form of folding of rocks and the rise of mountains in conjunction with fault movements at depth of the Earth. In fact, the highest frequency of earthquakes in Iran occurs in the Zagros region. However, because of the diffuse nature of this deformation (i.e., simultaneous movements along a number of sub-parallel faults over a wide area), the intensities of these tremors are generally low and are recordable only by sensitive seismic devices. The interior parts of Iran, however, respond to the plates colliding in a different manner. In the area known as Central-East Iran, deformation takes place largely in the form of strike-slip movements focused along a complex array of intersecting faults. In sharp contrast to that in Zagros, seismic activity associated with central Iranian faults is sporadic but much more localized and occurs at significantly higher magnitudes.

Figure 1 Maps indicating Arabian and Indo-Australian plate.

Vulnerability and Archaeoseismicity

The Islamic Republic of Iran's vulnerability to earthquakes is a historical fact that has for centuries caused the destruction of a huge quantity of habitats and claimed the lives of many inhabitants in this region. Iran is highly vulnerable to natural disasters, particularly earthquakes. It is one of the most arid regions of the world, where frequent droughts, floods, and landslides also occur. In the last few decades, the country has experienced many destructive earthquakes, resulting in the deaths of thousands of people and the destruction of many cities and villages, and causing extensive economical damage.

The vulnerability of the capital city of Tehran and other provincial cities such as Mashhad and Tabriz—which all are located next to several mapped seismogenic faults with documented history of several large-magnitude earthquakes—is scary. Major urban areas across the county are at high risk of being devastated by earthquakes and other natural hazards. The existence of the active North Tehran thrust, the active faults like Mosha and North and South Rey, the alluvium deposits of Tehran plain and Rey city, and the occurrence of severe past earthquakes all indicate the high seismicity of this region. The probability of occurrence of severe earthquakes with magnitudes over 7 is very high (Figure 2).

Since the beginning of this century, at least 126,000 people have lost their lives in destructive earthquakes in this region. The Tabas-e-Golshan earthquake of September 16, 1978, and the Rudbar-Tarom earthquake of June 20, 1990, were the most catastrophic earthquakes to have occurred in Iran in the twentieth century. The Tabas-e-Golshan earthquake destroyed or severely damaged about ninety villages, slightly damaged another fifty villages in the region, and completely demolished the oasis town of Tabas-e-Golshan, where 85% of the inhabitants (11,000 out of 13,000) perished. Total fatalities were more than 20,000, with thousands injured. This earthquake, strongly felt over an area of 1,130,000 square km, destroyed over 15,000 housing units and damaged one-third of the infrastructure in the epicentral region.

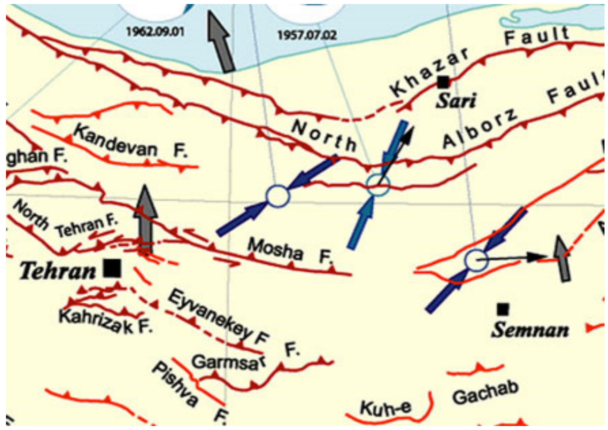

Figure 2 **Simplified structural map of Iran showing the location of major faults.**

The Rudbar-Tarom earthquake, the largest in this century to affect an urban area in Persia, killed over 40,000 people, injured 60,000, and left more than 500,000 homeless. The earthquake destroyed three towns (Rudbar, Manjil, and Lowshan), 700 villages, and damaged another 300 villages in Gilan and Zanjan provinces of northwest Persia, southwest of the Caspian Sea. The principal causes of vulnerability in Iran, which affects earthquake risk management, can be summarized as follows:

- Rapid and uncontrolled urbanization.
- Inexpensive and poorly constructed private dwellings that often fail even in the absence of earthquakes.
- A tendency of the government and general population to ignore the earthquake hazard due to more immediate and basic needs .
- Weak economy and lack of government funds to support earthquake hazard mitigation programs in cities, towns, and villages.
- Lack of or low awareness about the earthquake hazard.
- Lack of seismic rehabilitation programs for upgrading all highly vulnerable public buildings and multiple family residential buildings.
- Lack of enforcement of existing building codes.
- The degradation of the region's environment resulting from the mismanagement of natural resources.
- Lagging and misguided investments in infrastructure.

A proactive stance to reduce the toll of disasters in the region requires a more comprehensive approach that encompasses both pre-disaster risk reduction and post-disaster recovery. It is framed by new policies and institutional arrangements that support effective action. Such an approach involves the following set of activities:

- Risk analysis to identify the kinds of risks faced by people.
- Prevention and mitigation to address the structural sources of vulnerability.
- Risk transfer to spread financial risks over time and among different communities.

- Emergency preparedness and response to enhance the country's readiness to cope quickly and effectively in the event of an emergency.
- Post-disaster rehabilitation and reconstruction to support effective recovery and to safeguard against future disasters.

It has been observed that strengthening buildings and civic structures is the most effective approach to solving the underlying causes of their vulnerability and to effect earthquake disaster mitigation. This initiative is the most time and resource intensive issue; thus, more involvement is needed to raise public awareness and ensure the support and intervention of various stakeholders.

BUILDINGS AND POTENTIAL RISKS

In Iran, the vulnerability of building stock to earthquakes is widely known; however, it is not clear why such weak structures, especially residential buildings, are continuing to be built. Some of the key points related to vulnerability of the building stock in Iran can be summarized as follows:

Building Permits

Ironically, it is believed that the restriction of building permits increases the amount of poor construction. While most older building were built without construction permits, any new modifications in municipalities have strict permit requirements, and these permits are issued in accordance with existing building code; however, often the constructed buildings do not comply with the original design, and there is often collusion between the home owner—who would like to have addition floors— and the inspector and the contractor.

Construction Supervision

The construction supervision enforcement at the construction site and responsibilities are not clearly defined. Only major buildings such as office buildings and shopping centers, which are constructed by major companies, are built with high quality. Residential buildings are given less or little attention.

Earthquake-Resistant Code

Most of older buildings in Iran are made of either un-reinforced masonry or steel buildings constructed without seismic provisions or seismic regulations, which makes them extremely vulnerable to strong ground motion. Given that buildings are not built to code and do not adhere to the building permit process, the earthquake resistance of even newly constructed buildings cannot be verified.

Lack of Earthquake Resistance of Existing Buildings

Measures including retrofitting important facilities and infrastructure in order to secure their operational functionality in the event of an earthquake disaster have not been taken seriously. From an engineering perspective, most of the existing public buildings, particularly schools and hospitals constructed prior to 1995, need to be retrofitted or rehabilitated.

BUILDING STOCK IN TEHRAN

According to municipal statistics, 65% of the building stock in Tehran and 80% in the whole country are of weak or unreinforced masonry, which is considered one of the most vulnerable to earthquake-induced forces; 29% is steel construction and 6% is reinforced concrete. Approximately 90% of all buildings are residential. The inappropriate appraisal of the current system and lack of strict enforcement mechanisms of the seismic standards and codes are contributing factors that increase the physical vulnerability of the city. Hardly any building in Tehran meets the demand expected, because of the difference between the codes, design, material quality, method, and the quality of construction in Iran. Many older buildings of various types in Iran could be retrofitted, and the use of reinforced concrete has been a common practice in the construction of governmental, hospital, some schools, and newer residential buildings.

CONSTRUCTION TECHNIQUES

Most of the old buildings in Iran are of unreinforced masonry and are not engineered; construction of these buildings is based on what has been constructed in the past and there are no building plans. The numbers of stories are up to 4, excluding the basement. After the introduction of seismic code, the construction of engineered buildings using full beam-to column steel framing began. Initially the framing started with Khorjini connection framing but later changed to full beam-column framing.

Most of relatively new buildings are steel frame structures that have the structural deficiency of column beam connection points without forming a proper structural panel zone. High-strength steel profile or wide flange sections (H sections, etc.) are used for special projects, but they are imported. For typical buildings it is customary to use locally produced profiles with St-37 type and locally manufactured profile types, and the sizes are limited.

Even though there are relatively fewer reinforced concrete structures in Tehran, they are also structurally deficient because of inadequate shear walls. They are mostly made of bricks or hollow blocks, and the shearing resistance of such walls is minimal.

The single most important issue for these structures is the lack of quality control regarding the welds and generally poor workmanship. The secondary consideration is the lack of proper design due to the lack of seismic training for designers, in relation to the design of structural and non-structural elements.

Unreinforced Masonry Buildings

The unreinforced masonry buildings in Iran, which are largely built not in accordance with the design drawings, are extremely vulnerable to strong ground motion. The unreinforced masonry buildings are of two types: (1) the earlier version, which is very prevalent, reflects the buildings built prior to the enforcement of the Iranian seismic code. The floor joists are either I beams or concrete joists; and (2) recent versions of unreinforced masonry buildings use tie beams and/or tie beams plus tie columns per the requirements of Iranian seismic code. This type of construction is used in some residential and school buildings in Tehran. The Iranian seismic code only permits masonry structures up to two stories provided that they satisfy other specific limiting criteria.

Steel Structures

The great number of steel structures that were built before 1990 were not based on any seismic code. The older steel buildings are all saddle supported with brick infill. The infill walls are not tied to the framing and can easily separate from the framing during an earthquake. The framing of new steel structures that are built in compliance with seismic code consist of combining existing profiles of different sizes, or are sections made of steel sheets cut to size to form I beams or box sections. The majority of connections are simple supported (hinged) with bracing.

In nearly all of the steel framings the beam-to-column connection, even in most of the so-called moment resisting frames, have poor or inadequate welds; only rarely were full penetration welds observed at the connections. The welds appeared not to have been properly inspected. The quality of the majority of the welded connections is poor, and do not appear to have force and moment resisting capacity larger than the beam or column section. Hence, these connections appear to lack adequate ductility.

Reinforced Concrete Structures

Most of the reinforced concrete structures built in the past are government buildings, hospitals, and a few schools. Until approximately twenty years ago, all the reinforcing bars and stirrups were plain. Obviously, these older reinforced concrete buildings do not necessarily meet the recent seismic code requirements or the ductility demand expected at the connection point. In the last twenty years, the government has encouraged building reinforced concrete structures and they are now common. The older reinforced concrete buildings are regular framing with non-ductile connections and almost all lack shear wall. They use plain reinforcement with inadequate stirrups. This trend continued until the seismic code, which demanded ductile beam-to-column connection, was introduced. The floors of all buildings are jack arch, joist, and block and recently composite construction. In older buildings, the floor joists are not tied. The use of soft story in all types of buildings is very common, resulting in many failures.

Potential Deficiencies and Risks

The typical deficiencies in the buildings can be summarized as follows:

- Buildings’ dead weights are heavy due to thick walls and floors, such as solid brick covered with thick layer of clay mixed with gypsum.
- The infill walls and parapets are not tied to the structural framing system, thus there is no safeguard against their movement during an earthquake.
- The majority of steel joists are not tied together and do not provide diaphragm action.
- Using inadequately trained laborers for steel and concrete buildings has resulted in many defects in the workmanship.
- Lack of proper and frequent supervision by experienced and qualified engineers has left most of the workmanship defects in place.
- Defects in steel construction:
    - Short angle length (top and bottom)
    - Insufficient thickness of angle legs

  - Lack of top angle
  - Poor welding
- The main failure modes of construction are:
  - Buckling and lack of compression strength of slender bracing members, weak spliced bracing members, very weak welded connections, and brittle failure of bracing elements.
- Seismic design code: The implementation of the code is a major issue and in this regard effective training of professionals, providing additional guidelines for the code and effective construction control are essential.
- Lack of skilled labor and construction professionals: Most of the people working in the construction industry are unskilled and unlicensed. This results in poor material production and construction. A process should be implemented to train and license professional working in construction.

SEISMIC CODES

Standard No. 2800 Iranian Code of Practice for Seismic Resistant Design of Buildings, (same as UBC 1997) was established in 1989 after the Tabas earthquake (1978) and Naghan earthquake (1977). A second version was issued in 1999 after Manjil earthquake (1990). A third version was issued in 2005 and revised partially in 2008 after the Bam earthquake (2003). Standard 2800 encompasses the building of reinforced concrete, steel, wood, and masonry structures. The service life of building is considered 50 years. There are also several guidelines on the seismic codes and rehabilitation of existing structures. (Code 360, 390, 376 (Reinforced Masonry), 364)

Technical Observations on 2800 Code

- There are slight differences between the Standard 2800 code and Iranian Guidelines among which:
  - The Standard 2800 uses the behavior coefficient, R, to bring the nonlinear behavior into analysis. While the Iranian Guideline uses the partial ductility coefficient (m-factor) for this purpose. The behavior coefficient is constant for all members of an individual building. But the m-factor depends on the axial forces of the members.
  - The Standard 2800 code does not match the Iranian Guideline in terms of safety performance at the design hazard level.
  - Linear analyses are not reliable for the vulnerability assessment of building with moment resisting frames.
  - Nonlinear static and dynamic analyses show that the displacement coefficient method overestimates the target displacement.
- According to 2800 code, spectra is acquired through far-fault ground motions whereas the effects of near-fault ground motion is not considered:
  - Near-fault ground motions have more severe effects on short-period and long-period structures.

    - Inefficiency of designed structures under near-fault ground motions according to IRAN 2800 code, especially the short and tall buildings, verifies an essential revision in IRAN code to consider the near-source effects.

- The 2800 Standards overestimates the displacement of buildings and considering the vertical component of earthquake in far-fault areas can lead to an overestimation of axial force of columns that has no significant effect on the maximum displacement of stories.

DISASTER MITIGATION AND REDUCTION POLICIES

It is crucial to enhance preparedness in advance and increase resilience through mitigation and safe construction before an earthquake strikes. With proper mitigation and preparedness, the damage and losses caused by an earthquake can be minimized. In the Islamic Republic of Iran, the National Disaster Management Organization (NDMO) is responsible for defining policies, guidelines, and plans based on the overall policies of "prevention and reduction of the impact of natural disasters" endorsed by the supreme leader of the Islamic Republic of Iran, as well as the mandate forming the NDMO.

On the national level, disaster risk management in Iran is under the overall supervision of the Ministry of the Interior (MOI), as explained in the Law of Foundation of National Committee for Mitigation of Natural Disaster Effects. Two specialized bodies were created to provide support and organize the disaster management activities: The Bureau for Research and Coordination of Safety and Reconstruction Affairs (BRCRS), which has a broad mandate that includes research, formulation of preparedness and mitigation plans, collection, analysis and dissemination of related information, coordination of relief, and reconstruction and rehabilitation; it is encouraged to look for national and international alliances to achieve its mandate.

To ensure the sustainable development of Iran, since the early 1990s—and especially after the 1990 Manjil earthquake—a multidisciplinary risk reduction strategy with the objective of saving human lives and resources was initiated with an adaptable disaster management system. The government has adopted the National Plan on Natural Disasters Prevention that contains policies, actions, and programs with national, regional, and local focus that includes financial, educational and research aspects in the field of disaster prevention. It has three main components:

- Monitoring and early warning
- Risk assessment
- Mitigation and response

The annual budget for disaster risk reduction is generally the 2.5% of the total annual budget of the country; 1.5% of this sum is allocated for advocacy and damage reduction, and a portion of this amount is also used for emergency management.

Tehran

In Tehran, the Mayor is the official Commander for disaster management and the City Council work as a regulatory body. All activities related to disaster mitigation and management are managed at "Tehran Disaster Mitigation and Management Centre

(TDMMC)." The TDMMC falls under the direct control and guidance of the city's mayor. Its mandate includes mitigation, preparedness, emergency response, and reconstruction and rehabilitation activities.

The Master Plan for Urban Seismic Disaster Prevention and Management in Tehran has been prepared by the TDMMC with the support of the JICA, a disaster mitigation policy section that includes education, coordination capabilities, and institutional strengthening. Community-based activities for disaster preparedness, the reformulation of an emergency response plan for the city, and suggested implementation procedures for the master plan have been developed and are schedule to be completed by 2015. The challenges related to improving disaster preparedness and reducing the effects of disasters in Iran have many elements:

- Minimizing overlap of responsibilities between different administrative bodies.
- Lack of direct and effective involvement of local communities (development planning, construction, crisis management preparation, communication, population, etc.).
- The lack of dissemination of valid information on the direct and indirect consequences of earthquakes.
- Enforcing more efficiently the urban building codes designed to make buildings more earthquake-resistant and extending controls to the smaller towns and the countryside.
- Campaigning through schools, the media and local authorities for greater public awareness of the danger of disaster and of how ordinary citizens can participate in prevention and relief.
- The lack of active enhancement of a long-term (5-15 years) comprehensive action plan for sustainable urban development.

THE ROLE OF UN-HABITAT IN IRAN

About UN-Habitat

Established in 1978, the United Nations Human Settlements Programme (Habitat) is the lead agency within the UN system for coordinating activities in the field of human settlement development. It also serves as the focal point for monitoring progress on implementation of the Habitat Agenda—the global plan of action adopted at the Second United Nations Conference on Human Settlements (Habitat II), held in Istanbul, Turkey in 1996.

As an agency with global responsibilities, UN-HABITAT needs to find ways of maximizing its impact; its resources must be focused, and policy principles and approaches must be strategic. These principles are derived from UN-HABITAT's own experience of what works, and also from the experience of its partners. National governments, local authorities, non-governmental organizations (NGOs), community organizations, and the private sector are UN-HABITAT's partners.

Earthquake Risk Management and Education (I)

Mandate and Mission

HABITAT focuses on the following priority areas:

- Shelter and social services.
- Urban management.
- Environment and infrastructure.
- Assessment, monitoring, and information.

The UN-Habitat Disaster Mitigation Office, Tehran

The UN-HABITAT Disaster Mitigation Office in Tehran was established in April 2007 with an agreement between the Islamic Republic of Iran and UN-HABITAT, signed by Executive Director of UN-HABITAT and the Iranian Minister for Housing and Urban Development. The UN-HABITAT Disaster Mitigation Office in Tehran is focused on disaster mitigation, capacity-building in the area of earthquake resistant housing, with links to disaster mitigation with sustainable relief and reconstruction, and dissemination of earthquake-resistant technologies within the region.

Mandate and Mission

The primary responsibilities of the office pursuant to the mandate of UN-HABITAT related to the sustainable human settlements development are stated in the Article 3 of the Agreement:

- Strengthen the co-operation of the Islamic Republic of Iran and other United Nations Member States with UN-HABITAT and other UN agencies, programmes, and funds in the field of Earthquake resistant construction.
- Increase the possibilities for the interested Member States to provide development resources and contribute towards capacity enhancement in earthquake-resistant construction through technical and financial means.
- Promote participation of the experts, scientists, and urban managers in UN-HABITAT activities and more specifically in the field of earthquake-resistant construction.
- Promote UN-HABITAT mandated activities in the Islamic Republic of Iran.

Program

Technical cooperation projects coordinated by the UN-HABITAT Tehran Disaster Mitigation Office are related to rehabilitation of urban settlements in Iran, including improvement of Iran's preparedness for potential disasters and earthquakes through promoting the development, dissemination, and application of the expertise, experience, applied research and information on the earthquake-resistant construction, strengthening critical public facilities for earthquake resistance, and supporting measures for better enforcement of building codes and urban development. The Office has initiated a five-year work plan by dividing the above objectives into four main components:

Component A: Workshops, Seminars, and Sustainable Urban Development

The objective of this component is to undertake advocacy on earthquake resistant-housing retrofitting and reconstruction in both urban and rural areas through regional workshops, seminars, international conferences and publicity activities, and providing technical support and assistance by implementation of various programs relating to earthquake-resistant construction, which include:

- Regional workshops on international cooperation in the field of human settlements and post earthquake reconstruction.
- Workshops and conferences on disaster mitigation.
- Development of working groups and to widen cooperation for sustainable development of human settlements.

Component B: Project Management and Model Cities

The objective of this component is to support the Government to implement the project in an efficient and transparent manner, and build the institutional capacity to sustain the implementation of Seismic Risk Mitigation and Preparedness program beyond the life of the project, which includes:

- Project management support, including support for monitoring and evaluation.
- Implementation of activities on sustainable urban development by development of model cities and enhancing the capacity of government organizations.
- Facilitate the mobilization of financial resources for earthquake-resistant retrofitting and reconstruction.

Component C: Seismic Risk Mitigation for Public Facilities and Housing

The objective of this component is to reduce the risk of future earthquake damage to critical facilities and lifelines in order to save lives and ensure their continued functioning in the event of an earthquake. In the case of critical medical facilities where retrofitting is deemed to be unfeasible, some reconstruction may be included in this component. This component includes:

- Retrofitting or reconstruction of critical public facilities such as hospitals, clinics, schools, UN Buildings, foreign embassies, administration buildings, infrastructure, etc.
- Risk assessment of lifelines and vital infrastructure.
- Risk assessment of cultural heritage buildings.

Component D: Enforcement of Building Codes

The objective of this component is to support innovative approaches to better enforcement of building codes by promoting the development, dissemination, and application of expertise, experience, applied research, and information on earthquake-resistant construction. This component includes:

- Capacity building in the field of earthquake-resistant construction.
- Further development of regulatory framework.
- Facilitate the development of guidelines for construction of earthquake-resistant housing in urban and rural areas.
- Facilitate the development of guidelines for the retrofit of the existing building in urban and rural areas.
- Streamlining community re-planning, land adjudication mechanisms, and community-based disaster management systems.

FINAL REMARKS AND RECOMMENDATIONS

Final Remarks

UNHABITAT's support to the government of Iran is well placed in this regard, as it focuses on strategic planning of disaster risk mitigation to ensure progressive disaster risk reduction. The goals of the project will be reached through enhancement of Urban Earthquake Risk Mitigation program and projects with the following goals:

- Translating national disaster risk mitigation policies into local and intermediate level practices towards sustainable risk reduction.
- Increasing participation and awareness of local communities
- Enhancing coordination mechanisms among stakeholders at local and national levels.
- Developing a system for effective disaster risk management at all levels.
- Developing standards for reducing disaster risks across the country.
- Recognition as a proactive and responsive regional resource.
- Development of sustainable partnerships and networks in the region.

Recommendations

It is recommended that the following actions be considered during the overall implementation of Disaster Mitigation programs:

- First and foremost, the fundamental way for managing earthquake risk is that reactive approaches for handling natural disasters be replaced by a more proactive attitude against the risk.
- Periodic loss estimation exercises based on detailed hazard, vulnerability, and risk assessment need to be carried out.
- Building codes need to be enforced in both the design and construction process by engineers. The public should know that it is an essential task to have the building designs checked by qualified engineers.
- More stakeholders should get involved in key areas of earthquake risk reduction.

- Uncertainties are inherent with earthquakes. Earthquake magnitudes cannot be predicted precisely and their intensity may vary due to various factors. Therefore, complete risk mitigation is not practical unless authorities consider risk financing measures in larger cities in addition to physical risk reduction measures and policy interventions.

ACKNOWLEDGMENTS

The authors acknowledge the contributions made by the teams in their respective organizations in Tehran, Iran. We also acknowledge the inputs made by UN organizations and UNHABITAT Disaster Mitigation Office. A special tribute is made to the late Mr. Alireza Esmaeilzadeh (Chief, UN-HABITAT, Tehran, Iran) for his significant contributions to the sections of the role of UN-HABITAT.

REFERENCES

Building Housing Research Center (2007). Standard 2800, Iranian Code of Practice for Seismic Resistant Design of Buildings, 3rd ed., Iran.

JICA-CEST (1999-2004). Study on the seismic microzoning of the greater Tehran area."

Berberian, M. (2004). Opinion: earthquake management in Iran, *Iran Analysis Quarterly*, 1(2).

International Institute for Earthquake Engineering and Seismology, www.iiees.ac.ir/English/eng_index.html

Amiri, C.G., Motamed, R., Es-Haghi, H.R. (2007). Seismic hazard assessment of metropolitan Tehran, Iran, *J. Earthq. Engrg*., 7(3):347-372.

American Society of Civil Engineers (2006)., Seismic retrofit of existing buildings, ASCE-41, Reston, VA.

Haghipour, A., Aghanabati, A. (2007), Geological Map of Iran, 2nd ed., Tehran, Geological Survey of Iran, scale 1:2,500,000.

Jackson, J., McKenzie, D. (1984). Active tectonics of the Alpine-Himalayan Belt between western Turkey and Pakistan, Geophys. J. Royal Astro. Soc., 77:185-264.

UNDP Iran: see *www.undp.org.ir.*

National Geoscience Database of Iran: *http://www.ngdir.ir/.*

Tehran Disaster Mitigation and Management Organization: see *http://oldentdmmo.tehran.ir/.*

Risk Profile, Iran Prevention: see *http://www.preventionweb.net/english/countries/statistics/risk.php?iso=irn*

SEISMIC MICROZONATION CASE STUDIES

Atilla Ansal, Gökçe Tönük, and Aslı Kurtuluş

Kandilli Observatory and Earthquake Research Institute, Boğaziçi University, Istanbul, Turkey

INTRODUCTION

Seismic microzonation may be defined as the process for estimating the response of soil layers under earthquake excitations and the variation of earthquake characteristics on the ground surface. The main purpose of microzonation is to provide information for urban planning and for vulnerability assessment of the building stock for different hazard (performance) levels.

Relative variation of hazard due to differences of earthquake characteristics can be used to introduce earthquake effects as one factor in urban planning and land use management. Seismic microzonation of probable earthquake characteristics is also important for structural designers and builders to enable them to anticipate earthquake related problems. However, site-specific investigations to estimate design earthquake characteristics still need to be performed for the design of special and important buildings, and for rehabilitation and retrofit projects.

SEISMIC MICROZONATION CASE STUDIES

The adopted microzonation methodology is based on a grid system and is composed of three stages. In the first stage, regional seismic hazard analyses need to be conducted to estimate earthquake characteristics on rock outcrop for each cell. In the second stage, the representative soil profiles should be modelled based on available borings and *in-situ* tests. The third stage involves site response analyses for estimating the earthquake characteristics on the ground surface and the interpretation of the results for microzonation. In addition, microzonation maps with respect to spectral accelerations, peak accelerations, and peak velocities on the ground surface can be estimated to assess the vulnerability of the building stock [Ansal et al. 2006a] and lifeline systems [Ansal et al. 2008].

The proposed microzonation methodology was developed based on microzonation studies conducted in Turkey during the last decade, with significant improvements in the methodology during the DRM project and related pilot studies for Adapazarı and Gölcük after 1999 Kocaeli and Düzce earthquakes [Ansal et al. 2004; Studer and Ansal, 2004]. The proposed microzonation methodology was later applied to Zeytinburnu Municipality as a pilot project for Istanbul Earthquake Master Plan and to six municipalities during the World Bank project MEER. During this period, also a Microzonation Code was drafted for Istanbul Metropolitan Municipality. The methodology was further developed during EU FP6 LessLoss project [Ansal et al. 2007] and for the microzonation conducted for Bolu [Ansal et al. 2009].

A microzonation project generally starts with a regional seismic hazard study to estimate the detailed earthquake characteristics on the engineering bedrock outcrop for the adopted grid system. In the case of microzonation for urban planning, it is preferable to adopt probabilistic earthquake hazard assessment, since the purpose is to provide general guidelines for land use and urban planning. By definition, a probabilistic approach accounts for all possible earthquake source characteristics and ground motion probabilities to estimate earthquake characteristics at the site for different exceedance probabilities for a given time period. Independent of the methodology adopted for the earthquake hazard evaluation—whether it is probabilistic or deterministic, previously recorded, or simulated—suitable acceleration time histories are needed to conduct site response analyses for the investigated area.

As demonstrated by Ansal and Tönük [2007], if limited number of input acceleration time histories (e.g., 3 records as specified in some earthquake codes) are used (even with scaling to the same PGA amplitudes for site response analysis), the results in terms of ground shaking intensity can be different for different sets of input acceleration time histories. Therefore, it is preferable to use as many hazard compatible acceleration time histories (in terms of expected fault type, fault distance, and earthquake magnitude) as possible to conduct large number of site response analyses, taking into account the variability due to probable earthquake characteristics. In using real acceleration records, PGA scaling approach is adopted.

Site characterization needs to be performed for each cell based on available borings and other relevant information to define representative shear wave velocity profiles down to engineering bedrock. Two issues are important in determining local site conditions. The first issue is the soil classification for each layer encountered within the soil profile based on laboratory soil index tests performed on samples obtained from all borings. The second issue is the depth of the engineering bedrock, which can be defined as the layer with shear wave velocity, $Vs \geq 750$m/sec and the ground water level.

Site conditions are generally classified according the representative soil profiles selected for each cell based on the detailed assessment of the available geological and geotechnical data. The soil classification based on different earthquake codes is a Grade 1 type of microzonation with respect to ground shaking intensity [ISSMGE/TC4 1999]. Based on site classifications, these zonation maps are very similar to the zonation maps developed based on geological formations. Zonation maps based on site classification or geologic formations are very rough because both site classification in the earthquake codes and geological formations are defined within relatively large ranges, only involving one part of the microzonation problem by neglecting the effects of earthquake characteristics.

The site characterizations, as well as all the analyses performed, require various approximations and assumptions and, therefore, the absolute numerical values for the selected ground shaking parameters may not be very accurate and besides may not be needed for urban planning purposes. Their relative values are more important than their absolute values.

In this approach, variations of the calculated parameters for each cell are considered separately and their frequency distributions are used to determine the 33% and 67% percentiles to define the boundaries between the three zones. The zone A shows the most favorable 33 percentile (e.g., low spectral accelerations), zone B shows the intermediate 34% percentile and zone C shows the most unsuitable 33% percentile (e.g., high spectral accelerations). However, if the difference between 33% and 67% percentile values is less than 20%, the microzonation area is divided only into two zones, using 50% percentile value since definition of three zones based on relatively small differences may not be practically justifiable [Studer and Ansal, 2004].

Microzonation parameters are mapped using GIS techniques by applying linear interpolation among the grid points, thus enabling a smooth transition of the selected parameters. Soft transition boundaries are preferred to show the variation of the mapped parameters. Clearly defined boundaries are not recommended due to the uncertainties in all stages of the analyses to allow some flexibility to urban planners and avoid misinterpretation by the end users that may consider the clear boundaries as accurate estimations of different zones.

The purpose in assessing the ground shaking intensity is to estimate the relative effects of local site conditions on the level of earthquake characteristics. All available data for site characterization, such as average shear wave velocity (V_{s30}), and results of site response analyses conducted for each cell should be evaluated together to achieve practically applicable and consistent results.

Site response analysis, whether it is conducted by Shake91 [Idriss and Sun 1992] or using similar programs can sometimes yield relatively high spectral amplifications or low peak ground acceleration values depending on the thickness of the deposit, estimated initial shear moduli, and on the characteristics of the input acceleration time histories. Even though the amplification relationships such as the ones suggested by Borcherdt [1994] are more empirical, the spectral accelerations based on average shear wave velocity may yield consistent results for soil profiles.

The ground shaking intensity microzonation map reflecting the estimated relative shaking intensity levels is based on the combination of two parameters. The first parameter is peak spectral accelerations calculated from the empirical relationship proposed by Borcherdt [1994] using average shear wave velocities. The second parameter is average spectral accelerations calculated between the 0.1 sec and 1 sec periods of the average acceleration spectrum determined from all site response analyses conducted for each cell. The microzonation map with respect to ground shaking intensity is calculated by the superimposition of the microzonation maps with respect to these two parameters. The use of empirically and analytically calculated spectral accelerations is assumed to provide a realistic assessment of the variation of site effects in estimating the ground shaking intensity for urban planning and land use management as shown in Figure 1.

Figure 1(a) is microzonation map with respect to peak spectral accelerations based on Borcherdt [1994] produced in accordance with the relative mapping. For this case, since the difference between peak spectral accelerations calculated corresponding to 33% and 67% percentiles was less than 20%, the area was divided into two zones using 50% percentile as suggested by Studer and Ansal [2004]. In Figure 1(a), A_{BORCH} shows the most favorable zones and C_{BORCH} shows the most unsuitable zones with respect to peak spectral accelerations. In Figure 1(b), microzonation map with respect to the second microzonation parameter, the average spectral accelerations between 0.1sec and 1sec periods, determined from site response analyses is given for Zeytinburnu where A_{AVG} shows the most favorable zones C_{AVG} shows the most unsuitable zones.

The final microzonation map is the superimposed map of the average spectral acceleration microzonation map calculated by site response analyses and the short period spectral acceleration microzonation map calculated using Borcherdt [1994] formulation. The superimposed map is composed of three relative zones (A_{GS}, B_{GS}, C_{GS}) where A_{GS} shows the areas with lower ground shaking, and C_{GS} shows the areas with higher ground shaking intensity as shown in Figure 1(c).

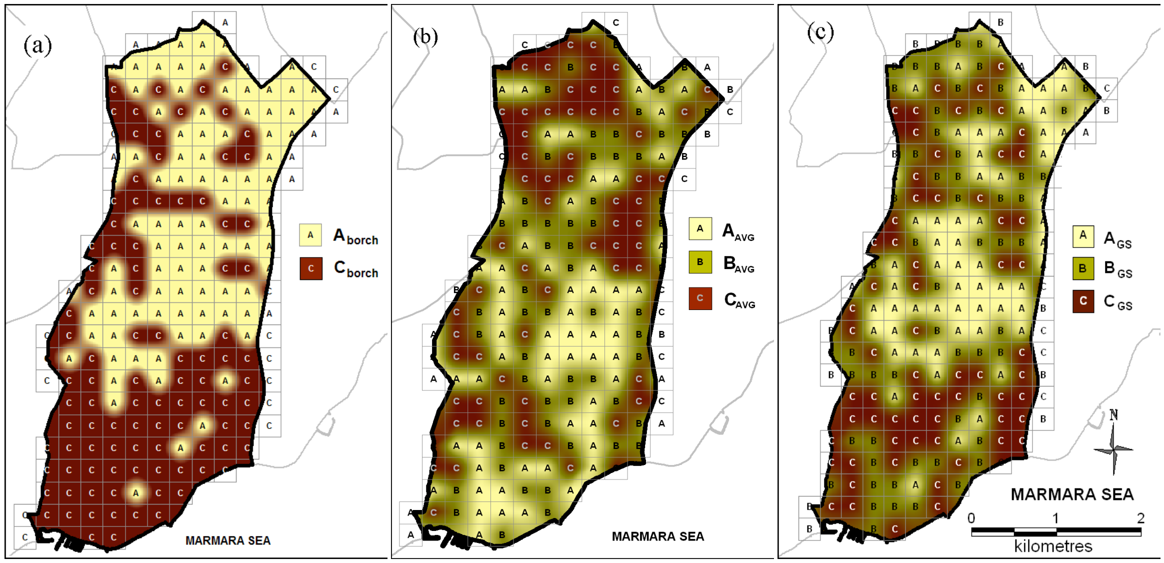

Figure 1 Microzonation with respect to ground shaking intensity for Zeytinburnu, Istanbul.

REFERENCES

Ansal A, Tönük G, Kurtuluş A (2009). Microzonation for urban planning, earthquakes and tsunamis, A.T. Tankut (ed.), *Geotechnical, Geological, and Earthquake Engineering Book Series*, Springer, pp.133-152.

Ansal A, Kurtuluş A, Tönük G (2008). Damage to water and sewage pipelines in Adapazari during 1999 Kocaeli, Turkey Earthquake, *Proceeding*, 6th Internationl Conference on Case Histories in Geotechnical Engineering, Arlington, Virginia, ABD, Paper No:3.17

Ansal A, Kurtuluş A, and Tönük G (2007). Earthquake damage scenario software for urban areas, *Computational Methods in Structural Dynamics and Earthquake Engineering*, M. Papadrakakis, D.C. Charmpis, N.D. Lagaros, Y. Tsompanakis (eds.), CRC Press.

Ansal A, Tönük G (2007). Source and site effects for microzonation, *Earthquake Geotechnical Engineering*, K.Pitilakis (ed.), Springer, pp.73-92.

Ansal A, Tönük G, Demircioglu M, Bayrakli Y, Sesetyan K, Erdik M. (2006). Ground motion parameters for vulnerability assessment, *Proceeding*, First European Conference on Earthquake Engineering and Seismology, Geneva, Switzerland, Paper No. 1790.

Ansal A, Erdik M, Studer J, Springman S, Laue J, Buchheister J, Giardini D, Faeh D, Koksal D. (2004). Seismic microzonation for earthquake risk mitigation in Turkey, *Proceeding*, 13th World Conference on Earthquake Engineering, Vancouver, Canada, CD Paper No.1428.

Borcherdt RD (1994). Estimates of site dependent response spectra for design (methodology and justification), *Earthq. Spectra*, 10(4):617-654.

Idriss I M, Sun JI (1992). *Shake91, A Computer Program for Conducting Equivalent Linear Seismic Response Analysis of Horizontally Layered Soil Deposits*, (modified based on the original SHAKE program Published in December 1972 by Schnabel, Lysmer and Seed.)

ISSMGE/TC4 (1999). *Manual for Zonation on Seismic Geotechnical Hazards, Tech. Com. for Earthquake Geotechnical Engineering* TC4, ISSMGE, Japanese Society of Soil Mechanics.

Studer J, Ansal A (2004). *Manual for Seismic Microzonation for Municipalities, Research Report for Republic of Turkey*, Ministry of Public Works and Settlement, General Directorate of Disaster Affairs prepared by World Institute for Disaster Risk Management, Inc.

CHALLENGES TO PUBLIC SEISMIC EDUCATION

William A. Anderson

National Research Council, National Academy of Sciences (Retired), USA

ABSTRACT

The United States is similar to many other seismically active countries regarding the need to further the resilience of vulnerable cities through the dissemination of science-based information that can enhance public awareness of the earthquake threat and provide guidance on risk reduction actions. Public seismic education in the U.S. is a multidisciplinary and multisectoral enterprise anchored by the National Earthquake Hazards Reduction Program. Some of the key challenges facing public earthquake education in the U.S. today include closing relevant knowledge gaps, furthering multidisciplinary cooperation, and determining when best to launch either single or multiple hazard education initiatives. Learning from and exchanging information with other societies, stakeholder relations with the mass media and the effective evaluation of educational initiatives present additional challenges.

INTRODUCTION

The United States is the third most populous country in the world and 81% of its population is urban, a key factor in its vulnerability to earthquakes and many other types of hazards. Large cities throughout the country, such as Los Angeles and San Francisco, California; Seattle, Washington; and Memphis, Tennessee, are exposed to significant earthquake risk. The U.S. shares this risk of urban-centered earthquakes with many other developed as well as developing countries.

The 2010 Haitian earthquake, with over 200,000 killed and billions of dollars in property losses, reminds us of this great threat to urban life throughout the world. The mitigation-oriented activities of the global Earthquakes and Megacities Initiative [EMI 2010] reflect the reality that many urban locales in both developed and developing countries are seriously endangered by earthquake hazards. The significance of this threat, of course, is that cities are the societal cornerstones because in them are found the key governmental, educational, industrial, and cultural institutions. Thus major losses incurred in urban areas can have widespread impact throughout society, as was the case in Haiti. Unfortunately, even many long-time residents of threatened urban areas throughout the world have inadequate awareness of the risk they face or what to do about it. This is why public earthquake education is so crucial.

The U.S. is similar to many other countries in terms of the need to further the resilience of populations in its vulnerable cities and other at-risk areas by disseminating scientifically credible information about the threat of earthquakes and how to counter it, not only to those in the relevant scientific and engineering communities but more broadly throughout society. This is the role of public earthquake education, a vital but sometimes underappreciated tool for furthering effective earthquake hazard reduction, preparedness, and response actions by a vulnerable population.

Public seismic education in the U.S. is the provision of earthquake information derived from multidisciplinary sources to the general public. Its purpose is to promote pre-disaster hazard awareness and such risk-wise behavior as mitigation and preparedness that can result in disaster resilience at the individual, household, organizational, and community level. It involves providing citizens guidance on protective actions that can be undertaken before, during, and after an earthquake.

Public earthquake education can be a daunting process. There is always more knowledge produced by the scientific community than will be put to use, either by other experts or the general public. And knowledge that is made available to the public by experts may not always produce the desired results. Thus it cannot be taken for granted that knowledge provided through public earthquake education is the most appropriate, that it is always producing the best results, and that it is furthering the resilience of vulnerable groups to the greatest extent possible. Such matters have to be assessed, as will be discussed later.

The public earthquake education system in the U.S. can be characterized as a collaborative network of government, private sector, and civil society organizations. It offers the general public such activities and products as hazard maps, earthquake safety handbooks and brochures, internet sites for children, videos, disaster kit information, home protection guides, museum programs, and reference materials and lesson plans for teachers [Anderson 2008]. Many of these efforts are focused on children, as is the case in many other countries.

This paper will focus on some of the key challenges facing public earthquake education in the U.S. Such challenges might be similar to those faced in other societies, including Iran and Turkey, but comparative research is required to determine the extent to which this is the case, as well as what different societies might learn from each other.

SCIENTIFIC FOUNDATION OF U.S. PUBLIC SEISMIC EDUCATION

Public earthquake education in the U.S., as elsewhere, requires a scientific underpinning that is multidisciplinary in nature. At a minimum, knowledge from the earth sciences, engineering, and the social and behavioral sciences is most relevant. The earth sciences contribute knowledge on the nature of the seismic hazard that the public needs to be made aware of, including the causes of earthquakes and where they are most likely to occur. Earthquake engineers contribute information on who is at risk and how the public's vulnerability can be reduced through science-based building design and construction practices for schools, living and work sites, and community infrastructure. Finally, even though this is often overlooked, the social sciences also have a vital role to play in public earthquake education in the U.S., providing knowledge on how the public perceives the earthquake risk, how the risk can be effectively communicated to the public, and how humans actually and should behave in the face of earthquakes and other hazards.

This paper will devote special attention to the role of the social and behavioral sciences in public earthquake education. Since public earthquake education is all about changing the behavior of the vulnerable in society to make them less so, it is ironic that the role of the social sciences in this regard is often overlooked, or at least not maximized, since human behavior is the research domain of social scientists.

Social and behavioral science research on earthquakes and other hazards has been conducted in a systematic way for over fifty years in the U.S., a short time compared to work in other relevant disciplines such as seismology and earthquake engineering, but still long enough so that a significant body of work has been produced [NRC 2006; Nathe et al. 1999]. Because of this research, public seismic education efforts in the U.S. can be grounded in a number of social science facts as well as those from the earth sciences and engineering. For example, social science-based facts that designers of public seismic education programs and campaigns in the U.S. can take into account include the following:

- Families are key decision making units in the hazards context.
- Families with children give more attention to earthquake preparedness.
- Disaster vulnerability varies among groups in society.
- Individuals with few social network connections are at higher risk to disaster.
- Social groups can vary significantly in their trust of disaster authorities.
- The public usually wants more information rather than less about hazards.
- People are more willing to take protective action when they feel that there is something they can do to reduce their vulnerability.
- Women and children are not only potential victims of disasters, but vital resources for dealing with them as well.
- Societal change produces both challenges and opportunities for adjusting to earthquakes and other hazards.

As a complement to these basic facts about risk-related human behavior, social scientists have, through their research on risk communication in the U.S., also produced important prescriptive knowledge to guide the development of public seismic education programs and campaigns [Nathe et al. 1999]. These include the following prescriptions:

- Complicated scientific and technical information should be explained in non-technical terms and communicated clearly to the public.
- Information should come from many credible sources.
- Information should be consistent and presented in many different media.
- Information should tell people what they can do before, during, and after an earthquake.
- Recent earthquakes should be used as “windows of opportunity” for public earthquake education.
- The effectiveness of educational initiatives should be assessed.

Since 1977, most of the knowledge developed by social and behavioral scientists in the U.S. related to earthquakes that can inform public earthquake education activities and those for many other natural hazards was made possible through financial support from the National Science Foundation (NSF), a participating agency in the U.S. National Earthquake Hazards Reduction Program (NEHRP).

A NEHRP ANCHOR

Public earthquake education policies and efforts have existed for several decades in the U.S. and have involved actors in government, the private sector, and civil society. The creation of the U.S. National Earthquake Hazards Reduction Program in 1977 was a major turning point because it then became possible for the four federal agencies that comprise the program to assume a leadership role in developing policies and programs related to public earthquake education along with various research programs and technology transfer activities. Besides NSF, the other agencies that comprise NEHRP are the National Institute of Standards and Technology (NIST), the U.S. Geological Survey (USGS), and the Federal Emergency Management Agency (FEMA).

Within NEHRP, FEMA was authorized by the U.S. Congress to assume the main responsibility for helping to bring public earthquake education efforts to states and local communities. Its early actions, for example, included working with and providing financial support to two regional organizations in California which carried out public earthquake education programs: the Southern California Earthquake Preparedness Program [Lambright 1985] and the Bay Area Regional Earthquake Preparedness Project. In 1993 these two activities were combined to form the Earthquake Program in what is now called the California Emergency Management Agency. Another example of FEMA's enabling efforts along these lines is its support of the Central U.S. Earthquake Consortium (CUSEC), which carries out public earthquake education activities in the eight participating states in the New Madrid Seismic Zone. The Northeast States Emergency Consortium which carries out all-hazards education activities, including earthquake- related ones, in eight states in the region is also supported by FEMA.

As part of NEHRP, USGS has played a vital part in public earthquake education and outreach in the U.S. This has involved taking a leadership role in developing earthquake preparedness handbooks, designing large-scale earthquake educational campaigns, providing information to the public through print, radio, and television media, and establishing educational partnerships with state and local governments and such nongovernmental organizations as the Red Cross.

As mentioned earlier, over the years NSF has been the principal supporter of earthquake-related social science research. The agency has also been the principal U.S. government supporter of major earthquake research centers and thus has been in a strong position to help guide the direction of the public outreach efforts of these important institutions. When the first earthquake engineering research center, the National Center for Earthquake Engineering Research, was created in 1986, NSF established the policy that the center must include a public earthquake education component. As a result, the center's public outreach included working with teachers and students. The same policy was applied in 1997 when NSF supported the creation of three new earthquake engineering research centers—the Multidisciplinary Center for Earthquake Engineering Research, Mid-America Earthquake Center, and the Pacific Earthquake Engineering Research Center—and earlier when the Southern California Earthquake Center was jointly funded with USGS in 1991. Though the resources made available to these centers by the sponsors for outreach and public education were significantly less than for its research activities, the policy requiring such educational programs was nevertheless important and drew attention to the need to increase public awareness of the earthquake hazard. A few years ago NSF ended its decade-long support of the three earthquake engineering research centers and they now rely on other sponsors. Only time will tell how long the centers will continue their public earthquake education programs now that they no longer receive major support from NSF and face the pressure from that agency to carry out such activities.

SOME KEY CHALLENGES

Turning now to some of the key challenges facing public seismic education and public education programs for other hazards in the U.S. today, it would not be a surprise to learn that such public education programs in other countries were faced with similar challenges.

Gaps in Knowledge Base

As mentioned previously, earth science, earthquake engineering, and social science knowledge related to earthquakes provide an important underpinning for public earthquake education in the U.S. Research is clearly needed in all of these disciplines if we are to understand and know how to adjust to the earthquake risk in the future. However, as one of the key building blocks, the social sciences in particularly stand out as in need of more attention. As previously noted, although much has been learned during their relatively short life as earthquake-relevant disciplines, much more knowledge is required from the social sciences to meet the needs of public earthquake education stakeholders.

For example, there has been little social science research in the U.S. on the behavior of children before, during, and after earthquakes and other kinds of disasters [Anderson 2005]. This is the case even though children are among the most vulnerable population groups in the U.S. and other countries, as recent earthquakes in China and Haiti have clearly demonstrated. It is important to note that the little social science research that has been conducted in the U.S. on children and youth to date suggests that children should not be seen as merely potential victims but as also having the capacity to learn self-protective actions if they are instructed properly and even play a role in communicating risk information to their families, thereby furthering earthquake planning and mitigation in their households and neighborhoods. Only recently have there been signs that social science researchers are beginning to put children on their research agendas and give this subject the attention it deserves [Ramirez et al. 2005; Peek 2008; Mitchell et al. 2008]. Increased knowledge on this vital subject could provide a more solid basis for designing public education policies and programs that meet the needs of children and their families.

Social scientists also need to give renewed attention to understanding risk communication in its broadest sense as it relates to public earthquake education in the U.S. This requires systematically investigating both traditional and new channels and tools for disseminating risk information. During the first few decades following NEHRP’s creation, social scientists gave a great deal of attention to risk communication and information dissemination, but their interest in these subjects has waned [NRC 2006]. As a result, updated knowledge on risk communication is now needed in light of the many recent societal changes that have taken place, including the development of the Internet, smart phones, geographic information systems, and social media.

For example, social scientists need to give attention to the implications of such social networking platforms as Twitter, Facebook, YouTube, and blogs for public earthquake education, including the challenges and opportunities they provide for increasing awareness and reducing vulnerability. This is particularly important because advocates have emerged in the U.S. calling for the increased use of social media as an additional source of risk information for the public. Indeed, both government and nongovernment organizations [Plan It Now 2010] are increasingly using Twitter, Facebook, and YouTube as well as other platforms to make earthquake, hurricane, and other hazard information more accessible to the public. Systematic social science research is needed to understand this changing face of public hazard education in the U.S. and to provide guidance for furthering the effective use of these new platforms.

Multidisciplinary Collaboration

Multidisciplinary cooperation is challenging for many reasons, including the fact that experts from various disciplines come from different academic cultures, bring different perspectives to their work, and even speak different technical languages. This is as true in the earthquake field as in many other technical areas. As a result, too often in the U.S. significant collaboration fails to evolve when public earthquake education activities are being designed and implemented. Experts from relevant disciplines are left out, or only participate marginally. Frequently, it is the social science expertise that is not represented when such programs are being developed, which can mean that behavioral issues will not be thoroughly considered and discussed, even though they may be crucial to program effectiveness and success.

Of course there are exceptions to this tendency which can offer lessons for future efforts. For example, leading social scientists have provided input to efforts led by USGS earth scientists to inform citizens in California about the earthquake threat [Nathe et al. 1999]. In 2008, the disciplinary barriers fell significantly when under the leadership of USGS leading earth scientists, earthquake engineers, social scientists, and state and local authorities developed an earthquake scenario of a magnitude 7.8 along the San Andreas Fault for a drill and several related activities called the Great Southern California ShakeOut [Jones et al. 2009]. Held on November 13, 2008, the drill is thought to have been the largest one conducted in the U.S., with an estimated 5 million or more participants. Similar statewide drills were held in California in 2009 and 2010, and are now expected to occur annually. This multidisciplinary effort has even inspired others. The CUSEC will be conducting its own drill called the Great Central U.S. ShakeOut in its eight-member states in 2011 [CUSEC 2010]. The experience with these campaigns shows that multidisciplinary earthquake education collaboration can be achieved in spite of the difficulties involved. Much more of this type of cross-disciplinary cooperation is needed in the U.S., and perhaps elsewhere as well. This can happen when trust and openness prevails among colleagues in different disciplines who are working on common problems.

Multihazard Risks

In addition to earthquakes, many urban as well as other areas of the U.S. are threatened by a variety of natural hazards, including hurricanes, tornados, floods, and wildfires. Los Angeles, for example, is at risk from not only earthquakes but floods and wildfires as well. Thus public education activities on the earthquake risk may stand alone, or be combined with education on other hazards. One advantage of such multihazard programs is that they may provide an opportunity for leveraging scarce resources. Another is that research has shown that persons at risk are more likely to adopt protective measures that counter many threats [Perry and Lindell 2007]. And as far as the education process is concerned, social science research has shown that many of the basic principles of risk communication are shared regardless of the disaster agent.

A challenge to those experts and decision makers dealing with the earthquake threat is determining when a single-hazard education focus, such as a state-wide earthquake campaign, makes sense and when to take advantage of promising opportunities to design combined hazards education programs, such as the dissemination of information on the Web and in schools to those exposed to multiple hazards. A related challenge is for earthquake and other single hazard experts to share experiences and lessons learned with each other in order to improve public hazard education across the board.

Cross-Cultural Learning

The U.S. is far from alone in the development of public earthquake or multihazard education programs. Other countries throughout the world have also done so, including our partners at this workshop [Hossieni et al. 2008; Parsizadeh 2009]. A recent U.N. document provides highlights on numerous education programs worldwide, many of them earthquake centered, that focus on children [ISDR 2007].

The challenge to U.S. experts in the field is to learn what is being done in other countries, consider adopting what is found to be promising and appropriate, and then make the necessary cultural adjustments once the decision is made to borrow and implement the new approach. In spite of language and other cultural barriers, U.S. experts have been fairly open to this for many years. For example, during the early years of NEHRP, the U.S. and Japan shared information on public seismic education programs, with each adopting some of the approaches designed by the other. Even though there is a history of such sharing, the U.S. could benefit from much more of it.

Another challenge is for such developed countries as the U.S. to take an increased leadership role in sharing their expertise with at risk developing countries. An example of what is possible is a tsunami guide book designed to educate local stakeholders and help them take the lead in preparing their coastal communities for tsunamis [Samant et al. 2007]. The guide was developed by GeoHazards International, which is a U.S.-based nonprofit organization, in response to the devastating 2004 Indian Ocean tsunami. Especially suited for developing countries, the guide is a compilation of relevant information from the physical sciences, engineering, and the social sciences offered in a fashion that is understandable to laypersons. The guide has been made available in both hard copy and through the Internet. Much more of this type of assistance is needed from developed countries like the U.S. to further public hazard education in risk-prone developing countries.

Mass Media Collaboration

Television, radio, and newspapers are a major source of disaster information for the U.S. public [Wenger 1980]. Such media help shape public perception of disasters in very significant ways. And many public earthquake education initiatives rely on the cooperation of the mass communication media. However, this can be a challenge to get right for many reasons. Pre-event earthquake education is not a priority for the media. Their preference is to focus on actual events because of their newsworthiness rather than on the far less dramatic mitigation and preparedness issues that the public also needs to learn about. Also, few media outlets have technical experts with an acquired interest in and understanding of earthquakes and other hazards. In addition, the media can be a channel for the spread of myths and rumors, such as overblown claims of looting and disorderly behavior following earthquakes and other disasters [Quarantelli and Dynes 1972].

Still, there is no getting around the fact that the media can play a key role in public earthquake education, both before and after an event. For example, the news media was an important partner in covering and calling attention to the previously mentioned Great

ShakeOut campaigns in California, and they are expected to continue to be so for future drills. And in spite of some of the myths they spread, the media brought many of the key earthquake issues to the forefront for the U.S. public following the 2010 earthquakes in Haiti and Chili, including the importance of earthquake hazard awareness, mitigation, and preparedness and the difficulties of designing effective reconstruction and recovery policies and activities. Similarly, researchers in Turkey found that the media played an important role in furthering public awareness following the devastating 1999 Marmara earthquake [Karanci and Aksit 2000].

Some organizations, such as the USGS, have become rather skilled at working with the news media and getting their educational messages out to the public through them, both before and after earthquakes. This is an important development, but many other public earthquake education stakeholders in the U.S. also need to spend time becoming more comfortable collaborating with the news media, especially at the local level.

Program Evaluation

The goals of public earthquake education activities include increasing the awareness of the hazard and changing the behavior of those at risk. The latter may involve undertaking mitigation and preparedness actions in such locations as schools, offices, and homes before an earthquake and self-protective actions during an actual event, such as is taught through Drop, Cover, Hold On drills. Some recent studies have reminded us of the importance of assessing hazard education programs rather than assuming that they are working as intended [Wachtendorf et al 2008; Ronan 2002]. This is the final challenge noted.

Too often the effects of public hazard education initiatives in the U.S. are not systematically evaluated to determine their overall value or if changes in approach might enhance their effectiveness [Perry and Lindell 2007; Coppola and Maloney 2009]. Frequently, there is a reliance on anecdotal information rather than sound data collected in a systematic and credible fashion.

Because of their importance, perhaps a focus on public hazard education initiatives aimed at children in the U.S. would be a good starting point for making progress in program evaluation [Anderson 2005]. Those activities that could be assessed include school and Internet-based programs, drill campaigns, as well as other initiatives launched by local and state authorities, federal agencies such as FEMA and USGS, and civil society organizations such as the Red Cross. Systematic assessments would enable the designers of such programs to know how many children are reached through them, how knowledgeable of the hazard they become as a result, and what consequences this has for the children's own behavior and their significant others, including those in their households. Such evaluations are long overdue for many programs, and could provide the basis for their improvement. A promising start in this direction was taken by researchers assessing some of the lessons learned from school participation in the 2008 Great Southern California ShakeOut drill [Green and Petal 2010]. Such efforts are rare, however, and the need is for program evaluation to become a standard practice when public earthquake and other hazard education initiatives are undertaken.

CONCLUSION

Like many countries, the U.S. has an array of public earthquake education programs. Such programs are sometimes combined with activities to educate the public about other hazards. Public earthquake education programs in the U.S. are designed by stakeholders in government, academia, the private sector, and civil society who sometimes work collaboratively or in parallel to promote the goals of public awareness and safety.

While these are the two most widely recognized goals of public earthquake education in the U.S., it should also be noted that this type of education might also help increase public support for disaster reduction legislation, policies, and public expenditures at the local, state, and national levels. With all of the other competing demands facing society, it is often difficult to get the public's attention regarding low probability events like earthquakes. However, in some cases sound public education efforts, like actual earthquake events, might facilitate putting earthquakes and other hazards more firmly on the public's agenda and generate more effective public participation in the hazards policy process. An informed public is more likely to participate in the process in a reasonable way, reducing the likelihood that a situation would arise as it did recently in Italy, where several scientists and technicians were put under criminal investigation for failing to predict an earthquake that occurred in central Italy on April 6, 2009 [EERI 2010]. Unfortunately, in this case the public was insufficiently aware of the limits of scientific knowledge in determining when and where earthquakes might occur and the precise impacts they might have. This resulted in the ill-advised assignment of blame to the scientific personnel by some in the public.

The noted challenges facing public earthquake education in the U.S. could be put into clearer perspective if they were rigorously compared with the educational challenges faced by other societies with large urban populations at-risk, such as Iran and Turkey. Perhaps we might even find that some of the challenges are shared. Such comparative analyses, which would require the involvement of multidisciplinary experts, could set the stage for significant cross-cultural learning and the transfer of culturally appropriate public earthquake education innovations across societies, thereby increasing earthquake safety for all.

Finally, Americans tend to think they live in a very child-centered society. Thus it is not too surprising that many of the public hazard education programs in the U.S. do indeed focus on children, in spite of the paradox that there has been only modest research on children and disasters to date. Much more needs to be done in the U.S. though to protect children from earthquakes and other disasters. For example, a comprehensive study by researchers found that even with the high earthquake risk in the state, professionals in many child care centers in California lack the knowledge to adequately plan for the safety of children in their charge [Junn and Guerin 1996]. The researchers recommend that legislation be passed to require child care centers to develop earthquake response plans.

Particularly since Hurricane Katrina brought widespread attention to the vulnerability of children to disasters in the U.S., many within and outside government have vigorously called for making disaster preparedness more children focused than it has been in the past. In 2007 the National Commission on Children and Disasters was established by the U.S. Congress to conduct a comprehensive review of federal disaster laws, programs and policies related to the needs of children and to make recommendations to deal with problem areas. The commission's recently issued report to the President and Congress, which has over one hundred on recommendations, calls for the integration of the needs of children across all government disaster management activities and operations and for the creation of a National Strategy for Children and Disasters to guide that process, which would involve the White House, Congress, federal agencies, and non-federal partners [NCCD 2010]. Most of the recommendations in the report are related to post-disaster issues, but pre-disaster education-oriented ones are also included. In terms of education, the commission recommends the full incorporation of the needs of children, such as at school and child care centers, into disaster planning, training, and exercises. Also included in the report are recommendations directed at specific agencies, such as requirements for FEMA to provide disaster preparedness and training resources to local and state organizations that serve children, and for the U.S. Department of Health and Human Services to enhance its research agenda relevant to children's disaster health risks.

Some of the legislative and policy changes proposed by the commission will certainly be challenging to achieve given competing societal needs. This makes it is difficult to predict the outcome of this call for action. However, if many of the recommendations actually become public policy, they could have a profound impact on the nature of public hazard education and the capacity to meet the disaster needs of children in the U.S. for years to come.

REFERENCES

Anderson WA (2005). Bringing children into focus on the social science disaster research agenda, *Inter. J. Mass Emergencies and Disasters*, 23, 159–175.

Anderson WA (2008). Public education for earthquake safety in the United States, *Proceedings*, 1st Iran-U.S. Seismic Workshop, Sharif University of Technology, Tehran, Iran.

Coppola DP, Maloney EK (2009). *Communicating Emergency Preparednes, Strategies for Creating a Disaster Resilient Public*, CRC Press, Boca Raton, Florida.

Central U.S. Earthquake Consortium (2010). See *www.cusec.org.*

Earthquake Engineering Research Institute (2010). Italian Seismologists Indicted, *EERI Newsletter*, 44, No. 7.

Earthquakes and Megacities Initiative (2010). See *www.emi-megacities.org.*

Green R, Petal M (2010). Lessons learned from school participation in the 2008 ShakeOut. See *www.wwu.edu*.

Karanci NA, Aksit B (2000). Building disaster-resistant communities: Lessons learned from past earthquakes in Turkey and suggestions for the future, *Proceedings*, *Inter. J. Mass Emergencies and Disasters*, 18:403–416.

Jones LM et al. (2009). Preparing a population for an earthquake like Chi-Chi: The great Southern California ShakeOut, *Proceedings,* U.S.-Iran Seismic Workshop, Irvine, California, Pacific Earthquake Engineering Research Center, Berkeley, CA.

Junn EN, Guerin DW (1996). Factors related to earthquake preparedness among child care professionals, *Inter. J. Mass Emergencies and Disasters*,, 14:343–359.

Hossieni M, Hosseini KA, Hosseinioon S (2008). Public participation in risk reduction and preparedness: Experience gained from projects in Tehran, *Proceedings,* 1st Iran-U.S. Seismic Workshop, Sharif University of Technology, Tehran, Iran.

International Strategy for Disaster Reduction (2007). *Towards a Culture of Prevention: Disaster Risk Reduction Begins at School-Good Practices and Lessons Learned.* See *www.unisdr.org*.

Lambright WH (1985). The Southern California earthquake preparedness project: Evolution of an earthquake entrepreneur, *Inter. J. Mass Emergencies and Disasters*, 3:75-94.

Mitchell T, Haynes K, Hall N, Choong W, Oven K (2008). The role of children and youth in communicating disaster risk, *Children, Youth and Environments,* 18:254-279.

Nathe S, Gori P, Greene M, Lemersal E, Mileti E (1999). Public education for earthquake aazards, *Natural Hazards Informer,* 2.

National Commission on Children and Disasters (2010). *2010 Report to the President and Congress*, August 23, 2010. See *hhs.gov/about.html.*

National Research Council (2006). *Facing Hazards and Disasters: Understanding Human Dimensions*, National Academies Press, Washington, D.C.

Parsizadeh F (2008). Public education and awareness program in Iran and its achievements, *Proceedings,* U.S.-Iran Seismic Workshop*,* Irvine, California, Pacific Earthquake Engineering Research Center, Berkeley, CA.
Peek L (2008). Children and disasters: Understanding vulnerability, developing capacities and promoting resilience – an introduction, *Children, Youth and Environments*, 18:1-29. See *www.colorado.edu/journals/cye.*
Perry RW, Lindell MK (2007). *Emergency Planning*, Wiley, Hoboken, N.J.
Plan It Now (2010). See *www.PlanItNow.org.*
Quarantelli EL, Dynes R(1972). When disaster strikes (it isn't much like what you've heard and read about). *Psychology Today*, 5:66-70.
Ramirez M, Kano M, Bourque LB, Shoaf KI (2005). Child and household factors associated with fatal and non-fatal pediatric injury during the 1999 Kocaeli earthquake, *Inter. J. Mass Emergencies and Disasters*, 23:129-147.
Ronan KR, Johnson DM (2002). Correlates of hazard education programs for youth, *Risk Analysis*, 21:1055-1064.
Samant LD, Tobin L, Tucker B (2007). *Planning Your Community for Tsunamis: A Guidebook for Local Advocates*, GeoHazards International. See*: www.geohaz.org*.
Watchtendorf T, Brown B, Nickle MC (2008). Big Bird, Disaster masters, and high school students taking charge: The social capacities of children in disaster education, *Children, Youth and Environments* , 18:457-469. See *www.colorado.edu/Journals/cye.*
Wenger D (1980). A few empirical observations concerning the relationship between the mass media and disaster fnowledge: A research report, *Proceedings,* Committee on Disasters and the Mass Media Workshop, February 1979, National Academy of Sciences, Washington, D.C.

PRIORITIZATION OF SEISMIC RISK IN URBAN BUILDING STOCKS

Haluk Sucuoğlu and Ahmet Yakut

Department of civil Engineering, Middle East Technical University, Ankara, Turkey

ABSTRACT

An efficient seismic risk prioritization procedure is developed herein for vulnerable urban building stocks. The method is valid for medium height reinforced concrete buildings essentially designed for gravity loads. It is basically a sidewalk survey procedure based on observing selected building parameters from the street side and calculating a performance score for determining the risk priorities for buildings. Statistical correlations have been obtained for measuring the sensitivity of damage to the assigned performance score by employing a database consisting of 454 damaged buildings surveyed after the 1999 Düzce earthquake in Turkey. The proposed procedure has been implemented to 125,000 concrete buildings in Istanbul during 2004-2009.

INTRODUCTION

The majority of the existing buildings in seismic regions do not satisfy modern code requirements. Yet, the ratio of severely damaged or collapsed buildings observed after a severe earthquake is much less than the ratio of substandard buildings. A rigorous loss estimation study for Istanbul [JICA 2002] revealed that the expected ratio of collapsed buildings under a scenario earthquake of magnitude 7.5 along the Marmara Sea segment of the North Anatolian fault is 7%, although the ratio of substandard buildings in Istanbul is significantly higher. Considering these large differences, it is proposed that a sound risk prioritization methodology for effective risk mitigation in urban environments focus on identifying the buildings with high damage risk.

A simple risk prioritization procedure is developed in this study for medium-rise (3-6 stories) ordinary reinforced concrete (RC) buildings with gravity design. The developed procedure produces a risk prioritization by evaluating selected building parameters that can be easily observed or measured during a systematic sidewalk survey. The survey is conducted by trained observers through walk-down visits where the time required for an observer for collecting the data of one building from the sidewalk is expected not to exceed 10 minutes. The acquired data is then processed for calculating a safety score for each building, which is in turn used for ranking the buildings in an urban stock with respect to their expected seismic damages (performances) under selected ground motion intensity.

RISK PRIORITIZATION PARAMETERS

Recent earthquakes in urban environments have revealed that building damage increase with the number of stories when the buildings lack the basic seismic resistant design features. Other factors that have significant contribution to damage are also well established. These are the presence of severe irregularities, such as the soft stories and heavy overhangs, other discontinuities in load paths, poor material quality, detailing and workmanship. It is usually difficult to quantify the sensitivity of damage to each parameter analytically, however, statistics helps. Fragility functions may be developed for determining damage probabilities, hence for estimating losses in certain building types under given ground motion intensities [Kircher et al. 1997; Akkar et al. 2005]. Fragility functions pertain to a group of buildings in a given area (cell) rather than a specific building. The scope of the study presented herein extends one step further, where several selected parameters are evaluated simultaneously to obtain a performance score for each building separately.

Some of the important parameters stated above that influence damage significantly can be determined quite easily, by visual observation. The simplest ones are the number of stories, soft stories, heavy overhangs, and the overall apparent quality of the building reflecting the quality of construction. They are discussed separately below.

The Number of Seismic Stories

Field observations after the 1999 Kocaeli and Düzce earthquakes revealed that there is a very significant correlation between the number of unrestrained stories and the severity of building damage. The increase in seismic demand with the number of stories is not balanced with the increase in seismic capacity in gravity designed buildings. After the 1999 Düzce earthquake, damage distribution for all of the 9685 buildings in Düzce was obtained by official damage assessors. This data was sorted then with respect to the number of stories [Sucuoğlu and Yılmaz 2001]. The results are shown in Figure 1 below, where the number of damaged buildings is normalized with the total number of buildings at a given story number.

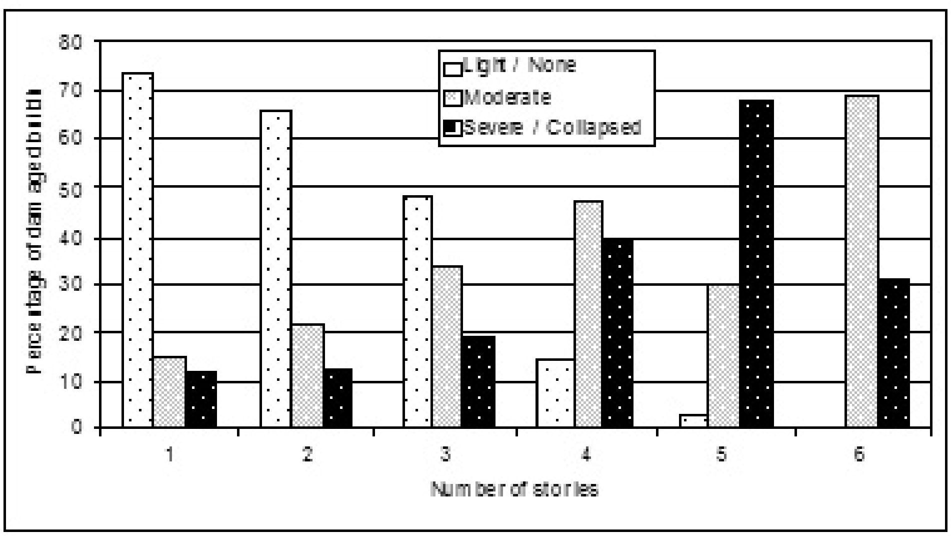

Figure 1 Damage distribution in Düzce after the 1999 earthquakes, with respect to the number of stories.

It can be observed that damage grades shift almost linearly with the number of stories. Although the objectivity of the assigned damage grades is not certain, there is a clear indication that the number of stories is a very significant, perhaps the most dominant, parameter in determining the seismic vulnerability of typical multistory concrete buildings. In this procedure the number of unrestrained stories in a building is identified as the number of "seismic" stories.

Soft Story

A soft story usually exists in a building when the ground story has less stiffness and strength compared to the upper stories. This situation arises mostly in buildings located along the side of a main street. Ground stories that have level access from the street are reserved as commercial space whereas residences occupy the upper stories. These upper stories benefit from the additional stiffness and strength provided by many partition walls, but commercial space at the bottom is mostly left open between the frame members for customer circulation. In addition, ground stories may have taller clearances and a different axis system causing further irregularity. From the earthquake engineering perspective, all these negative features have a compounded effect that identify as a soft story. All over the world, many buildings with soft stories have been observed to collapse due to a pancaked soft story from strong ground motion. During the street surveys, the presence of a soft story is evaluated on an observational basis, where the answer is either *yes* or *no*.

Heavy Overhangs

A common feature of mid-rise reinforced concrete urban buildings in Turkey and in several other countries is the difference between the footprint area and the floor area above the ground level. Larger space allowances in the upper floors are fulfilled by overhangs cantilevering outward from the exterior column axes. A typical building with heavy overhangs is shown in Figure 2. Heavy overhanging floors in multistory RC buildings cause discontinuities to develop in exterior frames (Figure 2b). Buildings with heavy overhangs sustained heavier damages during the recent Turkish earthquakes compared to buildings that were regular in elevation. This building feature can easily be observed during a walk-down survey and rated as either *yes* or *no*.

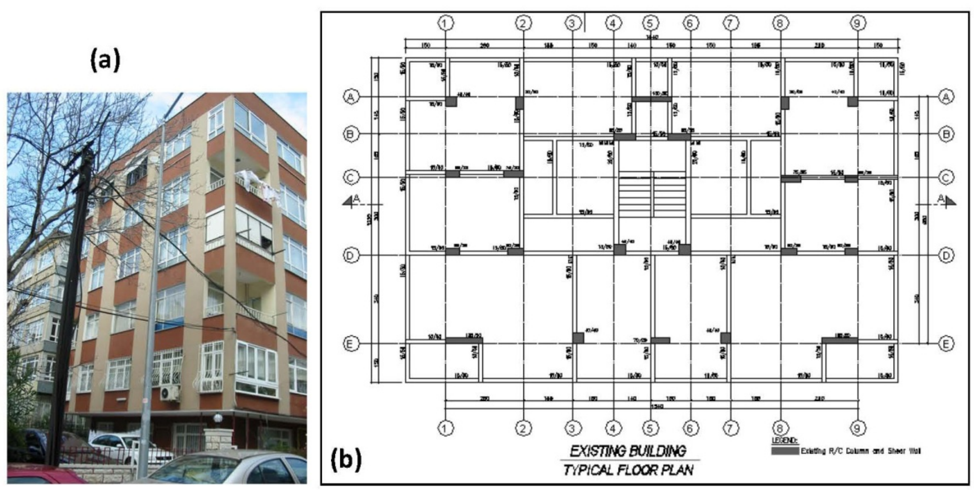

Figure 2 A building with heavy overhangs: (a) street view; and (b) floor plan.

Building Quality

The material and workmanship quality, and the care given to its maintenance reflect the apparent quality of a building. A well-trained observer can classify roughly the apparent quality of a building as *good*, *moderate*, or *poor*. A close relationship between the apparent quality and the damage experienced during the recent earthquakes in Turkey had been observed. A building with poor apparent quality can be expected to possess inherently weak material strengths and poor workmanship.

DÜZCE DAMAGE DATABASE

A district in Düzce with a total number of 454 three-to-six story RC buildings was surveyed after the 12 November 1999 Düzce earthquake. The strong-motion station was located in this district, where the maximum distance of a building from the station was less than 2 km. Soil conditions were uniform and topography was flat over the surveyed district. Building damage was classified in four grades, namely none, light, moderate, and severe or collapsed. A building with light damage can be occupied with minor repairs after the earthquake whereas a moderately damaged building requires structural repairs. The damage distribution of the investigated buildings with the number of stories is presented in Table 1.

Table 1 Damage distribution of the investigated buildings in Düzce.

Number of Stories	**Observed Damage** None	Light	Moderate	Severe/Collapse	Total
3	18	62	29	15	124
4	17	43	60	27	147
5 and 6	18	30	60	75	183
Total	**53**	**135**	**149**	**117**	**454**

The variation of damage in 454 buildings subjected to survey parameters was obtained independently for each parameter. Tge Düzce database did not represent all visually observable parameters such as pounding of adjacent buildings. Therefore, these parameters were not included in the following evaluation.

The distribution of damage with the number of stories is shown in Figure 3, confirming that damage was strongly correlated with the number of stories. Accordingly, it was decided to uncouple this parameter from the others. The data for the other parameters was sorted for each number of seismic stories separately in order to remove its effect on those parameters.

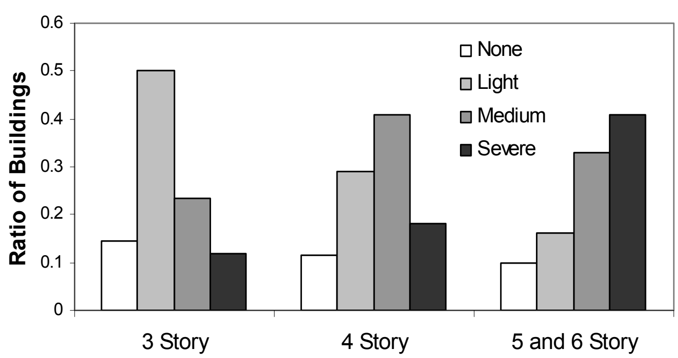

Figure 3 The distribution of damage with the number of stories in 454 buildings.

Among the 454 surveyed buildings, 230 buildings had soft stories. These buildings were grouped into two with respect to the observed damage grades as none/light, or moderate/severe for each number of stories, and then their number was normalized relative to the total number of buildings in each damage group. The reason for this damage classification is to separate buildings with high risk from the ones with low risk. As shown in Figure 4, the vertical axis shows the percentage of buildings with soft stories as normalized by the total number of buildings in each damage group. For all number of stories, it is evident that the buildings with soft stories were much more represented among the significantly damaged buildings than those in the lower damage group. This is a key important observation: if a building with a soft story is vulnerable to seismic damage, it is very likely that this damage will be significant.

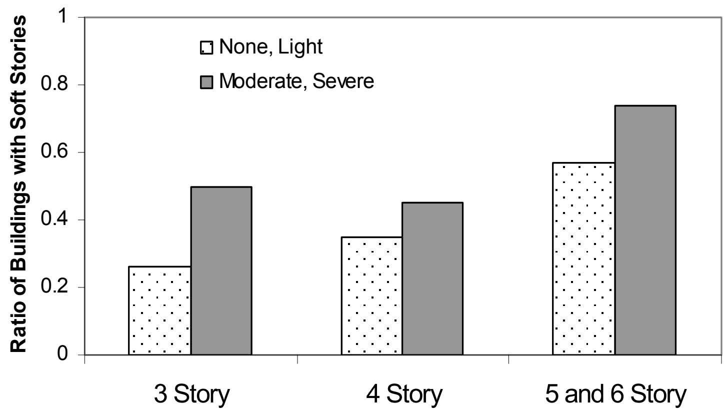

Figure 4 The effect of soft stories on damage distribution.

The quality classification of 454 surveyed buildings revealed that 59 were good, 372 were moderate, and 23 were poor. The observers usually chose the moderate rank when they were not very certain. Hence, the moderate group outnumbers the other two quality groups. These buildings are grouped with respect to the damage grades and the number of stories, and then their number is normalized relative to the total number of buildings in each quality group. The results are presented in Figure 5 for 5-story buildings. The data for 5-story buildings reveal that the severely damaged buildings were of lesser quality than the other damage groups. The effect of apparent quality on damage becomes more significant as the building height increases.

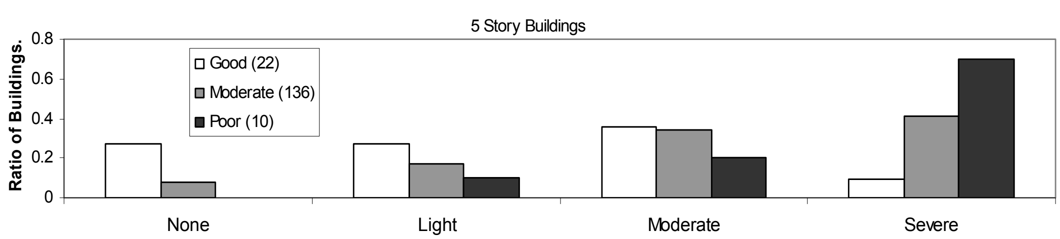

Figure 5 Correlation of damage with the apparent building quality.

There were 95 buildings with heavy overhangs among the total of 454. The data was sorted similar to the case for the presence of soft stories above. All of the undamaged buildings were free of heavy overhangs. The distribution of damage in buildings with heavy overhangs is presented in Figure 6. Evidently, buildings with heavy overhangs have about 30% share in the group of significantly damaged buildings, whereas their share is less than 12% in the lower damage group.

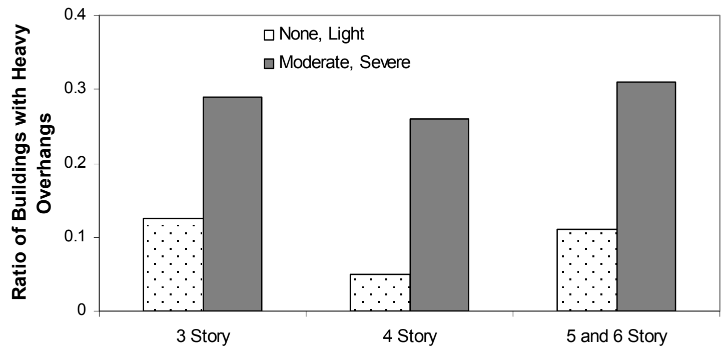

Figure 6 The effect of heavy overhangs on damage distribution.

STATISTICAL ANALYSIS

The objective of statistical analysis is to develop a performance score for prioritizing the buildings in an urban area, based on a set of vulnerability indicators that can be observed visually by a street survey. Multiple linear regression analysis is employed for developing a mean-value function that returns the expected value of the performance score. This function can be established by using the Düzce database.

MULTIPLE LINEAR REGRESSION ANALYSIS

A linear function is fitted to the Düzce damage database for calculating the expected performance scores (EPS) based on the presence of soft story (SS), apparent building quality (AQ), and the presence of heavy overhangs (HO) for groups of buildings with the same number of stories. In developing the linear regression functions, an "Observed Performance Score (OPS)" was assigned to each building according to its observed performance during the 1999 Düzce earthquake, as given in Table 2.

Table 2 Observed Performance Score Assignment

Observed Performance	Observed Performance Score (OPS)
None	100
Light	80
Moderate	50
Severe/Collapse	0

The mean-value function for the multi-linear regression analysis is

$$\mathrm{E}\left(PS \middle| SS = ss,\ AQ = aq,\ HO = ho\right) = EPS = \hat{\beta}_0 + \hat{\beta}_{SS}(ss) + \hat{\beta}_{AQ}(aq) + \hat{\beta}_{HO}(ho) \tag{1}$$

Here, $\mathrm{E}(PS|\ldots)$ is the expected performance score (*EPS*) of the building with a given set of "vulnerability indicators" ss, *aq* and *ho*; and $\hat{\beta}_0$, $\hat{\beta}_{SS}$, $\hat{\beta}_{AQ}$ and $\hat{\beta}_{HO}$ are the set of coefficients that minimize the weighted least squares error, Δ^2,

$$\Delta^2 = \sum_{i=1}^{n} \left(OPS_i - EPS_i\right)^2 \tag{2}$$

in which OPS_i is the observed performance score and EPS_i is the expected performance score of the *i*th building, respectively, and n is the total number of buildings in the group. The set of regression coefficients which minimize the least squares error in Equation (2) [Sucuoğlu et al., 2007] and the associated *R* values are presented in Table 3.

Table 3 Calculated set of regression coefficients.

Number of Stories	$\hat{\beta}_0$	$\hat{\beta}_{SS}$	$\hat{\beta}_{AQ}$	$\hat{\beta}_{HO}$	***R***
3	80.0	22.8	8.7	23.0	0.640
4	73.3	22.0	15.1	30.2	0.669
5 and 6	64.0	24.2	22.8	32.5	0.712

The expected performance score *EPS* for a building is then calculated from Equation (1), where $\hat{\beta}_0$, $\hat{\beta}_{SS}$, $\hat{\beta}_{AQ}$ and $\hat{\beta}_{HO}$ are given in Table 3 for different number of seismic stories. Note that $\hat{\beta}_0$ is an initial performance score for a building with no observed vulnerabilities, and the remaining terms in Equation (1) reduce the initial score for each indicated vulnerability *SS = ss, AQ = aq* and *HO = ho*. The value taken by *ss* is either -1 (soft story present) or 0 (no soft story), the value taken by *aq* is either -1 (poor quality), or 0 (moderate quality), or +1 (good quality), and the value taken by *ho* is either -1 (heavy overhangs present) or 0 (no heavy overhangs).

Risk Classification of the Buildings

Buildings in an inventory can be classified into two groups as "Low Risk" and "High Risk" after an earthquake, depending on the distribution of observed damage. These damage levels are generally selected as N (no damage) and L (light damage) for the low-risk buildings, and M (moderate damage) and S (severe damage or collapse) for the high-risk buildings. The expected performance scores (EPS) can be used for such a classification before an earthquake if a proper threshold score is selected to separate the low-risk and high-risk buildings. Such a threshold score should result in minimum misclassification of buildings. The EPS scores computed from Equation (1) can also be used to rank the buildings for seismic prioritization purposes.

Expected performance scores were computed for all 454 buildings in the Düzce database from Equation (1) using the set of $\hat{\beta}$ coefficients given in Table 3. For a specific threshold score TS, a building that has an EPS smaller than or equal to TS and classified as "High Risk" according to its observed damage level is a correctly classified as a "High Risk" building. Similarly, a building with an EPS greater than TS and classified as "Low Risk" according to its observed damage level is a correctly classified as a "Low Risk" building. The rate-of-correctness ratios were computed by normalizing the number of correctly classified buildings with the total number of buildings in those classes according to Düzce data.

The variation of the rate-of-correctness ratios with the expected performance score are presented in Figure 7. If the intersection of the two curves is selected as TS, which is 60, then 72% of those buildings with EPS<60 are correctly classified as high risk, and 72% of those buildings with EPS>60 are correctly classified as low risk.

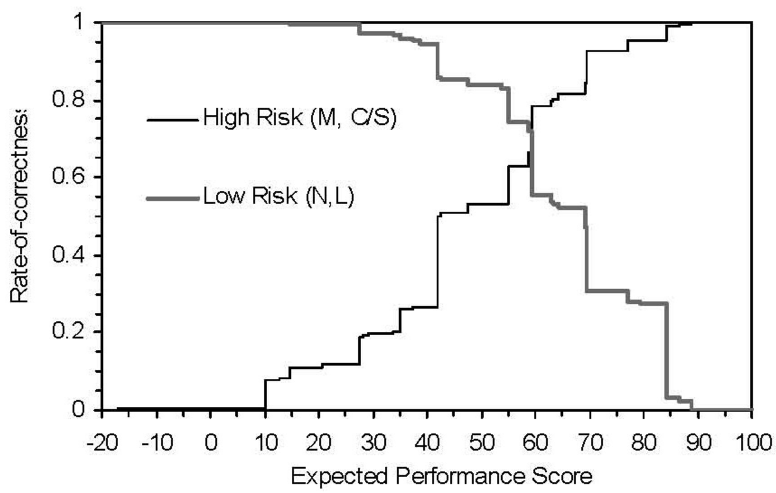

Figure 7 Variation of the rate-of-correctness ratios with the expected performance score for "Low Risk" and "High Risk" Buildings.

SCALING FOR THE GROUND MOTION INTENSITY

The 454 buildings surveyed after the 1999 Düzce Earthquake were in close proximity to the Düzce strong-motion station, which recorded PGA values of 341 and 525 cm/sec^2 and PGV values of 60 and 83 cm/sec along the 90 and 180 degree components, respectively. Düzce has a flat topography and soil conditions are uniform over the city [Sucuoğlu and Yılmaz 2001]. Therefore it may be assumed that the Düzce ground motion intensity was representative for the surveyed buildings. For different ground motion intensities, the results presented in Table 3 must be adjusted.

Recent studies have shown clear evidence that the structural damage is well correlated with PGV [Wald et al. 1999; Akkar and Ozen 2005]. Accordingly, it is decided to employ PGV in scaling the ground motion intensity in this study. The $\hat{\beta}$ values given in Table 3 were calculated for the 1999 Düzce earthquake ground motion where the geometric mean value of PGV for the horizontal components was 70.6 cm/sec. It was decided to keep the regression coefficients $\hat{\beta}_{SS}$, $\hat{\beta}_{AQ}$ and $\hat{\beta}_{HO}$ for the vulnerability indicators in Table 3 the same, but apply the intensity scaling to the initial performance scores $\hat{\beta}_0$ of 3-, 4-, 5-, and 6-story buildings in different PGV zones [Akkar and Sucuoğlu 2003; Sucuoğlu et al. 2007]. The results are presented in Table 4.

Table 4 Initial performance and vulnerability scores in different intensity zones.

Number of Stories	Initial Performance Score			Vulnerability Coefficient		
	60<PGV<80	40<PGV<60	20<PGV<40	Soft Story	Apparent Quality	Heavy Overhangs
3	80	107	138	23	9	23
4	73	91	115	22	15	30
5 and 6	64	76	92	24	23	33

CASE STUDY: KÜÇÜKÇEKMECE SUB-PROVINCE OF ISTANBUL

The prioritization procedure developed herein was implemented at the Küçükçekmece subprovince of Istanbul shown on the map in Figure 8. There were 40,800 reinforced concrete buildings in Küçükçekmece with 2-6 stories. The PGV values were calculated for each building for a scenario earthquake of M7.5 along the North Anatolian fault (Figure 8) by using ground motion prediction equations.

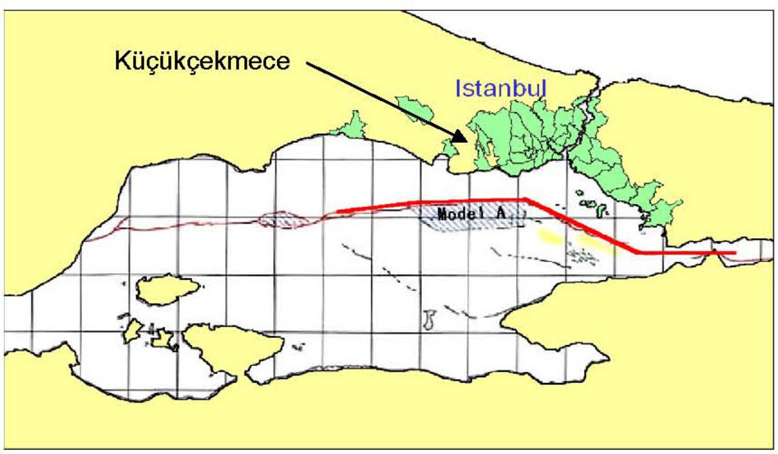

Figure 8 The geographical location of Küçükçekmece in Istanbul, and the fault model for the M7.5 scenario earthquake along the North Anatolian fault in the Marmara Sea.

The PGV values are marked on Figure 9 for each building with an increment of 20 cm/sec^2. There were only two PGV regions due to the close proximity of all buildings in the figure to the causative fault. The distances to the fault vary between 12-14v km for the buildings shown in Figure 9. Those buildings expected to sustain severe damage or collapse according to the proposed prioritization procedure are marked on Figure 10. Their number is 11,532 or

28% of the 3-6 story gravity designed RC buildings. Risk reduction efforts should begin with these buildings, either through replacement or retrofit.

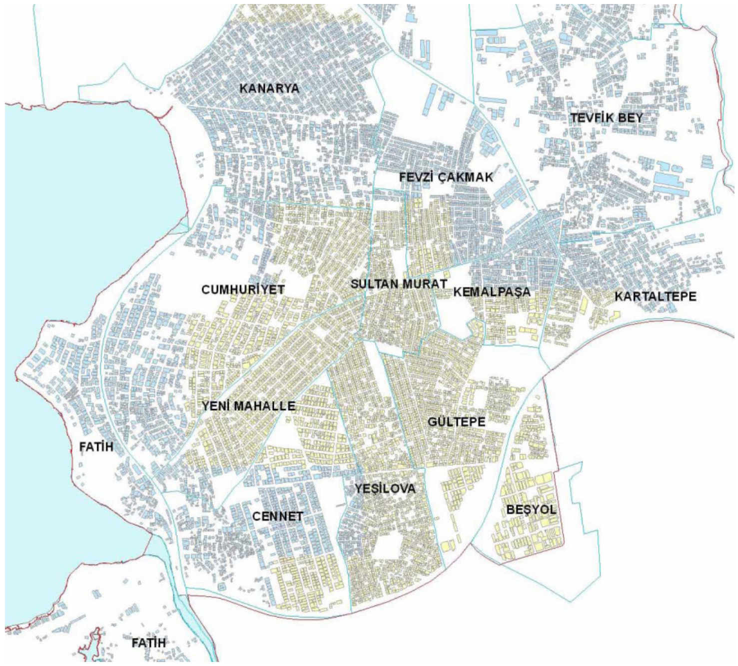

Figure 9 **The distribution of PGV values at the building sites in the populated southern tip of Küçükçekmece. Yellow is for 20<PGV<40 cm/sec and blue is for 40<PGV<60 cm/sec. There are about 40,000 building footprints in the figure.**

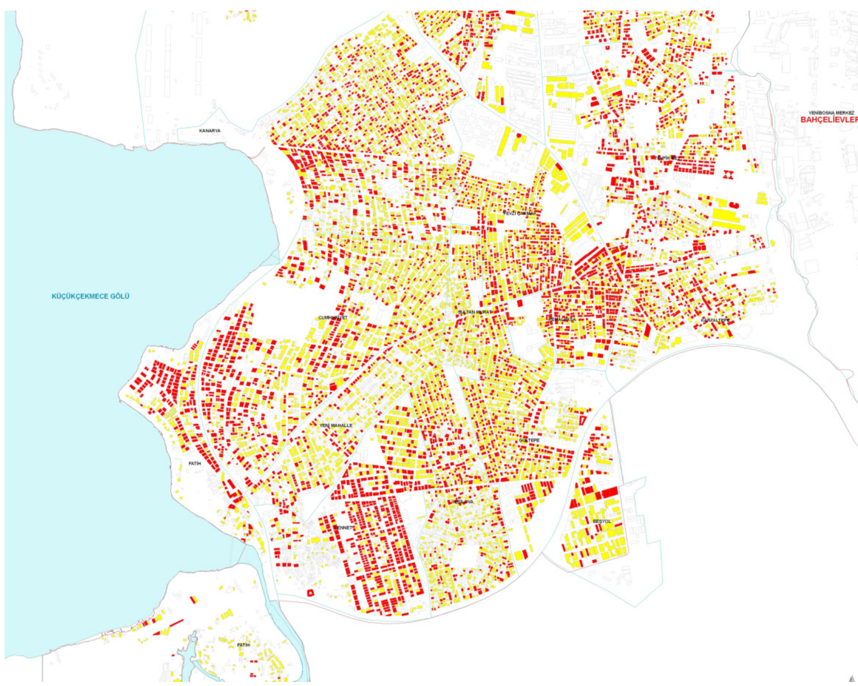

Figure 10 **The distribution of buildings with high seismic risk (red footprints) in Küçükçekmece (11,532 out of 40,800 buildings).**

CONCLUSIONS

A prioritization procedure is developed for 3-6 story gravity designed concrete buildings, which is based on a sidewalk survey of the vulnerable building stock in an urban environment. The proposed procedure is calibrated with field data compiled after the 1999 Düzce earthquake. The basic objective is to accelerate the vulnerability assessment studies in large urban regions populated with a very high number of vulnerable buildings. The method has been implemented to 125,000 concrete buildings in Istanbul during 2004-2009.

ACKNOWLEDGEMENTS

The work presented here is supported in part by TUBITAK (YMAU-ICTAG-1574) and NATO (SfP977231).

REFERENCES

Akkar S, Özen O (2005). Effect of peak ground velocity on deformation demands for SDOF systems, *Earthq. Engrg. Struct. Dyn.*, 34:1551–1571.

Akkar S, Sucuoğlu H (2003). PGV sensitive deformation demands and a rapid damage assessment approach, *Seismic Assessment and Rehabilitation of Existing Buildings*, NATO Science Series, Kluwer Academic Publishers, pp. 77–96.

Akkar S, Sucuoğlu H, Yakut A (2005). Displacement-based fragility functions for low- and mid-rise ordinary concrete buildings, *Earthq. Spectra*, 21:901–927.

Japan International Cooperation Agency and Istanbul Metropolitan Municipality (2002). *A Disaster Prevention/Mitigation Basic Plan in Istanbul including Seismic Microzonation,* Istanbul.

Kircher CA, Nassar AA, Kustu O, Holmes WT (1997). Development of building damage functions for earthquake loss estimation, *Earthq. Spectra*, 12:663–682.

Sucuoğlu H, Yılmaz T (2001). Düzce, Turkey: A city hit by two major earthquakes in 1999 within three months, Seismo. Res. Lett., 72:679–689.

Sucuoğlu H, Yazgan U, Yakut A (2007). A screening procedure for seismic risk assessment in urban building stocks, *Earthq. Spectra*, 23:441–418.

Wald DJ, Quitariano V, Heaton TH, Kanamori H, Scrivener CW, Worden CB (1999). Trinet Shake Maps: rapid generation of peak ground motion and intensity maps for earthquakes in Southern California, *Earthq. Spectra*, 15:537–555.

EMME-EARTHQUAKE MODEL OF MIDDLE EAST REGION: HAZARD, RISK ASSESSMENT, ECONOMICS AND MITIGATION

Karin Sesetyan[1] , Cuneyt Tuzun[1], Domenico Giardini[2], Mustafa Erdik[1]

[1] Boğazici University, Kandilli Observatory and Earthquake Research Institute, Istanbul,Turkey,
[2] Swiss Federal Institute of Technology, Zurich, Switzerland

ABSTRACT

As a consequence of the high probability of earthquake occurrence combined with high population growth, poor construction standards and practice, and lack of proper mitigation strategies, the Middle East and Caucasus represent one of the most seismically vulnerable regions worldwide. EMME (Earthquake Model of the Middle East Region) is a four-year project aimed at assessing seismic hazard, the associated risk in terms of structural damage, casualties and economic losses, and also evaluate the effects of relevant mitigation measures in the Middle East region in concert with the aims and tools of GEM (Global Earth Model). The EMME project is jointly directed by Eidgenössische Technische Hochschule Zürich (ETHZ) and Kandilli Observatory and Earthquake Research Institute (KOERI). A total of six work packages exist: Earthquake Catalog, Seismic Sources, Ground Motion Prediction Equations, Risk Assessment, City Scenarios, and Socio-Economic Impact, each of them being lead by a different partner institution. The core research group of the project consists of a large number of researchers from partner institutions of all EMME countries.

INTRODUCTION

Based on recent statistics, the number of people who have died in earthquakes and tsunamis worldwide in the last decade is about half a million. The majority of this loss of life occurred in developing countries where population and urbanization is increasing rapidly without any major control, increasing the risk of more casualties for the future. The Middle East region is located at the junction of major tectonic plates, namely the African, Arabian, and Eurasian plates, resulting in very high tectonic activity. Some of the major earthquake disasters in human history have occurred in the Middle East, affecting most countries in the region. Being one of the most seismically active regions of the world, the Middle East, extending from Turkey to India, is also a key region in terms of urbanization, energy reserves, and industrialization trend. The region under consideration involves world's most populated capitals and cities, with key economical importance such as Istanbul, Baghdad, Tehran, Jeddah, Riyadh, Cairo, Kabul, Karachi, and Lahore.

It is a well known fact that earthquakes cause not only direct damage on built environment such as buildings, infrastructure, or lifeline systems, resulting in human life and economic losses, but have also secondary effects such as social and economic losses. As a consequence of the high probability of earthquakes occurring combined with high population growth, poor construction standards and practice, and lack of proper mitigation strategies, the Middle East represents one of the most seismically vulnerable regions in the world.

Begun in earnest in the 1990s, seismic risk and associated mitigation strategies have been assessed on a worldwide scale through different initiatives funded and coordinated by international organizations such as the United Nations and World Bank. As a result of these projects, many valuable and applicable results have been obtained. As one of the latest initiatives, The Global Earthquake Model (GEM) aims at carrying former studies a step further by allowing meaningful comparisons between different regions through uniform data, methodologies, models, and training. Through interactive research activities performed by researchers from different disciplines, such as engineering and geosciences, the project will provide a comprehensive and uniform evaluation of the seismic risk and associated mitigation studies. The results of the project both in terms of risk evaluation and the developed IT structure will be widely used throughout the world especially in developing countries located in high seismicity regions.

The Earthquake Model of the Middle East Region (EMME) aims at assessing seismic hazard, the associated risk in terms of structural damages, casualties, and economic losses, and evaluates of the effects of relevant mitigation measures in the Middle East region in concert with the aims and tools of GEM. The EMME project encompasses several modules, such as the Seismic Hazard Module, Risk Module, Socio-Economic Loss Module, and the development of an IT infrastructure or platform for the integration and application of modules under consideration. The methodologies and software developments within the context of EMME will be compatible with GEM to enable the integration process. As such, a comprehensive interaction between the two projects is foreseen.

OVERALL GOALS

The EMME aims to contribute to and facilitate the seismic risk reduction through the realization of the following specific tasks:

- Calculate seismic hazard uniformly and with the highest standards.
- Rigorously validate earthquake and shaking probabilities using regional and global data.
- Communicate seismic risk clearly, accurately, and transparently to all users.
- Integrate local expertise in a regional and global context.
- Monitor and update changing infrastructure and vulnerability.
- Build seismic risk management capacity in the whole region.
- Enable dialog with decision-makers.
- Implement EMME as part of GEM.

The EMME will enable users to take the following specific actions to achieve risk-reducing outcomes:

- Improved earthquake preparation and response.
- Adoption and enforcement of building codes.
- Implementing seismic mitigation measures.
- Enabling accurate post-earthquake alerts and rapid assessment of direct and indirect losses.
- Increased earthquake insurance usage.

- Ensuring uniform comparability of seismic risk across multiple geographies.

The EMME's long-term impact is expected to be a more structured approach to seismic risk mitigation, leading to reduced monetary losses and casualties. Improved building construction practice and efficient risk allocation will lead to overall reduction of losses. Public policies for risk mitigation will be based on wider awareness and on more sound, integrated knowledge. Furthermore, a more robust post-earthquake financial infrastructure will reduce the reliance of developing nations on charity, thereby speeding their recovery and avoiding a downward spiral of environmental hazards and economic development.

The EMME is planned in such a way that it will form a living model, rather than a static study, with a flexible, modular architecture to allow addition and updating of components and datasets, and to maintain it continuously as state-of-the-art and in conformance with national developments and new international standards. As such, EMME also plans to allow multiple user types to derive updated products and outputs, and keep up with changing requirements. The users and beneficiaries of EMME will be broad, and include all those who make decisions based on seismic risk: seismic agencies, engineers and practitioners, government officials, insurance and finance industries, emergency responders, risk professionals, homeowners, investors, and the population at large.

The project is composed of three research modules (hazard, risk, and socio-economic impact), and a phase in which an IT infrastructure will be established for the application of the methodologies developed in each module. The EMME will set a uniform, independent standard methodology for seismic hazard and risk assessment both on the national and regional scale. The implementation of the methodology proposed in the project is based on a combination of regional and global elements, and integrates developments of scientific and engineering knowledge as well as IT processes and infrastructure. The hazard, risk, and socio-economic impact modules are divided into sub modules defining the various Work Packages (WPs), as presented in Figure 1. Each WP has a leading institution also given in Figure 1. The current partners of EMME are given in Table. Apart from the official partners cited in Table 1, researchers from the National Centre of Excellence in Geology. University of Peshawar, Pakistan and from the Civil Engineering Department, Jordan University of Science and Technology are actively contributing to the project. The American University of Beirut is also at the stage of joining the EMME consortium.

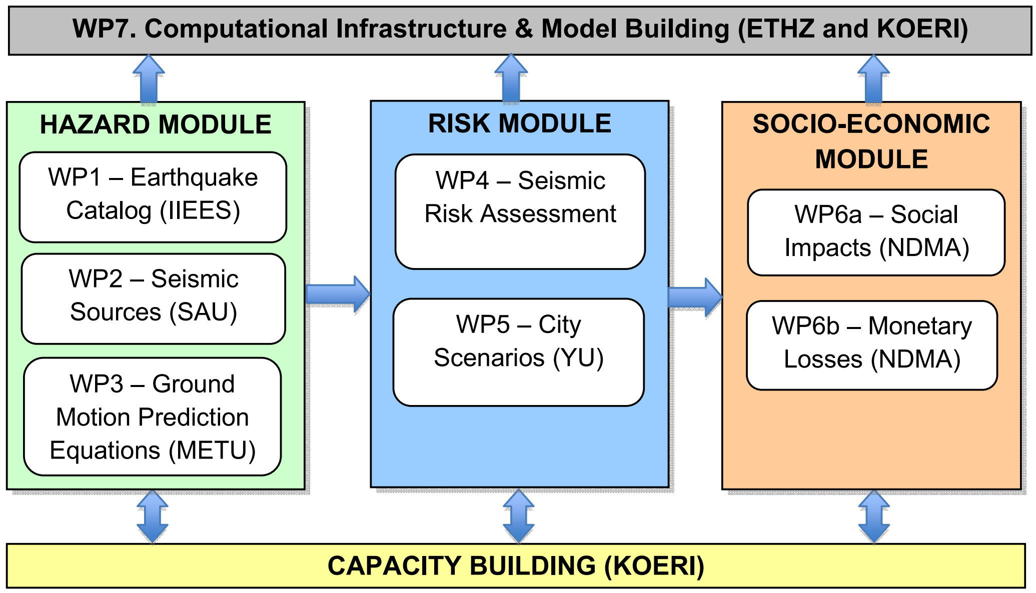

Figure 1 **Workflow of EMME.**

Table 1 **EMME-participating institutes.**

Partner Short Name	Partner Organization Full Name
ETHZ	Swiss Federal Institute of Technology, Zurich, Switzerland
KOERI	Kandilli Observatory and Earthquake Research Institute, Bogazici University, Istanbul, Turkey
IIEES	International Institute of Earthquake Engineering and Seismology, Tehran Iran
SAU	Department of Geophysical Engineering, Sakarya University, Sakarya, Turkey
METU	Department of Civil Engineering, Middle East Technical University, Ankara, Turkey
CUT	Department of Civil Engineering and Geomatics, Cyprus University of Technology, Nicosia, Cyprus
YU	Department of Earth and Environmental Sciences, Yarmouk University, Irbid, Jordan
NDMA	National Disaster Managment Authority, Islamabad, Pakistan
NED	Department of Civil Engineering, NED University of Engineering and Technology, Karachi, Pakistan
ACNET	Institute of Geophysics, Georgian Academy of Sciences, Tbilisi, Georgia
ANAS	Azerbaijan National Academy of Sciences, Ministry of Emergency Situations, Baku, Azerbaijan
SCI	Institute of Geological Sciences, National Acedemy of Sciences, Yerevan, Armenia

The EMME aims to compile the available data for the region and to concentrate the efforts on the homogenization of the data, with special attention on sharing and transferring experience throughout the region, the improvement of existing databases, and filling of possible gaps whenever possible. Compatibility with data requirements of the global projects (GEM) is also aimed at all stages. Technology and knowledge will be transferred from parallel projects such as NERIES, SHARE, and GEM. The ELER© (Earthquake Loss Estimation Routine) software developed by KOERI as a part of EU FP6 NERIES Project will be used for both regional and city scale earthquake damage and loss computations, whereas hazard computations will be done with the earthquake hazard computation software developed by GEM.

A main product of EMME will be the open source architecture, through which continuous refinement, analysis, and renewed studies can be implemented by risk professionals. The EMME also pays special care to have outputs for non-experts in order to disseminate the results widely. The outputs will be in the form of hazard maps, representing probability of ground shaking at various return periods for a suite of frequencies and with associated uncertainties, damage to the physical environment, casualties, affected and displaced population, and variations of economic indicators.

EMME WORK PACKAGES

The modules of the EMME project and the definitions of WP activities can be summarized as below.

Seismic Hazard Assessment Module

The EMME adopts the Probabilistic Seismic Hazard Assessment approach. The parameters required for that purpose are the definition of seismic source zones, determination of ground motion prediction models applicable to the region, and the choice of a proper probabilistic model. The seismic hazard module will consist of three Work Packages, the earthquake catalog, seismic sources, and ground motion prediction equations, which define the seismic activity rates (probability of occurrence of earthquakes in time and space) and earthquake hazard (annual probability of exceedance of a specific ground motion level). This separation of seismic hazard between events and shaking probabilities is justified on two principal grounds: (1) validation and testing of hazard can be conducted at the two separate levels of event and shaking probability; and (2) assessment of seismic risk based on scenario-based or intensity-based tools initiates from either individual events or occurrence probabilities.

The EU FP7 SHARE Project aims at developing a single computational infrastructure on a par and jointly with the OpenSHA program, a similar initiative supported by the USGS and SCEC in the United States. Initially located at SED-ETHZ, the SHARE computational infrastructure will be based on full accessibility and open availability of data, tools, and products, through a dedicated Portal fully connected with the portal for seismological data developed by the EMSC within the NERIES project. The software will be also open to be ported and installed in other centers, once fully tested and operational. The hazard assessment module of EMME will also make use of the methodologies developed within the context of SHARE, especially in terms of accessibility and open availability of databases and computational tools.

Work Package 1: Earthquake Catalog

Reliable seismic hazard studies depend on having a robust earthquake catalog. The longer the extent of the catalog and the more reliable the parameters are, the better it is for those doing seismic hazard analysis. There are two kinds of earthquake catalogs: one is the instrumental or recent catalog and the other is the historical catalog. In this study, the term "instrumental" or "recent" catalog refers to the time when seismic monitoring existed while "historical" refers to the pre-instrumental period.

The publication of earthquake catalogs in the Middle East region goes back to the preliminary efforts performed in late 1960s to early 1980s, mainly by the researchers conducted by Professor N. Ambraseys at Imperial College, London [Ambraseys and Melville 1982; Ambraseys 1988]. These catalogs provide detailed descriptive accounts of virtually all the earthquakes that are now known from the historical period and all subsequent analyses of seismicity up to the modern instrumental period. The earthquake catalogs for the Caucasus countries are also published mainly based on the former USSR earthquake catalogs. Regional catalogs were published in Armenia, Azerbaijan, and Georgia as well. The development of practical seismographic instrumentation around the turn of the 20th century led to the rapid growth of seismologic data, particularly for those events large enough to register at teleseismic distances on the early instruments.

For the EMME region, a new catalog is in the stage of being formed by combining both the global and regional catalogs. Catalog reliability, regional magnitude conversion rules, and regional catalog completeness issues are considered during the catalog formation process. The current state of EMME regional earthquake catalog for the period 1900–2010 is presented in Figure 2.

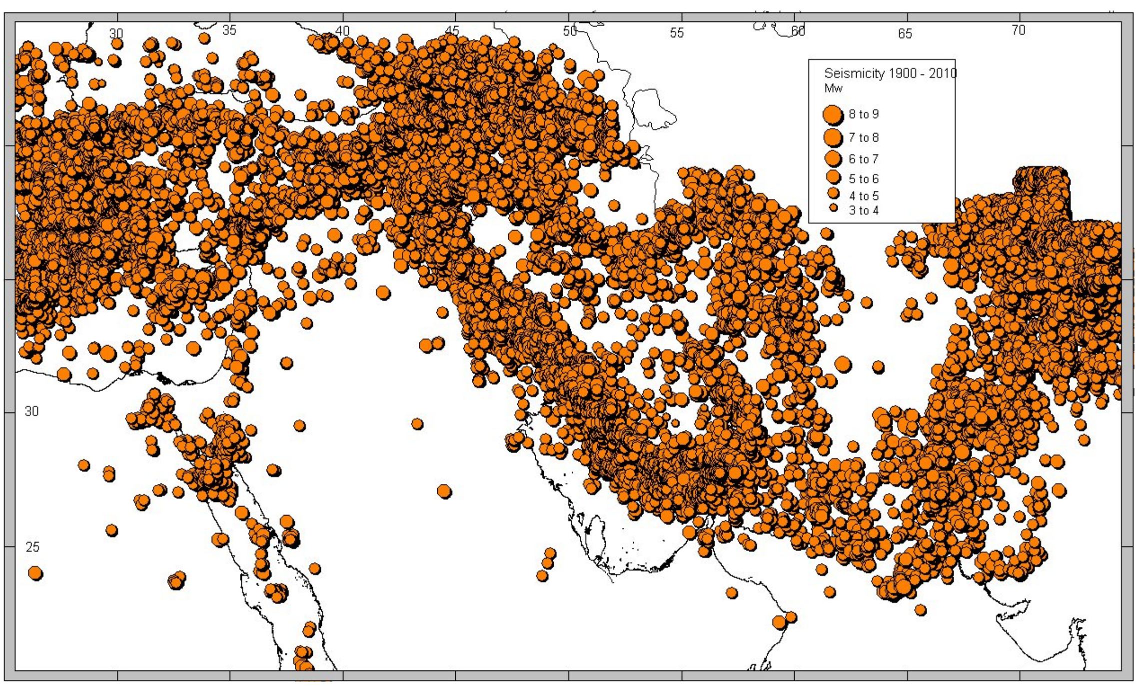

Figure 2 Earthquake catalog of the EMME region for the period 1900–2010.

Work Package 2: Seismic Sources

The delineation of seismic source zones can be accomplished providing that we have a thorough knowledge of geology, active tectonics, and complete record of seismicity (paleo+ historical+instrumental) of the region under consideration. The geodetic data obtained by Global Positioning System (GPS) measurements have also become a valuable data set to complement the other data sets in seismic hazard studies. The Seismic Sources Work Package of EMME is composed of the following tasks:

Task 2.1: Regional Compilation of Active Faults: Currently a database of fault parameters for active faults that are capable of generating earthquakes above a threshold magnitude *Mw* ≥ 5.5 for the entire EMME region is in the stage of development with the contribution of all partner institutes for their respective country and/or regions (Figure 3). This database includes information on the geometry and rates of movement of faults in a "Fault Section Database" and information on the timing and amounts of fault displacement in a "PaleoSites Database." In the "Fault Section Database" each entry contains the following information: fault name, fault trace, average dip estimate, average upper seismogenic depth estimate, average lower seismogenic depth estimate, average long term slip-rate estimate, average aseismic-slip-factor estimate, and average rake estimate.

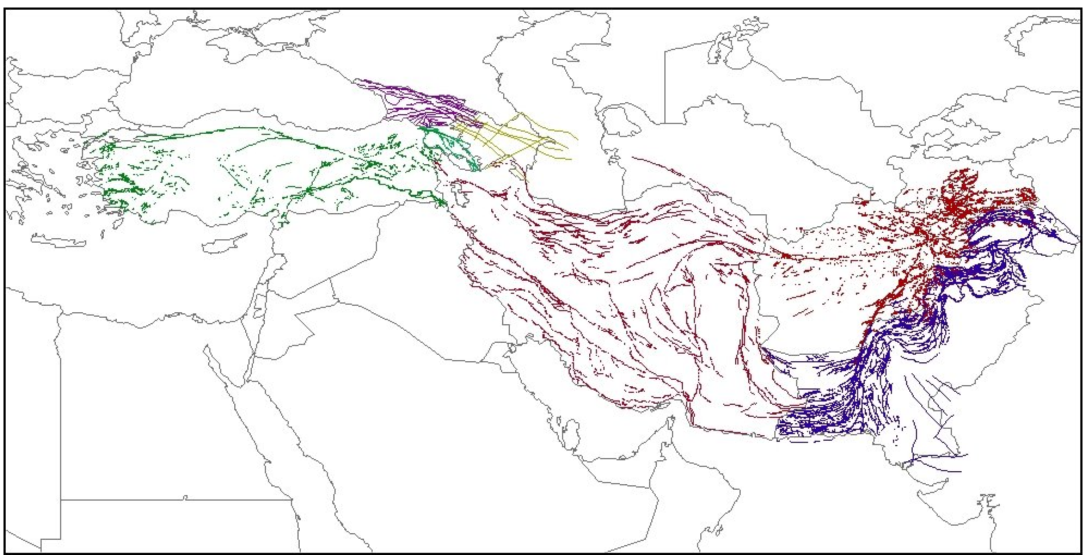

Figure 3 Active fault map of the EMME region.

Paleoseismic data for some major faults in the Middle East region have been acquired in several sites and published in the literature. These data are compiled and information on the timing and amounts of fault displacements will be provided in a "PaleoSites Database" that also includes the published recurrence intervals and their references.

Task 2.2: Regional Model of Strain and Slip Rates: Strain and slip rate models only exist for parts of the Middle East region. These models are either based on seismicity or GPS data. The comparison of the fault slip rates obtained by geological, seismic, and geodetic methods provide a good validation test. Especially the GPS data return realistic estimates of slip rates over large regions. All available data are currently being compiled in a map format for the Middle East region.

Task 2.3: Regional Model of Seismic Activity Rates: Once a uniform seismic catalogue is compiled and declustered for the Middle East region, in collaboration with the WP 1, fault activity parameters such as activity rate, *b*-value, and *Mmax* will be determined.

Task 2.4: Regional Model of Seismic Sources: The EMME region is not only seismically active but also geologically very complex that exhibits strong variations in rather short distances. In the construction of a homogeneous seismic zone model all the available data—including geological structure, seismotectonics, seismogenic faults, seismicity, and geodesy—will be taken into account. The existing seismic source zone models of the Middle East region will be assembled in terms of geometry and other parameters used in the description of seismic activity. New data and evidences will be interpreted to revise or modify the existing source models. A logic-tree approach will be utilized for the areas where there is no consensus to encompass different interpretations (e.g., the Sea of Marmara where there are several competing fault models).

Work Package 3: Ground Motion Prediction Equations

The objectives of Work Package 3 are to derive region specific ground-motion prediction equations for the Middle East and Caucuses by considering various ground-motion parameters that involve spectral acceleration, displacement, and peak ground-motion values, as well as to develop region specific tools useful for mapping local site conditions based on V_{s30} proxies, which are derived from the compilations of shallow geology and topography maps.

One of the goals in EMME is to devise methodologies for the estimation of seismic risk and loss that are tailored for different cities in the Middle East and Caucuses. To this end, the ground-motion prediction equations (GMPE) that provide hazard information to these methods should yield accurate ground motion estimates with low dispersion through simple functional forms that use the essential geophysical and seismological information. Based on this fact, the strategy of the work plan in developing the regional ground-motion models is schematized as:

- Level I: regions with different levels of seismic activity (low-to-high seismic activity) with abundant ground motions associated with well-defined geological, geotechnical and seismotectonic information.
- Level II: regions with different levels of seismic activity (low-to-high seismic activity) with poorly sampled strong-motion databases and/or poor geological, geotechnical and seismotectonic information.
- Level III: Seismic prone regions that lack data.

The prime methodology that followed in determining the level of sophistication in the regional GMPEs is to exploit the Level I ground-motion databases. Detailed studies on the performances of various GMPEs using these databases define the required level of complexity in the regional predictive model. The results and conclusions derived from the analysis of Level I datasets will be exported to Level II and III regions such that the most efficient model(s) will be used in these regions through rational calibration functions. The synthetics derived for the host-to-target relationships (through the consideration of source and radiation pattern features of the target region) form the most realistic calibrating functions to fulfill this objective. Such approaches have been implemented for eastern North America [Campbell 2003] and some regions in Europe [Douglas et al. 2006].

Seismic Risk Module

The risk module consists of two Work Packages: Seismic Risk Assessment (WP4), and Deterministic City Scenarios (WP5). The process will be performed by means of either deterministic risk scenarios for specific large earthquakes—depending on the models developed in hazard module—or probabilistic approach based on the same models and synthetic earthquake catalogs developed in hazards module. The seismic risk will be rigorously computed for selected cities.

Work Package 4: Seismic Risk Assessment

The objective of earthquake risk assessment and loss estimation studies is to assess the natural hazard and consequent risk due to the earthquake quantitatively. The output of these studies shall be used as a planning tool to execute management and mitigation policies of seismic disasters and damages within an area of interest.

Because the compilation of the inventories of the elements at risk forms one of the major components of seismic risk assessment, data under consideration will be obtained using existing databases and/or existing databases will be updated depending on the quality and quantity of the available data. Again the decisions concerning the determination of type of methodology and data to be used in the project are taken under the guidance of the regional experts. The elements at risk consist of the building stock, population, and infrastructure. The datasets of building stock, population, and infrastructure are currently being compiled by individual countries. For countries for which a grid-based distribution of building stock and population is available, that dataset is adopted. For other countries both local and globally available datasets are used to obtain a similar distribution. Some examples of building inventories developed are presented in Figure 4 and Figure 5. The building inventories are further classified in terms of major building types available in the region and associated vulnerability information is compiled from both macroseismic and analytical investigations. The databases are formed in terms of input requirements of the ELER© software to enable risk calculations to be performed with ELER© methodology [Erdik et al. 2010; Hancilar et al. 2010].

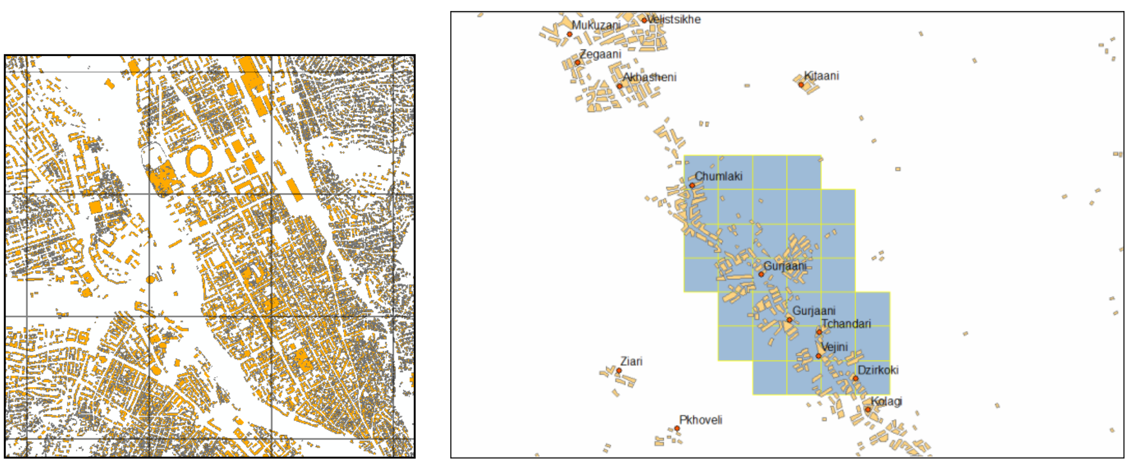

Figure 4 1x1 km grid based building inventory development for Tbilisi and county scale settlement based building inventory development for Georgia (study conducted by ACNET, Georgia).

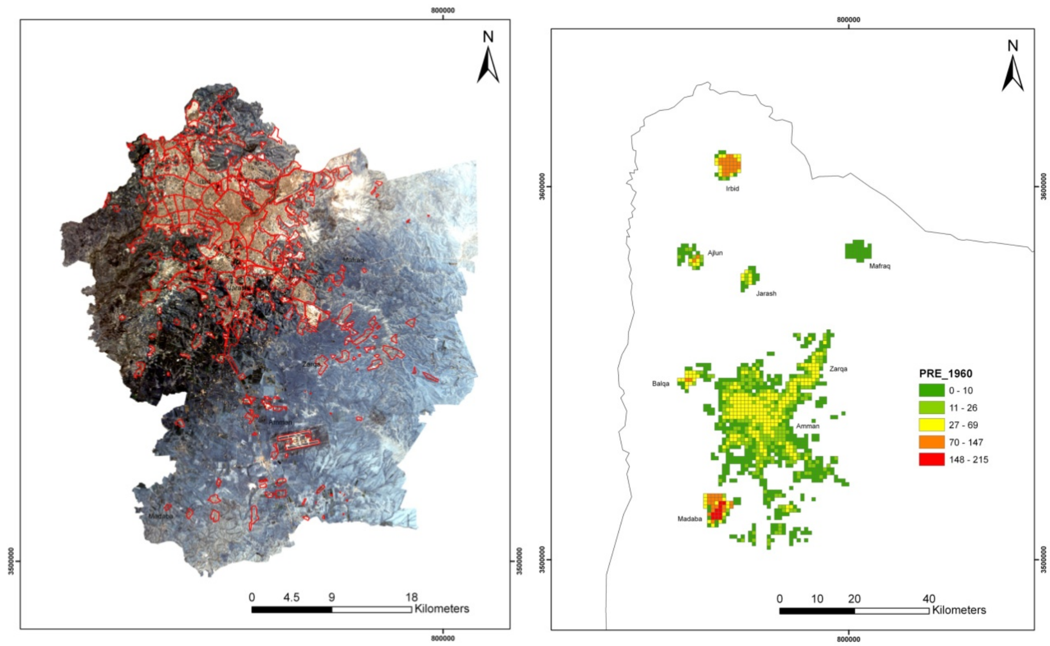

Figure 5 **Digitizing the populated urban areas from the satellite images in Irbid, Jordan, and distribution of buildings into urban areas (study conducted by YU and JUST, Jordan).**

Work Package 5: City Scenarios

City Scenarios Work Package forms one of the main components of EMME project Seismic Risk Module. The major aim of this work package is to achieve the main goals of EMME, which are the improvement of earthquake preparation and response, implementation of seismic mitigation measures, enabling accurate post-earthquake alerts and rapid assessment of direct and indirect losses, increase of public and administrative awareness on earthquake risk, and increase of earthquake insurance usage at the city level. As part of this component, deterministic seismic risk assessment will be carried out for risks associated with specified earthquake scenarios. The choice of scenarios will depend on the results of the Hazard Module Packages (WP1-3).To perform a city scenario application within the context of EMME, candidate cities were required to submit a proposal that would be subject to the approval of EMME’s Steering Committee. A guideline containing both the best practice city scenario reports (Istanbul and Amman) and the proposal format was prepared by September 30, 2009. A first call for City Scenario proposal was launched by September 30, 2009, and closed by May 31, 2010. Following the evaluation of the received proposals, the cities of Mashhad (Iran), Karachi (Pakistan), and Zarqa (Jordan) were selected to be supported. Further evaluation is in progress for the proposals of Tbilisi (Georgia), Yeravan (Armenia), and Baku (Azerbaijan).

Work Package 6: Socio-Economic Impacts

The general aim of the socio-economic impact module is to quantify socio-economic effects of earthquakes over the Middle East region. Specific tasks of the module are the development of tools and interfaces to the following end:

- Support risk-reducing decisions at an aggregate level in the Middle East.
- Calculate probabilistic and event-based financial losses.
- For cost/benefit analysis of mitigating actions such as strengthening/retrofit schemes; enforcement of building codes; urban development and transformation models.
- For the insurance sector to form the basis of development of new risk transfer mechanisms, to test the financial feasibility relatively new (i.e., cat-bonds) and existing (compulsory insurance) risk transfer models in the region. \

CURRENT STATUS AND FUTURE ACTIONS

The second year of the EMME project will end by March 2011. By that time a complete model of seismicity and active faults will be realized. By June 2011, the first three work packages of the project will be completed with all deliverables submitted, which will enable the computation of the seismic hazard with several models, logic tree considerations, sensitivity analyses, and deaggregration. The regional building inventories and associated building taxonomies will also be compiled by June 2011, allowing for building damage, casualty and loss calculations, and socioeconomic impact measurements to be conducted within the second half-term of the project.

REFERENCES

Ambraseys NN, Melville CP (1982). *A History of Persian Earthquakes*, Cambridge Univ. Press.

Ambraseys NN (1988). Engineering seismology, *Earthq. Engng. Struct. Dyn*., 17:1–105.

Campbell KW (2003). Prediction of strong ground motion using the hybrid empirical method and its use in the development of ground-motion (attenuation) relations in eastern North America, *Bull. Seism. Soc. Am*., 93(3)1012–1033.

Douglas J, Bungum H, Scherbaum, F (2006). Ground-motion prediction equations for southern Spain and southern Norway obtained using the composite model perspective, *J. Earthq. Engng*., 10:33–72.

EMME – Earthquake Model of the Middle East Project; see www.emme-gem.org.

Erdik M, Sesetyan, K, Demircioglu M, Hancilar U, Zulfikar C, Cakti E, Kamer Y, Yenidogan C, Tuzun C, Cagnan Z, Harmandar E. (2010) .Rapid earthquake hazard and loss assessment for Euro-Mediterranean region, *Acta Geophys*., 58:855–892.

GEM – Global Earthquake Model Project http://www.globalquakemodel.org

Hancilar U, Tuzun C, Yenidogan C, Erdik M (2010). ELER software–a new tool for urban earthquake loss assessment, *Nat. Hazards Earth Syst. Sci*., 10:1–20.

RECENT ADVANCES IN SEISMIC RISK ANALYSIS OF HIGHWAY SYSTEMS

Stuart D. Werner

Seismic Systems & Engineering Consultants, Oakland, California, USA

ABSTRACT

Since the mid-1990s, the United States Federal Highway Administration has been supporting research to develop methods for analysis and management of seismic risks to highway-roadway systems. This research has led to a new multi-disciplinary methodology and public-domain software package for deterministic or probabilistic seismic risk analysis of highway systems throughout the United States. This methodology estimates risks and losses due to earthquake-induced disruption of system-wide traffic flows and can be used to effectively manage these risks.

INTRODUCTION

Experience has shown that earthquakes can cause severe damage to individual highway components (e.g., bridges, tunnels, roadways, etc.) and that this damage can lead to significant risks to life safety (e.g., Figure 1a). Because of this, current practice for earthquake engineering for highway systems has focused on the reduction of these life safety risks. However, experience has also shown the earthquake damage can cause major traffic disruptions that, in turn, can adversely impact the region's economic recovery and emergency response (e.g., Figure 1b). These impacts will depend not only on the seismic performance of the highway components, but also on various characteristics of the highway system itself, such as its network configuration, the redundancies and traffic carrying capacities of the highways and roadways within the system, and the locations of the damaged components within the system.

Unfortunately, risks from earthquake-induced traffic disruption are typically not considered in seismic risk reduction activities for highway structures in the United States. One reason for this has been the lack of a technically sound and practical method for estimating these risks. To address this deficiency, since the mid-1990s the United States Federal Highway Administration (FHWA) has been supporting the development, testing, and application of a state-of-the-art methodology and public-domain software package for seismic risk analysis (SRA) and management of highway systems nationwide. This methodology is named REDARS (Risks of Earthquake DAmage to Roadway Systems). Detailed documentation of the REDARS methodology/software including an Import Wizard that facilitates input-data preparation is available in numerous reports and papers [e.g., Werner, et. al. 2006; Cho et al. 2006].

This paper describes the main features and applicability of the REDARS methodology. It is organized into three main sections. The first section summarizes the methodology, and the second section provides a demonstration analysis of an actual highway system that illustrates REDARS' applicability as a seismic risk management tool. The final section contains concluding comments that include a brief summary of current research and recommended directions for the continued development of the REDARS methodology and software in the future.

(a) (b)

(c)

Figure 1 Risks from earthquake-induced damage to highway systems: (a) life safety risks; 1989 Loma Prieta earthquake; (b) life safety risks, 1994 Northridge earthquake; and (c) risks from travel/traffic disruption (photo courtesy of Dave Brundsdon, New Zealand National Engineering Lifelines)

METHODOLOGY

Overview

The REDARS SRA methodology is shown in Figure 2. It includes input-data development and analysis setup (Step 1), system risk analysis for multiple simulations (Steps 2 and 3), and aggregation of the results from each simulation (Step 4). In this, a simulation is defined as the system SRA results for one set of uncertain input and model parameters. The numerical values of these parameters may differ from one simulation to another because of these uncertainties.

The heart of this methodology is four modules that contain the data and models needed to characterize: (a) the highway system and its post-earthquake traffic flows; (system module); (b) the ground motion and permanent ground displacement hazards (hazards module); (c) the component damage states, repair requirements, and traffic states; and (d) the losses due to traffic disruption and repair costs (loss module) (Figure 3). This modular structure enables inclusion of future upgrades to the REDARS models. Table 1 lists the multiple technical disciplines that are the basis for the models in each module.

The REDARS methodology uses a walkthrough process that is described in Taylor et al. [2001] and Werner et al. [2006]. This process is based on estimated earthquake occurrences over a time duration that is the order of thousands of years. For each year of the walkthrough, random samplings of a regional earthquake model are used to establish the number of earthquake occurrences during that year and each earthquake's magnitude and location. These data are stored in a "walkthrough table," which contains a year-by-year tabulation of these earthquake occurrences. Then, the following steps are used to develop a simulation for each occurrence.

- ***Uncertain Parameters:*** Values of all uncertain parameters are randomly selected.
- ***Seismic Hazards:*** Seismic hazard models from the Hazards Module are used to estimate site-specific ground-shaking and ground-deformation hazards at each component's site.
- ***Component Performance:*** Fragility models from the Component Module are used to estimate each component's damage state due to these hazards, along with its post-repair cost, downtime, and traffic state (ability to carry at least partial traffic at various post-earthquake times as the repairs proceed).
- ***System States:*** The component traffic states are used to develop post-earthquake "system states" that, at various post-earthquake times, represent which roadway links throughout the highway system are fully closed, partially closed, and open to traffic.
- ***Network Analysis:*** The network analysis model in the System Module is applied to each system state at each post-earthquake time, to estimate travel times, traffic flows, and trip demands.
- ***Loss Estimation:*** The network analysis results are used to estimate losses due to earthquake damage to the highway system (e.g., economic losses, increased travel times to/from key locations and along key routes, and reduced trip demands).

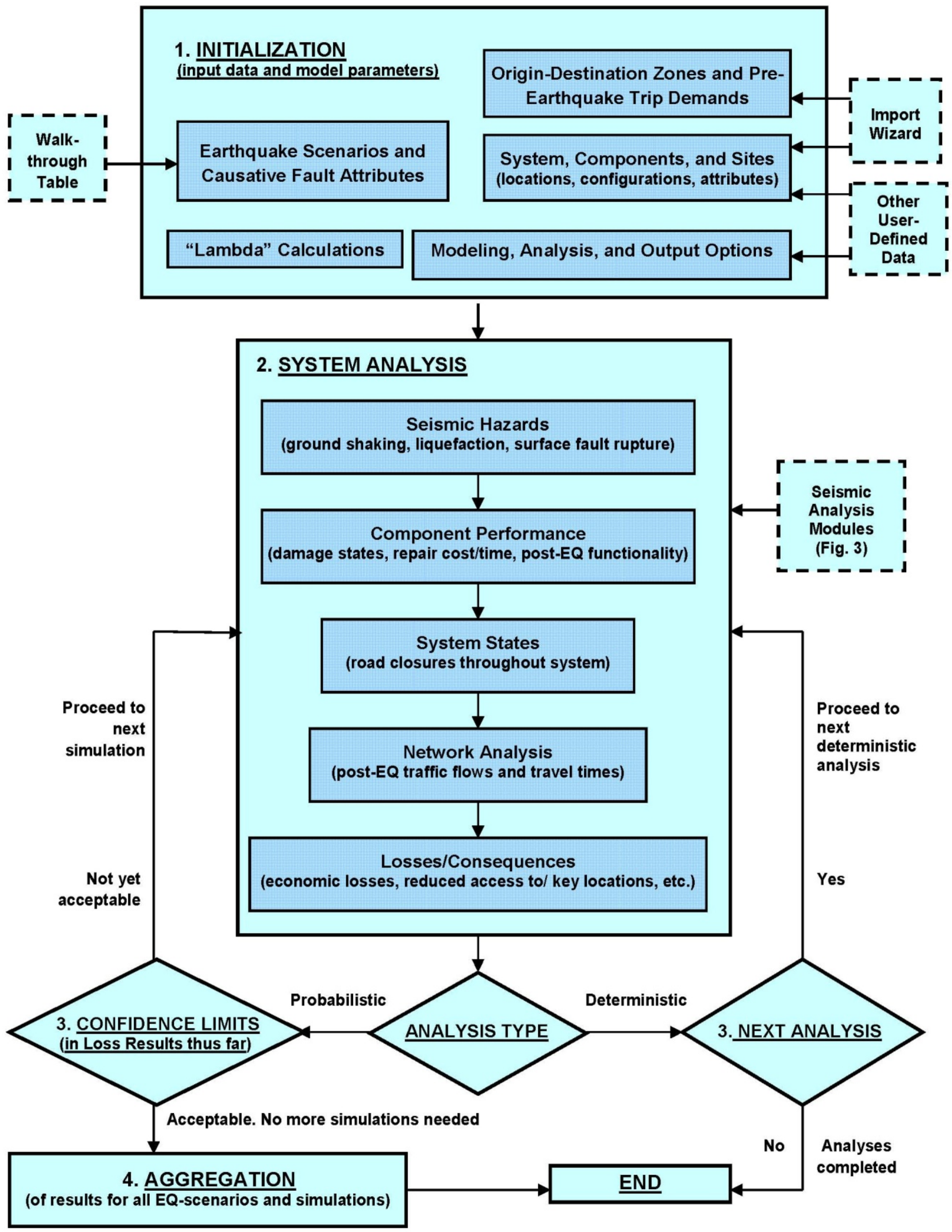

Figure 2 REDARS methodology for SRA of highway-roadway systems.

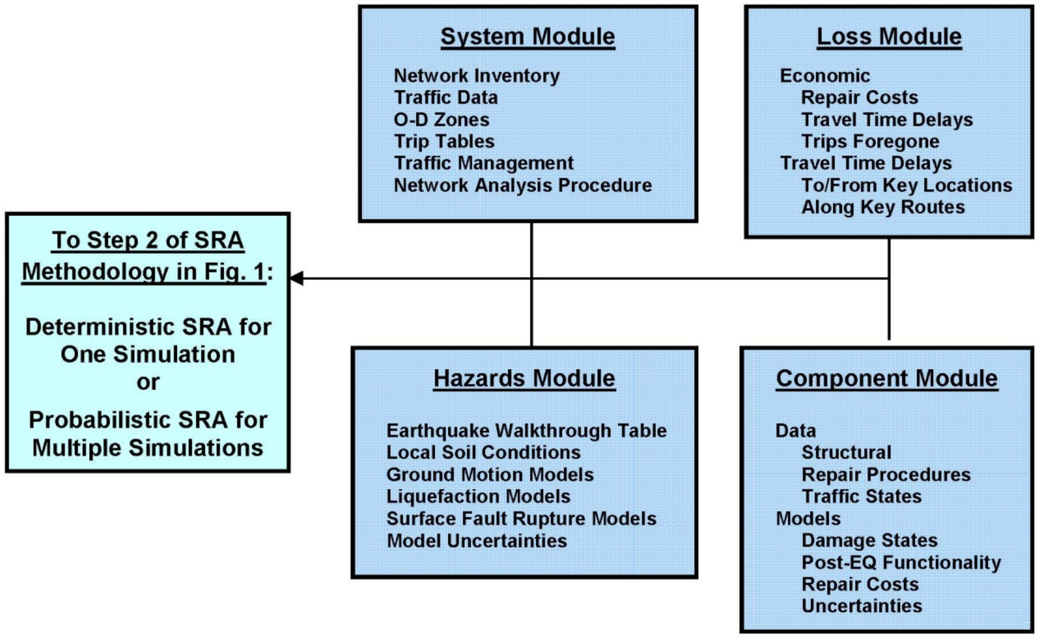

Figure 3 REDARS Seismic Risk Analysis Modules.

Table 1 The multiple disciplines that comprise the REDARS methodology.

Disciplines	Model	Description
• Geosciences	Earthquake Occurrences	• Table of EQ Occurrences over Time • Based on USGS & Regional EQ Models
• Geotechnical EQ Engineering	Seismic Hazards	• Ground Shaking • Liquefaction • Surface Fault Rupture
• Structural EQ Engineering	Component Vulnerability	• Bridges, Approach Fills, Tunnels, Roads • Damage States • Repairs (Costs, Durations, Traffic States)
• Transportation Engineering	Network Analysis	• Traffic Volumes • Travel Times • Trip Demands
	Loss Estimation	• Economic Losses • Reduced Access to/from Key Locations • Increased Travel Times along Key Routes • Reduced Trip Demands
• Risk Analysis	Probabilistic Risk Assessment	• Consideration of Uncertainties • Estimation of Confidence Levels

After each simulation, a variance-reduction procedure computes confidence intervals (CIs) in the economic-loss results. At any time during the analysis, the user can stop the SRA to examine these CIs and other results obtained thus far. If the CIs are judged to be acceptable, the SRA can be ended; otherwise, the SRA is restarted and additional simulations are developed. This iterative process continues until the user decides that further improvement of the CIs is no longer needed (Figure 2).

Initialization of Analysis (Step 1 of Figure 2)

Initialization of the analysis (Step 1 in Figure 2) includes the development of input data and the specification of various model and statistical analysis parameters. Input data for REDARS analyses include locations and traffic carrying capacities of all roadways in the system, locations and structural attributes of the bridges and tunnels along these roadways, pre-earthquake trip demands, soil conditions along the roadways, and scenario earthquake data. In the United States, the highway and bridge/tunnel data are obtained from national highway and bridge databases compiled by state transportation departments and maintained by the FHWA [FHWA, 2009, 2010a, 2010b]. Separate data for identifying those bridges that are seismically retrofitted are obtained from the state transportation department. Pre-earthquake trip demands on the system are obtained from regional Metropolitan Planning Organizations who subdivide their region into a series of traffic analysis zones (TAZs) and provide trip tables that define the number of daily trips from each TAZ to all other TAZs. System-wide soil conditions can be obtained from databases maintained by the state transportation department and from regional geologic data/maps.

The collection and manipulation of these data for input into the REDARS analysis can be extremely time consuming. However, REDARS substantially simplifies this effort through an Import Wizard that automates most of this data manipulation and provides a database that defines the study area's highway system, soils, bridges, and tunnels, and TAZ trip tables in a form that can be directly input into the REDARS core program [Cho et al. 2006].

Multiple scenario earthquakes used in probabilistic applications of REDARS are defined within an earthquake walkthrough table for the surrounding region. This table specifies earthquake occurrences (magnitudes and locations) over times on the order of thousands of years. For each earthquake, the table includes various parameters that characterize the faulting and the earthquake's hypocenter, epicenter, seismogenic depth, and center of energy release. These data are obtained from regional earthquake source models used by the United States Geological Survey (USGS) in their national seismic hazard mapping program, and also from regional earthquake centers. Scenario earthquakes used as input to deterministic applications of REDARS are defined in terms of their magnitude and the above faulting and earthquake source parameters.

System Analysis Procedure (Step 2 in Figure 2)

The REDARS system analysis procedure (Step 2 in Figure 2) is used to develop each simulation of a probabilistic analysis (with uncertain model parameters) and to perform a deterministic analysis (with fixed model parameters). To illustrate the procedure, this section summarizes results from a deterministic analysis of risks to the highway-roadway system in Los Angeles (LA), California, due to a Magnitude 6.6 earthquake along the Santa Monica Fault. Figure 3 shows the extent of this system and the location of the epicenter and surface fault rupture for this earthquake. The system includes the freeways and major arterials shown in Figure 3 and approximations of the effects of the traffic carrying capacities of the smaller roadways.

Figure 4 Los Angeles, California, highway-roadway system.

Seismic Hazards

Once the earthquake magnitude and location are defined, seismic hazard models are used to compute the intensities of the ground motions and permanent ground displacements due to liquefaction and surface fault rupture at the site of each component in the system. The system-wide seismic hazards due to the scenario earthquake for this analysis are displayed in Figure 5, which shows that the level of ground shaking at the bridges nearest to the surface fault rupture exceed 0.6*g* at several locations. Permanent ground displacements due to surface fault rupture zone are seen to exceed 12 in.

Component Performance

The damage state for each component is estimated as the median damage level that is obtained by applying the component's fragility model to its ground motion and permanent ground displacement hazards. Figure 6 displays damage states for this earthquake scenario in terms of HAZUS damage descriptors [FEMA 2010]. It highlights those bridges that are estimated to undergo "complete" (i.e., irreparable) damage due to strong ground shaking and surface fault rupture, as well as roadway segments (e.g., along Sunset Boulevard) that are estimated to undergo "complete" damage due to surface fault rupture.

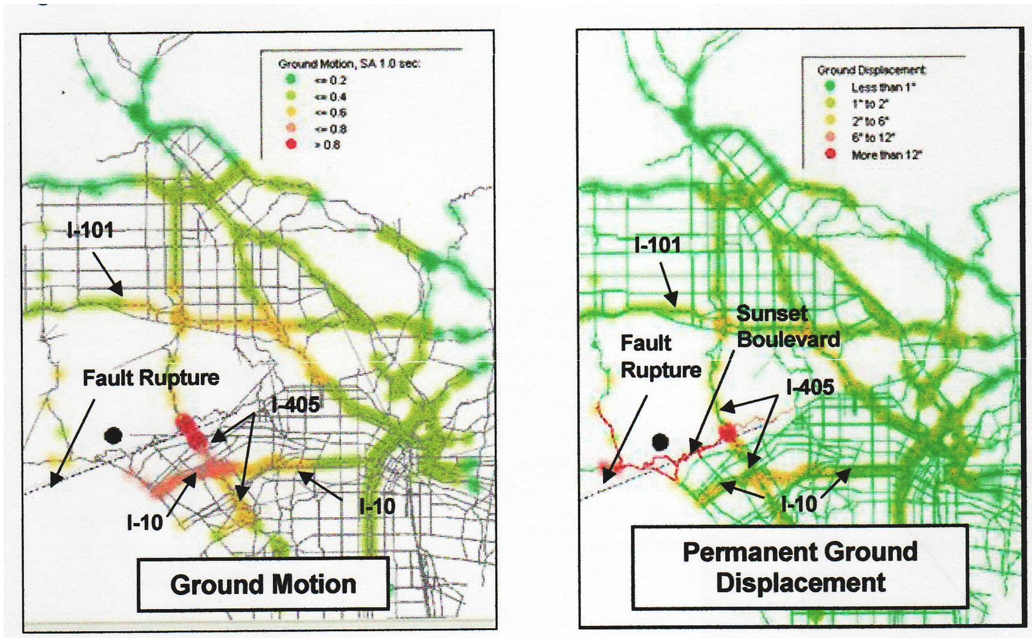

Figure 5 Seismic hazards.

After the component damage states are estimated, repair models are used to estimate corresponding component repair costs, downtimes, and post-earthquake traffic states (i.e., whether the component is fully closed, partially open, or fully open to traffic at various post-earthquake times). The repair models used in this example application were based on repair data provided by the California Department of Transportation

Network Analysis

In this step, system states at several post-earthquake times are developed as models of the highway system that use the component traffic states from the previous step to represent those roadway links throughout the system that are fully or partially closed to traffic at those times. Figure 7 shows system states at times of 7 days and 60 days after the earthquake. Then, transportation network analysis procedures are applied to each system state in order to estimate the traffic disruption and congestion due to the roadway closures at those times. The analysis also estimates how this increased congestion affects system-wide traffic flows, travel times, and trip demands. Figure 8 displays example network analysis results in terms of how system-wide traffic volumes are reduced relative to pre-earthquake volumes at times of 7 days and 60 days after the earthquake.

Losses

Losses due to highway system damage include: (a) economic losses due to increased travel times and reduced trip demands as well as repair costs; and (b) increased travel times to/from key locations and along key routes within the system that could affect regional emergency response and recovery. Figure 9 shows examples of losses that were computed from the network analysis results for this application.

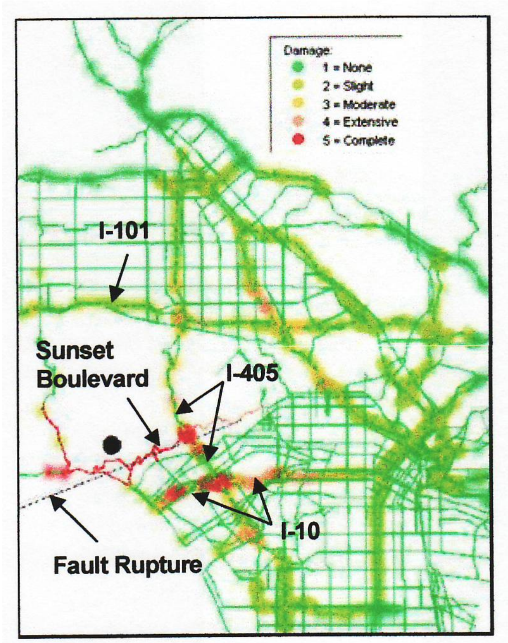

Figure 6 **Damage states.**

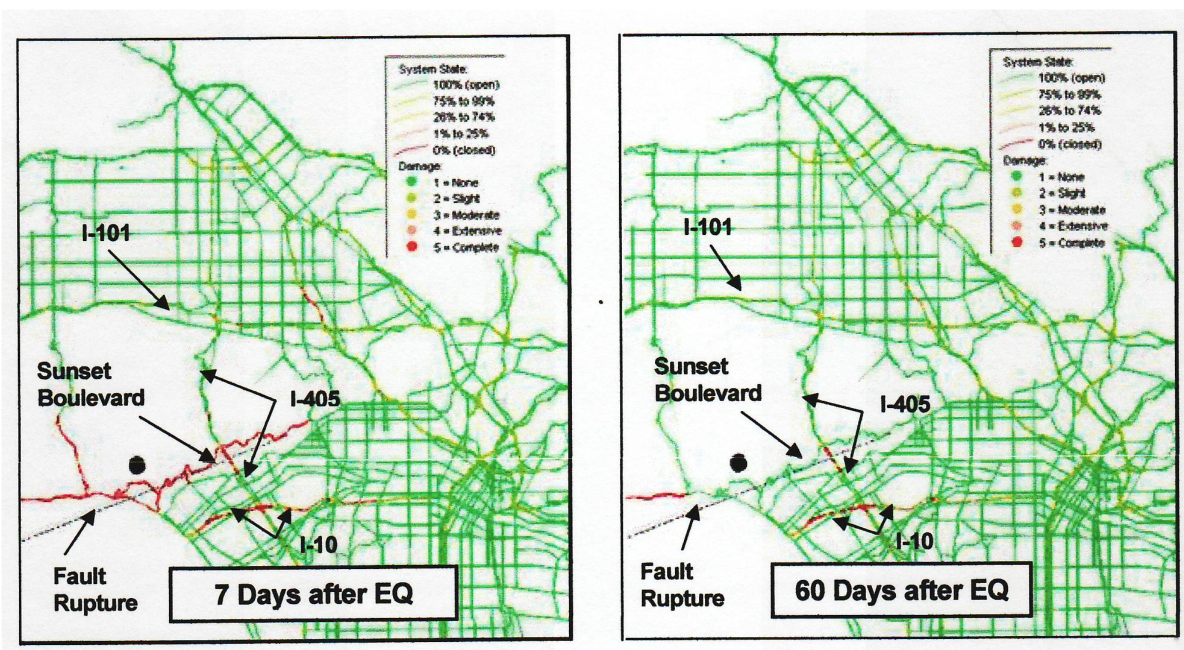

Figure 7 **Post-earthquake system states.**

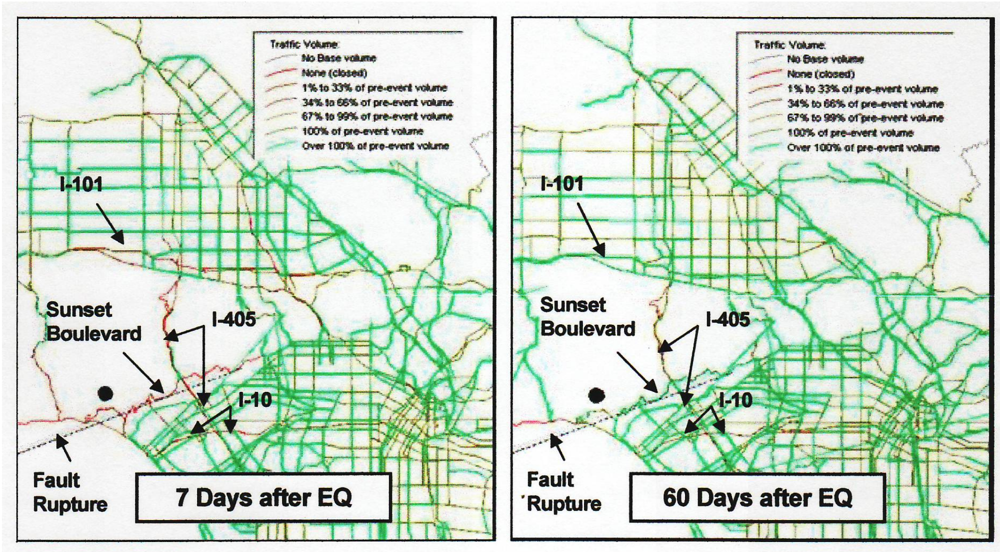

Figure 8 Network analysis results.

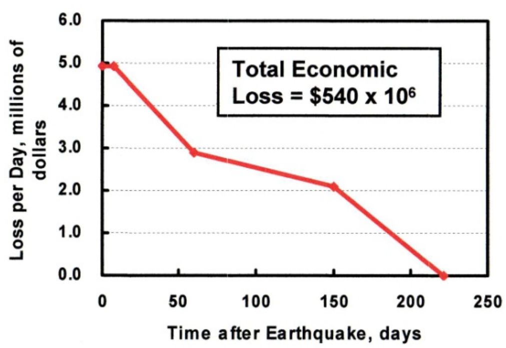

(a) Economic losses*

Route	Increase in Travel Time (relative to pre-EQ)			
	7-days after EQ	60-days after EQ	150-days after EQ	222-days after EQ
I-405 (San Diego Fwy) from I-10 to LA Airport	134.0%	63.6%	3.0%	0.0%
I-10 (Santa Monica Fwy) from Santa Monica to Downtown LA	209.7%	91.4%	37.6%	0.0%
I-5 (Golden State Fwy) from Burbank to Downtown LA	2.3%	2.0%	1.9%	0.0%

Location	Increase in Access Time (relative to pre-EQ)			
	7-days after EQ	60-days after EQ	150-days after EQ	222-days after EQ
UCLA Hospital	9.3%	9.3%	6.4%	0.0%
Van Nuys Airport	3.6%	0.3%	0.3%	0.0%
Encino Commercial Center	20.1%	0.5%	0.5%	0.0%

(b) Increased travel times between key locations and along key routes.

*Note: Economic losses are due to damage repair costs and to consequences of increased post-earthquake traffic congestion (increased travel times and reduced trip demands).

Figure 9 Losses due to earthquake-induced increases in traffic congestion.

SEISMIC RISK MANAGEMENT APPLICATION

An important benefit of the REDARS methodology is its applicability to the management of seismic risks to a highway system. In such applications, REDARS can be used to evaluate one or more seismic risk reduction options under consideration, by providing information on the relative effectiveness of each option in reducing losses due to transportation/traffic disruption. Options that can be evaluated in this way include: (a) prioritization of bridges for seismic retrofit; (b) establishment of component design or retrofit levels; (c) emergency response planning; (d) assessment of alternative post-earthquake repair strategies, such as the bonus-incentive program that Caltrans implemented after the Northridge Earthquake to replace collapsed bridges along major freeways; and (e) alternative system enhancement strategies. This section provides an example evaluation of an actual bridge retrofit program in the LA highway system, in order to demonstrate REDARS' applicability as a seismic risk management tool.

Statement of the Problem

The LA highway system considered in this example is shown in Figure 10. At the time of the Northridge Earthquake in January 1994, 57 bridges within this system had been retrofitted by column jacketing. Over a ten-year period after this earthquake, an additional 231 bridges within the system were column jacketed as part of a state-wide bridge retrofit program by the California Department of Transportation.

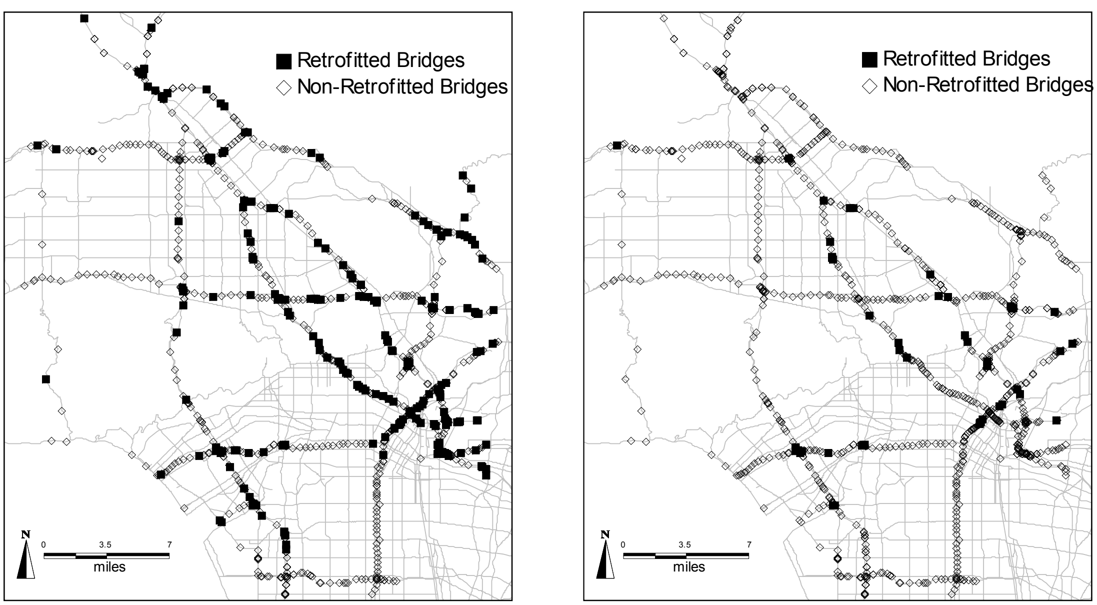

(a) Before Northridge Earthquake (early 1994). (b) Late 2004.

Figure 10 Column-jacketed bridges in LA highway system.

This example analysis uses REDARS probabilistic analysis procedures to examine the viability of these 231 bridge retrofits, in terms of their effectiveness in reducing economic losses due to earthquake-induced traffic disruption within this highway system. Thus, the analysis represents a "hindsight" evaluation of this bridge retrofit program that was completed approximately seven years ago.

Analysis Procedure

This evaluation is carried out from the perspective of a potential investor who is evaluating whether this retrofit program would be a good "investment", in terms of the potential for a good financial yield from the investment and whether the volatility of the investment is acceptably low. The evaluation procedure consists of the following steps.

- ***Cost of Investment:*** The total amount of this investment is the cost for retrofit of the 231 bridges. Based on data provided by Caltrans, the cost of this retrofit program is $11,000,000 [Bailey 2005].
- ***Probabilistic Analyses:*** REDARS is used to carry out probabilistic analyses of the potential losses due to earthquake damage to the highway system. Two analyses are carried out—one for the system before the additional 231 bridge retrofits are in place, and the other for the system after completion of these retrofits. Probabilistic estimates of economic losses due to increased post-earthquake traffic disruption (increased travel times and reduced trip demands) as well as repair costs are included.
- ***Financial Yield of Investment:*** In this analysis, the financial yield is measured by the effectiveness of the seismic retrofit program in reducing the present value of the average annualized loss (AAL) due to traffic disruption and repair cost. This reduction in AAL, which represents the "benefit" of the investment, can be compared to the cost of the investment in order to develop a benefit-cost ratio. An increasing benefit-cost ratio represents a more favorable investment from a financial yield perspective.
- ***Volatility of Investment:*** In this evaluation, this volatility of the investment is represented by the standard deviation of the economic losses due to traffic disruption and repair cost. The degree to which the standard deviation is reduced by the 231 bridge retrofits represents a more favorable investment from a reduced volatility perspective,
- ***Assessment of Investment:*** The above financial yield and financial volatility results are assessed together in order to decide whether this bridge retrofit program is economically viable.

Analysis Results

The financial yield of this investment as estimated according to the above procedure will depend on the discount rate and the exposure time for the investment. Table 2 shows the financial yield for three discount rates—2.5%, 4%, and 7%. Exposure times correspond to the estimated design life of a bridge in California which, according to Caltrans engineers, is about 75 years. To bracket this design life estimate, exposure times of 50, 75, and 100 years are considered.

Table 2 Benefit-cost ratios for use in evaluating potential financial yield of investment in retrofit of 231 Bridges in LA highway system.

Exposure Time	50 Years			75 Years			100 Years		
Discount Rate	2.5%	4%	7%	2.5%	4%	7%	2.5%	4%	7%
Benefit-Cost Ratio	3.90	3.19	2.41	4.45	3.42	2.45	4.74	3.51	2.46

Table 2 shows that the benefit-cost ratio is at least 2.4 for the highest discount rate, and is much larger for the lower discount rates shown in this table. In fact, in today's financial climate (February 2011) the discount rate is below 1%, which will further increase the benefit-cost ratios over those shown in Table 2. From this, it would seem that this bridge retrofit program is favorable from a financial yield perspective. Table 3 provides a comparison of the standard deviation of the losses for the LA highway system with and without the 231 bridge retrofits, which shows that the 231 retrofits reduce this standard deviation by about 38%, representing a substantial reduction in the volatility of this investment

Table 3 Standard deviation of losses for use in evaluating reduction in financial volatility of investment in retrofit of 231 bridges in LA highway system.

LA-Testbed System	Standard Deviation of Losses	Ratio of Standard Deviation of 2004 System to that of 1994 System
As of Early 1994 (prior to additional 231 bridge retrofits)	$218,634,766	0.616
As of End if 2004 (after completing additional 231 bridge retrofits)	$134,718,179	

Discussion of Results

The example represents one way in which REDARS can develop results for enabling transportation-department decision-makers to assess how various seismic-risk-reduction strategies may reduce potential losses caused by increased traffic disruption that can result from earthquake damage to the roadway system. Such results, when considered together with other relevant decision factors (e.g., life safety risks, various legal and political constraints, etc.) would enable these decision-makers to make a more informed selection of a preferred risk reduction strategy.

CONCLUDING COMMENTS

This paper has described and demonstrated the REDARS methodology for seismic risk analysis of highway systems. It has also shown how REDARS can be used as a tool for managing these risks by providing results that show the effectiveness of various seismic risk reduction options in reducing risks and losses due to earthquake-induced traffic disruption. The development of REDARS represents the first time that a technically sound and practical methodology and public-domain software package has been available to estimate and manage these important risks and losses for highway systems throughout the United States.

Research to continue the development of REDARS is proceeding. Current research is enabling REDARS to estimate the post-earthquake resilience of a highway system, and is also developing updated fragility models for bridges in the central and southeastern United States. These enhancements will be programmed into the REDARS software, and demonstration applications will be carried out to show the types of results provided by these enhancements and how they can be used in evaluation and management of seismic risks.

Much has been accomplished over the years to bring the REDARS to its present level of development. However, for REDARS to remain as a viable SRA tool in the future, the continued development of upgrades to its models, databases, and software will need to be an ongoing process. Vital to this continued development will be the future application of this software by transportation departments nationwide, and the suggestions and feedback that they provide. In addition, although REDARS has been developed to estimate losses and risks to earthquake damage, its methodology can be readily extended to also assess losses and risks from highway system damage due to other natural and man-made hazards such as flood, extreme wind, and explosion. Research to develop and apply these extensions is recommended.

ACKNOWLEDGEMENTS

The REDARS methodology and software has been developed under the sponsorship of the United States Federal Highway Administration under their ongoing Highway Seismic Research Programs, through contracts with the Multidisciplinary Center for Earthquake Engineering Research, and currently with the University of Nevada at Reno. The encouragement and support of Dr. Phillip Yen of the Federal Highway Administration (FHWA program manager), and Professor Ian Buckle of the University of Nevada at Reno (technical director of the program) throughout this research are gratefully acknowledged.

The procedures and applications described in this paper were developed as a team effort involving many individuals over the years. Key contributions to this work were made by Sungbin Cho of Southern California Association of Governments (transportation network analysis), Ronald Eguchi of ImageCat (internal review), Charles Huyck of ImageCat Inc. (Import Wizard developer and computer programming), Jean-Paul Lavoie of Geodesy (computer programming), James E. Moore II of the University of Southern California (transportation network analysis), and Craig E. Taylor of Natural Hazards Management Inc. (risk analysis).

REFERENCES

Bailey M (2005). Personal Communication to Stuart D. Werner, November 18.

Cho S, Ghosh S, Huyck CK, Werner SD (2006). *User Manual and Technical Documentation for the REDARS™ Import Wizard,* Report prepared for Multidisciplinary Center for Earthquake Engineering Research, Buffalo NY by ImageCat Inc., Long Beach CA.

Taylor CE, Werner SD, Jakubowski S (2001). The walkthrough method for catastrophe decision making, *Natural ASCE Hazards Review*, (2(4):193-202.

Federal Emergency Management Agency (2010). *HAZUS-MH MR4, Earthquake Model Technical Manual*, National Institute for Building Sciences, Washington D.C.

Federal Highway Administration (2009). The National Bridge Inventory Database, see www.nationalbridges.gov.

Federal Highway Administration (2010a). The National Highway Planning Network, see http://fhwa.dot.gov/planning/nhpn.

.Federal Highway System (2010b). Highway Performance monitoring system field manual for the continuing analytical and statistical database, *Report No. OMB21250028*, Washington D.C.

Werner SD, Cho S, Taylor CE, Lavoie J-P, Huyck CK, Chung H, Eguchi R (2006). *Technical Manual: REDARS™ 2 Methodology and Software for Seismic Risk Analysis of Highway Systems,* Report prepared for Multidisciplinary Center for Earthquake Engineering Research, Buffalo NY by Seismic Systems & Engineering Consultants, Oakland, CA.

VULNERABILITY AND RETROFITTING OF BURIED PIPELINES AND NETWORKS DURING EARTHQUAKES WITH EMPHASIZING ON URBAN AREAS

Fardin Jafarzadeh and Hadi Farahi Jahromi

Sharif University of Technology, Tehran, Iran

INTRODUCTION

Pipelines, considered as the main conveyance of energy, proved to be vulnerable to any transient loading. Loading can be divided to several categories including the traffic loads, earthquake loading, blasting, internal dynamic loading, etc. This paper discusses the impact of earthquake loading and dynamic excitations to pipelines. The paper is divided to three main parts: part one is devoted to the history of the events and the recorded damages to pipelines in several countries, while a brief description of hazards is also presented. Obviously, pipeline vulnerability to dynamic loading will be divided to four independent groups including: liquefaction, faulting, landslides, and wave propagation. In part two, a research performed at Sharif University of Technology will be presented. This study includes a dynamic sinusoidal excitation to a buried PVC pipeline. The pipe was buried in a laminar shear box, detail so which are presented in a related segment. The third part of this paper discusses an ongoing project considering the evaluation, analyzing, and the retrofitting of a gas pipeline system and network in Tehran megacity. This project is in progress by the Sharif University of Technology under the supervision of Tehran Gas Distribution Company, who is the client.

GENERAL FACTS REVEALING THE SEISMIC RESPONSE OF BURIED PIPELINES

According to the experience of many earthquakes (San Francisco 1906, Tokyo 1923, Manjil-Rudbar 1990, and Kobe 1995 as examples) the severity of damages and causalities were comprehensively increased due to damages and malfunctioning of lifelines. Pipelines are one of the main groups of lifelines and longitudinal structures passing through different geological areas with various risk of earthquake occurrence are very vulnerable to damage. Buried pipelines transmitting fuels (gas or oil), water, or as a part of sewage systems are among the lifelines whose damage could cause many problems and dangers, e.g., explosions, fire, flood, and environmental disasters. These elements could be generated by different mechanisms during strong ground motions as wave propagation, faulting, ground sliding, and liquefaction. Each item has diverse aspects, including the mechanism of occurrence, influential parameters, stabilizing methods, and the consequences of the event. In the following sections the four mentioned hazard will be discussed

Pipeline and Faulting Phenomenon

Permanent ground deformation includes the relative horizontal or vertical displacement of two sides of the earth occurring across a slip or fault plane (Figure 1). The faulting, which is divided to normal, transverse, and strike slip types, can occurred on both dry land seabed surfaces. In addition to the angle of intersection between the pipe and the fault, there are several other parameters that can affect the stresses and the consequent deformations on pipelines:

1. The situation of the pipe in operation or the shutdown state;
2. Normal or reverse-slip fault loading with longitudinal and vertical component to estimate the two-dimensional ground movement potential on the already snaked pipeline;
3. Ground oblique-slip fault loading with longitudinal, transverse, and vertical component to estimate three-dimensional ground movement potential on pipe stresses; and
4. A combination of above scenarios with maximum operational pressure/temperature conditions.

The main factor that determines the stresses on the pipe is the relative angle of the pipe axis and the orientation of the displacements. Bending and axial stresses are frequently imposed on the pipe, whether the axial tension or compression stresses occur depends on the relative displacement of the pipe and fault, type of faulting, and its orientation. Design of buried pipes against the peak ground displacement (PGD) is implemented by use of finite element analysis and the ASCE [1984] provisions. However the need for revision of the standard has led to further research, both experimentally and numerically.

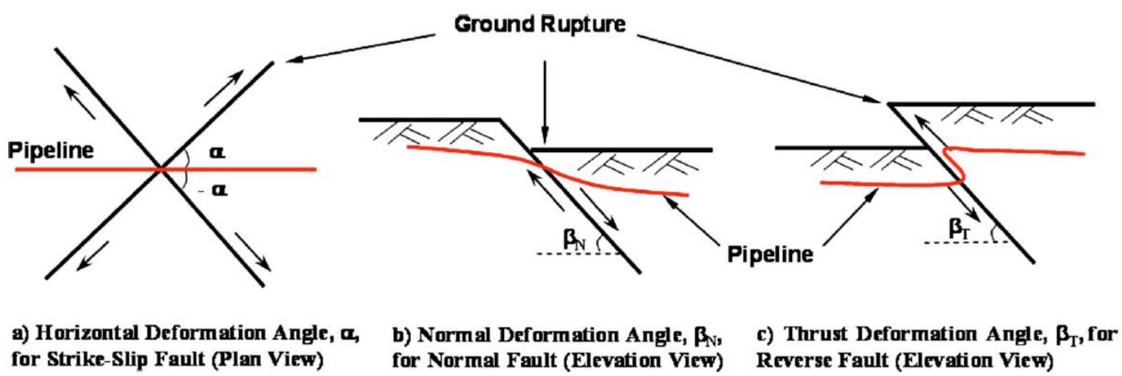

Figure 1 Different ground rupture patterns [Ha et al. 2008].

There are many catastrophe cases caused by fault interaction with pipelines. In the 1994 Northridge earthquake, there were 209 repairs required to metallic distribution lines and 27 repairs to polyethylene lines. There were 35 non-corrosion–related transmission pipeline repairs, of which 27 occurred on pipe joint with oxy-acetylene girth welds in pre-1930 pipelines. At one of those failures, gas leaked from a failed 56-cm line on Balboa Boulevard and was ignited by the ignition system on a nearby truck [O'Rourke and Liu 1994]; the resulting fire burned nearby houses (Figure 2). In Washington State, two high-pressure gas transmission line failures occurred in 1997, both resulting from ground movement. One of them resulted in an explosion. In 1999, a pipeline carrying gasoline failed due to damage caused by a third party during construction on adjacent facilities. The pipeline failure resulted in discharging 277,000 gallons of product into a creek bed. In the ensuing fire, two boys burned to death, and one young man was killed after he was overcome by fumes [SPA Risk 2008].

(a) (b)

Figure 2 (a) Balboa neighborhood burned by gas line in Northridge earthquake; and (b) fire ball that burned the neighborhood [SPA Risk 2008].

O'Rourke and Liu [2004] used the Rensselaer geotechnical centrifuge and a split container to model the horizontal displacement of faulting. In a more comprehensive test performed by Ha et al [2008], a container modeled the horizontal and vertical ground displacements. Figure 3 presents the configuration of the Rensselaer split-box and the HPDE pipe before and after the tests. They simulated the thrust block near a fault by pinning the pipe to the soil container. During each offset the axial and bending strains in the pipe and the axial force at the pipe end were measured during the tests. The pipe axial strains were a linear function of a longitudinal component of fault offset. Bending strain distribution was similar as the transverse component of fault offset. In addition, they compared the measured strains to the computed strains by Kennedy method, using tactile pressure sensors that measured the pressure distribution along and around the pipe. The *P*-*Y* relationship was also calculated based on the data from strain gauges and tactile pressure sensors and were compared with the charts proposed by both ASCE and Turner [2004].

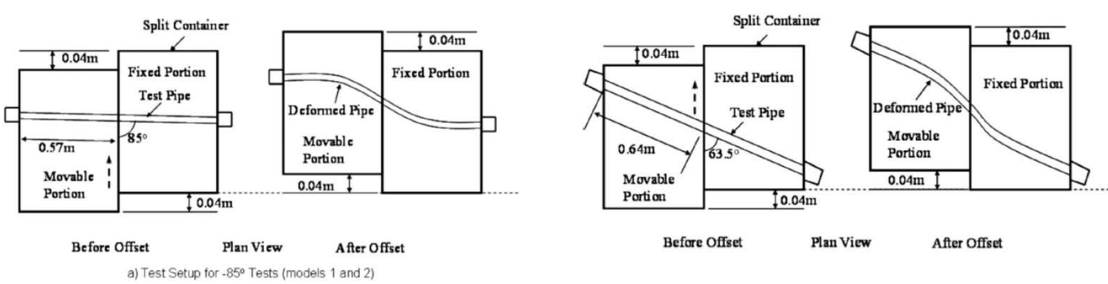

Figure 3 Configuration of the centrifuge model before and after offset, [Ha 2008].

Pipelines and Landslides

Landslides are also important factor to consider for crossing pipelines. Similar to faulting, here the important parameter affecting the pipeline behavior is the angle between the pipe axis and the loading direction. There is a major effective parameter that cannot be ignored: the slope's stability. Instability can occur due to two static and dynamic mechanisms; the major consideration is stability itself. Thus there are two ways to ensure the pipeline safety: first, control the parameters influencing the interaction between the pipe and the slope; and second, stabilize the slope to ensure that no excess loading will be imposed on pipeline in the future.

There are a few methods to control the interaction and many parameters exist for slope stabilization. The geological, hydrological, topographical, geometrical, and material characteristics can all influence slope stability. Any analysis of a slope's stability should rely on certain parameters These parameters can be accessed from available documents, field reconnaissance reports, field monitoring, subsurface investigation, and material testing [Ha 2008]. Slope stability analysis is divided into static and dynamic analysis. Each category also includes several sub-methods. For example, a static slope stability analysis can be performed by limit equilibrium and stress-deformation method. Similarly, dynamic analysis has two major sub-methods, including inertial and weakening of stability analysis. The inertial method includes pseudo-static, Newmark sliding block, Makdisi-Seed, and stress-deformation analysis. The weakening analysis has two sub-category methods, so-called flow failure and deformation failure analysis [Kramer 1996].

Provided that the interaction between the pipeline and the slope is of major consideration, the crossing angle, relative geometry of pipeline and the slope, type of pipeline (buried or above ground), and the pipeline characteristics should be considered. Some other items like internal pressure, duration of service, type of welding, and the pipe material can affect the durability and serviceability of pipeline during a dynamic event.

Stability analysis of the slope and crossing pipeline can be performed by two deterministic and probabilistic methods. In the first approach the whole system with its geometrical, mechanical, and geotechnical parameters is modeled. The result is only a safety factor implying whether the pipeline is safe or not. In a probabilistic approach, the result is a factor indicating the probability that the pipeline is to be injured in any type of loading. In both approaches, some structural analysis can be done to indicate the severity and type of damage to the pipeline. Although, practical stabilization techniques should be selected by an expert engineer, regarding numerical modeling and expertise, but subsequent cost-benefit analysis may suggest some revisions. The final plan should be re-analyzed to ensure the safety is fully provided.

The numerical approach is widely used by consultants and is the main method for slope stabilization. It is important to first chose the most advantageous approach and then analyze the system with known related parameters. Although this method has been proven to be successful, it is not particularly scientific. Physical modeling and numerical calculations are the two major types that are widely used by researchers. The ABACUS and FLAC3D programs—which are based on finite element or finite difference methods respectively—are used for numerical calculations; centrifuge and shaking table facilities can be used for dynamic physical modeling.

Figure 4 shows the physical model test configuration and the deployed sensors, performed by Qiao et al. [2008]. The shake table experiments used to model slope ground included a model pipe buried under the crest of the slope in a box, 1800 mm long × 600 mm wide × 800 mm high. The model ground consisted of 400-mm-thick sand in a 2H:1V slope, with its crest at the center of the box. Figure 4 presents a cross section of the ground, locations of pore water pressure gauges, the pipe, and accelerometers. Dynamic sinusoidal excitation had a frequency of 5 HZ. Several LVDTs in the model reported the lateral movement of the soil slope. This explanation is reported here to show an example of the arrangement and configuration of a typical model test found in the literature.

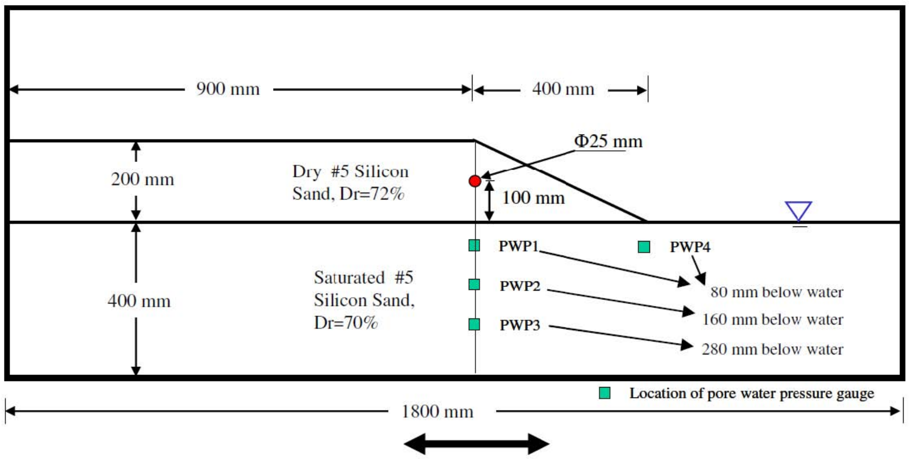

Figure 4 Shake table experimental equipment for the model slope ground and model pipe [Qiao et al. 2008].

Pipelines and Liquefaction

Generation of excess pore pressure under undrained loading condition is a hallmark of liquefaction occurrence. Liquefaction can be divided into two main groups: flow liquefaction and cyclic mobility. In addition to flow failures caused by liquefaction occurrence, there are three flow type failures that can damage structures. Local loosening, global loosening, and interface flow failures can damage structures by burying the structures or having the soil lean on the structure. Also, deformation failure—which is almost characterized as lateral spreading—can harm pipelines. Loosening in any mechanism, including the global and local, can alter the soil condition in a way that under the influence of gravity the lower part of the soil layer becomes denser and the upper part looser. Flow-type failures can occur when the shear strength of the interface between the liquefiable soil and a structure (in this case, a pipeline) becomes smaller than the shear stress required for equilibrium. As a result, the shear strength of the soil adjacent to pipeline will decrease and consequently the pipe support will fail. This condition will cause the pipe to experiences large deformations and damage will be inevitable. In addition; cyclic mobility can produce small, incremental deformations that may be sufficient to produce extensive damage. Lateral spreading causes the surficial layers to break into blocks that progressively move down slope or toward the free face. The ground surface may exhibit cracks at the head of the lateral spread, shear zones along its lateral margins, and compressed soil at the toe. So pipelines extending across or through the head of a lateral spread may be pulled apart, pipelines crossing lateral margins may be sheared, and pipelines near the toe may buckle [Kramer 1996].

In the case where a pipeline crosses the slope at 90 degree, it will not tolerate bending stresses. As an illustration, a perfect study reported by Mohri et al. [1995] of Hokkaido Nansei-Oki earthquake in 1993 showed that the pipes were separated from their supports, experienced torsion and upheaval even to the surface ground, or were laterally displaced at 20 to 30 cm [5]. Also manholes were displaced and the joints compressed. Soil strength, greatly influenced by relative density (D_r), acts as a support for buried pipes. Consequently, any reduction in relative density, which is common in liquefaction occurrence, directly decreases the soil strength, allowing the pipe to experience large deformations. Figure 5 shows displacement of a pipe after liquefaction has occurred.

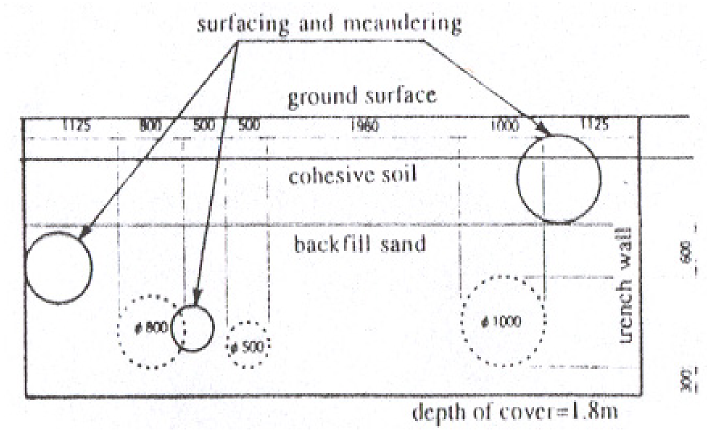

Figure 5 Pipe displacement after liquefaction occurrence [Mohri et al. 1995].

Pipelines and Wave Propagation

In the event that none of the scenarios discussed above occurs, the system is also vulnerable to wave propagation phenomenon. The relative deformation between plates occurs only in narrow zones near their boundaries. This deformation of plates can occur spasmodically in the form of earthquakes. Since this deformation occurs predominantly at the boundaries between the plates, it would be expected that the location of the earthquakes would be concentrated near the boundaries. While the theory of plate tectonics assigns the relative movement of plates to the form of spreading ridge boundaries, subduction zone boundaries, and transform fault boundaries, in some regions plate boundaries may be spread out, whereby edges of the plates have broken to form micro plates. Locally, the movement between two portions of crust will occur on new or existing offsets known as faults. Consequently, the most hazardous region for a pipeline and the related network will be in near-fault areas.

In addition to previous explanations, there are several micro faults in earthquake-prone areas, necessitating exact considerations. In addition to faults, pipelines are often buried in shallow depths, and movement of near-surface soils also impose stresses on them. As an illustration, a survey by O'Rourke and Liu [1994] established failure criterion for buried pipelines specific for urban areas [6]. Generally, a buried pipeline is subjected to both lateral and longitudinal PDGs, which, according to their study, a pipeline is more prone to failure in longitudinal than lateral deformations. The axial failure modes are divided to local and overall buckling and tension. Failure controlling parameters include δ (displacement), L (pipe length), δ_{cr} (critical displacement), pipe material (R/t), and burial specifications. They introduce critical length in which the longitudinal failure will take place, and effective length in which the maximum force is acting upon the pipe. Provided the effective length is more than the critical length or displacement is greater, the δ_{cr} buckling or wrinkling is expectable. In order to decrease damage, they advise using high strength steel, modern welding techniques, shallow burial depth, low-friction coefficient between soil and pipe and small (R/t).

RELATED RESEARCH IN SHARIF UNIVERSITY OF TECHNOLOGY

An extensive research for studying the geotechnical earthquake engineering aspects of buried pipelines began a few years ago and is currently in progress by researchers of the Civil Engineering Department of Sharif University of Technology. In a study reported here, soil structure interaction and wave propagation are simulated by using physical models. In this research, dynamic sinusoidal loading was applied to a soil container in which a PVC pipe was buried. The semi-infinite nature of the field was simulated using a laminar shear box. The soil used in the experiments was Babolsar coastal sand provided from Southern Caspian Sea shores; PVC pipe was selected due to their use in the field. Eight models were constructed. Four models had a uniform base. In the rest of models, the bed rock non-uniformities of real ground were simulated using a concrete pedestal installed at the very bottom of the shear box. Pipe deformations under dynamic loading, acceleration distribution in height, soil settlement, and horizontal displacements were measured by strain gauges, accelerometers, and displacement meters. With analyzing the obtained data, influence of different parameters of dynamic loading such as acceleration, frequency, soil density, base conditions, and shaking direction to pipe axis on the acceleration amplification ratio and pipe deformation were investigated. To study the effect of dynamic loading on two different materials (soil and pipe), horizontal strains were compared. Tests were conducted by using various apparatuses and sensors. T shaking table device, laminar shear box, PVC pipe, and supports are briefly explained below.

Shaking Table Device

The 4 m × 4 m shaking table in Sharif University of Technology was used to induce the desired excitations to the models. This table can sustain a model up to 20 tons in weight. The table has three degree of freedoms in x, y direction and rotation around the x-y plane vector, with a maximum displacement of 250 and 400 mm in the x and y directions; respectively.

Shear Box

A laminar shear box designed at Sharif University [Jourabchian 2002] includes 24 aluminum layers, each having the dimensions of $100 \times 100 \times 4$ cm^3. As shown in Figure 6, the laminar shear box is composed of a variety of equipment. Among them is a saturation-drainage system, horizontal supporting columns, and crossing elements on the top and horizontal displacement controlling planes between the layers to prevent the movement in desired direction.

Model Preparation

The container was filled by uniform sand and the pipe was fixed at the box bottom. The pipe was 80 cm long, 5.8 cm in diameter, and 0.178 cm thick, with E and υ equal to 18500 kg/cm^2 and 0.3; respectively. In order to obtain desired relative density, several calibration tests were performed and finally sieve #4 was selected through which sand was smoothly pluviated (see Figure 6).

(a) (b)

Figure 6 **(a) laminar shear box; and (b) Soil pouring in the box using the bucket [Jafarzadeh et al. 2010].**

Simulating the Topographical Conditions of the Pipe Base

Non uniformities of bedrock were simulated by providing a cast concrete pedestal with a parallelogram cross section, depicted in Figure7. The concrete pedestal was carefully placed in the soil container. Thus, the experiments were divided into two major categories. In the first series, in order to simulate a uniform condition of pipe trench, the concrete pedestal was not used, while in the second tests series the concrete pedestal was placed in the model to simulate the existence of bedrock.

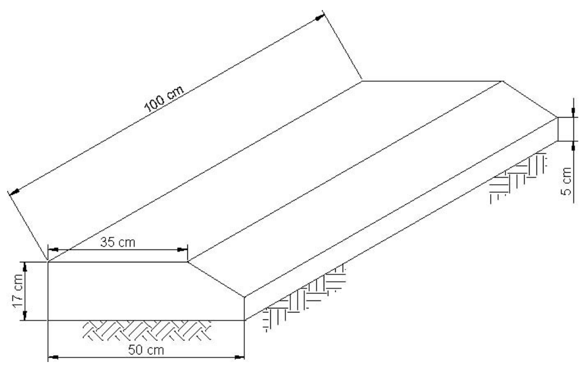

Figure 7 **Pedestal cross section.**

For the first group of tests in which the concrete pedestal was not used, the pipe was fixed between two bearings, as shown in Figure 8(a). By making a 5 cm deep, 5-cm-diameter hole in each support, a semi-rigid fixation was provided to serve as long buried pipe (Figure 8). In models with the concrete pedestal fixed in the shear box [Figure 8(b)], one end of the pipe remained unchanged, while the other was fixed on the pedestal. Figure 8 shows the details of the connection.

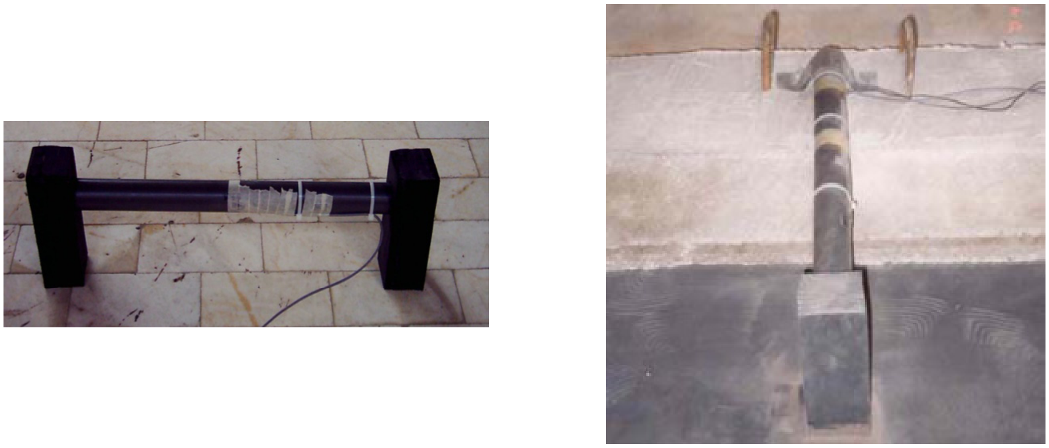

(a) (b)

Figure 8 The buried pipe and its two supports.

Instrumentation

Using the above mentioned method for model preparation, eight models were prepared. Several different measuring instruments were used in the experiments to monitor the behavior of the soil and pipe. The devices installed in the model include accelerometers, LVDT's, and strain gauges. The deployed instruments—showing the arrangement of pipe, sensors, and sand in the shear box during model construction—are shown in Figure 9.

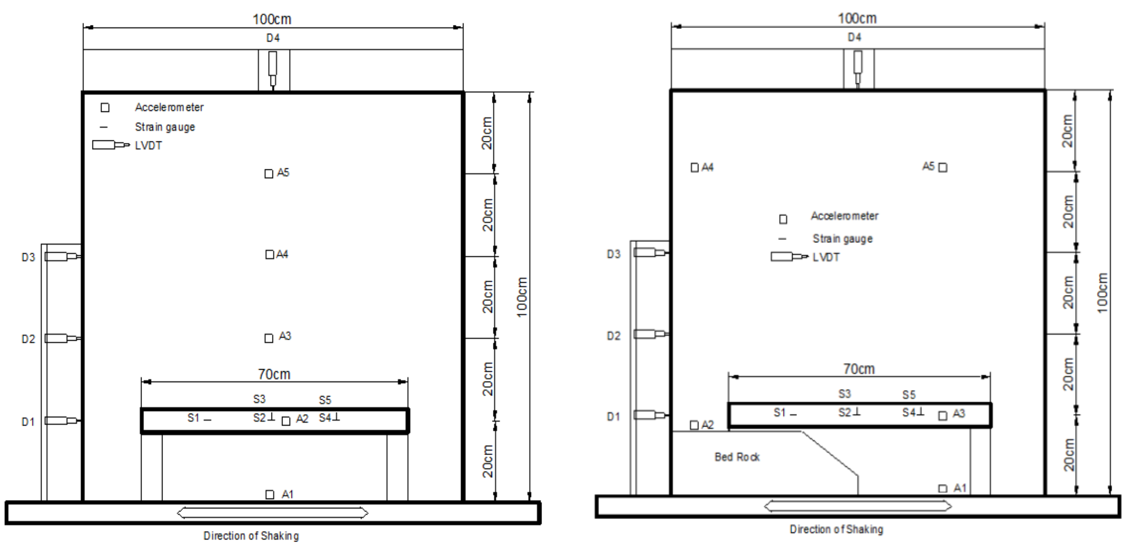

(a) (b)

Figure 9 Schematic cross section of the models and positioned sensors: (a) without pedestal; and (b) with pedestal.

Experimental Program

The tests were divided in two major groups, with and without the concrete pedestal (which acted as a bedrock in the model). Therefore, the loading plan was designed in such a way that the results recorded from these two model groups could be compared. In addition, according to the loading direction to pipe's axis, each model loading was divided in two minor sets. The loading direction, which could be either parallel or perpendicular to the axis, revealed the buckling and bending failure condition; respectively. The dynamic loading consisted of sinusoidal acceleration with amplitude in the range of 60 to 1100 gal, a frequency of 5 or 10 Hz, and the number of cycles of 10, 20, and 40. Table 1 summarizes the loading characteristics and model properties before and after each test.

Table 1 Dynamic loading characteristics and model properties before and after the tests.

Model No.	Number of Tests	Initial Dr (%)	Loading	Pipe Deformation	Final Dr (%)	Remarks
1	10	28.4	Harmonic	Bending	96.2	No Pedestal
2	17	16.0	Harmonic	Bending	90.7	No Pedestal
3	20	8.6	Harmonic	Buckling	92.7	No Pedestal
4	23	7.0	Harmonic	Buckling	92.9	No Pedestal
5	31	13.2	Harmonic	Bending	81.5	With Pedestal
6	32	11.0	Harmonic	Buckling	88.4	With Pedestal
7	12	8.2	Harmonic	Buckling	76.6	With Pedestal
8	15	9.2	Harmonic	Bending	80.3	With Pedestal

Test Results

Data obtained from data acquisition system were converted to physical parameters such as acceleration, displacement, and strains. Figures 10 and 11 demonstrate the typical recorded results for acceleration on the base, on the pedestal, near the pipe 60 or 80 cm high in the soil, the displacement of the soil layers at the pipe elevation, and the strains related to strain gauges No. 1 to 5 on the pipe. Figure10 pertains to those models where the pedestal was not used, with results with pedestal presented in Figure 11.

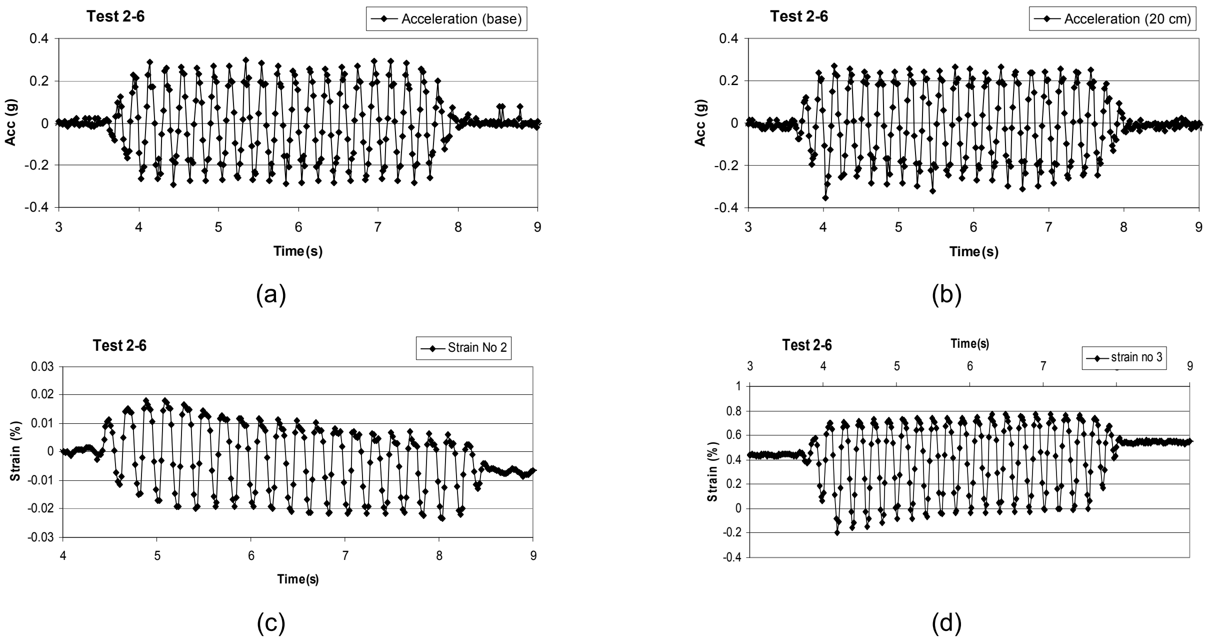

Figure 10 Recorded acceleration and strain time histories in soil and pipe for Test 2-6 at different points without pedestal: (a) base acceleration (A1); (b) acceleration near to pipe (A2); (c) longitudinal strain at the mid-height of pipe (S2); and (d) peripheral strain at the 0.25L of the pipe (S5).

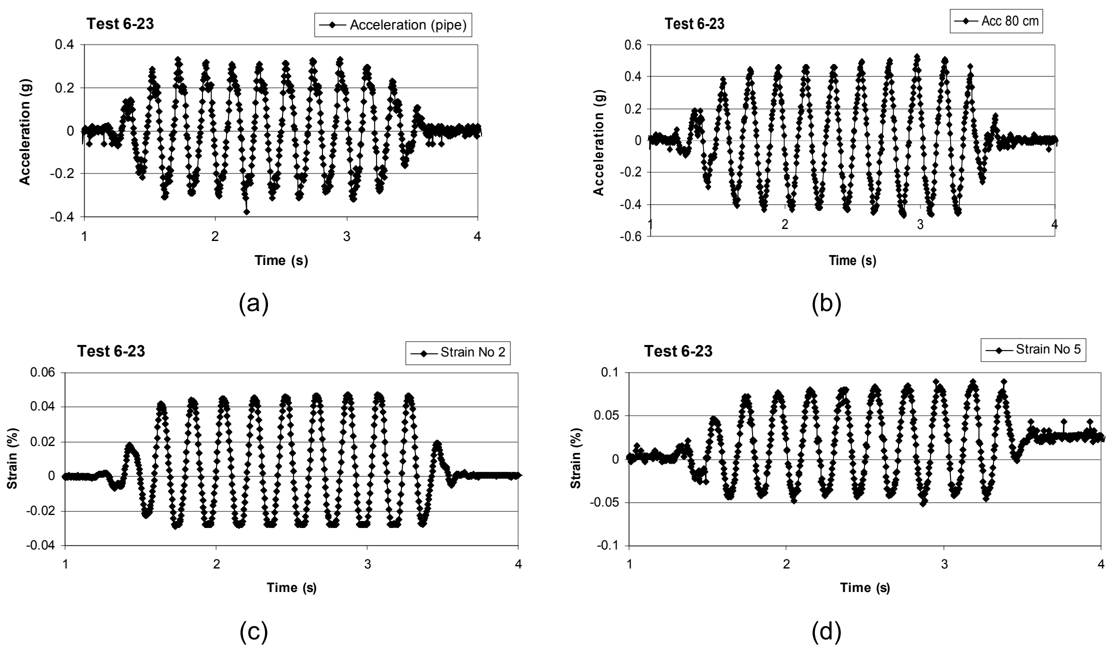

Figure 11 Recorded acceleration and strain time histories in soil and pipe for Test 6-23 at different points with pedestal: (a) acceleration near the pipe (A3); (b) soil acceleration in 80 cm height (A5); (c) longitudinal strain in the mid-height of the pipe; and (d) peripheral strain at the 0.5L of the pipe (S3).

Effect of Loading Direction to Pipe Axis on the Strains

Dynamic loading was applied parallel and perpendicular to the pipe axis. Thus the effect of the loading direction was verified by comparing the strains in the two sets of experiments. Figure 12 summarizes the data associated with the longitudinal strains having 5 Hz frequency and accelerations 0.3g to 0.5g, showing the strains of the models containing the concrete pedestal, It can easily be observed from these figures that the buckling mode of failure is dominant in models containing the concrete pedestal, which causes higher strains in the pipe. This conclusion however cannot be made in models without the concrete pedestal. Therefore, it is concluded that in areas where the trench base is composed of uniform soil, the perpendicular direction is more likely to cause failure. Unlike the previous case, the rigid rock movement parallel to the pipe axis caused higher strains in the buckling mode than the bending one.

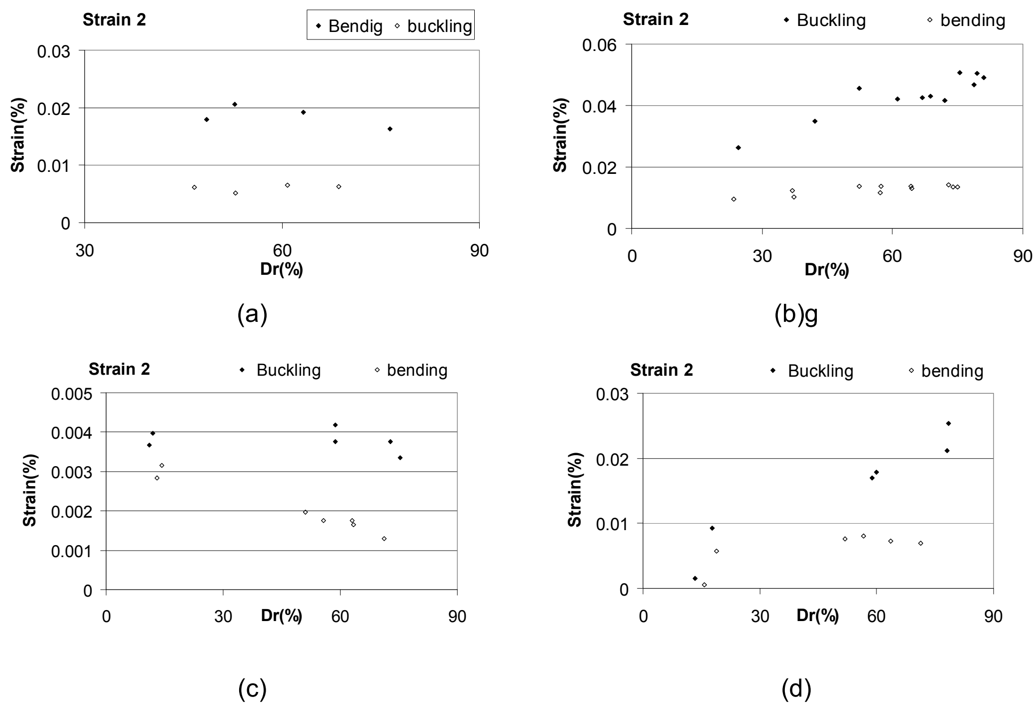

Figure 12 Loading direction effect various models (longitudinal strains): (a) f = 5 Hz without pedestal, a = 0.3g; (b) f = 5 Hz with pedestal, a = 0.3g; (c) f = 10 Hz without pedestal, a = 0.1g; and (d)) f = 10 Hz with pedestal, a = 0.3g.

Figure13 summarizes the results for circumferential strains measured at the mid-length of the pipe. Bending mode of loading caused critical conditions to the pipe, meaning that the pipe is likely to be damaged more in perpendicular loading to the pipe axis than the parallel direction. Thus, for all conditions of foundation and loading, perpendicular loading results in greater strains than the parallel one. In the parallel loading direction, the pipe is subjected to compression-tension stress cycles, while the main body of the pipe is kept undisturbed; however, in perpendicular loading, the pipe cross section experiences deformations. Thus, loading perpendicular to the pipe axis would be the critical failure mode that significantly deforms the pipe cross section.

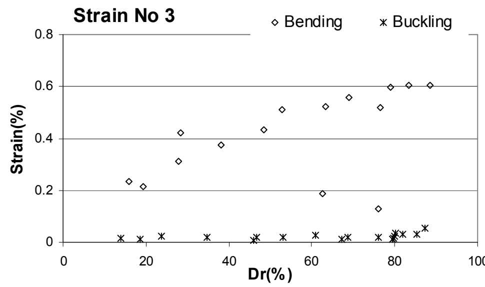

(a)

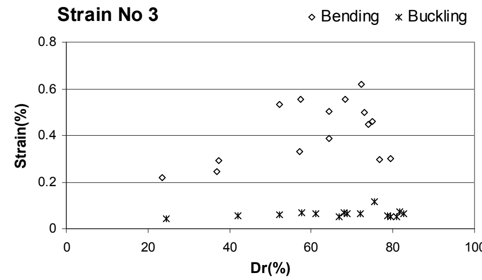

(b)

Figure 13: Loading direction effect on various models (peripheral strains): (a) f = 5 Hz, a = 0.1-0.5g without pedestal; and (b) f = 5 Hz, a = 03-0.4g with pedestal.

Effect of Concrete Pedestal on Pipe Strains

Provided the loading direction was parallel to pipe axis, the longitudinal strains induced on the pipe were higher for the model with the pedestal than for the model in the other cases, as shown in Figure 14. Regardless of acceleration values induced to models [see Figure 15(a)], the models with pedestal resulted in higher peripheral strain at the mid-length of the pipe. This is also seen in Figure 15(b), which proves that strain values for 240 gal acceleration loading and 10 Hz frequency in any relative density was higher in the models with pedestal than the ones that resemble the uniform base conditions.

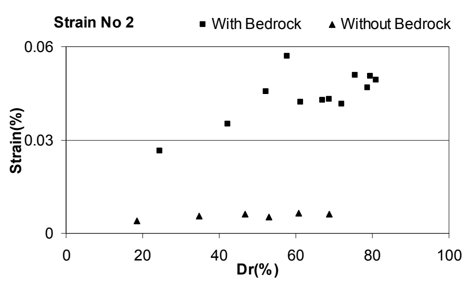

(a)

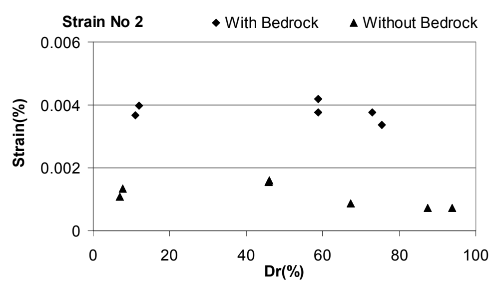

(b)

Figure 14 Pedestal effect on various models (longitudinal strains): (a) f = 5 Hz, a = 0.3g, buckling mode; and (b) f = 10 Hz, a = 0.1g, buckling mode.

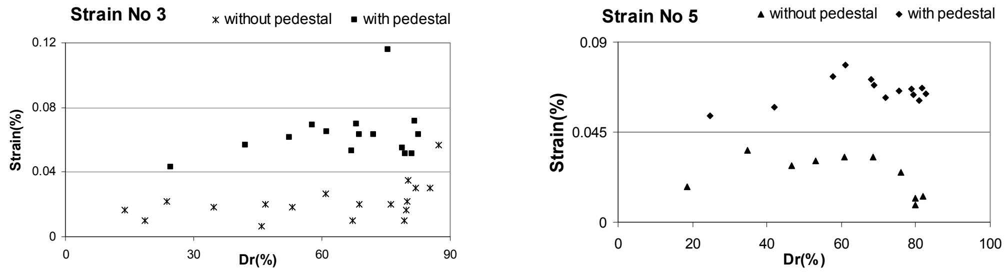

(a) (b)

Figure 15 Pedestal effect on various models – buckling mode (peripheral strains): (a) f = 5 Hz, a = 0.2-0.5g, buckling mode; and (b) f = 5 Hz, a = 0.24g, buckling mode.

Despite the above-mentioned results for buckling mode of loading, the recorded strains for the bending mode in strain gauge No. 2 were not as clear cut as the other results, and an obvious conclusion cannot be made in this case. This uncertainty also remains for the strain No. 3 (see Figure 16). This means that although the buckling mode presents an obvious result; for bending mode the strains for two cases are not so clear to yield in an incisive result.

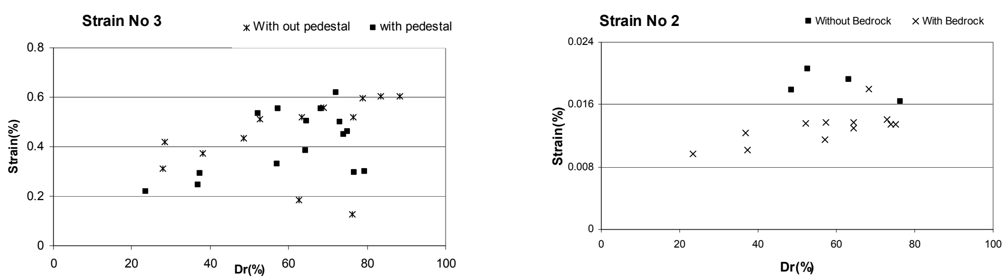

(a) (b)

Figure 16 Pedestal effect on various models- bending mode (peripheral strains): (a) f = 5 Hz, a = 0.2-0.4g, bending mode; and (b) f = 0.5 Hz, a = 0.3g, bending mode.

Comparison of Horizontal Strains for Soil and Pipe

The influence of dynamic loading on the soil and the pipe can be studied by comparing the longitudinal and shear strains on the pipe and the adjacent soil. Figure17 shows the strain distribution of the pipe and the adjacent soil versus relative density. The ratio of the two strains is illustrated. The average ratio of strains induced in sand is 10 times as much as those on the pipe; however, the maximum ratio is 31.2 for D_r=76% and acc=400 gal, while the minimum value is 1 for D_r=60% and acc=100 gal. The average strains for soil and pipe in the loose area are 0.09% and 0.0106%; respectively. These strains increase to 0.1% and 0.0192% for medium dense soil and to 0.15% and 0.025% for denser soil.

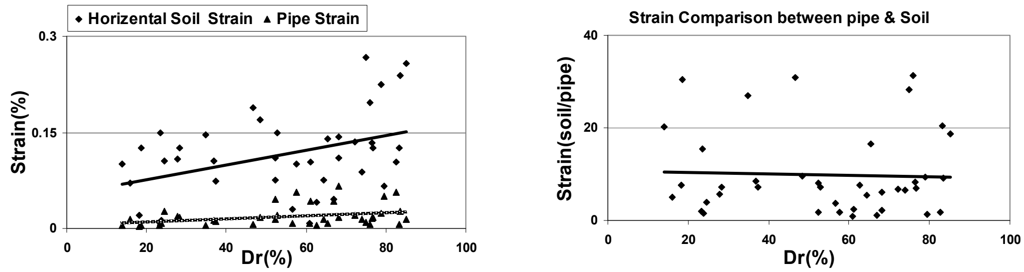

(a) (b)

Figure 17 Strain caparison for pipe and soil: (a) comparison of strains in pipe and soil; and (b) ration of soil to pipe strains versus D_r.

Besides the above discussion, acceleration amplification ratio in various height, acceleration effect and relative density effect on pipe strains are also reviewed, however all research aspects are not completely discussed. Main conclusions of this research are summarized as follows:

- The Raa (acceleration amplification ratio) values trend to unity as the relative density of the soil approaches 100%. But an evident trend could not be deduced for loose and medium dense soil since the calculated Raa records consisted of quantities both higher and lower than one.
- Regardless of the frequencies of the experiments, increasing the base acceleration caused more deformations to take place on the pipe.
- In models containing the pedestal, the buckling mode of loading induced higher strains on the pipe than the bending mode. However, if the pedestal was not used, then the bending mode was dominant and responsible for causing more deformations than the buckling mode.
- For circumferential strains, including models with and without pedestal, perpendicular loading led to higher strains than the parallel loading in all cases.
- As the density of the soil increased, its effect on the pipe strain diminished, meaning that the differences between the strains for two similar loading conditions could be more recognized for relative density in loose and medium dense areas. In dense areas where D_r>60%, the density effect on the strains attenuated.
- An investigation of the circumferential strain distribution on the pipe revealed that in bending mode the mid-length strains caused failure to occur, while in buckling mode the longitudinal strains along the pipe was constant.
- Comparing the strains in soil and pipe—two different materials with different constitutive behavior—demonstrated that the horizontal strains in the soil surrounding the pipe were, on average, ten times greater than the ones of the pipe.

THE PLAN FOR TEHRAN GAS NETWORK STUDIES

Tehran is the political and economical capital of Iran, with a population of more than 7 millions (more than 13 million in the Tehran province). It is ranked among the 20 most populous metropolitan cities of the world and has a widespread and dense gas network with related installations and elements. The basic grid is more than 10,000 km, with more than 700,000 local distribution points and more than 300 pressure control station. The high seismicity of Tehran and the surrounding area and the fact that no considerable strong ground motion occurred in this region during last 100 years is the main reason that authorities have supported many research and engineering projects for evaluating the seismic vulnerability and retrofitting strategies of Tehran and suburb gas network. In this framework, the earthquake and geotechnical groups of the Civil Engineering Department of Sharif University of Technology have recently engaged in a contract with Tehran Gas Company as client. Response and behavior of the pipeline network and related installations and stations to fault movements and landslides are the main objects. Although this research is in its primitive stage, a brief explanation of related previous research and planned activities and ongoing work is presented.

Project's Main Activities

The project will focus on "Damage Effect of Sliding on Gas Pipeline and Network." As a result, all physical tests and numerical modeling will be oriented to study the pipeline-soil interaction under static and dynamic loading. Generally, each pipeline has two underground and above ground support conditions. In addition, there are several variables that should be precisely considered in simulations, including the slope geometry, hydrology, topography, usage type, geological condition, and material type forming the slope. Shaking table apparatus will be used for conducting physical model tests and an advanced finite element or finite difference program such as ABACUS, FLAC3D will be used for numerical modeling.

The project is divided into several micro activities that will first review the operational problems and previous sliding history in the area of project. Main causes of a sliding event that probably could be the misconception of geological condition, prediction of earthquake loading parameters and residual soil-rock strength or the incorrect pipeline construction will be investigated by empirical analysis. This step will be followed by a first-stage numerical analysis that is planned to reveal the ambiguous aspects of slides. Slope stabilization methods will be suggested based on experience and the second-stage numerical calculations. Physical modeling will be performed to precisely examine the effectiveness of each proposal. Cost analysis and detail drawing are the two final steps, which will be done after the stabilization method selection. The main project activities are summarized below. These activities are scheduled so that the project is expected to be completed in 12 months.

- First stage studies and project planning.
- Sliding mechanism reconnaissance and classification, first in Tehran province and second in main pipelines in a country-wide span.
- Performing the first-step numerical modeling by means of appropriate advanced engineering programs.
- Planning and performing the physical tests and second-stage numerical modeling.
- Analysis and adding up the obtained result.
- Proposing the scientific and practical retrofitting method for vulnerable elements.
- Designing the instrumentation network for assessment of elements response under earthquake loading.

- Preparing the project report and detail drawings, papers, and relevant software for future usage.
- Detailed information data base preparation.
- Procurement of retrofit instructions and tender documents.

Project Justifications

Iran, a mountainous country, is located in an area prone to earthquakes. It experiences at least one destructing earthquake once a decade. It has great resources of natural gas and oil, emphasizing the role of pipelines as a mean for energy transportation route. Tehran, the capital of the country, has been established on many rock and soil slopes. The elevation difference between the highest and the lowest point is 700 m. Considering its population and political-economical importance, investigation of the vulnerability of the current gas pipeline and relevant network and probable retrofitting scheme is critical.

Concise Description of Previously Performed Projects [Takada et al. 1998]

Tehran, a city considered as being at high risk from earthquakes, has several faults. The fault geometry and characteristics were reviewed through geological maps (the map scales were 1:250,000 and 1:100,000), aerial photographs (1:55,000), all available documents were obtained from municipality of Tehran , relevant ministries, and engineering consultants. Based on the obtained geological investigations, the soil of Tehran is divided into four major categories, including alluvium type A, which is formed from conglomerates and cobbles, heterogeneous alluvium Type B, largely composed of gravel and cobbles, however, sand and clays are also evident. This formation is up to 60 m thick, which includes most of the slopes in the city. In addition, Tehran has two other formations named C and D, attributed to recent sedimentations formed by finer materials.

Pressure in the main gas pipelines in Tehran has been adjusted to 1000 psi, which is continuously decreased three times to reach the desired pressure for consumers (from 1000 psi to 250 psi and then to 60 psi and finally to fitted pressure appropriate for home consumers). Therefore, this, project will focus on three different pipe types, which probably have different material type, characteristics, and cross sections. According to test results, system equipment was divided into three main categories, with high, moderate, and low earthquake vulnerability.

Tehran's Faults

Determined by several studies, Tehran has several active faults including Mosha, Northern Tehran, Parchin, Northern and Southern Ray, Kahrizak, Niavaran, Mahmoodieh, Talv Payin, Shian and Kosar, Ghasre Firoozeh, Latian, Talv Bala, Sorkhe Hesar, and Southern Mehr Abad Faults. These faults are listed based on their importance and have caused several previous severe earthquakes, capable of producing events greater than magnitude 7 earthquakes. Gas pipelines cross these faults in several areas. Figure 18 generally illustrates the cross points in Tehran-span area.

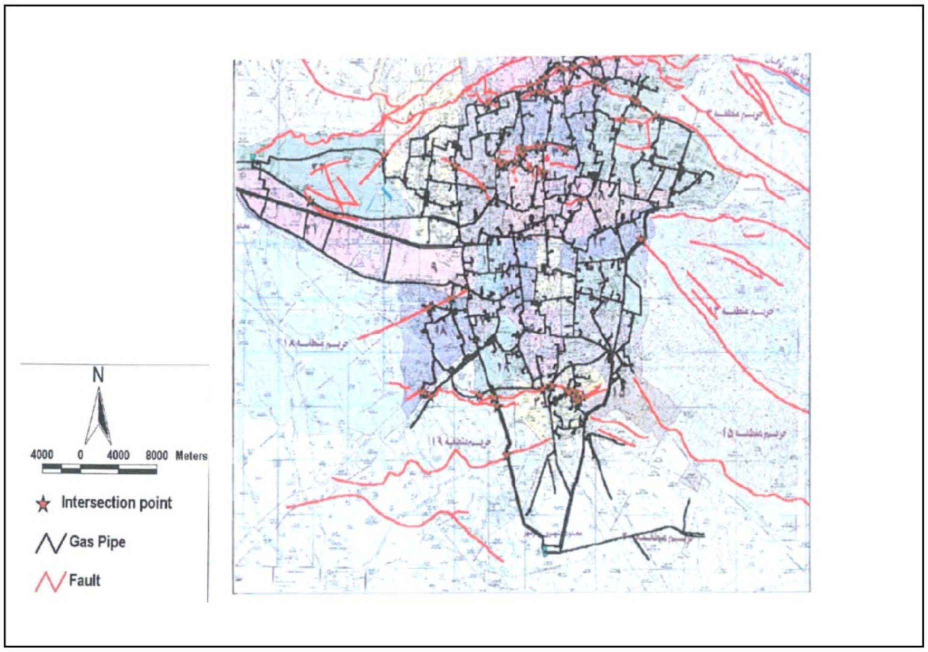

Figure 18 Cross points between Tehran's faults and gas pipelines [Takada et al. 1998].

Strong Ground Motion

Characterization of strong ground motions are basically performed based on statistical and artificially produced parameter approaches. Both methods were performed and consequently; the more deleterious result was selected for following calculations. In the first method, peak ground acceleration (PGA) was calculated based on the most probable event in a fixed period of time. The hazard risk for an event with magnitude of M and distance R from specific site was calculated and the most hazardous one was chosen. Figure 19 explains the event severity versus recurrence time period calculated from the mentioned method.

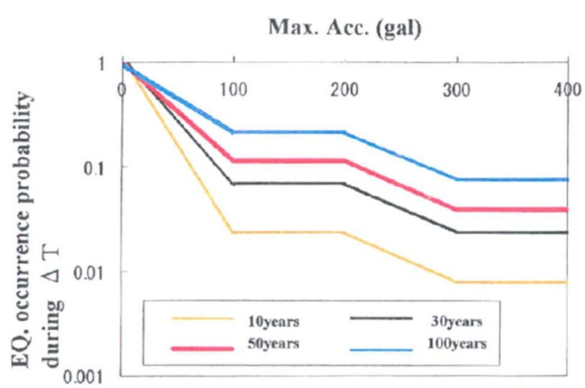

Figure 19 Probable event severity versus recurrence period for Tehran [Takada et al. 1998].

The second approach was performed based on the assumption of the most damaging fault. The basic parameters such as source-to-site distance and magnitude based on scientific methods and events history were selected. Events were divided to two main distant and near-field groups. The Tehran area was divided to 500×500 m blocks and subsequent calculations for artificial record production were performed by a computer program [Takada et al. 1998; Takada et al. 2001] and the Boore model [Boore 1983]. Figure 20 illustrates typical calculated results for bed rock acceleration distribution for the Mosha fault. Bed rock acceleration could then be multiplied by a local amplification factor that is related to damping, layer thickness, and depth of ground water table. Equivalent linear soil behavior was modeled by SHAKE program (Figure 21).

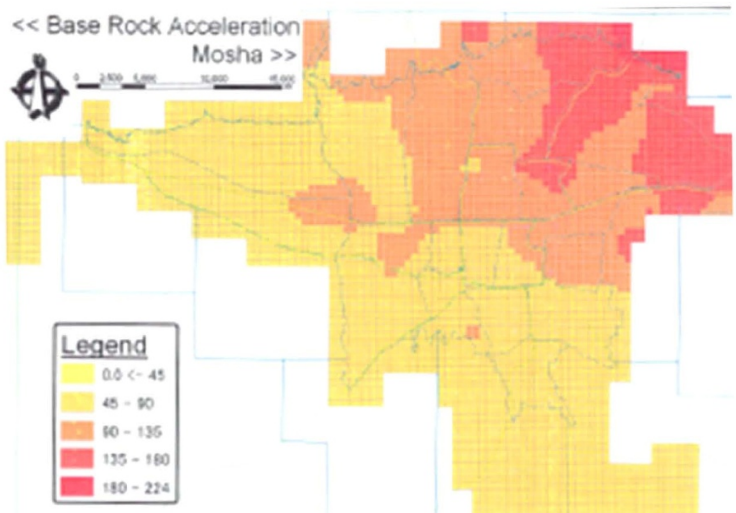

Figure 20 Bedrock acceleration distribution in Tehran based on the Mosha fault [Takada et al. 1998].

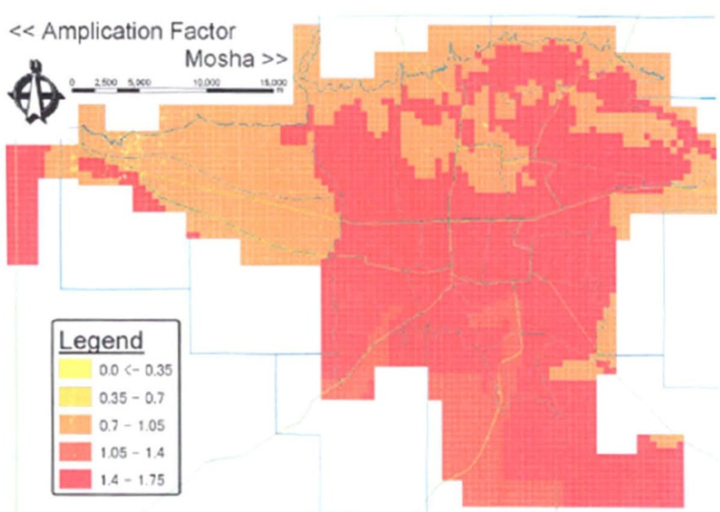

Figure 21 Amplification factor for a probable earthquake on the Mosha fault [Takada et al. 1998].

Besides the faulting phenomenon, liquefaction and sliding were also considered. A liquefaction hazard assessment was performed based on the SPT profile in bore holes, soil layer type and its characteristics, and maximum predicted acceleration. Two FL and PL approaches were combined to reach the liquefaction potential hazard, and lateral spreading was considered in the calculations. Figure 22 shows the calculated PL values for each block.

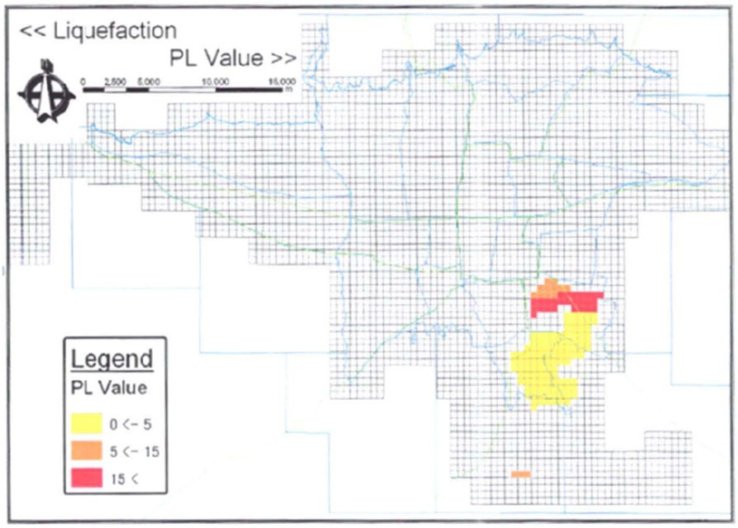

Figure 22 PL values after liquefaction calculations [Takada et al. 1998].

As previously mentioned, landslide hazard assessments were also a part of the project. The potential for landslides exists in northern part of Tehran, particularly in the areas nearer to the northern fault; the Abbas-Abad hills are considered vulnerable. Because of the low steep areas in southern Tehran, no hazard was assessed. Sliding potential is basically assessed according to the information on soil conditions, shear wave velocity, SPT values, depth of the rock beneath the soil layers, steepness of bed rock and upper alluvium layers, calculated acceleration, and amplification factor.

An informational data bank was also compiled, where any user has access to the raw data and calculated results. This information includes the geometrical and mechanical data of 60,100, 250 and 1000 psi pipes, material types (steel and polyethylene), length, thickness, diameter, distribution network, and gas company related buildings. Buildings are divided to four major groups of steel, concrete, other materials, and unknown categories. Each building category was analyzed on a scientific basis. These calculations were also performed for pipes and relevant equipments. Figure 23 is a typical example, showing a map of a damage assessment of buildings from an earthquake produced from northern Tehran fault.

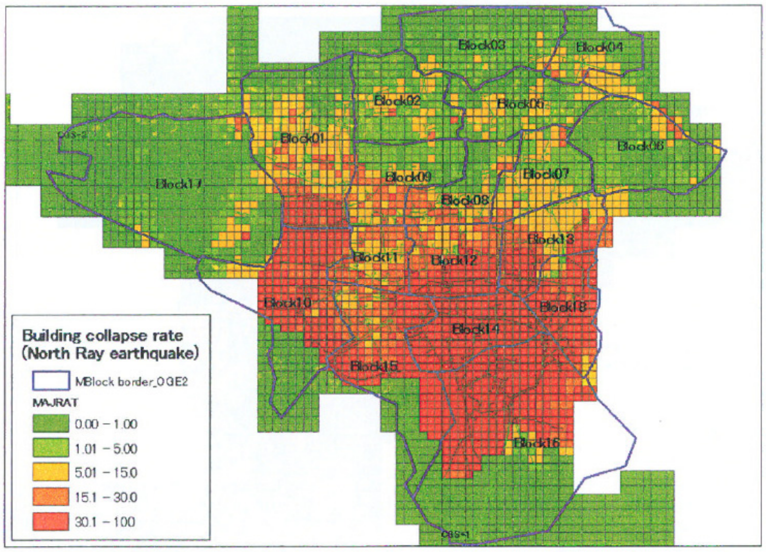

Figure 23 Map of damage assessment of buildings from an earthquake produced from the northern Tehran fault [Takada et al. 1998].

CONCLUSION

In this report the vulnerability of buried pipelines and networks to strong ground motion was discussed with an emphasis on urban areas. Three parts of the report focuses on different aspects of the phenomena. The first part discusses the main causes and mechanisms that cause damage to buried lifelines. The second part reports on the results of a related research project conducted on physical models at Sharif University of Technology. And finally, in the third part, a brief explanation about a recently started project for vulnerability assessment and retrofit of Tehran Gas Network was presented.

REFERENCES

Boore DM (1983). Stochastic simulation of high-frequency ground motion based on seismological models of radiated spectra, Bull Seismo. Am., 73(6):1856–1894.

Ha D et al. (2008). Centrifuge modeling of earthquake effects on buried high-density polyethylene (HDPE) pipelines crossing fault zones, ASCE, *J. Geotech. Geoenviro. Engng*., 134:1501.

Jafarzadeh F, Farahi Jahromi H, Abazari Torghabeh E (2010). Investigating dynamic response of a buried pipeline in sandy soil layer by 1g shaking table tests, *Inter. J. Civil Engng*., Iran University of Science and Technology, Tehran, Iran.

Jourabchian A (2002). Designing the laminar shear box for shaking table test, MSc. Thesis, Sharif University of Technology, Tehran, Iran.

Kramer SL (1996). *Geotechnical Earthquake Engineering*, Prentice Hall, Upper Saddle River, New Jersey.

Mohri Y, Yasunaka M, Tani S (1995). Damage to buried pipeline due to liquefaction induced performance at the ground by the Hokkaido–Nansei-Oki earthquake in 1993, *Proceedings of Earthquake Geotechnical Engineering*, Balkema, Rotterdam.

O'Rourke MJ, Liu X (1994). Failure criterion for buried pipe subjected to longitudinal PGD: Benchmark case history, *NCEER Report No. 94-0026*, 639 pages, State University of New York at Buffalo, Buffalo, NY.

Qiao L, Yuan C, Miyajima M, Zhai E (2008). Shake-table testing and FLAC modeling of liquefaction-induced slope failure and damage to buried pipelines, Geotechnical Earthquake Engineering and Soil Dynamics IV Congress, ASCE, GSP 181.
SPA Risk LLC (2008). The shake out scenario", prepared for United States Geological Survey and California Geological Survey.
Takada S, Fukuda K, Mori, K (1998). Estimating earthquake motion near fault in the light of frequency asperity, Research Report of Construction Engineering Research Institute, *No.40-B*, pp.23-39.
Takada S, Hasani N, Fukuda K (2000). Definition of fault near field based on seismic wave energy, *Earthq. Spectra*.

NUMERICAL MODELING OF THE LIQUEFACTION-INDUCED SETTLEMENTS OF BUILDINGS AND LATERAL SPREADING IN URBAN AREAS

Ali Pak[1], Hadi Shahir[2], and Omid Ghassemi Fare[1]

[1]Sharif University of Technology, Tehran, Iran, [2]Tarbiat Moallem University, Tehran, Iran

ABSTRACT

Structures located on loose saturated sands pose a real threat to seismic risk management in urban areas because of the possibility of liquefaction phenomenon. Liquefaction may cause general failure of structures due to loss of soil bearing capacity. In sloping grounds it usually causes large displacements in the direction of slope called lateral spread. In other situations liquefaction causes a wide range of structural damages such as settlement and/or tilt of the buildings, bridges, and roads.

A performance-based design (PBD) of building foundations requires understanding of the behavior of footings on liquefiable subsoil and predicting the anticipated settlement and/or tilt due to liquefaction. Also investigating the possibility of lateral spread due to liquefaction is important in urban areas.

A series of fully coupled hydro-mechanical dynamic numerical analysis has been conducted in order to investigate the seismic response of shallow foundations on liquefiable soils and evaluating the possibility of lateral spread due to liquefaction. The computer program OpenSees has been used for analyzing the three-dimensional seismic response of shallow foundations in conjunction with PISA, which has been used for two-dimensional lateral spread studies. In both cases, a well-calibrated critical state two-surface plasticity model has been used that is capable of accounting for the response of soil skeleton in a wide range of densities and confining pressures, using a single set of parameters. The variable soil permeability relation, introduced by the authors, has been used and its effects on the soil seismic response are incorporated in the analyses. Verification of the numerical models has been performed by comparing the numerical results against the centrifuge experimental observations and also VELACS no.2 test experiment. The obtained results reveal that the amount of settlements of footings resting on liquefiable or densified subsoil can be determined with a good accuracy. Also the key elements for predicting the amount of lateral spread due to liquefaction have been captured. Hence, the performance-based seismic design of foundations in urban areas, based on a reliable estimation of the liquefaction-induced displacement, has become feasible.

INTRODUCTION

Urban areas located on loose saturated sandy deposits are prone to liquefaction under earthquake loadings. Liquefaction—one of the most destructive phenomena—may cause large tilting of structures, sand boils, lateral spreading of the ground, and heavy damage to buildings, roads, bridges, and buried pipelines. The effects of liquefaction to the buildings may appear as large tilting (overturning) and complete failure due to total loss of the bearing capacity or excessive settlement of the ground. Since total loss of the bearing capacity does not always occur for a number of reasons, most of the damage observed in urban areas after earthquakes have been reported to be due to liquefaction-induced settlement of the residential or commercial buildings [Kishida 1966; Yasuda et al. 2001; Yoshimi and Tokimatsu 1977). Where liquefiable saturated soil layers are not horizontal, lateral spreading may occur during and/or after liquefaction.

Several factors may affect the amount of liquefaction-induced settlement of buildings, among which the natural relative density of sandy strata, the fine content in the sand, the thickness of unsaturated zone above the groundwater table, and the characteristics of seismic loading can be mentioned. Having a reasonable estimate of the liquefaction-induced settlement is very important in the design of buildings in urban areas. The importance partially comes from the performance-based design (PBD) approach that has gained momentum over the last decade in national building codes of Europe and elsewhere. The basic philosophy of PBD relies on the control of performance targets through a displacement-based design procedure. The PBD approach to design of building foundations enables the designer ensure a building's performance under critical conditions, and increase the reliability of the structure and safety levels of the inhabitants.

From a foundation design point of view, the PBD approach requires that the maximum horizontal and vertical displacements of foundation as well as its rotation are known under static and dynamic loadings. Also important is to identify the possibility of lateral spread and the maximum amounts of settlement and lateral ground displacement in order to prevent the failures that are associated with this phenomenon. Generally, the available methods for estimating of the liquefaction-induced settlements can be categorized as observational, experimental, and numerical.

Kishida [1966] classified the foundation damages during Nigata earthquake. A considerable amount of the observed settlement was less than 50 cm with a small tilt of less than 1°. In Adapazari city during the Kocaeli earthquake, the observed settlement and tilt of buildings without bearing capacity failure generally varied between 20 to 40 cm and 1° to 3°, respectively [Yasuda et al. 2001].

Yoshimi and Tokimatsu [1977] studied the amount of settlement of 35 reinforced concrete buildings that experienced damage during Nigata earthquake. By normalizing the average settlement and building width with respect to the depth of the liquefied sand, they established the relationship shown in Figure (1). As can be seen in the figure, for foundations with small width the bearing capacity loss failure mechanism prevails; however, for relatively large footings the damage mechanism tends to be settlement.

Some researchers have used centrifuge tests for studying the behavior of shallow foundations on liquefiable ground [Bouckovalas et al. 1991; Hausler 2002]. In these experimental endeavors the parameters affecting the loss of bearing capacity and settlement due to liquefaction have been studied in detail. Parameters such as width of the foundation, thickness of the liquefied soil, contact pressure beneath the footing, and building aspect ratio, etc., have been examined during these experimental studies.

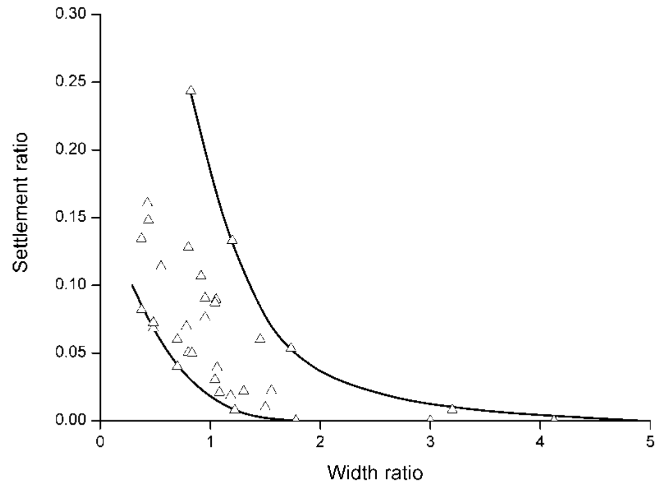

Figure 1 Variation of settlement ratio vs. width ratio for shallow foundations [Yoshimi and Tokimatsu 1977].

Numerical modeling of the behavior of foundations on liquefiable ground has been attempted during the last two decades. Liquefaction modeling by itself is a difficult task due to the complex behavior of saturated sand under cyclic excitation [Taiebat et al. 2007]. Clearly, by adopting a PBD approach, the interaction effects of foundation and soil play a significant role in the design process.

In some numerical investigations, the influence of soil liquefaction on the soil-structure interaction phenomenon has been studied [Koutsourelakis et al. 2002; Chakrabortty et al. 2004; Popescu et al. 2006; Lopez-Caballero and Modaressi 2008]. These models generally consist of simulation of the dynamic interaction between a homogeneous liquefiable soil layer and a structure resting on the ground surface using a two-dimensional (plane strain assumption) coupled finite element analysis. Elgamal et al. [2005] implemented a three-dimensional fully coupled numerical model to investigate the liquefaction-induced settlement of shallow foundations and effects of improvement by soil compaction. A main shortcoming of all of these studies is the lack of a verification process. Therefore, it is difficult to decide about using these numerical models in practice.

Quantitative analysis of liquefaction and lateral spreading can only be accomplished by considering the coupled interaction between the soil skeleton and the pore fluid. For this purpose, a suitable formulation for the behavior of the two-phase continuum and a proper constitutive model are required. Verified numerical models capable of simulating liquefaction phenomenon are valuable and robust tools for analyzing the settlement of foundations resting on liquefiable soil strata and also quantification of the amount of lateral ground movement due to lateral spread.

In this paper, mitigation measures for preventing the liquefaction phenomenon beneath the foundation and/or reducing the liquefaction-induced settlements and lateral deformations will be reviewed first. Then the fully coupled model used for analyzing the problem and its numerical features will be described. Finally, validity of the models in evaluating the liquefaction induced settlement of foundations on liquefiable and densified subsoil and estimating the amount of lateral spreading will be presented.

MITIGATION OF DAMAGES EXERTED ON BUILDINGS DUE TO LIQUEFACTION

There are a number of methods that are commonly employed for reducing the possibility of liquefaction and mitigating the destructive consequences of this phenomenon under buildings. These methods may be broadly categorized into two groups. In the first group the goal is prevent to excess pore water pressure generation. In the second group, however, the goal is to increase the resistance of soil skeleton subjected to seismic excitations.

The most common mitigating methods are mentioned below:

- Soil compaction/densification
- Grouting (solidification)
- Stone columns
- Lowering ground water table (GWT)

Among the above-mentioned mitigating measures, soil densification is the most economical one. Shallow and deep compaction methods increase the soil relative density and reduce the soil porosity. This happens because of collapsing the loose structure of sandy deposits under compaction loads. Densification is a permanent soil improvement that does not require any external component added to the ground. Another advantage of densification method is that it can be used over the whole area that is prone to liquefaction. Therefore, compaction is normally the most cost-effective method that can be used for mitigation.

The effectiveness of densification in mitigation of the effects of liquefaction can be demonstrated by reviewing the low level of damage of shallow foundations built on densified zones during the major seismic events as far back as the 1964 Niigata earthquake [Mitchell et al. 1995; Hausler 2002]. Because soil densification is one of the earthquake-damage mitigating measures that can be used in urban areas, it will be further discussed in the next sections.

SPECIFICATIONS OF THE NUMERICAL MODEL

In this study, OpenSees was used as a platform to conduct three-dimensional simulations of the behavior of foundations on liquefiable ground, and PISA was employed for two-dimensional lateral spreading analysis. Developed at the Pacific Earthquake Engineering Research Center (PEER) for simulating the seismic response of structural and geotechnical systems (*http://opensees.berkeley.edu*), OpenSees is an open-source software framework; PISA is a finite element software that was originally developed by Chan and Morgenstern [1988] under the name of SAGE. The subsequent versions of this program provided more possibilities for analyzing a wide variety of geotechnical problems. Pak [1997] increased the program capabilities by amending the formulation for analyzing thermal hydro-mechanical (THM) problems; Shahir [2001] added the dynamic analysis ability to the program and used PISA to model liquefaction phenomenon; and Ghassemi Fare [2010] further developed the program to analyze the lateral spreading phenomenon.

For a fully coupled hydro-mechanical analysis, the U-P formulation [Chan 1988] in which the displacement of solid phase (U) and pressure of fluid phase (P) are unknowns is used:

$$M\ddot{U} + \int_v B^T \sigma' \, dV - QP - f^{(s)} = 0 \tag{1a}$$

$$Q^T \dot{U} + HP + S\dot{P} - f^{(p)} = 0 \tag{1b}$$

where M is the mass matrix, U is the solid displacement vector, B is the strain-displacement matrix, σ' is the effective stress tensor, Q indicates the discrete gradient operator coupling the motion and flow equations, P is the pore pressure vector, S is the compressibility matrix, and H is the permeability matrix. The vectors $f^{(s)}$ and $f^{(p)}$ include the effects of body forces, external loads, and fluid fluxes.

A plasticity constitutive model developed by Dafalias and Manzari [2004] was employed to model the behavior of sand. The formulation of the model is based on the bounding surface plasticity theory [Dafalias 1986] within the critical state soil mechanics framework [Schofield and Wroth 1968]. A schematic representation of the two-surface model in the π-plane is shown in Figure 2.

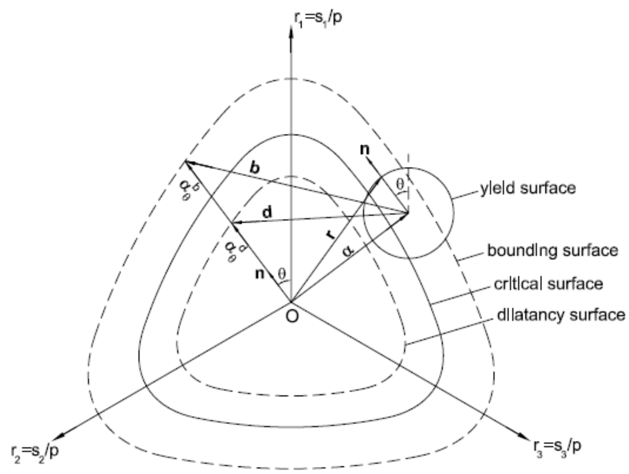

Figure 2 Schematic representation of the two-surface plasticity model in the π-plane [Dafalias and Manzari 2004].

In this constitutive model, the isotropic hypo-elasticity assumption is adopted with the elastic moduli as functions of current pressure and void ratio. The yield surface is a circular cone with its apex at the origin. The size of the yield surface is normally considered a constant (no isotropic hardening) having a rather small value in most applications. This model includes three other surfaces namely: bounding (peak), dilatancy, and critical surfaces. The critical surface is in direct correspondence to the critical stress ratio in the triaxial space. The critical state of a soil [Schofield and Wroth 1968] is attained when the stress ratio $\eta = q/p$ equals the critical stress ratio (M), which is a material constant. In the current model, the bounding and dilatancy stress ratios are related to the critical stress ratio by way of the "state parameter" as follows:

$$M^b = M \exp\left(-n^b \psi\right) \; ; \; M^d = M \exp\left(n^d \psi\right) \tag{2}$$

Where M^b and M^d are peak and dilatancy stress ratios and n^b and n^d are positive material constants. $\psi = e - e_c$ is the "state parameter" proposed by Been and Jefferies [1985], where e is the current void ratio of the soil element and e_c is the critical void ratio corresponding to the existing confining stress. The following power relation defines the Critical State Line (CSL):

$$e_c = e_0 - \lambda_c \left(\frac{p_c}{p_{at}} \right)^{\xi} \tag{3}$$

where e_0, λ_c, and ζ are critical state constants.

The state parameter includes the combined effect of density (void ratio) and the confining stress. Thus, one of the main features of the current constitutive model is its applicability to all densities and confining pressures with the same set of material constants.

The plastic modulus (K_p) and dilatancy coefficient (D) are related to the distance from the bounding and dilatancy surfaces as follows:

$$K_p = \frac{2}{3} ph\mathbf{b} : \mathbf{n} \tag{4}$$

$$D = A_d \mathbf{d} : \mathbf{n} \tag{5}$$

The vectors **b** and **d,** shown in Figure 2, are defined as the vectors connecting the current stress state to its image on the bounding and dilatancy surfaces, respectively. p is the mean effective stress and h is a positive scalar-valued function. A_d is a function including the effects of "fabric change phenomenon" arisen during stress increment reversal after a dilative plastic volumetric strain occurrence.

The model constants were calibrated for Nevada sand using the triaxial tests data performed under different conditions [Shahir 2009]. The list of the model constants is shown in Table 1. The model has 15 constants divided into 6 categories based on their functions.

Table 1 Material parameters of the critical state two-surface plasticity model for Nevada sand [Shahir 2009].

Constant	Variable	Value	Constant	Variable	Value
Elasticity	G_0	150	Plastic modulus	h_0	9.7
	ν	0.05		c_h	1.02
Critical state	M	1.14		n^b	2.56
	c	0.78	Dilatancy	A_0	0.81
	λ_c	0.027		n^d	1.05
	e_0	0.83	Fabric-dilatancy tensor	$z_{\max}$	5
	ξ	0.45		c_z	800
Yield surface	m	0.02			

VARIABLE PERMEABILITY FUNCTION

Numerical studies of liquefaction in which a variation in permeability has been considered are rare. Manzari and Arulanandan [1993] used findings of Arulanandan and Sybico [1992] and employed a variable permeability (as a function of time) for simulation of VELACS model No. 1. The proposed permeability function gave an increase to the permeability value only for the first seconds of liquefaction initiation, although the measured excess pore pressure ratios during the centrifuge experiment indicated that the liquefaction state was sustained for a long period. Also, in their analysis a unique permeability function was considered for all elements while different pore pressure responses were recorded along the soil column. They reported that by using their proposed permeability function, the measured settlement was simulated well. However, both rates of build-up and dissipation of pore pressure were overestimated when compared to the experimental measurements. To the best of the authors' knowledge, considering the variable permeability in numerical modeling of lateral spreading has not been attempted by other researchers before.

According to the study performed by Shahir et al. [2010], the variation of permeability coefficient in all pore pressure build-up, liquefaction, and dissipation phases can be expressed as a function of the excess pore pressure ratio. They proposed the following function for taking the variation of permeability into account in the numerical simulation of liquefaction:

$$\frac{k}{ki} = \begin{cases} 1+(\alpha-1)\times r_u^{\beta_1} & \text{in build-up phase } (r_u < 1) \\ \alpha & \text{in liquefied state } (r_u = 1) \\ 1+(\alpha-1)\times r_u^{\beta_2} & \text{in dissipation phase } (r_u < 1) \end{cases} \tag{6}$$

where k is the soil permeability coefficient during the process of liquefaction, k_i is initial (at-rest) permeability coefficient before shaking, and α, β_1, and β_2 are positive material constants. r_u is the excess pore pressure ratio defined as follows:

$$r_u = \frac{\Delta u}{\sigma'_{v0}} \tag{7}$$

where Δu is the excess pore water pressure, and σ'_{vo} is the initial vertical effective stress.

The above formulation was implemented into OpenSees and PISA for updating the coefficient of permeability at the end of each time step during seismic analysis. By comparing the numerical results with centrifuge experiment records, the constants were calibrated as $\alpha = 20$, $\beta_1 = 1.0$, and $\beta_2 = 8.9$ for Nevada sand

RESULTS AND DISCUSSION

For verification of the numerical model pertaining to liquefaction-induced settlement of footings, the centrifuge experiments accomplished by Hausler [2002] were considered. In these centrifuge experiments, the effects of densified depth (represented by higher D_r values on decreasing the foundation settlement) were studied.

The centrifuge model 1 consisted of a square rigid structure rested on approximately 20 m of liquefiable Nevada sand with initial relative density *(D_r)* of 30%, which was placed in a flexible container (Figure 3). In models 2 to 4, the soil beneath the structure was compacted up to a relative density of 85% with different depths of 6 m (0.3H improved), 14 m (0.7H improved) and 20 m (full depth improved). The initial relative density of the surrounding unimproved soil was 30%. The improved zone was square in plan and symmetric around the foundation axis, and the width of the improvement zone was approximately twice of the foundation width. The structure is a cubic rigid block with the same dimension of 8 m in all directions, embedded 1.0 m in the top dry soil, which exerts a bearing pressure of 96 kPa. A sketch of the geometry of the experiments is presented in Figure 3.

The pore fluid used in the experiments had a viscosity 10 times greater than that of water, and the model was spun up to a centrifuge acceleration of 40g. Considering the scaling laws in centrifuge modeling [Schofield 1981], this experiment simulates a soil deposit with a permeability coefficient four times greater than that of Nevada sand in prototype scale. All models were shaken with a scaled version of the 83 m depth, N-S component of 1995 Kobe Port Island earthquake with a peak ground acceleration of 0.15*g*. The prototype time history of the input motion is shown in Figure 4.

Numerical modeling of the centrifuge experiments were performed in prototype scale. A three-dimensional finite element mesh with 1960 8-node cubic elements was used in the analyses, as shown in Figure 5. Table 2 lists the properties of Nevada sand used in the analyses. To consider the effect of laminar box in the numerical simulation, the lateral boundaries perpendicular to the direction of shaking were constrained together to have the same displacement in the direction of shaking. The bottom boundary was assumed fixed. Full dissipation of pore pressure was allowed through the surface of sand layer and the lateral and bottom boundaries were supposed to be impervious. The structure was modeled by rigid brick elements connected rigidly to the adjacent soil nodes. The Young's modulus for the structure is chosen large enough so that the structure can be considered rigid.

Details of the verification process of the numerical model and its attributes has been demonstrated previously [Shahir 2009; Shahir and Pak 2010; Shahir et al 2010] and will not be dealt with here. The verification process revealed the capability of the model to predict the pore pressure variation as well as the settlement during the liquefaction process. Here, the results of the model pertaining to the settlement will be described as they are particularly important in PBD approach.

Table 2 Properties of Nevada sand used in the analyses [Hausler 2002].

Parameter	Value at D_r=30%	Value at D_r=85%
Void ratio	0.781	0.586
Saturated unit weight (kN/m^3)	19.0	20.15
Water permeability (m/sec)	4.0×10^{-5}	2.5×10^{-5}
Prototype permeability (m/sec)	1.6×10^{-4}	1.0×10^{-4}

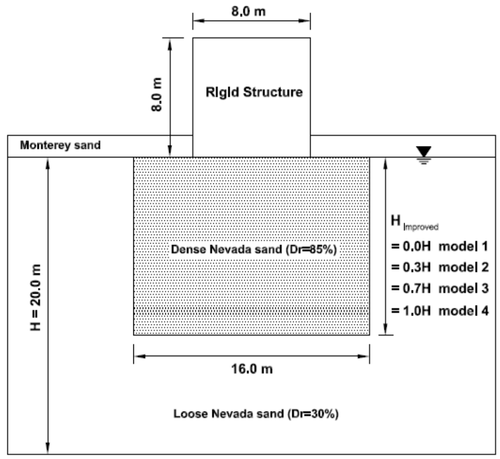

Figure 3 Geometry of the centrifuge experiments [Hausler 2002].

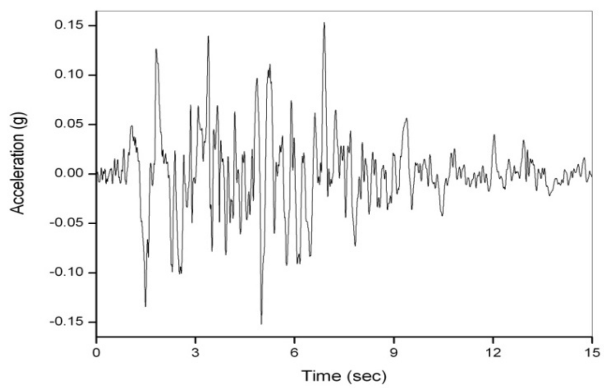

Figure 4 Prototype time history of the input motion.

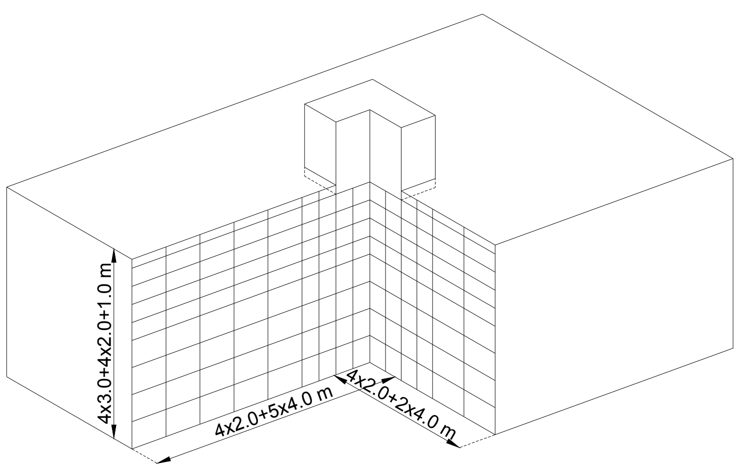

Figure 5 Cross section of the three-dimensional finite element mesh.

The variation of the final settlement of foundation (after fully dissipation of excess pore pressure) in all experiments versus normalized compaction depth is presented in Figure 6. The foundation settlement has decreased from 51 cm in the experiment without compaction to 9 cm in the experiment with full-depth compaction, i.e., the foundation settlement has decreased more than five times due to ground improvement. This indicates the effectiveness of densification in mitigation of liquefaction induced settlement. As observed in this figure, there is rather negligible reduction in settlement of foundation in the case of superficial compaction up to depth of 0.3H (H: total soil depth). The major reduction in the foundation settlement is achieved when the improved zone extends through 0.7H. Further compaction below the depth of 0.7H has a minor effect on reducing the amount of foundation settlement.

As depicted in Figure 6a, the measured and predicted foundation settlements match well with each other for models 3 and 4, however, some differences are observed between the results for model 1 and 2 (See also Figure 3). This difference can be due to the uncertainties in the measured characteristics for soil and/or input motion. This difference is also seen in the free field soil settlement. The measured free-field settlement in the experiments 1 to 4 is 24, 25, 20, and 21 cm, respectively. The predicted value by the numerical simulations is 18.6 cm for all models.

In an endeavor to omit the effects of these uncertainties, the settlements were normalized by the free field settlement. As observed in Figure 6b, the predicted normalized settlements are in good agreement with the experimental measurements, demonstrating that the influence of the uncertainties can be removed by normalization of settlement to the free-field soil settlement.

Numerical simulation of VELACS no. 2 experiment have been undertaken for analyzing the possibility of lateral spreading and quantification of displacements that take place. The general configuration of the experiment and the finite element mesh that was used are depicted in Figures 7 and 8, respectively.

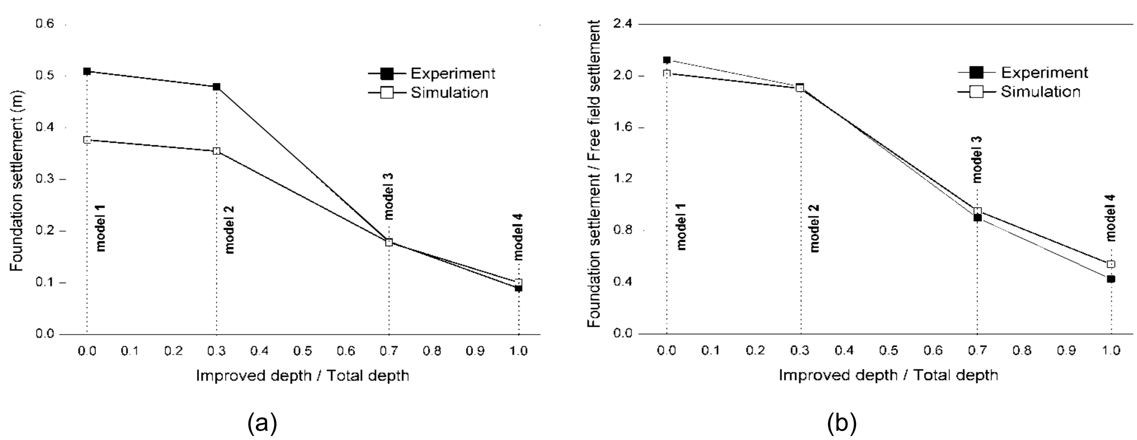

Figure 6 Measured and predicted liquefaction-induced settlements beneath shallow foundations resting on liquefiable and densified subsoils: (a) absolute settlement; and (b) normalized settlement.

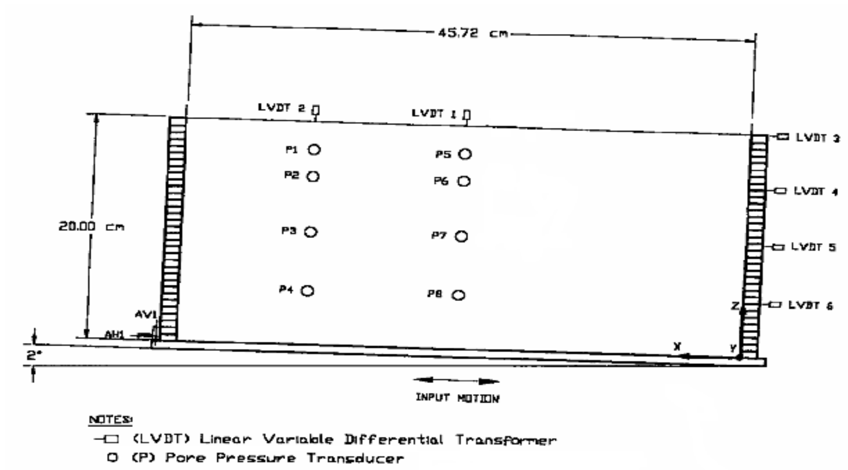

Figure 7 General configuration of VELACS no. 2 centrifuge experiment and instrumentations.

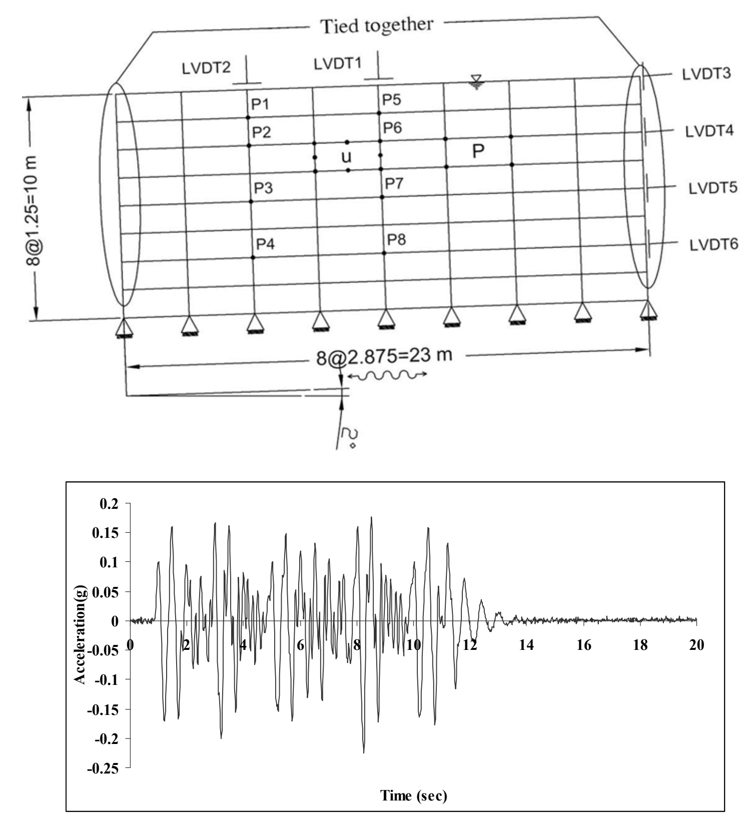

Figure 8 Finite element mesh and loading history used for numerical simulation.

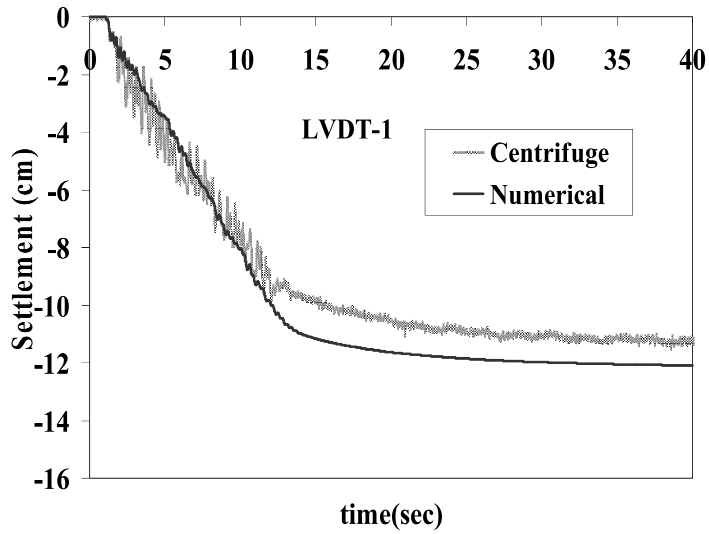

Figure 9 Comparing the computed and measured surface settlements at LVDT 1.

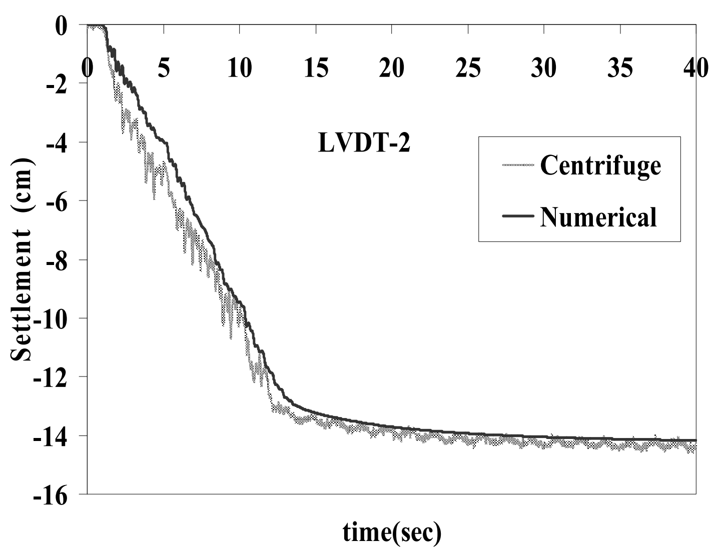

Figure 10 Comparing the computed and measured surface settlements at LVDT 2.

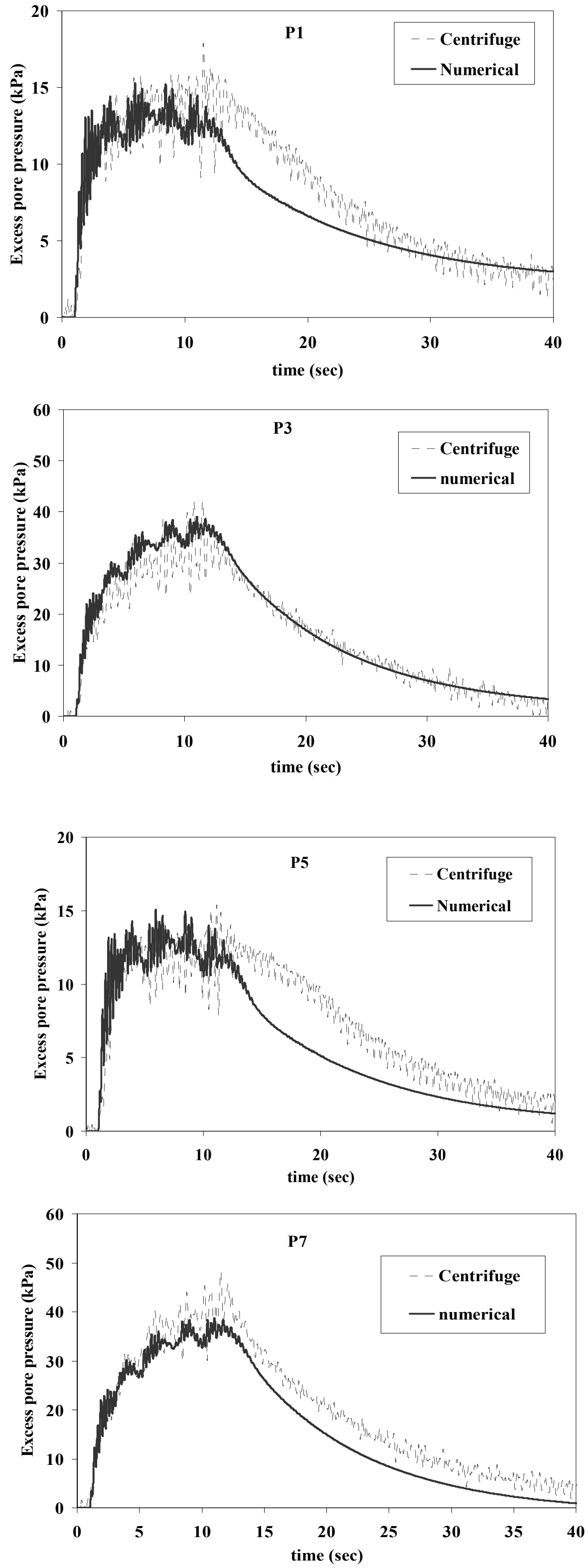

Figure 11 Comparison between the predicted and simulated pore pressure variations at different depths.

The finite element code PISA employing the constitutive model and variable permeability function mentioned above has been used here. The surface settlement results at two points shown in Figure 7 are illustrated in Figures 9 and 10. As can be seen there are very good agreement between the model predictions and experimental records. It should be emphasized that by using the above mentioned numerical procedures not only are the predicted displacements adequate, but also the pore pressure variations are simulated with a remarkable accuracy, as shown in Figure 11.

CONCLUSIONS

A PBD approach for designing shallow foundations for buildings in urban areas requires determination of the effects of liquefaction when buildings are built over loose saturated sandy strata. For an accurate modeling of liquefaction and its consequences, a number of preliminaries are required, namely:

- A fully coupled hydro-mechanical dynamic code for analysis of the behavior of saturated sand subjected to seismic excitations.
- A robust material constitutive model that is able to simulate the pore pressure generation and dissipation and also settlement simultaneously under different relative densities and applied stresses.
- Incorporating the variability of the coefficient of permeability during the liquefaction in the analysis.

In this study, it was shown that determination of the liquefaction-induced settlement of shallow foundations and the quantification of the displacements due to lateral spreading phenomenon are viable employing the developed computer programs which provide the required information for a reliable PBD design of the footings of buildings in urban areas that are at the zones of earthquake hazards. Also, it was shown that by using soil densification methods, it is possible to mitigate the liquefaction damage to the building and significantly reduce the amount of liquefaction-induced settlement beneath the foundations.

The results presented in this paper are the preliminary outcomes of on-going research with the aim of extracting simple applied relations for estimating the deformations exerted to the foundation of buildings in urban areas that may be subjected to liquefaction, to pave the way for safer and more reliable performance-based design of buildings.

REFERENCES

Arulanandan K, Sybico J Jr (1992). Post-liquefaction settlement of sand, *Proceeding*, Wroth Memorial Symposium, Oxford University, UK.

Been K, Jefferies MG (1985). A state parameter for sands, *Geotechnique*, 35(2): 99–112.

Bouckovalas G, Stamatopoulos C, Whitman RV (1991). Analysis of seismic settlements and pore pressures in centrifuge tests, ASCE, *J. Geotech. Engng*, 117(10):1492–1508.

Chakrabortty P, Popescu R, Prevost, JH (2004). Tower structures on liquefiable soil excited by random seismic input, *Proceedings*, 9th ASCE Specialty Conference on Probabilistic Mechanics and Structural Reliability, Albuquerque NM.

Chan AHC [1988]. A unified finite element solution to static and dynamic geomechanics problems, PhD Dissertation, University College of Swansea, Wales.

Chan D, Morgenstern N (1988). *SAGE : A Finite Element Program for Stress Analysis in Geotechnical Engineering, Program User Manual.* Geotechnical Group, University of Alberta, Canada.

Dafalias YF (1986). Bounding surface plasticity, I: Mathematical foundation and hypoplasticity, *J. Engng. Mech*., 112(9): 966–987.

Dafalias YF, Manzari MT (2004). Simple plasticity sand model accounting for fabric change effects, *J. Engng. Mech*., 130(6): 622–634.

Elgamal A, Lu J, Yang Z (2005). Liquefaction-induced settlement of shallow foundations and remediation: 3D numerical simulation., *J. Earthq. Engrg*., 9(1):17–45.

Ghassemi Fare O (2010), Numerical modeling of ground displacement due to liquefaction-induced lateral spreading, M.Sc. Thesis, Department of Civil Engineering, Sharif University of Technology, Iran.

Hausler EA (2002). Influence of ground improvement on settlement and liquefaction: A study based on field case history evidence and dynamic geotechnical centrifuge tests, PhD Dissertation, Department of Civil Engineering, University of California, Berkeley, CA.

Kishida H (1966). Damage to reinforced concrete building in Nigata City with special reference to foundation engineering, *Soils Found*, 1:71–88.

Koutsourelakis, S., Prevost J.H. & Deodatis, G. 2002. Risk assessment of an interacting structure-soil system due to liquefaction. Earthquake Engineering and Structures Dynamics 31(4): 851-879

Lopez-Caballero F, Modaressi Farahmand-Razavi A (2008). Numerical simulation of liquefaction effects on seismic SSI, *Soil Dyn. Earthq. Engng*., 28: 85–98.

Manzari MT, Arulanandan K (1993). Numerical predictions for Model No. 1. In: *Verification of Numerical Procedures for the Analysis of Soil Liquefaction Problems*. (K. Arulanandan and R. F. Scott, ed.), A.A. Balkema, Rotterdam, pp. 179–185.

Mitchell JK, Baxter CDP, Munson TC (1995). Performance of improved ground during earthquakes, *Proceeding*s, Soil Improvements for Earthquake Hazard Mitigation, ASCE, *Geotechnical Special Publication No. 49*, pp. 1–36

Pak A (1997). Numerical modelling of hydraulic fracturing. PhD thesis, Department of Civil and Environmental Engineering, University of Alberta, Canada.

Popescu R, Prevost JH, Deodatis G, Chakrabortty P (2006). Dynamics of nonlinear porous media with applications to soil liquefaction, *Soil Dyn. Earthq. Engng*., 26:648–665.

Schofield AN, Wroth CP (1968). *Critical State Soil Mechanics*. New York: McGraw-Hill.

Schofield AN (1981). Dynamic and earthquake centrifuge geotechnical modeling, *Proceedings*, International Conference on Recent Advances in Geotechnical Earthquake Engineering and Soil Dynamics, University of Missouri-Rolla, MO, pp.1081–1100.

Shahir H (2001). Dynamic analysis of porous media for numerical modeling of liquefaction, M.Sc. Thesis, Department of Civil Engineering, Sharif University of Technology, Iran.

Shahir H (2009). Assessment of effectiveness of compaction improvement for liquefaction mitigation of saturated sand deposits based on performance levels of shallow foundations, Ph.D. Thesis, Department of Civil Engineering, Sharif University of Technology, Iran.

Shahir H, Pak, A (2010). Estimating liquefaction-induced settlement of shallow foundations by numerical spproach, *Computers and Geotechnics*, 37:267-279.

Shahir H, Pak A, Taiebat M, Jeremic B (2010). Evaluation of variation of permeability in liquefiable soil under earthquake loading, submitted to *Computers and Geotechnics*.

Taiebat M, Shahir H, Pak A (2007). Study of pore pressure variation during liquefaction using two constitutive models for sand, *Soil Dyn. Earthq. Engng*., 27(1):60–72.

Yasuda S, Irisawa T, Kazami K (2001). Liquefaction-induced settlement of buildings and damages in coastal areas during the Kocaeli and other earthquakes, *Proceedings*, Satellite Conference on Lessons Learned from String Earthquakes, 15th ICSMGE, pp. 33–42.

Yoshimi Y, Tokimatsu K (1977). Settlement of buildings on saturated sand during earthquakes, *Soils Found*, 77(1):23–38.

GRAPHICAL USER INTERFACES FOR SOIL-STRUCTURE INTERACTION AND PERFORMANCE-BASED EARTHQUAKE ENGINEERING

Ahmed Elgamal[1], Jinchi Lu[1], and Kevin R. Mackie[2]

[1]*Department of Structural Engineering, University of California, San Diego, California;* [2]*Department of Civil and Environmental Engineering, University of Central Florida, Orlando, Florida.*

ABSTRACT

Three-dimensional nonlinear finite element simulations are becoming increasingly feasible for geotechnical applications. This paper presents versatile frameworks that help streamline the use of three-dimensional finite elements for analyses of soil and soil-structure systems. In this regard, a Windows-based graphical-user-interface (GUI) OpenSeesPL is developed for footing/pile-ground interaction analyses. The OpenSeesPL allows convenient studies of three-dimensional seismic (earthquake) and/or push-over pile analyses. Various ground modification scenarios may be also addressed by appropriate specification of the material within the pile zone. Building on OpenSeesPL, a new GUI is under development to combine nonlinear dynamic time history analysis of coupled soil-structure systems with an implementation of performance-based earthquake engineering (PBEE) for a single-column two-span bridge configuration. In this new interface, functionality is extended for analysis of multiple suites of ground motions and combination of results probabilistically using the Pacific Earthquake Engineering Research Center PBEE framework. Definition of the bridge, the underlying ground strata, and the material properties is greatly facilitated using this new interface. In addition, all stages of the involved analyses are conveniently executed in a systematic fashion, allowing the end user to investigate parametric or what-if scenarios on typical bridge configurations. In this paper, the main elements of the above numerical frameworks are presented. Aiming to highlight the GUI capabilities, a range of potential applications are also discussed.

INTRODUCTION

Soil-Foundation-Structure Interaction (SFSI) is an important aspect that affects the performance of structures such as buildings and bridges. With the recent developments in numerical modeling techniques and high-speed efficient computers, linear and nonlinear three-dimensional (3D) finite-element (FE) methods are becoming an effective technique for understanding the involved SFSI mechanisms Particularly suited to seismic applications, the open-source computational platform OpenSees [Mazzoni et al. 2006] provides such 3D simulation capabilities (*http://opensees.berkeley.edu*).

However, in conducting numerical simulations, preparation of the FE data file is a step that requires careful attention. A minor oversight might go undetected, leading to erroneous results. Numerous opportunities for such small errors abound, and a user-friendly interface can significantly alleviate this problem, and allow for high efficiency and much increased confidence.

On this basis, a user-interface "OpenSeesPL" [Elgamal et al. 2009c] has been developed (Figures 1 and 2) to allow for the execution of push-over and seismic footing/pile-ground simulations [Lu 2006; Lu et al. 2006]: *http://cyclic.ucsd.edu/openseespl*). The menu of soil materials in OpenSeesPL includes a complementary set of soil models/parameters representing loose, medium and dense cohesionless soils (with silt, sand, or gravel permeability), and soft, medium and stiff clay (J_2 plasticity cyclic-loading model). Various ground modification scenarios may be also studied by appropriate specification of the material within the pile zone.

More recently, an effort was initiated by the Pacific Earthquake Engineering Earthquake Center (PEER) to incorporate Performance-Based Earthquake Engineering (PBEE) analyses as an additional capability within the OpenSeesPL GUI environment [Mackie et al. 2010b; Lu et al. 2010], whereby PBEE aims to quantify the seismic performance and risk of engineered facilities using metrics that are of immediate use to both engineers and stakeholders. With significant PBEE tools for the next generation of design codes as applied to buildings already seeing rapid development and adoption recently (e.g., ATC-58 and ATC-63), an effort to address PBEE analysis and dissemination tools for bridges [Mackie et al., 2007; 2010a] was initiated (OpenSeesBridgePBEE). As such, the aim was to focus on a graphical environment for finite element modeling of coupled soil-structure systems as well as complete PBEE assessment for a single-column two-span bridge system. For that purpose, the main additional specific developments included [Mackie et al. 2010b; Lu et al. 2010]: (i) building a module for handling the needed input ground motion ensemble and for computing all salient characteristics, denoted as intensity measures (IMs); (ii) modifying the graphical interface to automatically generate user-defined bridge-ground FE models; and (iii) building the post-processing capability to display the seismic response ensembles, and the PBEE outcomes.

In the following sections, an overview of OpenSeesPL capabilities is presented, followed by a number of illustrative simulation scenarios. Elements of the new OpenSeesBridgePBEE framework are also presented. As such, the aim is to highlight the underlying analysis framework capabilities and range of potential applications.

COMPUTATIONAL FRAMEWORK

The open-source platform OpenSees (*http://opensees.berkeley.edu* [Mazzoni et al. 2006]) is employed throughout. A software framework for developing applications to simulate the performance of structural and geotechnical systems subjected to earthquakes, OpenSees can be used to study the performance of infrastructure facilities (bridges, buildings, etc.) under static loads, and during earthquake events. In the OpenSees platform, a wide range of linear and nonlinear soil and structural elements is available. The reported pre- and post-processing scenarios are generated by the user interface OpenSeesPL (*http://cyclic.ucsd.edu/openseespl*) which allows for: (i) convenient generation of the mesh and associated boundary conditions and loading parameters (FE input file); (ii) execution of the computations using the OpenSees platform; and (iii) graphical display of the results for the footing/pile and the ground system.

THE OPENSEESPL GUI

Modeling Configurations

The OpenSeesPL graphical interface (pre- and post-processor) is focused on facilitating a wide class of 3D studies. The basic default configuration is in the form of a 3D soil island with the possibility of including a footing/pile/pile-group model. Full-mesh, half-mesh, or quarter mesh configurations may be analyzed, as dictated by symmetry considerations (Figures 3 through 5).

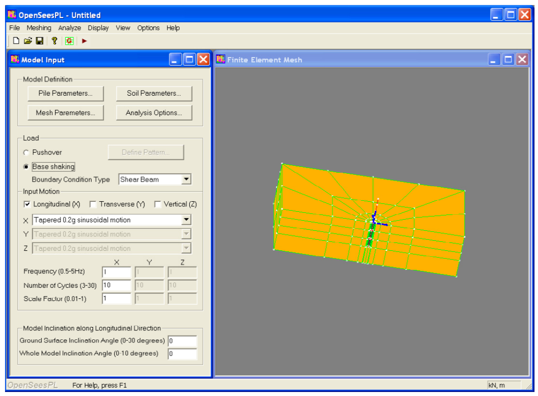

Figure 1 **OpenSeesPL user interface with mesh showing a circular pile in level ground [Lu et al. 2006].**

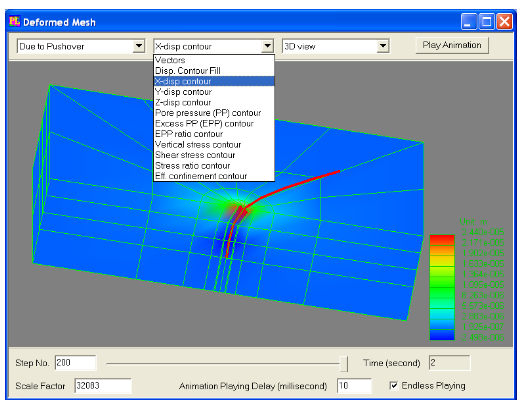

Figure 2 **Push-over analysis and deformed mesh window in OpenSeesPL [Lu et al. 2006].**

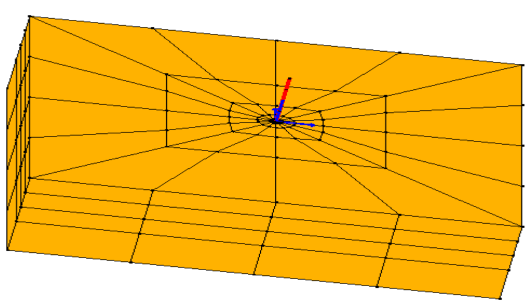

Figure 3 **Full 3D mesh-pile configuration.**

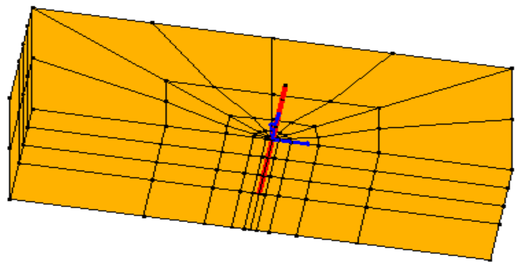

Figure 4 Half-3D mesh-pile configuration.

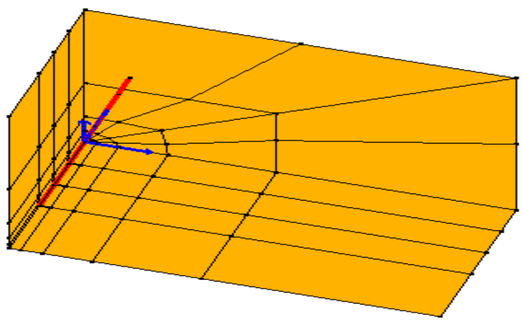

Figure 5 Quarter 3D mesh-pile configuration.

In OpenSeesPL, the mesh configuration may be easily modified to: (i) change the pile diameter, depth of embedment, height above ground surface, and number of pile beam-column elements; and (ii) refine the ground mesh domain in the lateral and vertical directions [Elgamal et al. 2009c]. In addition, square or circular pile cross-sections may be specified. As such, shallow foundations (rigid) in square or circular configurations may be also conveniently analyzed (Figures 6 and 7).

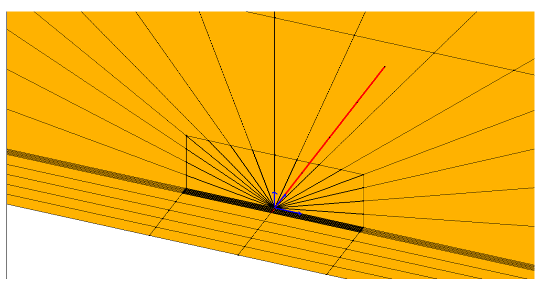

Figure 6 Building modeled as a bending beam on a shallow foundation embedded in the ground.

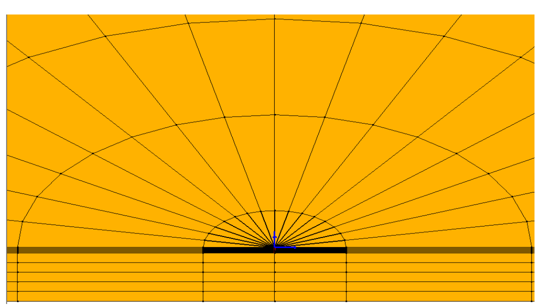

Figure 7 Circular shallow foundation model.

Independent control over the pile zone material may be exercised, allowing for a wide range of ground modifications studies (Figure 8). Of particular importance and significance in these scenarios is the ability to simulate the presence of a mild infinite-slope configuration, allowing estimates of accumulated ground deformation, efficacy of a deployed liquefaction countermeasure, pile-pinning effects, and liquefaction-induced lateral pile loads and resulting moments/stresses.

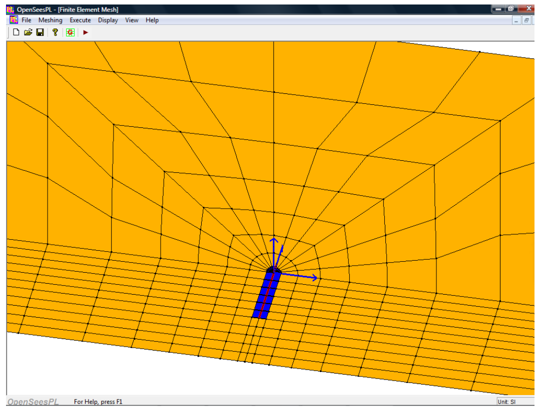

Figure 8 Control over specification of soil inside the pile zone.

Material for the pile-soil interfacing zone may be also specified by the user, permitting scenarios such as analysis of cylindrical foundations, and/or control over pile-soil friction and potential no-tension interaction during lateral deformation. In addition to the footing and single pile configurations, pile groups may be also represented in the free head or fixed-head configurations (Figure 9).

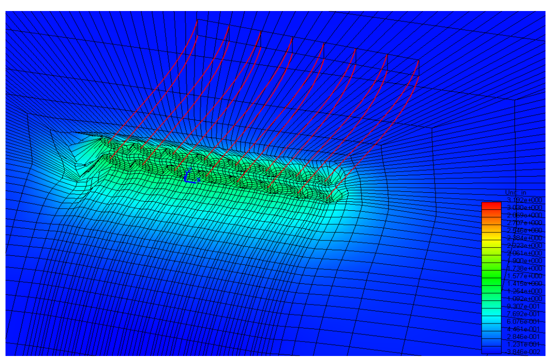

Figure 9 Large pile group model (1/2 mesh configuration.

Load Application

Static and dynamic loads may be applied. For static loading, push-over type analyses may be conducted where the loads/moments are directly applied to the pile top or footing surface, in force or in displacement modes. Capabilities are provided for monotonic loading, cyclic loading, and for user-defined load patterns to be uploaded as a text file. Push-over along the finite element mesh boundary may be also specified, for instance to explore loads on pile foundations due to lateral ground displacement [Elgamal et al. 2009c]. Dynamic and earthquake shaking may be also imparted along the soil lower boundary (base). Shaking is allowed in 3D with a small set of available motions, and a capability to upload user specified base shaking excitation (Figure 10).

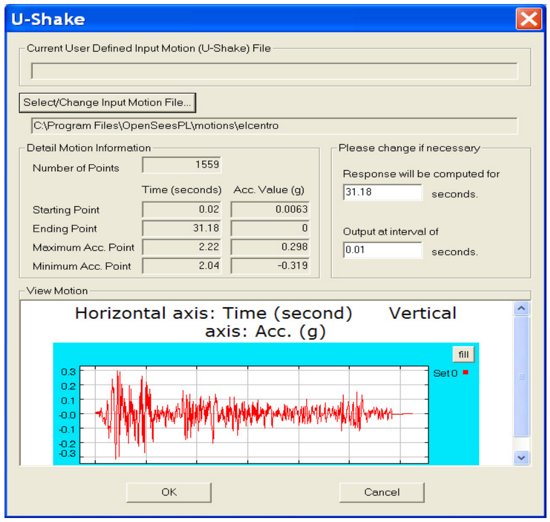

Figure 10 User-uploaded earthquake base excitation.

Soil Mesh Boundary Conditions

For static loading on the pile or footing system, a fixed boundary condition may be specified along the base and lateral boundaries of the soil mesh. For dynamic/earthquake excitation, ground motion is specified uniformly along the soil model base as mentioned earlier. Along the lateral boundaries, users can choose between fixed, shear beam, or periodic boundary conditions [Elgamal et al. 2009c].

Soil Properties

Linear and nonlinear elasto-plastic cyclic soil modeling capabilities are available. For nonlinear soil response, pressure independent (Mises or J_2) plasticity and pressure dependent (Drucker-Prager cone yield surface) models are available [Elgamal et al. 2003; Yang et al. 2003]. The available solid-fluid coupled formulation allows for conducting liquefaction-type analyses [Yang et al. 2003]. Selection may be made from a set of available soil model properties, or by user-defined input modeling parameters [Elgamal et al. 2009c].

Beam-Column Elements

OpenSeesPL employs state-of-the-art beam-column element formulations through the FE analysis engine OpenSees [Mazzoni et al. 2006]. In addition to static analysis, these elements allow for dynamic/cyclic earthquake-type simulations. Linear, bilinear hysteretic, and nonlinear fiber element formulations are available [Mazzoni et al. 2006], based on steel and concrete cyclic constitutive models. Using OpenSeesPL, the beam column modeling properties may be specified, and a display of the resulting moment-curvature relationship can be generated [Elgamal et al. 2009c].

Viscous Damping

For dynamic computations, viscous damping at the level of the entire model may be specified conveniently. A dedicated interface allows users to define damping ratios at two different frequencies, according to the Rayleigh mass-stiffness damping logic. Conversely, the mass and stiffness matrix viscous damping multipliers may be specified directly [Elgamal et al. 2009c].

Post-Processing

Upon specification of the model parameters, the interface accesses the FE OpenSees platform to conduct the computations. If needed, own weight is applied first (soil domain followed by super-structure), nonlinear material properties are activated, and the specified loading scenario is finally executed (static or dynamic/earthquake loading).

Upon completion of the computational phase, display of the results is initiated by OpenSeesPL. The structure response may be viewed as time histories and/or as response at various levels of the applied static load. The deformed mesh may be also viewed (Figures 2 and 9), with capabilities for animation and display of conditions after application of own weight only, and after execution of the static/dynamic load computations. Contour quantities such as displacement, strain, stress, pore pressure, and stress-ratio (stress-state relative to failure condition) may be viewed [Elgamal et al. 2009c].

Example Simulation Scenarios

Elgamal and Lu [2009a] conducted a pilot study of lateral loading on a 3x3 pile group. A single-pile FE model was first calibrated in the linear range based on the 3D analytical solution of Abedzadeh and Pak [2004]. Response of this linear pile in an idealized nonlinear undrained-clay material was then computed and compared to the linear solution. The corresponding 3x3 pile group response was also addressed (Figure 11), as a function of pile-spacing for the linear and nonlinear soil cases.

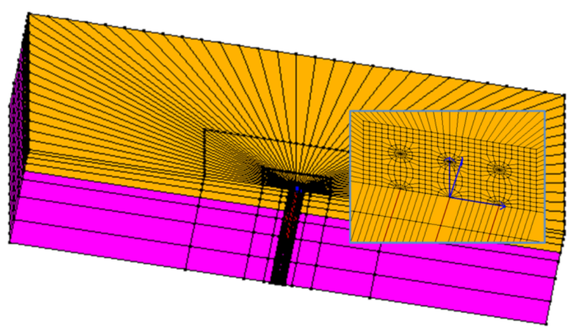

Figure 11 FE mesh of 3x3 pile group (1/2 mesh due to symmetry

Within a remediated area of large spatial extent, the periodic boundary technique offers an effective approach for conducting 3D analyses (i.e., symmetry allows the investigation of a representative remediated “cell”). As such, Elgamal et al. [2009b] conducted a 3D FE ground modification parametric study, to evaluate mitigation of liquefaction-induced lateral soil deformation by the stone column and the pile pinning approaches. An effective-stress plasticity-based formulation was employed. Using OpenSeesPL, a half-mesh was studied due to symmetry. A 10 m depth mildly-inclined (4 degrees) saturated layer was analyzed, with the remediated zone diameter maintained at 0.6 m throughout. Liquefaction-induced lateral deformation and remediation procedures for mildly sloping sand and silt strata were investigated under the action of an applied earthquake excitation. The extent of deployed remediation (area replacement ratio) and effect of the installed stone column permeability were analyzed. Effect of lateral spreading on the pile response was also investigated [Elgamal et al. 2009c].

THE OPENSEESBRIDGEPBEE GUI

Performance-based Earthquake Engineering Framework

Performance-based earthquake engineering considers seismic hazard, structural response, resulting damage, and repair costs associated with restoring a structure to its original function, using a fully consistent, probabilistic analysis of the associated parts of the problem [Cornell and Krawinkler 2000]. The uncertainty surrounding the PBEE framework components necessitates a probabilistic approach and acceptance criteria based on levels of confidence that probabilities of failure are acceptably small. Mackie and co-workers have pioneered the development of a bridge performance-based earthquake analysis framework [Mackie et al., 2007; Mackie et al. 2010a]. Based on the response of a series of typical pre-stressed, single-column bent, multi-span, box girder bridges in California, the data flows and requisite information were derived to relate response to damage of individual components within the structure, denoted as performance groups (PGs). Damage to these PGs were tied to explicit repair procedures and repair quantities that could then be used for cost estimation and repair effort necessary to return the bridge to its original level of functionality (direct costs). In addition, other PEER researchers used the same bridge configuration and model, but considered the pile-pinning effect at the abutments [Ledezma and Bray 2008] and the increase in repair costs due to the presence of a liquefaction-susceptible soil profile [Kramer et al. 2008].

A rigorous yet practical implementation of the PEER PBEE methodology was adapted for use in the new user interface OpenSeesBridgePBEE [Mackie et al. 2010b; Lu et al. 2010]. The methodology is subdivided to achieve performance objectives stated in terms of the probability of exceeding threshold values of socio-economic decision variables (DVs) in the seismic hazard environment under consideration. The PEER PBEE framework utilizes the total probability theorem to disaggregate the problem into several intermediate probabilistic models. This disaggregation of the decision-making framework outcome involves the following intermediate variables: repair quantities (Q), damage measures (DMs), engineering demand parameters (EDPs), and seismic hazard intensity measures (IMs). Consequently, engineers may choose to scrutinize probabilities of exceeding an EDP, such as strain, while an owner may choose to scrutinize probabilities of exceeding a DV, such as repair cost. An important step enabling effective aggregation of decision data is the association of structural elements and assemblies into performance groups (PGs) based on commonly used repair methods. The numerical implementation of the methodology is described in Mackie et al. [2010a].

The EDPs are computed directly from the ensemble of time history analyses performed. These are automatically associated with the PGs and the DSs for each. For example, additional bridge bents will automatically generate additional drift recorders and the distribution of maxima from multiple ground motion records will be compared to a set of damage fragility curves computed for each column PG. The data used to populate the relationships that associate EDPs to DMs and DMs to Qs were previously described in Mackie et al. [2007]. There exist default values for all of the built-in repair quantities, including the unit costs and production rates for each one of these items. However, the user has the ability to modify these if more state-specific or site-specific information is available [Mackie et al. 2010b; Lu et al. 2010].

Elements of the OpenSeesBridgePBEE GUI

The major components of a PBEE analysis are: specification of ground motions, mesh and soil constitutive model determination, bridge superstructure model and constitutive model determination, specification of PGs and the associated PBEE quantities, and the myriad of post-processing capabilities.

Specification of Ground Motion Input

The framework allows selection of individual ground motions, suites of ground motions, and bins of ground motions [Mackie et al. 2010b; Lu et al. 2010]. At the current time, all motions are obtained from the PEER NGA database (*http://peer.berkeley.edu/nga/*). An ensemble of 100 selected ground motions is employed in the PBEE analysis that is briefly discussed herein. Each motion is composed of three perpendicular acceleration time history components (two lateral and one vertical). These motions were selected through earlier efforts [Gupta and Krawinkler 2000; Mackie et al. 2007] to be representative of seismicity in typical regions of California. The motions are divided into 5 bins of 20 motions each with characteristics: (i) moment magnitude (M_w) 6.5-7.2 and closest distance (R) 15-30 km; (ii) M_w 6.5-7.2 and R 30-60 km; (iii) M_w 5.8-6.5 and R 15-30 km; (iv) M_w 5.8-6.5 and R 30-60 km; and v) M_w 5.8-7.2 and R 0-15 km. The user selects this motion ensemble by specifying the folder where the motion time histories have been stored in text files (Figure 12).

For each set of 3 orthogonal acceleration time histories, a large number of IMs are calculated, including peak ground acceleration (PGA), peak ground velocity (PGV), peak ground displacement (PGD), Arias intensity, strong motion duration ($D_{5\text{-}95}$), and cumulative absolute velocity (CAV). The IMs are calculated and displayed as a vector (one value for each shaking direction), and also in the form of the square root-sum-of-squares (SRSS) in the two horizontal directions (Figure 13). In addition, for each ground motion component, time histories and frequency domain (spectral) displays are provided (Figure 14) for acceleration, velocity, and displacement. The user can obtain this information by selecting any of the individual motions (Figure 12).

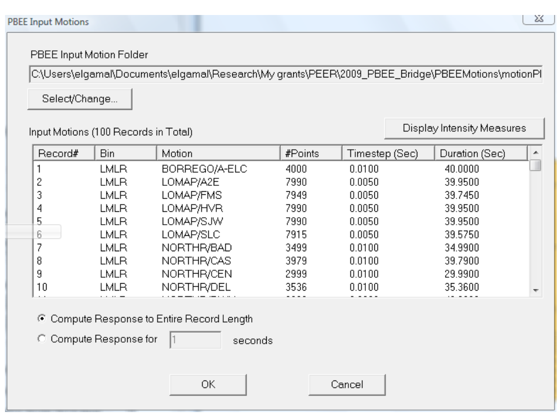

Figure 12 Ground motion selection screen.

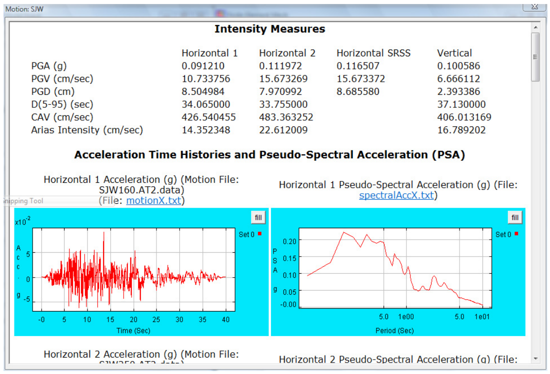

Figure 13 **IMs computed for SJW160 record (Loma Prieta 1989 Salinas J&W).**

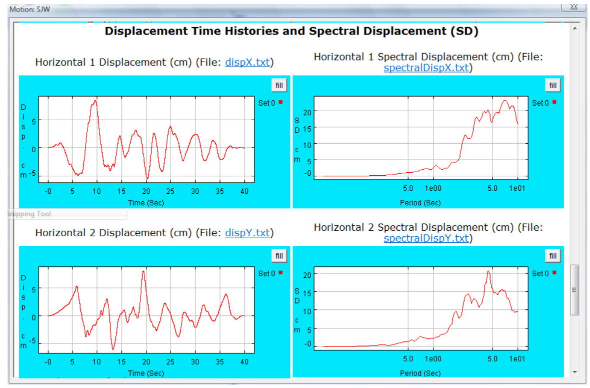

Figure 14 **Displacement time history and spectral displacement for SJW.**

While the ability to scrutinize individual records has numerous benefits, the use of PBEE necessitates the inclusion of multiple ground motions. Once these motions have been selected and/or binned, it is of interest to see the salient characteristics (IMs) of the group of ground motions. These characteristics of the entire ground motion ensemble are automatically generated and displayed in the form of histograms and cumulative distribution functions (CDF) for each of the IMs calculated. For example, the distribution of PGA values (Figure 15) shows the majority of records utilized have less than or equal 0.25 *g* PGA; however, the suite contains motions with PGAs as large as 1 *g*. Similarly, the histogram and CDF of PGV are shown in Figure 16.

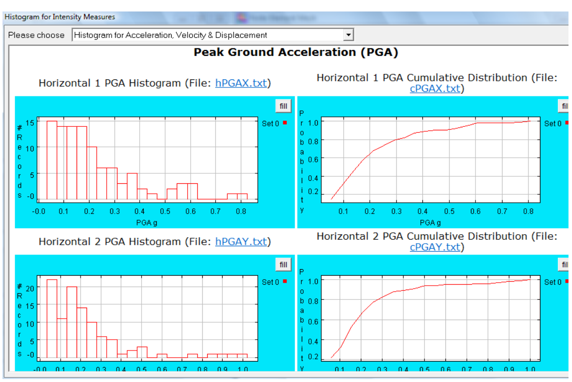

Figure 15 **100 motion PGA distribution.**

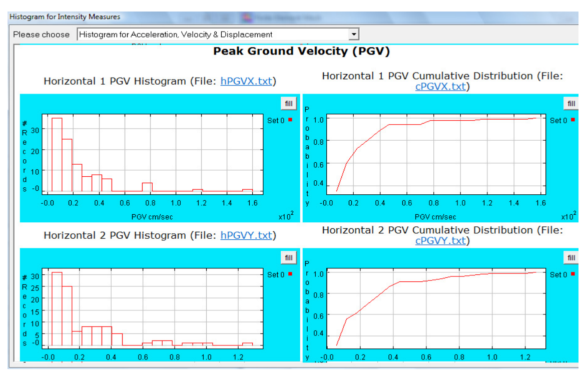

Figure 16 **100 motion PGV distribution**

Bridge-Ground Finite Element Model

The bridge-ground configurations available for construction in the user interface are currently based on single column bents extending into integral Type 1 pile shafts below grade. Mesh refinement is performed automatically surrounding each pile shaft in the ground. The columns are modeled as nonlinear beam-column elements with fiber cross sections. The user has the ability to configure the cross-sectional properties, shape, and materials. The current user interface supports reinforced concrete columns only. The deck is also modeled using two-noded beam-column elements discretized into five separate elements along each clear span. The deck is assumed to be capacity designed so that it responds in the elastic range. The gross or cracked section properties can be specified by the user. At the current stage of development, the approach ramp model connects the bridge longitudinal boundaries to the ground motion as specified by motion of the soil domain below the abutments (Figure 17). Several abutment models are currently available and provide the interface between the approach ramps and the bridge ends. These abutment options include a roller, elastic springs, gap and elastic-perfectly plastic resistance according to Caltrans Seismic Design Criteria (SDC) [2004], and a "spring model" that incorporates the SDC [2004] resistance along with that from user specified bridge-abutment bearings [Mackie et al. 2010b; Lu et al. 2010]. More details on the abutment models can be found in Aviram et al. [2008].

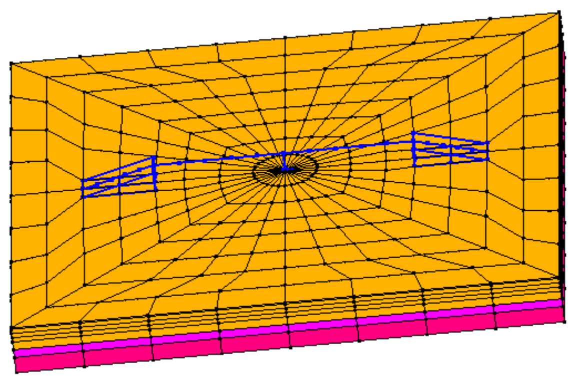

Figure 17 Perspective view of 3D bridge-ground domain with different soil layers

The ground domain is specified by: (i) definition of the zone occupied by the pile in terms of its diameter; (ii) definition of ground below the bridge; (iii) definition of the domain to support the approach ramp and abutment zones; (iv) definition of outer free-field lateral extent; and (v) definition of ground layer depth. A shear-beam type boundary condition is employed for the soil domain, i.e., at any given depth, displacement degrees of freedom of both sides of the longitudinal (and transverse) boundaries are tied together (both horizontally and vertically) to reproduce a 1D shear wave vertical propagation mechanism effect [Mackie et al. 2010b; Lu et al. 2010].

Performance-Based Earthquake Engineering Quantities

During transient analysis for each ground motion (either as a single ground motion analysis or as part of the ensemble of PBEE motions), response quantities are tracked at each time step. The response quantities of interest are tied directly the PGs that are used in the PBEE analysis for assessing damage and repair. Each major bridge component is grouped into a PG. Each PG contains a collection of components that reflect global-level indicators of structural performance and that contribute significantly to repair-level decisions. Currently, eleven performance groups are employed in OpenSeesBridgePBEE [Mackie et al. 2010b; Lu et al. 2010], including peak and residual column drift ratios, and peak deck-end/abutment relative displacements.

Discrete damage states (DS) are defined for each performance group. Each damage state has an associated repair method that also has a subset of different repair quantities (Qs). Once the Qs have been established for a given scenario (damage to different PGs), the total repair costs can be generated through a unit cost function. In addition, an estimate of the repair effort can be obtained through a production rate for each Q. The user has the ability to modify the default values specified for all of the repair quantities per damage state, unit costs, and production rates. More information on the derivation of the default DSs, Qs, unit costs, and production rates can be found in Mackie et al. [2007]. For the purposes of the user interface [Mackie et al. 2010b; Lu et al. 2010], an estimate of the replacement cost of the bridge is automatically generated based on the square footage of the deck and the Caltrans Comparative Bridge Costs (CBC) data, corrected to be consistent with the year 2007 cost data used in the calibration of the unit costs. The CBC includes a 10% mobilization cost but does not include any costs for demolition or removal of existing infrastructure.

Representative PBEE Results

Using the above user interface, repair cost and necessary Crew Working Days (CWD) for these repairs (may be displayed as a function of any of the available intensity measures. Figures 18 and 19 for instance display such an outcome with Peak Ground Velocity (PGV) as the Intensity Measure. From these figures, it is seen that: (i) maximum repair cost reaches as much as 60% of original cost at high PGVs; and (ii) 65 CWD are needed for making these repairs. Additional detailed PBEE results that are displayed by the user interface may be found in Mackie et al. [2010b] and Lu et al. [2010].

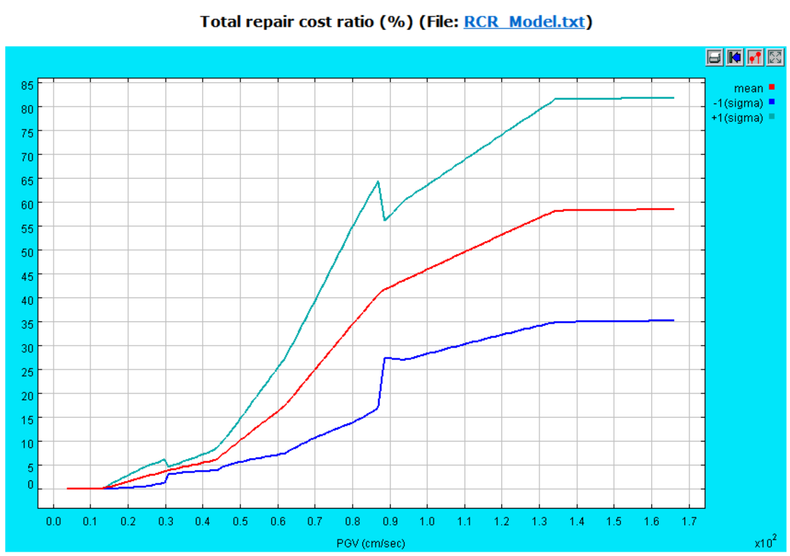

Figure 18 Repair const ratio (%) versus the IM of peak ground belocity.

Total repair time (CWD) (File: RT_Model.txt)

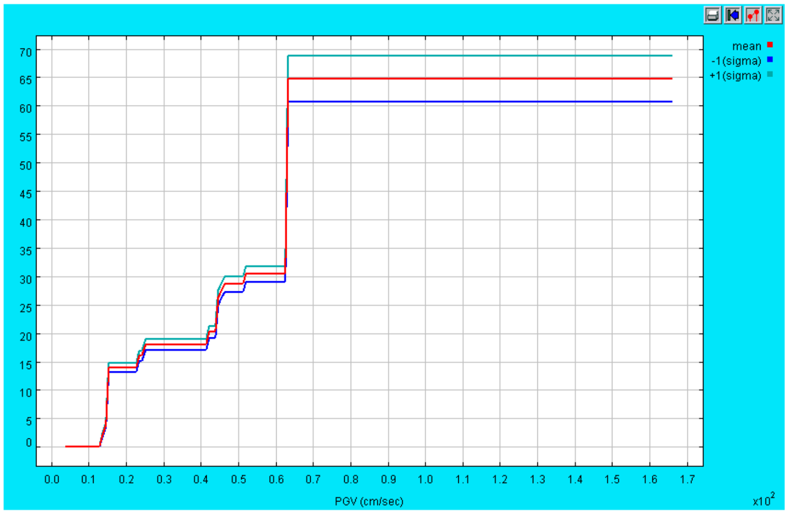

Figure 19 Necessary crew working days versus the IM of peak ground velocity.

SUMMARY AND CONCLUSIONS

A robust and versatile framework for computational analysis of pile-ground systems was presented. The open-source platform OpenSees is employed throughout. For illustration, scenarios of lateral response of piles, as well as ground remediation against liquefaction-induced lateral spreading were discussed. The conducted investigations aim to highlight the analysis framework capabilities and range of potential applications.

By coupling a refined graphical user interface for modeling of bridge-ground FE models with a PBEE framework, OpenSeesBridgePBEE has enabled more transparent access to performance-based assessment for typical twp-span single-column highway bridges. The elements of this new framework were presented in this paper. This new interface allows the user, be it a researcher or a practitioner, to focus on the PBEE outcomes and decision variable drivers rather than becoming inundated with the details of ground motion selection, FE modeling, constitutive model parameter calibration, and damage and repair data selection.

ACKNOWLEDGMENTS

The authors are grateful for the funding provided by the Pacific Earthquake Engineering Research (PEER) Center, the US National Science foundation Grant No. 0529995, and the PEER Lifelines program. Contributions, guidance, and feedback from PEER researchers working within the PEER Bridge Group, led by Professors Ross Boulanger and Stephen Mahin, are gratefully acknowledged. The data employed in this OpenSeesBridgePBEE user interface draws heavily from previous PEER projects and would not have been possible without collaboration with the California Department of Transportation. In particular, Mike Keever, Steve Sahs, Tom Shantz, and Richard Porter contributed the data needed to establish the repair cost and repair time databases.

REFRENCES

Abedzadeh F, Pak YS (2004). Continuum mechanics of lateral soil-pile interaction*, J. Engrg. Mech*.,130(11):1309–1318.
Aviram A, Mackie KR, Stojadinovic B (2008). Effect of abutment modeling on the seismic response of bridge structures, *Earthq. Engng. Engng. Vibration*, 7(4):395–402.
California Department of Transportation (2004). *Caltrans Seismic Design Criteria Version 1.3*, Sacramento, CA.
Cornell CA, Krawinkler H (2000). Progress and challenges in seismic performance assessment, *PEER Center News* 3(2).
Elgamal A, Yang Z, Parra E, Ragheb A (2003). Modeling of cyclic mobility in saturated cohesionless soils, *Inter. J. Plasticity*, 19(6):883–905.
Elgamal A, Lu J (2009a). A rramework for 3D finite element analysis of lateral pile system response, *Proceedings*, 2009 International Foundation Congress and Equipment Expo, Contemporary Topics in In Situ Testing, Analysis, and Reliability of Foundations, *ASCE GSP 186* (M. Iskander, D. F. Laefer, and M. H. Hussein, ed.), Orlando, FL, pp. 616–623.
Elgamal A, Lu J, Forcellini D (2009b). Mitigation of liquefaction-induced lateral deformation in a sloping stratum: 3D numerical simulation, ASCE *J. Geotech. Geoenviro. Engrg*., 135(11):672–1682.
Elgamal A., Lu J, Yang Z, Shantz T (2009c). Scenario-focused three-dimensional computational modeling in geomechanics, *Proceedings*, 4th International Young Geotechnical Engineers' Conference, Alexandria, Egypt.
Gupta, A., and Krawinkler, H., 2000. Behavior of ductile SMRFs at various hazard levels. *Journal of Structural Engineering*, 126(ST1), 98-107.
Kramer SL, Arduino P, Shin H-S (2008). Using OpenSees for performance-based evaluation of bridges on liquefiable soils. *Report No. 2008/07*, Pacific Earthquake Engineering Research Center, University of California, Berkeley, CA.
Ledezma CA, Bray JD (2008). Performance-based earthquake engineering design evaluation procedure for bridge foundations undergoing liquefaction-induced lateral spreading. *Report No. 2008/05*, Pacific Earthquake Engineering Research Center, University of California, Berkeley, CA.
Lu J, Yang Z, Elgamal, A. 2006. OpenSeesPL three-dimensional lateral pile-ground interaction version 1.00 user's manual, *Report No. SSRP-06/03*, Department of Structural Engineering, University of California, San Diego, La Jolla, CA.
Lu J, Mackie, KR, Elgamal A (2010). Performance-based earthquake evaluation of a single column bridge system, *Joint Conference Proceedings*, 7th International Conference on Urban Earthquake Engineering and 5th International Conference on Earthquake Engineering,Tokyo Institute of Technology, Tokyo, Japan.
Lu J (2006). Parallel finite element modeling of earthquake site response and liquefaction, PhD Thesis, Department of Structural Engineering, University of California, San Diego, CA.
Lu J, Yang Z, Elgamal A (2006). OpenSeesPL three-dimensional lateral pile-ground interaction version 1.00 user's manual. *Report No. SSRP-06/03*, Department of Structural Engineering, University of California, San Diego, CA.
Mackie KR, Wong J-M, Stojadinovic B (2007). Integrated probabilistic performance-based evaluation of benchmark reinforced concrete bridges, *Report No. 2007/09*, Pacific Earthquake Engineering Research Center, University of California, Berkeley, CA.
Mackie KR, Wong J-M, Stojadinovic B (2010a). Post-earthquake bridge repair cost and repair time estimation methodology, *Earthq. Engng. Struct. Dyn.*, 39(3):281–301.
Mackie KR, Lu J, Elgamal A (2010b). User interface for performance-based earthquake engineering: a single bent bridge pilot investigation, *Proceedings*, 9th US National and 10 Canadian Conference on Earthquake Engineering, Toronto, Canada.
Mazzoni S, McKenna F, Fenves GL (2006). *Open System for Earthquake Engineering Simulation User Manual*, Pacific Earthquake Engineering Research Center, University of California, Berkeley, CA (*http://opensees.berkeley.edu/*).
Yang Z, Elgamal A, Parra E (2003). A computational model for cyclic mobility and associated shear deformation, ASCE, *J. Geotech. Geoenviro. Engng*., 129(12):1119–1127.

EVALUATION OF LIQUEFACTION POTENTIAL AND PORE PRESSURE GENERATION OF SILTY SAND USING HOLLOW TORSIONAL TEST RESULTS

H. Sharafi[1] and M. H. Baziar[2]

[1]School of Faculty Engineering, Razi University, Kermanshah, Iran, [2] Professor, School of Civil Engineering, Iran University of Science and Technology, Tehran, Iran

ABSTRACT

This research presents an investigation on the effect of fines content on cyclic stress ratio (CSR), and excessive pore water pressure generation of Firouzkooh silty sands. Sixty stress-controlled cyclic hollow torsional tests were conducted to directly measure excess pore water pressure generation at different levels of CSR. The soil specimens were tested under three different confining pressures (σ'3= 60, 120, and 240 kPa), and different fines content at a constant relative density (Dr=60%). In this study, the effects of various parameters of soil such as confining pressure, fines content, void ratio, and the number of cycles required for liquefaction triggering on CRC of soil were studied. This research also presents a model to predict pore water pressure generation in non-plastic silty soil during cyclic loading. In general, beneficial effects of the silt were observed in the form of a decrease in excess pore water pressure. Modified models for pore water pressure generation model based on test results are also presented in this paper.

INTRODUCTION

Liquefaction is one of the main damage caused by strong earthquakes. Although liquefaction of non-cohesive soils was observed many years ago, it still has been a matter of great interest of geotechnical researchers for the last four decades since destructive Niigata, Japan, and Alaska, U.S., earthquakes. Such studies have mainly focused on clean sands or sands with a small portion of fines/gravel. However, recent earthquakes indicated that soils containing a significant percentage of silts may also liquefy due to shearing. Pioneer studies reported by Seed and his co-workers showed that sites containing silty sand behave differently from those containing relatively clean sand. This observation was later confirmed by other studies.

The primary framework for the energy-based liquefaction assessment approach was represented by previous researchers. The fact that the shear energy required to liquefy a soil deposit is independent of the stress history has become the main advantage of the energy approach. It was shown that there exists a unique relationship between the dissipated shear energy and the pore water pressure buildup which is independent of the shear stress history. In addition, Liang et al [1995] applied random and sinusoidal excitations to the samples of Reid Bedford sand; and concluded that the strain energy required for liquefaction triggering is independent of the applied load pattern (harmonic or random). Therefore, it is not necessary to decompose the time history of shear stress to find an equivalent number of cycles for a chosen average stress or strain level. Using energy procedure to determine the liquefaction resistance includes the following specific advantages [Baziar and Jafarian 2007]:

- Energy is associated with the quality of both shear stress and shear strain.

- Energy is a scalar quantity which can be associated with the main earthquake parameters such as focal distance and magnitude of the earthquake.

The objective of this research is to study the effect of fines content (from 0% to 100%) on the cyclic resistance of silty sand using energy methods. To achieve this goal, the observed relation between the cumulative strain energy, dissipated within the unit volume of sand-silt mixtures, and important parameters affecting liquefaction potential, such as fines content and effective confining pressure were studied.

TESTS RESULTS

The grain size distribution curves for the soils are shown in Figure 1. The variations of maximum and minimum void ratios versus fines content for the mixtures are shown in Figure 2. Typical results of the experiment conducted on a specimen composed of silty sand (Test No. 31 [Bazair and Sharafi 2011] are illustrated in Figures 3 through 8. The hysteresis loops of the test are shown in Figure 3, which is formed by plotting the shear stress variations versus shear strain. As observed in this figure, the secants shear modulus decreases with increase in the number of loading cycles and decrease in the effective stress. This cyclic degradation occurs due to increase in pore water pressure and finally causes the loops become flat after the occurrence of liquefaction. Figure 4 shows the shear stress in terms of time. The variations of the excess pore water pressure in terms of time for the same specimen are shown in Figure 5. These two figures indicate that the pore water pressure increased up to the confining pressure in which the shear resistance of the sample decreased suddenly. The variation of q' versus p' is plotted in Figure 6 for the same test. The variation of cyclic shear strain versus the number of cycles is also plotted in Figure 7. As seen in this figure, the amplitude of cyclic shear strain increases as the number of cycles increases, and for the same samples, such as the one presented in Figure 8, the double amplitude strain become more than 7.5%.

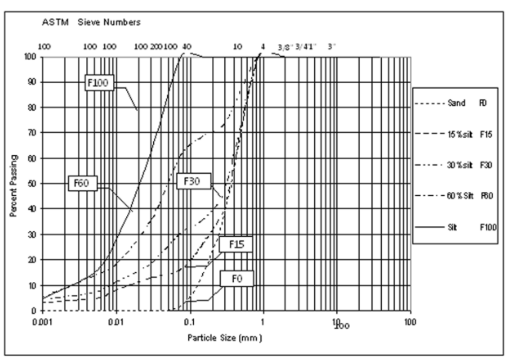

Figure 1 Grain size distribution of soils used.

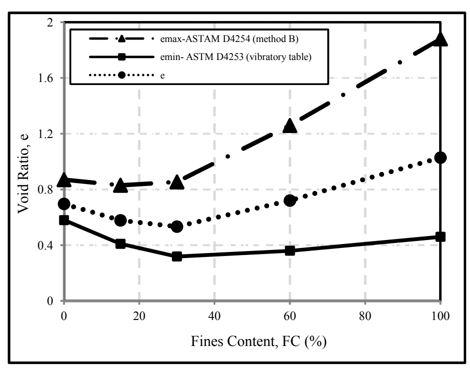

Figure 2 Maximum and minimum void ratios versus fines content for Firoozkooh sand and non-plastic.

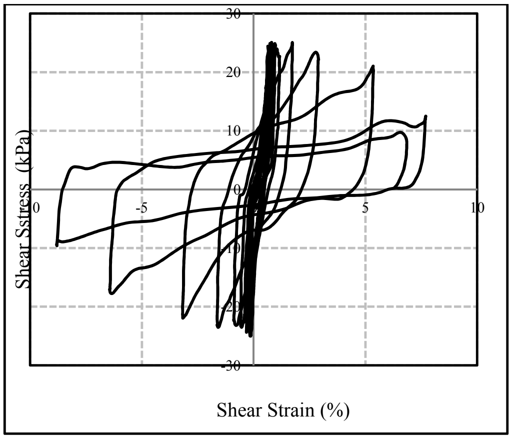

Figure 3 The hysteresis curve.

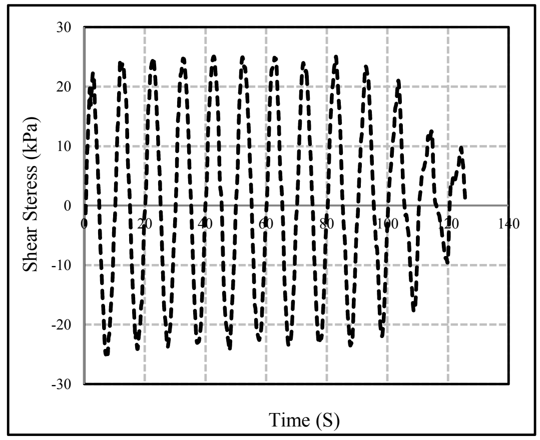

Figure 4 Cyclic shear stress variation versus time.

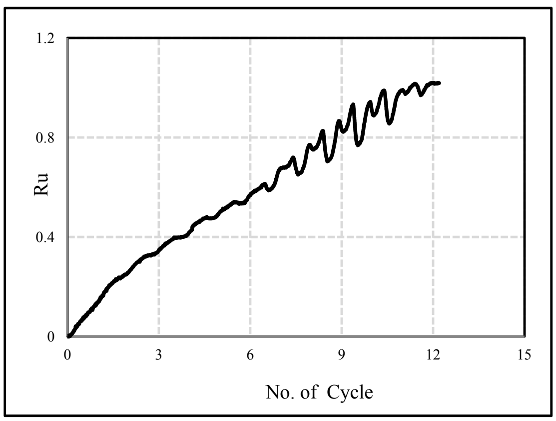

Figure 5 The excess pore water pressure per no. of cycle.

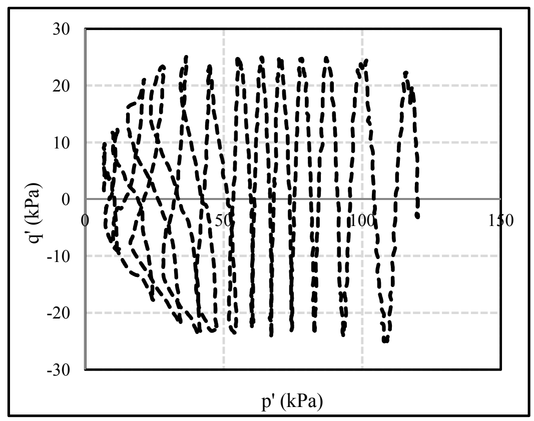

Figure 6 The variation of q' versus p'.

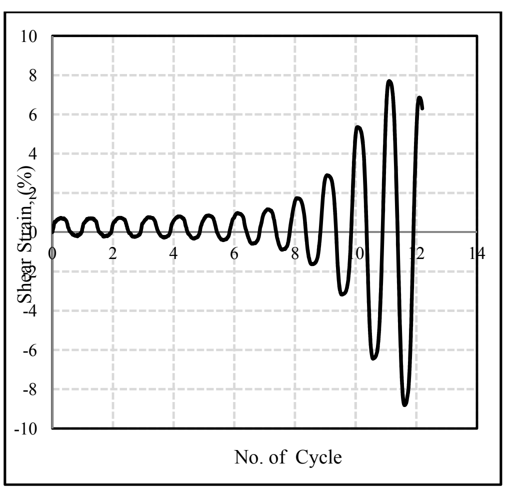

Figure 7 Cyclic shear strain stress variation versus cycle number.

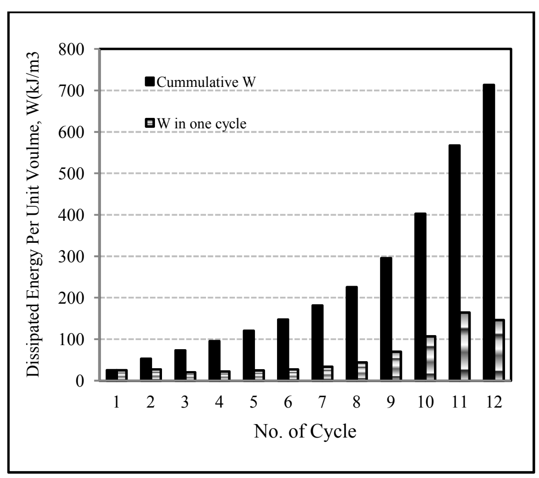

Figure 8 Dissipated shear energy in each cycle and cumulative dissipated shear energy after each cycle.

Figure 8 presents the dissipated shear energy in each cycle and cumulative dissipated shear energy after each cycle along with the number of cycle. Note that the dissipated shear energy in each cycle become greater within the first eleven cycles, finally causing liquefaction to occur, and then the dissipated shear energy in the 12 cycles decreased due to a very small shear resistance, while the resultant shear displacement in this cycle was greater (see Figures 4 and 7). Since the liquefaction triggered after the eleven cycles, the total shear energy within these eleven cycles (567.145 J /m^3) was regarded as the energy necessary for liquefaction triggering (W_{total}). The inter-particle resistance is reduced in accordance with the increasing in the pore water pressure. The obtained curves in Figure 8 (cumulative W) and also in Figure 5 (representing pore water pressure build up) are similar, whereby both of them meet their maximum values at the same time, indicating that the dissipated energy per volume is associated with the progression of pore water pressure and the consequent occurrence of liquefaction.

EFFECT OF FINES CONTENT ON CYCLIC RESISTANCE RATIO (CRR)

The effect of silts content on the liquefaction resistance at the constant relative density is shown in Figure 9. This figure indicates that for low values of fines content ($FC < FC_{th}$, where FC_{th} is threshold fines content for the change of behavior in silty sand), an increase in fines content, leads to decrease the liquefaction resistance. This behavior is similar to the one implied in the modified liquefaction resistance diagram presented by Polito and Martin [2001]. However, for higher values of fines content ($FC > FC_{th}$), an increase in fines content (almost 30 to 60%) at the same relative density, increases the liquefaction resistance. In contrast, an increase in fines content (more than 60%), decreases the liquefaction resistance. The effect of changing in the effective confining pressure on the liquefaction resistance of silty sands is shown in Figure 10. For 30% silt content, the change in confining pressure from 60 to 240 kPa causes an approximately 40% decrease in the cyclic resistance ratio, resulting in the occurrence of liquefaction after 15 cycles. This result is compatible with the observations reported by other researchers.

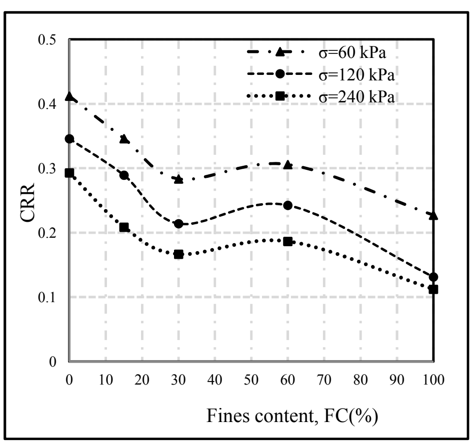

Figure 9 Fines content effect versus cyclic resistance ratio (CRR) with constant relative density.

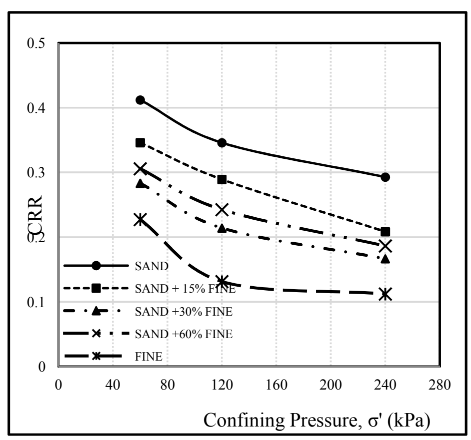

Figure 10 Confining pressure effect on the liquefaction resistance ratio (CRR) with constant relative density.

THE PORE PRESSURE MODEL PRESENTED IN THIS STUDY

Seed et al. [1970] developed an empirical model for predicting the rate of excess pore water pressure (r_u) using data from tests performed on clean sands. Equation (1) expresses their model.

$$r_u = \frac{1}{2} + \frac{1}{\pi}\arcsin\left[2(N/N_l)^{1/\alpha} - 1\right] \tag{1}$$

In their model, r_u is a function of the cycle ratio, which is the ratio of the number of applied uniform cycles of loading with constant amplitude (N) to the number of cycles with the same amplitude required to cause liquefaction in the soil (N_l), with an empirically parameter of α. Booker et al. [1976] proposed an alternative version of this model. This model is presented in Equation (2):

$$r_u = \frac{2}{\pi}\arcsin\left(\frac{N}{N_l}\right)^{\frac{1}{2\alpha}} \tag{2}$$

In this model, parameters of r_u, N, N_l, and α are also the same as Equation (2).

The two parameters α and N_l of both Equations (1) and (2) can be determined using results of stress-controlled cyclic triaxial tests, as well as other types of undrained cyclic tests. For a soil sample, N_l will be increased with increasing relative density, and it also decreases when the magnitude of stress increases (increase of CSR). The use of N_l has its drawback as it can only be applied to liquefiable soils such as loose sand and soils with non-plastic fines, which can still undergo significant pore pressure build up and deformation due to cyclic softening. Researchers showed that both Equations (1) and (2) produce good results when compared with the results of cyclic triaxial and cyclic simple shear tests on clean sand. Lee and Albaisa [1974] recommended an upper and lower bounds for residual pore pressure ratio for Monterey sand and Sacramento sand. These bounds and other bounds presented by Seed et al. [1974] and El Hosri et al. [1984] are shown in Figure 11. In addition to the two calibration parameters, implementation of either Equations (1) or (2) for the earthquake site response analyses requires that the earthquake motion be converted to an equivalent number of uniform cycles. Such load conversion procedures are outlined in Seed et al. [1983], Hancock and Bommer [2005], and Polito et al. [2008]. This required conversion is the greatest disadvantage in using either Equations (1) or (2) for predicting pore pressure generation in soils subjected to earthquake-type loadings.

Comparison of test results of current research with the bound from model of Seed et al. [1974], and model of El Hosri et al. [1984] are presented in Figures 11 to 15. These figures are for clean sand, pure silt, and sand samples with different silt content (15%, 30% and 60%). These figures show that both models cannot predict all the test results satisfactory. However predication of these models is better for clean sand and samples with silt content of less than 30%. In other words, the model of Seed et al. [1974] and EL Hosri et al. [1984] cannot be used for specimens with more than 30% silt content. It is clear that from these figures, pore pressure generation characteristics of silty sands up to 30% silt content are almost similar to that of clean sand. However, for the sandy silt specimens (silt ≥ 30%), the pore pressure generation patterns deviate from that of clean sand. The pore water pressure is much faster at the beginning of loading, and the rate slows down as considerable amount of pore water pressure builds up. It is interesting to note that pore water pressure build up curves for pure silt (Figure 16) is not much different from that of clean sand, which is in agreement with the literature, and follows the concept that non-plastic silt may be considered as a sand of very fine particles. However, it should be noted that in the field dissipation of pore water pressure for silt will be much slower compared with sand due to its low permeability. When it comes to natural silts, their behavior is much different from each other. This trend has been also observed for clayey silts. Due to this fact, using results of experimental tests presented in this work, it was tried to make possible correction on Equations (1) and (2) to predict the pore water pressure buildup for specimen in all range of silt content. This modified model will be explained in the next paragraph.

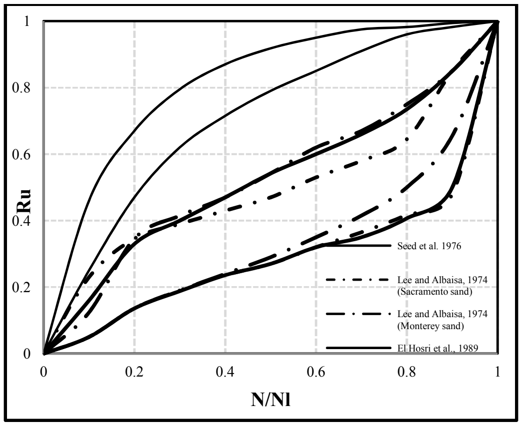

Figure 11 Pore pressure generation data for sands and clayey silts reported in the literature.

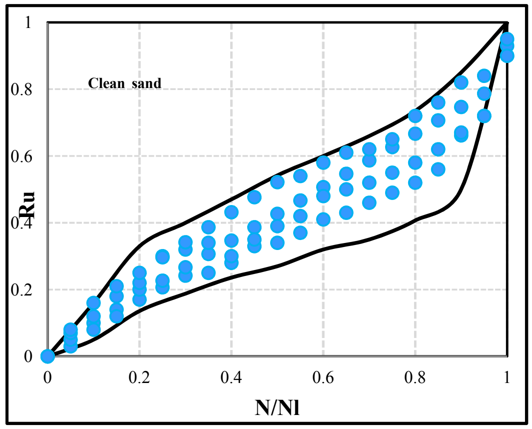

Figure 12 Excess pore water pressure generation data for clean sand.

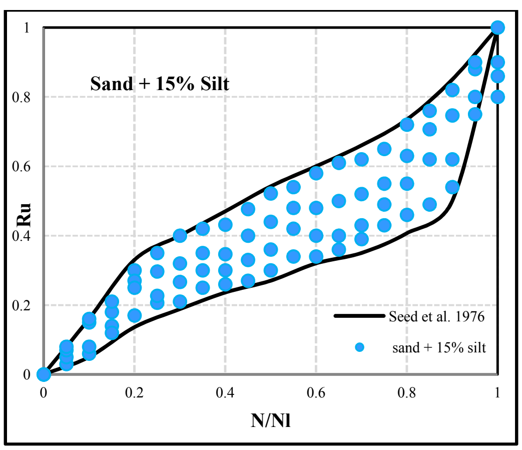

Figure 13 Excess pore water pressure generation dData for silty sands (sand + 15% fines).

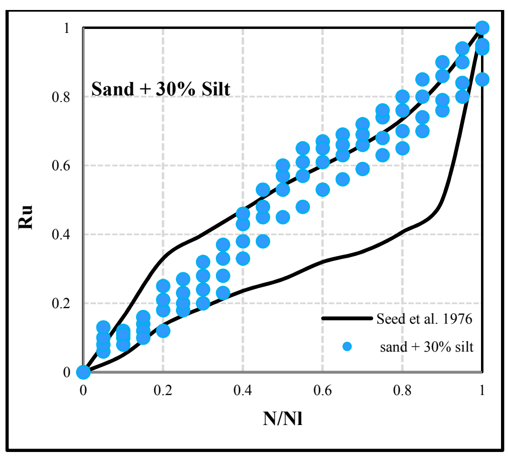

Figure 14 Excess pore water pressure generation data for silty sands (sand + 30% fines).

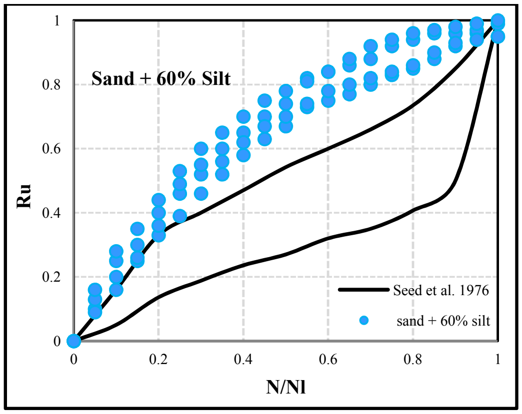

Figure 15 Excess pore water pressure generation data for silty sands (sand + 60% fines).

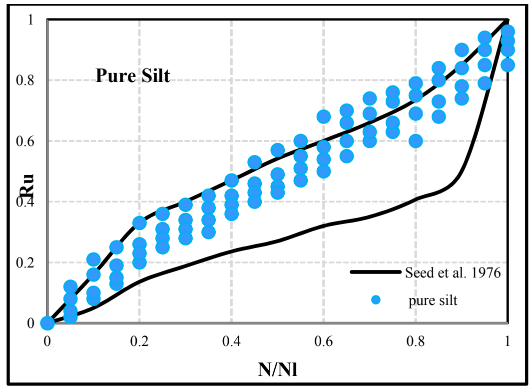

Figure 16 Excess pore water pressure generation data for pure silt.

The develop model of pore pressure build up data for clayey silt with plasticity index 5−15% reported in El Hosri et al. [1984] is shown in the Figure 11 for comparison purposes. It can be observed that this model is an upper bound for the generation patterns of non plastic silty soils. According to the above discussion, it can be concluded that an approximate pore water pressure generation pattern of any non-plastic soil or soil with very low plasticity can be obtained from the Figures 12 to 16. The presented tests results [Baziar and Sharafi 2010], implemented in the statistical software named DATAFIT, was carried out to modify the pore water pressure build up models. The output of this software is an equation that predicts r_u with maximum correlation coefficient (R^2).

The suggested equation is:

$$r_u = \left(\frac{u_g}{\sigma'}\right) = \frac{2}{\pi}\arcsin\left(\frac{N}{N_l}\right)^{1/2\alpha} + \beta\sqrt{\left(1 - \left(2\frac{N}{N_l} - 1\right)^2\right)} \tag{3}$$

In which u_g is excess pore water pressure, σ' is effective confining pressure, N is number of loading cycles, and N_l is number of cycles to liquefaction. In Equation 3, α and β are two constants that are defined for different types of soils based on their silt content in Table 1. Comparison of the modified model in this research with models of others researchers for different soil types are presented in Figures 17 and 18. As can be seen from Figure 18, the modified model presented in this study shows good predication for the pore water pressure in silty sands.

Table 1 Coefficients of *α* and *β*.

Soils	Seed	This study		R^2
	A	*α*	*β*	
Sand	0.6-1	0.6-0.8	0-0.25	0.94
sand+15%silt	0.6-1	0.3-0.6	0.2-0.3	0.92
sand+30%silt	0.6-1	0.2-0.4	0.25-0.3	0.9
sand+60%silt	0.6-1	0.2-0.4	0.45-0.6	0.91
Silt	0.6-1	0.6-0.8	0.1-0.2	0.92

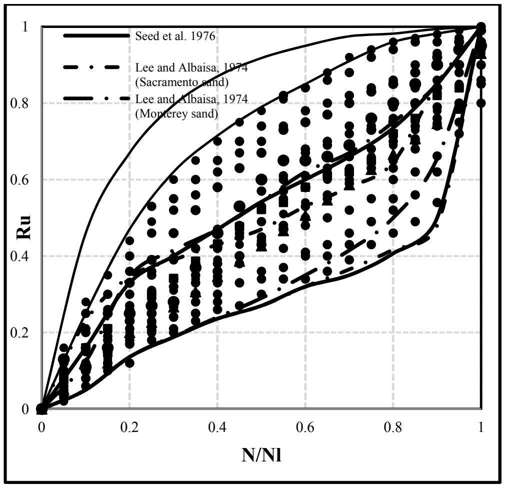

Figure 17 Excess Pore Water Pressure Generation Data for all specimens and Comparison with all model discussed in literature review

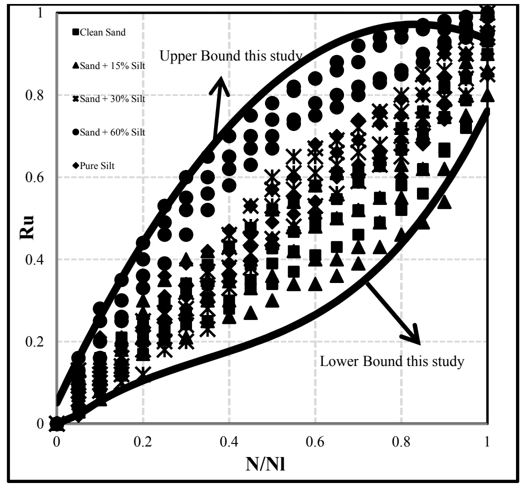

Figure 18 Excess Pore Water Pressure Generation Data for all specimens and Comparison with model presented.

CONCLUSION

Based on the experimental results of the current study, the following conclusions can be drawn:

1. The increase in silt content (percent passing the No.200 sieve) of the Firouzkooh sand caused the liquefaction resistance to decrease compared with clean sand, a result found similar in previous studies, as the confining pressure increases the liquefaction resistance of silty sand decreases.

2. For fines content lower than threshold limit ($FC < FC_{th}$), an increase in fines content at the same relative density led to a decrease in liquefaction resistance. This behavior is similar to the one implied in the modified liquefaction

resistance diagram of other researchers. A different trend is observed in the Figure 10, where it is demonstrated that for high values of fines content ($FC > FC_{th}$), an increase in fines content (almost 30 to 60%), at the same relative density, increases the liquefaction resistance and with more increase in fines content (more than 60%), the liquefaction resistance decreases.

3. The effect of silts content on required energy to liquefaction is exactly similar with the effect of silt content on cyclic resistance ratio for all the effective confining pressure tested here at the same relative density.

4. The liquefaction resistance of clean sand is much more than silty sand and pure silt, while several studies have indicated that sands deposits with silt content found to be more susceptible to liquefaction than clean sand.

5. The presence of silt indicated a decrease in excess pore water pressure generation.

6. The models of Seed et al. [1974] and EL Hosri et al. [1989] cannot be used for specimen with more than 30% silt content. It is clear that from this study, pore pressure generation characteristics of silty sands up to 30% silt content are almost similar to that of clean sand. However, for the sandy silt specimens (silt ≥ 30%), the pore pressure generation patterns deviate from that of clean sand.

7. The modified model presented in this study predicts well the pore water pressure build up in silty sands.

ACKNOWLEDGMENT

The laboratory tests reported in this research was conducted in Geotechnical Laboratory at International Institute of Earthquake Engineering and Seismology (IIEES) of Iran. This cooperation is gratefully appreciated. The study was funded by the Transportation Research Institute of Ministry of Road & Transportation, Islamic Republic of Iran. This support is gratefully appreciated.

REFERENCES

Baziar MH, Sharafi H (2011). Assessment of silty sand liquefaction potential using hollow torsional tests – An energy approach. *J. Soil Dyn. Earthq. Engrg.*

Baziar MH, Jafarian Y (2007). Assessment of liquefaction triggering using strain energy concept and ANN model: Capacity energy, *J. Soil Dyn. Earthq. Engrg*, 27:1056–1072.

Booker JR, Rahman, MS, and Seed HB (1976). GADFLEA—A computer program for the analysis of pore pressure generation and dissipation during cyclic or earthquake loading. *Rept. No. EERC 76-24*, Earthquake Engineering Research Center, University of California, Berkeley, CA.

El Hosri MS, Biarez J, Hicher PY (1984). Liquefaction characteristics of silty clay. *Proceedings,* 8th World Conference on Earthquake Engineering, San Francisco, CA., pp. 277–284.

Hancock J, Bommer JJ (2005). The effective number of cycles of earthquake ground motion, *Earthq. Engng. Struct. Dyn*., 34(6):637–664.

Lee KL, Albaisa A (1974). Earthquake induced settlements in saturated sands, ASCE, J. Geotech. Engrg. Div., 100(GT4):387–406.

Polito CP, Martin II JR (2001). Effects of non-plastic fines on the liquefaction resistance of sands, ASCE, *J. Geotech. Geoenviron. Engng*., 127(5):408–415.

Polito CP, Green RA, Lee J (2008). Pore Pressure generation models for sands and silty soils subjected to cyclic loading. J. Geotech. Geoenviron. Eng., 134(10), 1490-1500.

Seed HB, Idriss IM, Arango I (1983). Evaluation of soil liquefaction using field performance data, ASCE, *J. Geotech. Engng. Div*., 109(GT3):458–482.

Liang L, Figueroa JL, Saada AS (1995). Liquefaction under random loading: a unit energy approach, ASCE. *J. Geotech. Engng. Div.*, 121(GT11):776–781.

SEISMIC ISOLATION FOR HOUSING, SCHOOLS, AND HOSPITALS IN THE URBAN ENVIRONMENT

James M. Kelly and Dimitrios Konstantinidis

Pacific Earthquake Engineering Research Center, University of California, Berkeley, California.

ABSTRACT

We propose two types of multi-layer elastomeric isolation bearings where the reinforcing elements, normally thick and inflexible steel plates, are replaced by thin flexible reinforcement. The reinforcement in these bearings, in contrast to the steel in the conventional isolator (which is assumed to be rigid both in extension and flexure), is assumed to be completely without flexural stiffness. This is strictly correct for the first type where the reinforcement is provided by carbon fiber but not completely accurate for the second type where the standard steel shims are replaced by thin flexible steel sheets. In the second type there are fewer reinforcing layers than in conventional isolators, making them lighter, but the most important aspect of both types of bearings is that they do not have end plates, thus reducing their weight, but also they are not bonded to the upper and lower support surfaces. This at first sight might seem to be a deficiency of this design, but it has the advantage that it eliminates the presence of tensile stresses in the bearings. It is these tensile stresses and the bonding requirements that arise from them that lead to the high costs of conventional bearings.

A theoretical analysis of the ultimate displacement capacity of these bearings suggests, and test results confirm, that it is possible to produce in these ways a strip isolator that matches the behavior of a conventional steel-reinforced isolator. Tested bearings survived very large shear strains, comparable to those expected of conventional seismic isolators under seismic loading. However their cost is in the hundreds of dollars as compared to the cost of conventional isolators in the thousands of dollars.

The intention of this research is to provide low-cost lightweight isolation systems for the retrofit of housing and public buildings in highly seismic urban areas.

INTRODUCTION

Many large urban centers are extremely vulnerable to the damaging effects of large earthquakes. For example large cities such as Istanbul and Tehran have many thousands of buildings that were built prior to the enforcement of stringent building codes. Buildings in the range of two to six stories have been constructed using only vertical load designs and no provision for horizontal resistance. These are in many cases valuable buildings and are used as residences, offices and shops. There are so many of them that they cannot realistically be demolished and replaced, and retrofitting them by conventional methods would be highly disruptive to the occupants.

Modern methods of structural control would be much too expensive for these buildings, but it is possible that a system of inexpensive seismic isolation could be adapted to improve the seismic resistance of poor housing and other buildings such as schools and hospitals. In at least one retrofit project in Armenia, a large multi-family housing block was retrofitted using rubber isolators with no need for the families to leave while the work was done.

Development of low-cost seismic isolators that can be mass produced by a relatively simplified manufacturing process would stimulate world-wide application of the seismic isolation technology to the retrofit of existing structures with deficiencies and to new construction in lesser developed countries.

REALIZATION OF TWO TYPES OF POSSIBLE SYSTEMS FOR IMPLEMENTATION

This goal can be achieved in two ways both of which lead to low-cost isolation systems that can be mass produced and are lighter than conventional steel-reinforced bearings. The first is achieved by replacing the steel shim plates in rubber bearings with fiber reinforcement. The seismic effectiveness of the fiber-reinforced bearing has been demonstrated by an analytical model that estimates the vertical stiffness of the fiber-reinforced bearing and shows that the vertical stiffness of the bearing can be close to that of a conventional steel-reinforced bearing. In addition the results of an experimental research program conducted at the University of California, Berkeley [Kelly and Takhirov 2004], has confirmed that the main properties of the seismic isolators are preserved. Namely, the vertical stiffness is significantly greater than the horizontal one, providing the capacity to carry large vertical loads and provide isolation of the building from ground shaking in the horizontal direction.

The weight reduction is possible as fiber materials are available with an elastic stiffness that is of the same order as steel. Thus the reinforcement needed to provide the vertical stiffness may be obtained by using a similar volume of very much lighter material. The cost savings are also possible since the use of fiber allows a simpler, less labor-intensive manufacturing process. Another benefit of using fiber reinforcement is that it would then be possible to build isolators in long rectangular strips, whereby individual isolators could be cut to the required size. All isolators are currently manufactured as either circular or square. Rectangular isolators in the form of long strips would have distinct advantages over square or circular isolators when applied to buildings where the lateral resisting system is walls. When isolation is applied to buildings with structural walls, additional wall beams are needed to carry the wall from isolator to isolator. A strip isolator would have a distinct advantage for retrofitting masonry structures and for isolating residential housing constructed from concrete or masonry blocks (as shown in Figure 1).

The other system of low-cost isolators is the use of standard thermal expansion bridge bearings as isolators. The effectiveness of these isolators has been demonstrated by a theoretical analysis covering the mechanical characteristics of these bearings where the reinforcing elements, normally thick and inflexible steel plates, are replaced by thin flexible reinforcement. The reinforcement in these bearings, in contrast to the steel in the conventional isolator (which is assumed to be rigid both in extension and flexure), is assumed to be completely without flexural stiffness. This is of course not completely accurate but allows the determination of a lower bound to the ultimate lateral displacement of the isolator. In addition, there are fewer reinforcing layers than in conventional isolators, making them lighter, but the most important aspect of these bearings is that they do not have end plates which again reduces the weight but the main difference from conventional isolators is that they are not bonded to the upper and lower support surfaces. This at first sight might seem to be a deficiency of this design, but it has the advantage that it eliminates the presence of tensile stresses in the bearings. It is these tensile stresses and the bonding requirements that arise from them that lead to the high costs of conventional bearings.

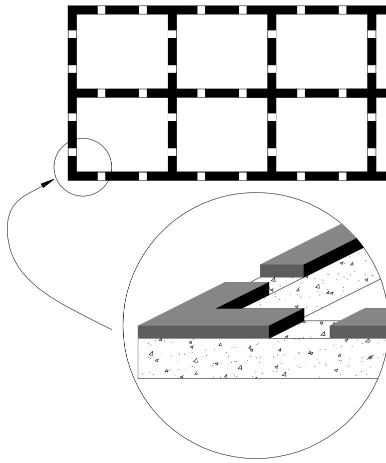

Figure 1 One of the proposed installations of the strip bearings.

Thermal expansion bridge bearings in contrast to seismic isolation bearings are much less expensive. The in-service demands on these bearings are, of course, much lower, but the tests have shown that even if displacements of seismic-demand magnitude are applied to them, they can deform without damage. The primary reason for this is the fact that the top and bottom surfaces can roll off the support surfaces, and no tension stresses are produced. The unbalanced moments are resisted by the vertical load through offset of the force resultants on the top and bottom surfaces. These bearings were tested at the University of California, San Diego [Konstantinidis, Kelly and Makris 2008] and were shown to be able to survive very large shear strains comparable to those expected of conventional seismic isolators under seismic loading. However, their cost was in the hundreds of dollars as compared to the cost of conventional isolators in the thousands of dollars.

THEORETICAL ESTIMATION OF EFFECTIVE COMPRESSION MODULUS

To calculate the effective vertical stiffness of a steel-reinforced bearing, an approximate analysis is used that assumes that each individual pad in the bearing deforms in such a way that horizontal planes remain horizontal and points on a vertical line lie on a parabola after loading. The plates are assumed to constrain the displacement at the top and bottom of the pad. Linear elastic behavior with incompressibility is assumed, with the additional assumption that the normal stress components are approximated by the pressure. This leads to the well-known “pressure solution”, which is generally accepted as an adequate approximate approach for calculating the vertical stiffness. It is shown that the extensional flexibility of the fiber reinforcement can be incorporated into this approach, and that predictions of the resulting effective compression modulus be made [Kelly and Takhirov 2001]. The vertical stiffness of the bearing, K_V, can be defined as [Kelly 1996]

$$K_V = \frac{E_c A}{t_r}$$

where E_c is the compression modulus of the bearing (steel- or fiber-reinforced), A is the area of the bearing, and t_r is the total thickness of rubber material in the bearing.

For a steel-reinforced strip isolator the effective compression modulus, E_c^s, can be estimated from the following expression [Kelly 1996]:

$$E_c^s = 4GS^2$$

where G is a shear modulus of rubber, S is a shape factor defined through half width of the strip, b, and thickness of single rubber layer, t, as follows

$$S = b / t$$

The experimental study conducted earlier [Kelly and Takhirov 2004] shows the thickness variation of the shims in steel-reinforced bearings does not cause significant variation of the bearing's vertical stiffness. This fact supports the idea of possibility to replace steel shims with a fiber reinforcement that can stretch during vertical loading of the bearing. In the fiber reinforced isolator the effective compression modulus, E_c^f, can be estimated from the following expression [Kelly and Takhirov 2001]:

$$\frac{E_c^f}{4GS^2} = \frac{3}{\alpha^2}\left(1 - \frac{\tanh\alpha}{\alpha}\right)$$

Where the dimensionless parameter α is defined through the tension elastic modulus of the fiber, E_f, and the thickness of the fiber reinforcement, t_f, in the following form

$$\alpha^2 = \frac{12Gb^2}{E_f t_f t}$$

The dimensionless ratio E_c^f / E_c^s for various values of parameter α is presented in Figure 2.

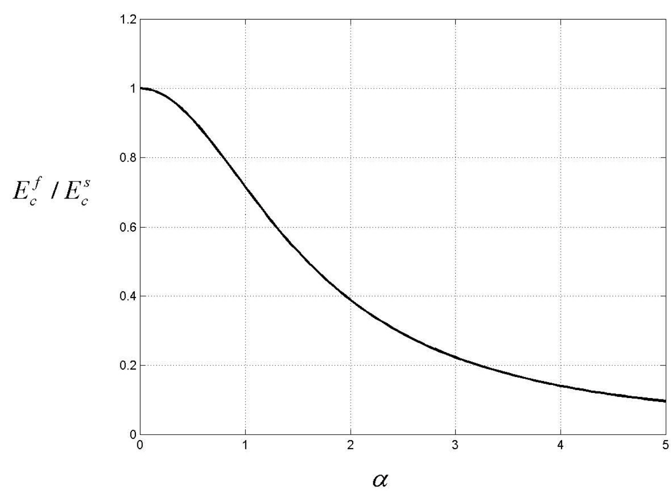

Figure 2 Dimensionless ratio of fiber-reinforced and steel reinforced compression moduli as function of parameter *α*.

ULTIMATE DISPLACEMENT OF UNBONDED BEARINGS

The highly favorable response of an isolator which is not bonded to the top or bottom plates is due to the elimination of tension in the elastomer. In a bonded bearing under the simultaneous action of shear and compression, the presence of an unbalanced moment at both top and bottom surfaces produces a distribution of tensile stresses in the triangular region outside the overlap between top and bottom. The compression load is carried through the overlap area, and the triangular regions created by the shear displacement provide the tensile stresses to balance the moment. These tensile stresses must be sustained by the elastomer and also by the bonding between the elastomer and the steel reinforcement plates. These bonding requirements are the main reason for the high cost of current designs of isolator bearings for buildings. With the elimination of these tension stresses, the bonding requirements for this new type of bearing are reduced.

In these bearings, the steel reinforcing plates are relatively thin as compared to the reinforcing in current designs of building seismic isolators. This flexibility allows the unbonded surfaces to roll off the loading surfaces and thus relieves the tensile stresses that would be produced if the top and bottom surfaces of the bearing were bonded; this in turn puts much lower demands on the internal bonding between elastomer and reinforcing.

The experimental results show that the roll-off response is limited by the fact that the free edge of the bearing rotates from the vertical towards the horizontal with increasing shear displacement, and the limit of this process is reached when the originally vertical surfaces at each side come in contact with the horizontal surfaces at both top and bottom. Further horizontal displacement beyond this point can only be achieved by slip. The friction factor between rubber and other surfaces often can take very large values, possibly as high as 1, and slip can produce damage to the bearing through tearing of the surface distortion of the reinforcing steel and heat generated by the sliding. Thus the maximum displacement for a bearing of this type can be specified as that which transforms the vertical free edge to a horizontal plane. In the normal situation, where the bearing thickness is small in comparison to the plan dimension in the direction of loading, this can be estimated by studying only the deformation of one side and neglecting the interaction between the deformations at each end.

The basic assumptions used in the development of the prediction of the limiting shear deformation are

- the material is incompressible.
- the plates are completely flexible.
- the free surface of the roll-off portion is stress free.

The first two are reasonable for the elastomer and reinforcement of these bearings, and the third means that the displacement when the vertical surface touches the horizontal support is the length of the curved arc of the free surface.

The geometry assumed in the derivation is shown in Figure 3. The thickness of the bearing is 1. We assume that the curved free surface is a parabolic arc, then in the coordinate system x, y shown in the figure, the curved surface is given by

$$y = \frac{x^2}{a^2}; \quad x = a\sqrt{y}$$

The area of the region enclosed by the curved arc of length Δ is

$$A = \int_0^1 \int_0^{a\sqrt{y}} dxdy = \frac{2}{3}a$$

The requirement of compressibility means that the volume before deformation and after is preserved, thus

$$\frac{1}{2}\Delta = \frac{2}{3}a \quad \text{or} \quad a = \frac{3}{4}S$$

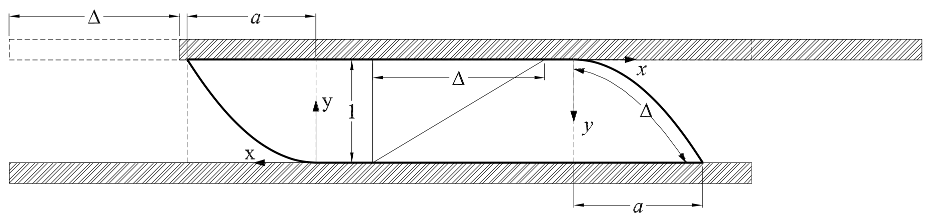

Figure 3 Geometry assumed in the derivation.

The curved arc length Δ is given by

$$d\Delta = \sqrt{dx^2 + dy^2}$$

where

$$dy = \frac{2x}{a^2}dx$$

So

$$\Delta = \int_0^a \sqrt{1 + \left(\frac{2x}{a^2}\right)^2} dx$$

Using the change of variable $u = 2x / a^2$, we have

$$\Delta = \frac{a^2}{2} \int_0^{2/a} \sqrt{1 + u^2} du$$

Let $u = \sinh t$. Then

$$\Delta = \frac{a^2}{2} \int_0^{\sinh^{-1} 2/a} \cosh^2 t \, dt$$

Since $\cosh^2 t = \left(\cosh 2t + 1\right)/2$, this leads to

$$\Delta = \frac{a^2}{4} \left[\sinh t \cosh t + t\right]_0^{\sinh^{-1} 2/a}$$

and with $\cosh t = \sqrt{1+\sinh^2 t}$, we have

$$\Delta = \frac{a^2}{4} \left(\frac{2}{a} \sqrt{1+\frac{4}{a^2}} + \sinh^{-1} \frac{2}{a} \right)$$

The incompressibility condition requires that $\Delta = 4a/3$, leading to an equation for a in the form

$$\sinh^{-1} \frac{2}{a} = \frac{16}{3a} - \frac{2}{a} \sqrt{1+\frac{4}{a^2}}$$

Replacing $2/a$ by t and inverting the equation leads to a transcendental equation for t in the form

$$t = \sinh\left[\left(\frac{8}{3} - \sqrt{1+t^2}\right) t\right]$$

which after solving for t gives a and in turn Δ. The solution to a high degree of accuracy is $t = 1.60$, $a = 1.25$ and $\Delta = 1.67$. This is the overall shear strain. Since the steel will not deform in shear, the shear in the elastomer is increased by the ratio of the total thickness (steel plus rubber) to rubber thickness. For the bearings in this study, the rubber and steel thicknesses are 12 mm and 1.9 mm, respectively. Thus the limiting shear strain based on the thickness of rubber is 1.92.

The conclusion is that in broad terms these bearings with small thickness compared to their plan dimension can experience a displacement of twice the thickness of rubber before they run the risk of damage by sliding. This is quite comparable to the shear maxima usually imposed on building bearings in current practice in the United States although it is somewhat less than that permitted in Japan. It is also worth noting that this is a lower bound to the maximum displacement of the second type of isolator since in that case the reinforcement is not completely flexible, and the small but finite bending stiffness will allow the bearing to displace further.

STABILITY OF HORIZONTAL DISPLACEMENT

The basic premise for the analysis of these bearings is that the regions of the bearing that have rolled off the rigid supports are free of all stress, and that the volume under the contact area has constant shear stress. Under this assumption, the active area that produces the force of resistance F to displacement Δ, is $B-\Delta$ and thus the force (per unit width of the bearing) is $F = G\gamma\left(B-\Delta\right)$, but $\gamma = \Delta / t_r$, thus $F = G\left(B-\Delta\right)\Delta / t_r$, and consequently the force displacement curve has zero slope when

$$\frac{dF}{d\Delta} = \frac{G}{t_r}\left(B-2\Delta\right) = 0, \quad \text{i.e., when } \Delta = B/2$$

The implication of this result is that the bearing remains stable in the sense of positive tangential force-displacement relationship so long as the displacement is less than half the length in the direction of the displacement.

DESIGN CRITERIA FOR FIBER REINFORCED BEARINGS

As a result of the two limiting displacement criteria outlined in the previous two sections, it is possible to determine a simple design criterion for this type of bearing. We need only to determine a maximum required design displacement which normally would depend on the site, the anticipated isolation period and damping. If we denote this by Δ, then the requirement for positive incremental horizontal stiffness requires that the width B of the bearing in the direction of the displacement be at least twice the displacement, i.e., $B \geq 2\Delta$, and the requirement that the vertical faces should not contact the horizontal support surfaces means that the total rubber thickness t_r should be not less than half of the displacement, i.e. $t_r \geq \Delta / 2$.

CONCLUSIONS

This paper has described two potential approaches to the provision of low-cost, light-weight rubber isolation systems. Both types have been extensively tested in laboratory test programs and have also been verified by finite element studies. They both have much less severe bonding requirements than conventional isolators and have the potential of lending themselves to mass production manufacturing, which will be required for any type of retrofit of vulnerable buildings in the urban environment.

The most important aspects of both types of these bearings are that they do not have thick end plates, they are not bonded to the top and bottom support surfaces, and their reinforcement mechanisms are very flexible. These aspects at first sight might seem to be deficiencies of their design, but they in fact have the advantage that they eliminate the presence of tensile stresses in the bearing by allowing it to roll off the supports. This reduces the costly, stringent bonding requirements that are typical for conventional bearings. The weight and the cost of isolators is reduced by using fiber reinforcement or very thin steel reinforcing plates, no end-plates and no bonding to the support surfaces, thereby offering a low-cost light-weight isolation system for retrofit in large cities such as Tehran and Istanbul and also for new housing and public buildings in developing countries.

REFERENCES

Kelly JM (1996). *Earthquake Resistant Design with Rubber*. 2nd ed., London: Springer-Verlag.

Kelly JM, Takhirov SM (2001). Analytical and experimental study of fiber-reinforced strip isolators, *Report No. PEER 2001/11*, Pacific Earthquake Engineering Research Center, University of California, Berkeley, CA.

Kelly JM, Takhirov SM (2004). Experimental study of steel reinforced rubber bearings with various shim thicknesses, *Proceedings*, SEM X International Congress and Exposition on Experimental and Applied Mechanics. Costa Mesa, CA.

Konstantinidis D, Kelly JM, Makris N (2008). Experimental investigations on the seismic response of bridge bearings, *Report No. EERC 2008/02*, Earthquake Engineering Research Center, University of California, Berkeley. CA.

DYNAMIC RESPONSE CONTROL OF BASE ISOLATED STRUCTURES CARRYING CYLINDRICAL LIQUID TANKS VIA FLUID/STRUCTURE INTERACTION

Nader K. A. Attari[1] and Fayaz R. Rofooei[2]

[1] *Structural Engineering Lab, Building and Housing Research Center (BHRC), Tehran, Iran,*
[2]*Department of Civil Engineering, Sharif University of Technology, Tehran, Iran*

ABSTRACT

Dynamic response of a base-isolated system containing a rigid circular cylindrical liquid tank under harmonic excitations is considered in the presence of fluid/structure interaction. The governing differential equations of the system is derived considering the first three liquid sloshing modes (1, 1), (0, 1) and (2, 1) under harmonic excitations. The dynamic response of the system is investigated in the neighborhood of 1:2 and 1:1 internal resonance between the first mode of base isolated system and the first asymmetric liquid sloshing mode. The efficiency of the liquid sloshing modes in reducing the maximum seismic response of the base isolated system is numerically demonstrated. Additionally, the transfer of energy from the structure to liquid due to nonlinear interaction is investigated.

INTRODUCTION

The application of sloshing-induced hydrodynamic forces to control the dynamic response of structures has been explored during the last few decades. Different types of nonlinear interactions could exist for a liquid tank placed on an elastic structure. The interaction of liquid sloshing modes with the modes of the supporting structure that is of highest interest, could lead to different types of free liquid surface motion exhibiting energy exchange between the interacting modes. Therefore, the fluid/structure resonances can be used as a mean to reduce the vibration of different structural system such as satellites, towers and tall buildings.

Various analytical and computational models have been proposed for the dynamic behavior of shallow and deep water containers mounted on the top floor of different building structures. Applications of tuned liquid dampers (TLD) in controlling the response of tall building structures have been investigated by various researchers. Modi and Munshi [1998] used a barrier for increasing the energy dissipation in a rectangular TLD system. Kaneko et al. [1999] presented an analytical model describing the effectiveness of Deep water rectangular and cylindrical TLDs (DTLD) with a submerged net for the horizontal response reduction of structural system. Ibrahim et al. [1988; 2005] examined the nonlinear interaction in the elevated water tanks subjected to vertical sinusoidal ground motion in the neighborhood of internal resonances. They showed that the liquid sloshing modes and the vibrating modes of the supporting structure were coupled through inertial nonlinearity. This nonlinearity can be generated through the presence of the concentrated or distributed masses in the equations of motion, or in the boundary conditions, depending on the coordinate system used and the orientation of the body forces such as gravity. Free surface condition in fluids is considered to be a nonlinear boundary condition [Ikeda and Ibrahim 2005]. Also, the acceleration of the fluid particles includes a nonlinear convective term as well.

The internal resonance among the interacting modes caused by inertial nonlinearity can be determined using the condition $\sum_{j=1}^{n} k_j \omega_j = o$, in which k_j is an integer and ω_j is the j^{th} natural frequency of the coupled fluid/structural modes. Ibrahim showed that the dynamic response of a system such as elevated water tank, subjected to vertical excitation, and under parametric resonance of the first normal mode, would behave as a hard nonlinear system [Ibrahim et al. 1988]. However, upon the parametric excitation of the second normal mode, the system would perform as a soft nonlinear model. They also studied the random response characteristics of an elevated water tower subjected to wide band random excitation. They showed that at certain internal resonance cases, the nonlinear modal interaction would happen, leading to energy exchange between the normal modes [Ibrahim 2005]. On the other hand, various issues such as modal couplings, modal saturation, and transfer of energy among different modes should be considered in nonlinear modeling.

The random vertical excitation of an elastic structure carrying a cylindrical liquid tank has been numerically studied by Ikeda and Ibrahim. They demonstrated that the liquid motion can act as a nonlinear vibration absorber of the structure response over a narrowband of the excitation frequency [Ikeda and Ibrahim 2005]. Ikeda and Murakami investigated the influences of the liquid level and a detuning parameter on the theoretical resonance curves. They showed that the frequency response curves depend on the liquid level and a small deviation of the tuning condition may cause amplitude and phase modulated motions and chaotic vibrations [Ikeda and Murakaim 2005].

Attari and Rofooei studied the lateral response of a SDOF structural system containing a rigid circular cylindrical liquid tank, under harmonic and earthquake excitations. They showed the efficiency of the sloshing modes of cylindrical tanks in reducing the seismic response of the SDOF system to a large extent, especially when the fundamental frequency of the SDOF system is close to the dominant earthquake excitation frequency. They also observed the transfer of energy from structure to liquid due to nonlinear interaction and showed that considering three sloshing modes are necessary for having accurate results. [Attari et al. 2008; Roffoei and Attari 2008].

In this study, the nonlinear interaction between a base isolated structural model carrying a circular cylindrical liquid tank and the sloshing modes of the liquid is investigated. Response of this model under horizontal harmonic excitation is studied considering three sloshing modes in the neighborhood of 1:2 internal resonances. In addition, energy transfer from the structure's fundamental mode to the first unsymmetrical sloshing mode of liquid is investigated for this system.

GOVERNING DIFFERENTIAL EQUATIONS OF MOTION

A SDOF system resting on a base isolation system is considered. The SDOF system could be assumed as a representation of the dominant mode of a more general MDOF system, as we are concern with the internal resonances between the fundamental structural mode and the liquid sloshing modes. Using base isolation system makes the fundamental natural mode of the whole system even more dominant (larger effective modal mass).

A circular cylindrical tank with liquid depth *h* and radius *R*, is placed on the SDOF system as it is shown in Figure 1. The liquid is assumed to be irrotational, non-viscous and incompressible. The effect of wave breaking caused by intense excitation is ignored in this study. Thus, the governing differential equation of motion for the liquid becomes the Laplace equation. Also, equivalent linear viscous damping term is considered in the decoupled equations of motion of the first 3 sloshing modes of the liquid.

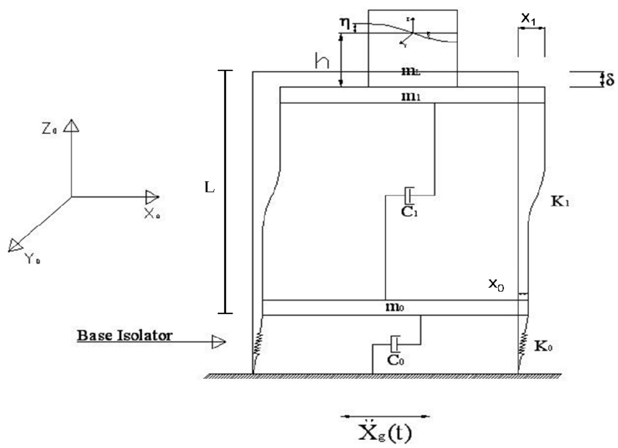

Figure 1 The base isolated structural model with the cylindrical tank and the used coordinate systems.

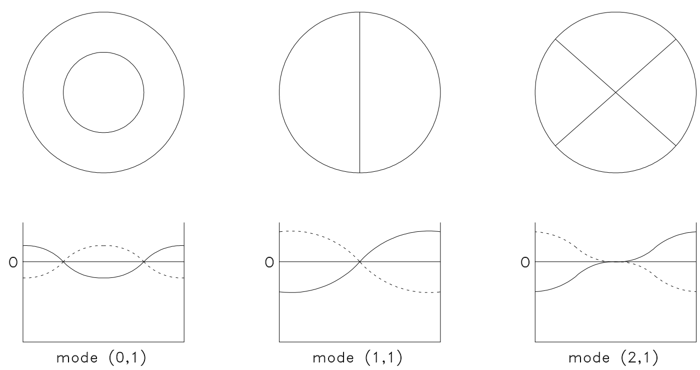

Figure 2 The first three sloshing modes considered in this study.

A Cartesian system of coordinates (*x,y,z*) is considered for the base-isolated structural system, while a cylindrical (r,θ,z) system of coordinates on the free surface of liquid is assumed for the liquid as it is shown in Figure 1. The wave amplitude with respect to the liquid stationary level h in any location(r,θ) is represented by η. The tank is assumed to be rigid and the effects of the first three sloshing modes are considered in this study. The previous experimental studies have shown that if the first asymmetric sloshing mode (1,1) be assumed as the primary mode, then the (0,1) and (2,1) sloshing modes shown in Figure 2 are considered to be of second order. The other sloshing modes, as Equation 1 shows, are of higher orders, thus their effects in problem formulation can be neglected [Attari and Roffoei 2008]:

$$a_{11},\alpha_{11}=\mathrm{O}(\eta) \quad a_{01},\alpha_{01},a_{21},\alpha_{21}=\mathrm{O}(\eta^2) \quad a_{mn},\alpha_{mn}=\mathrm{O}(\eta^m) \tag{1}$$

where, α_{mn} and a_{mn} are the modal amplitude of the liquid wave and velocity potential function respectively. The *m and n* indicate the number of diametric nodal lines and the number of nodal concentric circles correspondingly. Also, x_0 and x_1 are the relative lateral displacements of the base isolation and the structural system respectively.

Application of Newton's second law to the liquid particle in a non-viscous liquid leads to:

$$\frac{\partial\varphi}{\partial t}+\frac{1}{2}\left\{\left(\frac{\partial\varphi}{\partial r}\right)^2+\frac{1}{r^2}\left(\frac{\partial\varphi}{\partial\theta}\right)^2+\left(\frac{\partial\varphi}{\partial z}\right)^2\right\}+\frac{p}{\rho}+(g-\ddot{\delta})z+\ddot{x}_0 r\cos\theta=0 \tag{2}$$

where ρ, P. and φ are the liquid's density, pressure and velocity potential, respectively. The governing differential equation of motion for an incompressible liquid is the Laplace equation:

$$\nabla^2\varphi=0 \;\Rightarrow\; \frac{\partial^2\varphi}{\partial r^2}+\frac{1}{r}\frac{\partial\varphi}{\partial r}+\frac{1}{r^2}\frac{\partial^2\varphi}{\partial\theta^2}+\frac{\partial^2\varphi}{\partial z^2}=0 \tag{3}$$

Also, the differential equation of the motion for base isolated system is:

$$m_0\ddot{x}_0+(k_0+k_1)x_0-k_1x_1+(c_1+c_0)\dot{x}_0-c_1\dot{x}_1=-m_0\,\ddot{x}_g(t) \tag{4}$$

$$(m_1+m_L)\ddot{x}_1+\frac{36}{25l^2}x_1(\dot{x}_1^{\,2}+x_1\ddot{x}_1)+c_1\dot{x}_1-c_1\dot{x}_0+k_sx_1-k_sx_0=F_L-(m_1+m_L)\ddot{x}_g(t) \tag{5}$$

Where, m_0, k_0, c_0 and m_1, k_1, c_1 are the mass, stiffness and damping constant of the base isolation system and the structural system respectively. Also,

$$k_s=k_1-k_f=k_1-\frac{6}{5L}Mg \quad , M=m_1+m_L \tag{6}$$

Where k_s is the effective stiffness of the structure, and the k_f represents the stiffness reduction due to vertical displacement of structural mass. F_L shows the hydrodynamic force acting along the tank's walls and can be determined by integrating the liquid pressure distribution over the related wall surface.

$$F_L=\int_0^{2\pi}\int_{-h}^{0}R.P(r,\theta,z,t)\Big|_{r=R}.\cos\theta.\,d\theta\,dz+\int_0^{2\pi}R[\eta.P(R,\theta,0)+\frac{\eta^2}{2}.P_z(R,\theta,0)+O(\eta^4)].\cos\theta.d\theta \tag{7}$$

BOUNDARY CONDITIONS

The relative velocity of the liquid along the walls and the bottom of the rigid tank is equal to:

$$\left.\frac{\partial\varphi}{\partial r}\right|_{r=R}=0 \qquad \left.\frac{\partial\varphi}{\partial z}\right|_{z=-h}=0 \tag{8}$$

The kinetic boundary condition at the liquid surface level is:

$$\frac{\partial n}{\partial t}=\frac{\partial\varphi}{\partial z}-\frac{\partial\varphi}{\partial r}\frac{\partial n}{\partial r}-\frac{1}{r^2}\frac{\partial\varphi}{\partial\theta}\frac{\partial n}{\partial\theta} \tag{9}$$

meaning that the vertical component of the liquid surface velocity be equal to the vertical velocity of the liquid particle on the liquid surface. Also, at the free surface ($z=\eta$) the pressure is equal to zero. Therefore:

$$\frac{\partial\varphi}{\partial t}+\frac{1}{2}\left\{\left(\frac{\partial\varphi}{\partial r}\right)^2+\frac{1}{r^2}\left(\frac{\partial\varphi}{\partial\theta}\right)^2+\left(\frac{\partial\varphi}{\partial z}\right)^2\right\}+(g-\ddot{\delta})\eta=\ddot{x}_0 r\cos\theta \tag{10}$$

NON-DIMENSIONALIZING THE EQUATIONS OF MOTION

The equations of motions, i.e., Equations (2) through (4), with the related boundary conditions provided by Equations (6) though (8), are non-dimensionalized for parametric studies, using the following parameters:

$$\begin{aligned}
&\bar{x}_0=\frac{x_0}{R}\quad \bar{x}_1=\frac{x_1}{R}\quad \bar{r}=\frac{r}{R}\quad M=m_1+m_L\quad \bar{h}=\frac{h}{R}\\
&\bar{z}=\frac{z}{R}\quad \bar{\eta}=\frac{\eta}{R}\quad \mu_1=\frac{m_1}{M}\quad \mu_2=\frac{m_L R}{\pi M h}\quad \mu_3=\frac{m_0}{M}\\
&\bar{\varphi}=\frac{\varphi}{R^2\omega_{11}}\quad m_L=\pi\rho R^2 h\quad \bar{l}=\frac{L}{R}\quad \bar{\delta}=\frac{\delta}{R}\quad \zeta_1=\frac{c}{M\,\omega_{11}}\\
&\zeta_0=\frac{c_0+c_1}{M\,\omega_{11}}\quad \bar{k}_0=\frac{k_0}{M\,\omega_{11}^2}\quad \bar{k}_1=\frac{k_1}{M\,\omega_{11}^2}\quad \bar{p}=\frac{p}{\rho R^2\omega_{11}^2}\\
&\tau=\omega_{11}t\quad \varepsilon_{mn}=\lambda_{mn}R\quad \Omega=\frac{\Omega_0}{\omega_{11}}\quad \bar{\ddot{x}}_g=\frac{\ddot{X}_g}{MR\omega_{11}^2}\\
&f_L=\frac{F_L}{mR\omega_{11}^2}\quad \omega=\frac{\omega_{mn}}{\omega_{11}}\quad \bar{\omega}_{11}=1
\end{aligned} \tag{11}$$

in which, m_L and M are the liquid mass and total mass of the system, respectively. The parameter ω_{11} is the first unsymmetrical liquid frequency defined as:

$$\omega_{11}^2=\frac{g\,\varepsilon_{11}}{R}\tanh\left(\varepsilon_{11}\frac{h}{R}\right) \tag{12}$$

Also, λ_{mn} is the n*th* positive root of the derivative of Bessel function $\left.\frac{\mathrm{d}J_m(\lambda_{mn}r)}{\mathrm{d}r}\right|_{r=R}=0$.

SOLVING THE DERIVED DIFFERENTIAL EQUATIONS

One could solve the Laplace equation, Equation (3), with the boundary conditions given by Equation (8). Using the linear part of Equation (9) for calculating η, expanding Equations (9) and (10) around $\eta=0$ and equating the coefficients of $J_0(\varepsilon_{01}r)$, $J_1(\varepsilon_{11}r)\cos\theta$ and $J_2(\varepsilon_{21}r)\cos 2\theta$ to zero, and finally omitting the redundant parameters a_{11}, a_{01}, a_{21} from equations would result in the following five governing differential equations for the system. The bar sign (-) is omitted from all parameters for simplicity. As it was mentioned before, a viscous modal damping coefficient was considered for the sloshing modes.

$$\mu_3 \ddot{x}_0 + (k_0 + k_1)x_0 - k_1 x_1 + \zeta_0 \dot{x}_0 - \zeta_1 \dot{x}_1 = -\mu_3 \ddot{x}_g (t) \tag{13}$$

$$\begin{aligned}
& G_0 \ddot{x}_1 + \frac{36}{25l^2} x_1 ({\dot{x}_1}^2 + x_1 \ddot{x}_1) + k_1 x_1 - k_1 x_0 + \frac{G_2}{\psi_{11}} \ddot{\alpha}_{11} + \zeta_1 \dot{x}_1 - \zeta_1 \dot{x}_0 + G_2 S_2 \ddot{\alpha}_{01} + G_2 S_3 \ddot{\alpha}_{21} \\
& + G_2 S_6 \ddot{\alpha}_{11} \alpha_{11} + G_2 S_6 {\dot{\alpha}_{11}}^2 + \left(\frac{G_3}{\psi_{01} \psi_{11}} + (S_4 + S_7) G_2 \right) \dot{\alpha}_{01} \dot{\alpha}_{11} + \left(\frac{G_4}{\psi_{21} \psi_{11}} + (S_5 + S_8) G_2 \right) \dot{\alpha}_{21} \dot{\alpha}_{11} \\
& + \left(\frac{G_3 Q_{21}}{\psi_{01} {\psi_{11}}^2} + \frac{G_4 Q_{22}}{\psi_{21} {\psi_{11}}^2} + 2S_9 G_2 \right) \alpha_{11} {\dot{\alpha}_{11}}^2 + G_2 S_4 \ddot{\alpha}_{01} \alpha_{11} + G_2 S_5 \ddot{\alpha}_{21} \alpha_{11} + G_2 S_7 \ddot{\alpha}_{11} \alpha_{01} \\
& + G_2 S_8 \ddot{\alpha}_{11} \alpha_{21} + G_2 S_9 \ddot{\alpha}_{11} {\alpha_{11}}^2 + G_5 \frac{\alpha_{11}^2 \ddot{\alpha}_{11}}{\psi_{11}} + G_6 \frac{\alpha_{11} \dot{\alpha}_{11}^2}{\psi_{11}^2} = -\ddot{x}_g (t)
\end{aligned} \tag{14}$$

$$\begin{aligned}
& \ddot{\alpha}_{11} + {\omega_{11}}^2 \alpha_{11} + G_1 \psi_{11} \ddot{x}_1 + 2\zeta_{11} \dot{\alpha}_{11} (t) + G_1 \psi_{11} [\ddot{x}_g (t) + \frac{36}{25l^2} x_1 ({\dot{x}_1}^2 + x_1 \ddot{x}_1)] \\
& - \frac{6}{5l} ({\dot{x}_1}^2 + x_1 \ddot{x}_1) \alpha_{11} + \psi_{11} S_6 {\dot{\alpha}_{11}}^2 + \psi_{11} S_2 \ddot{\alpha}_{01} + \psi_{11} S_3 \ddot{\alpha}_{21} + \psi_{11} S_6 \ddot{\alpha}_{11} \alpha_{11} + \\
& \left(\frac{Q_4}{\psi_{01}} + S_4 \right) \psi_{11} \alpha_{11} \ddot{\alpha}_{01} + \left(\frac{Q_{21} Q_4}{\psi_{01}} + \frac{Q_{22} Q_7}{\psi_{21}} + Q_8 + \psi_{11} S_9 \right) \ddot{\alpha}_{11} {\alpha_{11}}^2 + \left(\frac{Q_9}{\psi_{01}} + \psi_{11} (S_4 + S_7) \right) \dot{\alpha}_{01} \dot{\alpha}_{11} \\
& + (Q_5 + S_7 \psi_{11}) \ddot{\alpha}_{11} \alpha_{01} \left(\frac{Q_{21} Q_4}{\psi_{01}} + \frac{Q_{22} Q_7}{\psi_{21}} + \frac{Q_{22} Q_{10}}{\psi_{21} \psi_{11}} + \frac{Q_{11}}{\psi_{11}} + \frac{Q_9 Q_{21}}{\psi_{01} \psi_{11}} + 2S_9 \psi_{11} \right) \alpha_{11} {\dot{\alpha}_{11}}^2 \\
& + (Q_6 + S_8 \psi_{11}) \ddot{\alpha}_{11} \alpha_{21} + \left(\frac{Q_7}{\psi_{21}} + S_5 \right) \psi_{11} \ddot{\alpha}_{21} \alpha_{11} + \left(\frac{Q_{10}}{\psi_{21}} + \psi_{11} (S_5 + S_8) \right) \dot{\alpha}_{21} \dot{\alpha}_{11} = 0
\end{aligned} \tag{15}$$

$$\begin{aligned}
& \ddot{\alpha}_{01} + {\omega_{01}}^2 \alpha_{01} + 2\zeta_{01} \omega_{01} \alpha_{01} (t) - \frac{6}{5l} ({\dot{x}_1}^2 + x_1 \ddot{x}_1) \psi_{01} \alpha_{01} + \left(\frac{Q_{21} + \psi_{01} Q_{12}}{\psi_{11}} \right) \alpha_{11} \ddot{\alpha}_{11} \\
& + (Q_{21} + Q_{12} \psi_{01}) S_6 \ddot{\alpha}_{11} \alpha_{11}^2 + \left(\frac{Q_{21}}{\psi_{11}} + \frac{Q_{13} \psi_{01}}{{\psi_{11}}^2} \right) {\dot{\alpha}_{11}}^2 + (Q_{21} + Q_{12} \psi_{01}) S_2 \alpha_{11} \ddot{\alpha}_{01} \\
& + (Q_{21} + Q_{12} \psi_{01}) S_3 \alpha_{11} \ddot{\alpha}_{21} + \left(Q_{21} S_2 + \frac{2S_2 Q_{13} \psi_{01}}{\psi_{11}} \right) \dot{\alpha}_{11} \dot{\alpha}_{01} \\
& + \left[(Q_{21} + Q_{12} \psi_{01}) S_6 + S_6 Q_{21} + \frac{2S_6 Q_{13} \psi_{01}}{\psi_{11}} \right] \alpha_{11} {\dot{\alpha}_{11}}^2 + \left(Q_{21} S_3 + \frac{2S_3 Q_{13} \psi_{01}}{\psi_{11}} \right) \dot{\alpha}_{11} \dot{\alpha}_{21} = 0
\end{aligned} \tag{16}$$

$$\begin{aligned}
& \ddot{\alpha}_{21} + {\omega_{21}}^2 \alpha_{21} + 2\zeta_{21} \omega_{21} \alpha_{21} (t) - \frac{6}{5l} ({\dot{x}_1}^2 + x_1 \ddot{x}_1) \psi_{21} \alpha_{21} + \left(\frac{Q_{22} + \psi_{21} Q_{14}}{\psi_{11}} \right) \alpha_{11} \ddot{\alpha}_{11} \\
& + (Q_{22} + Q_{14} \psi_{21}) S_6 \ddot{\alpha}_{11} \alpha_{11}^2 + \left(\frac{Q_{22}}{\psi_{11}} + \frac{Q_{15} \psi_{21}}{{\psi_{11}}^2} \right) {\dot{\alpha}_{11}}^2 + (Q_{22} + Q_{14} \psi_{21}) S_2 \alpha_{11} \ddot{\alpha}_{01} \\
& + (Q_{22} + Q_{14} \psi_{21}) S_3 \alpha_{11} \ddot{\alpha}_{21} + \left(Q_{22} S_2 + \frac{2S_2 \psi_{21} Q_{15}}{\psi_{11}} \right) \dot{\alpha}_{11} \dot{\alpha}_{01} \\
& + \left[(Q_{22} + \psi_{21} Q_{14}) S_6 + Q_{22} S_6 + \frac{2S_6 Q_{15} \psi_{21}}{\psi_{11}} \right] \alpha_{11} {\dot{\alpha}_{11}}^2 + \left(Q_{22} S_3 + \frac{2S_3 Q_{15} \psi_{21}}{\psi_{11}} \right) \dot{\alpha}_{21} \dot{\alpha}_{11} = 0
\end{aligned} \tag{17}$$

All the coefficients are defined in Appendix I. Equations (13) to (17) can be numerically solved to obtain the responses of the base isolated structural system and the amplitude of liquid sloshing modes.

MODEL VERIFICATION

Part of Kaneko and Mizota's [2000] work in analyzing the DTLD system is considered here to verify the accuracy of the derived equations of motion. They investigated the harmonic response of a liquid tank with and without submerged net with a number of shaking table tests. Figure 3a, shows the test result of the rigid tank without submerged net (*h/R* =0.3, *R*=0.48 m, $\Omega \approx \omega_{11}$, excitation amplitude = 0.0033 m, $\omega_{11} = 4.34708$ rad/sec), while Figure 3b shows the results obtained from numerical solution of the derived equations, using the same tank size and excitation parameters. That was achieved by largely increasing the stiffness of the structural system and base isolation, so that they behave as a rigid support for the liquid tank, and adjusting the coefficients of the derived equations to the first liquid sloshing frequency of the tank under the shaking table test. As the results show, the proposed mathematical model can accurately capture the beating phenomena and the liquid wave amplitude.

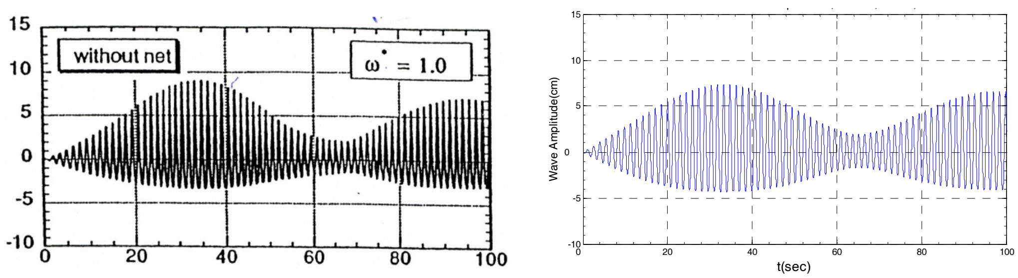

(a) (b)

Figure 3 Comparison of the sloshing wave amplitude obtained from the mathematical model with those from the shaking table test for h/R =0.3, *R*=0.48 m, $\Omega \approx \omega_{11}$, excitation amplitude=0.0033 m, $\omega_{11} = 4.34708$ rad/sec): (a) shaking table test [Kaneko and Mizota 2000]; and (b) the response obtained in this study.

NUMERICAL EXAMPLE

For the numerical part, the derived governing differential equations of motion are parametrically analyzed using MATLAB 7.0 software subject to harmonic excitation input at the internal resonance cases of 1:2 and 1:1 (between the first mode of base isolated system and the first liquid sloshing mode). The study is carried out for liquid mass ratio m_L=0.1*M*, and the height to tank radius ratio *h/R*=1.

The response of elastic base isolated SDOF system carrying the liquid tank is compared with those for the case of base isolated system alone. This study is performed for two damping coefficients of %2 and %0.5 of the elastic system. In addition, the modal damping coefficients of the liquid sloshing modes, ε_0, ε_1 and ε_2 are all considered to be equal to %1. Analyses have been carried out for two level of the non-dimensional external excitation $\left[f = \dfrac{F_0}{M\,\omega_{11}^2 R^2} \quad \text{and} \quad \ddot{X}_g(t) = f\cos(\omega t) \right]$. The m_0 and k_0, mass and stiffness of base isolation system is assumed to be 0.1M and 0.1k_1 .

Harmonic Excitation (Resonance case 1:2)

In this resonance case, the frequencies of the coupled system are determined from the following equations that are the linear part of the governing differential equations of the system (Equations 13-17) by omitting the higher order terms.

$$G_7\,\ddot{x}_0 + (k_0 + k_1)x_0 - k_1 x_1 = 0 \tag{18}$$

$$G_0\,\ddot{x}_1 + k_1\,x_1 - k_1\,x_0 + \frac{G_2}{\psi_{11}}\ddot{\alpha}_{11} = 0 \tag{19}$$

$$\ddot{\alpha}_{11} + \omega_{11}{}^2\,\alpha_{11} + G_1\,\psi_{11}\,\ddot{x}_{11}\ddot{x}_1 = 0 \tag{20}$$

The non-dimensional natural frequencies of the base isolated system without the liquid tank are $\omega_{1S} = 1.9320$, $\omega_{2S} = 23.0219$, while, the frequencies of the base-isolated system with liquid tank would change to: $\omega_{11} = 0.9929$, $\omega_{2S} = 1.9858$, $\omega_{3S} = 23.0622$ in which ω_{11} is the first asymmetric sloshing frequency. One should observe the slight shift in natural frequencies of the base isolated structure that could change their overall seismic response. However, the objective of current study is to examine the effect of possible internal resonances between the structural and sloshing modes of the system on its dynamic response under harmonic excitation. Since any structural response reduction is due to the energy transfer from structural modes to liquid sloshing modes, thus an increase in the amplitude of liquid sloshing modes would be expected. The external excitation frequency Ω is assumed to be equal to the first system's natural frequency ω_{1S}, and twice the frequency of the first sloshing mode of the liquid, i.e., $2 \times \omega_{11} = 2 \times 0.9929 = 1.9858$. The non-dimensional external excitation amplitudes are considered to be $f = 0.005$ and 0.01 for 2 different loading cases.

Figure 4 shows the response of the SDOF system and the base isolator (x_1 and x_0), the wave amplitude η at one of the tank sides, and their Fourier amplitude for the case of $f_0 = 0.005$ and $\xi = 0.02$. As the Figure 4b, Figure 4d, and Figure 4f indicate, there is a peak in the Fourier amplitude of the structural response at a frequency equal to the half of the excitation frequency, and the energy transferred from structural modes to liquid mode due to nonlinear interaction.

Figure 5 compares the structural response of the base-isolated system with and without liquid tank for $f_0 = 0.005$ and $\xi = 0.02$. As it is shown, using a liquid tank with 1:2 frequency ratio clearly reduces the structural response, with part of the seismic energy being transferred to the system. Table 1 also shows the comparison of the structural response of the base isolated system with and without tank under different damping ratios and excitation intensities.

As one can see from Table 1, structural responses are reduced around 40% for different damping ratios and excitation levels due to energy transfer to the liquid. The results indicate that the system works even better under tense external excitation. But, in some cases the wave heights become larger than *0.7h,* in which the wave breaking could occur, and the derived equations would not be valid anymore. However, although the computed structural response amplitude would not correct if the wave breaking occurs, but in reality the structural response would be reduced even more due to larger amount of dissipated energy caused by wave breaking.

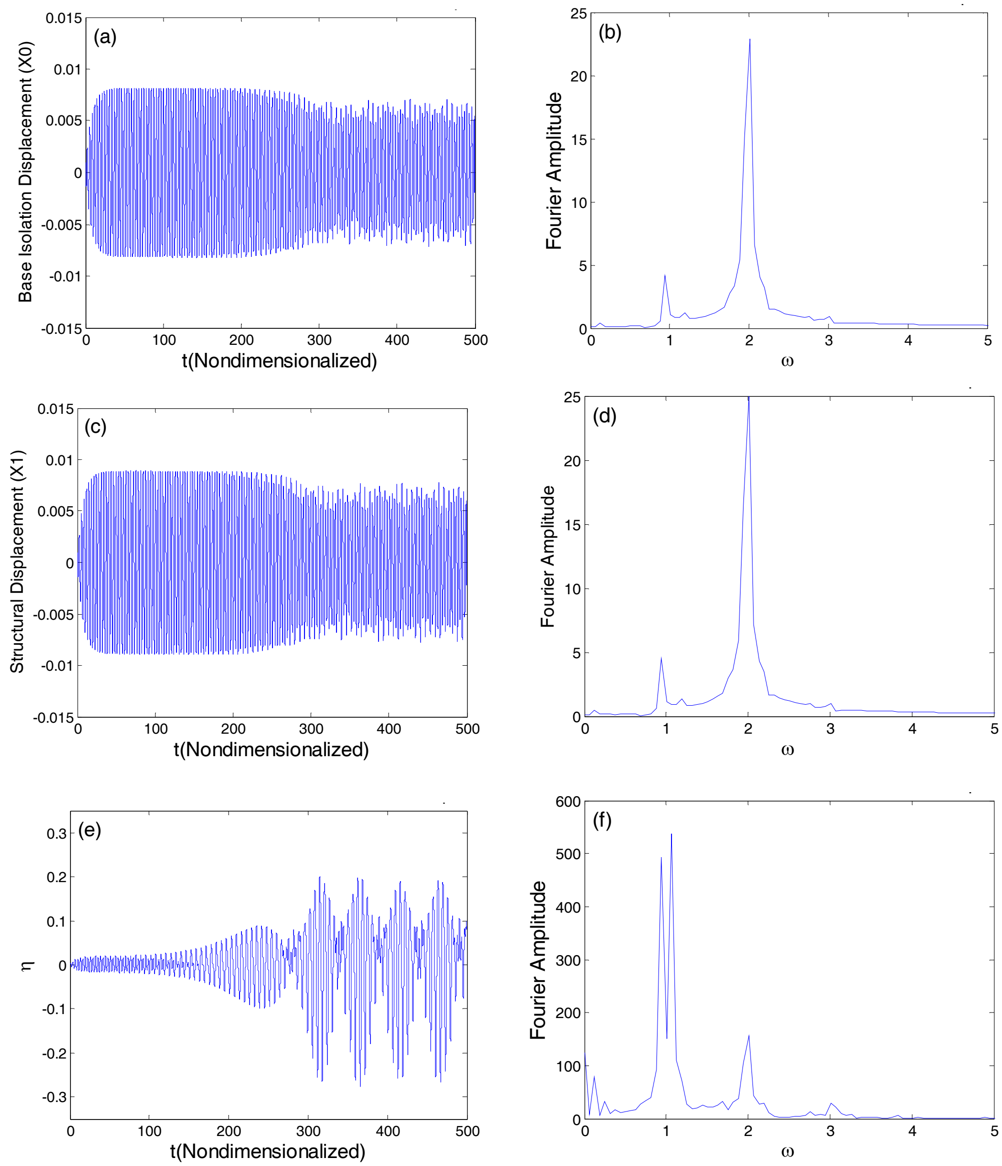

Figure 4 The response parameters of the base isolated system at 1:2 resonance case with f_0=0.005 and ,ξ=0.02. (a) base isolator displacement x_0 ; (b) Fourier amplitude of x_0; (c) displacement of structure x_1 ; (d) Fourier amplitude of x_1 ; (e) liquid wave amplitude η, and (f) Fourier amplitude of η.

The obtained results show that the combination of DTLD and base isolation system could resolve the concern over the large lateral displacements of base isolated structural systems to a large extent.

Harmonic Excitation (Resonance case 1:1)

In this resonance case, the main frequency of isolated structure ω_{1s}, the first asymmetric liquid sloshing mode ω_{11}, and excitation frequency are assumed to be equal, i.e.,

$\omega_{11} = \omega_{1s} = \Omega$. Thus, the system response parameters are determined for the same level of system damping and the excitation forces as the case with 1:2 resonance state. As Table 2 indicates, in this resonance case around 80% reductions in different structural response parameters is achieved that is mainly due to shift in frequencies. However, in case of seismic input, the results would highly be depended on the frequency content of the earthquake records that in turn are influenced by the soil type and site-to-source distance. Also, the results show that the system effectiveness is slightly better for lower level of excitations and structural damping.

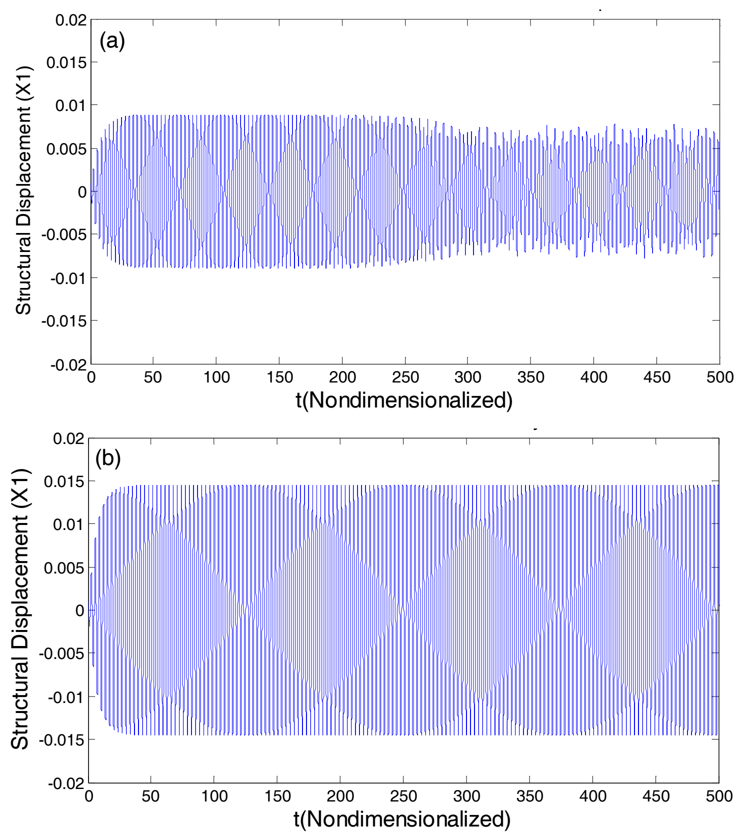

Figure 5 Comparison of structural response under harmonic excitation for 1:2 resonance case and f_0=0.005 *and* ,ξ=0.02: (a) base-isolated system with tank; and (b) base-isolated system without tank.

Table 1 **Comparison of maximum response parameters under harmonic excitation for resonance case 1:2 ($2\omega_{11}=\omega_{1s}=\Omega$) for base-isolated structure with and without tank.**

Harmonic Excitation-Resonance Case 1:2—Base Isolated Structure *h/R*=1, m_L=0.1M									
Model Properties		Response Parameters						Reduction (%)	
		x_0	x_1	η	α_{11}	α_{01}	α_{21}	x_0	x_1
$f=0.005$ $\xi=\%2$	Structure with Tank	0.0082	0.0090	0.2768	0.3284	0.1291	0.1976	38.3	37.9
	Structure without Tank	0.0133	0.0145	-	-	-	-	-	–
$f=0.005$ $\xi=\%0.5$	Structure with Tank	0.0310	0.0339	0.6268	0.7259	0.4607	0.9522	41.6	41.5
	Structure without Tank	0.0531	0.0579	-	-	-	-	-	–
$f=0.01$ $\xi=\%2$	Structure with Tank	0.0164	0.0179	0.3742	0.5000	0.1844	0.2987	38.5	38.3
	Structure without Tank	0.0267	0.0290	-	-	-	-	-	–
$f=0.01$ $\xi=\%0.5$	Structure with Tank	0.0687	0.0750	1.4651	1.9849	1.4651	1.5050	(wave breaking)	
	Structure without Tank	0.1062	0.1159	-	-	-	-	-	–

Table 2 **Comparison of maximum response parameters at harmonic excitation for resonance case 1:1 ($\omega_{11}=\omega_{1s}=\Omega$) for the base-isolated structure with and without rank.**

Harmonic Excitation- Resonance Case 1:1—Base Isolated Structure, *h/R*=1, m_L=0.1M									
Model Properties		Response Parameters						Reduction (%)	
		x_0	x_1	η	α_{11}	α_{01}	α_{21}	x_0	x_1
$f=0.002$ $\xi=\%2$	Structure with Tank	0.0075	0.0082	0.1209	0.1815	0.0296	0.0126	88.7	88.7
	Structure without Tank	0.0665	0.0726	-	-	-	-	-	-
$f=0.002$ $\xi=\%0.5$	Structure with Tank	0.0084	0.0092	0.1347	0.1990	0.0349	0.0149	96.7	96.7
	Structure without Tank	0.2532	0.2784	-	-	-	-	-	-
$f=0.005$ $\xi=\%2$	Structure with Tank	0.0331	0.0361	0.2381	0.3001	0.1350	0.0381	80.1	80.1
	Structure without Tank	0.1664	0.1816	-	-	-	-	-	-
$f=0.005$ $\xi=\%0.5$	Structure with Tank	0.0785	0.0860	1.5633	1.2076	0.9938	2.8584	(wave breaking)	
	Structure without Tank	0.6637	0.7245	-	-	-	-	-	-

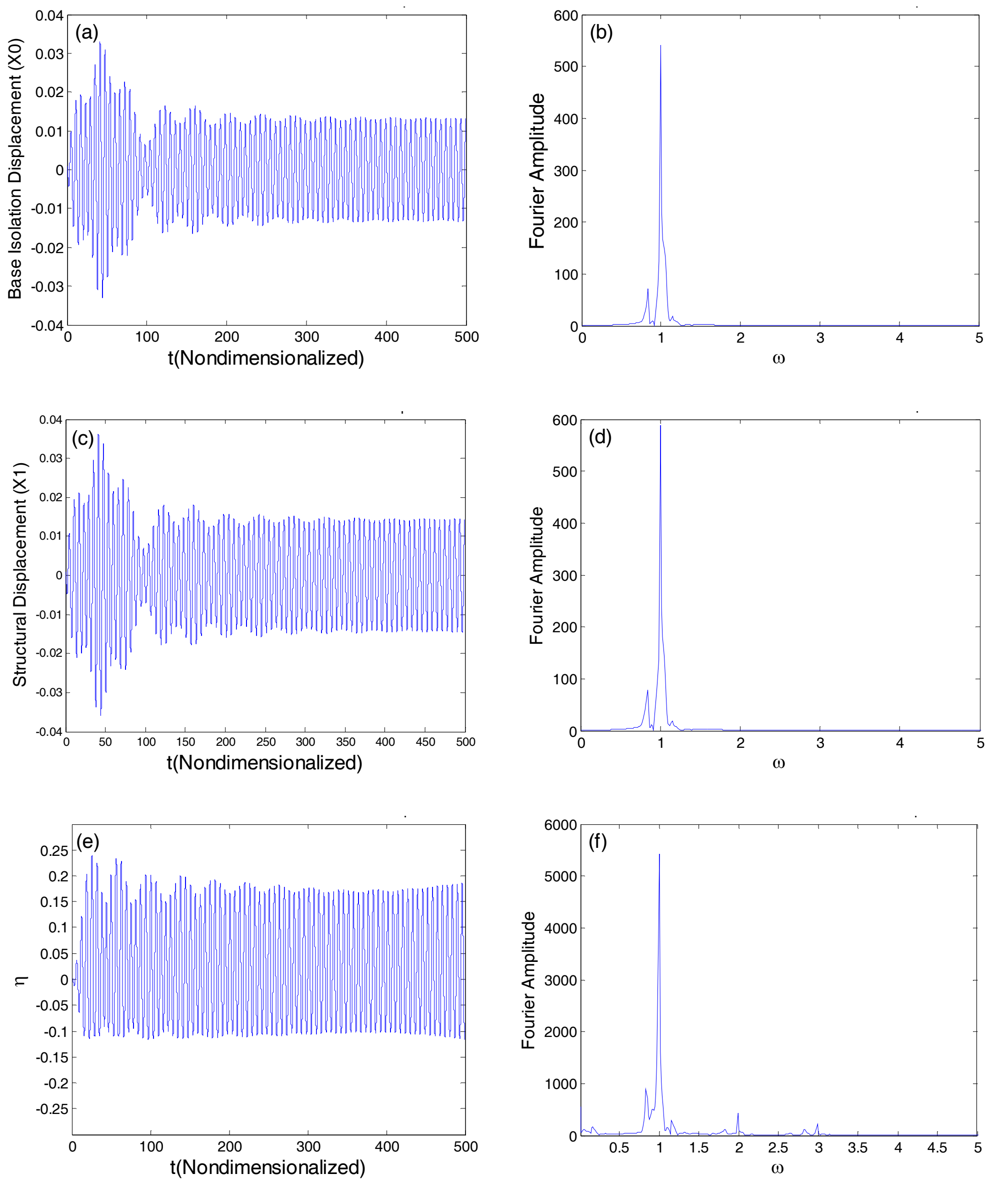

Figure 6 The response parameters of the base-isolated system at 1:1 resonance case with $f_0 = 0.005$, and ξ=0.02: (a) base isolator displacement x_0; (b) Fourier amplitude of x_0; (c) displacement of structure x_1; (d) Fourier amplitude of x_1; (e) liquid wave amplitude η; and (f) Fourier amplitude of η.

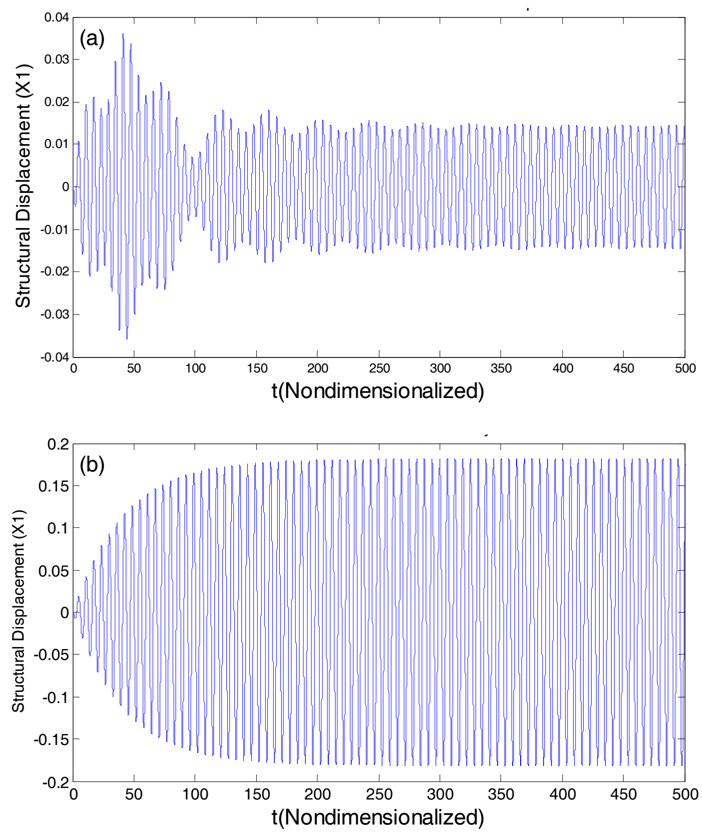

Figure 7 Comparison of structural response under harmonic excitation at 1:1 resonance case and f_0=0.005, ξ=0.02: (a) base-isolated system with tank; and (b) base-isolated system without tank.

CONCLUSIONS

The governing differential equations of motion of an elastic base isolated structural system containing a liquid cylindrical tank are presented. These equations are numerically solved for harmonic excitation input at internal resonance cases 1:2 and 1:1. The study is carried out for different structural damping ratios ξ, and external excitation amplitudes f_0. It is shown that at 1:2 resonance case, the structural response parameters are largely reduced for different damping ratios and excitation amplitudes. The Fourier amplitude of the displacement of the base-isolated structure clearly shows the transfer of energy from the base isolated structural system to the liquid due to the nonlinear interaction between the liquid and structural modes. That would lead to an increase in the liquid response amplitude while reducing the base isolated structure's response. The performance of the liquid tanks improves by increasing the intensity of the external excitation, as long as there is no wave breaking in the free liquid surface. On the other hand, in case of 1:1 resonance state, and because of a frequency shift, the structural response parameters are significantly reduced. However, the effectiveness of the proposed system for earthquake excitation would be highly depended on the frequency content of the earthquake records that in turn are influenced by the soil type and site-to-source distance. For the resonance case 1:2, and due to energy transfer from base isolated structure to the liquid tank, one could expect that the structural response would always be reduced.

REFERENCES

Attari NKA, Rofooei FR (2008). On lateral response of structures containing a cylindrical liquid tank under the effect of fluid/structure resonances, *J. Sound and Vibration*, 318:1154–1179**.**

Kaneko S, Yoshida O (1999). Modeling of deepwater-type rectangular tuned liquid damper with submerged net, *J. Pressure Vessel Tech*., 121:413–422.

Kaneko S, Mizota Y (2000). Dynamical modeling of deep water-type cylindrical tuned liquid damper with a submerged net, *J. Pressure Vessel Tech*.,122:96–104.

Ibrahim RA, Gau JS, Sounararajan A (1988). Parametric and autoparametric vibrations of an elevated water tower,Part I, nonlinear parametric response, *J. Sound and Vibration*, 121:413–428.

Ibrahim RA (2005). *Liquid Sloshing Dynamic*, Cambridge University Press, United Kingdom.

Ikeda T, Ibrahim RA (2005). Nonlinear random responses of a structure parametrically coupled with liquid sloshing in a cylindrical tank, *J. Sound and Vibration*, 284:75–102.

Ikeda T, Murakami S (2005). Autoparametric resonances in a structure/fluid interaction system carrying a cylindrical liquid tank, *J. Sound and Vibration*, 285:517–546.

Modi VJ, Munshi SR (1998). An efficient liquid sloshing damper for vibration control. *J. Fluids Struct.*, 12: 1055–1071.

Rofooei, F.R., Attari, N.K.A.: Using the Fluid/Structure Interaction to mitigate the Seismic Response of Structures Equipped with Cylindrical Liquid Tanks. EASEC-11, Eleventh East **A**sia-Pacific Conference on Structural Engineering & Construction, Building a Sustainable Environment, November 19-21, Taipei, TAIWAN (2008)

APPENDIX I

$$G_{m1} = \int_0^1 r\, J_m{}^2\left(\varepsilon_{m1}\, r\right)\mathrm{d}r \qquad g_{m1} = \int_0^1 1/r\, J_m{}^2\left(\varepsilon_{m1}\, r\right)\mathrm{d}r$$

$$K_m^{ijk} = \frac{\int_0^1 r\, J_0{}^i\left(\varepsilon_{01} r\right) J_1{}^j\left(\varepsilon_{11} r\right) J_2{}^k\left(\varepsilon_{21} r\right)\mathrm{d}r}{G_{m1}} \qquad U_m^{ijk} = \frac{\int_0^1 1/r\, J_0{}^i\left(\varepsilon_{01} r\right) J_1{}^j\left(\varepsilon_{11} r\right) J_2{}^k\left(\varepsilon_{21} r\right)\mathrm{d}r}{G_{m1}}$$

$$\Gamma_m^{ijkl} = \frac{\int_0^1 r\, J_i\left(\varepsilon_{i1} r\right) J_j\left(\varepsilon_{j1} r\right)\frac{\partial}{\partial r}\left[j_k\left(\varepsilon_k r\right)\right]\frac{\partial}{\partial r}\left[J_l\left(\varepsilon_{l1} r\right)\right]\mathrm{d}r}{G_{m1}} \quad \gamma_m^{ijk} = \frac{\int_0^1 r\, J_i\left(\varepsilon_{i1} r\right)\frac{\partial}{\partial r}\left[J_j\left(\varepsilon_{j1} r\right)\right]\frac{\partial}{\partial r}\left[J_k\left(\varepsilon_{k1} r\right)\right]\mathrm{d}r}{G_{m1}}$$

$$\psi_{mn} = \varepsilon_{mn}\tanh\left(\varepsilon_{mn}\, h\right) \qquad \omega_{mn}^2 = \frac{\psi_{mn}}{\psi_{11}}$$

$$G_0 = \mu_1 + \mu_2\,\pi h \qquad G_1 = \frac{2}{\left(\varepsilon_{11}{}^2 - 1\right) J_1\left(\varepsilon_{11}\right)} \qquad G_2 = \pi\,\mu_2 \frac{J_1\left(\varepsilon_{11}\right)\psi_{11}}{\varepsilon_{11}{}^2}$$

$$G_3 = \pi\,\mu_2 \frac{\varepsilon_{01}\,\varepsilon_{11}}{\varepsilon_{01}{}^2 - \varepsilon_{11}{}^2} \times \left[\left(\psi_{01} - \psi_{11}\right)\frac{\mathrm{dJ}_1\left(\varepsilon_{11} r\right)}{\mathrm{d}r}\frac{\mathrm{dJ}_0\left(\varepsilon_{01} r\right)}{\mathrm{d}r} + \left(\frac{\varepsilon_{01}{}^2\psi_{11} - \varepsilon_{11}{}^2\psi_{01}}{\varepsilon_{01}\,\varepsilon_{11}}\right) J_1\left(\varepsilon_{11} r\right) J_0\left(\varepsilon_{01} r\right)\right]$$

$$G_4 = \pi\,\mu_2 \frac{\varepsilon_{11}\,\varepsilon_{21}}{\varepsilon_{11}{}^2 - \varepsilon_{21}{}^2} \times \left[\frac{1}{2}\left(\psi_{11} - \psi_{21}\right)\frac{\mathrm{dJ}_1\left(\varepsilon_{11} r\right)}{\mathrm{d}r}\frac{\mathrm{dJ}_2\left(\varepsilon_{21} r\right)}{\mathrm{d}r} + \left(\psi_{11} - \psi_{21}\right) J_1\left(\varepsilon_{11} r\right) J_2\left(\varepsilon_{21} r\right) + \frac{1}{2}\left(\frac{\varepsilon_{11}{}^2\psi_{21} - \varepsilon_{21}{}^2\psi_{11}}{\varepsilon_{11}\,\varepsilon_{21}}\right) J_1\left(\varepsilon_{11} r\right) J_2\left(\varepsilon_{21} r\right)\right]$$

$$G_5 = \frac{3\pi}{8}\mu_2 J_1^3\left(\varepsilon_{11} r\right)\psi_{11} \qquad G_6 = \frac{3\pi}{8}\mu_2 [J_1^3\left(\varepsilon_{11} r\right)\left(\frac{1}{3} + \psi_{11}{}^2\right) + \varepsilon_{11}{}^2 J_1\left(\varepsilon_{11} r\right)\left(\frac{\mathrm{dJ}_1\left(\varepsilon_{11} r\right)}{\mathrm{d}r}\right)^2$$

$$G_7 = \frac{m_0}{M} \qquad G_8 = \left(1 + \frac{c_0}{c_1}\right)$$

$$Q_4 = \psi_{01} K_1{}^{120} \quad Q_5 = \psi_{11} K_1{}^{120} \quad Q_6 = \frac{1}{2}\psi_{11} K_1{}^{021} \quad Q_7 = \frac{1}{2}\psi_{21} K_1{}^{021} \quad Q_8 = \frac{3}{8}\varepsilon_{11}{}^2 K_1{}^{040} \quad Q_9 = \gamma_1{}^{110}\varepsilon_{01}\varepsilon_{11} + K_1{}^{120}\psi_{01}\psi_{11}$$

$$Q_{10} = \frac{1}{2}\gamma_1{}^{112}\varepsilon_{11}\varepsilon_{21} + u_1{}^{021} + \frac{1}{2}K_1{}^{021}\psi_{11}\psi_{21} \quad Q_{11} = \frac{3}{4}\varepsilon_{11}{}^2\psi_{11}\Gamma_1{}^{1111} + \frac{1}{4}u_1{}^{040}\psi_{11} + \frac{3}{4}\varepsilon_{11}{}^2\psi_{11}K_1{}^{040} \quad Q_{12} = \frac{1}{2}\psi_{11}K_0{}^{120}$$

$$Q_{13} = \frac{1}{4}\varepsilon_{11}{}^2\gamma_0{}^{011} + \frac{1}{4}u_0{}^{120} + \frac{1}{4}\psi_{11}{}^2 K_0{}^{120} \quad Q_{14} = \frac{1}{2}\psi_{11}K_2{}^{021} \quad Q_{15} = \frac{1}{4}\varepsilon_{11}{}^2\gamma_2{}^{211} - \frac{1}{4}u_2{}^{021} + \frac{1}{4}\psi_{11}{}^2 K_2{}^{021}$$

$$Q_{16} = \gamma_1{}^{110}\varepsilon_{01}\varepsilon_{11} - \varepsilon_{01}{}^2 K_1{}^{120} \quad Q_{17} = \gamma_1{}^{110}\varepsilon_{01}\varepsilon_{11} - \varepsilon_{11}{}^2 K_1{}^{120} \quad Q_{18} = \frac{1}{2}\gamma_1{}^{112}\varepsilon_{11}\varepsilon_{21} + u_1{}^{021} - \frac{1}{2}\varepsilon_{11}{}^2 K_1{}^{021}$$

$$Q_{19} = \frac{1}{2}\gamma_1{}^{112}\varepsilon_{11}\varepsilon_{21} + u_1{}^{021} - \frac{1}{2}\varepsilon_{21}{}^2 K_1{}^{021} \quad Q_{20} = \frac{3}{4}\varepsilon_{11}{}^2\psi_{11}\Gamma_1{}^{1111} + \frac{1}{4}u_1{}^{040}\psi_{11} - \frac{3}{8}K_1{}^{040}\psi_{11}\varepsilon_{11}{}^2$$

$$Q_{21} = \frac{1}{2}\varepsilon_{11}{}^2\gamma_0{}^{011} - \frac{1}{2}\varepsilon_{11}{}^2 K_0{}^{120} + \frac{1}{2}u_0{}^{120} \quad Q_{22} = \frac{1}{2}\varepsilon_{11}{}^2\gamma_2{}^{211} - \frac{1}{2}\varepsilon_{11}{}^2 K_2{}^{021} - \frac{1}{2}u_2{}^{021}$$

$$S_2 = \frac{Q_{16}}{\psi_{01}\psi_{11}} \quad S_3 = \frac{Q_{19}}{\psi_{21}\psi_{11}} \quad S_4 = \frac{Q_{16}}{\psi_{01}\psi_{11}}\left(\frac{Q_{16}Q_{21}}{\psi_{01}\psi_{11}} + \frac{Q_{19}Q_{22}}{\psi_{21}\psi_{11}}\right) \quad S_5 = \frac{Q_{19}}{\psi_{21}\psi_{11}}\left(\frac{Q_{16}Q_{21}}{\psi_{01}\psi_{11}} + \frac{Q_{19}Q_{22}}{\psi_{21}\psi_{11}}\right)$$

$$S_6 = \frac{1}{\psi_{11}}\left(\frac{Q_{16}Q_{21}}{\psi_{01}\psi_{11}} + \frac{Q_{19}Q_{22}}{\psi_{21}\psi_{11}}\right) \quad S_7 = \frac{Q_{17}}{\psi_{11}{}^2} \quad S_8 = \frac{Q_{18}}{\psi_{11}{}^2} \quad S_9 = \frac{Q_{20}}{\psi_{11}{}^2}$$

IMPROVED INTEGRATION METHODS FOR ACCURATE IDENTIFICATION OF DYNAMIC PROPERTIES OF STRUCTURAL COMPONENTS USING SEISMIC HYBRID SIMULATION

M. Ahmadizadeh[1] and G. Mosqueda[2]

[1]School of Civil Engineering, Sharif University of Technology, Tehran, Iran; [2]Department of Civil, Structural and Environmental Engineering, University at Buffalo, The State University of New York, Buffalo, New York, USA

ABSTRACT

Hybrid simulation combines numerical and experimental methods for cost-effective, large-scale laboratory testing of structures under simulated earthquake loading. One of the more challenging aspects of hybrid simulation has been the development of suitable integration methods that can effectively incorporate the experimental substructures into the simulation. Direct application of fully implicit integration methods to hybrid simulation has been partially limited by the requirement to iterate with experimental substructures and difficulties in estimating the experimental tangent stiffness matrix during simulation. Consequently, explicit integrators have been widely applied for pseudo-dynamic testing because they are the easy to implement. However, their conditional stability limits their application to simple structural models. Other methods such as the operator-splitting method have also been developed, in which the initial experimental stiffness matrix is used as an approximation of the tangent stiffness matrix during the simulation. These methods have better stability properties, but their application is limited to structural systems with mild nonlinear behavior. This paper presents numerical integration methods with improved accuracy and stability of hybrid simulation, leading to better identification of dynamic properties of the experimental substructure. These methods include combined implicit or explicit steps for hybrid simulation, improved operator splitting method using experimental tangent stiffness, and full implicit integration using experimental tangent stiffness. Numerical and hybrid simulations are used to demonstrate that the above-mentioned procedures provide better stability and accuracy properties and capture the component behavior more accurately. In particular, the stability of integrators using combined implicit and explicit steps is demonstrated in the presence of random errors expected in a hybrid simulation.

INTRODUCTION

The increasing need for identification of seismic performance of novel and existing structural systems has resulted in highly sophisticated dynamic test procedures. Further, advanced design methods, such as performance-based design require a better understanding of the behavior of structures well into their nonlinear response range. As a result, various forms of hybrid simulation [Nakashima 2001; Shao et al. 2006; Mahin et al 1989; Shing et al. 1991; Takanashi and Nakashima 1987; Shing et al. 1996] and effective force testing methods have been of special interest in recent years. Hybrid simulation is an efficient method for assessment of the dynamic and rate-dependent behavior of structural systems subjected to earthquake excitation. The method separates a structure into physical (experimental) and numerical substructures, only requiring the experimental simulation of parts of the structure that are difficult to model (Figure 1). By utilizing an incremental time-stepping solution technique and communication of interface forces and displacements, a parallel simulation can be carried out, which takes advantage of numerical simulation for the well-identified parts of the structure, and experimental evaluation of complicated and nonlinear parts.

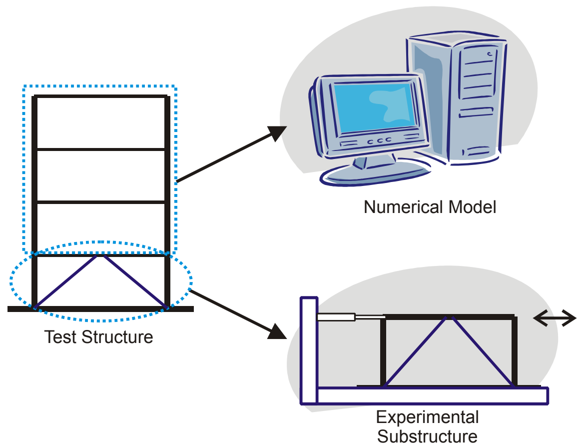

Figure 1 Illustration of hybrid structural simulation.

A real-time hybrid test may have significant advantages over an earthquake simulation test using a shake table in terms of the size, geometry, and required physical mass of structures that can be tested [Nakashima 2001]. Substructure testing can also result in a better understanding of component behavior while interacting with the entire system, contrary to shaking table tests that provide information about the overall behavior of the test structure. On the other hand, performing an accurate and reliable hybrid simulation can be a challenging task, due to (a) the presence of both numerical and experimental errors, (b) difficulties in applying proper boundary conditions, (c) use of numerical integration methods with limited accuracy and stability, and (d) lack of a general and user-friendly software interface for hybrid simulations.

Since in a hybrid simulation the identification of the dynamic properties of the experimental substructure is of primary concern, the accuracy of the employed numerical integration methods in capturing this behavior is very important. This paper presents improved numerical integration methods that have better stability properties compared to the widely used explicit methods, and eliminate the initial stiffness approximation as customary in the conventional operator-splitting approach [Nakashima et al. 1990]. These methods include combined implicit or explicit steps for hybrid simulation, improved operator splitting method using experimental tangent stiffness, and a fully implicit integration method. The difficulties of implementing implicit integrators in a hybrid simulation are addressed at the element level by introducing a safe iteration strategy and using an efficient procedure for online estimation of the experimental tangent stiffness matrix. Numerical and hybrid simulations are used to demonstrate that the proposed procedures provide better stability and accuracy properties and capture the actual behavior of the experimental components.

PSEUDO-DYNAMIC HYBRID SIMULATION

In a hybrid simulation, the equation of motion of the combined numerical and experimental structure model can be expressed as:

$$\mathbf{Ma}+\mathbf{Cv}+\mathbf{Kd}+\mathbf{r}=-\mathbf{M}^{\mathrm{t}}\boldsymbol{\iota}\ddot{u}_g \tag{1}$$

in which $\mathbf{M}$, $\mathbf{C}$ and $\mathbf{K}$ are mass, damping, and stiffness matrices of the numerical substructure, $\mathbf{M}^{\mathrm{t}}$ is the total mass matrix of the structural model (including the experimental mass), $\boldsymbol{\iota}$ is the influence vector, $\mathbf{d}$, $\mathbf{v}$, and $\mathbf{a}$ are displacement, velocity and acceleration vectors, respectively; $\ddot{u}_g$ is the input ground acceleration and $\mathbf{r}$ is the restoring force measured in the experimental substructures. In a displacement controlled experiment (also called pseudo-dynamic—since the dynamic inertial forces can be entirely modeled in the numerical module), the displacements computed by the numerical model are applied to the physical specimen, and the resisting force is measured and fed back into the numerical model.

NUMERICAL INTEGRATION

The formulation of α-method by Hilber et al. [1977] used in the proposed integration algorithms is presented in this section. In this method, the time-discrete equation of motion and finite difference relations for determination of displacement and velocity at step n are given by:

$$\mathbf{Ma}_n+\mathbf{Cv}_n+\mathbf{Kd}_n+\alpha\left[\mathbf{C}\left(\mathbf{v}_n-\mathbf{v}_{n-1}\right)+\mathbf{K}\left(\mathbf{d}_n-\mathbf{d}_{n-1}\right)\right]=-\mathbf{M}^{\mathrm{t}}\boldsymbol{\iota}\ddot{u}_g\left(t_n+\alpha\Delta t\right) \tag{2}$$

$$\mathbf{d}_n=\mathbf{d}_{n-1}+\Delta t\mathbf{v}_{n-1}+\Delta t^2\left[\left(1/2-\beta\right)\mathbf{a}_{n-1}+\beta\mathbf{a}_n\right] \tag{3}$$

$$\mathbf{v}_n=\mathbf{v}_{n-1}+\Delta t\left[\left(1-\gamma\right)\mathbf{a}_{n-1}+\gamma\mathbf{a}_n\right] \tag{4}$$

in which Δt is the integration time step and subscripts denote the step number. This method provides numerical energy dissipation controllable by the parameter α. If the parameters are selected such that $-1/3\le\alpha\le 0$, $\gamma=\left(1-2\alpha\right)/2$, and $\beta=\left(1-\alpha\right)^2/4$, an unconditionally stable, second-order accurate scheme results. In a hybrid simulation, Equation (2) should be modified to include the restoring force vector from the experimental substructure:

$$\begin{aligned}&\mathbf{Ma}_n+\mathbf{Cv}_n+\mathbf{Kd}_n+\mathbf{r}_n+\\&\alpha\left[\mathbf{C}\left(\mathbf{v}_n-\mathbf{v}_{n-1}\right)+\mathbf{K}\left(\mathbf{d}_n-\mathbf{d}_{n-1}\right)+\mathbf{r}_n-\mathbf{r}_{n-1}-\mathbf{M}^{\mathrm{e}}\left(\mathbf{a}_n-\mathbf{a}_{n-1}\right)\right]=-\mathbf{M}^{\mathrm{t}}\boldsymbol{\iota}\ddot{u}_g\left(t_n+\alpha\Delta t\right)\end{aligned} \tag{5}$$

where $\mathbf{M}^{\mathrm{e}}=\mathbf{M}^{\mathrm{t}}-\mathbf{M}$ is the experimental mass matrix. In a fast pseudo-dynamic test, the inertial mass effect should be removed from the incremental feedback force vector in Equation (5), so that the remainder will only include strain-dependent and damping effects.

The integration methods presented in this paper work similarly [Ahmadizadeh and Mosqueda 2008; Mosqueda and Ahmadizadeh 2007; Ahmadizadeh and Mosqueda 2011] in that they first apply a predictor displacement on the experimental substructure given by an explicit expression:

$$\tilde{\mathbf{d}}_n=\mathbf{d}_{n-1}+\Delta t\mathbf{v}_{n-1}+\frac{1}{2}\Delta t^2\mathbf{a}_{n-1} \tag{6}$$

and then attempting to correct the displacement to account for the remaining implicit terms obtained by a non-zero β. After the corrector step, the final (or converged) displacement vector (which satisfies the implicit formulation) will be:

$$\mathbf{d}_n = \tilde{\mathbf{d}}_n + \beta \Delta t^2 \left(\mathbf{a}_n - \mathbf{a}_{n-1} \right) \tag{7}$$

In a fully numerical simulation of a nonlinear structure, an iterative procedure is usually employed to determine the final (converged) displacement vector from the initial displacements. This is to ensure the satisfaction of Equations (3)-(5) at the end of each integration step. However, alternative methods should be used in hybrid simulations to avoid physical iterations on the experimental substructures to avoid damages to these components or erroneous energy dissipation in cases of displacement overshoot, or simulation interruptions resulting from convergence failure. In this study it is attempted to address these issues by selecting a safe iteration strategy and switching to alternative solution approaches in cases of convergence failure.

Integration Method with Combined Implicit or Explicit Steps

The major challenge in implementing implicit integration algorithms in a hybrid simulation is that iterative displacement reversals may result in unrecoverable damage to experimental specimens or erroneous energy dissipation. Therefore, it is not advisable to measure experimental restoring forces in iterations, $\mathbf{r}_n^i$, by physically imposing the iterative displacements. In the implicit integration method [Mosqueda and Ahmadizadeh 2007] presented in this section, recent experimental measurements are used to capture the instantaneous behavior of experimental substructures and estimate forces corresponding to iterative displacements.

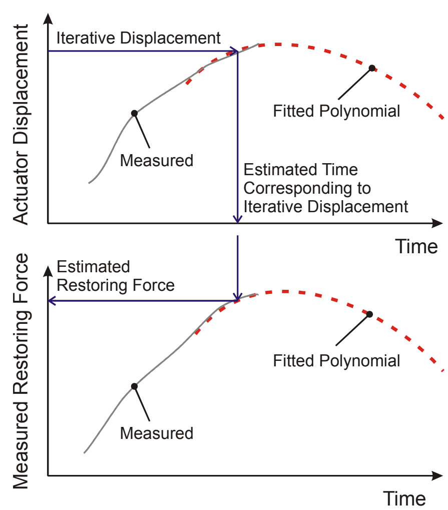

Figure 2 Estimation of force corresponding to the desired displacement using measurements.

The iterations are implemented numerically, without physical imposition of iterative displacements on the experimental substructures using the following procedure. In each integration step, first, the actuator command displacements are predicted using an explicit expression [Equation (6)] to load the experimental substructures. Second, the displacements and forces measured through the load path are used in the iterative scheme to satisfy an implicit formulation, given by Equations (3) through (5). Instead of physically applying the iterative displacements, a force estimation procedure for iterative displacements is followed using the recent measurements. For this purpose, second-order polynomials are fitted to both measured displacement and force histories in actuator local coordinates. The fitted polynomials are then used to estimate forces corresponding to each of the iterative displacements by using time stamps as a parameter relating force and displacement polynomials, as shown in Figure 2. The iterative procedure is repeated until a convergence criterion is satisfied, such as:

$$\frac{\left\| \mathbf{d}_n^i - \mathbf{d}_n^{i-1} \right\|}{\left\| \mathbf{d}_n^i \right\|} < \varepsilon \tag{8}$$

where ε is the convergence tolerance for the normalized displacement increment, and superscripts denote the iteration number.

As with most iterative integration schemes for nonlinear systems, convergence cannot be guaranteed in each step, especially for a hybrid simulation that also involves experimental errors. The failed integration steps can be identified by detection of excessive time parameter variation, or convergence failure after maximum number of iterations. An alternate solution strategy is necessary for the simulation to continue in case the iterative solution scheme fails. Here, it is proposed to revert to an explicit procedure by selecting the displacement of Equation (6) as the final solution for the step. The measured restoring force vector $\mathbf{r}_n$ is then directly used to determine acceleration and velocity vectors at step n using Equation (4) and:

$$\mathbf{a}_n = \mathbf{A}^{-1} \left\{ \begin{aligned} & \mathbf{M}^{\mathrm{t}} \boldsymbol{\iota} \ddot{u}_g \left(t_n + \alpha \Delta t \right) \\ & - \left[\mathbf{C} \left(\mathbf{v}_{n-1} + (1+\alpha) \frac{\Delta t}{2} \mathbf{a}_{n-1} \right) + (1+\alpha) \left(\mathbf{K} \mathbf{d}_n + \mathbf{r}_n \right) + \alpha \left(\mathbf{M}^{\mathrm{e}} \mathbf{a}_{n-1} - \mathbf{K} \mathbf{d}_{n-1} - \mathbf{r}_{n-1} \right) \right] \end{aligned} \right\} \tag{9}$$

where

$$\mathbf{A} = \mathbf{M} + (1+\alpha) \frac{\Delta t}{2} \mathbf{C} - \alpha \mathbf{M}^{\mathrm{e}} \tag{10}$$

If the initial stiffness matrix of the system is available, an operator-splitting method can also be utilized in the steps with failed implicit iterations to update the state vectors [Mosqueda and Ahmadizadeh 2007].

Operator-Splitting Integration with Estimation of Experimental Stiffness Matrix

The integration method described in this section takes advantage of the experimental measurements to update a condensed experimental tangent stiffness matrix [Ahmadizadeh and Mosqueda 2008]. The tangent stiffness is then used in an operator-splitting method to improve its accuracy for testing nonlinear systems. Following a procedure similar to the previous section, the predictor displacement of Equation (6) is applied on the experimental substructure and the restoring force is measured. In the corrector step, Equation (7) is used to update the displacement vector. As a result of this change in displacement vector, force vector $\tilde{\mathbf{r}}_n^l$ should also be updated in the corrector step:

$$\mathbf{r}_n^l = \tilde{\mathbf{r}}_n^l + \mathbf{K}_n^l \left(\mathbf{d}_n^l - \tilde{\mathbf{d}}_n^{l,m} \right) \tag{11}$$

where $\mathbf{d}_n^l$ is the displacement vector given by Equation (7), $\tilde{\mathbf{d}}_n^{l,m}$ is the measured displacement vector, and $\mathbf{K}_n^l$ is the experimental stiffness matrix at step n, all expressed in the actuator coordinate system. Note that in a conventional operator-splitting method, $\mathbf{K}_n^l$ is simply the initial experimental stiffness matrix. By using the measured displacement vector $\tilde{\mathbf{d}}_n^{l,m}$, Equation (11) not only updates the force vector due to displacement modification of Equation (7), but also attempts to make correction for actuator tracking errors. The corrected restoring force vector is then transformed to the global coordinate system using $\mathbf{r}_n = \mathbf{T}^T \mathbf{r}_n^l$, and used in Equations (4), (5), (7) and (11) to update the states.

Online Estimation of Tangent Stiffness Matrix

For use in the integration procedures presented in this and the next sections, an experimental tangent stiffness matrix is estimated that satisfies the following incremental force-displacement relation at the n^{th} integration step:

$$\Delta \mathbf{r}_n^l = \mathbf{K}_n^l \Delta \mathbf{x}_n^l \tag{12}$$

where $\Delta \mathbf{r}_n^l$ and $\Delta \mathbf{x}_n^l$ are incremental force and displacement vectors of the experimental substructure in actuator local coordinate system, respectively, and $\mathbf{K}_n^l$ is the $m \times m$ stiffness matrix of the experimental substructure, m being the number of actuators (and load cells). Knowing that an online stiffness estimation procedure should estimate the tangent stiffness only using $m \times 1$ vectors of measured force and displacement data, it is first attempted to reduce the number of unknowns required to update the tangent stiffness matrix. For this purpose, the stiffness matrix $\mathbf{K}_n^l$ of the experimental substructure in the actuator coordinate system is expressed as:

$$\mathbf{K}_n^l = \mathbf{T}_p^T \mathbf{P}_n \mathbf{T}_p \tag{13}$$

where $\mathbf{P}_n$ is a diagonal $p \times p$ matrix of essential stiffness parameters. The transformation matrix $\mathbf{T}_p$ transform displacements from the local actuator (substructure) coordinate system to an intrinsic (parameter) coordinate system with a presumed diagonal stiffness matrix $\mathbf{P}_n$. In order to obtain the transformation matrix $\mathbf{T}_p$, it may be necessary to identify the source of stiffness and nonlinear behavior of the experimental substructure [Ahmadizadeh and Mosqueda 2008]. Examples of such sources are the stiffnesses in a shear building, or the overall behavior of lateral resisting elements within a frame. In the absence of such information of the experimental substructure, one can use the classical approach of matrix diagonalization, in which a general choice of the transformation is the modal matrix, i.e.,

$\mathbf{T}_p = \mathbf{\Phi}_n^{\mathrm{T}}$, where $\mathbf{\Phi}_n = [\boldsymbol{\varphi}_1 \boldsymbol{\varphi}_2 \cdots \boldsymbol{\varphi}_m]_n$. Note that the eigenvectors of a symmetric stiffness matrix are orthogonal, which simplifies the calculations.

In order to calculate the terms of the diagonal stiffness matrix $\mathbf{P}_n$, the incremental displacement and force vectors should be transformed to the above-mentioned intrinsic coordinate system. For displacements, the transformation can be carried out through the same transformation matrix described above:

$$\Delta\mathbf{x}_n^p = \mathbf{T}_p \Delta\mathbf{x}_n^l \tag{14}$$

in which $\Delta\mathbf{x}_n^l$ and $\Delta\mathbf{x}_n^p$ are the displacement increment vectors in actuator and intrinsic coordinate systems, respectively. The transformation of displacements from global to actuator coordinate system can be carried out using $\Delta\mathbf{x}_n^l = \mathbf{T}\Delta\mathbf{x}_n$.

For statically determinate structures, the intrinsic forces can simply be found by equilibrium, and the transformation of local incremental force vector $\Delta\mathbf{r}_n^l$ to intrinsic coordinates ($\Delta\mathbf{r}_n^p$) is:

$$\Delta\mathbf{r}_n^p = \mathbf{T}_p^{(-T)} \Delta\mathbf{r}_n^l \tag{15}$$

where the superscript $(-T)$ represents a pseudo-inverse of the matrix transpose. If the experimental substructure is statically indeterminate, the calculation of forces in intrinsic coordinates requires the stiffness matrix of the system for a structural analysis. In this case, the structure should be analyzed to find local displacements from the measured local force vector, $\Delta\mathbf{r}_n^l$. The resulting local displacements can then be transformed to the intrinsic coordinate system using Equation (14). The intrinsic forces will be the forces corresponding to the intrinsic displacement vector using diagonal stiffness matrix $\mathbf{P}_n$:

$$\Delta\mathbf{r}_n^p = \mathbf{P}_n \mathbf{T}_p \left(\mathbf{K}_n^l\right)^{-1} \Delta\mathbf{r}_n^l \tag{16}$$

Note that to omit the iterative procedure involved in the use of the above equation, it can be approximately replaced by $\Delta\mathbf{r}_n^p = \mathbf{P}_{n-1} \mathbf{T}_p \left(\mathbf{K}_{n-1}^l\right)^{-1} \Delta\mathbf{r}_n^l$, updated once at the beginning of each integration step. After determination of forces and displacements in the intrinsic coordinate system, each diagonal element of the updated parameter matrix can be found by dividing the corresponding elements of force vector by the displacement vector. The global stiffness matrix of the experimental substructures can then be found using $\mathbf{K}_n = \mathbf{T}^T \mathbf{K}_n^l \mathbf{T}$, where $\mathbf{T}$ is the displacement transformation matrix. Note that the above stiffness estimation procedure is carried out in steps with significant displacement increments [Ahmadizadeh and Mosqueda 2008] to reduce the effects of experimental errors in the estimations.

Fully Implicit Integration

This section presents a fully implicit integration procedure for hybrid simulation [Mosqueda and Ahmadizadeh 2011] that can be incorporated seamlessly in the commercial finite element analysis software developed for purely numerical simulations. Fully implicit iterative solution scheme leads to more accurate correlations between the states and proper detection of the behavior of the experimental substructure in the simulation. For this reason, it is attempted to provide an efficient implementation of implicit integrators for hybrid simulations of large structural systems that can accurately capture large nonlinearities distributed throughout the structure. This procedure makes use of the procedures of the two methods presented in the previous sections to achieve this goal.

Similar to the other integration method presented herein, each step of the fully implicit integration procedure begins with calculation of the desired displacement vector from Equation (6) and its application on the experimental substructures. The measured experimental displacements and restoring forces are then used to solve Equations (3)-(5) iteratively, and obtain the converged states at the current time step.

In iterations, the calculation of the experimental restoring forces is carried out in two steps. First, the experimental restoring force vector is updated according to the new iterative displacement vector using the same procedure described in Figure 2. Then, the experimental iterative force-displacement pairs are then used in the stiffness estimation procedure outlined in the previous section to determine experimental stiffness matrix. This stiffness matrix is then used in Equation (11) with $\mathbf{d}_n^l$ being the iterative displacement vector, and $\mathbf{K}_n^{e,l}$ is the experimental tangent stiffness matrix determined in each iteration. The iterations are repeated until the convergence criterion [Equation (8)] is satisfied. Again, if the iterations are not successful in an integration step, an alternative solution method is adopted in that step to continue the simulation.

In addition to providing all the necessary requirements for incorporating experimental substructures into commonly used finite element analysis software, the benefits of the proposed integration method becomes clear considering: (a) this integration method uses symmetric tangent stiffness matrix to estimate the experimental restoring forces, thus providing a more meaningful relation between experimental forces and displacements, and (b) a one-step correction using the tangent stiffness matrix as proposed by Ahmadizadeh and Mosqueda [2008] may yield inaccurate results if the tangent stiffness matrix significantly changes between predictor and corrector displacements, while this method updates the tangent stiffness matrix within an integration step as many times as necessary.

ACCURACY AND STABILITY

The proposed integration methods for hybrid simulation use well-known numerical integration algorithms, whose accuracy and stability properties are well established for linear systems. However, stability criteria for linear systems cannot be directly extended to hybrid simulation of nonlinear systems with experimental errors such as servo-hydraulic actuator delay, tracking errors and measurement noise. In addition, the proposed integration methods sometimes switch between implicit, explicit, or operator splitting approaches to maintain the continuity of the simulation. Consequently, the stability and accuracy of these integration methods have been studied in several nonlinear hybrid simulations. These experiments have shown excellent performance by the presented integration methods in the accurate detection of the dynamic properties of the experimental substructure and in maintaining an accurate and stable hybrid simulation, by (a) showing excellent agreement between actual and converged hysteresis behavior of the experimental substructure [Ahmadizadeh and Mosqueda 2008; Mosqueda and Ahmadizadeh 2007; Mosqueda and Ahmadizadeh 2011], (b) good agreement between the estimated tangent stiffness and the stiffness of numerical models of the experimental substructure [Mosqueda and Ahmadizadeh 2011] , and (c) maintaining the energy balance of the system throughout the simulation [Ahmadizadeh and Mosqueda 2009].

In this section, a procedure from the field of structural control is also implemented to numerically investigate the stability of the combined integration algorithm. The combination of explicit and implicit integration steps for solving the equation of motion can be considered as a particular type of "variable structure control system" [Utlin 1977]. Combining several control laws has the advantage of utilizing the useful properties of each of the control systems, namely the stability of the implicit procedure, and the simplicity and guaranteed continuity of the alternative explicit (or operator-splitting) approach. For the analysis of stability and accuracy in the presence of experimental random errors, the equation of motion of a linear system is expressed as:

$$\mathbf{M}\mathbf{a}_n + \mathbf{C}\mathbf{v}_n + \mathbf{K}\mathbf{d}_n - \mathbf{u}_n^{\mathrm{err}} = \mathbf{0} \tag{17}$$

where $\mathbf{u}_n^{\mathrm{err}}$ is an $N \times 1$ vector of random disturbance signals representing errors in force measurements. For simplicity, Newmark integration relations can be put in a state-space form as follows:

$$\begin{bmatrix} \mathbf{x} \\ \dot{\mathbf{x}} \end{bmatrix}_n = \mathbf{A}_{\mathrm{D}} \begin{bmatrix} \mathbf{x} \\ \dot{\mathbf{x}} \end{bmatrix}_{n-1} + \mathbf{B}_{\mathrm{D}} \begin{bmatrix} \mathbf{u}_n^{\mathrm{err}} \\ \mathbf{u}_{n-1}^{\mathrm{err}} \end{bmatrix} \tag{18}$$

where $\mathbf{x}$ and $\dot{\mathbf{x}}$ are column vectors of displacements and velocities, respectively, and $\mathbf{A}_{\mathrm{D}}$ and $\mathbf{B}_{\mathrm{D}}$ are time-discrete state equation matrices given by:

$$\mathbf{A}_{\mathrm{D}} = \mathrm{diag}\left[\begin{pmatrix} \mathbf{M} + \gamma\,\Delta t\,\mathbf{C} \\ +\beta(\Delta t)^2\,\mathbf{K} \end{pmatrix}^{-1}\right] \begin{bmatrix} \begin{array}{l} \mathbf{M} + \gamma\,\Delta t\,\mathbf{C} - \left(\frac{1}{2} - \beta\right)(\Delta t)^2\,\mathbf{K} \\ +\left(\beta - \frac{1}{2}\gamma\right)(\Delta t)^3\,\mathbf{C}\mathbf{M}^{-1}\mathbf{K} \end{array} & \begin{array}{l} \Delta t\,\mathbf{M} - \left(\frac{1}{2} - \gamma\right)(\Delta t)^2\,\mathbf{C} \\ +\left(\beta - \frac{1}{2}\gamma\right)(\Delta t)^3\,\mathbf{C}\mathbf{M}^{-1}\mathbf{C} \end{array} \\ \begin{array}{l} -\Delta t\,\mathbf{K} \\ +\left(\frac{1}{2}\gamma - \beta\right)(\Delta t)^3\,\mathbf{K}\mathbf{M}^{-1}\mathbf{K} \end{array} & \begin{array}{l} (\beta - \gamma)(\Delta t)^2\,\mathbf{K} - (1-\gamma)\,\Delta t\,\mathbf{C} \\ +\mathbf{M} + \left(\frac{1}{2}\gamma - \beta\right)(\Delta t)^3\,\mathbf{K}\mathbf{M}^{-1}\mathbf{C} \end{array} \end{bmatrix} \tag{19}$$

$$\mathbf{B}_\mathrm{D} = \mathrm{diag}\left[\begin{pmatrix}\mathbf{M}+\gamma\,\Delta t\,\mathbf{C}\\ +\beta(\Delta t)^2\,\mathbf{K}\end{pmatrix}^{-1}\right]\begin{bmatrix}\beta(\Delta t)^2\,\mathbf{I} & \left(\frac{1}{2}-\beta\right)(\Delta t)^2\,\mathbf{I}+\left(\frac{1}{2}\gamma-\beta\right)(\Delta t)^3\,\mathbf{CM}^{-1}\\ \gamma\,\Delta t\,\mathbf{I} & (1-\gamma)\,\Delta t\,\mathbf{I}+\left(\beta-\frac{1}{2}\gamma\right)(\Delta t)^3\,\mathbf{KM}^{-1}\end{bmatrix} \tag{20}$$

When $\beta = 1/4$ and $\gamma = 1/2$ in the above equations, the state equation takes the implicit form, while for $\beta = 0$ and $\gamma = 1/2$ an explicit formulation results. Fully explicit and fully implicit simulations have been carried out for a 5-story structure, with $(\omega\Delta t)_{\max} \approx 2$ and 5% of critical damping (stiffness-proportional). The multi-degree-of-freedom structural model is selected to demonstrate the stability problem in the presence of high-frequency modes. Random signals with zero mean and RMS amplitude of 10% of initial restoring forces are used for $\mathbf{u}_n^{\mathrm{err}}$. The phase diagrams of the top story states are shown in Figure 3 for an initial displacement (90 mm at the top). This figure shows that the simulation using implicit method remains stable up to the vicinity of the origin, where the response continues to oscillate due to the disturbance signals $\mathbf{u}^{\mathrm{err}}$. The explicit simulation becomes unstable, although it should remain stable according to numerical stability limit of $\omega\Delta t = 2$ for undamped structures.

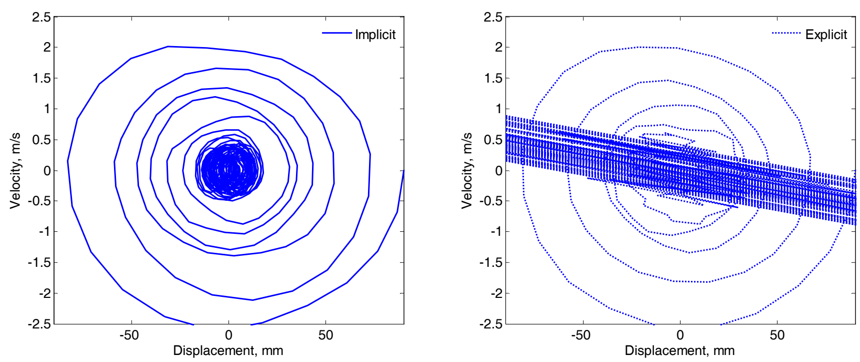

Figure 3 Phase diagram of a free vibration response with fully implicit or fully explicit integration methods – $(\omega\Delta t)_{\max} \approx 2$.

In the proposed integration method with combined implicit or explicit steps, the control structure is selected based on the possibility of using the implicit solution scheme. That is, only if the implicit structure control system fails, the explicit approach is admitted. Figure 4 shows the phase diagram of a simulation with combined implicit or explicit integration steps. Here, the selection of implicit or explicit control system is made using a random decision logic, providing a 20% probability for explicit steps. This probability is more than what is expected to occur in hybrid simulations with properly tuned experimental setups. As illustrated, similar to a fully implicit procedure, the combined method results in a stable simulation. It is shown that the implicit steps (shown by solid lines) are occasionally interrupted by one or more explicit steps (shown by dotted lines). Since the explicit steps are sparsely distributed, the accumulation of errors is prevented, and the simulation remains stable.

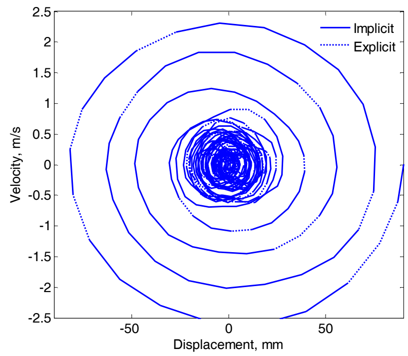

Figure 4 Phase diagram of a free vibration response with combined implicit or explicit integration steps – $(\omega\Delta t)_{\max} \approx 2$.

Simulations with higher-frequency modes or longer time steps also show that the combined integration method can produce stable results when explicit procedures fail. The simulation results shown in Figure 5 are determined for the same structure as above, but with $(\omega\Delta t)_{\max} = 2.79$. The explicit results are shown to immediately become unstable, while the combined integration remains stable throughout the simulation.

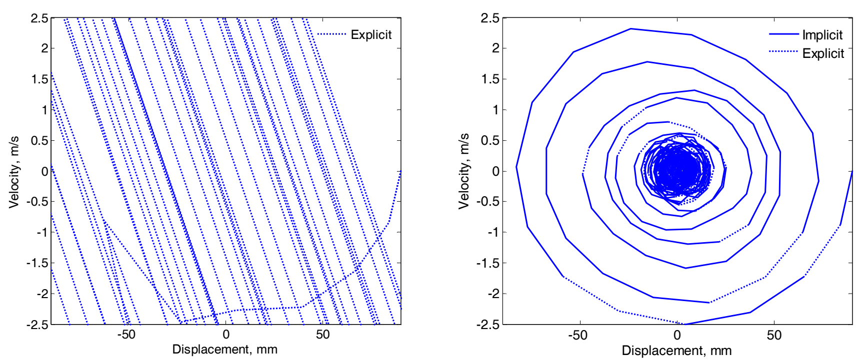

Figure 5 Phase diagram of a free vibration response with fully explicit and combined implicit or explicit integration steps – $(\omega\Delta t)_{\max} = 2.79$.

To further study the accuracy and stability properties of the combined integration method, a series of parametric studies has been carried out. In these analyses, the same simulation model and initial conditions as above are considered. The unbalanced energy [Ahmadizadeh and Mosqueda 2009] errors of 5-second simulations with different integration time steps and probabilities for explicit steps are calculated and shown in **Error! Reference source not found.**. As shown, the energy balance error shows a consistent increase with increase of $\omega\Delta t$ or the probability of explicit integration steps. Note that large errors and the instability of the explicit integration method occurs before the numerical limit of $\omega\Delta t = 2$ due to the existence of an error signal, although the assumed damping of 5% of critical should expand this stability limit. It can be seen that when the percentage of explicit steps is limited to 20% or less, stable results can be obtained over a relatively wide range of $\omega\Delta t$.

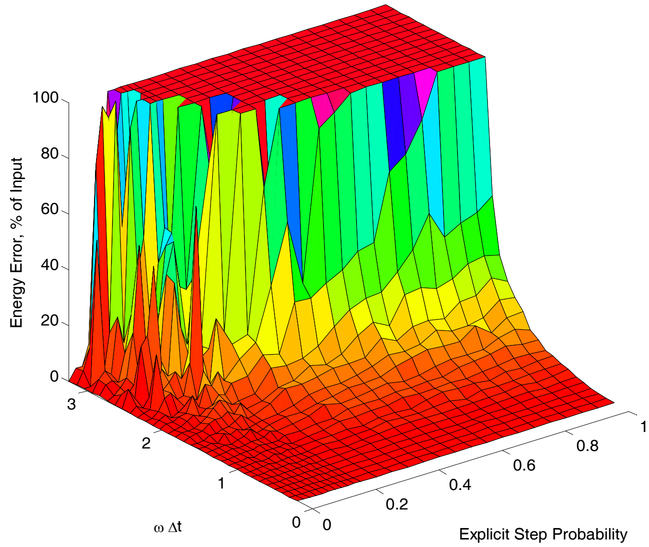

Figure 6 Energy error as a function of explicit step probability and $\omega\Delta t$.

CONCLUSIONS

Improved numerical integration methods were presented for seismic hybrid simulation of structures. Through polynomial interpolations and extrapolations on recently measured data, these integration methods eliminate the need for physical application of the iterative displacements on the experimental substructure. An efficient method was also outlined for online and accurate estimation of experimental tangent stiffness matrix using the readily-available force and displacement measurements. These integration methods attempt to solve each simulation step using implicit expressions and an updated experimental tangent stiffness matrix, but revert to an alternative solution scheme to complete the integration steps with failed convergence (or stiffness estimation) and maintain the continuity of the simulation. Through several numerical and experimental simulations, these methods were shown to have excellent performance in accurately estimating the experimental tangent stiffness matrix and capturing the dynamic behavior of the experimental components. Furthermore, computation of the energy balance in a simulation with relatively large and nonlinear structures indicates that both numerical and experimental errors are small.

A parametric numerical study of the accuracy and stability of the integration methods that may switch to alternative (e.g., explicit) approaches in certain steps for simulation continuity was also carried out. This study showed that as long as the implicit integration is successful in the majority of the integration steps and the explicit steps are sparsely distributed throughout the simulation, the properties of the resulting simulation are similar to those of a fully implicit approach. Hence, although they may use alternative approaches to complete a number of integration steps, the presented integration methods provide improved stability and accuracy in hybrid simulations.

REFERENCES

Ahmadizadeh M, Mosqueda G (2008). Hybrid simulation with improved operator-splitting integration using experimental tangent stiffness matrix estimation, ASCE, *J. Struct. Engng*., 134(12):1829−1838.

Ahmadizadeh M, Mosqueda G (2009). Online energy based error indicator for assessment of numerical and experimental errors in hybrid simulation, *Engng*. *Structures*, 31(9):1987−1996.

Hilber HM, Hughes TJR, Taylor RL (1977). Improved numerical dissipation for time integration algorithms in structural dynamic, *Earthq. Engrg. Struct. Dyn.*, 5(3):283−292.

Mahin SA, Shing PSB, Thewalt CR, Hanson RD (1989). Pseudodynamic test method - current status and future direction, ASCE, *J. Struct. Engng*., 115(8):2113−2128.

Mosqueda G, Ahmadizadeh M (2007). Combined implicit or explicit integration steps for hybrid simulation, *Earthq. Engrg. Struct. Dyn.*, 36(15):2325−2343.

Mosqueda G, Ahmadizadeh M (2011). Iterative implicit integration procedure for hybrid simulation of large nonlinear structure, *Earthq. Engrg. Struct. Dyn.*, in press.

Nakashima M (2001). Development, potential, and limitations of real-time online (pseudo-dynamic) testing. *Phil. Trans. Royal Soc. London Series A-Math. Phys. Engng. Sci.*, 359(1786):1851−1867.

Nakashima M, Kaminoso T, Ishida M, Kazuhiro A (1990). Integration techniques for substructure online test, Proceedings, *4th US National Conference of Earthquake Engineering*, Palm Springs, CA.

Shao X, Reinhorn AM, Sivaselvan M (2006). Real time dynamic hybrid testing using force-based substructuring, *Proceedings*, 8th National Conference on Earthquake Engineering, San Francisco, CA.

Shing PSB, Vannan MT, Cater E (1991). Implicit time integration for pseudodynamic tests, *Earthq. Engrg. Struct. Dyn.*, 20(6):551−576.

Shing PSB, Nakashima M, Bursi O (1996). Application of pseudodynamic test method to structural research, *Earthq. Spectra*,12:29−56.

Takanashi K, Nakashima M (1987). Japanese activities on online testing, ASCE, *J. Engng. Mech.*, **113**(7):1014−1031.

Utkin V (1977). Variable structure systems with sliding modes. *Proceedings,* IEEE Transactions on Automatic Control, 22(2):212−222.

RECENT ADVANCES IN SEISMIC ASSESSMENT OF STRUCTURES BY ENDURANCE TIME METHOD

Homayoon E. Estekanchi1[1], Abolhassan Vafai[2], Vahid Valamanesh[3], Amin Mirzaee[4], Amin Nozari[5], and Amirali Bazmuneh[6]

[1]Associate Professor, Sharif University of Technology, Tehran, stkanchi@sharif.edu, [2]Professor, Sharif University of Technology, Tehran, vafai@sharif.edu, [3]PhD candidate, Department of Civil Engineering, Sharif University of Technology, Tehran, valamanesh_1@yahoo.com, [4]PhD candidate, Department of Civil Engineering, Sharif University of Technology, Tehran, Email: mirzaee61@gmail.com, [5]PhD candidate, Department of Civil Engineering, Sharif University of Technology, Tehran, bsamin2000@yahoo.com, [6]PhD candidate, Department of Civil Engineering, Sharif University of Technology, Tehran, amirgimt@yahoo.com

SUMMARY

The endurance time (ET) method is a dynamic analysis procedure in which structures are subjected to predesigned intensifying excitation functions and their performance is assessed based on their response at different excitation levels. The concept of the ET method is analogous to the exercise test used in medicine for assessing the fitness of athletes or patients. Endurance time excitation functions (ETEFs) that are ground motion response spectrum compatible have been produced using numerical optimization procedures. The basic concepts and overview of the development of this procedure has been explained. Recent developments including the extension to multi-component analysis and performance based design applications are also addressed. Advantages and limitations of the procedure are discussed. By significantly reducing the analysis effort required for a multi level response history analysis, this method can pave the way towards practical application of response history based analysis in seismic design applications.

INTRODUCTION

In earthquake engineering, the need for developing better and more effective structural analysis tools seems to be a never ending endeavour [Newmark 1971]. This need is magnified by two major factors: first, the increasing demand for building structures that are more complex due to various architectural or functional requirements, and secondly by the development and growing trend in using sophisticated seismic mitigation technologies. Various limitations of traditional seismic design procedures, along with remarkable advances in the field of computational technology, have encouraged researchers and engineers to seek more reliable and consistent analysis methods for the design of structures with optimal seismic performance. Nonlinear pushover and time-history analyses are gradually becoming prevalent in structural design offices. Various procedures are now available for predicting nonlinear response of the structure by a pushover analysis [Chopra and Goel 1999; Chopra and Goel 2003]. Incremental dynamic analysis procedure is another method to provide a more realistic estimation of seismic response of structures [Vamvatsikos and Cornell 2003; Vamvatsikos and Cornell 2005]. Extensive research is underway in the direction of performance-based seismic engineering objectives [Bertero and Bertero 2002; Bozorgnia and Bertero 2004]. Recent developments have made it possible for engineers to incorporate various significant nonlinear material and geometric behaviour characteristics into their models, and perform a more realistic analysis of structural behaviour corresponding to realistic seismic events [Chopra 1995; FEMA 2005].

A brief comparison of the available analysis procedure options and their limitations suggests that nonlinear response-history based procedures are the way to go in future, in spite of their complexity and huge computational demand. This is due to the fact that response-history analysis is the only procedure that makes it possible to directly incorporate nearly all sources of nonlinear and time dependant effects in the analysis. The endurance time (ET) method is a response-history based procedure that strives to improve on complexity and computational demand of this category of analysis procedures.

The concept of endurance time is quite straightforward and is similar to the well-known exercise test in medicine. That is, subjecting the system into an increasing demand and monitoring its response stage by stage. A basic question is that if such a simple procedure turns out to be so useful in medicine, then, is it possible to develop a similarly simple procedure for structural engineering. The answer, most probably, must be true, so the next step is to think of a way to provide a practical implementation of the concept. During the last few years, this basic concept has been evolved into a working procedure that offers three major benefits:

- Significant reduction of the computational demand required in order to make a realistic estimation of seismic response at multiple intensity levels.
- Simplicity and sensibility of the concept for engineering applications.
- Applicability to virtually all types of structures and dynamic systems regardless of their complexity.

In this paper, the basic concepts of ET method, its implementation, and recent advances in its developments will be explained.

THE CONCEPT

In order to explain the concept of ET, consider a hypothetical test in which, prototypes of three design alternatives for a structure are placed on a shaking table and subjected to an intensifying excitation until complete failure of all of them. Based on the order in which these structures fail, one can comparatively categorize them as the worst, average, and the best performer. Figure 1 shows a numerical presentation of what happens in the exercise test. If the variations of appropriate engineering demand parameters (EDPs) are monitored, then it can be readily seen which design works better and approximately by how far. It should be mentioned that these increasing demand curves represent the maximum absolute value of response from the start up to a particular time.

The concept seems to be simple enough. Now, the next big question is whether it is possible to establish a meaningful correlation between the intensity of an intensifying excitation and those of ground motions. It turns out that the concept of response spectrum can be used quite effectively in producing intensifying acceleration functions that practically work. The point is that the response spectrum strongly reflects two major characteristics of any ground motion, i.e., the intensity and the frequency content. Two dynamic excitations, with similar response spectrum, produce almost similar responses in most structures. Thus, if the response spectrum of ET excitation functions (ETEFs) at that particular time can be made to match a particular response spectrum corresponding to say the average response spectrum of a set of ground motions, then the response it produces at that time can be considered a good estimator of the expected average response of the particular structure when subjected to those ground motions. As will be explained below, this idea is a good starting point in producing useful intensifying acceleration functions.

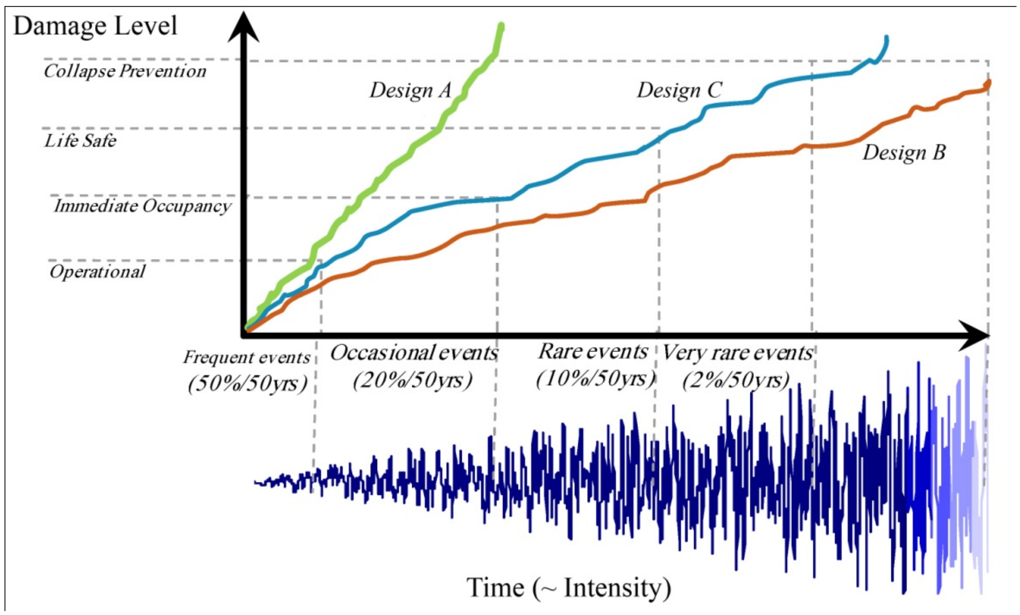

Figure 1 Basic concept of ET analysis.

The basic concepts of the method were published in 2004 [Estekanchi et al. 2004]. Then after successful production of second generation of ETEFs and its application considering linear behaviour was published in 2007 [Estekanchi et al. 2007]. A preliminary study of nonlinear analysis and predicting various damage indexes were published in 2008 [Estekanchi et al. 2008]. Nonlinear analysis of SDOF systems considering different material models was published in 2009 [Riahi et al. 2009]. This was followed by application to and analysis of MDOFs in 2010 [Riahi and Estekanchi 2010]. The procedure has recently been extended for multi-component analysis [Valmanesh and Estekanchi 2010a; Valamanesh and Estekanchi 2010b]. In the next sections, a brief introduction to the characteristics of currently available ETEFs will be followed by a description of some recent advances in this area.

ET EXCITATION FUNCTIONS

The first step in implementing the concept of ET is to produce usable intensifying ETEFs, which in this case translates into meaningful correspondence between the responses of a structure at a particular time in ET analysis to the average response to ground motions representing the seismicity of a particular site at certain hazard level. As explained in the previous section, the concept of response spectrum can be used effectively in providing a preliminary formulation of the problem. A typical code design spectrum can be considered a good starting point. In this way, the problem reduces to generating an intensifying acceleration function that produces a response spectrum matching the code design spectrum at a particular time. This particular time will be called hereafter the target time, i.e. t_{Target}. At all times the response spectrum produced by ETEF should be less before the target time, and after the target time should be greater than the considered design spectrum at all times.

It is possible to consider different target spectra at different times pertaining to different hazard levels. As a preliminary trial, the same target spectrum scaled linearly with the time will be assumed here. This means that the overall shape of the target spectrum is assumed to remain the same, and target spectrums at various times are scaled versions of the same spectrum that called here the template spectrum. This means that while the response produced by ETEF at target time t_{Target}, should match the considered design spectrum at a time equal to ½ of the t_{Target}, it should produce a response spectrum that matches the design spectrum with a scale factor of ½; similarly a linear scaling should apply at all other times. This requirement can be formulated as follows:

$$S_{aC}(T,t) = \frac{t}{t_{Target}} S_{aC}(T) \tag{1}$$

In which $S_{aC}(T)$ is the template spectrum, and $S_{aC}(T,t)$ is the target spectrum to be approached at time t of ETEF. This formula simply states that the acceleration response produced by ETEF at a particular time t should remain proportional to the considered template spectrum and scaled in a linear manner as a function of time. Obviously these simplifications are not an inherent part of the concept behind the ET method, but are just being made in order to synthesize a preliminary ETEF function.

The Displacement spectrum is also a very important consideration in characterizing a dynamic excitation. Target displacement spectrum can be defined as a function of template acceleration spectrum considering linear behavior and common simplifications applied in structural dynamics as shown in Equation 2:

$$S_{uC}(T,t) = \frac{t}{t_{Target}} S_{aC}(T) \times \frac{T^2}{4\pi^2} \tag{2}$$

Here, $S_{uC}(T,t)$ is the target displacement spectrum to be induced at time t by ETEF. Equations 1 and 2 define what is required of a basic ETEF at its simplest form. The next big question is if and how such a record can actually be created. Obviously, from analytical viewpoint, this is a formidably complicated problem to be tackled by future mathematicians. However, for the moment, the virtue of numerical optimization can be used to seek a possible solution.

This problem can be formulated as shown in Equation 3 considering acceleration data points as variables. For a record of about 20 sec considering a time interval of 0.01 sec, about 2000 acceleration data points are required. These are to be treated as variables in the optimization problem.

Minimize

$$F(a_g) = \int_0^{T_{\max}} \int_0^{t_{\max}} \{[S_a(T,t) - S_{aC}(T,t)]^2 + \alpha[S_u(T,t) - S_{uC}(T,t)]^2\} dt\, dT \tag{3}$$

In which α is a weight factor considered equal to unity in this research [11]. The target function in this formulation is a fundamentally more difficult one to satisfy as compared to the case of creating an artificial accelerogram because the acceleration function is required to produce a specific response at each particular time. In effect, each ETEF includes many artificial accelerograms condensed into a single acceleration function. Now the next question is whether the working solution can be achieved by solving the optimization problem formulated in Equation 3? The response spectra of a typical ETEF produced by the above procedure is shown in Figure 2. As can be seen in this figure, the resulting ETEF fits with the target spectrum in a reasonably well manner.

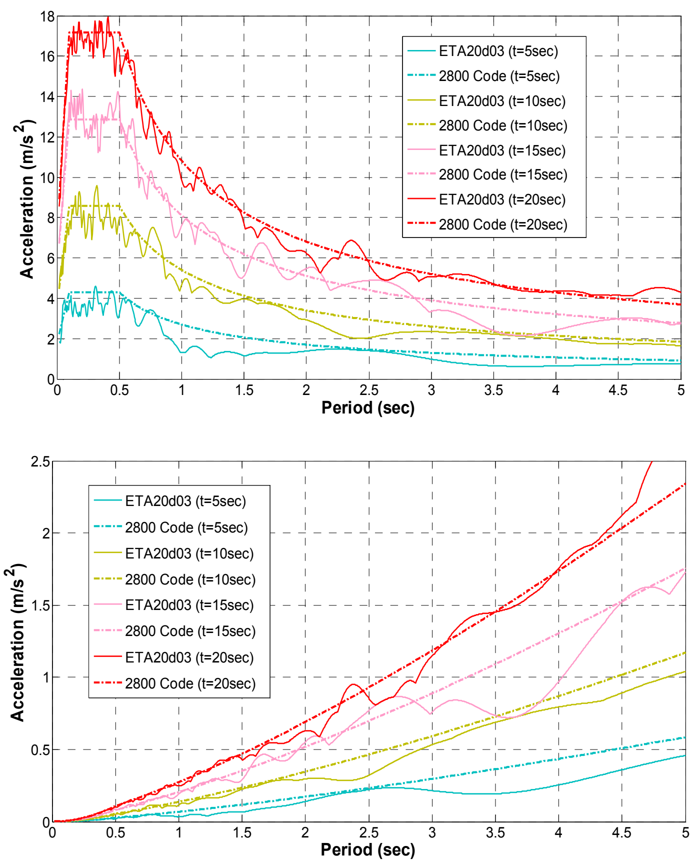

Figure 2 Response spectra of ETA20d03 at 5th, 10th, 15th and 20th sec: (a) acceleration; and (b) displacement.

It is not clear how much better ETEFs can be produced using advanced optimization procedures. However it seems that even with current level of fit, the produced ETEFs can be put into practical use. In order to reduce the level of scatter, various alternative schemes can be adopted. One of the simplest procedures in this regard is to average the result from several ETEFs in order to reduce the level of a scatter around the target. Preliminary studies show that by averaging the results from three ETEFs, a reasonably accurate estimate of the response can be made [Estekanchi et al. 2007]. The average response from three different ETEFs with equal target spectrum is shown in Figure 3. As can be seen, the average response has a better fit with the target spectrum.

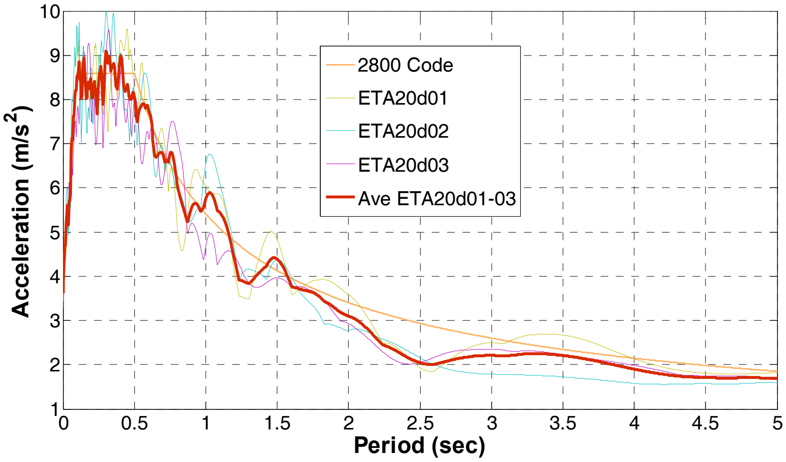

Figure 3 **Acceleration response spectra of ETA20d01-03 at the target time (the 10th sec).**

A typical 20-sec-long ETEF is shown in Figure 4 where the maximum acceleration has been indirectly made to follow an almost linear increasing pattern as a result of constraining the spectrum per Equations 1 through 3.

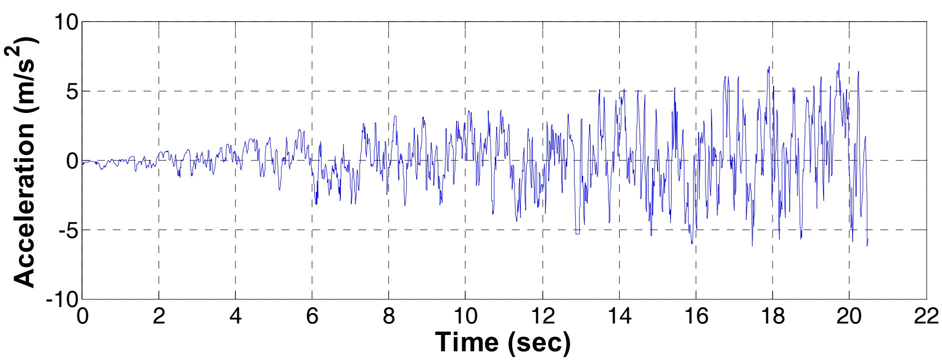

Figure 4 **A typical intensifying acceleration function (ETA20a03).**

The production of ETEFs has evolved during the past few years. Table 1 categorizes the type of ETEF records into four generations:

Table 1 Various generations of ETEFs.

Category	Description	Example Records
1st Generation	Essentially a profiled filtered white noise. Just demonstrated the concept with little numerical significance.	acc1, acc2, acc3
2nd Generation	Made to produce a consistent response spectrum that grows with time using optimization in linear range. Produced good results in nonlinear range when long periods included.	ETA20a01-3, ETA20e01-3, ETA20f01-3, …
3rd Generation	Optimized directly in nonlinear range. Nonlinear results improved approximately 20%.	ETA20en01-3, ETA20inx01-3, …
4th Generation	Include duration consistency with intensity.	Under investigation

The first generation of ETEFs were essentially profiled filtered white noises produced in order to describe the concept of using an intensifying dynamic excitation for seismic evaluation of structures [Estekanchi et al. 2004]. In the second generation of ETEFs, the concept of response spectrum and numerical optimization were introduced and numerically significant results were achieved [Valamanesh et al. 2010]. By extending the range of period of vibration into very long periods of about 100 sec, records in this generation also produced very reasonable estimates in the nonlinear range of behavior [Riahi and Estekanchi 2010]. In the third generation, nonlinear response spectra was directly included in the optimization procedure. While theoretically important, only a 20% improvement to be achieved over the already good estimates that could be made by second generation records. In the fourth generation of records, it is intended to include duration consistency with intensity. This means that, instead of following an arbitrary linear intensification pattern, the ETEFs are to be made to produce desired intensity at a time that is consistent with the duration of the ground motions that can be considered a representative of that intensity on the average. Production of this fourth generation is under investigation.

OPTIMIZATION IN NONLINEAR REGION

As mentioned in the last section, optimization of ETEFs in the nonlinear range has been applied in the third generation of ETEFs and is still under investigation. The effect of optimization in nonlinear range at a typical level of non-linearity (i.e. for R=4) is shown in Figure 5, where the second generation ETEF somewhat underestimates the displacement for periods of above 1.5 sec. When optimization in nonlinear range as applied, the results are improved in the long-period range, while inconsistencies in the periodic range of 1 to 1.5 sec is somewhat increased. Although the fit of the curves to the target curve is not especially good here, it should be noted that there are too many targets to be matched at different times and at different levels of nonlinearity [Nozari 2008].

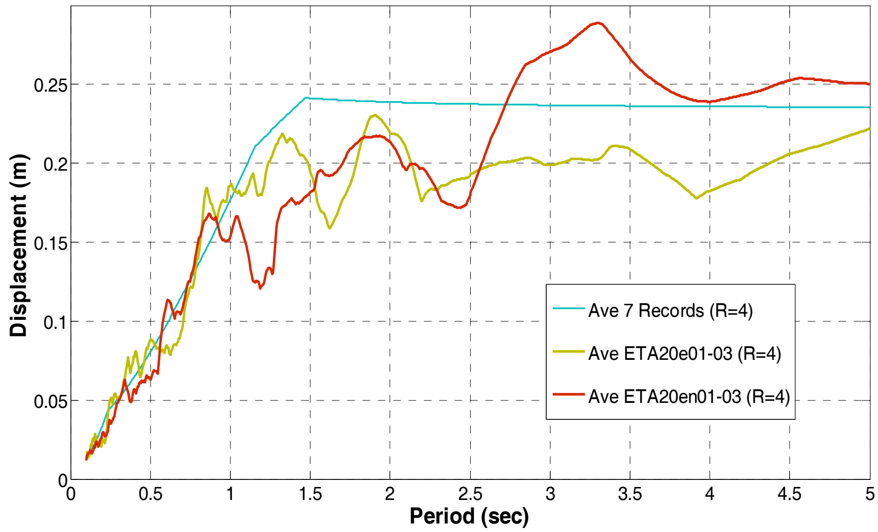

Figure 5 Comparison of displacement spectra of 'e' and 'en' series for R=4.

The comparison of the improvement achieved through nonlinear optimization can be made by considering Tables 2 and 3. In these tables absolute and relative average deviations from target displacement spectrum for a second and a third generation ETEF are provided. As can be seen in Table 2, the total relative error for ETA20e series is about 24%, while Table 3 shows that this relative error is about 16% in ETA20en series as a result of applying numerical optimization in nonlinear range in producing this third generation ETEF.

Table 2 Absolute and relative errors of ETA20e01-03 in the nonlinear range.

Error	Strength ratio	Acceleration function			
		ETA20e01	ETA20e02	ETA20e03	Average
Absolute (m)	R=1	0.0397	0.0504	0.0384	0.0428
	R=2	0.0570	0.0667	0.0559	0.0599
	R=4	0.0650	0.0811	0.0675	0.0712
	R=6	0.0731	0.0848	0.0688	0.0756
	R=8	0.0847	0.0864	0.0709	0.0807
Relative	R=1	15.06%	17.22%	14.10%	15.46%
	R=2	19.64%	20.70%	19.58%	19.97%
	R=4	23.93%	25.58%	27.62%	25.71%
	R=6	25.43%	27.46%	30.00%	27.63%
	R=8	27.40%	30.65%	30.80%	29.62%
Total absolute error (m)		0.0657	0.0759	0.0623	0.0680
Total relative error		22.47%	24.50%	24.73%	23.90%

Table 3 Absolute and relative errors of ETA20en01-03 in the nonlinear range.

Error	Strength ratio	Acceleration function			
		ETA20en01	ETA20en02	ETA20en03	Average
Absolute (m)	R=1	0.0398	0.0385	0.0379	0.0387
	R=2	0.0438	0.0452	0.0435	0.0442
	R=4	0.0491	0.0449	0.0427	0.0456
	R=6	0.0459	0.0458	0.0487	0.0468
	R=8	0.0331	0.0372	0.0386	0.0363
Relative	R=1	15.93%	13.01%	12.90%	13.95%
	R=2	16.75%	15.51%	15.82%	16.03%
	R=4	17.04%	16.12%	16.83%	16.66%
	R=6	15.81%	17.33%	17.71%	16.95%
	R=8	12.57%	14.21%	16.17%	14.32%
Total absolute error (m)		0.0451	0.0443	0.0431	0.0442
Total relative error		15.98%	15.71%	16.16%	15.95%

EXTENSION TO MULTI-COMPONENT ANALYSIS

Three dimensional modelling has become a standard in structural engineering design practice partly because the interaction of translational and torsional modes of vibration can produce complicated effects that cannot be predicted with acceptable accuracy considering a simplified two dimensional model. For seismic loading, in the past unidirectional excitation applied to a three dimensional model has been considered as an acceptable practice for regular structures with limited height. However, considering recent advances in understanding the nature of earthquakes and availability of more powerful analysis software, it seems that more realistic multi-component seismic loading will prevail in the near future.

The extension of the concept of applying an intensifying excitation function to a structure to two- and three-directional loading is relatively straightforward [Valamanesh et al. 2010]. Preliminary studies demonstrate that by applying a set of ETEFs simultaneously in three directions to a structure, a reasonably well estimate of the response of the structure when subjected to ground motions considering two or three components of ground motion can be achieved. Figure 6 shows a sample 15 stories irregular building used in a study of multi-component ET analysis [Valamanesh et al. 2010a].

In Figure 7, internal forces the structural members of the structure shown in Figure 6 using ET analysis is compared with those of response history analysis using a set of seven ground motions recorded on soil type C. As can be seen in this figure, ET analysis results match reasonably well with those of complete response-history analysis. Even though the results are from a linear analysis compared at a single intensity level, considering the findings in two dimensional nonlinear studies, it can be expected that the usable level of accuracy can also be achieved in a multi-component nonlinear case. This subject is also currently under investigation and the results will shortly become available.

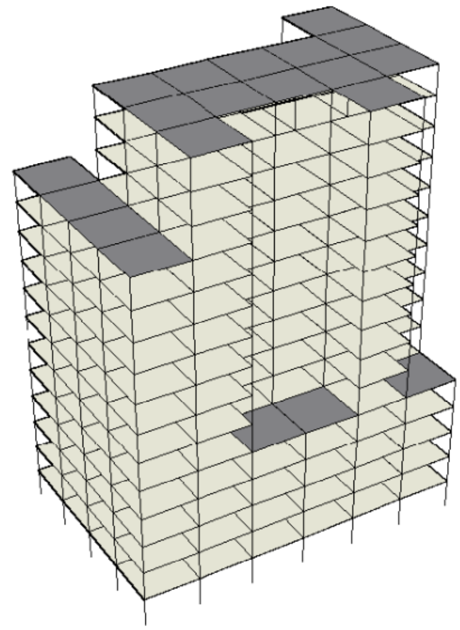

Figure 6 Irregular 15 stories steel frame.

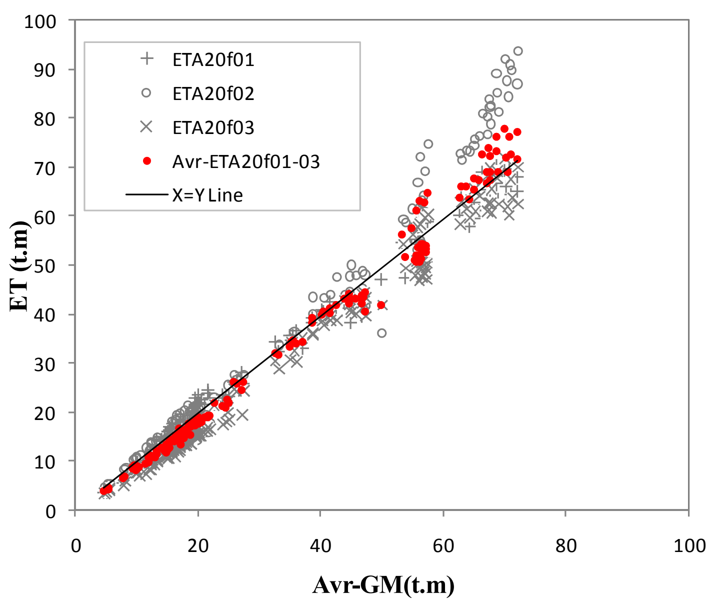

Figure 7 Beam moments of irregular 15 story building from ET and ground motion analysis.

APPLICATIONS IN PERFORMANCE BASED DESIGN

One of the interesting applications of ET method is in performance based design of structures, where structural and non-structural performance is to be evaluated at various different levels of excitation. The ET analysis turns out to be very efficient in these cases since it inherently produces estimates of the response as a continuous function of intensity [Estekanchi et al. 2011]. A general methodology for application of the ET method for practical design is given in Figure 8. Considering the relatively high computational demand required in producing ETEFs, it is not expected that normally the designer should require producing ETEFs for design. For practical application, ETEFs compatible with standard seismic codes and design spectra should be generated and be made available for design applications.

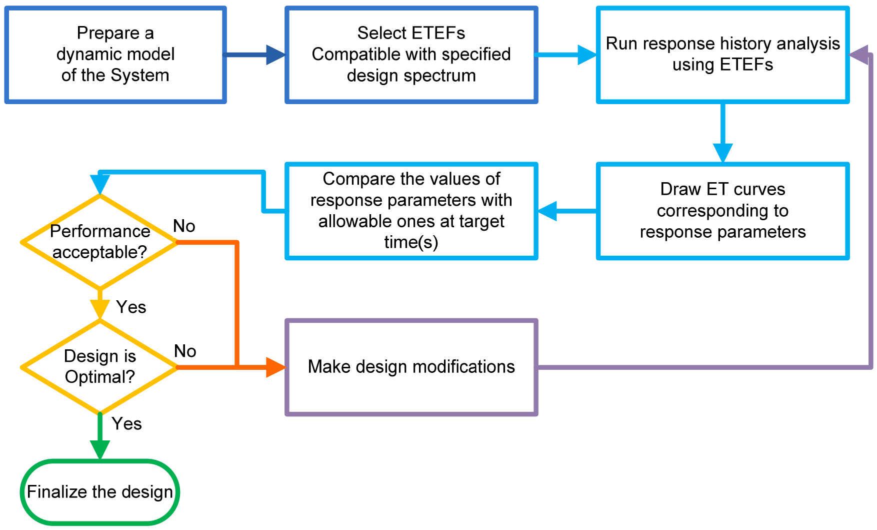

Figure 8 General methodology of ET design procedure.

As mentioned above, ET defines engineering demand as a continuous function of applied intensity. The target performance can also be better presented in the form of a continuous function rather than discreetly. While of little practical significance considering current design requirements, this kind of presentation seems to be more sensible from engineering standpoint. Figure 9 shows a sample ET analysis result curve along with a continuous target performance curve. It can be readily observed that in this case, the performance requirement at IO level has not been satisfied while there is a relatively large margin of safety considering LS and CP level requirements [Mirzai et al. 2010].

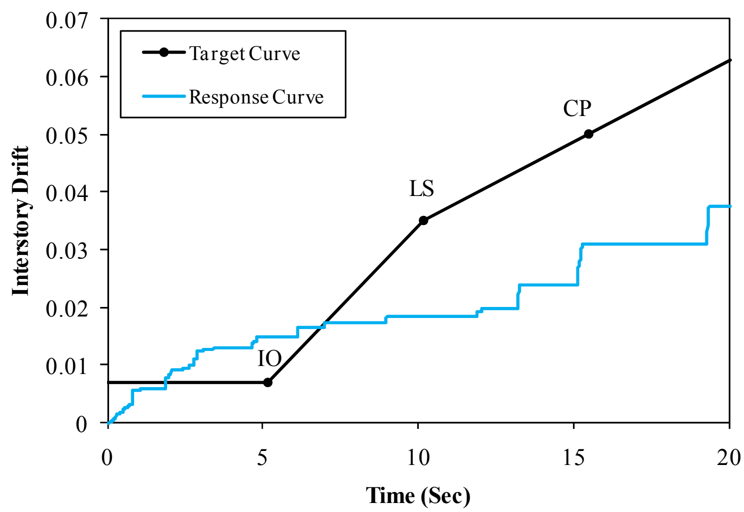

Figure 9 Target and concurrent performance curves.

In practice, various different demand parameters should be compared in order to assess the performance at the particular intensity level. To provide a better presentation of overall performance on a single graph, demand parameters can be normalized so that many of them can be presented on the same axis. Figure 10 shows the presentation of interstory drift and maximum plastic joint rotation using a normalized vertical axis where interstory drift is the critical parameter at IO level; in this case, plastic joint rotations become more critical at LS and CP levels. Note that while in ET method, time is a representative of intensity level. It can be more versatile to use equivalent S_a or, better still, the equivalent return period for horizontal axis. This can be readily achieved by comparing the response spectrum of the applied ETEF to the response a spectrum expected at various return periods. However, there are some technicalities involved in this transformation of coordinates that is under investigation, and the results are expected to be published in the near future.

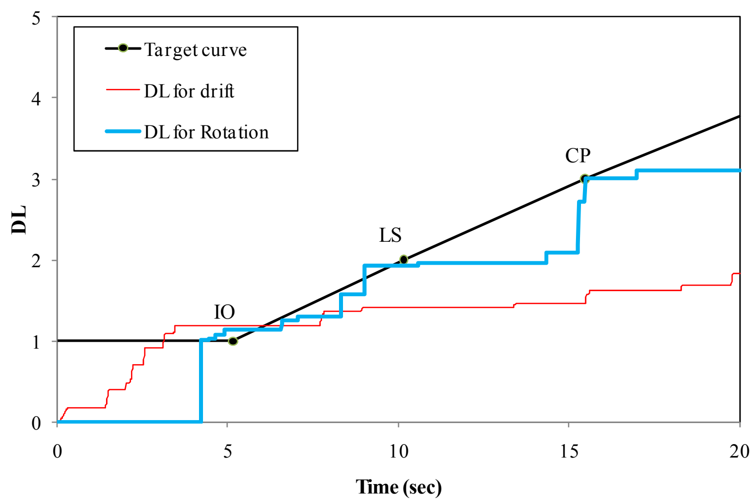

Figure 10 Performance curves considering plastic rotations and drift in a typical 3 story 1 bay frame.

SUMMARY AND CONCLUSIONS

In this paper, basic concepts and some recent advances in seismic assessment of structures using the Endurance Time (ET) method was explained. The ET method is a dynamic pushover procedure in which structures are subjected to predesigned intensifying excitation functions (ETEFs) and their performance is assessed based on their response at different excitation levels. This method is a response-history based procedure and provides some improvements on complexity and computational demand of these categories of analysis procedures. Major benefits that can be achieved by applying this procedure include significant reduction of the computational demand, simplicity and sensibility for engineering application, and applicability to a broad range of structures regardless of their complexity. The procedure can also be very beneficial in experimental studies where practical test cases have to be reduced to a minimum. Currently available ETEFs are produced by using numerical optimization procedures. The estimated response at various levels of intensities matches well with ground motions analysis results in linear and nonlinear analysis. Production of improved ETEFs that produce more precise estimates of seismic response at different equivalent intensity levels remains an open topic. Recent developments in application of the procedure in multi-component analysis and performance based design were also explained.

REFERENCES

Bazmuneh A, Estekanchi HE (2009). Application of endurance time method in performance based design with an example of special concentric braced frame (in Persian), *Proceedings*, 4th National Conference on Seismic Resistant Design of Buildings (Standard 2800), Building and Housing Research Center, Tehran, Iran, No. EC22–05.

Bertero RD, Bertero VV (2002). Performance-based seismic engineering: the need for a reliable conceptual comprehensive approach, *Earthq. Engng. Struct. Dyn.*, 31(3):627–652.

Bozorgnia Y, Bertero VV (2004). *Earthquake Engineering: from Engineering Seismology to Performance-based Engineering*, CRC Press, USA.

Chopra AK (1995). *Dynamics of Structures: Theory and Applications to Earthquake Engineering*, Prentice Hall International Series in Civil Engineering and Engineering Mechanics, Prentice Hall, Englewood Cliffs, NJ.

Chopra AK, Goel RK (1999). Capacity-demand-diagram methods for estimating seismic deformation of inelastic structures: SDF systems, *Report No. PEER-1999/02*, Pacific Earthquake Engineering Research Center, University of California, Berkeley, CA.

Chopra AK, Goel RK (2003).A modal pushover analysis procedure to estimate seismic demands for buildings: Summary and Evaluation, *Proceedings*, Fifth National Conference on Earthquake Engineering, May 26-30, Istanbul, Turkey.

Estekanchi HE, Vafai A, Sadeghazar M (2004). Endurance time method for seismic analysis and design of structures, *Scientia Iranica*, 11(4):361–370.

Estekanchi HE, Valamanesh V, Vafai A (2007). Application of endurance time method in linear seismic analysis, *Engng. Struct.,* 29(10):2551–2562.

Estekanchi HE, Arjomandi K, Vafai A (2008). Estimating structural damage of steel moment frames by endurance time method, *J. Construct. Steel Res.,* 64(2):145–155.

Estekanchi HE, Basim MC (2011). Optimal damper placement in steel frames by the endurance time method, *The Structural Design of Tall and Special Buildings*, doi:10.1002/tal.689.

Federal Emergency Management Agency (2005). Improvement of nonlinear static seismic analysis procedures, *FEMA-440*, Washington DC.

Mirzai A, Estekanchi HE, Vafai A (2010). Application of endurance time method in performance based design of steel moment frames, *Scientia Iranica*, 17(6):482–492.

Newmark NM (1971). *Fundamentals of Earthquake Engineering*, Prentice-Hall, Englewood Cliffs, NJ.

Nozari A (2008). Optimization of ET accelerograms using classic and heuristic approaches, M.S. thesis, Dept of Civil Engineering, Sharif University of Technology, Tehran, Iran.

Riahi HT, Estekanchi HE, Vafai A. (2009). Endurance time method - Application in nonlinear seismic analysis of SDOF systems, *J. Appl. Sci*., 9(10):1817–1832.

Riahi HT, Estekanchi HE (2010).Seismic assessment of steel frames with endurance time method, *J. Construct. Steel Res*., 66(6):780–792.

Valamanesh V, Estekanchi HE (2010a). A study of endurance time method in the analysis of elastic moment frames under three-directional seismic loading, *Asian J. Civil Engng*., 11(5):543–562.

Valamanesh V; Estekanchi HE, Vafai A (2010a). Characteristics of second generation endurance time accelerograms, *Scientia Iranica*, 17(1):53–61.

Valamanesh V, Estekanchi HE (2010b). Compatibility of the endurance time method with codified seismic analysis approaches on three-dimensional analysis of steel frames, *The Structural Design of Tall and Special Buildings*, doi:10.1002/tal.666.

Vamvatsikos D, Cornell CA (2003). Incremental dynamic analysis, *Earthq. Engng. Struct. Dyn*., 31:491–514.

Vamvatsikos D, Cornell CA (2005). Seismic performance, capacity and reliability of structures as seen through incremental dynamic analysis, The John A. Blume Earthquake Engineering Center, Stanford University, Stanford, CA.

PERFORMANCE ASSESSMENT OF IRREGULAR BUILDINGS USING AN ADAPTIVE PUSHOVER METHOD

Reşat A. Oyguç and Hasan Boduroğlu

Istanbul Technical University, Earthquake Engineering and Disaster Management Institute, Maslak 3469 Istanbul, TURKEY

ABSTRACT

In recent years, performance-based design methods have been started to be used widely among the engineers. Those methods rely on nonlinear static analysis procedures. Although, nonlinear time history analysis is known as the most accurate way to determine the structural capacity, it needs expertise in computation procedure. Today it is a well-known fact that conventional procedures are only adequate when the fundamental mode is predominant. They neglect the progressive changes in the modal properties and the higher mode effects. Recent studies rely on adaptive pushover procedures, which take into account the higher mode effects, and update the load pattern at instantaneous states of inelasticity with a less computational time. A newly proposed adaptive pushover procedure by Shakeri et al. [2010] has been developed for accounting the three-dimensional irregularity effects of existing reinforced concrete structures. The computer code named NASAP has been developed for implementing the mentioned procedure. Results are compared with time-history domain analysis demonstrating that conventional analysis overestimates the base shear forces by 20%.

INTRODUCTION

During last decades, nonlinear static (pushover) analysis has been the most popular tool for seismic performance evaluation of buildings because of its simplicity. The methods rely on pushing the structure with incremental static lateral loads. Nonlinear time-history analysis is an accurate way to assess the seismic demand.

However, recent studies have shown that conventional pushover design procedures are not dependable because conventional procedures neglect the progressive changes in the modal properties and the higher mode effects. This makes the deformation results inaccurate. In the conventional procedure, damage is a function of the lateral deformation only. It neglects the duration effects. Papanikolaou et al. [2005] stated that conventional pushover analysis implies a separation between structural capacity and earthquake demand. Many researchers have showed a correlation between structural capacity and demand of an earthquake. Although static pushover procedures neglect the dynamic effects, it is not possible to take into account the kinetic energy and viscous damping energy changes during a monotonic static push. Pushover analyses give inaccurate results for three-dimensional (3D) structures. Torsional effects and irregularities make the results of the analysis suspicious.

To overcome all this deficiencies, several researchers [Papanikolaou et al. 2005a; Papanikolaou et al. 2005b; Papanikolaou et al. 2006; Jeong and Elnashai et al. 2004] have suggested a combination of pushover analysis with fiber models, where the moment-curvature response is derived from the material characterization. Chopra et al. [2000; 2002] developed multi-mode pushover analyses. Later studies rely on adaptive pushover procedures, which take into account the higher mode effects, and update the load pattern at instantaneous states of inelasticity. Also, Incremental Response Spectrum Analysis (IRSA), has been developed by Aydınoğlu [2003]. Here, pushover analysis is performed according to the incremental displacements and instantaneous inelastic spectral displacements are used to calculate the modal story displacements in each step. Then the capacity curves are transformed to response spectrum format.

REVIEW OF THE PREVIOUS STUDIES

Non-adaptive Modal Pushover Procedures

Due to higher mode effects, Paret et al. [1996] and Sasaki [1998] suggested multi-mode pushover procedure (MMP).As shown in Figure 1, Sasaki et al. [1998] illustrated the conversion of capacity curve to spectral acceleration spectral displacement. Capacity curves based on elastic mode shapes are determined separately by conventional pushover analysis. Then each capacity curve is compared with the demand spectrum using the Capacity Spectrum Method (CSM). This way, the critical mode is obtained. Procedure takes into account the higher mode effects but neglects the modal changes during plastification.

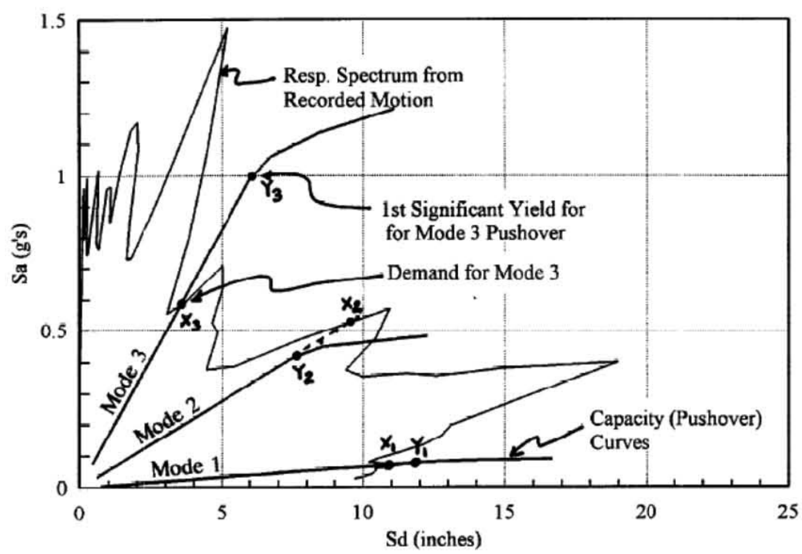

Figure 1 Capacity and demand curves in ADRS format [Sasaki et al. 1998].

Moghadam [2002] proposed a modal combination procedure, Pushover Results Combination (PRC), for multi-mode pushover analysis. According to this method, several pushover analyses are carried out by using the modal load pattern. The maximum response is estimated by combining the pushover results.

Chopra and Goel [2002] conducted Modal Pushover Analysis Procedure (MPA). The procedure is nearly same to Paret et al. [1996], except the modal capacity curves are idealized as bilinear, as shown in Figure 2. Total demand is calculated by combining the modal responses using the SRSS rule. Because MPA lacks the effect of reversal, the modal interaction Modified Modal Pushover Analysis Procedure has been proposed by Chopra and

Goel [2004]. The only difference between MPA and MMPA is that the higher modes effects are computed under the assumption that the system is elastic. Then the analysis becomes identical to classical modal analysis for linear systems, and pushover analysis for higher modes is not needed.

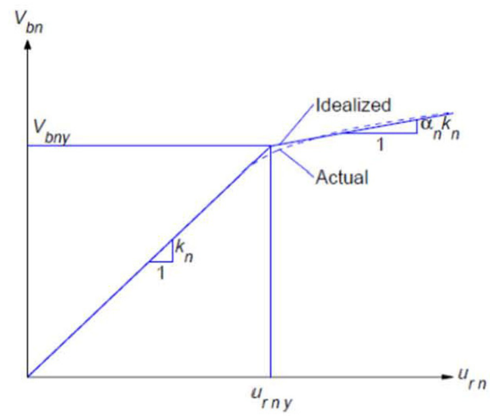

Figure 2 Idealized pushover curve [Goel and Chopra 2004].

Adaptive Pushover Procedures

Reinhorn [1997] used an incremental lateral load pattern during response spectrum analysis (RSA). Modal story forces are then combined using the rule SRSS, combined lateral forces are then executed to the system. Bracci et al [1997] proposed an adaptive procedure, where the equivalent elastic story shear and drift demand curves are determined using modal superposition. Story capacities are then superimposed with the story response demand curves and the performance point is calculated. Satyarno et al. [1998] proposed a procedure, where the modal properties updated constantly due to the simultaneous changes through a modified Rayleigh method. Requena and Ayala [2000] established a procedure that takes into account the instantaneous higher mode effects.

Gupta and Krawinkler [2000] proposed a methodology where the applied load pattern is derived from the RSA. The derived load pattern is simultaneously updated, depending on the instantaneous dynamic properties of the structure. After performing eigenvalue analysis, the modal participation factor for that mode is calculated. Using the modal participation factor, story forces at each level for each *n* mode is determined. Modal base shears are then computed, and they are combined using the SRSS to derive the structural base shear. Before performing a static analysis, the story forces are scaled using a scaling ratio. This means, for modes other than the fundamental mode, the structure will be pushed and pulled simultaneously. In Figure 3, the drift profiles of SAC20 under various analyses are compared. As it can be seen from the figure, the uniform load pattern is only applicable where higher mode effects are not significant.

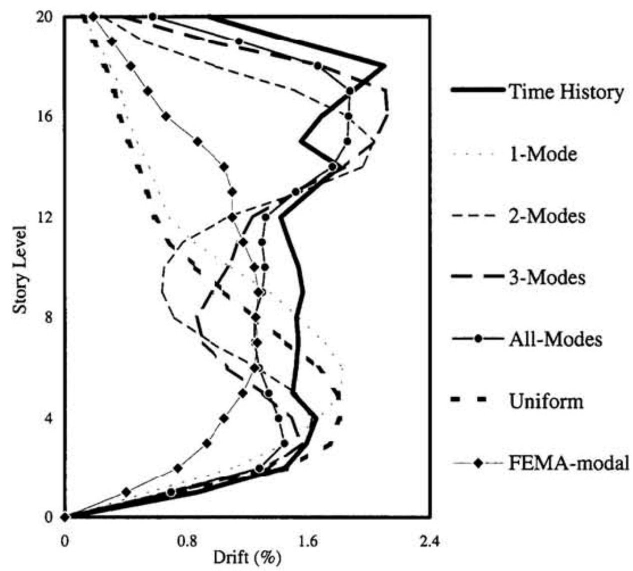

Figure 3 **Story drifts of SAC20 building for different procedures [Gupta and Krawinkler 2000].**

Elnashai et al. [2001] proposed a force-based adaptive procedure, where inelasticity is spread through the element length and across the section depth. In Figure 4, a comparison of conventional and adaptive pushover analysis results is given. For more detailed information, Papanikolaou et al. [2005a]. Regarding the fault effect, it can be stated from the figure that adaptive pushover approach performs better than the conventional ones, especially at lower drift levels.

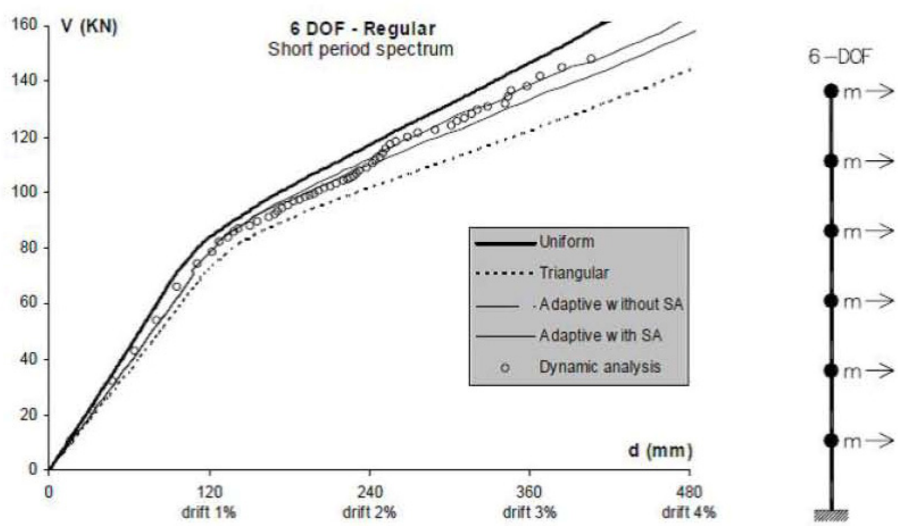

Figure 4 **Comparative plot among conventional pushover, adaptive pushover and dynamic analysis [Mwafy and Elnashai 2001].**

Antoniou and Pinho [2004a] proposed a modal adaptive pushover procedure, which is similar to Reinhorn's, with the only difference being in the incremental scaling approaches. Aydınoğlu [2003] studied an incremental RSA procedure, similar to Gupta and Krawinkler's procedure. However, in this procedure, the pushover analysis is performed according to incremental displacements where in each step inelastic spectral displacements are used to determine the modal story displacements. Antoniou and Pinho [2004b], Pinho et al. [2006], and Ferracuti et al. [2009] developed a displacement-based adaptive pushover method (DAP) where at each step; displacement load pattern is applied to the structure. Story forces are calculated as a response of the displacement loads. Figure 5 shows the comparative results of force based and displacement based pushover analysis with the dynamic analysis for four story reinforced concrete structure. More details about the structural properties can be found in their paper.

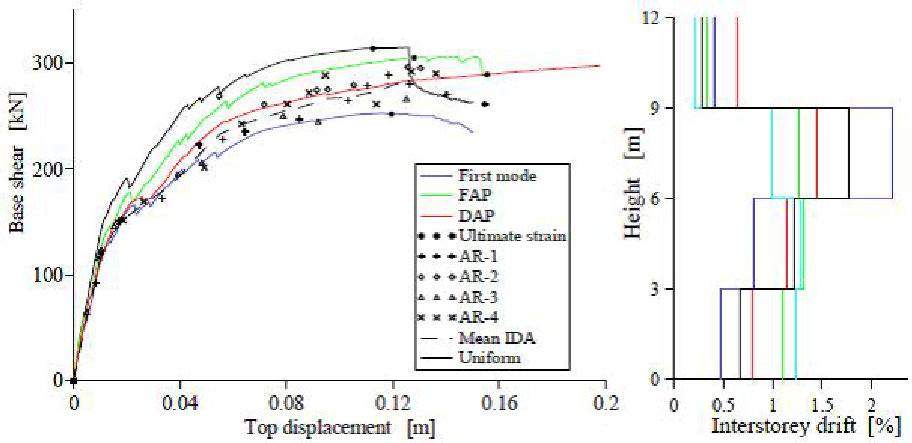

Figure 5 Comparative results of a 4 story frame [Ferracuti et al. 2009].

Shakeri et al. [2010] proposed a story shear-based adaptive procedure for nonlinear static analysis. It is a single run adaptive pushover procedure, where at each step the load pattern is derived from the modal story shears of the instantaneous step. The sign changes in the higher modes are taken into account.

A STORY SHEAR BASED ADAPTIVE PUSHOVER PROCEDURE

The procedure mainly consists of three parts [Shakeri et al 2010]. First, based on the modal story shear profile, the load pattern is updated at each analysis step. Secondly, by using the previous load pattern, the mode shape is derived and the last step is converting the capacity curve of multi degree of freedom system (MDOF) to an equivalent single degree of freedom system (SDOF). The procedure considers the contribution of the higher modes and reversal effects. At each analysis step, the story shears are calculated from the associated mode by using

$$F_{ij} = \Gamma_j \emptyset_{ij} m_i Sa_i \qquad SS_{ij=} \sum_{k=i}^{n} F_{kj} \quad SS_i = \sqrt{\sum_{j=1}^{m} SS_{ij}^2}$$

Here, i is the story number, j is the mode number, $\emptyset_{ij}$ is the ith component of the jth mode shape, m_i is the mass of the ith story, S_{aj} is the spectral acceleration corresponding to the jth mode, Γ_j is the modal participation factor for the jth mode, SS_{ij} is the story shear in level i associated with mode j, and SS_i is the modal story shear in level i associated with all the considered modes. The required story forces are calculated by subtracting the combined modal shear of consecutive stories using the equation below:

$$F_iS_i - SS_{i+1} \qquad i = 1, 2, \ldots(n-1)$$

$$F_n = -SS_n \qquad i = n$$

The lateral load pattern is normalized with respect to its total value by

$$\bar{F}_i = \frac{F_1}{\sum F_1}$$

$$\Delta F_i = \Delta V_b x \bar{F}_1$$

Here; ΔV_b is the incremental base shear, ΔF_i is the ith component of the incremental applied load at each step.

The proposed SSAP methodology is given as a flowchart in Figure 6.

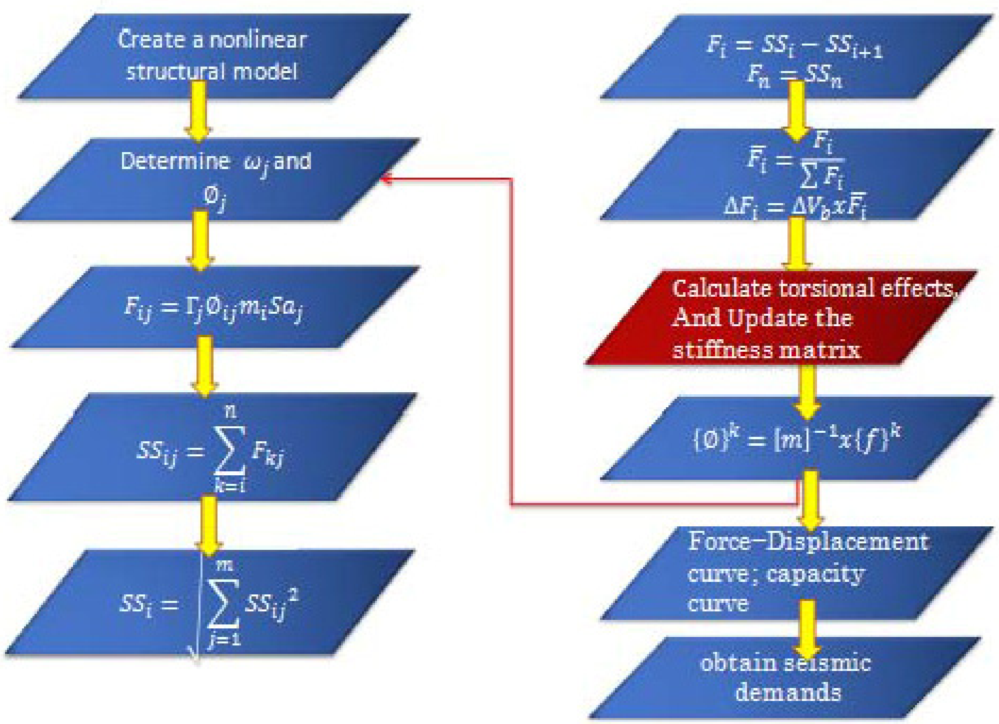

Figure 6 The proposed SSAP process.

PROPOSED METHOD: NONLINEAR ADAPTIVE STRUCTURAL ANALYSIS PROGRAM (NASAP)

The main objective of this study is to develop a procedure that takes into account the higher mode effects besides the torsional response of a 3D building. The results of the 3D pushover analysis are compared with the nonlinear time history results of the considered building. The torsional effects are induced in the updated stiffness matrix at each adaptive analysis steps as described by Fajfar and Gaspersic [1996]. Effective eccentricities are used in order to improve the results of the pushover analysis as Fajfar proposed. As a well-known issue, torsional responses in fundamental mode shapes under dynamic loadings cannot be determined by conventional analysis methods. The software package used in the present work is NASAP. This is a tool for finite element analysis of structural elements, meaning "Nonlinear Adaptive Structural Analysis Program". Figure 7 shows the NASAP model of the SPEAR building, a 3D frame tested in 2003 within the European network project "Seismic Performance Assessment and Rehabilitation (SPEAR)." The structure is a three-story building that is representative of older construction in southern Europe without earthquake design provisions. It was designed by Fardis and Paolo [2005]. It has large eccentricity in plan and irregularity in elevation. Figure 8 shows the overview of the test model.

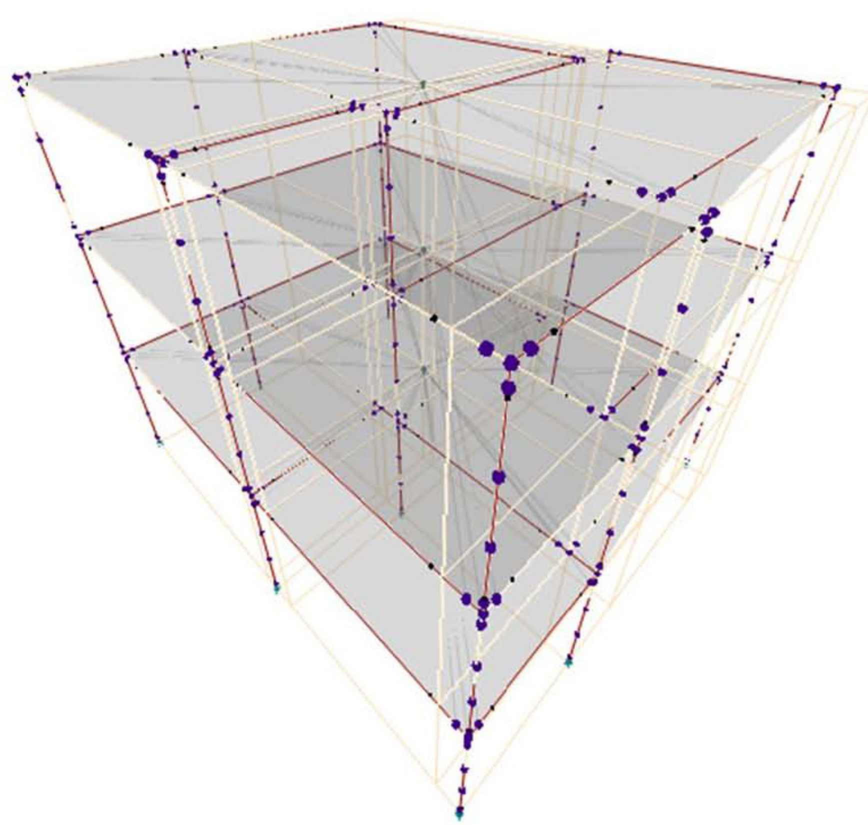

Figure 7 Print screen from NASAP program.

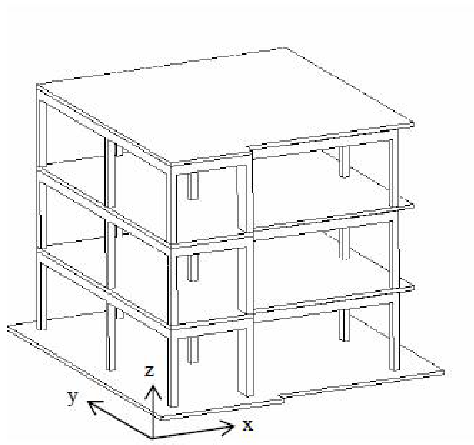

(a) 3D view of the test model

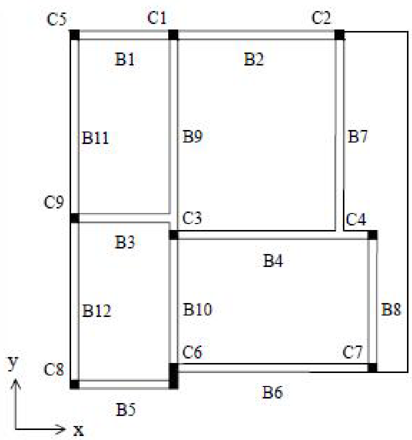

(b) Plan of the test model

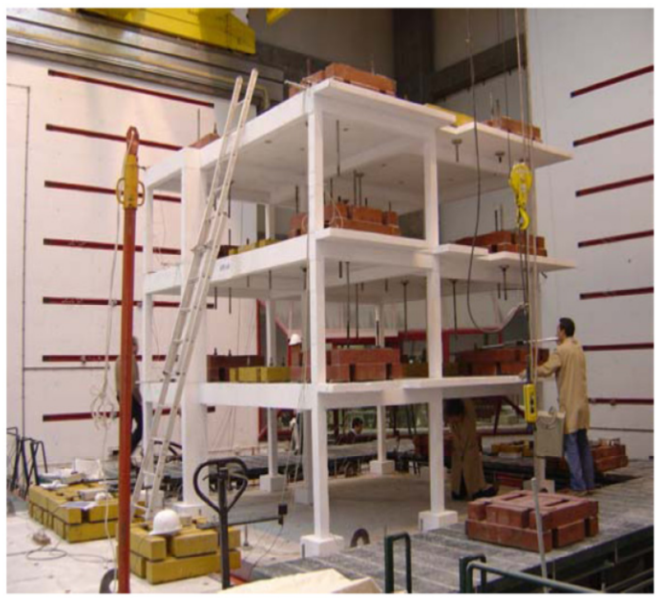

Figure 8 Overview and plan of SPEAR [Fardis and Paolo 2005].

The NASAP program performs nonlinear analysis using a concentrated plastic hinge concept. Story shear-based adaptive pushover procedure which is proposed by Shakeri et al. [2010] has been utilized in developing NASAP. Torsional effects are also induced into the program code. A non-adaptive pushover analysis option has been added to NASAP. It also performs the non-adaptive analysis by the procedures described in SSAP. The needed target displacement for both adaptive and non-adaptive pushover analysis is calculated by the formulas given in FEMA. P-Delta effects are neglected in the analysis. Time-history analysis are conducted with PERFORM 3-D (CSI). The results of the time-history analysis are compared with the adaptive and non-adaptive pushover results of NASAP.

In the test structure, columns are slender and not strong enough to carry a large magnitude of bending caused by lateral forces due to earthquakes, and they are more flexible than the beams. For the modeling of beams, a reinforced concrete T-section was utilized. The P-MM properties for the column 25×75 are shown in Figure 9, and the M-κ properties of the beams used in the analysis is given in Figure 10.

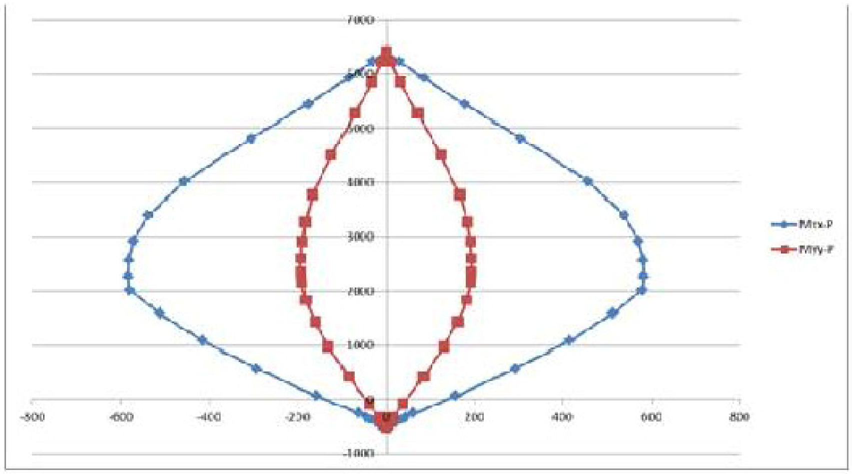

Figure 9 P-MM properties of the column 25*75.

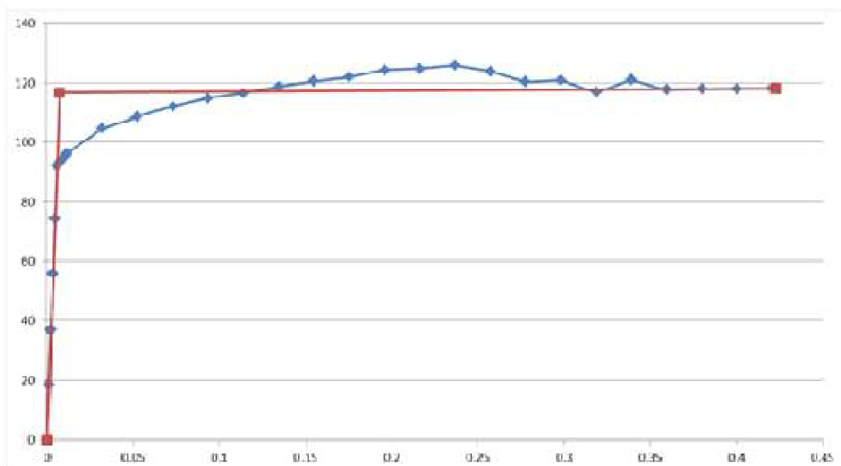

Figure 10 M-κ properties of the beams.

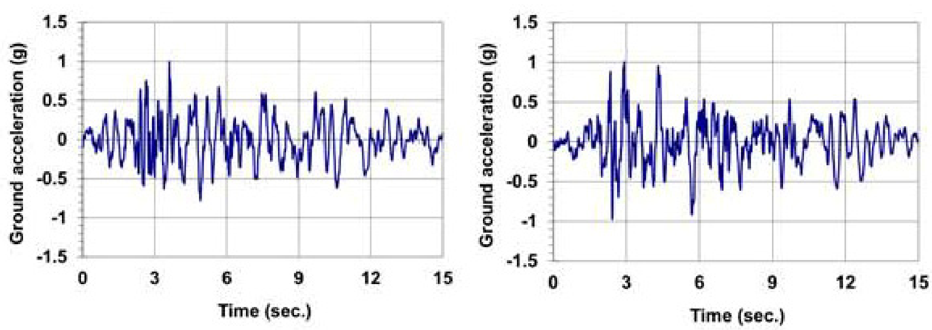

Figure 11 1979 Montenegro record scaled to 1g, longitudinal and translational components.

The SPEAR building was subjected to the 1979 Montenegro record. The record consists of two orthogonal components (longitudinal and translational) of horizontal accelerations and modified from natural records to be compatible to the EC8 Type 1 design spectrum, soil type C and 5% damping. The latter records were normalized to peak ground acceleration of 1.0g on rock site, which means that PGA is 1.15g on soil type C, as shown in Figure 11.

The capacity curves were calculated by following the procedures described by Gupta and Kunnath [16]. According to the procedure, the intersection of the inelastic spectrum and the demand curve gives the first iteration point for the calculated target displacement value. This procedure has been implemented, and the capacity curves of SPEAR building for both longitudinal and transverse ways were calculated.

CONCLUSIONS

Comparisons of adaptive and conventional pushover curves for the SPEAR building can be seen in Figures 12 and 13. It is obvious that, conventional pushover analysis overestimates the base shear forces. Conventional analysis overestimates the base shear by approximately20%.

Uniform load pattern may only be applicable when higher mode effects are not significant. Ignoring the higher modes can result in highly inaccurate estimates of deformation demands. Force-based adaptive procedures use SRSS to combine the modal story effects. In addition, the majority of adaptive pushover analyses taking in account torsional effects are not so common. Here, a 3D adaptive pushover procedure takes into account the irregularity effects.

Comparison of the drift profile of SPEAR building using story shear based adaptive pushover analysis with the drift profile obtained by the time history domain analysis is an ongoing research project.

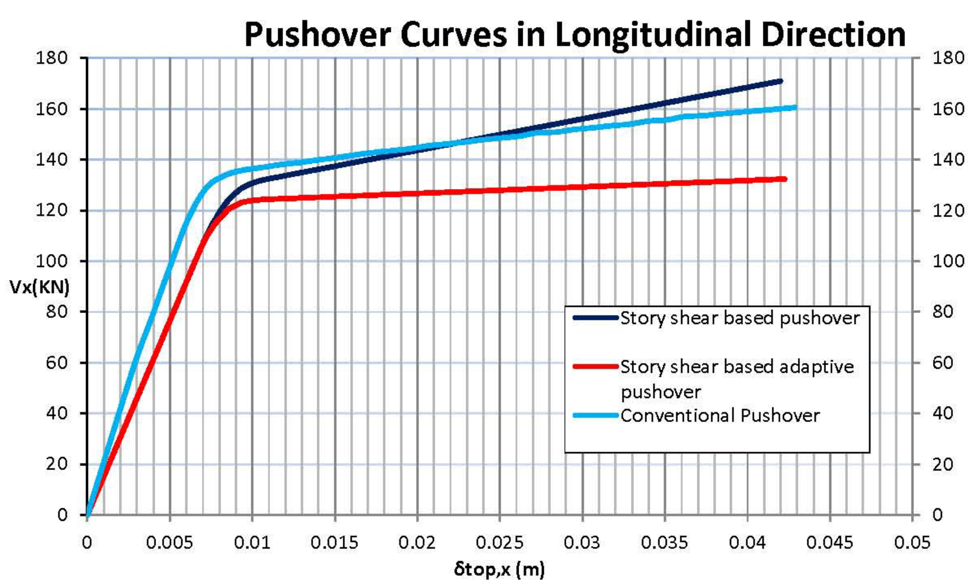

Figure 12 Pushover curves in longitudinal direction.

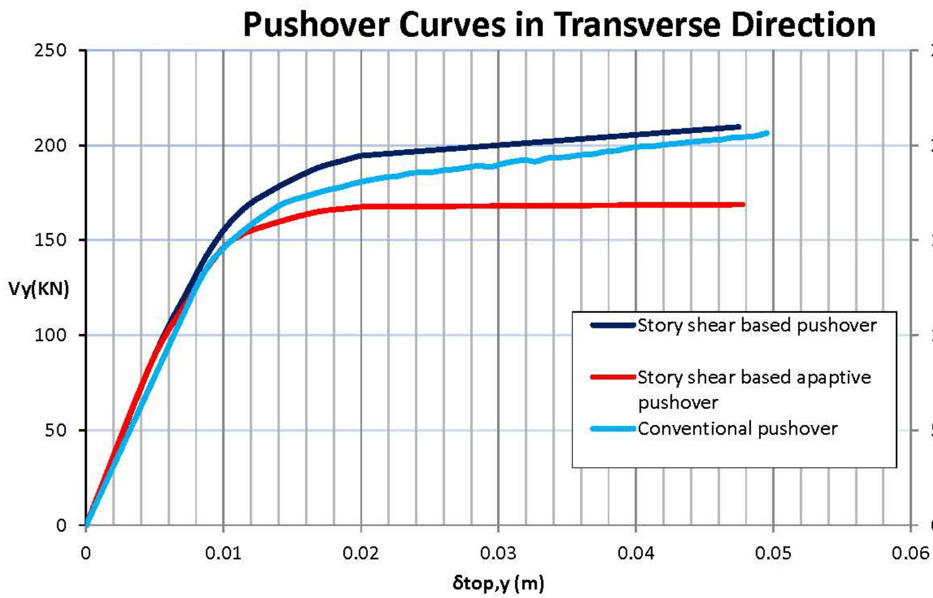

Figure 13 Pushover curves in transverse direction.

REFERENCES

Antoniou S, Pinho R (2004a). Advantages and limitations of adaptive and non-adaptive force-based pushover procedures, J Earthquake Eng 8 (4) (2004), pp. 497–522.

Antoniou S, Pinho R (2004b). Development and verification of a displacement-based adaptive pushover procedure, *J. Earthq. Engng*., 8(5):643–661.

Aydınoğlu N (2003). An incremental response spectrum analysis procedure based on inelastic spectral displacements for multi-mode seismic performance evaluation, *Bull. Earthq. Engng.,* 1:3–36.

Bracci JM, Kunnath SK, Reinhorn AM (1997). Seismic performance and retrofit evaluation of reinforced concrete structures, ASCE, *J. Struct. Engng*. ASCE 123(1): 3–10.

Chopra A, Goel R, Chinatanapakdee C (2000). Evaluation of a modified MPA procedure assuming higher modes as elastic to estimate seismic demands, *Earthq. Spectra*, 20:757–778.

Chopra A, Goel R (2002). A modal pushover analysis procedure for estimating seismic demands for buildings, *Earthq. Engng. Structural Dyn*., 31:561–582.

Fajfar P, Gaspersic P (1996). The N2 method for the seismic damage analysis of RC buildings, *Earthq. Engng. Structural Dyn*., 25:31-46.

Fardis M, Paolo, N (2005). *Seismic Performance Assessment and Rehabilitation of Existing Buildings*.

Ferracuti B, Pinho R, Savoia M, Francia R (2009). Verification of displacement-based adaptive pushover through multi-ground motion incremental dynamic analyses, *Engng. Struct*., 31:1789–1799.

Goel R, Chopra A (2004). Evaluation of modal and FEMA pushover analysis: SAC buildings, *Earthq. Spectra*, Vol. 20.

Gupta A, Krawinkler H (2000). Estimation of seismic drift demands for frame structures, *Earthq. Engng. Structural Dyn*., 29:1287–1305.

Jeong S, Elnashai A (2004). Analytical assessment of an irregular RC full scale 3D test structure, *Mid-America Earthquake Center Report*, University of Illinois at Urbana-Champaign, Urbana, IL.

Moghadam AS (2002). A pushover procedure for tall buildings, *Proceedings*, 12th European Conference on Earthquake Engineering.

Mwafy AM, Elnashai A (2001). Static pushover versus dynamic collapse analysis of RC buildings, *Engng. Struct*., 23:407–424.

Papanikolaou V, Elnashai A., Pareja J (2005). Evaluation of conventional and adaptive pushover analysis Part-I, *J. Earthquake Engng*.

Papanikolaou V, Elnashai A, Pareja J (2006). Evaluation of conventional and adaptive pushover analysis Part-II Comparative Results, *J. Earthquake Engng*.

Papanikolaou V, Elnashai A., Pareja J (2005). Limits of applicability of conventional and adaptive pushover analysis for seismic response assessment, *Mid-America Earthquake Center Report*, University of Illinois at Urbana-Champaign, Urbana, IL.
Paret T, Sasaki K, Elibeck D, Freeman S (1996). Approximate inelastic procedures to identify failure mechanism from higher mode effects, *Proceedings*, 11th World Conference on Earthquake Engineering.
Pinho R, Antoniou S, Pietra D (2006). A displacement-based adaptive pushover for seismic assessment of steel and reinforced concrete buildings, *Proceedings*, 8th US National Conference on Earthquake Engineering.
Reinhorn AM (1997). Inelastic analysis techniques in seismic evaluations, *Proceedings*, International Workshop on Seismic Design Methodologies for the Next Generation of Codes.
Requena M, Ayala G (2001). Evaluation of a simplified method for the determination of the non-linear seismic response of RC frames, *Proceedings*, 12th World Conference on Earthquake Engineering.
Sasaki KK, Freeman SA, Paret TF. Multi-mode pushover procedure (MMP)—A method to identify the effects of higher modes in a pushover analysis, *Proceedings,* 6th US National Conference on Earthquake Engineering, 1998.
Satyarno I, Carr AJ, Restrepo J (1998). Refined pushover analysis for the assessment of older reinforced concrete buildings, *Proceedings*, New Zealand Society of Earthquake Engineering Technology Conference.
Shakeri K, Shayanfar M, Kabeyasawa T (2010). A story shear-based adaptive pushover procedure for estimating seismic demands of buildings, *Engng. Struct*., 32:174–183.

PROBABILISTIC APPROACH ON SEISMIC DESIGN PARAMETERS OF RC FRAMES

Ali Bakhshi and Payam Asadi

Civil Engineering Department, Sharif University of Technology, Tehran, Iran

ABSTRACT

There are many parameters that are used to improve the performance of structures under earthquake excitations in seismic provisions. General considered parameters in seismic provisions are peak ground acceleration (PGA), important factor (I), and typical inherent overstrength and global ductility capacity (R). It is well recognized that the main intent of designing structures under seismic excitation is probabilistic rather than deterministic; therefore, the probability of structural damage decreases when such parameters are used to design structures. In this paper to evaluate these parameters, fragility curves are developed. Fragility curves are used for various probability parameters. These diagrams are used to demonstrate when a coefficient or some parameters are used to improve performance level of a structure, it guarantees that probability of exceedance of limit states decreases, as is expected. These diagrams can also show the effect of uncertainty of parameters on the design After introducing fragility curves and the procedure used to produce them, the effect of uncertainty of PGA is displayed and discussed. Results are shown that increasing the important factor (I) for hospital structures versus office structures does not guarantee a decrease in damage probability of exceedance.

INTRODUCTION

Seismic provisions have several parameters used to control or improve the performance of the structures under seismic excitations. Many studies have shown that the damage index of a structure can be decreased by changing these parameters. But all the earthquake properties and behavior of the structures when earthquake occurred are probabilistic rather than deterministic. At source of earthquake, the inherent of earthquake caused from fault movement is also stochastic. This uncertainty is in the whole property of earthquake record like peak ground acceleration (PGA) and frequency content. In the next step, the whole property of structure-like element details, material properties, and hysteresis or ductility behaviors are indecisive. By neglecting all these uncertainties, a meaningful evaluation of structures cannot be done.

Also there is no sufficient guarantee that considering such parameters included in seismic provisions improves the performance of structures to a precise degree. A decrease in damage index does not mean that the probability of exceedance and loss estimation can be ignored. For surveying the entire effect of these parameters, this paper introduces a new procedure where fragility curve will investigate assessing the efficiency of these coefficients on the probability of exceedance of limit states.

Many studies have used fragility curves to evaluate structures under seismic excitation with random parameters. In general, these studies have been done in three categories. The first category uses observation data on structures experiencing earthquake motions. In this category, databases of the damage index of structures are produced after the earthquake occurs. For each damaged structure, a level of seismic excitation is chosen. Fragility curve for such structures are produced by statistical handouts. This category is often used to evaluate bridge structures after an earthquake occurs. Shinozuka et al. [1999] studied the effects after Northridge earthquake for bridges in lifeline bridges in Los Angeles for four limit states (low, medium, high, and collapse) and developed fragility curves. Basöz et al. [1998] conducted similar studies on the probability of exceedance of bridge damage.

The second category to produce fragility curve is based on experimental data. This category is usually used when nonstructural elements are evaluated. In this category, structural or non-structural specimens are tested under simulated earthquake excitations in experimental situation like on shake tables. Then for each level of excitation damage indexes are extracted. A sample of this category is Chong et al. study [2000] on unrestrained equipment in critical facilities. They have shown that by testing these equipments on shake tables under variable accelerations, vulnerability curves of these structures under seismic excitation and performance and loss estimation of them can be calculated.

The last category is an analytical-based procedure. In this procedure, based on experimental or designing parameters, fragility curves are displayed by analyzing selected systems. These systems can be equipment, bridge, building structures, or lifeline structures. Analysis must be static or dynamic nonlinear one. In the past, Hwang and Huo [1994] displayed an analytical method for showing fragility curves based on numerical simulations of the dynamic behavior of specific structures. The uncertainties are quantified by using the parameters in the system as random. Karim and Yamazaki [2001] have developed an analytical approach to construct vulnerability curves for highway bridge piers of specific bridges. The simulation method makes use of the nonlinear dynamic response of an equivalent single-degree-of-freedom system of the pier obtained by static pushover analysis. One of the specific studies is presented by Barron et al. [2000] where fragility curves were used for evaluating of various structural retrofitting techniques. By comparing damage exceedance of each technique, the appropriate one was selected. This method demonstrates the influence of retrofitting on decreasing the probability of damage exceedance. This investigation has been done by Hueste et al. [2007] for a five-story building.

The main point of all categories and studies is to use fragility curves for evaluation of existing structures under earthquake excitation. In this research a new approach is developed where fragility curves are used for evaluating structures while under design, considered the effects of changing of general parameters. These design parameters can be random or fixed. Peak ground acceleration is the main random parameter. The global ductility coefficient and important factor are fixed parameters that are very important for seismic design of structures.

With respect to actual treatment of elements in earthquake and by using ACI318-99 provision, first the current procedure developed a squad of structures. For nonlinear dynamic analysis of these structures, a sufficient group of records were selected. In the next step, by selecting probabilistic parameters, a fragility curve of the structure under varying these parameters was evaluated. Finally, the results of analyses are discussed.

FUNDAMENTAL OF FRAGILITY CURVE FORMULATION

Fragility curves as well known are diagrams that show probability of exceedance of damage of structures under earthquake excitation. For that, damage distribution of structure should be assumed by calculating mean and variance, also for each level of damage criteria probability of exceedance should be produced. The main concept of relationships is similar, but there is a difference between fragility formulations in distribution and assumed variance.

Hwang and Huo [1994] used cumulative absolute velocity (CAV) and described probability exceedance of damage from i^{th} for an earthquake PF_{ij} with equal CAV v_j as follows:

$$CAV = \int_0^T |a(t)dt| \tag{1}$$

$$PF_{ij} = prob\big(DT \geq DT_i \big| CAV = v_j\big) = F_{DT}\big|CAV = v_j) \tag{2}$$

where DT is damage index, and F is function of probability distribution. Considering normal distribution PF_{ij} derivate as:

$$PF_{ij} = 1 - \Phi\left(\frac{Ln(DI_i) - \overline{Ln(DI)}}{\sigma_{Ln(DI)}}\Big|CAV = v_j\right) \tag{3}$$

The damage probability matrix is obtained by the following procedure:

$$PDS_{ij} = \begin{cases} PF_{ij} - PF_{i+1\ j} & (i \leq 4) \\ PF_{ij} & (i = 5) \end{cases} \tag{4}$$

It is important to know that PGA can be used as seismic parameter instead of CAV. Wen et al. [2004] used more detailed function:

$$P(LS/S_a) = 1 - \Phi\left(\frac{\lambda_{CL} - \lambda_{D/Sa}}{\sqrt{\beta_{D/Sa}^2 + \beta_{CL}^2 + \beta_M^2}}\right) \tag{5}$$

where $P(LS/S_a)$ is the probability of exceeding a specified limit state given the spectral acceleration, Φ is the standard normal cumulative distribution function, λ_{CL} is the ln(damage index of limit state (in that paper rotation of elements), $\lambda_{D/Sa}$ is the ln(calculated damage index(in that paper rotation of elements), $\beta_{D/Sa}$ is the uncertainty associated with the fitted power law equation used to estimate demand damage index=$\sqrt{}$(ln(1+σ2), β_{CL} is the uncertainty associated with the damage index taken as 0.3 for that study, β_M = is the uncertainty associated with the analytical modeling the structure, taken as 0.3 for that study. In that study, since each parameter was considered independently, the relationship developed by Hwang and Huo [1994] is used and a lognormal distribution is assumed.

STRUCTURAL MODELS

For preparing the structural models, two squad of structure were designed with respect to ACI318-99 seismic provisions. The first squad was an ordinary office structure and the second squad was an important safety-related structure, e.g., a hospital. Weight loads were extracted from usual details for office and hospital structures. Earthquake design loads and control parameters were taken from earthquake code provision of the 2800 Iranian standard. The hazard level was assumed as the highest earthquake hazard in the 2800 Iraninan standard: a PGA=0.35g. and soil type I, which is equivalent to type C of 200 IBC code.

For designing the structures, a general finite element program was used and for nonlinear dynamic analysis of structures under earthquake excitation, open source software, IDARCV7.0 [Valles et al. 1996] was implemented. The design parameters are listed in Table 1, and the main characteristics of structures are shown in Table 2.

Table1 Main design parameters.

Structure type	Ductility coefficient	Story	Dead load (da N/m)	Live load (da N/m)	Base Shear coefficient	f′c (MPa)	Fy (MPa)	Story height (m)
Office	7	3	4200	1500	0.123	25	400	3.5
	10	3	4200	1500	0.086	25	400	3.5
	7	7	4200	1500	0.081	25	400	3.5
	10	7	4200	1500	0.057	25	400	3.5
	7	10	4200	1500	0.067	25	400	3.5
	10	10	4200	1500	0.047	25	400	3.5
	7	15	4200	1500	0.055	25	400	3.5
	10	15	4200	1500	0.039	25	400	3.5
Hospital	10	3	4200	2100	0.0107	25	400	4.5
	10	7	4200	2100	0.070	25	400	4.5
	10	10	4200	2100	0.058	25	400	4.5
	10	15	4200	2100	0.048	25	400	4.5

Table 2 Main characters of the structures.

Structure type	Ductility coefficient	Story (ID)	1^{st} mode period(sec)	Base section of cols.(mmxmm)	First story beams section	Drift demand	Allowable drift
Office	7	3	0.75	500X500	50X50	0.003	0.0051
	10	3	1.04	500X500	40X40	0.0031	0.0036
	7	7	1.39	600X500	60X50	0.0030	0.0041
	10	7	1.57	600X500	60X50	0.0028	0.0029
	7	10	1.85	700X700	70X50	0.0039	0.0041
	10	10	1.83	700X700	70X50	0.0024	0.0029
	7	15	2.70	800X800	70X50	0.0039	0.0041
	10	15	2.69	800X800	70X50	0.0028	0.0029
Hospital	10	3	0.91	600X600	50X50	0.0028	0.0029
	10	7	1.52	700X700	70X60	0.0026	0.0029
	10	10	1.83	800X800	80X60	0.0027	0.0029
	10	15	2.36	900X900	90X70	0.0026	0.0029

When considering the effect of special and intermediate ductility of structures in the models, hysteresis diagram and parameters were used.

There are six type of hysteresis behavior in IDARC [1996] program. These types include: the three-parameter Park model, the tri-linear steel model, bilinear model, the Kelvin model, the Maxwell model, and the smooth hysteretic model. These behaviors are used in different types of structures. For instance, for structures that include viscous-elastic dampers, the Maxwell or Kelvin model is suitable; the smooth hysteretic model is good for structures with infill materials. Reinforced concrete frames may have several degradations in the hysteresis diagrams. In the general case, these degradations included stiffness, strength, and pinching degradation. In this research, the three-parameter Park model for beams and column was used. This model includes all main parameters to control the behavior of element in each branch of the hysteresis diagram: stiffness and strength degradation (see Figures 1 and 2), modeling of slip or pinching behavior, and an overall monotonic three-line skeleton.

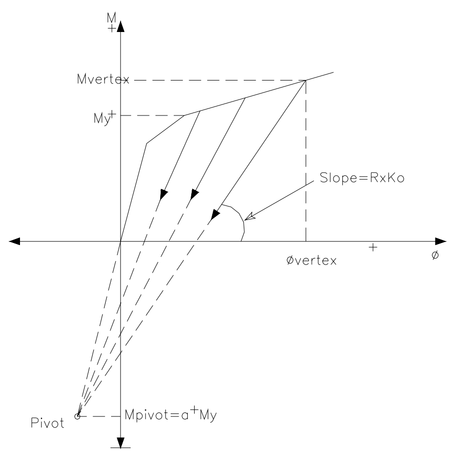

Figure 1 Shape of stiffness degradation.

When considering these parameters in modeling of the hysteresis diagram, parameters were calculated with respect to available hysteresis diagram, which were drawn from tested elements according to the details of the elements in each type of ductility. For this purpose, the IDARC technical report [1996] and Wan et al. [2001] paper were used. Accordingly, the stiffness degradation was formulated as below:

$$R_K^+ = \frac{M_{cur}+\alpha M_y}{K_0\varphi_{cur}+\alpha M_y} \tag{6}$$

α can be found as follows:

$$\alpha=(M_{cur} - R_k K_0 \varphi_{cur})/(M_y (R_k-1)) \tag{7}$$

and the strength degradation introduced with below equation and shape (Figure 2):

$$M_y^{+/-} = M_y^{+/-}\left[1-\left(\frac{\varphi_{max}^{+/-}}{\varphi_u^{+/-}}\right)^{\frac{1}{\beta_1}}\right]\left[1-\frac{\beta_2}{1-\beta_2}\frac{H}{H_{ult}}\right] \tag{8}$$

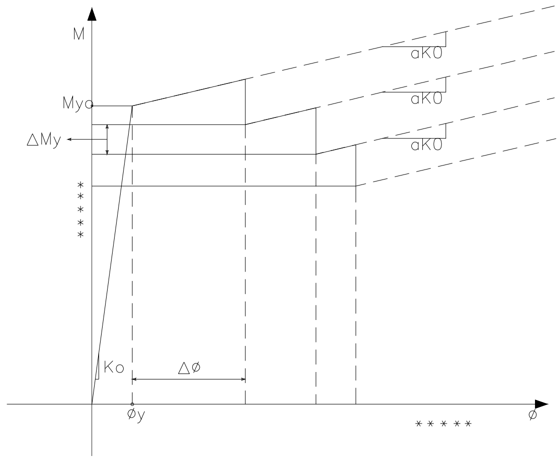

Figure 2 **Shape of strength degradation.**

It is very difficult to obtain this coefficient by this equation. Wan et al. [2001] introduced the simple relation for strength degradation based on ductility as follows:

$$M_s = M_u\,(1 - \eta\,\lambda) \tag{9}$$

Wan et al.[2001] introduced another energy based strength degradation coefficient:

$$\phi_a^* = \phi_a + \beta\,\frac{\Delta E}{M_y} \tag{10}$$

where the β coefficient is:

$$\beta = M_y\,(\varphi_a^{\;*} - \varphi_a)\,/\,\Delta E \tag{11}$$

The last parameter—pinching—has the following shape (Figure 3):

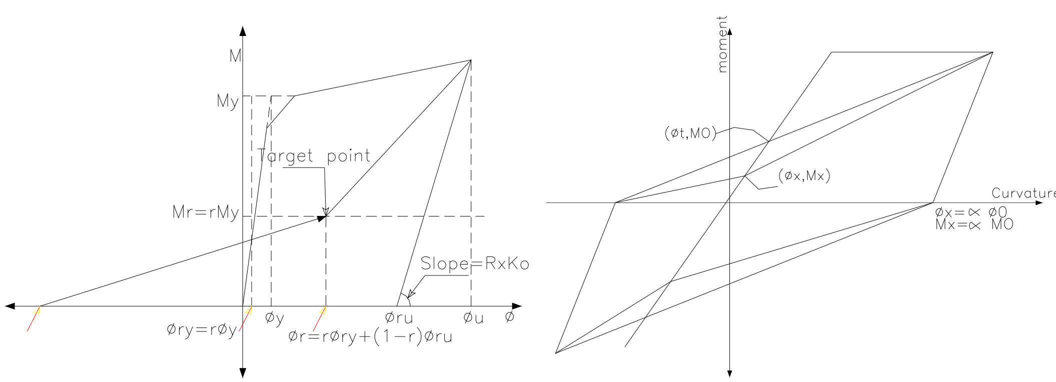

Figure 3 **Shape of properties of pinching parameter.**

For a simple estimation of pinching parameter (γ) the following procedure was done using software (Figure 4):

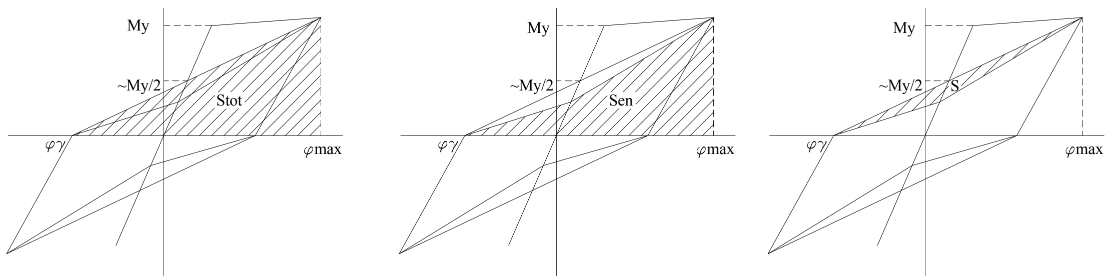

Figure 4 Shape of estimation of pinching parameter.

$$S_{tot} = My * (\varphi_{max}+\varphi_{\gamma})/2 \;\rightarrow\; S = S_{tot} - S_{en}$$

$$\Rightarrow \gamma = 1 - 2 * S / \left[(\varphi_{max} + \varphi_{\gamma})*(M_y/2)\right] \qquad (12)$$

Model Verification

Figure 5 and 6 show experimental data fitting for procedure that was used for the relations established above. According to intermediate and special details and provisions, two hysteresis diagrams were selected from Washington test.

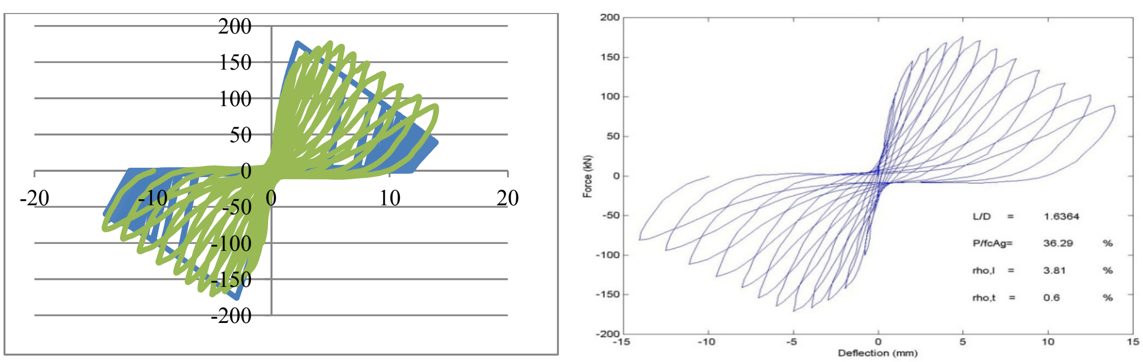

Figure 5 Arakawa et al. [1988] model No.27 (α=41,λ=1.0,β=0.9,γ=0.0).

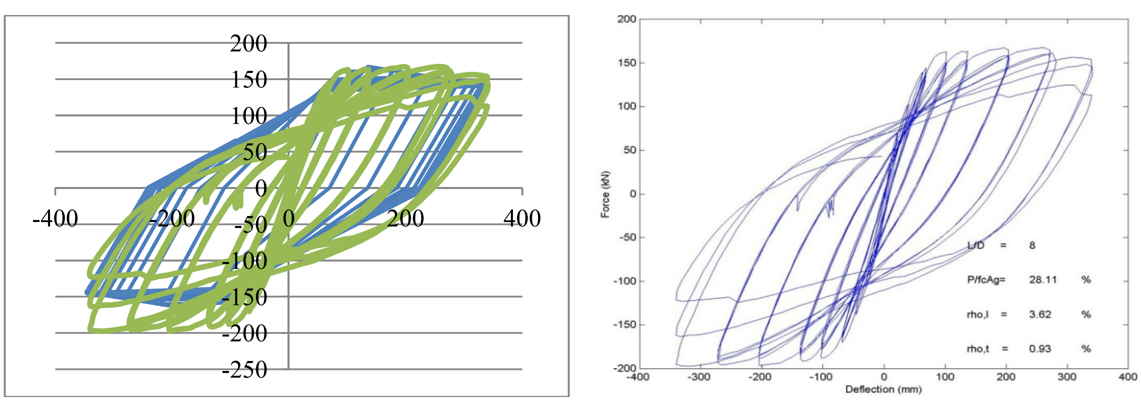

Figure 6 Kowalsky model No.FL3 (α=1.17,λ=1.0,β=0.9,γ=1.0) [1999].

Figure 7 displays the main shape and estimated diagram.

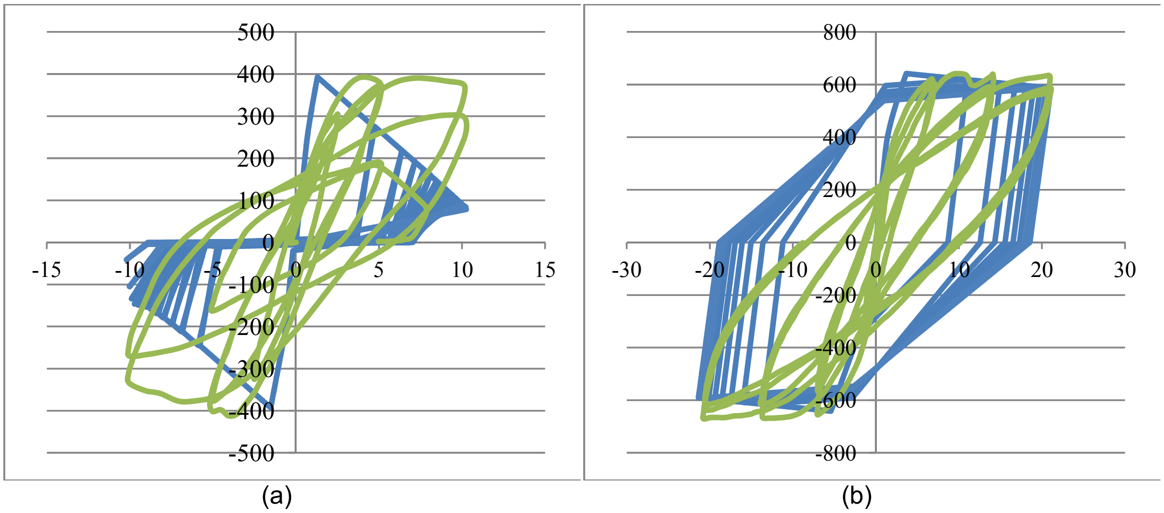

Figure 7 **Main shape and estimated hysteresis diagram: (a) intermediate [Sakai et al. 1990]; and (b) special hysteresis diagram [Gill et al. 1979].**

Randomness Parameters

To evaluate structures, random parameters should be selected. These random parameters are extracted from natural specification of structures and earthquake excitations. In this paper, the random parameters include: record of earthquake, global ductility factor, important factor, and PGA error probability. The first usual random parameter is the record of earthquake excitation. For this purpose, 23 earthquake records were chosen considering type of soil category as adapted from the design properties. For scaling these records, a power spectra response is used, shown in Figure 8. By using this random parameter, the effect of general design parameters (i.e., important factor) can be evaluated on fragility curve of the structure.

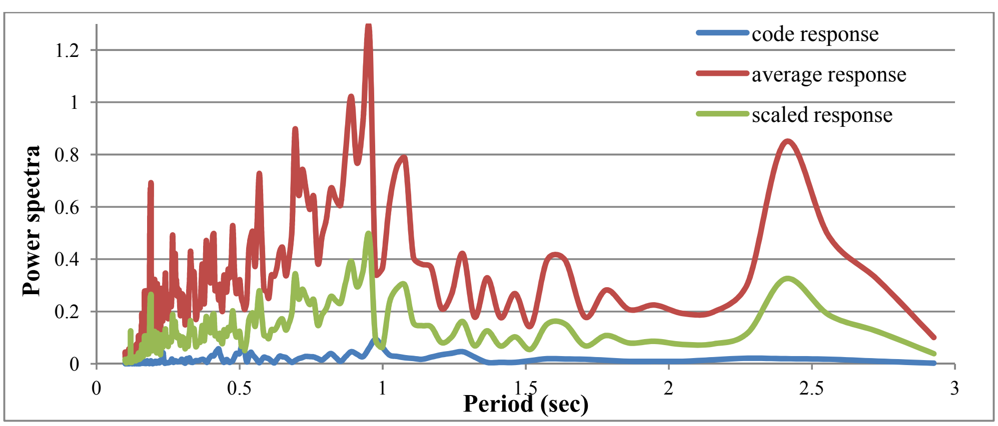

Figure 8 **Diagram of scaling with power spectra.**

Effect of Important Factor

To improve behavior of structures under earthquake excitation, seismic code proposed methods. One of general methods for improvements is increasing important factor. Seismic provisions assume that probability of damage of structure under earthquake decreases if the important factor is increased, and thus increasing the base shear. Comparing the fragility curves of the office structure and hospital structure displays the effect of this parameter, as shown in Figure 9. Because of higher probability damage of the 4- and 7-story hospital building compared to the 4- and 7-story office buildings, the design base shear for these structures increases by 15% (PGA = 0.4 g). Figure 10 shows that over estimating the base shear works very well to decrease probability of damage.

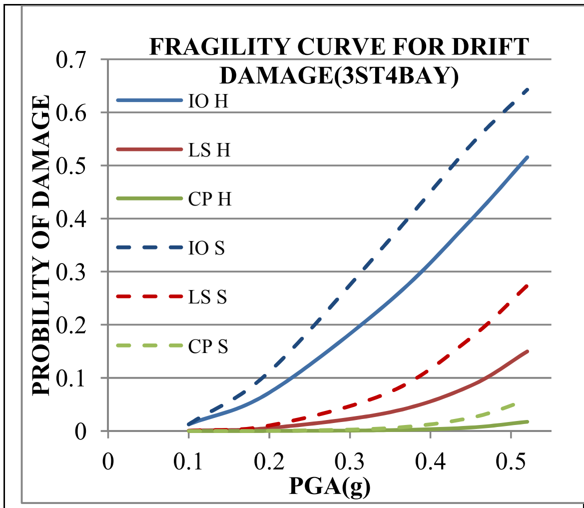
FRAGILITY CURVE FOR DRIFT DAMAGE(3ST4BAY)
PROBILITY OF DAMAGE
PGA(g)
IO H
LS H
CP H
IO S
LS S
CP S
0
0.1
0.2
0.3
0.4
0.5
0.6
0.7

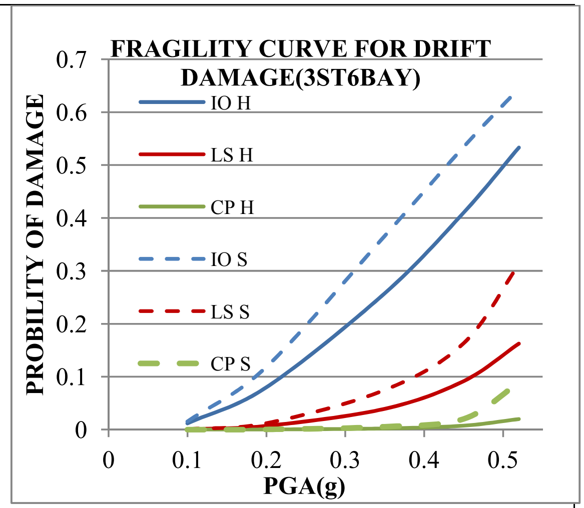
FRAGILITY CURVE FOR DRIFT DAMAGE(3ST6BAY)
PROBILITY OF DAMAGE
PGA(g)
IO H
LS H
CP H
IO S
LS S
CP S
0
0.1
0.2
0.3
0.4
0.5
0.6
0.7

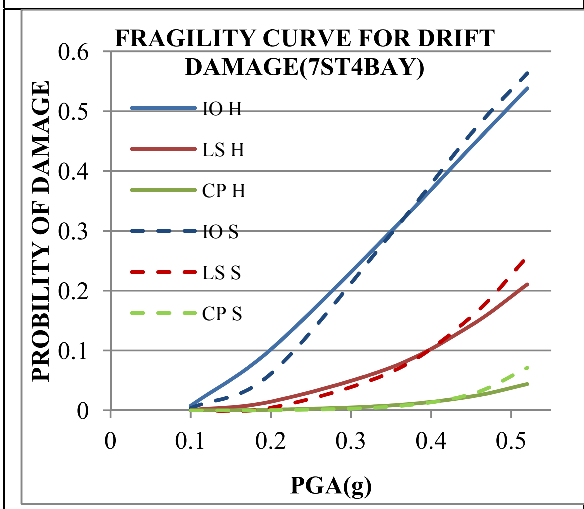
FRAGILITY CURVE FOR DRIFT DAMAGE(7ST4BAY)
PROBILITY OF DAMAGE
PGA(g)
IO H
LS H
CP H
IO S
LS S
CP S
0
0.1
0.2
0.3
0.4
0.5
0.6

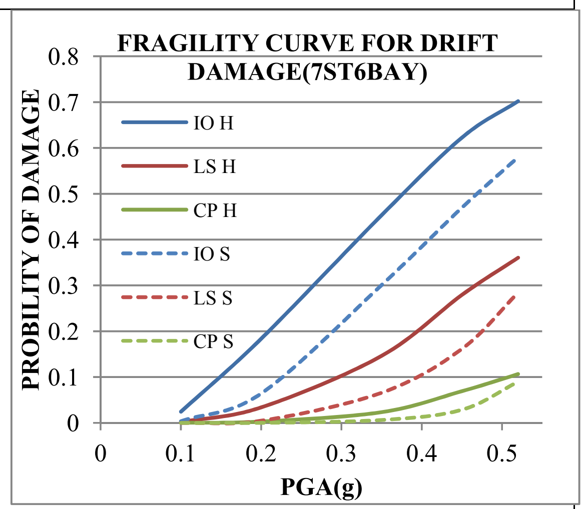
FRAGILITY CURVE FOR DRIFT DAMAGE(7ST6BAY)
PROBILITY OF DAMAGE
PGA(g)
IO H
LS H
CP H
IO S
LS S
CP S
0
0.1
0.2
0.3
0.4
0.5
0.6
0.7
0.8

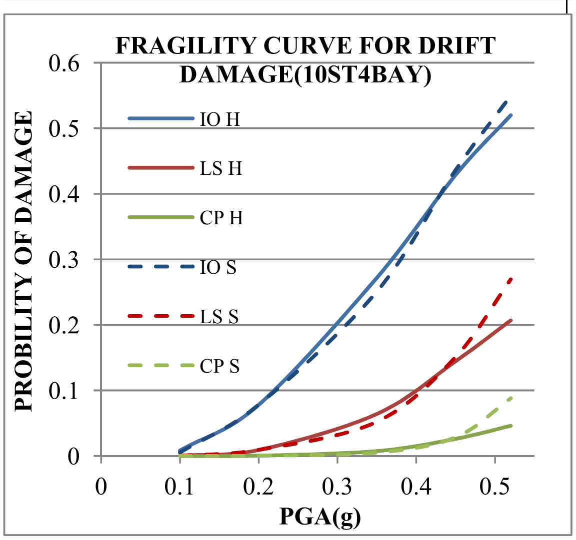
FRAGILITY CURVE FOR DRIFT DAMAGE(10ST4BAY)
PROBILITY OF DAMAGE
PGA(g)
IO H
LS H
CP H
IO S
LS S
CP S
0
0.1
0.2
0.3
0.4
0.5
0.6

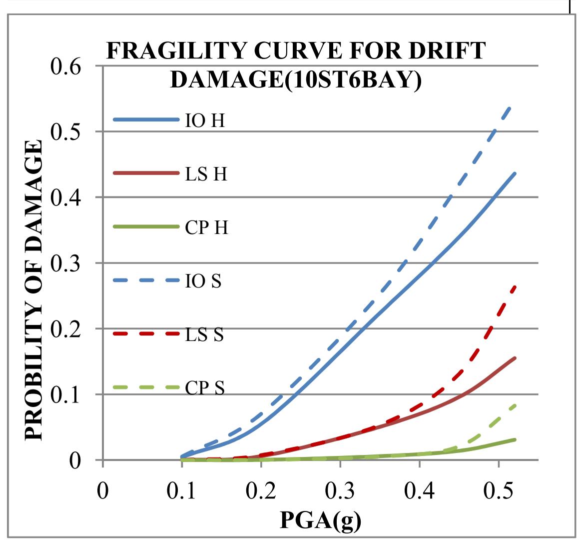
FRAGILITY CURVE FOR DRIFT DAMAGE(10ST6BAY)
PROBILITY OF DAMAGE
PGA(g)
IO H
LS H
CP H
IO S
LS S
CP S
0
0.1
0.2
0.3
0.4
0.5
0.6

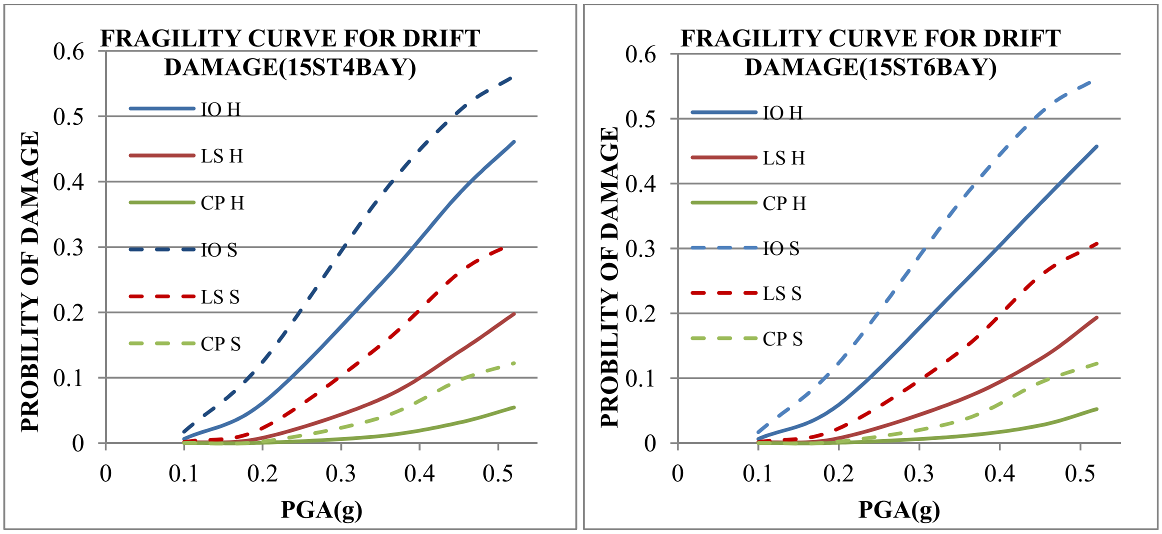

Figure 9 Effect of direct important factor on fragility curve of structures.

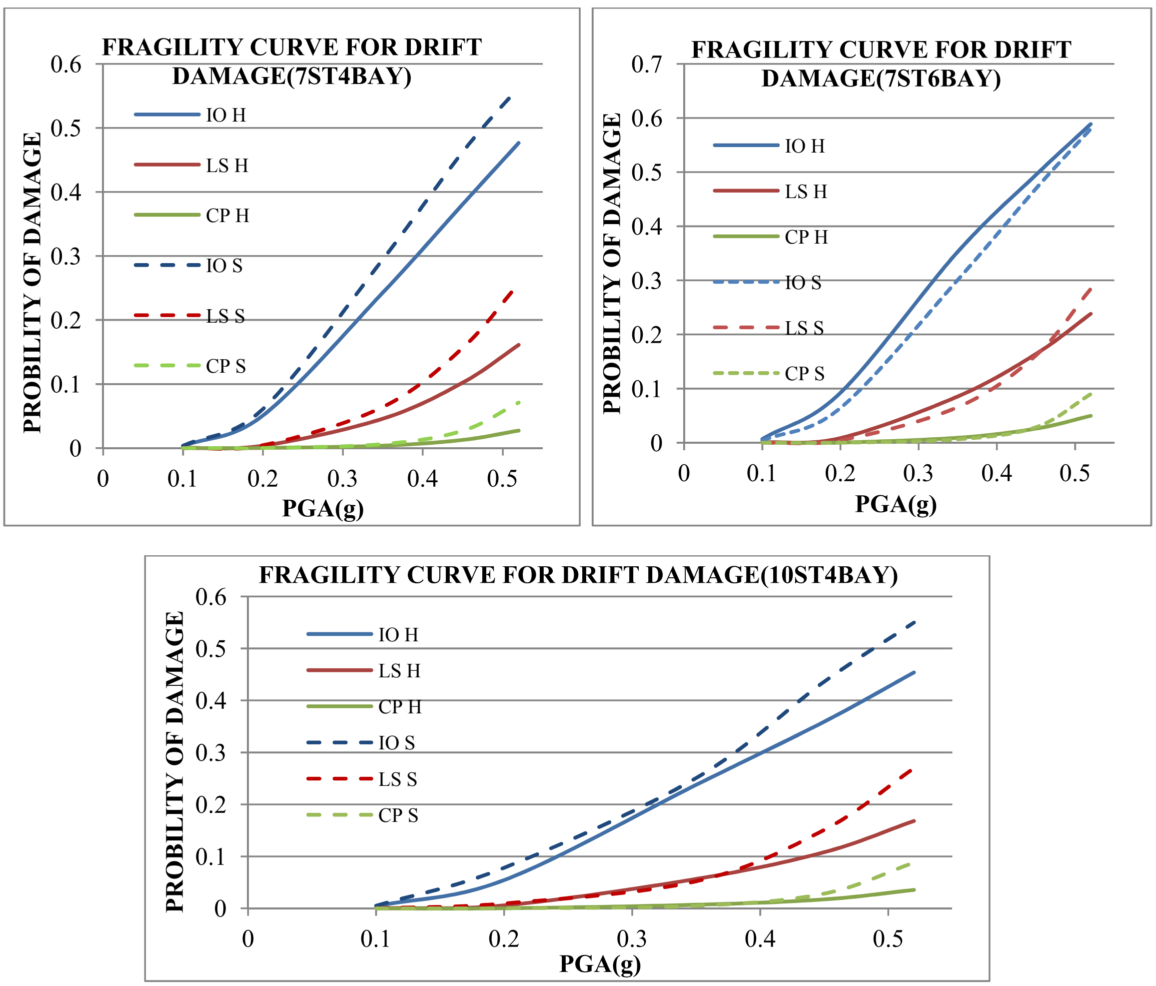

Figure 10 Effect of over estimating the design base shear on the fragility curve for 7- and 10-story structures.

DISCUSSION AND CONCLUSION

Seismic provisions have several parameters to control or improve the performance of the structures under seismic excitations, but earthquake properties and behavior of the structures under earthquake excitation are probabilistic. Damage caused by earthquakes from the movement of is random. There are also many uncertainties in earthquake records like content frequency. Other uncertainties include structural elements, general structural hysteresis diagram, and/or global ductility coefficient.

The main object of this research is to consider the parameters included in seismic provisions to improve the performance of structures do not sufficiently guarantee that a structure will not be damaged in the event of an earthquake. Decrease in the damage index does not mean that the probability of damage exceedance and loss estimation is met. In this paper, a procedure to survey of the effect of all these parameters is introduced. In this procedure, fragility curve is investigated for assessing the efficiency of these coefficients on the damage probability of exceedance of limit states.

Using the 2800 Standard Iranian Earthquake Code with a very high seismic hazard and soil type II, a number of structures were designed. Those structures had 4 and 6 bays, 3, 7, 10 and 15 stories. According to ductility details and hysteresis diagrams, perfect parameters adapted using the IDARC computer program were selected, including stiffness degradation, strength deterioration based on ductility, strength deterioration based on energy, and the pinching factor. By selecting a random parameter, the effect of this parameter on the fragility curves was displayed.

The random parameter examined here was the impact factor. Hospital structures with a 1.4 impact factor and special ductility details were compared with office structures with a 1.0 impact factor and special ductility details. Earthquake records were selected to this parameter were adapted with a soil type in earthquake code. The fragility curve results demonstrated that probability of damage exceedance in the 7- and 10-storey hospital structures had more probability of damage than the office structures due to the greater mass and height. These results are for mid-rise structures because of the properties of the earthquake records and frequency content of records. By increasing the design base shear of the hospital structures by 15%, the damage probability of exceedance decreased. This was confirmed by a redesign of the 7- and 10-story hospital structures and was confirmed by the fragility curves.

REFERENCES

Arakawa T, He MX, Arai Y, Mizoguchi M (1998). Shear resisting behavior of reinforced concrete columns with spiral hoops, *Trans. Japanese Conc. Institute*, 10:155–162.

Barron R, Reinhorn A. (2000). Spectral evaluation of seismic fragility of structures, *Technical Report*, Multidisciplinary Center for Earthquake Engineering Research, Buffalo, NY.

Basöz N, Kiremidjian AS (1998). Evaluation of bridge damage data from the Loma Prieta and Northridge, California, earthquake, *Technical Report MCEER-98-0004*, Multidisciplinary Center for Earthquake Engineering Research, Buffalo, NY.

Chong WH, Soong TT (2000) Sliding fragility of unrestrained equipment in critical facilities, *Technical Report,* Multidisciplinary Center for Earthquake Engineering Research, Buffalo, NY.

Gill WD, Park R, Priestley MJN (1979). Ductility of rectangular reinforced concrete columns with axial load, *Report 79-1*, Department of Civil Engineering, University of Canterbury, Christchurch, New Zealand, 136 pgs.

Hueste MBD, Bai JW (2007). Seismic retrofit of a reinforced concrete flat-slab structure: Part I—seismic performance evaluation, *Engng. Struct.,* 29:1165–1177.

Hwang HHM, Huo JR (1994). Generation of hazard-consistent fragility curves, *Soil Dyn. Earthquake Engng*., 13:345–354.

Karim KR, Yamazaki F (2001). Effect of earthquake ground motions on fragility curves of highway bridge piers based on numerical simulation, *Earthq. Engng. Struct. Dyn*., 30(12):1839−1856.

Kowalsky MJ; Priestley MJN; Seible F (1999). Shear and flexural behavior of lightweight concrete bridge columns in seismic regions, *ACI Struct. J*., 96():136−148.

Sakai Y; Hibi J, Otani S, Aoyama H (1990). Experimental study on flexural behavior of reinforced concrete columns using high-strength concrete, *Trans. Japanese Conc. Institute*, 12:323−330.

Shinozuka M, Feng M, Kim H, Uzawa T, Ueda T (1999). Statistical analysis of bridge fragility curves, *Technical Report*, Multidisciplinary Center for Earthquake Engineering, Buffalo, NY.

Valles RE, et al. (1996). IDARC2D version 7.0: a computer program for the inelastic damage analysis of buildings,*Report No. NCEER-96-0010*, State University of New York at Buffalo, Buffalo, NY.

Wan S, Loh CH, Peng SY (2001). Experimental and theoretical study on softening and pinching effects of bridge column, *Soil Dyn. Earthq. Engng*., 21:75−81.

Wen YK, Ellingwood BR, Bracci JM (2004). Vulnerability function framework for consequence-based engineering, *DS-4 Report,* Mid-America Earthquake Center, Urbana, IL.

BEYOND R-FACTOR: DESIGN THEORY FOR DAMAGE-BASED SEISMIC DESIGN OF RC BUILDINGS

Mahmoud-Reza Banan

Civil and Environmental Engineering Department, Shiraz University, Shiraz, Iran
bananm@shirazu.ac.ir

INTRODUCTION

Recent significant earthquakes have shown that the seismic risk in urban areas is increasing. More reliable seismic specifications for seismic evaluation, design and retrofit of structures and their stringent implementation for complete engineering of existing and new structures can effectively reverse this situation. Development and implementation of new seismic codes must consider design aspects namely design philosophy, theory, and provisions and construction aspects namely structural detailing, constructability, inspection, and maintenance.

In past two decades, seismic codes have moved from strength-based design toward ductility-based design using empirical force reduction factors or *R*-factors to determine the strength demand of the structure required to ensure a satisfactory performance for presumed levels of over-strength and ductility capacities. Such capacities are assumed to be provided based on the broad classification of the building system (such as Ordinary Moment-Resisting Frame (MRF); Intermediate MRF; Special MRF; Special Reinforced Concrete Shear Walls). The *R*-based seismic design is still a force-based approach that predicts the strength demand of the structure. Although *R*-factors have been refined by many researchers to be function of structural period, soil-structure interaction, and seismic hazard parameters, the design approach suffer from many shortcomings. The R-based approach is suited for buildings satisfying implicit requirements of ductility and regularity; however such requirements are not well defined and required by existing codes. A single-valued factor cannot represent ductility and performance of complex structures due to the wide diversity of structural forms and the large number of uncertainties involved. The *R*-based approach is too rigid to consider the economics of loss for a given building.

The most accurate seismic analysis is nonlinear time-history analysis. However, such analysis suffers from high computational intensity and need for ground motions. In order to develop practical analytical methods, researchers have used simplified equivalency relationships for seismic behavior of nonlinear structures. Structural systems with long periods are likely to follow equal displacement equivalency, while those with average periods follow equal energy equivalency. For structures with short periods, ductile behavior is limited and equal acceleration equivalency with R=1 may be assumed. These equivalency relations are used to estimate response of a nonlinear structure from response of a linear structure.

Developments in performance-based design in the past two decades have led to understanding by seismic design researchers that all buildings can be custom-made to behave according to the required performance during seismic event and to have structural conditions that are reasonably predicted for its serviceability, reparability, and damage intensity, and distribution after the earthquake. Although such achievement is no longer farfetched, a side effect of such diversified researches has been the addition of numerous aspects to the design process that used to be hidden during design process to the mainstream design engineer. These aspects are related to measures for seismic hazard, structural performance, damage spread, safety hazards, and loss. Due to existence of uncertainties, non-uniformities, incompleteness, indeterminacies, unknowns, time dependencies, deteriorations, variations, varieties, accumulations, and recurrences; the mathematical models representing seismic response of a building, seismic design of such a building, and loss due to building damages need to be probabilistic. Furthermore, not a single design approach can include all of these listed complexities.

It has been shown that robust probability-based design procedures are needed for developing design codes, however such design approaches are not practical for day-to-day designs. Some researchers have concentrated on developing such probability-based approaches namely the Pacific Earthquake Engineering Research Center (PEER) robust methodology for performance-based earthquake engineering [Moehle and Deierlein 2004]. Probabilistic design approaches can be effectively used to tune main factors of deterministic design approaches, as has been done for development of LRFD codes. Meanwhile; deterministic design approaches have been developed for day-to-day designs and/or modification of existing codes namely, drift-based or damage-index-based or displacement based design approaches.

For development of a robust and practical performance-based seismic design approach for buildings, a practical deterministic design approach should define the main framework of the design procedure while probability-based methods should be used to tune main factors of such a deterministic approach. This article discusses the aspects of the deterministic approach that has been successfully used for seismic retrofit of toll road bridges in California in 1995−1996 and later on, became the framework for the Caltrans seismic design criteria for bridges [Caltrans 2006] and recently has been adopted as an alternate to the seismic provisions in the AASHTO LRFD Bridge Design Specifications [AASHTO 2010]. It differs from the current procedures in the LRFD Specifications by using ductility-based design procedures, instead of the traditional force-based *R*-Factor method. It includes guidance on earthquake resisting elements and systems, global design strategies, demand modeling, and capacity calculation. Capacity design procedures underpin the methodology including prescriptive detailing for plastic hinging regions and design requirements for capacity protection of those elements that should not experience damage.

For reinforced concrete (RC) buildings located in high seismic zones, the framework of the highlighted deterministic performance-based design approach can be summarized in following steps:

1. Hazard study to set code-based or site-specific ground motions or earthquake spectrum considering:
   - Site and building design characteristics
2. Identification of the earthquake resisting system consisting of:
   - Ductile members with plastic hinges (commonly beams and column and shear wall bases)
   - Essentially-elastic members (columns, beam-column joints, soil-foundation assemblies, and floor slabs)
3. Linear dynamic analysis to estimate:
   - Demand curvatures for plastic hinges

- o Demand drifts for ductile members, building stories, and the building

4. Equivalent nonlinear static analyses to determine:
   - o Expected capacity curvatures for plastic hinges and expected capacity displacements for earthquake resisting subsystems and systems
   - o Reduction of capacity curvature for plastic hinges due to P−Δ effect
   - o Over-strength shear demands for ductile members and over-strength design forces for essentially-elastic members
5. Performance-based design to check:
   - o Concrete and rebar strains for plastic hinges based on required damage level
   - o Displacement demand-capacity ratios for ductile members and earthquake resisting subsystems and systems
   - o Minimum required capacity displacement ratios
6. Strength-based reinforced concrete design to:
   - o Check shear strength of ductile members (including effect of ductility demands on concrete capacities)
   - o Design essentially-elastic members and connections according to the governing RC code
7. Detailing of all members and components for:
   - o Development of stable and ductile plastic hinges
   - o Eliminating brittle failures (such as loss of confinement failure, splice failure, inadequate anchorage, inadequate rebar development, rebar buckling)

This design approach uses fundamental of reinforced concrete behavior and robust and practical analyses. It avoids preset tables and values for establishing seismic performance. It can be used for different structural systems.

For seismic design of RC buildings, a coordinated research based on this framework has been started at the structural engineering division of the Civil and Environmental Engineering Department at the Shiraz University. Currently, main efforts are concentrated on Steps 3 through 6 to provide conservative designs with realistically accurate estimations of demands and capacities. In the following, summary of investigations for (a) different procedures for equivalent static analysis and (b) development of curvature damage index intervals for different performance levels based on concrete and rebar strains for RC frame members are presented.

INVESTIGATION OF RESPONSE ESTIMATION ERRORS OF DIFFERENT NONLINEAR EQUIVALENT STATIC ANALYSES

For seismic evaluation and design of building structures, simplified design-oriented modeling procedures using static analyses are more practical than nonlinear dynamic modeling procedures. Nonlinear equivalent static analysis (NESA) is used to determine realistic displacement capacities and to estimate demand displacements. The NESA is an incremental nonlinear analysis which captures the overall nonlinear behavior of the structure and its elements through each limit state. The NESA model includes the redistribution of forces as each limit state is reached. Foundation effects may also be included in the model.

Engineering demands are based on simplified analysis techniques, including static and linear analysis methods; where dynamic or nonlinear methods are used, calibrations between calculated demands and component performance are largely lacking. Our coordinated investigations are concentrated on estimation of conservatism and accuracy of following well-established NESA procedures [Momtahen et al. 1008; Kashkooli et al. 2011]:

- FEMA-440 Modified Coefficient Method (MCM) for uniform and triangular loading pattern [2005]
- Modal Pushover Analysis (MPA) [Chopra and Goel 2002]
- Displacement-based Adaptive Pushover Analysis (DAPA) [Antoniou and Pinho 2004] combined with FEMA440 Capacity Spectrum Method (CSM)
- FEMA440 with CSM nonlinear static analysis using first-mode loading pattern [2005]
- Force-based Adaptive Pushover Analysis (FAPA) [Antoniou and Pinho 2004]

Various studies investigate the effect of frame irregularity in height on accuracy and conservatism of these selected NESA procedures for predicting frame target displacement, story drifts, and frame base shear. In order to have a thorough investigation of frame irregularity, 22 irregularity layouts are considered for a 5-story steel moment resisting frame, as shown in Figure 1. Each irregular frame is designed to represent low and high values of response reduction factor (*R*). Models from 0 to 21 are designed for seismic loads to have low R-value and models 22 to 43 are designed for gravity loads to have high *R*-values. For each frame model, nonlinear dynamic analyses for 14 ground motions (7 pairs) whose information is shown in Table 1 and their spectra scaled to match code spectrum are shown in Figure 2.

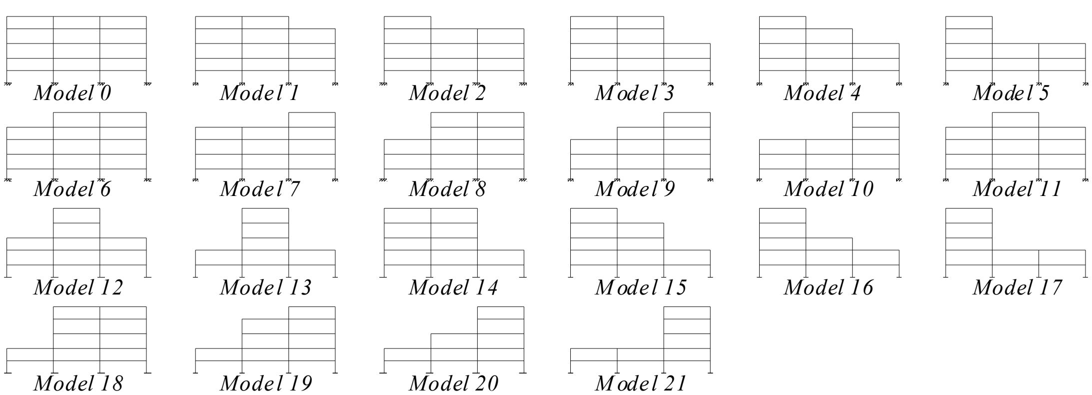

Figure 1 Selected frame models.

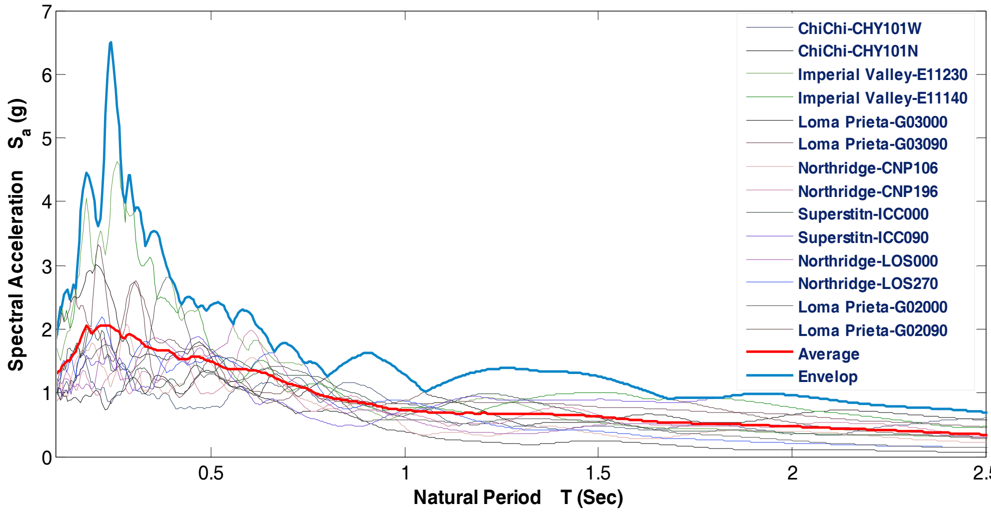

Figure 2 Scaled ground motion spectra.

Table 1 Selected ground motions

	Earthquake	Identifier	Magnitude	Distance (Km)	PGA (g)	Scaled PGA (g)
1	Chi-Chi, Taiwan	CHY101W	Ms= 7.6	11.1	0.353	0.596
2	Chi-Chi, Taiwan	CHY101N	Ms= 7.6	11.1	0.440	0.596
3	Imperial Valley	E11230	Ms= 6.9	12.6	0.380	1.154
4	Imperial Valley	E11140	Ms= 6.9	12.6	0.364	1.154
5	Loma Prieta	G03000	Ms= 7.1	14.4	0.555	0.813
6	Loma Prieta	G03090	Ms= 7.1	14.4	0.367	0.813
7	Northridge	CNP106	Ms= 6.7	15.8	0.356	0.562
8	Northridge	CNP196	Ms= 6.7	15.8	0.420	0.562
9	Superstitn	ICC000	Ms= 6.6	13.9	0.358	0.750
10	Superstitn	ICC090	Ms= 6.6	13.9	0.258	0.750
11	Northridge	LOS000	Ms= 6.7	13.0	0.410	0.664
12	Northridge	LOS270	Ms= 6.7	13.0	0.482	0.664
13	Loma Prieta	G02000	Ms= 7.1	12.7	0.367	0.705
14	Loma Prieta	G02090	Ms= 7.1	12.7	0.322	0.705

For each frame model, nonlinear static pushover analysis up to the target displacement predicted by the selected NESA procedure are performed using computer programs IDARC-2D and OpenSEES. Although for the sake of reducing computational efforts, all analyses are done for steel moment resisting frames with nodal plastic hinges, the results could be generalized to RC frames with well-confined plastic hinges under moderate axial stresses and no brittle failures. In other words, this part of research is interested in estimating the equivalency of NESA methods to nonlinear dynamic analyses for frames with plastic hinges.

Over 25,000 nonlinear time histories and static pushover analyses were performed. The results of nonlinear static analyses are compared with the results for nonlinear dynamic analyses to evaluate the accuracy and conservatism of these selected NESA procedures. Correlations and errors of predicted measures with respected to results from nonlinear dynamic analyses are computed for all models and also each model. Sample of results for base shears predicted for MPA procedure are shown in Figures 3 through 5. Some of conclusions are:

- Summary of estimated median errors and correlation values are shown in Table 2 for different NESA procedures. When error is negative, the results from NESA are conservative, i.e. greater than the results from nonlinear dynamic analyses.
- All studied NESA methods have good correlation values for base shear.
- MPA has the best correlation values for roof displacement, base shear, and story drifts.
- All NESA methods are generally unconservative for estimating dispalcement responses of irregular frames for a computed target displacement. Therefore, such methods are generally conservative for estimating story and frame displacement capacities (although DAPA would not be a good choice for story capacity analyses).
- Except for DAPA, all NESA methods are generally unconservative for estimating base shear. Consequently, such methods are not conservative for estimating over-strength member forces. The most promising NESA procedure is DAPA whose success could be related to the use of capacity spectrum method (CSM). Such an observation need to be investigated for ultimate over-strength forces which occured when a frame reaches its plastic hinging mechansim.
- It has been observed that adaptivity of loading pattern cannot improve the performance of NESA methods at least for the investigated frame response measures. Such adaptivity may improve plastic hinging approximation, which needs to be studied.

The errors for all response measures relate to the frame dynmaics and plastic hinging. Such relationship should depend on story masses, stiffnesses, and lateral capcities distributions. Such relationships are under development through ongoing research while more complicated frames are being analyzed to enrich the existing database.

Estimation error for all NESA methods is partially due to occurance of incomplete plastic hinging mechanisms. Quantification of irregularity and defining modification coefficients representing irregularity are needed for increasing the accuracy of NESA methods. Such irregularity modification procedures are under invetigation.

The accuracy and conservatism of NESA methods for estimating displacement capacities for frame ductile members, frame stories, and the entire frame need to be investigated by enriching the current ongoing research for more complicated frames. The results for FEMA-440 CSM with first mode and FAPA methods are not presented here. Furthermore, the correlations of different NESA methods with one another are also not presented for the sake of clarity and briefness.

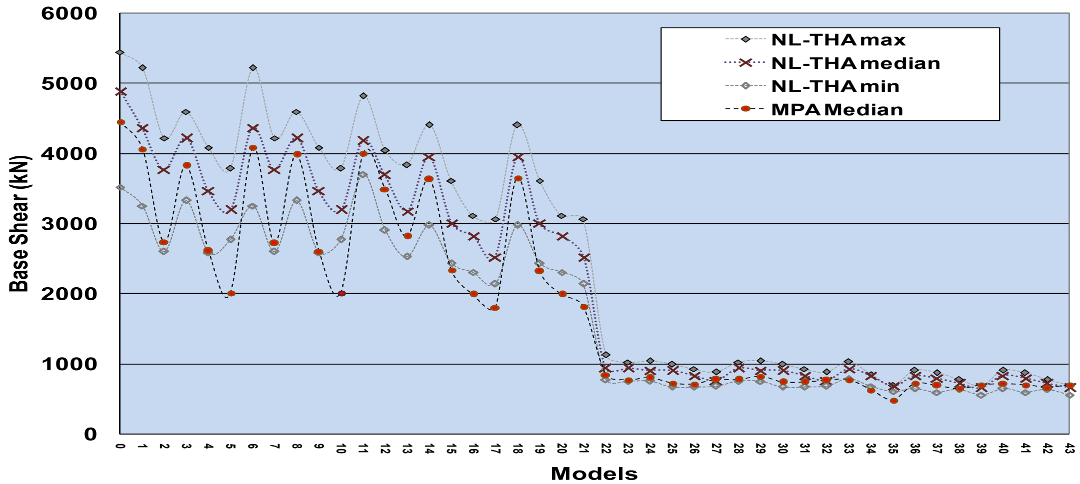

Figure 3 **Comparison of predicted MPA base shear with maximum, median, and minimum base shears computed by the nonlinear time history analyses for all frame models.**

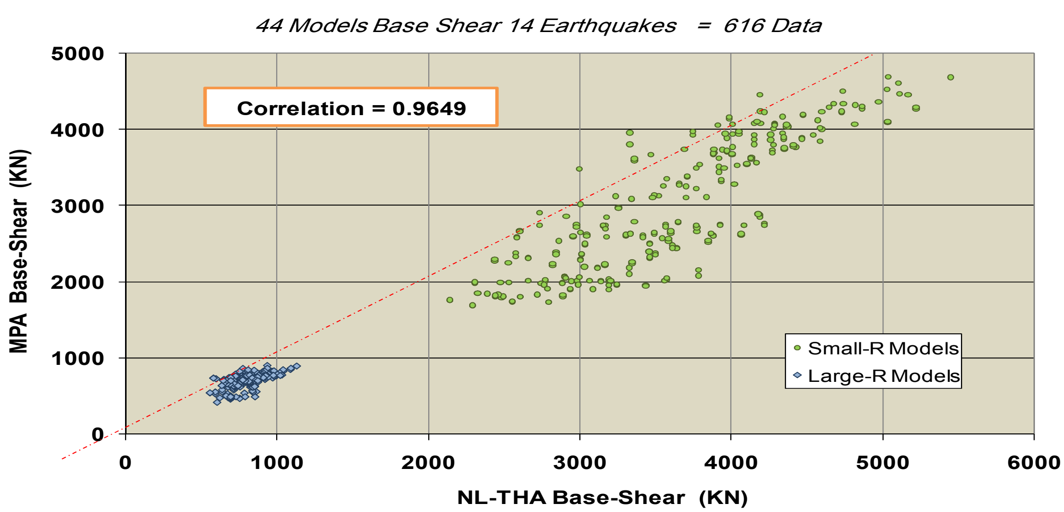

Figure 4 **Comparison of base shears estimated by MPA and determined by nonlinear time-history analysis for all frame models.**

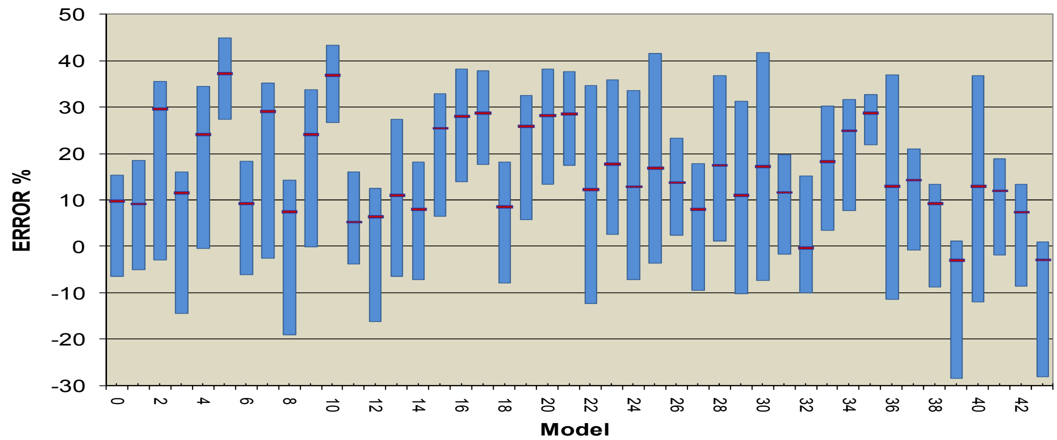

Figure 5 Relative errors of base shears estimated by MPA for all frame models.

Table 2 Median errors and correlation values for different NESA procedures.

NESA Procedure	Median Error (%)			Correlation Value		
	Roof Displacement	Base Shear	Story Drifts	Roof Displacement	Base Shear	Story Drifts
FEMA440 MCM	8 to 30	-8 to 36	-4 to 41	0.69	0.86	0.69
MPA	-22 to 18	-4 to 37	2 to 42	0.81	0.96	0.82
DAPA with CSM	-8 to 60	-25 to 0	-30 to 25	0.81	0.95	0.51

DEVELOPMENT OF CURVATURE DAMAGE INDEX INTERVALS FOR DIFFERENT PERFORMANCE LEVELS BASED ON CONCRETE AND REBAR STRAINS FOR RC FRAME MEMBERS

For designing ductile RC frame members, the required damage level needs to be translated to computable damage indices. Such damage indices need to be defined for plastic hinge sections, frame member, frame subassemblies, and the overall building frame. Damage indices are collapse indices normalized such that a value of zero indicates an undamaged state while a value of one indicates failure. Many different damage indices have been introduced in recent years utilizing different response measures for sections, members, and sub-systems of structural systems. Damage index for sections of RC members is fundamental to define damage level for the members and sub-systems. However, damage due to shear-torsional failures, plastic P-Δ effects, bond failures, and joint failures cannot be represented by section damage indices. For the sake of clarity, in the following, we only discuss selection issues for section damage index.

Demand-capacity ratios for sectional curvature and hysteretic energy dissipated by plastic deformation are extensively used to define section damage index [Power and Allahabadi 1988; Park and Ang 1985]. It is well established that for RC sections reasonably detailed, the curvature damage index is adequately accurate to represent the sectional damage level. For well accepted performance-based design levels of operational, immediate occupancy, life-safety, and collapse prevention; values of the damage index needs to be selected. However such a selection needs to be based on a sound engineering approach instead of arbitrary levels selected in the literatures.

Damage level of an RC section depends on its strength and stiffness degradation, residual deformation, concrete spalling, and crack width. While spalling controls by concrete cover strain, the other major damages are associated to rebar tensile strain and concrete core compression strain in the core concrete. In our coordinated investigations, the correlation of damage level to concrete core and rebar strains is used to recommend damage index intervals associated to performance levels. The results from cyclic lateral loading analyses of a large number of cantilever columns have been used to establish such a correlation. The cyclic analyses have been performed using the computer program UC-win/FRAME (3D) while material and failure models have been calibrated using the test results collected in the PEER database [Berry et al. 2004].

The column design parameters taken into account and their ranges are shown in Table 3. Two types of column sections are considered: (a) square sections with cross sections of 300×300, 400×400, 500×500, 600×600, and 700×700mm^2 and (b) circular sections with 300, 400, 500, 600, and 700 mm diameters. The yield strength and clear cover of transverse reinforcements are set to be 400 MPa and 30 mm, respectively. The rebar ultimate strain is set to be 0.09. The layouts of longitudinal and transverse reinforcement are satisfied the detailing requirements of ACI-318 provisions.

For five selected limit points on the stress-strain curve of confined concrete core, as shown in Figure 6, the associated rebar tensile rebar and curvature damage index are calculated for each cyclic analysis. The curvature, rebar and concrete stresses and strains are calculated at the lower integration point of the fiber element representing the plastic hinge of the cantilever column. The five selected limit points are:

1. No damage state where concrete core strain is less than $0.15\varepsilon_{cc}$
2. Operational level where concrete core strain is less than $0.35\varepsilon_{cc}$
3. Immediate Occupancy level where concrete core strain is less than ε_{cc}
4. Life Safety or repairable damage level where concrete core stress is reduced from peak f_{cc} by 20% to $0.8f_{cc}$
5. Collapse Prevention level where concrete core stress is reduced from peak f_{cc} by 50% to $0.5f_{cc}$, as an upper bound for core crushing.

Where the stress-strain relationship for confined concrete is adopted from Hoshikuma, et al. [1997], while the stress-strain relationship for tensile rebar is based on formula proposed by Mander, et al. [1984], and the relationship for compression rebar is based on formula proposed by Dhakal and Maekawa [2002].

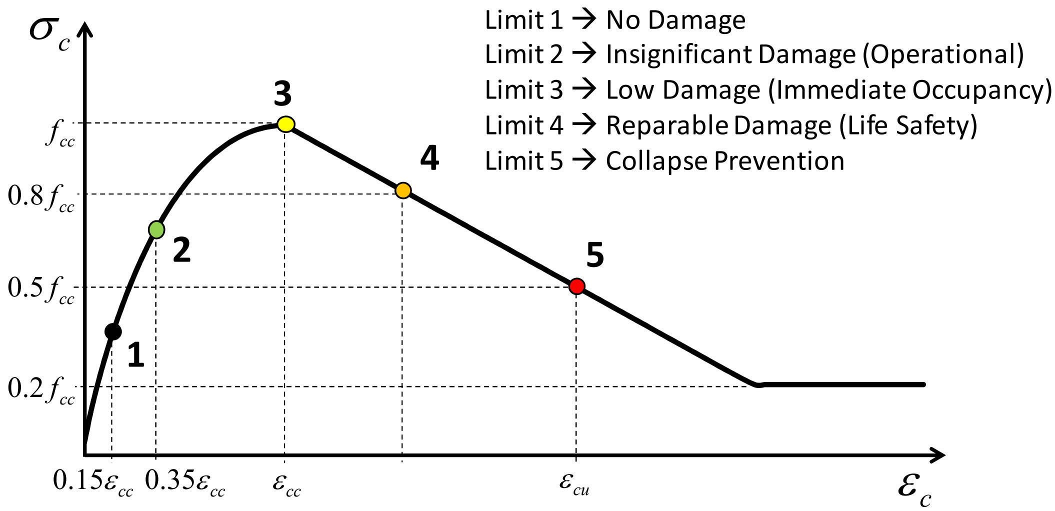

Figure 6 Proposed limit points for confined concrete core stress-strain curve.

Table 3 Column design parameters for the damage index study.

Column Design Parameter	Studied Range
Longitudinal reinforcement ratio (ρ)	1% to 3%
Volumetric transverse reinforcement ratio (ρ_s)	0.2% to 2%
Column axial load ratio to gross concrete compressive strength ($P/A_g f_c'$)	0.0 to 0.5
Concrete compressive strength (f_c')	20 to 30 MPa
Longitudinal rebar yield strength (f_y)	400 to 500 MPa
Column aspect ratio ($\frac{L_c}{D}$)	3 to 5

More than 23,900 square columns and 34000 circular columns were analyzed. The analyses were terminated for: (a) Main rebar rupture $\varepsilon_s=\varepsilon_{su}$, (b) Core crushing $\varepsilon_c=\varepsilon_{cu}$; (c) Significant lateral capacity reduction determined by 20% reduction of column lateral capacity from its peak value. In the performed parametric study, for 99.3% of square columns and 90.5% of circular columns the core crushing was the cause of column failure. Therefore, relating column damage level to the concrete core state of strain and stress should be a governing observation, especially for building frame members. Whereas for large column sections used for bridge piers, rebar strain should also be controlled for the state of crack width and consequently reparability. The effect of column size and shape on determination of damage level is under investigation.

The density functions of the distribution of curvature damage indices for each limit point of core concrete for square and circular columns are shown in Figures 7 and 9, respectively. The average and standard deviation of the estimated density functions are also shown in Figures 7 and 9. The average value minus 1.64 times standard variation (95% confidence level) has been used to recommend damage index intervals for different performance levels for seismic design of buildings. Such interval values may be relaxed to the average values for seismic evaluation and retrofit of buildings

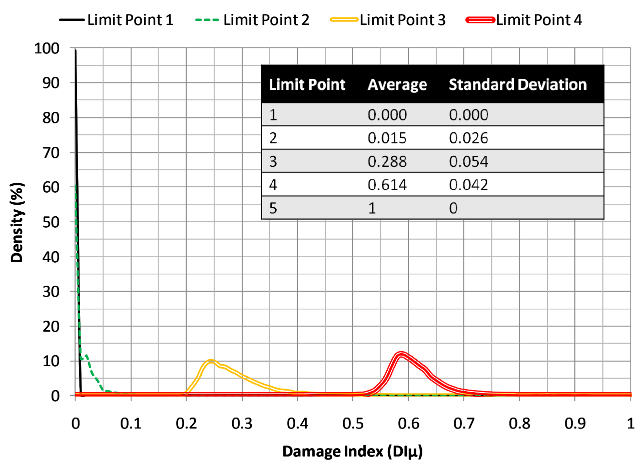

Figure 7 Density functions of damage index for each limit point of core concrete (square columns).

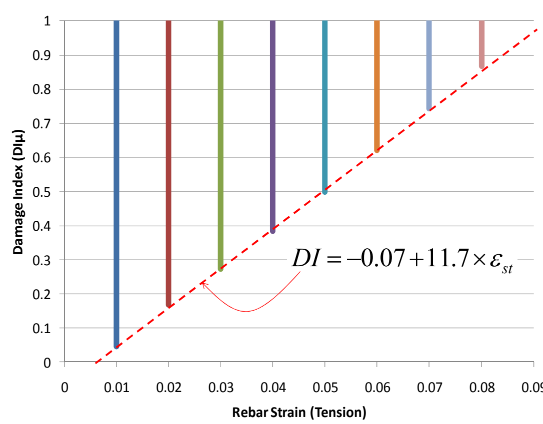

Figure 8 Damage index-rebar strain relation for square columns.

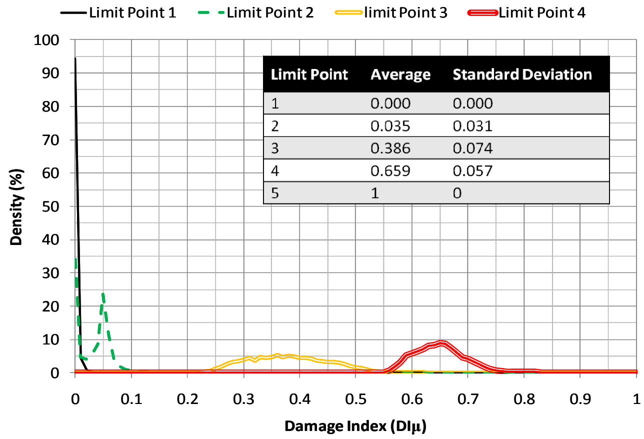

Limit Point	Average	Standard Deviation
1	0.000	0.000
2	0.035	0.031
3	0.386	0.074
4	0.659	0.057
5	1	0

Figure 9 Density functions of damage index for each limit point of core concrete (circular columns).

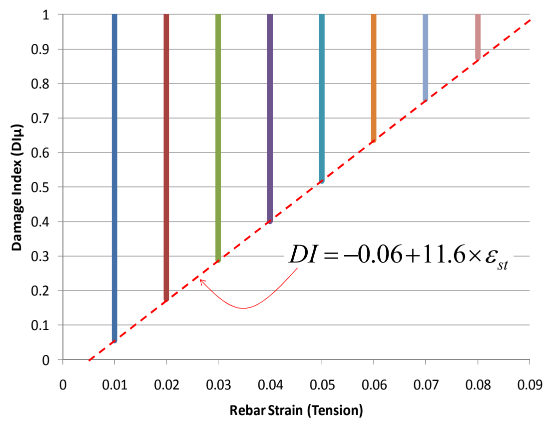

Figure 10 Damage index-rebar strain relation for circular columns.

Furthermore, the variations of damage indices with respect to rebar strain are shown in Figures 8 and 10 for square and circular columns, respectively. The lower bounds of damage indices for each selected rebar strain linearly vary with rebar strain values. Such linear relationships are shown in Figures 8 and 10. It can be observed that for a selected rebar strain, curvature damage index could range from a minimum value to its maximum of 1.0. Therefore damage index is not directly correlated to the rebar strain however for each damage index value there is an upper bound for rebar strain which can be used to limit the crack width. The value of the crack width depends on parameters such as concrete strength, rebar diameter, rebar spacing, reinforcement ratio, and rebar strain (stress). By knowing the maximum rebar strain (stress) for a given damage index, the maximum potential crack width can be estimated which can be controlled by rebar diameter and spacing, and reinforcement ratio.

Proposed damage index intervals and their associated concrete core stress and strain limits and rear strain limits for different performance levels are summarized in Table 4 for square and circular columns. These recommendations are for columns whose design parameters within the limitation shown in Table 3. It has been shown that the fundamentals of reinforced concrete behavior can be used to establish damage levels. Furthermore, the general approach of setting design intervals for a given damage index based on concrete and steel rebar can be used for RC structural members with different shapes and dimensions.

Table 4 Proposed damage index intervals and concrete core and rebar strains for different performance levels.

Performance Level	Damage Index Intervals		Concrete Core Compression Limits	Rebar Strain Limit	
	Square Columns	Circular Columns		Square Columns	Circular Columns
Operational	DI = 0		$0 < \varepsilon_c \leq 0.35\varepsilon_{cc}$	$\varepsilon_s \leq 0.06\varepsilon_{su}$	$\varepsilon_s \leq 0.06\varepsilon_{su}$
Immediate Occupancy	0 < DI ≤ 0.20	0 < DI ≤ 0.25	$0.35\varepsilon_{cc} < \varepsilon_c \leq \varepsilon_{cc}$	$\varepsilon_s \leq 0.25\varepsilon_{su}$	$\varepsilon_s \leq 0.31\varepsilon_{su}$
Life Safety	0.20 < DI ≤ 0.55	0.25 < DI ≤ 0.55	$\varepsilon_{cc} < \varepsilon_c \leq \varepsilon_{cu}$ $f_{cc} \geq \varepsilon_c > 0.8f_{cc}$	$\varepsilon_s \leq 0.58\varepsilon_{su}$	$\varepsilon_s \leq 0.58\varepsilon_{su}$
Collapse Prevention	0.55 < DI ≤ 1.0		$\varepsilon_{cc} < \varepsilon_c \leq \varepsilon_{cu}$ $0.8f_{cc} \geq \varepsilon_c > 0.5f_{cc}$	$\varepsilon_s \leq \varepsilon_{su}$	$\varepsilon_s \leq \varepsilon_{su}$

SUMMARY

The aspects of a robust and practical performance-based deterministic seismic design approach for RC buildings have been discussed. The proposed design approach can be used for different structural systems by using fundamentals of reinforced concrete behavior and practical analyses. Summary of findings by the coordinated research at the Shiraz University for tuning some steps of the proposed seismic design approach has been presented.

REFERENCES

AASHTO (2010). *AASHTO Guide Specifications for LRFD Seismic Bridge Design*, *1st Edition, with 2010 Interim Revisions*, Association of State Highway and Transportation Officials, Washington, D.C.

Antoniou S, Pinho R (2004). Development and verification of a displacement-based adaptive pushover procedure, *J. Earthq. Engng*., 8(5):643-661.

Antoniou S, Pinho R (2004). Advantages and limitations of adaptive and non-adaptive force-based pushover procedures, *J. Earthq. Engng*., 8(4):497–522.

Berry M, Parrish M, Eberhard M (2004). *PEER Structural Performance Database User's Manual: Version 1.0*, Pacific Earthquake Engineering Research Center, University of California, Berkeley, CA.

Caltrans (2006). *Seismic Design Criteria, Version 1.4*, California Department of Transportation, Sacramento, CA.

Chopra AK, Goel RK (2002). A modal pushover analysis procedure for estimating seismic demands for buildings, *Earthq Engrg. Struct. Dyn.,* 31:561–582.

Federal Emergency Management Agency (2005). *Improvement of Nonlinear Static Seismic Analysis Procedures*, FEMA-440, Washington, D.C.

Dhakal R, Maekawa K (2002). Modeling for post-yield buckling of reinforcement, ASCE, *J. Struct. Engrg*., 128:1139–1147.

Hoshikuma J, Kawashima K, Nagaya K, Taylor AW (1997). Stress-strain model for confined reinforced concrete in bridge piers. ASCE, *J. Struct. Engng*., 123(5):624–633.

Kashkooli NA, Banan MaR, Banan MR (2011). Effect of frame irregularity on accuracy of modal equivalent nonlinear static seismic analysis, *Proceedings*, 8th International Conference on Structural Dynamics EURODYN 2011, Leuven, Belgium.

Mander JB, Priestley MJN, Park R (1984). Seismic design of bridge piers. *Research Report 84-2*, Department of Civil Engineering, University of Canterbury, Christchurch, New Zealand.

Moehle J, Deierlein GG (2004). Framework methodology for performance-based earthquake engineering, *Proceedings*,13th World Conference on Earthquake Engineering, Vancouver, B.C., Canada.
Momtahen A, Banan MR, Banan MaR (2008). Evaluation of FEMA440 equivalent nonlinear static seismic analysis for irregular steel moment resisting frames, *Proceedings*,14th World Conference on Earthquake Engineering, Beijing, China.
Park YJ, Ang AHS (1985). Mechanistic seismic damage model for reinforced concrete, ASCE, *J. Struct. Engrg*., 111(4):722–739.
Powell GH, Allahabadi R (1988). Seismic damage prediction by deterministic methods: Concepts and procedures, *Earthq Engrg. Struct. Dyn.,* 16:719–734.
Sharifi A. (2010). Damage-index-based seismic design and assessment of RC rrames designed according to code, PhD Thesis, Civil and Environmental Engineering Department, Shiraz University, Iran.

AN EXPERIMENTAL INVESTIGATION OF THE BEHAVIOR OF ECCENTRICALLY BRACED FRAMES

Shahrokh Maalek

School of Civil Engineering, University of Tehran, maalek@ut.ac.ir

ABSTRACT

The results of a number of experiments on full scale single story-single span eccentrically braced frames (EBFs) have been reported. The work consists of three distinguishable parts. The first part is concerned with a number of proofs of concept tests in order to demonstrate the problems associated with the use of open web beams as short or long links. An appropriate retrofitting method has been proposed for the seismic retrofit of a rather large number of steel buildings composed of EBFs with castellated link beams, which have been constructed in Iran during the last two decades. The second part of the project underscores the importance of full-scale testing of complete EBF specimens in order to reveal characteristics of the system that cannot be observed through testing of isolated link beams. In this part, in addition to an examination of the suitability of the use of IPE sections to DIN (1025-4)—widely produced in Iran—emphasis has been laid upon some observations made during the tests that have not been reported previously. In particular, premature fracture at the positions of welded bracing to beam connections—where high ductility demands are to be induced—is a matter of concern and highlights need for assessing EBFs constructed by such welded connections during the last two decades all over the world. When such welded connections provide partial fixity, they also affect the overall behavior of EBFs. An investigation of the behavior of EBF specimens composed of double IPE sections is the subject matter of the third part of this work. It was demonstrated that such double sections can be used as the link beams of EBFs not only to relax the lateral bracing requirements, but also to increase the clear height of braced frame by reducing the depth of the link beam. This also makes it possible to use smaller sections when larger sections are not available. An examination of the hysteretic curves pertaining to shearing force versus link rotation for the three EBF specimens fabricated with the same link beam and bracing sections but with short, medium and long length links reveals that the energy absorption capacity, strength and initial stiffness of the EBF specimens increase substantially as the link lengths decrease.

INTRODUCTION

Background

Through observations of the seismic behavior of structures and the lessons learnt from the past catastrophic earthquakes, the so called eccentrically braced frames (EBFs) emerged as a result of the recognition of importance of ductility and energy absorption capability of structures at large by the structural engineering community worldwide; in particular in late 1970s and early 1980s. Mainly, the works of the late Professor Popov and his colleagues provided the basis for the 1992 AISC Seismic Provisions [AISC 1992] on the design of EBFs. In the works of Hjelmstad and Popov [1984], Kasai and Popov [1986a; 1986b], and Popov and Engelhardt [1988], the fundamental concepts of the behavior of EBFs were developed on the basis of a series of experiments on isolated link beams with idealized boundary conditions and related supporting theoretical studies. Consequently, many important properties of EBFs such as elastic stiffness, ductility, and the behavior of the link beam under combined shear, bending and axial actions were investigated, together with proposed detailing and further developments followed (e.g., Ghobarah and Ramada [1991] and Engelhardt and Popov [1992] among others) and design recommendations were provided and elaborated [AISC 1992; 1997a; 2002; 2005a).

Previous experimental works on EBFs were mostly concerned with the study of the behavior of wide flange sections as the link beam and the experiments based on which the Seismic Provisions on the design of EBFs were developed [AISC 1992; UBC 1997; AISC 1997; AISC 2002; AISC 2005] had been carried out either on isolated link beams with idealized boundary conditions, or a subassembly of the braced frame. Up to the initiation of the present work in1999, no detailed experimental work on a complete EBF in full scale had been reported in the published literature, except the work reported by Foutch [1989] on a six story building initially designed, constructed and tested as a concentrically braced frame (CBF) system; which had provided a general, but not detailed, overview of the behavior of buildings composed of EBFs.

A number of more recent works were reported during the course of the present investigation. Itani et al. [2003] reported the results of tests on two built up specimens each of which included a subassembly composed of a one half of EBF bay in full scale. Also, proof of concept test was reported by Berman and Bruneau [2007] involving a RHS tubular link that did not require lateral bracing. The work also included an analytical investigation of the use of such members as link beams. In another work [Okazaki and Engelhardt 2007], a number of isolated link specimens constructed from different wide flange sections of ASTM A992 steel with link lengths varying from short shear yielding link to long flexure yielding ones were tested and the potential role of material properties on the fracture of the web was discussed and some design suggestions were proposed.

Objectives and Scope of Present Investigation

With the official approval of the system and its appearance in the AISC Seismic Provisions, we witnessed a period of slowdown in related researches; as if no unresolved problems remained to require further investigations. Enjoying many advantages of the EBF system, such as good balance between stiffness and ductility, high response modification (and behavior factor) assigned by the seismic design codes, more architectural freedom than CBFs, etcetera, engineers began to design EBFs resulting in the wide and rapid spread of the use of EBFs around the earthquake prone areas of the world. Now, after two decades, the author would like to raise the following general question:

> "*Has the research based on the Seismic Provisions for the design of EBFs been developed sufficiently to assure the intended level of reliability of the seismic design and behavior of such systems*"?

In this context, some relevant questions are referred to below:

- <u>Question 1</u>: *Do we expect that the previous experiments on isolated links or subassemblies of EBFs would sufficiently represent the true behavior of EBFs?*

  <u>Comment on Question 1</u>: The actual behavior of the link beam cannot be independent from the actual end boundary conditions and the interaction of all the elements and

components involved. The best way to compare the actual behavior with the behavior of an isolated link is full scale testing that can account not only for the end conditions of links, but also for the effects of the imposed rotation at the top ends of bracing members that may cause premature buckling. Through such tests, the validity of the over-strength factor proposed by the Provisions (AISC, 1997, 2002 and 2005) can also be examined.

- Question 2: *While almost all the previously reported tests were carried out on the Wide Flange sections to the AISC Specification, that are not available in many countries other than the US, can one use any other available non-wide-flange sections that merely satisfy the requirements of Compact and/or Plastic Sections as the link beam of EBFs?*

  Comment on Question 2: Since no general confirmation could be made with full certainty, qualifying tests may be carried out in the context of design assisted by testing for any potentially candidate section.

- Question 3: *Is there any concern about the use of welded gusset plate connections as recommended by many researchers and used frequently in the construction of EBF structures during the past two decades?*

  Comment on Question 3: The author has been concerned about the potentialities of fracture failure of such joints due to the high ductility demand imposed on the joint; particularly premature failure as a result of low cycle fatigue and/or as a consequence of the initiation of web or flange buckling.

- Question 4: *The use of web doubler plates has been prohibited by the AISC Seismic Provisions for the link beam. What about the use of double I sections?*

  Comment on Question 4: In the Provisions, the use of web doubler plates has been prohibited based on a reason that is not necessarily applicable to double beam sections. The AISC Provisions have made no reference to the design and use of double sections. We may conduct appropriate tests and observe the behavior of such double sections as link beams of EBFs.

This work is composed of three parts:

Part I focuses on the misuse of EBFs in Iran where castellated beams have been frequently used as the link beams of EBFs. Part II attempts are made to deal with the Questions 1, 2, and 3 raised above. Part III is concerned with the Question 4 above.

PART I: MISUSE OF THE CONCEPT: EBFS COMPOSED OF CASTELLATED LINK BEAMS

The castellated beam has been widely used in many countries for quite a few decades and in a variety of applications. Requirements for the analysis, design and fabrication of castellated beams appeared as an appendix to the Iranian specification for the design and construction of steel structures [Maalek 1991] and later in the body of the Iranian Specification [Maalek 2008) based on a comprehensive program of tests on castellated beams [Maalek 1986; Maalek 1990; Maalek and Burdekin 1991] carried out to investigate different aspects of the behavior, analysis and design of these beams. Also, for the first time, indeterminate structures composed of castellated beams were studied theoretically, numerically and experimentally by

Maalek [1989], Maalek [1993], Maalek [2000 a, b, and c], and Maalek [2002]. Also a series of related investigations were conducted and supervised by the author through a series of research works reported in his postgraduate students' theses, (a total of more than 20 Master's theses accomplished on the subject in the University of Tehran between 1992 and 2008), only a few of which have been published [Maalek et al. 2002; Maalek and Rajabi 2006].

Castellated Links

Castellated beams have been used as the link beam of the EBFs for residential, administrative and educational buildings of up to 14 stories in Iran for almost two decades. As a matter of fact, after the introduction of EBFs a number of engineers in this country began to take advantage of the possibility of providing some openings by adopting various forms of EBFs but they largely disregarded the recommendations clearly specified by the Seismic Provisions [AISC 1992, 1997, 2002, and 2005] prohibiting the use of any web openings in the link beam. This misuse of the concept rapidly spread all over the country to an extent that only in a single day of the summer of 2005 the author observed more than 70 buildings under construction by this system in the central Tehran from 5-story to 14-story residential/administrative/commercial buildings, up to 4 story school buildings and in one occasion a fire-fighting station! Figure 1 shows only one of many in which a rather long (flexural) castellated link is used with no web stiffener whatsoever. On the other hand, it can be seen that the bracings are quite slender and prone to premature buckling. They are installed at an angle of inclination out of the range proposed by the Seismic Provisions in a way that they are not much effective in increasing the stiffness of the unbraced frame to a desirable amount.

Figure 1 An example of many steel buildings constructed with castellated link beam.

The webs of the castellated beams in Figure 1 have been strengthened by doubler plates only near the beam to column connections, at a position outside the link. There are also conceptual deficiencies in the design and erection of the bracing to beam and other connections. It is interesting to note that here the beams in the neighboring panel have solid webs! Apparently, this practice of design and construction leads to a school building which is prone to high damage during a not so severe earthquake, resulting in huge loss of lives. The author hardly worked through explanation of potential problems associated with the use of the castellated beam as the link of an EBF in numerous lectures and workshops around the country and at the same time, by planning and conducting experiments on such deficient systems in order to provide the designers with observable proofs of his words.

Experimental Program

The experimental program included testing of six full scale single-span single story eccentrically braced frames with short to long castellated link beams with the geometry of cut specified in the Iranian Standard [INBC 1991-2008]. Another two specimens were also fabricated with all the castellations along their link lengths in-filled with hexagonal infill plates. For the latter specimens, web stiffeners were also provided along the length of the link at an interval equal to the center to center of the web posts. The re-entrant corners for all specimens were cut with the minimum radius of 0.07 times the initial height of the rolled section as recommended by the author in the Iranian National Code of Practice [Maalek 1992-2008].

Figure 2 shows one of the specimens with a rather short castellated link beam. In this specimen, the web panels at both ends of the link were filled with infill plates along the length of the bracing to beam connections. Also web stiffeners were provided at these positions. The reason for such strengthening was to ensure failure at the link beam. The bracings had been designed to resist the lateral force and its equivalent base shear calculated by the equivalent static method of the estimation of earthquake forces pertaining to a five story residential building with an appropriate number of such braced spans at each major perpendicular direction to be built on firm soil, assuming a response modification factor corresponding to a non-ductile braced frame structural system. Tests were carried out under cyclic lateral loading to ATC-24 (1994). Lateral supports for both top and bottom flanges were provided by means of rather long anchored cables on both sides of the plane of the frame.

Figure 2 An overall view of a specimen and the test setup.

Numerical Results

A series of detailed nonlinear finite element analyses was carried out attempting to estimate the behavior of such test specimens under lateral loading [Maalek and Tafazoli 2002; Maalek 2006]. The resulting mode of failure for a specimen with all its castellations left open and unstiffened is presented graphically in Figure 3. The failure is found to be controlled by lateral torsional buckling of the web along the length of the link.

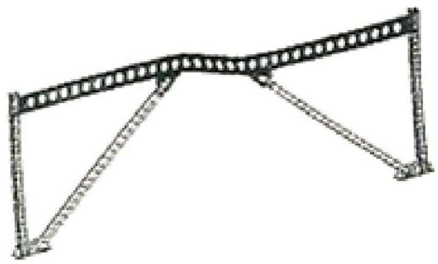

Figure 3 Finite element representation of the deformed shape of the test specimen and the lateral torsional buckling of the link webs under monotonically increasing lateral loading.

The Observed Behavior of the Test Specimens during the Experiments

The after test residual deformed shape of the specimen of Figure 2 is shown in Figure 4. It can be seen that the mode of failure predicted by numerical analysis has been reproduced in the experiment as well [Ghaedian 2002; Maalek 2006]. Note that the specimens with infill plates and web stiffeners along the length of the link acted satisfactorily as a ductile link in the EBF. Hence, as far as the expanded beam satisfies the requirements of compact sections, the seismic retrofit by adding infill plates together with web stiffeners at the positions of the center lines of the web posts not only leads to the elimination of lateral torsional buckling of the web but also provides the required conditions for energy absorption through web yielding along the length of the link. In the tested specimens strengthened by this retrofitting method, not only the strengths increased by about 2.5 times but also the specimens exhibited sufficient ductility. Hence, the author suggests retrofitting of such buildings by this method. This may need to be accompanied by the provision of sufficient lateral supports for both top and bottom flanges.

Tests on the specimens with a rather long castellated link beams showed much less initial stiffness, as expected. The observed behavior included the formation of plastic hinges at both ends of the link followed by the formation of a vierendeel type of mechanism at the end panels. Before the exhibition of any noticeable plastic rotation, premature buckling of the flanges occurred that limited the load carrying capacity of the specimen (Figure 5). Here, the purpose of the author has been the presentation of proof of the concept test results. Details of the geometric and material properties of the specimens along with detailed test results can be provided to interested individuals and/or bodies upon request.

Figure 4 Lateral torsional buckling of the end panel of the web posts of the short castellated link.

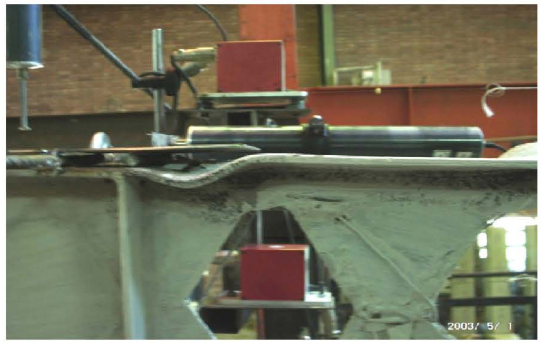

Figure 5 Buckling of the flange at the long castellated link.

Remark on Part I Experiments

As a result of these tests, and the efforts made to demonstrate the potential danger associated with the use of open web beams as the link beam of braced frames of usual forms and configurations suitable for EBFs, such misuse of the concept has been largely reduced if not completely eliminated from the normal practice of steel designers of this country.

PART II: EXPERIMENTS ON EBFS WITH IPE LINK BEAMS

In this part, the results of a number of experiments on full scale single span - single story EBFs with shear link beams are reported. The tests were carried out in order to observe the behavior of a particular type of the link beam under actual boundary conditions and investigate the performance of connections, bracing members and the effects of their interaction in the overall behavior of the EBF specimens.

The previous experimental works had been concerned with wide flange (WF) sections to the AISC specification (AISC, 1997b), which may not be available world-wide. With the consideration of the availability of IPE sections to the German Standard (DIN, 1994) in many developing countries and regarding their geometric and dimensional properties, a study on the feasibility of the use of such sections was conducted; so that structural designers in many parts of the world may be encouraged to employ EBFs in their designs with the use of available sections.

Attention has also been paid to the observed modes of failure, particularly due to premature buckling or fracture of the members and connections and their effects on the energy absorption and the ductility capacity of the system. The type of the bracing member to beam connection details employed here utilizes welded gusset plates.

Experimental Program

A schematic diagram of the test set up is shown in Figure 6. The IPE 270 mm profile to the German standard (DIN, 1994) has been employed as the beam, both along the link length, *e*, and outside of the link, for all the specimens. The section satisfies the requirements for seismically compact sections, set by the AISC seismic provisions [AISC 2005a] and AISC specification [AISC 2005b]. In the series of tests reported here, the bracing to beam connections have been chosen to be of welded type, as suggested in many related works (e.g., Engelhardt and Popov [1992]), due to its more relaxed tolerance in real steel construction. The tests were carried out under cyclic lateral loading and under displacement control. In order to eliminate the effect of unrealistic compression in the beam and uneven response of bracing members, the test set up was designed to enable the application of equal displacements at both ends of the beam at the positions of the beam to column connections. A device was designed to enable the application of required equal displacements at both sides of the test specimen by means of four compressive hydraulic jacks as shown in Figure 6.

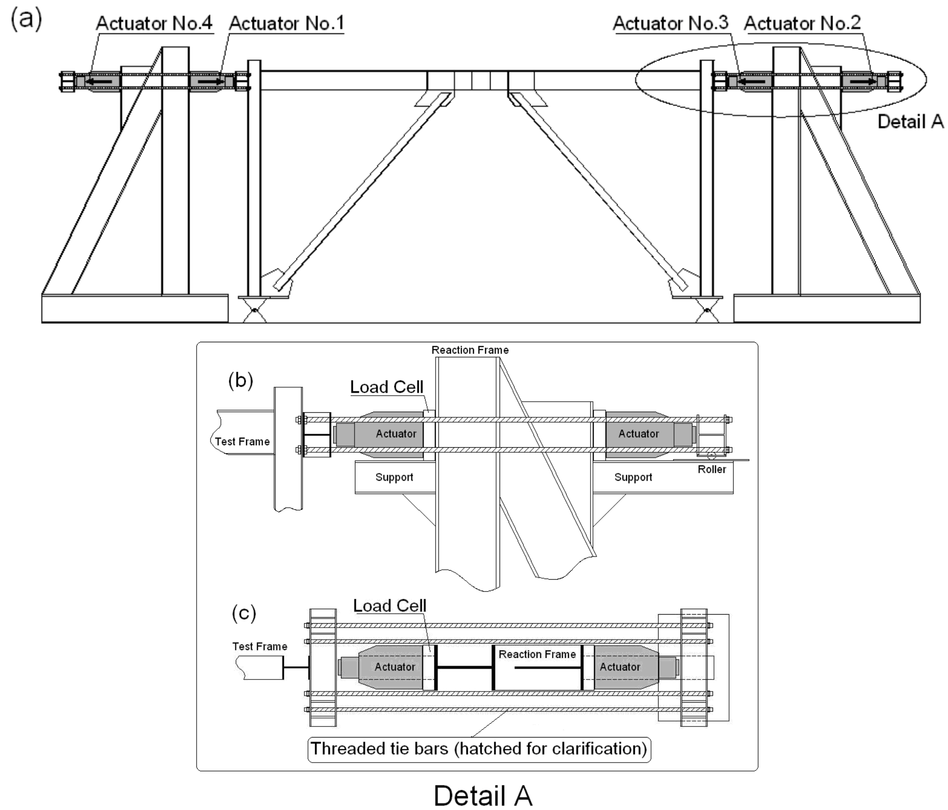

Figure 6 A schematic diagram of the test setup: (a) general overall view; (b and c) detail A-side and plan views.

Loading History

The behavior of the specimens was studied under the action of cyclic lateral loading. At the time when the tests reported here were in process, the available AISC seismic provisions was the 1997 edition [AISC, 1997a] in which the specified loading sequence was identical to that specified in the ATC-24. Hence, the cyclic loading history was adopted based on the ATC-24 [1992] recommendations for the test specimens Nos. 2, 3, and 4. This type of loading had also been used in the works reported by Ghobarah and Ramadan [1991] and Berman and Bruneau [2007], among others. Specimen No.1, were loaded differently. It is also to be noted that in both the 2002 and 2005 provisions, the loading sequence specified in ATC-24 has been considered as an acceptable alternative to those prescribed in Section S6.3 of both provisions (see also AISC [2000]). Loading was applied under displacement control.

Some Theoretical Background

Denoting by e the link length, the nominal shear strength of the link (V_n) is taken as the smaller of the plastic link shear strength, V_p **,** and $2M_p / e$ [AISC 1997a; 2005a]**,** where for a beam section with depth, d, flange thickness, t_f , and web thickness, t_w ,:

$$V_p = 0.6F_y(d - 2t_f)t_w \tag{1}$$

and

$$2\frac{M_p}{e} = \frac{2ZF_y}{e} \tag{2}$$

$M_p = ZF_y$ represents the plastic moment of resistance of the link beam section with a plastic section modulus Z and the yield stress F_y **.** According to AISC [2005a], a link of length $1.6\ M_p\ /\ V_p$ or less is classified as a shear link, and a link of length $2.6\ M_p\ /\ V_p$ or more is categorized as a moment link. Substituting for M_p and V_p the corresponding values for the standard IPE 270 section (to DIN 1024) used for the test specimens, it can be seen that in the design of the test specimens, the length of the link beam has been so chosen to be slightly less than $1.6\ M_p/\ V_p$ and hence, the link is to be categorized as a shear yielding one:

$$\mathrm{e} = 750 \leq \frac{1.6\mathrm{M_p}}{\mathrm{V_p}} = 783\ \mathrm{mm} \tag{3}$$

Some Important Observations

The following is an outline of the observations made during the experiments [Maalek 2006; Moslehi 2005; Adib-rad 2010; Maalek et al. 2011].

Test Specimen No. 1

The application of cyclic loading with increasing amplitude was accompanied by considerable plastic deformations of the web until a crack was noticed at the weld which had joined the gusset plate stiffener to the lower flange of the beam (Figure 7a). The crack initiated from the toe of the fillet weld and propagated inwards and extended towards the weld between the gusset plate and the bottom flange of the beam. It is to be mentioned that the specimens had been manufactured by the manufacturer as a normal manufacturing process with no special precautions. The gusset plate stiffener had close square butt preparation with no V-preparation, but had been welded to the bottom flange of the beam with Manual Metal Arc welding using deep penetration electrodes to achieve some but not full penetration in addition to the fillet welding at both sides. The imposition of the inelastic link rotation at this stage on the connection tended to apply a considerable end rotation on the bracing member through the connection together with the corresponding moment in the plane of the frame inducing additional tension on the weld in excess of the tensile force produced in the bracing member, requiring a high ductility demand well above the ductility capacity of such a welded connection. The high intensity of the stress field at the positions of hot spots due to the geometry of connection, loading condition and probable welding defects are to be considered as the main cause for the initiation of crack. This crack propagated rather rapidly resulting in the fracture of the weld at this position. At this stage, the test was paused, the fractured weld was repaired and the test was continued. With the continuation of the test, extensive plastic deformations were observed, whereas out of plane displacement of the link beam had been observed at both ends of the link beam from the initial stages of yielding of the web due to the insufficiency of lateral supports that resulted in premature lateral torsional buckling of the link beam followed by the reduction of resistance. As displacement was increasing, the reinforced weld fractured suddenly at the same position that had fractured earlier.

Test Specimen No. 2

In this test, in order to prevent lateral torsional buckling of the beam, the distance between the lateral supports was reduced. At the same time, the stiffness of the lateral supports was increased substantially with the use of additional oblique brace members in order to limit the out of plane deformation of the top and bottom flanges of the beam to a negligible value. During the experiments, the adequacy of the lateral support provided was confirmed. In this experiment, with the extension of plasticity in the web of the link beam and the increase in the beam rotation angle, inelastic deformations were also observed in the connection plate followed by the occurrence of the local bucking in the flanges at both ends of the beam. Shortly after, the fracture of the fillet weld between the bracing connection plate stiffener and the flange occurred. The crack propagated to the welded joint between the gusset plate and the flange in the longitudinal direction as shown in Figure 7b.

Following the fracture of the weld, the specimen was unloaded, the fractured weld was repaired and the test was continued. With the continued cyclic loading, more pronounced flange buckling was observed at both ends of the link beam. After extensive plastic deformations, the web also buckled at the two end panels. The reduction of the lateral load bearing capacity of the test specimen was accompanied by substantial increase in the lateral displacement (storey drift) of the braced frame and the rotation angle of the link beam until the test was terminated. At this stage, inelastic deformation of the web had been extended along the link beam and across the full height of the web. In close observation of the specimen after dismantling, it was found that cracking had occurred at the welded joint between the web stiffener and the link web at one side of the middle web panel.

Test Specimen No. 3

In this specimen, a bigger fillet weld size was used to increase its load carrying capacity. After the development of extensive plastic deformation along the link web, the local buckling of the end web panels was noticed through the measured values of strains corresponding to back to back strain gauges located at the middle of the end panels. This was followed by the initiation of buckling of the flange. Due to a rather large deformation observed in one of the column bases under tension, the test was continued under monotonically increasing loading applied in the direction causing the base plate to remain under compressive actions until the attainment of the ultimate lateral load. With the increase of monotonically applied load, the deformation of the bottom flange at the vicinity of the connection plates became considerable as the ultimate load was reached and unloading occurred. The applied lateral displacement was continued with a gradual decrease in strength. At this stage, the specimen was unloaded. The considerable deformation of the end panel led to the bending deformation of the web stiffeners and after a considerable plastic deformation, the reinforced fillet weld that connected the gusset plate stiffener to the bottom flange of the link beam fractured at the other end. Fracture propagated to the weld connecting the gusset plate to the bottom flange rather abruptly (Figure 7c).

An investigation of the results recorded through the strain gauges installed across this section reveals the fact that at the attainment of the ultimate load, a plastic hinge had been formed completely at this section.

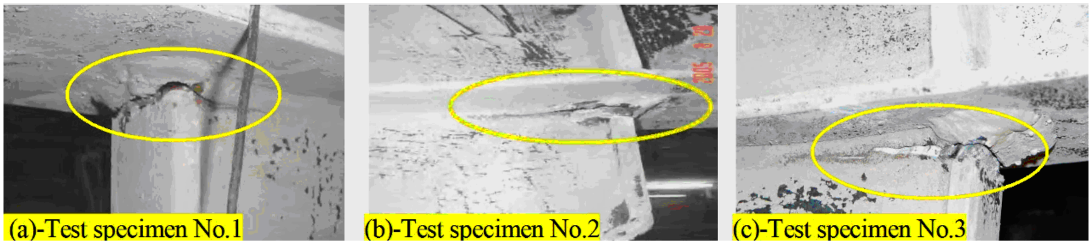

Figure 7 Fracture of the transverse fillet welds at the connections between the gusset plate stiffener and the beam bottom flange followed by the propagation of fracture towards the longitudinal weld connecting the gusset plate to the flange.

Test Specimen No. 4

In the fabrication of this test specimen, in order to prevent fracture at the welded bracing to beam connection, use was made of two triangular plates at both sides of the gusset plate stiffener (Figure 8). In this manner, the length of the weld increased substantially.

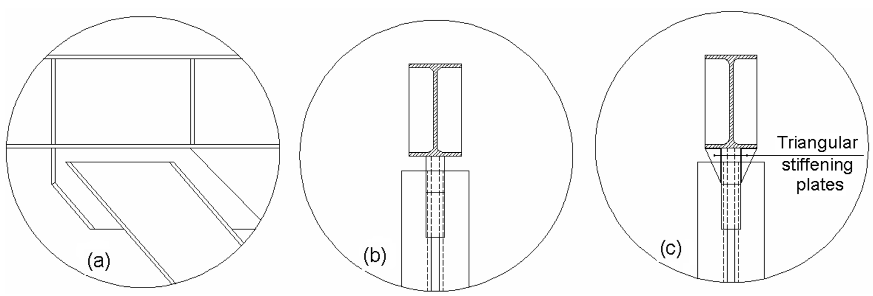

Figure 8 Bracing to beam connection details: (a) side view; (b) section through the link; and (c) section through the link after the addition of the triangular stiffening plates.

In this test, following the penetration of plastic deformations and the formation of plastic hinges at end sections, the buckling of the web occurred at the end panels followed by the buckling of the flanges in such a manner as expected in cyclic tests (Figure 9). With the continued application of the predetermined incremental cyclic lateral displacements and the increase in lateral displacements and the local buckling related deformation, the fracture of the weld connecting a web stiffener to the web of the link beam occurred at the position just above the bracing to beam connection. With the consideration of the large deformation demand at the locations of the fracture, the initiation and propagation of such cracks can be expected at such positions where hot spots exist due to geometrical characteristics and welding defects. In particular, the heat affected zone (HAZ), in which a high temperature gradient may have been induced during welding and may have caused the micro structure of the base metal to experience embitterment, is not expected to be able to accommodate with such a considerable ductility demand. In the bottom part of the welded joint of the web stiffener, the crack initially propagated rather aligned with the welded joint and then branched and deviated from that direction and propagated rather horizontally through the web. The final deformed shape of the link beam is shown in Figure 9, which also shows the combined effects of flexure and shear after buckling of the web at both end panels. In the same figure, the additional triangular plates used for the strengthening of the weld (by increasing the welded length) can also be seen. It is to be noted that with the aid of these additional triangular plates and the resulting increase in the weld length, no fracture occurred at this critical position in this test.

The behavior of the test specimen can be traced through the hysteretic curves concerning the variation of the web shear force with respect to the plastic angle of rotation as shown in Figure 10.

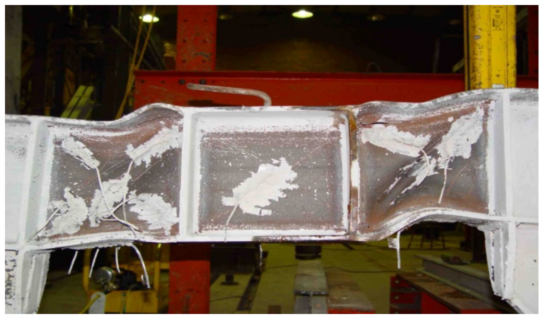

Figure 9 Final residual deformed shape of the link beam (Test No.4).

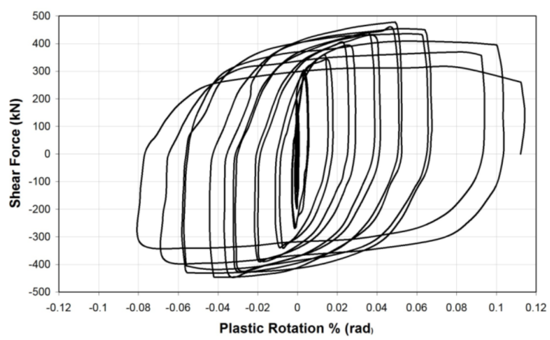

Figure 10 Hysteretic relationship between the web shearing force and the plastic angle of rotation (Test No.4).

Remarks on Part II Experiments

- With regard to the limitations of the production of hot rolled steel sections in many developing countries, which prevents the use of a variety of sections available in international standards or national standards of industrialized countries, tests on the IPE section carried out here, which is the most popular rolled section produced in Iran and probably some other countries, provided us with the required information in relation to its behavior and suitability of use as a link beam and some quantitative data corresponding to the load carrying capacity and its cyclic behavior. A study of the data gathered and processed during the series of experiments reported in this part [Maalek 2006; Moslehi 2005; Adib-rad 2010; Maalek et al. 2011] demonstrates that, although the depth to thickness ratios of IPE sections are usually higher than those of WF sections; however, they are still expected to be capable of the development of full shear yielding of the web in short (shear) links with sufficient margin of safety against failure through web buckling or fracture at the end panels, to satisfy the requirements of the Seismic Provisions [AISC 1992, 1997, 2002, and 2005a], provided that sufficient lateral support is present to prevent premature lateral- torsional buckling of the beam. Further investigations are needed under dynamic loading to observe the actual dynamic behavior of such EBFs.

- The observations made during the tests on specimens 1, 2 and 3 concerning the fracture failure of the welds at the joint between the gusset plate stiffeners to the bottom flanges of the link beams -the zones where high ductility demands are induced—would lead to a subject matter of concern. These observations emphasize the fact that such type of gusset plate connections are expected to be seismically vulnerable. Hence, more studies seem to be essential in order to assess the seismic behavior of these EBFs that have been constructed over the past 20 years with conceptually similar bracing to beam connection details. The success in the achievement of the desired performance of such structures may be highly dependent upon the detailing of connections. At the same time, the penetration and propagation of plasticity in the gusset plate and the probability of buckling of rather thin gusset plates need further attentions. However, it is to be emphasized that in the experiments, the fracture of weld occurred in specimens Nos. 1, 2, and 3 under values of lateral loads, and their corresponding plastic rotations, well in excess of the values pertaining to the achievement of V_p. However, in the case of Specimen No. 4, for which additional triangular plates had been included as shown in Figure 8c, weld fracture did not occur at this position and the specimen failed by other modes as described below.
- The pronounced mode of failure of the link beam of the test specimen No. 4 was the web buckling of the end panel after an extensive plastic deformation followed by the flange buckling. The fracture of the web initiated from the weld of the web stiffeners. With the consideration of the large deformation demand at the locations of the fracture, the initiation and propagation of such cracks can be expected at such positions where hot spots exist due to geometrical characteristics and welding defects. In particular, the heat affected zone is not expected to be able to accommodate with such a considerable ductility demand. Excessive deformation has resulted in a considerable crack opening displacement. In fact the type of fracture observed was a combination of the in plane and out of plane modes of fracture including the tearing due to the out of plane buckling of the web panel. The buckling of the web at the end panels of the IPE sections had occurred in a stage of loading when a comprehensive amount of energy had already been dissipated through shear yielding of the link beam. It was noticed that after the initiation of web buckling, a considerable post buckling strength existed which was accompanied by the capability of the absorption of energy through further deformations and rotations, with gradual loss of strength; that is, without any abrupt reduction of strength. As long as sufficient space is available for welding of the web stiffeners, there seem to be no difficulties associated with the installation of stiffeners at shorter intervals to prevent buckling; however, the more welding applied in critical locations, the more welding defects are expected to be introduced in those critical areas (such as the end panels) which may cause the initiation of premature facture. These observations suggest the need for further investigation of the post buckling behavior of the web and its influence on the fracture of the weld as well as the fracture behavior of the web at the end panels on the basis of principles of elastic-plastic fracture mechanics which shall provide a means for the investigation of the low cycle fatigue behavior of such EBFs.
- With regard to the type of the bracing to beam connections with partial fixity employed in the specimens, the considerable plastic shear deformations of the link

beam in an EBF, imposes rotations at the top ends of the bracing members about an axis perpendicular to the plane of the braced frame. On one hand, this partial fixity may affect the reduction of the effective length of the bracing member, but on the other hand, by the application of an end moment and its corresponding end rotation, it may reduce the desired margin of safety in connection with the over-strength factor and the reserve of strength against in-plane buckling. At the same time, this joint partial fixity may affect the behavior of the link beam and the connection welds. This requires more investigation through quantitative analytical methods with supporting experimental studies.

PART III: TESTS ON SPECIMENS WITH LINKS COMPOSED OF DOUBLE IPE SECTIONS

Bearing in mind that in the seismic provisions, the use of web doubler plates has been prohibited, the present work is concerned with an investigation on the competitiveness and suitability of the use of double I sections as the link beam of EBFs. In case if such double sections comply with the seismic requirements and exhibit sufficient capabilities to act as a satisfactory link beam, the followings may be considered as immediate advantages associated with the use of double sections as the link beam of EBFs:

- The more relaxed lateral support requirements due to its much higher warping and torsional strength compared with single web-open sections such as Wide Flange sections.
- The possibility of the use of available smaller I sections where the larger size sections are not available in the rolled form.
- Even if large size rolled sections are available, one may find it beneficial to use an equivalent double section to reduce the beam height and provide more clearance.

Experimental Program

In the work reported here, three single story-single span test specimens have been constructed in full scale with their link beams chosen to be double IPE 180-mm sections welded together along the joints between both the top and bottom flange edges and along the full length of the link. The shear area of this section is very close to a single IPE 270-mm section that had also been tested prior to this work and reported in Part II above [Maalek et al. 2011).

In the first specimen, the length of the double section link was so chosen to be representative of a shear dominant link (500 mm in this case); while in the second and the third ones, the link lengths were adopted to represent a combined moment-shear link (750 mm) and a moment link (1000 mm) respectively. The tests were carried out under cyclic lateral loading under displacement control. Here, the observed behavior of the specimens has been demonstrated with emphasis on their energy absorption capacities. The test set up and loading history were the same as used for specimens tested and discussed in Part II of this work.

Experimental Results

Figures 11 and 12 show the deformed shape of the short and the long link beams respectively at the final stages of testing. Figures 13 a, b, and c, respectively, represent the hysteretic curves exhibiting the cyclic behavior of the specimens comprising the short, medium, and long double sections as their link beams [Maalek 2006; Adib-rad 2010; Maalek et al. 2011).

Figure 11 The after-test residual deformed shape of the short link.

Figure 12 The after-test residual deformed shape of the long link.

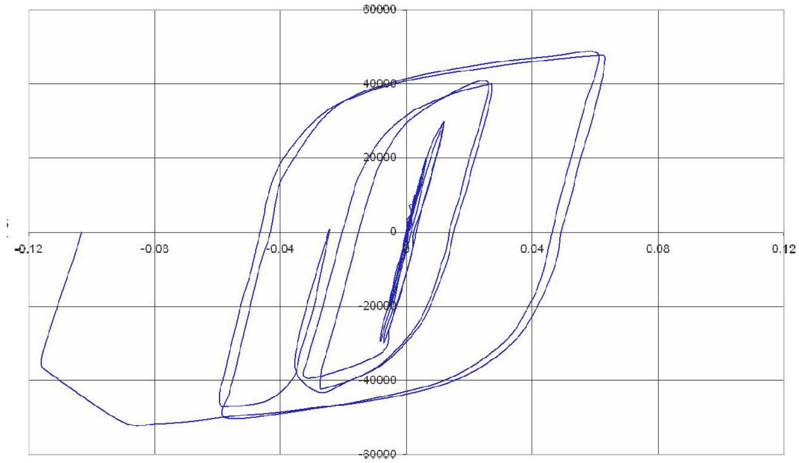

(a)

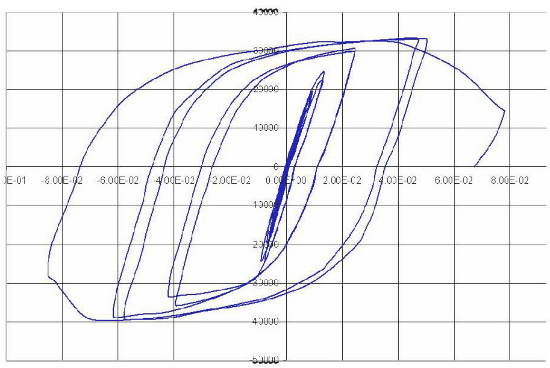

(b)

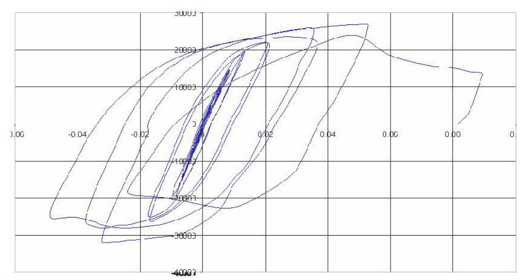

(c)

Figure 13 Hysteretic relationships between the shearing force and the angle of rotation for (a) short, (b) medium, and (c) long length links composed of double IPE sections. Note that the curves have been drawn approximately to the same scale.

Remarks on Part III Experiments

The results obtained from the tests with a rather short, medium, and long double I sections indicate that:

- The test specimen with shear link exhibited the highest stiffness, strength and ductility, due to its higher energy absorption capacity and the lesser angle of inclination of the bracing members in comparison with the other specimens with longer link beams.
- In contrast, the experimental results reveal that the specimen with the longest link absorbed the least internal energy, showed the lowest ultimate strength and the lowest initial stiffness compared with the specimens with shorter links.
- As expected, in the case of the specimen with a link length in the range of the evident shear-moment interaction, the corresponding values of relevant quantities were found

to be in between those of the specimens with the shortest and the longest link beams tested.

- In all the three tests, the ultimate loads were reached after the achievement of the specified link rotation (AISC, 2005a) with a rather gradual loss of strength.
- Observations made during these experiments has revealed that the laterally well supported double rolled I section of the IPE type tested here satisfies the requirements of the seismic provisions and hence can be used as the link beam of appropriately designed EBFs.
- The observed modes of failure of the tested specimens were related to extensive plastic deformations, local buckling of webs and flanges at the link end panels and in the case of the shorter link, the fracture failure initiating from the weld joining the gusset plate stiffener to the lower flange, extending to the flange and propagating to the web just after the achievement of the maximum permitted rotation angle prescribed by the seismic provisions. Therefore, the observed behavior reported here too reflects the potential danger of the type of welded bracing to beam connections through gusset plates, which is not expected to be capable of accommodating the imposed large ductility demand at a stage when the specimen has undergone extensive plasticity and the local buckling and/or fracture failure has initiated.

CONCLUSIONS

- The experimental work reported above consisted of three parts. In part one, a misuse of the concept, which was common in this country for a rather long period of time, was discussed through experimental works as well as numerical analysis. As a result, the serious problems associated with the use of castellated beams as the link beam of EBFs were demonstrated clearly. Although the use of open web link beams had been clearly prohibited in the Seismic Provisions, this important matter had been disregarded by the steel designers in this country. The work was carried out to prevent further construction of such deficient systems to reduce the risk of collapse. As a matter of fact, this objective was met successfully. Also in this part, a retrofit measure was introduced for the seismic retrofit of several structures already built with castellated link beams. However, since these buildings have been built only recently (i.e. during the last two decades), there are no tendencies among the designers and the bodies who had approved their designs to disclose their mistake! Most of such vulnerable buildings have been constructed by builders, who have already sold the buildings and have disappeared with no regard to their responsibilities. On the other hand, most of the owners are not aware of the quality of the structural design and construction of their buildings. Thus, the author has not yet encountered even a single building of this category that has been retrofitted by the suggested method or any other measures. As a consequence, these buildings are being used while they are highly prone to disastrous seismic hazards.
- In part II, in addition to the examination of the suitability of the use of laterally well supported IPE sections to DIN standards, which are produced in Iran, as short links of EBFs, warnings were given in relation to the potentialities of premature fracture of weld and local buckling of web and flanges at the end panels of the link. During the experiments on three specimens out of the four specimens tested here, it was observed that fracture of weld between the gusset plate stiffener and the bottom flange of the

beam occurred and propagated rather abruptly to the weld connecting the gusset plate itself to the bottom flange. In one of the specimens, a substantial increase in the welded length, by the addition of triangular plates as shown in Figure 8c, prevented such premature fracture failure. However, before any general recommendations can be made, further investigations are necessary in relation to weld quality requirements with due consideration of the high ductility demands imposed on the welded joints as the link rotation reaches to its permitted values. Such investigations should include a comprehensive program of tests with different weld qualities and connection details (including bolted connections) under dynamic lateral loading. In the specimen for which the fracture of the weld discussed above was prevented, after substantial plastic deformation, the weld between the web stiffener and the web fractured together with the buckling of the web and flanges. The high deformability demand on the web weld resulted in the propagation of crack towards the web, and the excessive out of plane deformation of the buckled web led to eventual tearing of the web. On the one hand, one may reduce the distance between the web stiffeners to prevent buckling and its consequent tearing; however, care must be exercised in excessive use of welding (due to the probability of introducing welding defects) in areas that are expected to act in a ductile fashion. On the other hand, the gradual loss of strength and yet energy absorption capability of the specimen No. 4 leads us to the necessity of better understanding of the post buckling behavior of such critical panels through further studies. It is to be noted here that the recommendations concerning the over-strength factor specified in the Seismic Provisions was confirmed quantitatively; that is, the test results were found to be in close agreement with the values of over-strength factors obtained in accordance with the Provisions for four different types of bracing members employed in the test specimens (Maalek, et al., 2011).

- In part III it was demonstrated that laterally well supported double IPE sections acted satisfactorily as the link beam of the EBF specimens tested here. In these specimens, the joints between the top and bottom flange edges of the IPE sections had been welded together uninterruptedly along the length of the link. Hence, there seem to be no difficulties associated with the use of double sections as the link beam of EBFs provided that each single section satisfies the requirements set by the Provisions (AISC, 2005a) and the Specification (AISC, 2005b) concerning compact sections and preferably plastic sections. Hence, designers may use such double sections and benefit from the advantages mentioned in Part III above (Section 4); that is, much more relaxed lateral support requirements, the possibility of the use of available smaller I sections and the reduction of the beam height compared with single web links to provide more clearance. Also, a glance at the hysteretic relations between the shearing force and the link rotation for the test specimens shown in Figures 13a, b, and c indicates the considerable differences between the energy absorption capacities, strengths and initial stiffnesses of the EBF specimens fabricated with the same link beam and bracing sections but with short, medium and long length links.
- Observations made during the Test 1 of the part III experiments and the Tests Nos. 1, 2 & 3 of the series of experiments reported in part II suggest that the seismic behavior of welded gusset plate connection details proposed by many researchers - due to the ease of fabrication and greater fabrication and erection tolerances compared with bolted connections - is a subject matter of concern. This has to be reminded that in a considerable number of EBF buildings constructed during the past 20 years similar welded connection details have been used at the brace to beam connections. With due consideration of the observations made during the tests reported in this work, it has

been found that the seismic behavior of such connections is to be considered as a subject matter that needs particular attention and further investigation. Related observations reported here in this context may be regarded as sufficient warning signs of the potential danger associated with the structures constructed with such details that may need proper seismic retrofit.

- It was shown that full scale testing on the whole EBF specimens could clarify the effects of the end boundary condition of the link and the influence of connection details on the system behavior including the link beam, the bracings and their connections. Apparently, such observations could not be made by mere testing of isolated links. Also, for a more realistic prediction of the most probable behavior of EBFs during devastating earthquakes, the importance of experimental works under well simulated dynamic loading cannot be overemphasized.
- Here, due to limited space, only a description of the main test results and the observed behavior were presented from a conceptual standpoint concentrating on qualitative aspects of the observed behavior. Detailed quantitative results can be provided for interested readers upon request.
- In conclusion, the researches based on which the current seismic provisions have been developed, have addressed many important aspects of the behavior of EBFs to be considered in design practice and hence have attracted so much attention of the structural engineers in an international level and hence have received particular appreciation. However, there are still some, if not many, issues that need further investigations as mentioned above in order to increase the level of reliability in the design and construction of buildings composed of EBFs.

ACKNOWLEDGEMENTS

The experimental work reported here, was a part of a program of research proposed and conducted by the author and approved by the earthquake subcommittee of the National Disaster Mitigation Committee of Iran. The tests were carried out in the heavy structure laboratories of the Building and Housing Research Center. The test specimens were fabricated in Coopal steel construction limited.

REFERENCES

Adib-rad M H (2010). An experimental and theoretical investigation of the hysteretic behavior of eccentrically braced frames, PhD Dissertation, School of Civil Engineering, University of Tehran.

AISC (1992). *Seismic Provisions for Structural Steel Buildings*, American Institute of Steel Construction, Chicago, IL.

AISC (1997a). *Seismic Provisions for Structural Steel Buildings*, American Institute of Steel Construction, Chicago, IL.

AISC (1997b). *Specification for Structural Steel Buildings*, American Institute of Steel Construction, Chicago, IL.

AISC (2000). *Supplement No.2 to the 1997 AISC Seismic Provisions*, American Institute of Steel Construction, Chicago, IL.

AISC (2002). *Seismic Provisions for Structural Steel Buildings*, American Institute of Steel Construction, Chicago, IL.

AISC (2005a), *Seismic Provisions for Structural Steel Buildings*, American Institute of Steel Construction, Chicago, IL.

AISC (2005b). *Specification for Structural Steel Buildings*, American Institute of Steel Construction, Chicago, IL.
Applied Technology Council (1992). Guidelines for seismic testing of components of steel structures, *ATC-24*, Redwood City, CA.
Berman JW, Bruneau M (2007). Experimental and analytical investigation of tubular links for eccentrically braced frames, *Engng. Struct*.; 29(8):1929−1938.
DIN-1025-4 (1994). *Hot Rolled I and H Sections, Dimensions, Mass and Static Parameters.*
Engelhardt MD, Popov EP (1992). Experimental performance of long links in eccentrically braced frames, ASCE, *J. Struct. Engng.*, 118(11):3067−3088.
Engelhardt MD, Popov EP (1989). Behavior of long links in eccentrically braced frames, *Report UCB/EERC-89/0,* Earthquake Engineering Research Center, University of California, Berkeley, CA.
Foutch DA (1989). Seismic behavior of eccentrically braced steel building, ASCE, *J. Struct. Engng.*, 115(8):1857−1876.
Ghaedian D (2002). An experimental investigation of the cyclic behavior of eccentrically braced rrames composed of castellated beams, MSc Thesis, School of Civil Engineering, University of Tehran, Tehran, Iran.
Ghobarah A, Ramadan T (1991). Seismic analysis of links of various lengths in eccentrically braced frames, *Canadian J. Civil Engng*.; 18(1):140−148.
Hjelmstad KD, Popov EP (1984). Characteristics of eccentrically braced frames, ASCE, *J. Struct. Engng.*, 110(2):340−353.
International Conference of Building Officials (1997). Uniform Building Code, Whittier, CA.
Iranian National Building Code (1991). *Design and Construction of Steel Structures*, Part 10, Appendix A, by S. Maalek.
Iranian National Building Code (2008). *Design and Construction of Steel Structures*, Part 10.
Itani AM. Elfass S, Douglas BM (2003). Behavior of built-up shear links under large cyclic displacement. AISC, *Engmg. J*., 40(4):221−234.
Kasai K, Popov EP (1986a). General behavior of WF steel shear link beams, ASCE, *J. Struct. Engng.*, 112(2):362−382.
Kasai K, Popov EP (1986b). Cyclic web buckling control for shear link beams, , ASCE, *J. Struct. Engng*, 112(3):505−523.
Maalek S. & Burdekin, F. M. (1986), "Weld Quality Requirements and Design of Castellated Beams", Technical Report, Department of Civil and Structural Engineering, UMIST, November.
Maalek S (1989). A formex formulation for substructure analysis of open web grids*, Inter. J. Space Structures*, (1):43−64.
Maalek S (1990). Finite element analysis of modular structures and the behaviour of castellated beams, PhD Thesis (UK)/Dissertation (US), UMIST.
Maalek S, Burdekin FM (1991). Weld quality requirements for castellated beams, *The Struct. Engineer*; 69(13):243−254.
Maalek S (1993). A formex approach to substructuring, *Space Structures 4*; Vol. 2, Thomas Telford, London, pp. 1073−1084.
Maalek S (2000a). On the behavior, analysis and design of castellated beams–A state-of-the-art report, *Proceedings*, 5th International Conference on Civil Engineering, Ferdowsi University, pp. 364-377.
Maalek S (2000b) Detailed finite element and experimental stress analysis of castellated beams, *Proceedings*, 5th International Conference on Civil Engineering, Ferdowsi University, pp. 378−388.
Maalek S (2000c). Automated multi-level substructuring, *Proceedings*, 1st National Conference on Space Structures; Tehran University, pp. 20−41.
Maalek S (2002). The analysis of modular structures, *Space Structures 5*; Vol. 2, Thomas Telford, London, pp 1593−1604.
Maalek S, Tafazoli N (2002). The behavior of eccentrically braced frames composed of castellated beams, *Res. Bull. Seismo. Earthq. Engng*., International Institute of Earthquake Engineering & Seismology, 5(2):13−24.
Maalek S; Haddad-Kolur H; Kamyab-Moghaddam K, Pour-Afshari MR (2004). A finite element study of the nonlinear behavior of frames composed of castellated beams, *J. Faculty of Engng*., University of Tehran; 38(2):281−295.
Maalek S, Rajabi H (2006). Cyclic behavior of frames composed of castellated beams, *Proceedings*, 7th International Conference on Civil Engineering, Tarbiat Modarres University, Tehran, Iran.

Maalek S (2006). An investigation of the cyclic behavior of eccentrically braced frames with various link beams, bracing members and connections—An experimental and numerical study, *Research Report St-EBF-09,* Vol. 10, Building and Housing Research Center and National Disaster Mitigation Committee, Tehran, Iran.

Maalek S, Adib-rad MH, Moslehi Y (2011). An experimental investigation of the behavior of EBFs, in press: *Structures and Buildings*, Proceedings of the Institution of Civil Engineers.

Moslehi Y (2005). An experimental investigation of the cyclic behavior of eccentrically braced frames, MSc Thesis, School of Civil Engineering, University of Tehran, Tehran, Iran.

Okazaki T. Engelhardt MD (2007). Cyclic loading behavior of EBF links constructed of ASTM A992 steel, *J. Const. Steel Res*., 63:751−765.

Popov EP. Engelhardt MD (1988). Seismic eccentrically braced frames, *J. Const. Steel Res*., 10:321−354.

TURKISH CATASTROPHE INSURANCE POOL

İsmet Güngör

ABOUT THE TURKISH COMPULSORY INSURANCE POOL

Because of the geologic and topographic structure and climate attributes of Turkey, it is frequently confronted with natural disasters that lead to immense losses of life and property. Natural disasters that affect Turkey can be put in order according to their severity: earthquakes, landslides, water floods, rock sliding, fires, avalanches, storms and underground water movements. Within the past sixty years, when the statistics of the structural damage caused by the natural disasters are taken into consideration, it is observed that 2/3 of these damages occur due to earthquakes. As a result, in Turkey when natural disasters are mentioned, the first thing that comes to mind is earthquakes. When basing the seismic zone maps that are in effect at the present time, 96% of the territories of the country are inside the seismic zones that possess various ratios of risk, and that 98% of the inhabitants are located in these areas. These ratios dramatically reveal the fact that Turkey is an earthquake country.

The effects of the earthquakes in Turkey are not only felt in the disaster originated regions but the whole country, and, therefore, all residents living in the country are affected by the consequences of an obvious and considerable extent. Compensating the material damages, getting back to regular life in seismic zones, alleviating the needs of those who require emergency assistance, etc., incurred expenditures brings an immense financial burden to the national economy and the state. The August 17, 1999, Marmara earthquake is the most recent example, which has been deemed as the disaster of the last century, causing widespread devastation in terms of economic losses and social disruption.

Subsequent to the Marmara earthquake, great numbers of precautions were taken in order to minimize the damages of earthquakes by the public authority. One of the most significant precautions is the execution of the Turkish Compulsory Insurance Pool (TCIP). Within the Marmara Earthquake Emergency Reconstruction Project, the World Bank assisted Turkey in designing an insurance program to be able to manage its own national catastrophic exposure. The project consisted of two main objectives: one was technical assistance to the General Directorate of Insurance in establishing TCIP and ensuring sound management of the pool for the first five years. The second was to provide initial capital through contingent loan facility. The project was the first World Bank project to have components of financial risk management, disaster mitigation, and emergency preparedness.

Immediately after the devastating earthquake, on August 27, 1999, Law No.4452 stated: “Measures to be taken Against Natural Disasters and Authorization in Regards to Arrangements to be done in Overcoming the Damages Caused by Natural Disasters Law” was enacted giving three months of provisional authority to the Council of Ministers to orginise and establish a legal framework against natural disasters. With this power of authority, Decree Law No.587, “Decree Law Relating to Compulsory Earthquake Insurance” entered into force by being published on December 27, 1999, giving birth to the TCIP.

The tariffs and regulations were published on September 8, 2000, and as of September 27. 2000, the TCIP began offering coverage after 9 months of formation process following the decree law. The following year, on March 27, 2001, earthquake insurance became compulsory for dwellings described in the decree law. Currently, 29 accredited insurance companies and their agents are providing Compulsory Earthquake Insurance in the name and on behalf of the TCIP. This newly formed system produced a victorious performance in a short time and has been proposed as a model solution for many countries by the international organizations.

THE PURPOSE OF THE TCIP

Compulsory Earthquake Insurance is a system that was created to ensure the compensation of the material damages on dwellings caused by earthquakes. Following comprehensive research, this system is created with the cooperation of the World Bank, Turkish Government, and the insurance sector. Its fundamental purposes are as follows:

- In order to give insurance protection against the earthquake for all the residences, subject to compulsory earthquake insurance, in return for an affordable premium.
- To provide risk sharing mechanism within the country, at the same time transferring financial burden caused by the earthquake damages to the international reinsurance and capital markets through the insurance system.
- Reducing the state's financial burden caused by the earthquakes
- To use the insurance system as an instrument in increasing the quality of construction of houses.
- Ensuring long-term fund accumulation for compensation of earthquake damages.
- To contribute to the development of insurance awareness in the society.

With the application of the Compulsory Earthquake Insurance, without relying on the budgetary means of the government, a concrete protection is provided by immediately compensating the material losses in residences. Until sufficient internal sources are accumulated, a significant portion of the risk is transferred to the international markets through re-insurance schemes. Because the financial burden incurred on the national budget as a result of earthquakes is reduced, potential additional taxes are prevented.

STRUCTURE OF THE TCIP

The fundamental structure of TCIP is based on the public-private partnership initiation (see below):

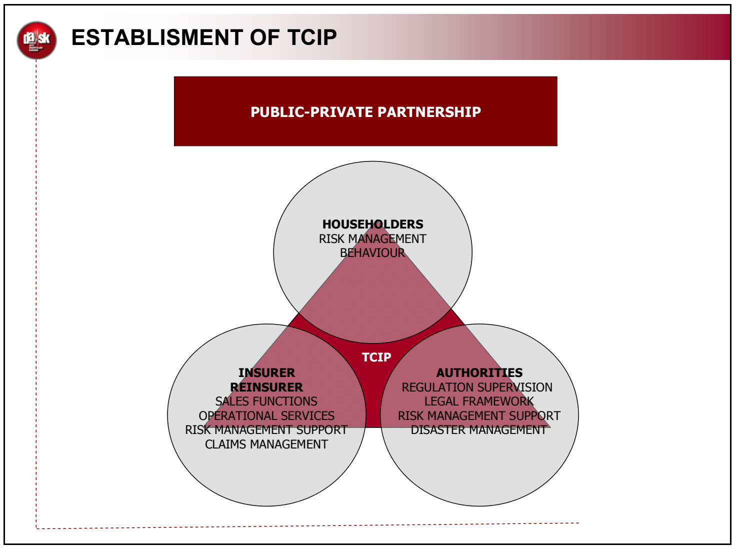

Board of Directors

The TCIP is administered by the "Turkish Catastrophe Insurance Pool Board of Directors," which consists of 7 members. The Board Of Directors comprise the representatives of; Prime Ministry, Under secretariat of the Treasury, Ministry of Public Works and Settlement, The Association of the Insurance and Reinsurance Companies of Turkey, Middle East Technical University, Capital Markets Board of Turkey, and General Manager of Eureko Insurance Company (Pool Management Company) . Four members of the Board of Directors are high-level public officials who are experts in different subject matters; two of the members are private sector representatives and one of them is a university representative. Formation of the Board of Directors and representation of all concerned parties are significant in order to successfully conduct the Compulsory Earthquake Insurance Program.

Pool Management Company

The government decided to outsource all operational tasks to private insurers. The decision necessitated engagement of a manager to handle all technical tasks in the TCIP's daily operations. The government appointed Milli Re as the Pool Management Company for five years until 2005. From 2005, these tasks have been moved to responsibility of the Eureko Insurance Company in the capacity of Manager of Pool until year 2015. See below: Operational Structure of TCIP.

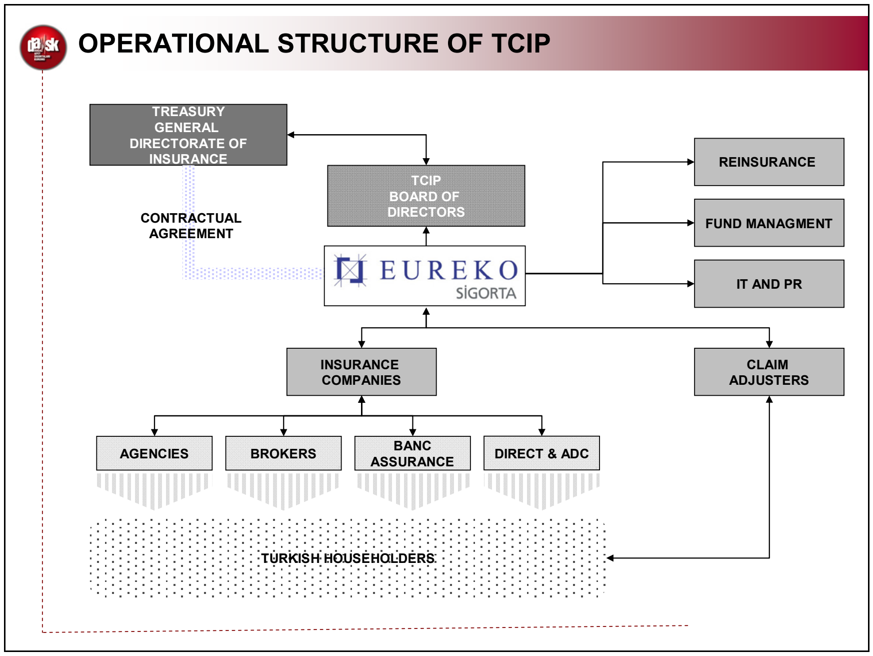

IT Infrastructure

The TCIP's IT system enables real-time on line policy production, premium booking, claim management, and reporting. Presently, 23,500 (including bank branches) agents throughout Turkey are able to reach through Web access to the central database and application software provided by TCIP. However, those insurance companies with high technical capacity may incorporate policy production unit into their main application by using real-time data, thereby transferring that function of the TCIP system. See below IT structure of TCIP.

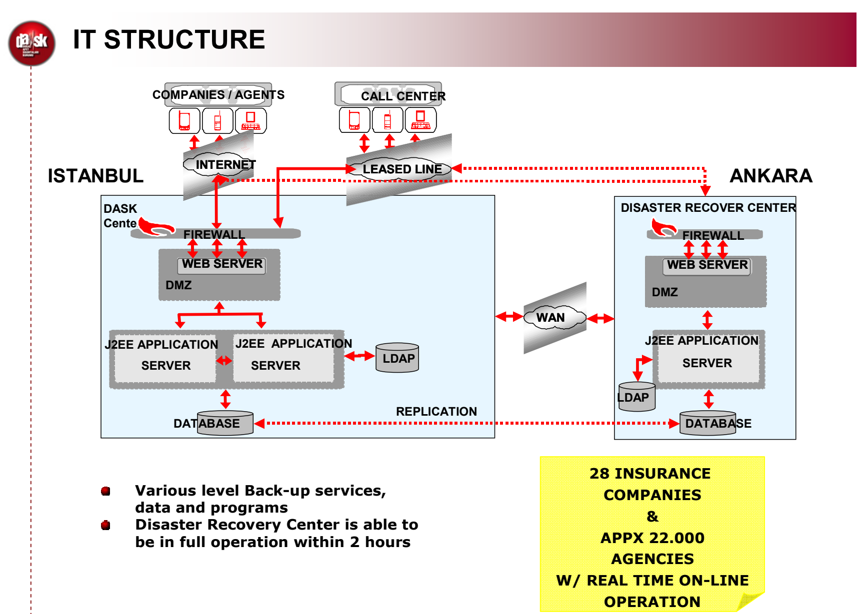

DETAILS OF COMPULSORY EARTHQUAKE INSURANCE

Insurable Property

Compulsory Earthquake Insurance constitutes a system of insurance that is in general in meaning, intended for dwellings that remain inside the boundaries of the municipality. Buildings and dwellings subject to compulsory earthquake insurance are as follows:

- Buildings constructed as dwellings on lands subject to private ownership and have registered title deeds.
- Independent sections within the context of the Condominium Law No: 634.
- Independent sections situated inside residential buildings but used as small business establishments, bureaus, and similar purposes.
- By reason of natural disasters, properties built by the government or built by housing credit.

Uninsurable Property

Properties that fall outside the Compulsory Earthquake Insurance are as follows:

- Dwellings belonging to public body and institutions.
- Dwellings built in residential areas of villages.
- Dwellings entirely used for commercial and industrial purposes (block of offices, business centers, administrative service buildings, training center buildings etc.).
- Dwellings that are still under construction.
- Independent units and dwellings that were built after December 27, 1999, without any construction permit granted within the framework of the legislation.

Compulsory insurance for the dwellings built in residential areas of villages is not anticipated because currently there is not a municipal inspections and building inspection system, and because who live in these areas are anticipated to have a low level of income. However, if they wish, homeowners who reside in these areas may obtain earthquake insurance from insurance companies in the market. Owners of commercial and public buildings are not required to buy earthquake insurance, but they can voluntarily purchase it from private insurance companies.

Scope of Coverage

With the Compulsory Earthquake Insurance;

- earthquakes
- fires as a result of earthquakes
- explosions as a result of earthquakes
- landslides as a result of earthquakes

Material damages to the insured buildings are covered up to the sum insured by the TCIP, including foundations, main walls, common walls separating independent sections, ceilings and bases, stairs, platforms, halls, roofs, and chimneys.

Exclusions

- Removal of debris expenses
- Loss of profit
- Loss of income
- Loss of rent
- Alternative residence and work place expenses
- Financial liabilities and all other similar indirect damages brought forward
- All sorts of movable goods, furnishings and other items
- All personal injury including death
- Claims of damages for pain and suffering

Maximum Sum Insured

The intent of the Compulsory Earthquake Insurance is to have a standard coverage with a minimal premium. Consequently, the TCIP grants cover in specified maximum sum insured determined by using unit cost of building construction. As of January 1, 2011, maximum sum insured amount granted by TCIP policies in all structure types is determined as 150.000 Turkish Lira. The sum insured is determined according to the magnitude and structure type; it cannot exceed the maximum sum insured amount of the dwellings. If the value of the dwelling exceeds the sum insured amount given by TCIP, the insured optionally can get additional cover for the exceeding amount from the insurance companies.

Tariff Rates and Premiums

The TCIP's premium tariff is determined by the Treasury Under secretariat and 3 factors determine the insurance premium amount:

- Location of the building according to earthquake risk zones
- Construction type of the building
- Gross square area of the dwelling

Descriptions of the structure styles that are indicated in the tariff are as follows:

> A—Steel, Reinforced Concrete Frame Structures: These structures are made up of steel or reinforced concrete bearing frames.
>
> B—Masonry Stone Structures: These are structures that do not have frames, bearing walls made by rubble stones, hewn stone, brick or filled, unfilled concrete briquette, and floorings, stairs and ceilings made up of concrete or reinforced concrete.

C—Other Structures: Structures that do not enter into the above mentioned groups.

There are 15 tariff rates determined according to 5 risk zones and 3 different construction types. See below pricing Table of TCIP

PRICING TABLE					
REGION BASED RATES ACCORDING TO CONSTRUCTION TYPE (‰)	**ZONE 1**	**ZONE 2**	**ZONE 3**	**ZONE 4**	**ZONE 5**
A- Steel, Reinforced Concrete Frame Structures	2.20	1.55	0.83	0.55	0.44
B- Masonry Stone Structures	3.85	2.75	1.43	0.60	0.50
C- Other Structures	5.50	3.53	1.76	0.78	0.58

Allocation of the risk zones is based on the "Turkey Seismic Zones Map" (see below) which is prepared by the Ministry of Public Works and Settlement.

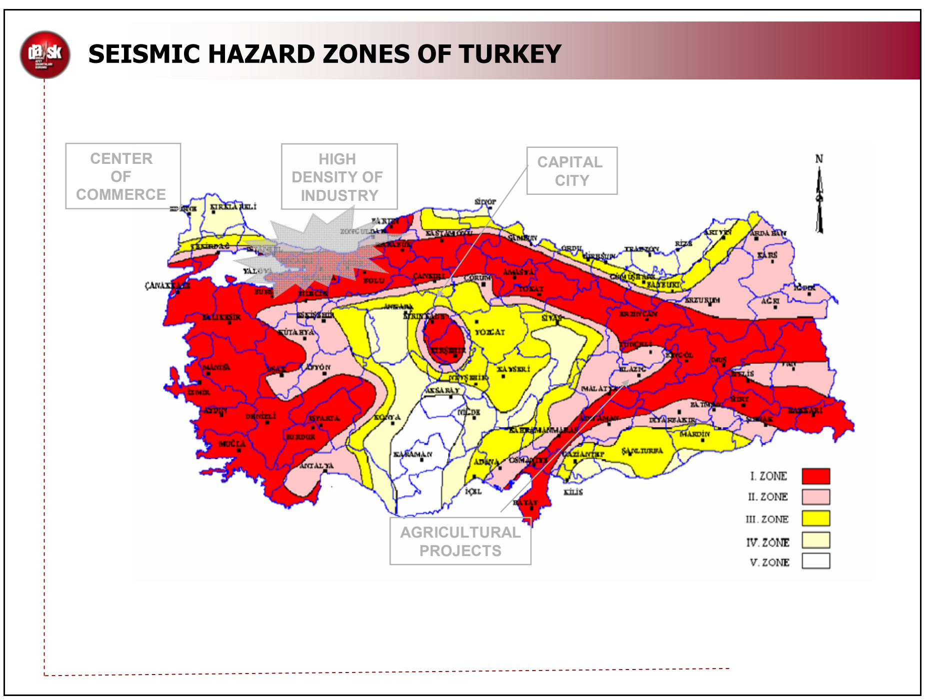

The policy sum insured is obtained by multiplying the unit square meter costs with the gross square meter area of the dwelling.

As of January 2, 2011, the unit square meter costs which are settled according to the structure type and used in calculation of the insurance compensation are as follows:

A- Steel, Reinforced Concrete Frame Structures: 590 TL
B- Masonry Stone Structures: 425 TL
C- Other Structures: 220 TL
(Maximum sum insured for all construction type is determined as 150 thousand TL.)

The above indicated gross square meter values that are used as base in calculation of the insurance compensation, determined annually according to changes in the ratios of the "Building Construction Cost Index," statements made by the State Institute of Statistics and announced in the Official Gazette. Base policy premium is obtained by multiplying the sum insured with the tariff rate. Hence, there is a fix premium amount to be added to this base policy premium in order to reach final policy premium. Fix premium for risks in Istanbul is 15 TL and 10 TL for risks in other cities.

- Premium Amounts According to the Risk Zones and Construction Types (for Istanbul). See below, Unit Construction Cost for Sum Insured.

UNIT CONSTRUCTION COST FOR SUM INSURED				
FOR ISTANBUL PREMIUM AMOUNT FOR 100 SQUARE METER RESIDENCE (TL)				
CONSTRUCTION TYPE	SUM INSURED	RISK ZONES AND PREMIUM (TL)		
		I	II	III
Steel, R.C.	(100 m² x 590 TL) 59.000	145	106	64
Masonry Stone	(100 m² x 425 TL) 42.500	179	132	76
Others	(100 m² x 220 TL) 22.000	136	93	54

- Premium Amounts According to the Risk Zones and Construction Types (Outside of Istanbul)

UNIT CONSTRUCTION COST FOR SUM INSURED						
OTHER CITIES PREMIUM AMOUNT FOR 100 SQUARE METER RESIDENCE (TL)						
CONSTRUCTION TYPE	SUM INSURED	RISK ZONES AND PREMIUM (TL)				
		I	II	III	IV	V
Steel, R.C.	(100 m² x 590 TL) 59.000	140	101	59	42	36
Masonry Stn	(100 m² x 425 TL) 42.500	174	127	71	36	31
Others	(100 m² x 220 TL) 22.000	131	88	49	27	25

As per the Property Law, no. 634, apartment blocks and building complexes (housing estates) have been entitled for a 20% discount over the designated tariff rates for group insurance that are arranged by administrators and consist of minimum eight independent sections and policies renewed within 30 days upon expiry thereof will be entitled to a further discount of 20% over designated tariff rates. Minimum premium on a TCIP policy is 25 TL.

Essential Information and Documents for Insurance Policy

Essential information is as follows:

- Name, address, telephone number and mobile phone number of the insured
- Tax ID number and Turkish Republic ID number of the insured
- Full address of the residence that is to be insured
- Title deed information (block, plot, parcel, page number) (dwelling title deed or land title deed)
- Construction year of the building (1975 and before, between 1976–1996, between 1997–1999, 2000 and after)
- The construction type of the building (Steel, Reinforced Concrete Frame Structures, Masonry Stone Structures, others)
- Total number of floors in the building
- The damage condition of the building (free of damage, slightly damaged, moderately damaged)
- Gross square meter (m2) of the dwelling (apartment)
- Type of usage of the dwelling (apartment) (residential home, business establishment, office and others)

Distribution Channels

Compulsory Earthquake Insurance policies are arranged through the accredited insurance companies, and agents belonging to these companies in the name and on behalf of the TCIP. Currently 29 accredited insurance companies and their agents are providing Compulsory Earthquake Insurance in the name and on behalf of TCIP. The TCIP has contractual agreement with the insurance companies. Insurance companies are obliged to pay the sum of monthly premium production to TCIP at the beginning of the following month.

LOSS AND CLAIM PAYMENT

Notice of Claims

The citizens whose homes are damaged as a result of an earthquake and those who have Compulsory Earthquake Insurance policy should consult one of the indicated options as soon as possible:

- TCIP Call Center
- Website of TCIP
- An insurance company or agent who issued the Compulsory Earthquake Insurance policy on behalf of TCIP

Required Documents for Notice of Claims

In case of damage the documents and information to be forwarded to the TCIP:

- Notice of Claim Information

- Photocopy of the policy
- Photocopy of the title deed
- Full address of the damaged location in order for the expert to find the damaged location easily and to assess the damage
- Telephone number or cell phone number to get in touch with the insured

Assessment of Loss and Claim Payments

Loss adjustment is one of the most critical issues in the whole operation of the TCIP system. Accuracy, speed, and homogeneity in calculation of loss increase the public confidence. The basic task of a TCIP loss adjuster is to determine the cost of damage. The TCIP retains loss adjusters already employed in the property insurance industry. The TCIP launches training program for individuals who possess professional civil engineering knowledge.

The TCIP is a first loss policy and the loss amount is determined on new construction value and there is a deductible of 2% of sum insured value. In claim adjustment, new construction cost of the building according to actual market price prevailing at the time and location of the earthquake is taken into account.

Notice of claims taken directly or through the accredited insurance companies is evaluated by the TCIP, who then opens claim files and employs claim adjuster. After the assessment of claim, claim payments are made as soon as possible usually within one month and in case of further assessment of damages advance payments are made to the insured.

REINSURANCE

Risk charge depends primarily on the probable maximum loss (PML), In the case of the TCIP, the PML is defined as the largest likely loss to insured dwellings from an earthquake with a 200-year return period.

STATISTICS ABOUT THE PORTFOLIO OF TCIP

Basic Figures

- Total No. of Policies 3.349.677
- Total Annual Premium 149.860.000 €
- Avg. Sum Insurance 27.700 €
- Avg. Premium 45 €
- Total number of Paid Claim Files 11.114
- Total Claims Paid (from 2000) 9.650.000 €

For further information and statistics please visit: ***www.tcip.gov.tr***

ACTIVE-SOURCE SURFACE WAVE DISPERSION METHODS FOR EARTHQUAKE SITE-RESPONSE AND LIQUEFACTION ASSESSMENT

Robert Kayen

U.S. Geological Survey, Menlo Park, CA, USA, and University of California, Los Angeles, CA USA

ABSTRACT

Geotechnical engineering methods develop through comparison of field-response and sub-surface geotechnical properties with advances in numerical and theoretical modeling. Recent advances in non-invasive sub-surface quantitative stiffness characterization allow us to rapidly and inexpensively map these spatial and physical properties for urban ground notion site response studies. In this paper, new technologies used at the U.S. Geological Survey (USGS) and the University of California, Los Angeles (UCLA) employ surface wave methods to characterize soil stiffness. The power of the active-source surface wave methods are their ability to non-invasively and rapidly characterize the stiffness of the ground; to be relatively portable, lightweight, and efficient in deployment; and to accurately profile earth materials including difficult materials such as gravely deposits, rock, and stiff soils where conventional invasive methods are not possible or practical. The two active-source spectral analysis of surface waves (SASW) systems used on our projects are a small-to-large parallel array of harmonic-wave shakers that serve as a signal source; and a seafloor harmonic-wave source system. Active source surface methods allow us to directly relate ground-motion site-response and liquefaction potential with the shear wave velocity properties of the ground.

INTRODUCTION

In this paper, two active-source surface wave systems, onshore and offshore, are described that are used to model the dispersion of surface waves, and these in-turn allow for modeling of the shear wave velocity structure of the underlying ground for site response and soil liquefaction studies. The two active source surface wave systems described are based on the same continuous harmonic wave test using computer-controlled electro-mechanical vibrators [Kayen et al. 2005; 2009]. Onshore, a trailer-mounted parallel array of shakers is used for profiling shallow V_{s30} site response and potential ground failure measurements, and deeper profiles to several hundred meters depth for V_{s100}-V_{s200} measurement. For urban micro-zonation studies, the onshore system can be easily transported to the field in portable, deployable modular units. A second seafloor system is designed for profiling sediment in sub-aqueous settings to water depths of 100 and sub-seafloor depths of up to 30 m.

Spectral Analysis of Surface Waves (SASW)

Spectral Analysis of Surface Waves (SASW) is an efficient method for non-invasive investigation of soil properties that is strongly linked to earthquake engineering analysis of stiffness and its effect on site response and liquefaction potential. Our surface wave test systems are based on a computer-controlled electromechanical vibrator source manufactured by CLD Dynamics. The test is performed along linear arrays where the harmonic wave-source is placed at the end of the array line. A harmonic wave signal from a sine-function generator is sent to the shaker, after being boosted from a milliWatt level to end-to-end 50

Volts range and 20 Amps current by an amplifier. The electro-motor on the shaker drives reaction weights that are suspended on silicon bands and causes them to slide up and down, producing gentle harmonic-surface wave. In the SASW test, vertical seismometer receivers are used to pick up the waveform of the surface waves. As the test progresses through a suite of stepped frequencies, each signal is analyzed using the Fast Fourier Transform (FFT) to compute linear spectra, cross power spectra, phase lag (wrapped or unwrapped phase), and frequency response. This allows for the calculation of phase lag across the frequency range for any pair of seismometers [Nazarian and Stokoe 1984]. The harmonic wave vibrator is used to sweep through a range of low frequencies, typically 2-100Hz, to capture the surface wave dispersion characteristics of the ground. The ability to perform near real-time frequency domain calculations and monitor the progress and quality of the test allows us to adjust various aspects of the test to optimize the capture of the phase data. These aspects include the source-wave generation, frequency step-size between each sine-wave burst, number of cycles-per-frequency, total frequency range of all the steps, and receiver spacing.

The test apparatus consist of 1-Hz seismometers, a low frequency spectrum analyzer/signal generator, and one or more computer-controlled electro-mechanical shakers and amplifiers (Figure 1). The 1-Hz Kinemetrics receivers we normally use are designed for capturing low frequency vertical motions. The shaker(s) are arrayed at the end of an SASW test line of seismometers. Spacing between the receivers, and the first receiver and source, are stepped geometrically from 1 m to 128 m. Each pair of two seismometers, separated by distance, δ, and the source is usually placed at a distance of d from the inner seismometer. Rayleigh wavelengths (λ) are computed by relating the seismometer spacing (δ) and the phase angle (θ, in radians determined from the peak of the cross-power spectrum) between the seismometers:

$$\lambda = 2\pi\delta/\theta \tag{1}$$

The surface wave velocity, V_r, is the product of the frequency and its associated frequency dependent wavelength:

$$V_r = f\lambda \tag{2}$$

Computing the averaged grouped dispersion curve for a site requires that we collect a suite of individual dispersion data sets for specific array geometries. Regardless of the array dimensions, we compute phase velocities for phase angles between 120° and 1080°, corresponding to wavelengths of 3d and d/3 respectively. If the data are not optimal, the range is narrowed to 180° and 720°, or 2d and d/2. For example, if the array separation was 3 m, velocities are inverted for Rayleigh wavelengths of 1 to 9 m under ideal conditions, or 1.5 to 6 m of the site is difficult to test. Longer wavelengths sound more deeply in the ground and are extend the overall profile to greater depths. These long wavelength data are associated with low frequencies and large array separations. The array is lengthened between tests, and a group of individual dispersion curves are captured to cover the target range of wavelengths. The averaged grouped dispersion curve is calculated from these profiles and is the basis for inverting the velocity structure of the ground. Dispersion curves are the surface wave velocities calculated using Equation 2, plotted against frequency or wavelength.

An inversion method is used to estimate the soil stiffness by comparing a theoretical-dispersion curve with the experimental dispersion data collected in the field. That is, we invert a shear wave velocity profile that provides the best-fit between the shear wave velocity dependent theoretical and averaged field dispersion curve. The term “best-fit” means the least squares of the residuals from the differences between the theoretical and experimental dispersion curves. Several inversion algorithms are used to compute theoretical shear wave velocity profiles.

Figure 1 Electromechanical shakers act as a source. Sensors, on the right, are arrayed in lines to collect dispersion data (Patras December 2010).

Large Parallel Arrayed-Source for Harmonic Wave SASW

The SASW test is ultimately limited by the inability of the signal of the lowest frequency waves to reach the outermost sensor. To address this problem, some practitioners will try to use larger energy source in the form of construction equipment, a large drop weight, or a large vibration source. The USGS uses a novel approach to this problem by building a large parallel array of in-phase sources on a trailer to increase the dynamic force on the ground. On a trailer, we array up to 8 individual units that receive a simultaneous waveform signal from the spectrum analyzer (Figure 2). The advantage of this approach is that the system is considerably more portable than units based on a single large static mass or large hydraulic vibrator. The electromechanical shaker can vibrate consistently at frequencies as low as 1 Hz, difficult for large mass systems. With a modular system, a single vibration source is adequate until the test progresses to low frequencies and large array separations (Figure 3). At that point, additional vibrators are turned on to provide a strong signal to the receivers.

To transport the parallel shaker array to the field, we use a large trailer that houses the eight vibrator source units, amplifiers, generators, and the receiver cables. A hydraulic unit lifts the trailer off its suspension similar to a CPT truck so that a rigid contact is made with the ground. The total static weight of the trailer, generators, and amplifiers load the contact with the ground, and this improves the signal transmission from the shakers into the soil. The large parallel array of harmonic vibrators can be used to collect surface wave wavelengths of several hundred meters and routinely allows for the inversion of shear wave velocity to depths in excess of one hundred meters.

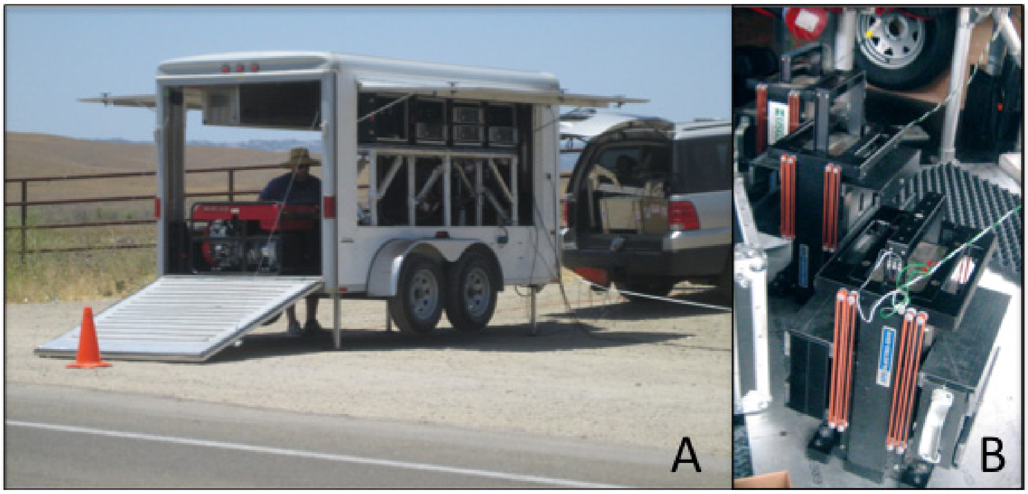

Figure 2 **Large parallel arrayed sources are mounted to the floor of the Velociraptor trailer. (A) Hydraulic legs lift the trailer off the suspension. (B) Shakers are arrayed in a chevron pattern in the trailer floor.**

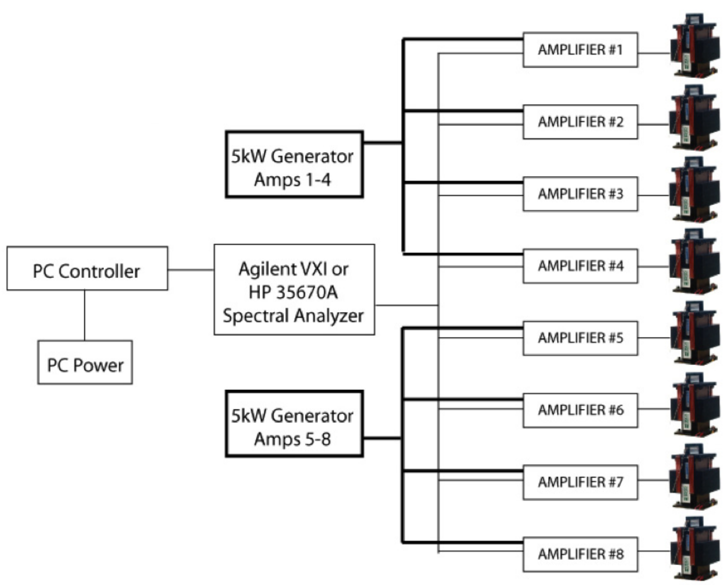

Figure 3 **Schematic of large parallel array harmonic wave sources for SASW testing. Arrays of 6-8 shakers are transported to a site by a trailer with generators, receivers, and amplifiers pre-wired to improve testing efficiency.**

Seafloor SAIW

Earthquake effects are often most extreme in the sub-aqueous environment of ports, harbors and open waters where saturation is 100% and extremely soft sediment are deposited. These sediments are often overlain with critical transportation infrastructure and transmission lifelines, including pipelines, sewer outfalls, airports, bridges, causeways, marine container facilities and fishing ports. Accumulations of seafloor sediment can result in very low SV velocity and long natural periods, and these motions can be extremely damaging to large long-period engineering structures. The USGS has developed a new system for gathering the dispersive characteristics of Scholte interface-waves that propagate along the seafloor-seawater interface. The field acquisition system is based on the same electromechanical vibrator that is used in the large parallel-array source spectral analysis of interface waves (SAIW) test, described above.

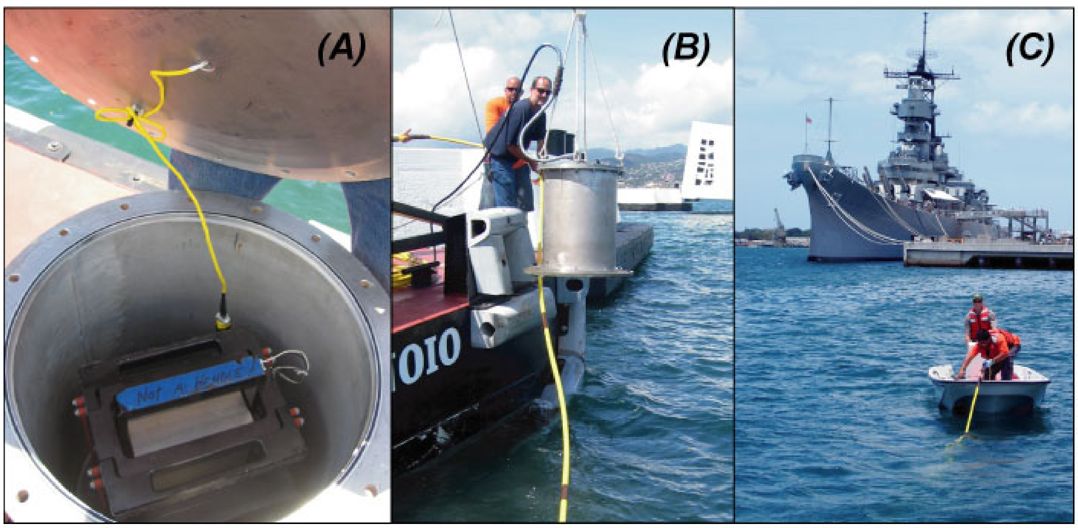

Figure 4 Deployment of the seafloor SASW system at the USS Arizona Memorial: (A) a single harmonic wave vibration source is sealed in a gasket-lined aluminum pressure vessel and (B) deployed over the side of a research platform. The multi-channel streamer cable is (B) Yale-gripped to the vibration source and (C) straightened into a linear array using a launch. The streamer is weighted to sink into the seafloor sediment.

The three unique components of the seafloor SAIW apparatus are a large cylindrical containment vessel for the harmonic-vibrator, the use of a lead-weighted 36-channel geophone streamer cable for the receivers, and a 300 m conductor cable for powering the shaker and acquiring the transmitted waveforms (Figure 4). The pressure vessel is made of a 24 in.- (79-cm) inner -diameter, 0.5 in.- (1.27-cm) thick aluminum cylindrical section with a base plate welded to the bottom and a gasketed aluminum cover plate. The power supply is delivered to the vibrator through a marine cable-connect mounted on the cover plate. The other end of the power cable is connected to the shaker-amplifier unit. A weighted geophone cable with 36 individual 4-Hz receivers is placed on the seafloor. Channels 1−24 are spaced 1 m apart and the remaining channels 25-36 are spaced 2 m apart, for a total array separation length of 48 m. The test can be run in multichannel analysis of interface waves (MAIW-mode), gathering all the channels simultaneously, or 2 or 4 channel SAIW-mode. To run the test in MAIW or SAIW-mode, we built a custom multichannel streamer breakout-box to collect data for different seismometer (Figure 5).

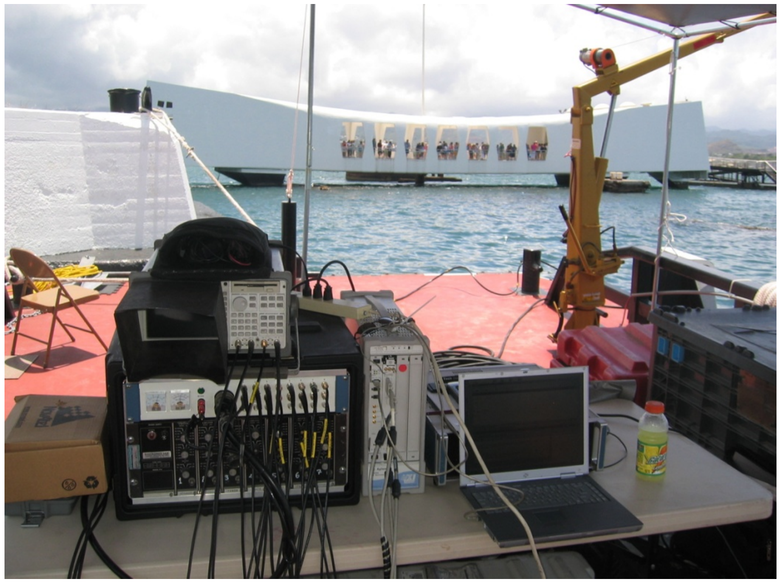

Figure 5 Data acquisition unit for the seafloor MAIW/SAIW system includes an Agilent VXI digital recorder for MAIW; custom breakout box for the multichannel streamer; channel amplifier box; and a 4 channel spectral analyzer for SAIW.

The seafloor system is designed for continental shelf water depths of 100 m or less. To account for currents and drift of an anchored deployment vessel, the conducting cable has 300 m of scope. The long conducting cable requires that the signal from the receivers is amplified, and this is accomplished with an in-line amplification unit. The maximum design hydrostatic pressure that can load the pressure vessel without causing leakage is 100 m. In order to reach deeper depths, a thicker walled cylinder or a non-conducting oil filled chamber would be needed.

Inversion Procedure

The inversion procedures used to estimate the soil-stiffness compute theoretical-dispersion curves that are best-fit with the experimental dispersion data collected in the field. The term "best-fit" refers to the minimum sum of the squares of residuals from the differences between the theoretical and experimental dispersion curves (Figure 6). Inversion of soil stiffness is concerned with the estimation of shear and compression wave velocities, Poisson ratio, density, and appropriate layering parameters based on a set of field observations. This is possible because we can calculate the forward problem that relates the model parameters to the measurements. The surface wave inversion problem is an "ill-posed" inverse problem meaning that solutions are non-unique and can be unstable. Suites of methods have been proposed for solving ill-posed inversions - termed regularization methods [Lai and Rix 1998; Hayashi and Kayen 2003; Zhdanov 2002].

The stiffness model parameters are chosen that minimize the difference between the observations and the output of the forward problem, a procedure termed optimization. It is important that the stiffness model parameters in the final model fit the observed data and are physically realistic, as solutions can reach an acceptable least squares solution minimization of error and still be unrealistic. Examples of this include models with shear wave velocity oscillations that indicate instability, are not consistent with other observations of the site (Figure 7).

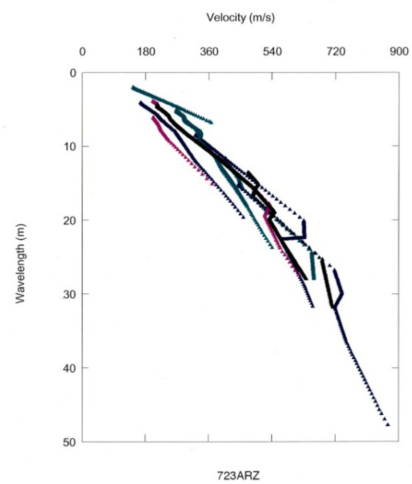

Figure 6 Example of grouped experimental dispersion curves from one site beneath the bow of the USS Arizona, Pearl Harbor, HI.

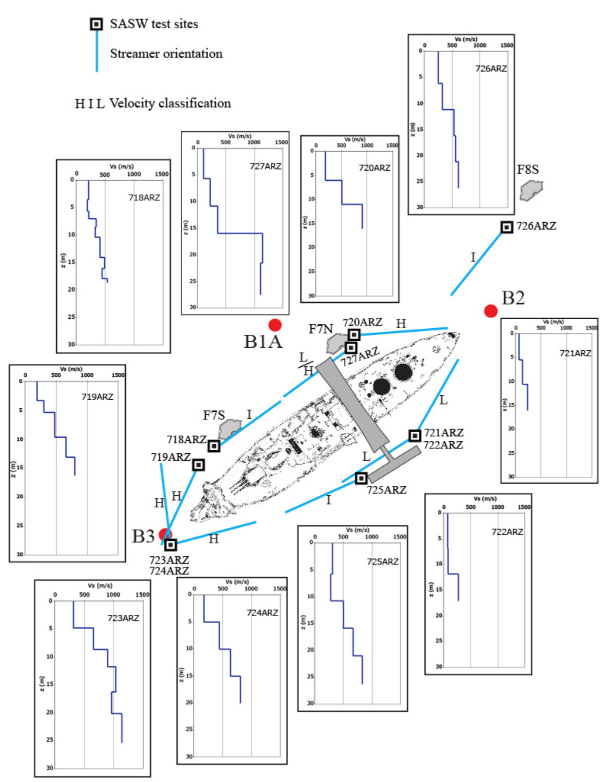

Figure 7 Example of shear wave velocity profile data from the seafloor test system measured along the perimeter of the USS Arizona Memorial, Pearl Harbor, HI.

CONCLUSIONS

This paper describes methods used at the USGS to characterize sub-surface stiffness properties of the ground using large parallel arrays of shakers as a source for SASW, and seafloor spectral analysis of Scholte interface waves SAIW). These new technologies are transportable to sites for sub-aerial and subaqueous site investigation. The test systems described here are all based on the same electro-mechanical harmonic wave shaker. For onshore profiling to 100 m depth we array multiple shakers in parallel-array configuration multiple shakers. A trailer at the USGS is designed to array up to 8 sources in a large parallel circuit that can profile the stiffness properties of the ground to typically 100–200 m. A parallel circuit is used to generate in-phase harmonic waves among the large array of shakers that together can generate a dynamic force of 1600 lb.

The most difficult soil environments to profile properties for geotechnical earthquake engineering and other studies are sub-aqueous. A system we developed at the USGS is designed to profile in water depths up to 100 m. The elements of this system are a 36 multi-channel omni-directional geophone cable, a custom pressure vessel for one harmonic shaker, and a 300-m conductor power cable. This system is useful for shallow sub-30 m profiling of the sediment.

REFERENCES

Hayashi K, Kayen R (2003). Comparative test of three surface wave methods at Williams Street Park in San Jose, USA, Joint Meeting of Japan Earth and Planetary Science, University of Tokyo, Tokyo, Japan 2003 Joint Meeting, *Paper S051-009, 2003*.

Kayen R (2005). The spectral analysis of surface waves measured at William Street Park, San Jose, California, using swept-sine harmonic waves, in: Asten and Boore, eds., Blind comparisons of shear-wave velocities at closely-spaced sites in San Jose, California, *US Geological Survey Open-File Report 2005–1169*, 6 pgs., [http://pubs.usgs.gov/of/2005/1169/].

Kayen R, Scasserra G, Stewart JP, Lanzo G (2008, revised 2009). Shear wave structure of Umbria and Marche, Italy, strong motion seismometer sites affected by the 1997-98 Umbria-Marche, Italy, earthquake sequence, *U.S. Geological Survey Open-File Report 2008–1010*, v. 1.1, 51 pgs., [http://pubs.usgs.gov/of/2008/1010/].

Lai CG, Rix GJ (1998). Simultaneous inversion of Rayleigh phase velocity and attenuation for near-surface site characterization, *Report No. GIT-CEE/GEO-98-2*, Georgia Institute of Technology, School of Civil and Environmental Engineering, 258 pgs.

Nazarian S, Stokoe KH (1984). In situ shear wave velocities from spectral analysis of surface waves, *Proceedings*, 8th World Conference on Earthquake Engineering, 3:31–38, Prentice-Hall, Englewood Cliffs, NJ

Zhdanov MS (2002). Geophysical inverse theory and regularization problems, Methods in Geochemistry and Geophysics, Vol. 36, first ed., Elsevier Science.

PREPARING ISTANBUL FOR FUTURE DISASTERS: ISTANBUL SEISMIC RISK MITIGATION AND EMERGENCY PREPAREDNESS PROJECT (ISMEP)

Fikret Azili[1]

Istanbul Governorship Special Provincial Administration, Istanbul Project Coordination Unit, Istanbul, Turkey, fazili@ipkb.gov.tr

ABSTRACT

Throughout its history Turkey has experienced frequent natural disasters, which have resulted in unacceptable loss of life, injuries and property damages. Earthquakes, floods, landslides, rock falls, drought, and snow avalanches are leading natural hazards. As for Istanbul, the biggest metropolis of Turkey, with the distinction of being the center of culture, economy and industry; on the other hand, because of its seismic-prone location nearby the North Anatolian Fault, it has a high earthquake risk.

The Istanbul Seismic Risk Mitigation and Emergency Preparedness Project (ISMEP) is a significant attempt to implement essential principles of comprehensive disaster management financed by the World Bank, European Investment Bank and Council of Europe Development Bank. The main objectives are to improve the city of Istanbul's preparedness for a potential earthquake through enhancing the institutional and technical capacity for disaster management and emergency response, strengthening critical public facilities for earthquake resistance, and supporting measures for better enforcement of building codes and land use plans.

INTRODUCTION

Because of its geological structure, topography and climate conditions, Turkey always faces different types of natural hazards. Throughout its history Turkey has experienced frequent natural disasters, which have resulted in unacceptable loss of life, injuries and property damages. The importance of natural disaster hazards and risks again have been come to the fore in Turkey with the August 17, 1999 İzmit Bay earthquake (magnitude 7.4) and November 12, 1999 Duzce earthquakes (magnitude 7.2).

After Marmara Earthquakes experience, beside recovery and response studies, mitigation and preparedness studies approach is also adopted in disaster management. Beside many actions taken in Turkey, for disaster preparedness, implementation and development of scientific research projects which could set an example worldwide are being carried out in Istanbul. As the first risk reduction project implemented in Turkey, Istanbul Seismic Risk Mitigation and Emergency Preparedness Project (ISMEP) is the most important of them.

In this framework, "Istanbul Seismic Risk Mitigation and Emergency Preparedness Project" (ISMEP) is an important step forward to improve the city of Istanbul's preparedness for a potential earthquake and to reduce disaster-related impacts. Within this project, the main focus lies on the implementation of preventive and supporting measures on preparedness, mitigation, response and recovery activities covering pre-disaster, disaster, and post-disaster periods.

The Government of Turkey (GOT) and International Bank of Reconstruction and Development (IBRD) agreed upon a loan (€ 310 Million) on September 18, 2005, to implement and finance the “Istanbul Seismic Risk Mitigation and Emergency Preparedness Project” (ISMEP). The Project started on February 3rd, 2006 and is implemented by the Istanbul Project Coordination Unit established under the Istanbul Special Provincial Administration. On March 12, 2008, the Republic of Turkey and the European Investment Bank (€ 300 Million), and then on September 16, 2010, the Council of Europe Development Bank signed a loan agreement (€ 250 Million) to support the ISMEP activities. Consequently the ISMEP budget reached to € 860 Million.

The project aims to enhance the institutional and technical capacity of the emergency management related institutions; raise public awareness in emergency preparedness and response, feasibility studies of the priority public buildings against seismic risks and as to assessment reports the retrofitting or reconstruction of these buildings; support to the national disaster activities; inventory of cultural heritage buildings, carry out seismic risk assessment of selected cultural heritage buildings, prepare retrofitting project designs; and to take supportive measures for effective building code enforcement to prepare Istanbul for a potential earthquake.

The project consists of the following components and activities:

- **Component A:** “Enhancing Emergency Preparedness” aims to enhance the effectiveness and capacity of the provincial and municipal public safety organizations in Istanbul to prepare for, respond to and recover from significant emergencies, especially those arising from earthquakes
- **Component B,** “Seismic Risk Mitigation for Priority Public Buildings” covers risk mitigation activities on priority public buildings and some of the buildings under cultural and historical heritage.
- **Component C,** “Building Code Enforcement” aims to improve technical and professional capacity of pilot municipalities (Bağcılar and Pendik) for streamlining building permit issuance procedures and cover public awareness activities on urban planning and construction for disaster mitigation and preparedness which are designed and implemented for three target groups (local decision makers, technical staff and community representatives).

PROJECT ACTIVITIES

Under Component A of the ISMEP, enhancement of disaster and emergency communication systems (Subcomponent A1), design and deployment of emergency management information systems (Subcomponent A2), enhancement of operational capability of the Governor’s Provincial Disaster Management Center (DMC-ADM) (Subcomponent A3), enhancement of emergency response capacity of the first responder institutions (Istanbul Search and Rescue Unit (ISARU), Istanbul Health Directorate (IHD), Istanbul Police Department (IPD), Turkish Red Crescent, etc.) (Subcomponent A4) and public awareness/training studies (Subcomponent A5) are being carried out.

Under A1 subcomponent, the current analogue radio communication infrastructure of the public institutions have been enhanced by the procurement of analogue area relays, mobile relays, multimode digital radios, relays and peripheral communication devices, communication switches, HF/SSB Radios and communication vehicles. By extending and investing the current security video network of the IPD, Istanbul DMC has gained the capability to monitor the video streams of the IPD network spread all over Istanbul city.

Under A2 subcomponent, Istanbul Disaster Management System software has been developed and deployed to Istanbul DMC. The system aims to gather information from all the public institutions that may be needed for collaboration and command control during a disaster or emergency situation.

Under A3 subcomponent, dedicated to “Enhancing the institutional capacity of Istanbul Provincial Disaster Management Center”, a new building was constructed and furnished in the campus area of the Governorship. IT equipments like display wall system; servers, active devices, communication devices, etc. have been procured to make the DMC fully operational. The Istanbul Governorship designated two locations, one on the Asian and one on the European side, to be used as new emergency management centers. The construction of HASDAL DMC started in April 2010.

Under A4 subcomponent, many procurement packages have been completed and the goods have been delivered to the public institutions.

For Istanbul Health Directorate:

1. Isolated Containers (50 items)
2. Various Medical equipment
3. Vehicles (Electrical and diesel forklifts, 4x4 health rescue vehicles, emergency health service vehicles, heavy duty health service trucks.)
4. Mobile Lighting Towers
5. Cold Air Depot (To keep vaccine and blood products)

For Istanbul Disaster Management Center:

1. Vehicles (Mobile communication, mobile broadcast, survey, transport, operation vehicles)
2. Various Communication Devices (Radio handsets, car radios, communication switches, antennas and antenna near products, etc.)

For Istanbul Search and Rescue Unit:

1. Vehicles (Off-road Equipped Search and Rescue, Water Rescue, K-9 Rescue, NBC Rescue, Mobile communication, survey and operation vehicles)
2. Various Communication Devices (Radio handsets, car radios, HF/SSB radios, etc.)
3. Various Search, Rescue and Camping Equipment
4. Diving Equipment
5. IT Equipment (PCs, laptops, cameras, video cameras, printers, etc.)

With the help of these procurements, on-disaster and post-disaster responses of the related public institutions have been enhanced. Such procurements are still being carried out with close coordination of the public agencies.

To minimize probable life and economic losses due to earthquakes, it is very significant not only to construct new buildings in accordance with building codes and regulations, but also to retrofit or reconstruct vulnerable existing buildings. Accordingly, **Component B**, as an important part of the project, includes the retrofitting or reconstruction of priority public buildings (schools, hospitals, dormitories, administrative and social service buildings). The prioritization studies, which form the basis of the retrofitting works, were carried out under MEER Projected financed by the World Bank: the total number of evaluated buildings was 2694.

Table 1 Feasibility Studies within the scope of the ISMEP.

	COMPLETED		ON GOING		TOTAL	
Building Type	Campus	Building	Campus	Building	Campus	Building
Schools	653	969	151	214	**804**	**1183**
Hospitals	29	282	2	28	**31**	**310**
Polyclinics-Healthpost	18	19	70	70	**88**	**89**
Administrative Buildings	28	63	6	6	**34**	**69**
Dormitories & Service Buildings	18	61	1	6	**19**	**67**
TOTAL	**746**	**1394**	**230**	**324**	**976**	**1718**

The buildings are reviewed with respect to the “Regulation on Buildings to be Constructed in Earthquake Zones”. Accordingly, the retrofitting designs were prepared in line with the regulation for buildings which did not have retrofitting designs and those financially feasible decided to be retrofitted. The decision for reconstruction was given when retrofitting was not financially affordable, economically justifiable, technically feasible, and socially acceptable.

Table 2 Retrofitting of buildings within the scope of the ISMEP.

Building Type	RETROFITTING WORKS							
	Completed		Ongoing		Tender Stage		Total	
	Campus	Building	Campus	Building	Campus	Building	Campus	Building
Schools	311	379	108	137	-	-	**419**	**516**
Hospitals	5	10	3	10	1	4	**9**	**24**
Polyclinics-health centers	3	3	2	2	6	6	**11**	**11**
Administrative buildings	10	19	6	13	1	4	**17**	**36**
Dormitories & social service buildings	13	32	1	3	-	-	**14**	**35**
TOTAL	**342**	**443**	**120**	**165**	**8**	**14**	**470**	**622**

Figure 1 Retrofitting work: column jacketing and shear wall.

Table 3 Reconstruction of Buildings within the scope of the ISMEP.

Building Type	RECONSTRUCTION WORKS							
	Completed		Ongoing		Tender Stage		Total	
	Campus	Building	Campus	Building	Campus	Building	Campus	Building
Schools	43	43	28	28	36	38	**107**	**109**
Hospitals	-	-	-	-	1	1	**1**	**1**
Polyclinics-health centers	1	1	-	-	1	1	**2**	**2**
Administrative buildings	-	-	-	-	1	1	**1**	**1**
Dormitories & social service buildings	-	-	2	6	1	6	**3**	**12**
TOTAL	44	44	30	34	40	47	114	125

Besides, a commentary guideline for the **"Seismic Retrofit Design for School and Hospital Facilities in Istanbul"** was prepared under B component as a part of the consultancy service contracts in order to prepare seismic retrofitting principles of education and health buildings under ISMEP.

Moreover, within the context of the B Component, the inventory of 26 cultural heritage buildings (176 buildings) of which are under the protection of the Ministry of Culture and Tourism were carried out. The data will be shared, depending on the level of confidentiality, with the public, universities and other public institutions. The retrofitting designs of Topkapı Palace, 4th Court–Mecidiye Kiosk, Archeological Museum Additional and Classical Building and Haggia Sophia Museum Directorate–Saint Irene Monument are still being prepared.

In this framework, UNESCO – ICOMOS Joint Mission who visited the World Heritage Property of the Historic Areas of Istanbul in May 2008 prepared the report referred to the World Bank funded ISMEP. Turkey is a State Party to the "Convention Concerning the Protection of the World Cultural and Natural Heritage and the Historic Areas of Istanbul was inscribed on the UNESCO World Heritage List. The mission declared that risk assessments of cultural heritage buildings under ISMEP were being implemented by appropriately qualified international expert consultancies and were designed as pilot projects for replication more widely in Turkey. Also the mission commended Turkey for this innovative and comprehensive initiative in risk mitigation, which would provide a model for emulation in other large and complex World Heritage properties exposed to earthquake risk.

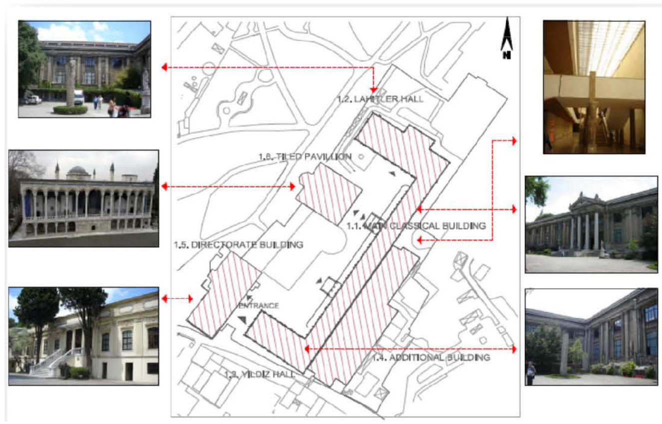

Figure 2 **Field survey-sample drawings of Archeological Museum Complex.**

Component C of the ISMEP covers the activities on streamlining of building permit issuance, planning and land use development procedures under the strong coordination and cooperation with two pilot municipalities (Bagcilar and Pendik) which were selected by determined criteria (such as; located nearby disaster prone areas, high distribution of dangerous materials, high population density and growth). In that, firstly, a need analysis and evaluation study was executed in pilot municipalities to improve existing building permit issuance and application processes. Then, in compliance with the results of this study, software and IT related hardware, system room construction, local area network (LAN) backbone implementation and Disaster Recovery System hardware were provided to the pilot municipalities in order to build necessary IT infrastructure to achieve expected project results. Projects are being implemented, such as geo-referenced data (spatial and non spatial data) integration and updating and collection services covering establishment of digital archive system for documents of land use development activities. After this project, a documentation management system will be established and integrated into existing GIS based system to monitor land use development processes and increase service capacity of the municipalities to their community.

Under Component C, "Public Land Management Project", introduces models and options based on sustaining public benefits for better/efficient management of public lands of public buildings to be relocated or to be demolished because of being exposed to disaster and having low accessibility within the city centre. In that, existing national and international policies and tools were analyzed and evaluated in terms of legal and institutional framework with their opportunities and restrictions.

In addition, training programs are being organized and implemented under the protocol signed with the Ministry of Public Works and Settlement and IPCU, aiming to increase the education level of civil engineers on "Regulation on Buildings to be constructed in Earthquake Zones." Training materials were designed and prepared. Up to now a total of 2660 engineers have been trained in the determined cities throughout Turkey.

Social Aspect and Contribution

ISMEP with its three components gives importance to accomplishing social dimensions of ongoing technical and institutional works and to increase public awareness on disaster mitigation activities.

Under the scope of Component A, it is aimed to spread a disaster volunteering system throughout Istanbul, and to develop a conceptual, administrative and practical model for its integration with "Provincial Disaster Management Center. Within this context, a Search Conference for Evaluation for Volunteer Systems in Disaster Response was organized on May 24 2007. The search conference where Istanbul Governorship gathered with the executives of the entities in direct relation with the disaster volunteering system and exchanged information showed the interest and significance attached to the subject by the participants with their opinions and their evaluations on the suggested system for improvement of the disaster volunteering system. Besides this, under this component, disaster public awareness training materials and trainings were developed, those trainings and public awareness campaigns are being carried out.

Under component B, a study on the social aspects of retrofitting were initiated in order to reduce the problems arising from the retrofitting works and to inform the beneficiaries. Seminars were made within different groups with school directors, parent unions, members of schools and the Provincial Directorate of Education, District Directors of Education to increase their awareness about retrofitting activities. Brochures, awareness booklets and comic books were prepared and distributed for the schools being retrofitted. Moreover, Social Impact Assessment Surveys were conducted to evaluate the social impacts of retrofitting works executed at schools and to identify the retrofitting/reconstruction work procedures. According to the survey results, this social guidance study also is being carried out in host schools. The content of the seminars differs from in retrofitting and host schools in terms of the target group needs. Approximately two hundred fifty thousand people have been trained since 2009.

Under Component C, for urban planning and construction; training programs were prepared for three target groups: local decision makers, technical staff of the municipalities and community representatives. These training programs were carried out in two municipalities (Bağcılar and Pendik) chosen as pilot municipalities within project. Approximately 740 people were trained.

As mentioned before, under the scope of Components of A and C, disaster public awareness trainings for different target groups are organized in İstanbul to raise public awareness for disaster preparedness, urban planning and construction for disaster mitigation. Training modules and materials include participant, instructors, books, posters, brochures, information cards, power point presentations with technical drawings and spot films were prepared in Turkish and English. Training Modules and Materials for Public Awareness are given below;

1. First 72 Hours for the Individual and a Family in an Earthquake
2. First 72 Hours for Disabled People in an Earthquake
3. Non- structural Risk Mitigation Against Earthquake
4. Structural Retrofitting Against Earthquake
5. Structural Risk Mitigation Against Earthquake
6. Survival Under Extraordinary Conditions
7. Psychological First Aid in Disasters
8. Disaster Emergency Aid Planning Guide for Educational Institutions
9. Disaster Emergency Aid Planning Guide for Healthcare Organizations
10. Disaster Emergency Aid Planning Guide for Industries and Working Place
11. Disaster Preparedness for Local Disaster Volunteers

12. Compulsory Earthquake Insurance Awareness
13. Urban Planning and Construction for Disaster Mitigation for Local Decision Makers
14. Urban Planning and Construction for Disaster Mitigation for Technical Staff
15. Urban Planning and Construction for Disaster Mitigation for Community Representatives

Several public awareness campaigns in Istanbul are implemented. Istanbul Governorate with the support of the ISMEP organized the first campaign on August 16-17, 2008, the anniversary of the 1999 Marmara Earthquake to raise public awareness in life safety issues. The campaign motto was “A Step Forward for a Safe Life” which will be used at each planned future campaign.

The second campaign was a Public Awareness Campaign organized at the tenth Anniversary of 1999 Marmara Earthquake and had two basic activities; the first was “Safe City Safe Life Istanbul 2009 Meeting” which aimed to introduce ISMEP’s activities to institutions and to bring together all related institutions, to introduce training programs and to invite related institutions to share the training programs. In “Safe City Safe Life Istanbul 2009 Meeting” also “Safe Life Volunteers” training and communication campaign was introduced. The second was stand and field activities, which aimed to introduce ISMEP’s activities to public. In addition, trainings materials were delivered during the campaign.

The third campaign was a Public Awareness Campaign that was a duplication of August Campaign, was realized on November 12, 2009. During this campaign, again stand and field activities, material distribution activities were carried out. During the campaign, Safe Life Volunteer training was given to actors and actresses who are opinion leaders of our society and also defender of our project. The motto of these campaigns was “A step forward for a safe life: Get a training.”

CONCLUSION

ISMEP pursues a pro-active approach to mainstreaming risk mitigation and prevention for a potential earthquake in İstanbul. The activities of ISMEP have crucial importance in terms of the prevention of potential loss of lives and mitigation of social, economic and financial impacts. Additionally, ISMEP will be an outstanding model for the design and implementation of other national and international projects and activities in the field of disaster risk mitigation.

TSUNAMI THREAT TO ANATOLIAN COASTS: ESTABLISHING A TSUNAMI WARNING SYSTEM IN TURKEY

Nurcan Meral Özel[1], Öcal Necmioğlu [1]; Ahmet Cevdet Yalçıner[2], and Mustafa Erdik[1]

[1]Boğaziçi University, Kandilli Observatory and Earthquake Research Institute, Istanbul-Turkey, 2 Middle East Technical University, Civil Engineering Department; Ocean Engineering Research Center, Ankara-Turkey

ABSTRACT

This report provides a summary of the Tsunami Hazard in the Eastern Mediterranean and its connected seas (Aegean, Marmara and Black Sea) by providing brief information on some of the historically and instrumentally recorded significant tsunamigenic events surrounding Turkey, together with the activities on the establishment of a National Tsunami Warning Center (NTWC) / Regional Tsunami Watch Center (RTWC) by KOERI under the UNESCO Intergovernmental Oceanographic Commission—Intergovernmental Coordination Group for the Tsunami Early Warning and Mitigation System in the North Eastern Atlantic, the Mediterranean and Connected Seas (ICG/NEAMTWS) initiative. In addition, results of some tsunami modeling are also presented here.

INTRODUCTION

It was only after the tragic event of Sumatra in 2004 that most of the people realized the real threat of a tsunami, even though tsunamis were well known among the earth-science community before the Indonesian Tsunami led to the death of more than 200,000 people, caused damage of property and business in more than $4.4 billion, and left hundreds of thousands people homeless, leaving unprecedented damage to the economy and infrastructures of the region. It was these numbers sending a strong signal to the policy makers that they have to do something about it, and as a result of this, tsunami mitigation, preparedness and early warning initiatives have begun at the global scale. Turkey, as a country with a history of devastating earthquakes, has been also effected by tsunamis in its past, and a possible tsunami effecting the coastal areas of Turkey may cause considerable damage, especially considering the densely populated coastal areas, infrastructure and harbours. More than 30 sunken ships were found in Theodosius Harbour during the construction of the Marmara Rail-Tube Tunnel at Yenikapi location of Istanbul. Furthermore, the sedimentary sequence discovered at archaeological excavations contains significant records of sea level change due to various reasons, among which the content of one layer suggest an abrupt event [Algan et. al. 2009). This abrupt event was interpreted as a tsunami event caused by the AD 553 Istanbul earthquake, [Perincek et al. 2007]. In the Aegean and Eastern Mediterranean, volcanic eruption, such as the one in Santorini in around 1600 B.C, was also an important tsunami source, resulting in the destruction of the Minoan culture of the Bronze Age and even affecting the Levantine. A strong earthquake in 1956 generated a tsunami in the Aegean Sea [Soloviev, et. al. 2000] and two third of the towns were destroyed and thousands of inhabitants were killed in Antiochia after a destructive earthquake on August 23, 1822, where tsunami was observed in Beirut, Iskenderun, and on the Island of Cyprus [Karnik 1971; Soloviev et al. 2000]. Historical assessment of the tsunami hazard indicates the importance of the tsunami modeling in this region, hence we have applied tsunami numerical model NAMI DANCE in two nested domains for a possible tsunami source area between Rhodes and southwest of Turkey. Also, we have simulated the 300 m collapse of the 10-km-diameter Thera (Santorini) caldera using a 900 m grid resolution of Aegean Sea bathymetry and calculated the distribution of maximum positive amplitudes of water elevations.

HISTORICAL TSUNAMI EVENTS AROUND ANATOLIA

Turkey is a peninsula surrounded by Black, Aegean, and Mediterranean Seas, which are all historically proven to be locations of tsunamigenic sources (see Figure 1). During an observation period of over 3000 years, historical records clearly indicate that the coastal and surrounding areas of Turkey have been affected by more than ninety tsunamis. These tended to cluster around the Marmara Sea, the city of Istanbul and the gulfs of Izmit, Izmir, Fethiye, and Iskenderun [Altinok and Ersoy 2000]. Not all of the tsunamis were well recorded, and there are some indications that a considerable percentage of the cases found in the literature concerning the tsunamis in the Marmara Sea are to be ruled out as spurious events [Ambraseys 2002]. Nevertheless, this region remains one of the European areas with the highest tsunami activity, and most vulnerable to tsunami attacks [Tinti et al. 2006; Yalciner et al. 2001]. Reliable and extensive information is especially available for the tsunamis associated with the Istanbul earthquakes of 1509 and 1894, the Eastern Marmara earthquake in 1963, and that of Izmit in 1999, all effective in the Marmara Sea; and the 1939 Erzincan and 1968 Bartin earthquakes, in Eastern Anatolia and Amasra on Black Sea coast, respectively [Altinok and Ersoy 2000].

The historical documents regarding at least 22 tsunamis in the basin of the Black Sea suggest a significant tsunami hazard and nine of the 22 occurred in the twentieth century [Yalciner et al. 2004]. According to Ambraseys and Finkel [1995], the Amasya earthquake in 1598, which led to the Black Sea Tsunami, was a major earthquake in central northern Anatolia but there was not enough data to assess its size.

The Erzincan earthquake (Ms=8) occurred on December 26–27 1939, at 02.00 a.m. local time and caused the Fatsa tsunami (see Figure 2). Related sea disturbances were observed and reported in various studies [Parejas et al. 1942; Eyidogan et al. 1991]. Murty [1977] states that the tsunami amplitudes were smaller on the Russian coasts than in Turkey. The initial rise of the sea level was recorded at six tidal stations on the northern coast of the Black Sea [Altinok and Ersoy 2000; Yalciner et al. 2002a].

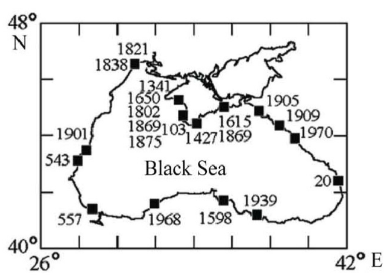

Figure 1 **Sites and years of observation of tsunamis on the Black-Sea coast without instrumental recording of the oscillations of sea level [Dotsenko and Ingerov 2007].**

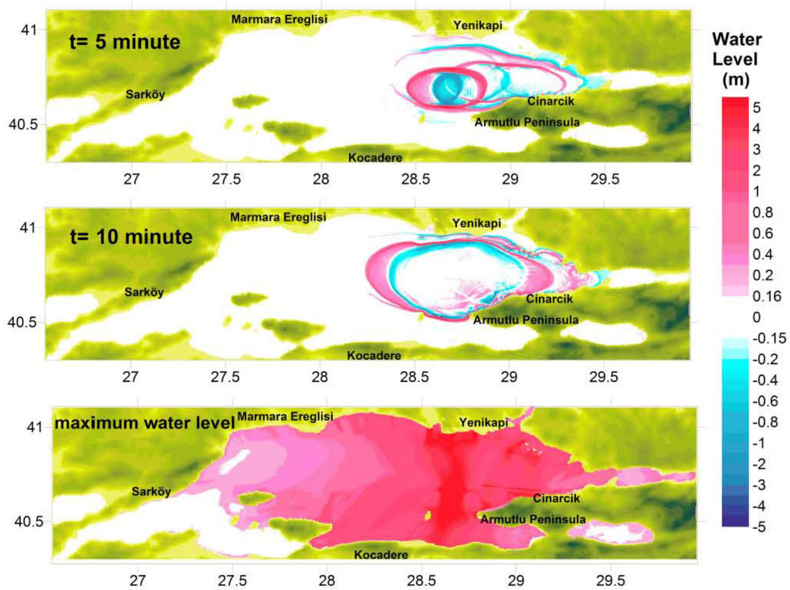

Figure 2 Recorded oscillations of the sea level at various sites of the Black-Sea coast caused by the tsunami of December 26, 1939; (◆) beginning of the seaquake generating the tsunami wave, (↓) time of arrival of the tsunami wave at the points of observation [Dotsenko and Ingerov 2007].

The Istanbul Earthquake on September 10, 1509 was one of the largest and most destructive earthquakes of the last five centuries in the eastern Mediterranean. Along the coast, the sea flooded the shores and waves crashed against the walls in the narrows between Pera and Istanbul [Ambraseys and Finkel 1995]. Waves overtopped the walls in Yenikapi and Aksaray was flooded. The walls of Izmit Castle on the shore were damaged beyond repair, the quay walls of the shipyard collapsed, and waves flooded the dockyard and the lower districts of the city. The tsunami waves of the earthquake overtopped the sea walls in Yenikapi, the wave height was most probably more than 6.0 m, and the magnitude of the earthquake was close to 8.0 [Oztin and Bayulke 1991].

Another earthquake in Istanbul occurred at 12.24 a.m. on July 10, 1894, damaged Istanbul and the surrounding area, and was felt at Ioanina, Bucharest, Crete, Greece, Konya, and most of Anatolia [Öztin 1994]. Reports indicate that, along the coast, many disturbances were seen in many parts; the sea receded up to 50 m and then returned. In another part, the sea rose and then receded. There was no permanent change to the coastline. The hypocentral depth was estimated as 34 km. According to Mihailovic in 1927, the sea rose up and inundated 200 m, and after a few disturbances became normal. The tsunamis were observed to occur around the Prince Islands and on the northern coast of the Marmara Sea from Buyukcekmece to Kartal. During the earthquake, at first the sea was at a low level, and then later a strong wave hit the shore to the west of Istanbul. There was definitely a tsunami, though probably a small one. The tsunami height was less than 6.0 m, and the earthquake magnitude was less than 7.0 [Oztin and Bayulke 1991; Altinok and Ersoy 2000].

It has been shown that the Kocaeli 1999 Earthquake with an M_w = 7.4 also created a tsunami in Izmit Bay [Altinok et al. 2001; Tinti et al. 2006]. A possible future earthquake occurring in the Marmara Sea has a direct tsunamigenic potential, and, furthermore, may set in motion submarine masses (landslides or slumps), with additional possibility to produce tsunamis [Tinti et al. 2006; Yalciner et al 2001].

Yalciner et al. [2002a] determined the slope failure potential as a possible tsunamigenic source in the Sea of Marmara by utilizing multi-beam bathymetry, shallow, and deep seismic reflection data. On the basis of the landslide geomorphology, they tested the generation, propagation, and coastal amplifications of tsunamis related to earthquake and slope failure scenarios by using tsunami simulation model TWO_LAYER and obtained maximum water surface elevations (Figure 5) near the shores along the north and south coasts according to the selected scenarios of tsunami generation by using available data [Yalciner, et al. 2002a].

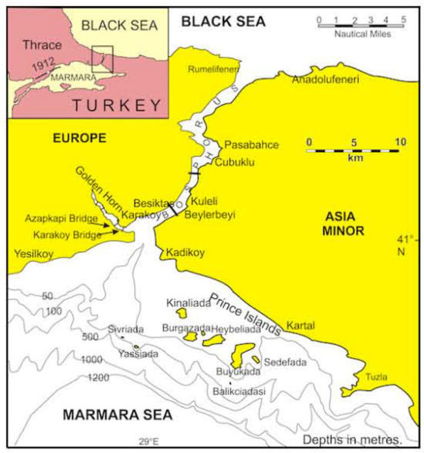

Figure 3 Places for Tsunami reports in and around the city of Istanbul [Altinok et al. 2003).

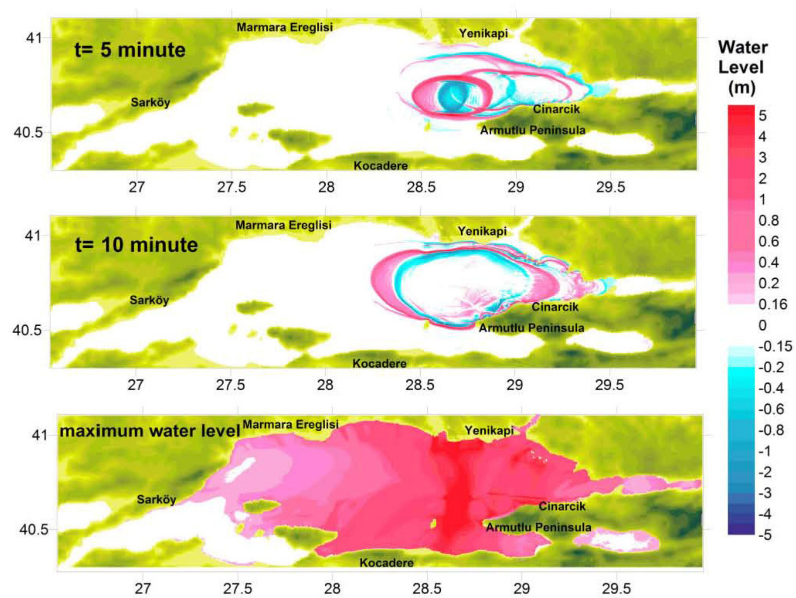

Figure 4 Sea state at 1, 5, 10, 15th minutes of tsunami propagation according to fault break and underwater landslide scenario at offshore Armutlu Peninsula.

In the Aegean Sea, tsunamis are not only generated by earthquakes but also by volcanic eruptions. The well-known giant eruption of the Santorini volcano approximately in 1600 B.C. was accompanied by a strong earthquake and a huge tsunami, resulting in the destruction of the Cretan-Mycenaean (Minoan) culture of the Bronze Age. We have performed a simulation using 900 m grid resolution of Aegean Sea bathymetry with a 300 m collapse of 10 km diameter of Thera (Santorini) Volcano. Figure 5 shows the distribution of maximum positive amplitudes of water elevations in the duration of four hours simulation of this tsunami in the Aegean Sea (Figure 6)**.** In 1956, a strong earthquake in the Aegean Sea generated a destructive tsunami [Soloviev et al. 2000]. A destructive earthquake took place on August 13, 1822, in particular in Antiochia, where two third of the towns were destroyed and thousands of inhabitants were killed. A tsunami was observed in Beirut, Iskenderun and on the Island of Cyprus [Karnik 1971; Soloviev et al. 2000]. Tsunamis have caused severe damage and flooded lowlands in many segments of the Mediterranean coasts. Historical documents, and geological, archaeological and many trench studies demonstrate that parts of the Turkish coastlines have suffered from disastrous sea-waves several times in the past [Yolsal et al. 2007; Yalciner et al. 2002; 2004; Boschi et al. 2005; Guidoboni and Comastri 2005; Scheffers and Kelletat 2005; Fokaefs and Papadopoulos 2007; Papadopoulos et al. 2007].

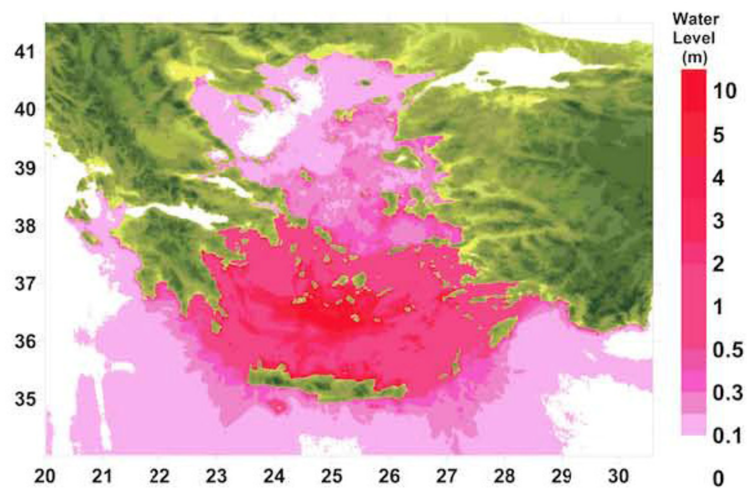

Figure 5 Distribution of maximum positive amplitudes of the water elevations computed in the duration of four hours simulation of Santorini originated (caldera collapse) tsunami in the Aegean Sea.

The earthquake of August, 8 1303, in Crete proves to be one of the largest and best-documented seismic events in the history of the Mediterranean area [Yolsal et al. 2007]. It has been suggested that the epicenter was probably near the island of Crete, and after this event tsunami waves were reported to be seen as far as the coastlines of Crete, the Peloponnese, Rhodes, Antalya (SW Turkey), Cyprus, Acre, and Alexandria–Nile delta (in Egypt. In addition, this earthquake and associated damage distributions are listed in most descriptive and parametric catalogues for the Mediterranean basin. However, the orientations of active faults vary along the concave part of the Hellenic arc (e.g., Pliny and Strabo trenches) in accordance with subduction of remnants of old lithospheric slab (Taymaz et al. 1990; 1991). Hence, the Hellenic trench in the vicinity of Crete should be considered to be a seismogenic zone of considerable importance in the Mediterranean region [Guidoboni and Comastri 1994].

TSUNAMI MODELING CASE STUDY: AN EARTHQUAKE BETWEEN RHODES AND SOUTHWEST OF TURKEY

A possible tsunami source area is selected between Rhodes and southwest of Turkey for modeling, with the epicenter at 27.5°E,37.80°N and rupture parameters of 140 km length, 40 km width, 40° strike, 50 km focal depth, 30° dip angle, 90° rake angle, and 6 m displacement. In order to understand the arrival time and coastal amplification of this tsunami in one of the tsunami forecast areas at Southwest of Turkey (the towns of Marmaris and Kas), the tsunami numerical model NAMI DANCE is used in two nested domains. The largest domain is bounded 20° and 36.3° in easting direction, and 30° and 41.5° in northing direction with 1800 m grid size. The smaller domain covers a selected tsunami forecast area bounded 28.23° and 29.7° in easting direction, and 36.08° and 36.86° in northing direction with 600 m grid size. The maximum positive amplitude is computed as 1.13 m and maximum negative amplitude is -0.5 m at the tsunami source (Figure 7). The initial wave and distribution of maximum positive amplitudes in the eastern Mediterranean computed in four hours simulation are given in Figure 10. The directivity of this tsunami is towards SE and NW directions.

The distribution of maximum positive amplitudes of the water surface elevations in the selected tsunami forecast area and time histories of water level fluctuations near selected locations (the towns of Marmaris, Dalaman, Fethiye and Kas) are given in Figure 8. As seen in Figure 10, the maximum positive amplitude near the coast in the selected forecast area exceeds 3.5 m. The arrival time of maximum wave to Marmaris and Dalaman, is 10 minutes, while for Fethiye and Kas tois 15-20 minutes. The maximum positive amplitudes near the shallow region around 10 m depth are 3 m (Marmaris), 1m (Dalaman), 2 m (Fethiye) and 1 m (Kas).

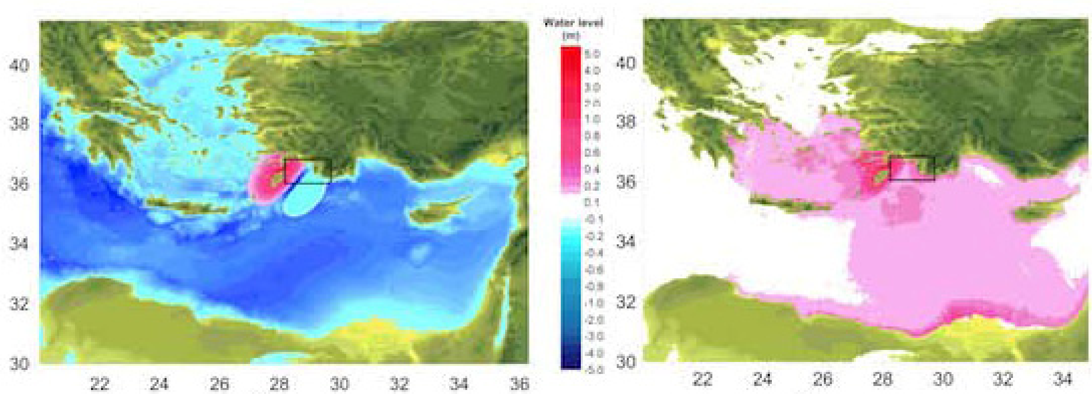

(a) (b)

Figure 6 The selected tsunami source (a) on the bathymetry in Eastern Mediterranean and (b) the distribution of maximum positive amplitudes of the water elevations (right) in Eastern Mediterranean in the duration of four-hour simulation. The rectangle bounds the tsunami forecast area.

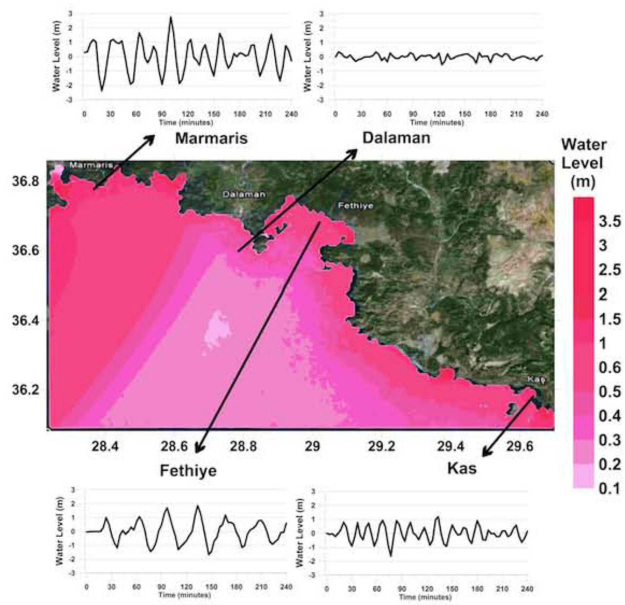

Figure 7 Distribution of maximum positive amplitudes of the water elevations in the selected tsunami forecast area and time histories of water level fluctuations at selected locations (the towns of Marmaris, Dalaman, Fethiye, and Kas).

ESTABLISHING A TSUNAMI WARNING CENTER IN TURKEY

Historical documents, seismicity and modeling studies show a clear necessity of understanding and preparedness for the tsunami hazard in Turkey. Turkey was ready to join and contribute to the initiative of a Tsunami Warning System in the North-eastern Atlantic, the Mediterranean and connected seas region (ICG/NEAMTWS) at its very beginning, and Kandilli Observatory and Earthquake Research Institute (KOERI), as the leading Earthquake Research Institute in Turkey, was ready to lead related national institutions for the establishment of a National Tsunami Warning System. ICG/NEAMTWS is responsible for the implementation of a tsunami warning system controlled by the Intergovernmental Oceanographic Commission of UNESCO (IOC-UNESCO). It has been formally established by the IOC Assembly during its twenty-third Session (June 21-30, 2005). Its first session was held in Rome, Italy in November 2005, and its last session took place in Paris, France, in November 2010. Currently, it has four working groups responsible for Hazard Assessment and Modeling (WG 1), Seismic and Geophysical Measurements (WG 2), Sea Level Data Collection and Exchange, Including Offshore Tsunami Detection and Instruments (WG 3), Public Awareness, Preparedness and Mitigation (WG 4) and two task teams responsible for the Regional Tsunami Warning System Architecture and Communication Test and Tsunami Exercises. KOERI is now a candidate to become a Regional Tsunami Watch Center (RTWC), providing coverage to Eastern Mediterranean, Aegean and Black Sea.

The first coordination meeting for the establishment of a National Tsunami Warning Center was held in March 2008 at KOERI, Istanbul and was attended by Office of Navigation, Hydrography and Oceanography (ONHO), General Directorate of Disaster Affairs-Earthquake Research Department (GDDA-ERD), State Planning Organization (SPO), Directorate of Disaster and Emergency Management (DDEM), General Command of Mapping and Middle East Technical University (METU), Department of Civil Engineering, Ocean Engineering Research Center (OERC) and the Institute of Marine Science (IMS). A road-map was set, and accordingly, a Tsunami Working Group was established at KOERI. The group held several internal meetings, conducted studies and investigations to evaluate the existing capacity of KOERI in terms of instrumentation, software and hardware, and identified the areas to be improved. Four different sub-working groups referenced to NEAMTWS working groups were established with the support of contributing national institutions mentioned above. As a result of all these efforts, a project proposal was submitted to the Prime Ministry State Planning Organization for the establishment of a Regional Tsunami Watch and Evaluation Center and was accepted at the end of 2009.

The sixth session of the ICG/NEAMTWS was held in Istanbul, Turkey on November 11–13, 2009, which also launched a program of communication exercises to test the communication capability of the warning system. Two communication test exercises were held on June 24, and September 30, 2010, with the successful participation of candidate RTWCs, simulating the dissemination of tsunami messages by one candidate RTWC and its timely reception by the NTWCs. During the sixth session, the importance of the multi-hazard approach for the NEAMTWS, especially in relation to storm surges that affect Members States around the North-eastern Atlantic was also confirmed. In relation to the multi-hazard approach the ICG/NEAMTWS called for strengthened cooperation with the World Meteorological Organization (WMO), the European Commission (EC), especially regarding the Flood Directive, and the European Space Agency (ESA). ICG/NEAMTWS-VI decided on the establishment of a Tsunami Information Centre for the North-eastern Atlantic, the Mediterranean and connected seas (NEAMTIC) at the IOC Secretariat. NEAMTIC will take advantage of the expertise of the UNESCO/IOC International Tsunami Information Centre (ITIC) working on adapting its existing awareness and educational products to the Mediterranean context and will be responsible for the collection and dissemination of information on international warning activities for tsunamis and other sea-level related hazards, particularly in the NEAM region, foster identification and exchange of best practices in preparedness for tsunamis and other sea-level related hazards, and act as an information resource for the development and distribution of awareness, educational and preparedness materials, and will collect data of tsunami events. The relevant project proposal was approved by the European Commission in 2010.

During the seventh session of NEAMTWS held in Paris between November 23–25, 2010 a Task Team on the Multi-hazard Approach to Coastal Inundation in NEAMTWS was also established, emphasizing the need to link tsunami warning and preparedness with other types or related coastal inundation within a multi-hazard approach. It has also been concluded to conduct Communication Test Exercises during 2011 involving the Tsunami Warning Focal Points (TWFP) and to set up procedures for the first NEAM Tsunami Exercise to be conducted in 2012.

MONITORING AND ANALYSIS CAPABILITIES OF THE KOERI

The KOERI has been monitoring the seismic activity in and around Turkey more than 80 years. At the moment, KOERI Seismic Network comprises 108 broadband and 22 short-period seismometers and satellite systems are being used for the communication since 2004. An increase in number of seismic stations, especially through the coastal ranges of Turkey, is foreseen. A protocol has been signed with the General Directorate of Disaster Affairs—Earthquake Research Department, according to which data from ten seismic stations along the coastal areas of Turkey will be integrated into KOERI's existing network to increase the density of the station distribution across the country. SeisComp3 software, provided by GFZ, is now being used successfully in the National Earthquake Monitoring Center (NEMC). Currently NEMC is receiving real-time data from 72 stations from 10 networks in SeisComp3 compiled by GEOFON, reaching up to 107 stations with the agreements concluded with some other countries in the region. We are able to produce analysis within 2 minutes for earthquakes in Turkey and within 30 sec. to 15 minutes for earthquakes in its surrounding region according to the event magnitude and distance. Both zSacWin and SeisComp3 software are utilized at the NEMC and besides event location, duration, local, surface wave and moment magnitudes are calculated automatically and are ready to be sent in 3 to 5 minutes as an average after the event time. (mb is calculated by SeisComp3 at the moment) zSacWin performs automatic phase picking and interactive analysis is performed as soon as an event is observed. In this case, the reviewed event analysis is ready for distribution in 2-10 minutes average depending on the size of the earthquake and experience of the analyst. SeisComp3 produces automatic solution after recording seven P arrivals, namely after 30 sec–2 minutes in average. The quality of this location is highly dependent on the magnitude of the event and station coverage. Currently, irregular interactive analysis is performed also on SeisComp3 output based on the interest to the specific event, however, this can be done on a routine basis anytime needed.

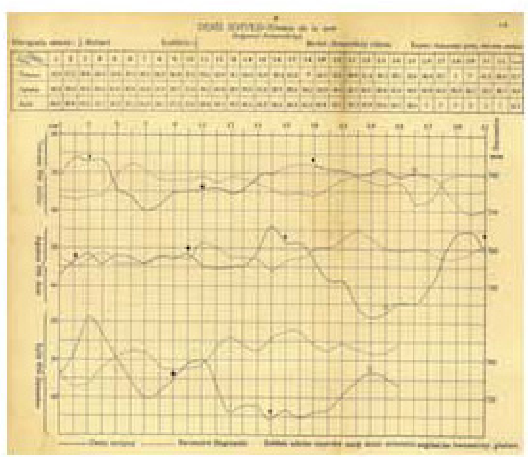

Figure 8 An example KOERI sea-level measurement from 1934 at Arnavutkoy-Istanbul tide-gauge.

Another important element of the Tsunami Early Warning System is the use of sea-level measurement especially important for the verification of the warning messages and improving the modeling outputs. The KOERI had an experience of sea-level monitoring around Marmara Sea during the first half of the twentieth-century in the 1930s (Figure 8). We have initiated cooperation with ONHO, which is responsible for the sea level measurements in Turkey currently operating 19 tide-gauges. Data from three tide-gauges (at Sinop, Marmara Ereglisi, and Bodrum) are currently being transmitted to KOERI using ftp protocol and real-time data transmission will be established soon. Data is sampled at every 15 sec intervals and transferred using GPRS modems. The sampling rate will be increased to 1 Hz, and KOERI is assisting ONHO in establishing satellite communication for data transfer. Sea-level data have been tested by Middle East Technical University in Tsunami modeling and its suitability was verified. We hope that sea-level data from the three tide-gauge stations listed above will be publically available within this year. The NAMI-DANCE Tsunami Simulation / Visualization Code was installed at the National Earthquake Monitoring Center of KOERI, and a NAMI-DANCE workshop took place at KOERI.

The NAMI DANCE was developed specifically for tsunami modelling in a collaborative effort between the Ocean Engineering Research Center, Middle East Technical University, Turkey, and the Institute of Applied Physics, Russian Academy of Science, Russia by Professors Andrey Zaytsev, Ahmet Yalciner, Anton Chernov, Efim Pelinovsky, and Andrey Kurkin. It has been tested and verified parallel to TUNAMI-N2 at international workshops. Some of those workshops are (i) benchmark problems for tsunami numerical models [i.e., Synolakis et al. In 2004 and Liu et al. in 2008] and (ii) testing and verification of tsunami numerical models in EU TRANSFER Project. The model has also been applied to several case studies Yalciner et al., 1995, 2006, 2007; Zaytsev et al. 2008; Yolsal et al. 2007].

It provides direct simulation and efficient visualization of tsunamis to the user and for the assessment, understanding and investigation of tsunami generation and propagation mechanisms. In addition to the computations of necessary tsunami parameters, NAMI DANCE also computes the distributions of current velocities and their directions at selected time intervals, relative damage levels according to drag and impact forces, and it also prepares 3D plots of sea state at selected time intervals from different camera and light positions, and animates the tsunami propagation from source to target for visualization. Further info about NAMI DANCE is available at http://namidance.ce.metu.edu.tr.

The proposed Tsunami Warning System in Turkey will function in the following way: A bulletin indicating the possibility of a tsunami will be disseminated to the Disaster and Emergency Management Presidency of Turkey (AFAD) based on the automatically obtained magnitude, location and focal depth information (from which the type of the message will also be determined) with reference to the draft decision matrix currently being developed by the NEAMTWS Task Team on the Regional Tsunami Warning System Architecture. Until the tsunami scenario/model database is fully developed, which is expected to be accomplished by the end of 2011, the initial bulletin will be updated using the source parameters obtained from seismological analysis and tsunami modeling will be performed based on these parameters and tsunami height and arrival time will be calculated for the pre-defined Tsunami Forecast Points (TFP). Using this information, the initial bulletin will be updated. Currently, TFPs are determined based on the initial modeling studies; however, KOERI is cooperating with AFAD in order to determine the criteria for the selection of TFPs. Once the scenario database is created, the tsunamigenic zone in which the event is located will be identified automatically based on the preliminary earthquake information, and output of the previously obtained scenario model created for the same magnitude will be used automatically at the initial bulletin. After obtaining the source parameters from the seismological analysis, an assessment of the deviation from the initial model will be made to determine the need for a re-run of the tsunami model. The criteria for this assessment will be obtained during the course of the scenario-database creation. If necessary, the message will be updated and/or cancelled.

Decision Matrix for the Mediterranean

Depth	Location	Mw	Tsunami Potential	Tsunami Message Type		
				Local	Regional	Basin-wide
<100 km	Under or very near the sea (D < 30 km)	5.5-6.0	Small potential for a destructive local tsunami	Advisory	Information	Information
		6.0-6.5	Potential for a destructive local tsunami	Watch	Advisory	Information
		6.5-7.0	Potential for a destructive regional tsunami	Watch	Watch	Advisory
		>7.0	Potential for a destructive basin-wide tsunami	Watch	Watch	Watch
	Inland (D<30 km)	≥5.5	No tsunami potential	Information	Information	Information
≥100 km	All locations	≥5.5	No tsunami potential	Information	Information	Information

Figure 9 Draft decision matrix for the Eastern Mediterranean proposed by the ICG/NEAMTWS Task Team on the Regional Architecture of the NEAMTWS – unpublished material.

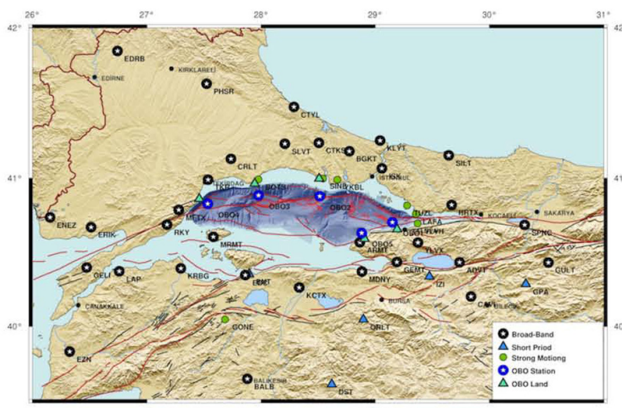

Figure 10 Distribution of seismic stations and sea floor observation system in Marmara region.

Figure 11 Scenes from the deployment of the first sea floor observation system element in November 2009.

DEPLOYMENT OF THE SEA BOTTOM OBSERVATION SYSTEM IN MARMARA SEA

The KOERI is also in the process of enhancing its observational capabilities with the deployment of five sea bottom observation systems in the Sea of Marmara, including broadband seismometers and differential pressure meters, pressure transducer, strong-motion sensor, hydrophone, temperature measurement device, and flow meter. The deployment phase was finalized in December 2010, and the system is fully operational. The seismic component of the sea bottom observation system will improve the spatial distribution of the existing seismic network, especially after the integration with the land-based stations. We also expect to reduce the early warning time and the minimum magnitude threshold down to 1.0 in the Marmara Sea, which especially close to the northern branch of North Anatolian fault and which is the most active fault zone in the Marmara Sea. Once all observatories are deployed and data communication to KOERI has been established, research work on noise and signal analysis will be initiated, together with seismologic and seismotectonic studies.

CONCLUSIONS AND FUTURE CHALLENGES

The KOERI has a sufficient and reliable seismic network and is able to monitor earthquake activity in the region on a 24/7 basis. With very dense seismic, strong-motion instrumentation and five sea bottom multi-parameter measurement systems, the Marmara Sea and its surrounding area are becoming a natural laboratory. Concerning sea-level measurement, data transmission to KOERI from ONHO is established through ftp connection. NAMI DANCE Tsunami Simulation / Visualization Code have been installed in KOERI. Despite all these efforts and the considerable progress achieved, it is important to emphasize that tsunami observations and warning and/or watch activities require a multidisciplinary approach, and hence KOERI will increase the number of researchers from oceanography and hydrology in the near future and will increase the interaction with the meteorological resources it currently has.

With more than 140 years of history, KOERI has always recognized the need of an improved and close scientific collaboration among scientific institutions. We believe that the comprehensive and precise real-time monitoring of the seismicity in the region is very important, and KOERI is prepared to function as a Regional Tsunami Warning Center covering the Black Sea, Sea of Marmara, the Aegean Sea and the Eastern Mediterranean on 24/7 basis; however, online seismic and sea-level data from the northern part of the Black Sea and North and North-East Africa are needed to enhance detection capability. In this respect, KOERI has concluded new agreements with neighbouring countries' institutions to share seismic data in addition to the previous agreements, involving thirteen broadband stations from Romania to help better coverage of Aegean Sea and Black Sea region, respectively. In addition to this, KOERI has established an agreement with Georgia to share at least two stations in real time. We would like to continue to work together especially with the Northern African countries towards real-time exchange and sharing of broadband seismological data from the mutually selected and agreed seismological stations. To accomplish this, KOERI officially contacted institutions from Algeria, Tunisia, Libya, and Egypt.

As for the future plans, the followings will be considered:

- identification and segmentation of the seismic sources related to tsunami generation.
- updating and enhancing the bathymetric and topographic database for the near-shore regions
- customization of the computational tools for the better and effective performance in Regional Tsunami Warning Center.
- determination of the tsunami scenarios for simulations.
- performing simulations and obtaining database of computed tsunami parameters (distribution of coastal amplitudes, runup values, inundation distances, etc.) of each scenario.
- installing and operation of the tsunami modeling tools in cooperation with seismic and sea level data.

Information on tsunamigenic sources is of crucial importance, especially considering the short arrival times in the Marmara and Aegean Seas. To overcome the difficulties caused by short arrival times, an extensive modeling study is being initiated at KOERI that will help to produce a Tsunami Hazard Map for the Eastern Mediterranean, Aegean, Marmara, and Black Seas. The goal of this study is not only to review the existing tsunami zones and re-evaluating existing studies, but also concentrating on regions where previously such hazard assessments were not made. Tsunami modeling will be performed on each tsunami source region based on deterministic approach and a Tsunami Risk Map for Turkey will be created initially.

This paper sought to inform the reader about the past tsunami events around Turkey together with historical and modern studies in order to understand and analyze the tsunami hazard. Also included were the results of a model of selected tsunamigenic regions. There is no doubt that the establishment of a Tsunami Warning Center will broaden the existing knowledge and opportunities concerning tsunami related studies, leading towards a higher level of cooperation among national and international institutions, after which the global scientific community will benefit considerably.

ACKNOWLEDGMENTS

We would like to thank to the State Planning Organization, Republic of Turkey–Prime Ministry, for providing support to the “Regional Tsunami Monitoring and Evaluation Center” Project (Project Number: 2010K140200). Professor Yalciner would like to thank Professors C. Synolakis, F. Imamura, N. Shuto, and E. Pelinovsky for their long-term collaboration and contributions in tsunami research. Drs A. Zaitsev and A. Chernov are also sincerely acknowledged for their outstanding efforts on development of tsunami model NAMI DANCE.

REFERENCES

Algan O, Namık Yalcin M, Ozdogan M, Yilmaz I, Sari E, Kirci-Elmas E, Ongan D, Bulkan-Yesiladalı O, Yilmaz Y, Karamut I (2009). A short note on the geo-archeological significance of the ancient Theodosius harbour (Istanbul, Turkey); *Quaternary Research*, 72:457–461.

Altınok Y, Ersoy S (2000). Tsunamis observed on and near the Turkish coast, *Nat. Hazards,* 21:185–205.
Altinok Y; Alpar B; Yaltirak C (2003). Sarkoy-Murefte 1912 Earthquake's Tsunami, extension of the associated faulting in the Marmara Sea, Turkey; *J. Seismol*., 7: 329–346.
Ambraseys NN (2002). Seismic sea-waves in the Marmara Sea region during the last 20 centuries. *J. Seismol*, 6:571– 578.
Ambraseys NN, Finkel, C (1995). The seismicity of Turkey and adjacent areas. A historical review, 1500–1800, *Eren Yayıncılık*, Istanbul.
Boschi E, Tinti S, Armigliato A. et al. (2005). A tsunami warning system for the Mediterranean: a utopia that could be implemented in a short time. EGU-2005 General Assembly, NH6.01 Tsunamis, *Geophysical Research Abstracts*, Vol. 7.
Dotsenko SF, Ingerov AV (2007). Spectra of the Black-Sea tsunamis, *Phys. Oceanography*, 17(5): 269-277.
Eyidogan H, Guclu U, Utku Z, Degirmenci E (1991). Türkiye Büyük Depremleri Makro-Sismik Rehberi (Macro-Seismic guide of big earthquakes in Turkey) (1990–1988), ITU Maden Fak. Jeofizik Muhendisligi Bolumu, Istanbul.
Fokaefs A, Papadopoulos GA (2007). Tsunami hazard in the Eastern Mediterranean: strong earthquakes and tsunamis in Cyprus and the Levantine Sea, *Nat, Hazards*, 40:503–526.
Guidoboni E, Comastri A, Trania G (1994). *Catalogue of Ancient Earthquakes in the Mediterranean Area up to 10th Century*, Instituto Nazionale di Geofisica, Rome
Guidoboni E, Comastri A (2005). *Catalogue of Earthquakes and Tsunamis in the Mediterranean Area from the 11th to the 15th Century,* Istituto Nazionale di Geofisica e Vulcanologia—Storia Geofisica Ambiente (INGV-SGA), Italy.
Karnik V (1971). Tsunamis. In: Seismicity of the European Area. Part II, D. Reidel Publ. Co., Dordrecht, pp. 203-206.
Mihailovic J (1927). Memoir-Sur les Grands Tremblement de Terre de la Mer de Marmara, Beograd, pp. 215–222.
Murty TS (1977). *Seismic Sea Waves Tsunamis, Department of Fisheries and the Environment Fisheries and Marine Service*, Scientific Information and Publication Branch, Ottawa, Canada.
Oztin F, Bayulke N (1991). Historical earthquakes of Istanbul, Kayseri, Elazıg, *Proceedings*, Workshop on Historical Seismicity and Seismotectonics of theMediterranean Region, (Istanbul), Turkish Atomic Energy Authority, Ankara, pp. 150–173.
Oztin F (1994). 10 Temmuz 1894 Istanbul Depremi Raporu, T.C. Bayindirlik ve Iskan Bakanligi, Afet Isleri Genel Mudurlugu, Deprem Arastırma Dairesi, (Report on 10 July 1894 Istanbul Earthquake by Ministry of Public Works and Settlement, General Directorate of Disaster Affairs, Department of Earthquake Research), Ankara.
Papadopoulos GA, Daskalaki E, Fokaefs A, Giraleas N (2007). Tsunami hazard in the Eastern Mediterranean: strong earthquakes and tsunamis in the east Hellenic Arc and Trench system, *Natural Hazards and Earth System Sciences*, 7:57–64.
Perincek D, Meric E, Pulak C, Korpe R, Yalciner AC, Gokcay M, Avsar N, Nazik A, Kozanlı C., Kapan Yesilyurt S, Gokgoz Z (2007). Yenikapı Antik Liman Kazılarında Jeoarkeoloji Çalışmaları ve Yeni Bulgular (Geoarcheological studies in the Yenikapı Ancient Harbour Excavations and New Findings). 60. Türkiye Jeoloji Kurultayı, Ankara.
Scheffers A, Kelletat D (2005). Tsunami relics on the coastal landscape west of Lisbon (Portugal), *Science of Tsunami Hazard*, 23(3).
Soloviev SL, Solovieva ON, Go CN, Kim KS, Shchetnikov NA (2000). *Tsunamis in the Mediterranean Sea 2000 B.C.-2000 A.D*., Springer Verlag.
Taymaz T, Jackson JA, Westaway R (1990). Earthquake mechanisms in the Hellenic trench near Crete, *Geophys. J. Inter.*, 102:695–731.
Taymaz T, Jackson JA, Mckenzie D (1992). Active tectonics of the north and central Aegean Sea, *Geophys. J. Inter.*, 106:433–490.
Tinti S, Armigliato A, Manucci A, Pagnoni G, Zaniboni F, Yalçıner AC, Altinok Y (2006). The generating mechanisms of the August 17, 1999 Izmit bay (Turkey) tsunami: Regional (tectonic) and local (mass instabilities) causes, *Marine Geology*, 225:311– 330.
Yalciner AC, Synolakis, CE, Alpar B, Borrero J, Altinok Y, Imamura F, Tinti S, Ersoy S, Kuran U, Pamukcu S, Kanoglu U (2001). Field surveys and modeling of the 1999 Izmit Tsunami. *Proceedings*, International Tsunami Symposium, Seattle, Washington, pp. 557–564.
Yalcıner AC, Alpar B, Altinok Y, Ozbay I Imamura F (2002a). Tsunamis in the Sea of Marmara: historical documents for the past, models for the future, *Marine Geology*, 190:445–463.
Yalciner AC, Cakir TE (2002b). Eyewitness report of 1956 Southern Aegean tsunami in Bodrum peninsula, Turkey, International Symposium on Natural and Human Made Hazards HAZARDS 2002, Antalya, Turkey.

Yalciner AC, Pelinovsky E, Talipova T, Kurkin A, Kozelkov A, Zaitsev A (2004). Tsunami in the Black Sea: comparison of the historical, instrumental and numerical data, *J. Geophys. Ress*, 109.

Yolsal S, Taymaz T, Yalciner AC 2007. Understanding tsunamis, potential source regions and tsunami-prone mechanisms in the Eastern Mediterranean, *Geo. Soc., London, Special Publications,* 291:201-230

Insurance, Field Measurement, Retrofit, Urban Renewal, and Tsunami Issues

PEER REPORTS

PEER reports are available individually or by yearly subscription. PEER reports can be ordered at http://peer.berkeley.edu/publications/peer_reports.html or by contacting the Pacific Earthquake Engineering Research Center, 325 Davis Hall mail code 1792, Berkeley, CA 94720. Tel.: (510) 642-3437; Fax: (510) 665-1655; Email: peer_editor@berkeley.edu

PEER 2011/07 *Seismic Risk Management in Urban Areas. Proceedings of a U.S.-Iran-Turkey Seismic Workshop.* September 2011.

PEER 2011/06 *The Use of Base Isolation Systems to Achieve Complex Seismic Performance Objectives.* Troy A. Morgan and Stephen A. Mahin. July 2011.

PEER 2011/05 *Case Studies of the Seismic Performance of Tall Buildings Designed by Alternative Means.* Task 12 Report for the Tall Buildings Initiative. Jack Moehle, Yousef Bozorgnia, Nirmal Jayaram, Pierson Jones, Mohsen Rahnama, Nilesh Shome, Zeynep Tuna, John Wallace, Tony Yang, and Farzin Zareian. July 2011.

PEER 2011/04 *Recommended Design Practice for Pile Foundations in Laterally Spreading Ground.* Scott A. Ashford, Ross W. Boulanger, and Scott J. Brandenberg. June 2011.

PEER 2011/03 *New Ground Motion Selection Procedures and Selected Motions for the PEER Transportation Research Program.* Jack W. Baker, Ting Lin, Shrey K. Shahi, and Nirmal Jayaram. March 2011.

PEER 2011/02 *A Bayesian Network Methodology for Infrastructure Seismic Risk Assessment and Decision Support.* Michelle T. Bensi, Armen Der Kiureghian, and Daniel Straub. March 2011.

PEER 2011/01 *Demand Fragility Surfaces for Bridges in Liquefied and Laterally Spreading Ground.* Scott J. Brandenberg, Jian Zhang, Pirooz Kashighandi, Yili Huo, and Minxing Zhao. March 2011.

PEER 2010/05 *Guidelines for Performance-Based Seismic Design of Tall Buildings.* Developed by the Tall Buildings Initiative. November 2010.

PEER 2010/04 *Application Guide for the Design of Flexible and Rigid Bus Connections between Substation Equipment Subjected to Earthquakes.* Jean-Bernard Dastous and Armen Der Kiureghian. September 2010.

PEER 2010/03 *Shear Wave Velocity as a Statistical Function of Standard Penetration Test Resistance and Vertical Effective Stress at Caltrans Bridge Sites.* Scott J. Brandenberg, Naresh Bellana, and Thomas Shantz. June 2010.

PEER 2010/02 *Stochastic Modeling and Simulation of Ground Motions for Performance-Based Earthquake Engineering.* Sanaz Rezaeian and Armen Der Kiureghian. June 2010.

PEER 2010/01 *Structural Response and Cost Characterization of Bridge Construction Using Seismic Performance Enhancement Strategies.* Ady Aviram, Božidar Stojadinović, Gustavo J. Parra-Montesinos, and Kevin R. Mackie. March 2010.

PEER 2009/03 *The Integration of Experimental and Simulation Data in the Study of Reinforced Concrete Bridge Systems Including Soil-Foundation-Structure Interaction.* Matthew Dryden and Gregory L. Fenves. November 2009.

PEER 2009/02 *Improving Earthquake Mitigation through Innovations and Applications in Seismic Science, Engineering, Communication, and Response. Proceedings of a U.S.-Iran Seismic Workshop.* October 2009.

PEER 2009/01 *Evaluation of Ground Motion Selection and Modification Methods: Predicting Median Interstory Drift Response of Buildings.* Curt B. Haselton, Ed. June 2009.

PEER 2008/10 *Technical Manual for Strata.* Albert R. Kottke and Ellen M. Rathje. February 2009.

PEER 2008/09 *NGA Model for Average Horizontal Component of Peak Ground Motion and Response Spectra.* Brian S.-J. Chiou and Robert R. Youngs. November 2008.

PEER 2008/08 *Toward Earthquake-Resistant Design of Concentrically Braced Steel Structures.* Patxi Uriz and Stephen A. Mahin. November 2008.

PEER 2008/07 *Using OpenSees for Performance-Based Evaluation of Bridges on Liquefiable Soils.* Stephen L. Kramer, Pedro Arduino, and HyungSuk Shin. November 2008.

PEER 2008/06 *Shaking Table Tests and Numerical Investigation of Self-Centering Reinforced Concrete Bridge Columns.* Hyung IL Jeong, Junichi Sakai, and Stephen A. Mahin. September 2008.

PEER 2008/05 *Performance-Based Earthquake Engineering Design Evaluation Procedure for Bridge Foundations Undergoing Liquefaction-Induced Lateral Ground Displacement.* Christian A. Ledezma and Jonathan D. Bray. August 2008.

PEER 2008/04 *Benchmarking of Nonlinear Geotechnical Ground Response Analysis Procedures.* Jonathan P. Stewart, Annie On-Lei Kwok, Youssef M. A. Hashash, Neven Matasovic, Robert Pyke, Zhiliang Wang, and Zhaohui Yang. August 2008.

PEER 2008/03 *Guidelines for Nonlinear Analysis of Bridge Structures in California.* Ady Aviram, Kevin R. Mackie, and Božidar Stojadinović. August 2008.

PEER 2008/02 *Treatment of Uncertainties in Seismic-Risk Analysis of Transportation Systems.* Evangelos Stergiou and Anne S. Kiremidjian. July 2008.

PEER 2008/01 *Seismic Performance Objectives for Tall Buildings.* William T. Holmes, Charles Kircher, William Petak, and Nabih Youssef. August 2008.

PEER 2007/12 *An Assessment to Benchmark the Seismic Performance of a Code-Conforming Reinforced Concrete Moment-Frame Building.* Curt Haselton, Christine A. Goulet, Judith Mitrani-Reiser, James L. Beck, Gregory G. Deierlein, Keith A. Porter, Jonathan P. Stewart, and Ertugrul Taciroglu. August 2008.

PEER 2007/11 *Bar Buckling in Reinforced Concrete Bridge Columns.* Wayne A. Brown, Dawn E. Lehman, and John F. Stanton. February 2008.

PEER 2007/10 *Computational Modeling of Progressive Collapse in Reinforced Concrete Frame Structures.* Mohamed M. Talaat and Khalid M. Mosalam. May 2008.

PEER 2007/09 *Integrated Probabilistic Performance-Based Evaluation of Benchmark Reinforced Concrete Bridges.* Kevin R. Mackie, John-Michael Wong, and Božidar Stojadinović. January 2008.

PEER 2007/08 *Assessing Seismic Collapse Safety of Modern Reinforced Concrete Moment-Frame Buildings.* Curt B. Haselton and Gregory G. Deierlein. February 2008.

PEER 2007/07 *Performance Modeling Strategies for Modern Reinforced Concrete Bridge Columns.* Michael P. Berry and Marc O. Eberhard. April 2008.

PEER 2007/06 *Development of Improved Procedures for Seismic Design of Buried and Partially Buried Structures.* Linda Al Atik and Nicholas Sitar. June 2007.

PEER 2007/05 *Uncertainty and Correlation in Seismic Risk Assessment of Transportation Systems.* Renee G. Lee and Anne S. Kiremidjian. July 2007.

PEER 2007/04 *Numerical Models for Analysis and Performance-Based Design of Shallow Foundations Subjected to Seismic Loading.* Sivapalan Gajan, Tara C. Hutchinson, Bruce L. Kutter, Prishati Raychowdhury, José A. Ugalde, and Jonathan P. Stewart. May 2008.

PEER 2007/03 *Beam-Column Element Model Calibrated for Predicting Flexural Response Leading to Global Collapse of RC Frame Buildings.* Curt B. Haselton, Abbie B. Liel, Sarah Taylor Lange, and Gregory G. Deierlein. May 2008.

PEER 2007/02 *Campbell-Bozorgnia NGA Ground Motion Relations for the Geometric Mean Horizontal Component of Peak and Spectral Ground Motion Parameters.* Kenneth W. Campbell and Yousef Bozorgnia. May 2007.

PEER 2007/01 *Boore-Atkinson NGA Ground Motion Relations for the Geometric Mean Horizontal Component of Peak and Spectral Ground Motion Parameters.* David M. Boore and Gail M. Atkinson. May. May 2007.

PEER 2006/12 *Societal Implications of Performance-Based Earthquake Engineering.* Peter J. May. May 2007.

PEER 2006/11 *Probabilistic Seismic Demand Analysis Using Advanced Ground Motion Intensity Measures, Attenuation Relationships, and Near-Fault Effects.* Polsak Tothong and C. Allin Cornell. March 2007.

PEER 2006/10 *Application of the PEER PBEE Methodology to the I-880 Viaduct.* Sashi Kunnath. February 2007.

PEER 2006/09 *Quantifying Economic Losses from Travel Forgone Following a Large Metropolitan Earthquake.* James Moore, Sungbin Cho, Yue Yue Fan, and Stuart Werner. November 2006.

PEER 2006/08 *Vector-Valued Ground Motion Intensity Measures for Probabilistic Seismic Demand Analysis*. Jack W. Baker and C. Allin Cornell. October 2006.

PEER 2006/07 *Analytical Modeling of Reinforced Concrete Walls for Predicting Flexural and Coupled–Shear-Flexural Responses.* Kutay Orakcal, Leonardo M. Massone, and John W. Wallace. October 2006.

PEER 2006/06 *Nonlinear Analysis of a Soil-Drilled Pier System under Static and Dynamic Axial Loading.* Gang Wang and Nicholas Sitar. November 2006.

PEER 2006/05 *Advanced Seismic Assessment Guidelines.* Paolo Bazzurro, C. Allin Cornell, Charles Menun, Maziar Motahari, and Nicolas Luco. September 2006.

PEER 2006/04 *Probabilistic Seismic Evaluation of Reinforced Concrete Structural Components and Systems.* Tae Hyung Lee and Khalid M. Mosalam. August 2006.

PEER 2006/03 *Performance of Lifelines Subjected to Lateral Spreading.* Scott A. Ashford and Teerawut Juirnarongrit. July 2006.

PEER 2006/02 *Pacific Earthquake Engineering Research Center Highway Demonstration Project.* Anne Kiremidjian, James Moore, Yue Yue Fan, Nesrin Basoz, Ozgur Yazali, and Meredith Williams. April 2006.

PEER 2006/01 *Bracing Berkeley. A Guide to Seismic Safety on the UC Berkeley Campus.* Mary C. Comerio, Stephen Tobriner, and Ariane Fehrenkamp. January 2006.

PEER 2005/16 *Seismic Response and Reliability of Electrical Substation Equipment and Systems.* Junho Song, Armen Der Kiureghian, and Jerome L. Sackman. April 2006.

PEER 2005/15 *CPT-Based Probabilistic Assessment of Seismic Soil Liquefaction Initiation.* R. E. S. Moss, R. B. Seed, R. E. Kayen, J. P. Stewart, and A. Der Kiureghian. April 2006.

PEER 2005/14 *Workshop on Modeling of Nonlinear Cyclic Load-Deformation Behavior of Shallow Foundations.* Bruce L. Kutter, Geoffrey Martin, Tara Hutchinson, Chad Harden, Sivapalan Gajan, and Justin Phalen. March 2006.

PEER 2005/13 *Stochastic Characterization and Decision Bases under Time-Dependent Aftershock Risk in Performance-Based Earthquake Engineering.* Gee Liek Yeo and C. Allin Cornell. July 2005.

PEER 2005/12 *PEER Testbed Study on a Laboratory Building: Exercising Seismic Performance Assessment.* Mary C. Comerio, editor. November 2005.

PEER 2005/11 *Van Nuys Hotel Building Testbed Report: Exercising Seismic Performance Assessment.* Helmut Krawinkler, editor. October 2005.

PEER 2005/10 *First NEES/E-Defense Workshop on Collapse Simulation of Reinforced Concrete Building Structures.* September 2005.

PEER 2005/09 *Test Applications of Advanced Seismic Assessment Guidelines.* Joe Maffei, Karl Telleen, Danya Mohr, William Holmes, and Yuki Nakayama. August 2006.

PEER 2005/08 *Damage Accumulation in Lightly Confined Reinforced Concrete Bridge Columns.* R. Tyler Ranf, Jared M. Nelson, Zach Price, Marc O. Eberhard, and John F. Stanton. April 2006.

PEER 2005/07 *Experimental and Analytical Studies on the Seismic Response of Freestanding and Anchored Laboratory Equipment.* Dimitrios Konstantinidis and Nicos Makris. January 2005.

PEER 2005/06 *Global Collapse of Frame Structures under Seismic Excitations*. Luis F. Ibarra and Helmut Krawinkler. September 2005.

PEER 2005//05 *Performance Characterization of Bench- and Shelf-Mounted Equipment.* Samit Ray Chaudhuri and Tara C. Hutchinson. May 2006.

PEER 2005/04 *Numerical Modeling of the Nonlinear Cyclic Response of Shallow Foundations.* Chad Harden, Tara Hutchinson, Geoffrey R. Martin, and Bruce L. Kutter. August 2005.

PEER 2005/03 *A Taxonomy of Building Components for Performance-Based Earthquake Engineering.* Keith A. Porter. September 2005.

PEER 2005/02 *Fragility Basis for California Highway Overpass Bridge Seismic Decision Making*. Kevin R. Mackie and Božidar Stojadinović. June 2005.

PEER 2005/01 *Empirical Characterization of Site Conditions on Strong Ground Motion.* Jonathan P. Stewart, Yoojoong Choi, and Robert W. Graves. June 2005.

PEER 2004/09 *Electrical Substation Equipment Interaction: Experimental Rigid Conductor Studies.* Christopher Stearns and André Filiatrault. February 2005.

PEER 2004/08 *Seismic Qualification and Fragility Testing of Line Break 550-kV Disconnect Switches.* Shakhzod M. Takhirov, Gregory L. Fenves, and Eric Fujisaki. January 2005.

PEER 2004/07 *Ground Motions for Earthquake Simulator Qualification of Electrical Substation Equipment.* Shakhzod M. Takhirov, Gregory L. Fenves, Eric Fujisaki, and Don Clyde. January 2005.

PEER 2004/06 *Performance-Based Regulation and Regulatory Regimes.* Peter J. May and Chris Koski. September 2004.

PEER 2004/05 *Performance-Based Seismic Design Concepts and Implementation: Proceedings of an International Workshop.* Peter Fajfar and Helmut Krawinkler, editors. September 2004.

PEER 2004/04 *Seismic Performance of an Instrumented Tilt-up Wall Building.* James C. Anderson and Vitelmo V. Bertero. July 2004.

PEER 2004/03 *Evaluation and Application of Concrete Tilt-up Assessment Methodologies.* Timothy Graf and James O. Malley. October 2004.

PEER 2004/02 *Analytical Investigations of New Methods for Reducing Residual Displacements of Reinforced Concrete Bridge Columns.* Junichi Sakai and Stephen A. Mahin. August 2004.

PEER 2004/01 *Seismic Performance of Masonry Buildings and Design Implications.* Kerri Anne Taeko Tokoro, James C. Anderson, and Vitelmo V. Bertero. February 2004.

PEER 2003/18 *Performance Models for Flexural Damage in Reinforced Concrete Columns.* Michael Berry and Marc Eberhard. August 2003.

PEER 2003/17 *Predicting Earthquake Damage in Older Reinforced Concrete Beam-Column Joints.* Catherine Pagni and Laura Lowes. October 2004.

PEER 2003/16 *Seismic Demands for Performance-Based Design of Bridges.* Kevin Mackie and Božidar Stojadinović. August 2003.

PEER 2003/15 *Seismic Demands for Nondeteriorating Frame Structures and Their Dependence on Ground Motions.* Ricardo Antonio Medina and Helmut Krawinkler. May 2004.

PEER 2003/14 *Finite Element Reliability and Sensitivity Methods for Performance-Based Earthquake Engineering.* Terje Haukaas and Armen Der Kiureghian. April 2004.

PEER 2003/13 *Effects of Connection Hysteretic Degradation on the Seismic Behavior of Steel Moment-Resisting Frames.* Janise E. Rodgers and Stephen A. Mahin. March 2004.

PEER 2003/12 *Implementation Manual for the Seismic Protection of Laboratory Contents: Format and Case Studies.* William T. Holmes and Mary C. Comerio. October 2003.

PEER 2003/11 *Fifth U.S.-Japan Workshop on Performance-Based Earthquake Engineering Methodology for Reinforced Concrete Building Structures.* February 2004.

PEER 2003/10 *A Beam-Column Joint Model for Simulating the Earthquake Response of Reinforced Concrete Frames.* Laura N. Lowes, Nilanjan Mitra, and Arash Altoontash. February 2004.

PEER 2003/09 *Sequencing Repairs after an Earthquake: An Economic Approach.* Marco Casari and Simon J. Wilkie. April 2004.

PEER 2003/08 *A Technical Framework for Probability-Based Demand and Capacity Factor Design (DCFD) Seismic Formats.* Fatemeh Jalayer and C. Allin Cornell. November 2003.

PEER 2003/07 *Uncertainty Specification and Propagation for Loss Estimation Using FOSM Methods.* Jack W. Baker and C. Allin Cornell. September 2003.

PEER 2003/06 *Performance of Circular Reinforced Concrete Bridge Columns under Bidirectional Earthquake Loading.* Mahmoud M. Hachem, Stephen A. Mahin, and Jack P. Moehle. February 2003.

PEER 2003/05 *Response Assessment for Building-Specific Loss Estimation.* Eduardo Miranda and Shahram Taghavi. September 2003.

PEER 2003/04 *Experimental Assessment of Columns with Short Lap Splices Subjected to Cyclic Loads*. Murat Melek, John W. Wallace, and Joel Conte. April 2003.

PEER 2003/03 *Probabilistic Response Assessment for Building-Specific Loss Estimation.* Eduardo Miranda and Hesameddin Aslani. September 2003.

PEER 2003/02 *Software Framework for Collaborative Development of Nonlinear Dynamic Analysis Program.* Jun Peng and Kincho H. Law. September 2003.

PEER 2003/01 *Shake Table Tests and Analytical Studies on the Gravity Load Collapse of Reinforced Concrete Frames.* Kenneth John Elwood and Jack P. Moehle. November 2003.

PEER 2002/24 *Performance of Beam to Column Bridge Joints Subjected to a Large Velocity Pulse.* Natalie Gibson, André Filiatrault, and Scott A. Ashford. April 2002.

PEER 2002/23 *Effects of Large Velocity Pulses on Reinforced Concrete Bridge Columns.* Greg L. Orozco and Scott A. Ashford. April 2002.

PEER 2002/22 *Characterization of Large Velocity Pulses for Laboratory Testing.* Kenneth E. Cox and Scott A. Ashford. April 2002.

PEER 2002/21 *Fourth U.S.-Japan Workshop on Performance-Based Earthquake Engineering Methodology for Reinforced Concrete Building Structures*. December 2002.

PEER 2002/20 *Barriers to Adoption and Implementation of PBEE Innovations.* Peter J. May. August 2002.

PEER 2002/19 *Economic-Engineered Integrated Models for Earthquakes: Socioeconomic Impacts.* Peter Gordon, James E. Moore II, and Harry W. Richardson. July 2002.

PEER 2002/18 *Assessment of Reinforced Concrete Building Exterior Joints with Substandard Details.* Chris P. Pantelides, Jon Hansen, Justin Nadauld, and Lawrence D. Reaveley. May 2002.

PEER 2002/17 *Structural Characterization and Seismic Response Analysis of a Highway Overcrossing Equipped with Elastomeric Bearings and Fluid Dampers: A Case Study.* Nicos Makris and Jian Zhang. November 2002.

PEER 2002/16 *Estimation of Uncertainty in Geotechnical Properties for Performance-Based Earthquake Engineering.* Allen L. Jones, Steven L. Kramer, and Pedro Arduino. December 2002.

PEER 2002/15 *Seismic Behavior of Bridge Columns Subjected to Various Loading Patterns.* Asadollah Esmaeily-Gh. and Yan Xiao. December 2002.

PEER 2002/14 *Inelastic Seismic Response of Extended Pile Shaft Supported Bridge Structures.* T.C. Hutchinson, R.W. Boulanger, Y.H. Chai, and I.M. Idriss. December 2002.

PEER 2002/13 *Probabilistic Models and Fragility Estimates for Bridge Components and Systems.* Paolo Gardoni, Armen Der Kiureghian, and Khalid M. Mosalam. June 2002.

PEER 2002/12 *Effects of Fault Dip and Slip Rake on Near-Source Ground Motions: Why Chi-Chi Was a Relatively Mild M7.6 Earthquake.* Brad T. Aagaard, John F. Hall, and Thomas H. Heaton. December 2002.

PEER 2002/11 *Analytical and Experimental Study of Fiber-Reinforced Strip Isolators*. James M. Kelly and Shakhzod M. Takhirov. September 2002.

PEER 2002/10 *Centrifuge Modeling of Settlement and Lateral Spreading with Comparisons to Numerical Analyses***.** Sivapalan Gajan and Bruce L. Kutter. January 2003.

PEER 2002/09 *Documentation and Analysis of Field Case Histories of Seismic Compression during the 1994 Northridge, California, Earthquake.* Jonathan P. Stewart, Patrick M. Smith, Daniel H. Whang, and Jonathan D. Bray. October 2002.

PEER 2002/08 *Component Testing, Stability Analysis and Characterization of Buckling-Restrained Unbonded Braces*^{TM}. Cameron Black, Nicos Makris, and Ian Aiken. September 2002.

PEER 2002/07 *Seismic Performance of Pile-Wharf Connections.* Charles W. Roeder, Robert Graff, Jennifer Soderstrom, and Jun Han Yoo. December 2001.

PEER 2002/06 *The Use of Benefit-Cost Analysis for Evaluation of Performance-Based Earthquake Engineering Decisions*. Richard O. Zerbe and Anthony Falit-Baiamonte. September 2001.

PEER 2002/05 *Guidelines, Specifications, and Seismic Performance Characterization of Nonstructural Building Components and Equipment*. André Filiatrault, Constantin Christopoulos, and Christopher Stearns. September 2001.

PEER 2002/04 *Consortium of Organizations for Strong-Motion Observation Systems and the Pacific Earthquake Engineering Research Center Lifelines Program: Invited Workshop on Archiving and Web Dissemination of Geotechnical Data, 4–5 October 2001.* September 2002.

PEER 2002/03 *Investigation of Sensitivity of Building Loss Estimates to Major Uncertain Variables for the Van Nuys Testbed.* Keith A. Porter, James L. Beck, and Rustem V. Shaikhutdinov. August 2002.

PEER 2002/02 *The Third U.S.-Japan Workshop on Performance-Based Earthquake Engineering Methodology for Reinforced Concrete Building Structures*. July 2002.

PEER 2002/01 *Nonstructural Loss Estimation: The UC Berkeley Case Study.* Mary C. Comerio and John C. Stallmeyer. December 2001.

PEER 2001/16 *Statistics of SDF-System Estimate of Roof Displacement for Pushover Analysis of Buildings.* Anil K. Chopra, Rakesh K. Goel, and Chatpan Chintanapakdee. December 2001.

PEER 2001/15 *Damage to Bridges during the 2001 Nisqually Earthquake.* R. Tyler Ranf, Marc O. Eberhard, and Michael P. Berry. November 2001.

PEER 2001/14 *Rocking Response of Equipment Anchored to a Base Foundation.* Nicos Makris and Cameron J. Black. September 2001.

PEER 2001/13 *Modeling Soil Liquefaction Hazards for Performance-Based Earthquake Engineering.* Steven L. Kramer and Ahmed-W. Elgamal. February 2001.

PEER 2001/12 *Development of Geotechnical Capabilities in OpenSees.* Boris Jeremić. September 2001.

PEER 2001/11 *Analytical and Experimental Study of Fiber-Reinforced Elastomeric Isolators*. James M. Kelly and Shakhzod M. Takhirov. September 2001.

PEER 2001/10 *Amplification Factors for Spectral Acceleration in Active Regions.* Jonathan P. Stewart, Andrew H. Liu, Yoojoong Choi, and Mehmet B. Baturay. December 2001.

PEER 2001/09 *Ground Motion Evaluation Procedures for Performance-Based Design.* Jonathan P. Stewart, Shyh-Jeng Chiou, Jonathan D. Bray, Robert W. Graves, Paul G. Somerville, and Norman A. Abrahamson. September 2001.

PEER 2001/08 *Experimental and Computational Evaluation of Reinforced Concrete Bridge Beam-Column Connections for Seismic Performance*. Clay J. Naito, Jack P. Moehle, and Khalid M. Mosalam. November 2001.

PEER 2001/07 *The Rocking Spectrum and the Shortcomings of Design Guidelines.* Nicos Makris and Dimitrios Konstantinidis. August 2001.

PEER 2001/06 *Development of an Electrical Substation Equipment Performance Database for Evaluation of Equipment Fragilities*. Thalia Agnanos. April 1999.

PEER 2001/05 *Stiffness Analysis of Fiber-Reinforced Elastomeric Isolators.* Hsiang-Chuan Tsai and James M. Kelly. May 2001.

PEER 2001/04 *Organizational and Societal Considerations for Performance-Based Earthquake Engineering.* Peter J. May. April 2001.

PEER 2001/03 *A Modal Pushover Analysis Procedure to Estimate Seismic Demands for Buildings: Theory and Preliminary Evaluation.* Anil K. Chopra and Rakesh K. Goel. January 2001.

PEER 2001/02 *Seismic Response Analysis of Highway Overcrossings Including Soil-Structure Interaction.* Jian Zhang and Nicos Makris. March 2001.

PEER 2001/01 *Experimental Study of Large Seismic Steel Beam-to-Column Connections.* Egor P. Popov and Shakhzod M. Takhirov. November 2000.

PEER 2000/10 *The Second U.S.-Japan Workshop on Performance-Based Earthquake Engineering Methodology for Reinforced Concrete Building Structures.* March 2000.

PEER 2000/09 *Structural Engineering Reconnaissance of the August 17, 1999 Earthquake: Kocaeli (Izmit), Turkey.* Halil Sezen, Kenneth J. Elwood, Andrew S. Whittaker, Khalid Mosalam, John J. Wallace, and John F. Stanton. December 2000.

PEER 2000/08 *Behavior of Reinforced Concrete Bridge Columns Having Varying Aspect Ratios and Varying Lengths of Confinement.* Anthony J. Calderone, Dawn E. Lehman, and Jack P. Moehle. January 2001.

PEER 2000/07 *Cover-Plate and Flange-Plate Reinforced Steel Moment-Resisting Connections.* Taejin Kim, Andrew S. Whittaker, Amir S. Gilani, Vitelmo V. Bertero, and Shakhzod M. Takhirov. September 2000.

PEER 2000/06 *Seismic Evaluation and Analysis of 230-kV Disconnect Switches.* Amir S. J. Gilani, Andrew S. Whittaker, Gregory L. Fenves, Chun-Hao Chen, Henry Ho, and Eric Fujisaki. July 2000.

PEER 2000/05 *Performance-Based Evaluation of Exterior Reinforced Concrete Building Joints for Seismic Excitation.* Chandra Clyde, Chris P. Pantelides, and Lawrence D. Reaveley. July 2000.

PEER 2000/04 *An Evaluation of Seismic Energy Demand: An Attenuation Approach.* Chung-Che Chou and Chia-Ming Uang. July 1999.

PEER 2000/03 *Framing Earthquake Retrofitting Decisions: The Case of Hillside Homes in Los Angeles.* Detlof von Winterfeldt, Nels Roselund, and Alicia Kitsuse. March 2000.

PEER 2000/02 *U.S.-Japan Workshop on the Effects of Near-Field Earthquake Shaking.* Andrew Whittaker, ed. July 2000.

PEER 2000/01 *Further Studies on Seismic Interaction in Interconnected Electrical Substation Equipment.* Armen Der Kiureghian, Kee-Jeung Hong, and Jerome L. Sackman. November 1999.

PEER 1999/14 *Seismic Evaluation and Retrofit of 230-kV Porcelain Transformer Bushings.* Amir S. Gilani, Andrew S. Whittaker, Gregory L. Fenves, and Eric Fujisaki. December 1999.

PEER 1999/13 *Building Vulnerability Studies: Modeling and Evaluation of Tilt-up and Steel Reinforced Concrete Buildings.* John W. Wallace, Jonathan P. Stewart, and Andrew S. Whittaker, editors. December 1999.

PEER 1999/12 *Rehabilitation of Nonductile RC Frame Building Using Encasement Plates and Energy-Dissipating Devices.* Mehrdad Sasani, Vitelmo V. Bertero, James C. Anderson. December 1999.

PEER 1999/11 *Performance Evaluation Database for Concrete Bridge Components and Systems under Simulated Seismic Loads.* Yael D. Hose and Frieder Seible. November 1999.

PEER 1999/10 *U.S.-Japan Workshop on Performance-Based Earthquake Engineering Methodology for Reinforced Concrete Building Structures.* December 1999.

PEER 1999/09 *Performance Improvement of Long Period Building Structures Subjected to Severe Pulse-Type Ground Motions*. James C. Anderson, Vitelmo V. Bertero, and Raul Bertero. October 1999.

PEER 1999/08 *Envelopes for Seismic Response Vectors.* Charles Menun and Armen Der Kiureghian. July 1999.

PEER 1999/07 *Documentation of Strengths and Weaknesses of Current Computer Analysis Methods for Seismic Performance of Reinforced Concrete Members.* William F. Cofer. November 1999.

PEER 1999/06 *Rocking Response and Overturning of Anchored Equipment under Seismic Excitations.* Nicos Makris and Jian Zhang. November 1999.

PEER 1999/05 *Seismic Evaluation of 550 kV Porcelain Transformer Bushings.* Amir S. Gilani, Andrew S. Whittaker, Gregory L. Fenves, and Eric Fujisaki. October 1999.

PEER 1999/04 *Adoption and Enforcement of Earthquake Risk-Reduction Measures.* Peter J. May, Raymond J. Burby, T. Jens Feeley, and Robert Wood.

PEER 1999/03 *Task 3 Characterization of Site Response General Site Categories.* Adrian Rodriguez-Marek, Jonathan D. Bray, and Norman Abrahamson. February 1999.

PEER 1999/02 *Capacity-Demand-Diagram Methods for Estimating Seismic Deformation of Inelastic Structures: SDF Systems.* Anil K. Chopra and Rakesh Goel. April 1999.

PEER 1999/01 *Interaction in Interconnected Electrical Substation Equipment Subjected to Earthquake Ground Motions.* Armen Der Kiureghian, Jerome L. Sackman, and Kee-Jeung Hong. February 1999.

PEER 1998/08 *Behavior and Failure Analysis of a Multiple-Frame Highway Bridge in the 1994 Northridge Earthquake.* Gregory L. Fenves and Michael Ellery. December 1998.

PEER 1998/07 *Empirical Evaluation of Inertial Soil-Structure Interaction Effects.* Jonathan P. Stewart, Raymond B. Seed, and Gregory L. Fenves. November 1998.

PEER 1998/06 *Effect of Damping Mechanisms on the Response of Seismic Isolated Structures.* Nicos Makris and Shih-Po Chang. November 1998.

PEER 1998/05 *Rocking Response and Overturning of Equipment under Horizontal Pulse-Type Motions.* Nicos Makris and Yiannis Roussos. October 1998.

PEER 1998/04 *Pacific Earthquake Engineering Research Invitational Workshop Proceedings, May 14–15, 1998: Defining the Links between Planning, Policy Analysis, Economics and Earthquake Engineering.* Mary Comerio and Peter Gordon. September 1998.

PEER 1998/03 *Repair/Upgrade Procedures for Welded Beam to Column Connections.* James C. Anderson and Xiaojing Duan. May 1998.

PEER 1998/02 *Seismic Evaluation of 196 kV Porcelain Transformer Bushings.* Amir S. Gilani, Juan W. Chavez, Gregory L. Fenves, and Andrew S. Whittaker. May 1998.

PEER 1998/01 *Seismic Performance of Well-Confined Concrete Bridge Columns.* Dawn E. Lehman and Jack P. Moehle. December 2000.

ONLINE REPORTS

The following PEER reports are available by Internet only at http://peer.berkeley.edu/publications/peer_reports.html

PEER 2011/106 *Self Compacting Hybrid Fiber Reinforced Concrete Composites for Bridge Columns.* Pardeep Kumar, Gabriel Jen, William Trono, Marios Panagiotou, and Claudia Ostertag. September 2011.

PEER 2011/105 *Stochastic Dynamic Analysis of Bridges Subjected to Spacially Varying Ground Motions.* Katerina Konakli and Armen Der Kiureghian. August 2011.

PEER 2011/104 *Design and Instrumentation of the 2010 E-Defense Four-Story Reinforced Concrete and Post-Tensioned Concrete Buildings.* Takuya Nagae, Kenichi Tahara, Taizo Matsumori, Hitoshi Shiohara, Toshimi Kabeyasawa, Susumu Kono, Minehiro Nishiyama (Japanese Research Team) and John Wallace, Wassim Ghannoum, Jack Moehle, Richard Sause, Wesley Keller, Zeynep Tuna (U.S. Research Team). June 2011.

PEER 2011/103 *In-Situ Monitoring of the Force Output of Fluid Dampers: Experimental Investigation.* Dimitrios Konstantinidis, James M. Kelly, and Nicos Makris. April 2011.

PEER 2011/102 *Ground-motion prediction equations 1964 - 2010.* John Douglas. April 2011.

PEER 2011/101 *Report of the Eighth Planning Meeting of NEES/E-Defense Collaborative Research on Earthquake Engineering.* Convened by the Hyogo Earthquake Engineering Research Center (NIED), NEES Consortium, Inc. February 2011.

PEER 2010/111 *Modeling and Acceptance Criteria for Seismic Design and Analysis of Tall Buildings.* Task 7 Report for the Tall Buildings Initiative - Published jointly by the Applied Technology Council. October 2010.

PEER 2010/110 *Seismic Performance Assessment and Probabilistic Repair Cost Analysis of Precast Concrete Cladding Systems for Multistory Buildlings.* Jeffrey P. Hunt and Božidar Stojadinovic. November 2010.

PEER 2010/109 *Report of the Seventh Joint Planning Meeting of NEES/E-Defense Collaboration on Earthquake Engineering. Held at the E-Defense, Miki, and Shin-Kobe, Japan, September 18–19, 2009.* August 2010.

PEER 2010/108 *Probabilistic Tsunami Hazard in California.* Hong Kie Thio, Paul Somerville, and Jascha Polet, preparers. October 2010.

PEER 2010/107 *Performance and Reliability of Exposed Column Base Plate Connections for Steel Moment-Resisting Frames.* Ady Aviram, Božidar Stojadinovic, and Armen Der Kiureghian. August 2010.

PEER 2010/106 *Verification of Probabilistic Seismic Hazard Analysis Computer Programs.* Patricia Thomas, Ivan Wong, and Norman Abrahamson. May 2010.

PEER 2010/105 *Structural Engineering Reconnaissance of the April 6, 2009, Abruzzo, Italy, Earthquake, and Lessons Learned.* M. Selim Günay and Khalid M. Mosalam. April 2010.

PEER 2010/104 *Simulating the Inelastic Seismic Behavior of Steel Braced Frames, Including the Effects of Low-Cycle Fatigue.* Yuli Huang and Stephen A. Mahin. April 2010.

PEER 2010/103 *Post-Earthquake Traffic Capacity of Modern Bridges in California.* Vesna Terzic and Božidar Stojadinović. March 2010.

PEER 2010/102 *Analysis of Cumulative Absolute Velocity (CAV) and JMA Instrumental Seismic Intensity (I_{JMA}) Using the PEER–NGA Strong Motion Database.* Kenneth W. Campbell and Yousef Bozorgnia. February 2010.

PEER 2010/101 *Rocking Response of Bridges on Shallow Foundations.* Jose A. Ugalde, Bruce L. Kutter, and Boris Jeremic. April 2010.

PEER 2009/109 *Simulation and Performance-Based Earthquake Engineering Assessment of Self-Centering Post-Tensioned Concrete Bridge Systems.* Won K. Lee and Sarah L. Billington. December 2009.

PEER 2009/108 *PEER Lifelines Geotechnical Virtual Data Center.* J. Carl Stepp, Daniel J. Ponti, Loren L. Turner, Jennifer N. Swift, Sean Devlin, Yang Zhu, Jean Benoit, and John Bobbitt. September 2009.

PEER 2009/107 *Experimental and Computational Evaluation of Current and Innovative In-Span Hinge Details in Reinforced Concrete Box-Girder Bridges: Part 2: Post-Test Analysis and Design Recommendations.* Matias A. Hube and Khalid M. Mosalam. December 2009.

PEER 2009/106 *Shear Strength Models of Exterior Beam-Column Joints without Transverse Reinforcement.* Sangjoon Park and Khalid M. Mosalam. November 2009.

PEER 2009/105 *Reduced Uncertainty of Ground Motion Prediction Equations through Bayesian Variance Analysis.* Robb Eric S. Moss. November 2009.

PEER 2009/104 *Advanced Implementation of Hybrid Simulation.* Andreas H. Schellenberg, Stephen A. Mahin, Gregory L. Fenves. November 2009.

PEER 2009/103 *Performance Evaluation of Innovative Steel Braced Frames.* T. Y. Yang, Jack P. Moehle, and Božidar Stojadinovic. August 2009.

PEER 2009/102 *Reinvestigation of Liquefaction and Nonliquefaction Case Histories from the 1976 Tangshan Earthquake.* Robb Eric Moss, Robert E. Kayen, Liyuan Tong, Songyu Liu, Guojun Cai, and Jiaer Wu. August 2009.

PEER 2009/101 *Report of the First Joint Planning Meeting for the Second Phase of NEES/E-Defense Collaborative Research on Earthquake Engineering.* Stephen A. Mahin et al. July 2009.

PEER 2008/104 *Experimental and Analytical Study of the Seismic Performance of Retaining Structures.* Linda Al Atik and Nicholas Sitar. January 2009.

PEER 2008/103 *Experimental and Computational Evaluation of Current and Innovative In-Span Hinge Details in Reinforced Concrete Box-Girder Bridges. Part 1: Experimental Findings and Pre-Test Analysis.* Matias A. Hube and Khalid M. Mosalam. January 2009.

PEER 2008/102 *Modeling of Unreinforced Masonry Infill Walls Considering In-Plane and Out-of-Plane Interaction.* Stephen Kadysiewski and Khalid M. Mosalam. January 2009.

PEER 2008/101 *Seismic Performance Objectives for Tall Buildings.* William T. Holmes, Charles Kircher, William Petak, and Nabih Youssef. August 2008.

PEER 2007/101 *Generalized Hybrid Simulation Framework for Structural Systems Subjected to Seismic Loading.* Tarek Elkhoraibi and Khalid M. Mosalam. July 2007.

PEER 2007/100 *Seismic Evaluation of Reinforced Concrete Buildings Including Effects of Masonry Infill Walls.* Alidad Hashemi and Khalid M. Mosalam. July 2007.

The Pacific Earthquake Engineering Research Center (PEER) is a multi-institutional research and education center with headquarters at the University of California, Berkeley. Investigators from over 20 universities, several consulting companies, and researchers at various state and federal government agencies contribute to research programs focused on performance-based earthquake engineering.

These research programs aim to identify and reduce the risks from major earthquakes to life safety and to the economy by including research in a wide variety of disciplines including structural and geotechnical engineering, geology/seismology, lifelines, transportation, architecture, economics, risk management, and public policy.

PEER is supported by federal, state, local, and regional agencies, together with industry partners.

PEER reports can be ordered at http://peer.berkeley.edu/publications/peer_reports.html or by contacting

Pacific Earthquake Engineering Research Center
University of California, Berkeley
325 Davis Hall, mail code 1792
Berkeley, CA 94720-1792
Tel: 510-642-3437
Fax: 510-642-1655
Email: peer_editor@berkeley.edu

ISSN 1547-0587X